

STEREOSELECTIVE ADDITION OF SIMPLE AMINES TO UNACTIVATED
ALKENES

by

ALEXANDER REZNICHENKO

A Dissertation submitted to the
Graduate School-New Brunswick
Rutgers, The State University of New Jersey
in partial fulfillment of the requirements

for the degree of

Doctor of Philosophy

Graduate Program in Chemistry and Chemical Biology

written under the direction of

Professor Kai C. Hultsch

and approved by

New Brunswick, New Jersey

October 2012

ABSTRACT OF THE DISSERTATION

Stereoselective Addition of Simple Amines to Unactivated Alkenes

By ALEXANDER REZNICHENKO

Dissertation Director:

Professor Kai C. Hultsch

The facile and atom-economic synthesis of amines via direct addition of an amine N–H or C–H moiety to an unactivated alkene belongs to the major challenges of organometallic catalysis. In this thesis we summarize our efforts towards the development of efficient stereoselective catalysts for the addition of the amine N–H-fragment to alkenes, which is known as a catalytic hydroamination reaction. We have performed a detailed mechanistic study of the rare earth metal-catalyzed stereoselective hydroamination/cyclization with particular focus on the kinetic resolution of racemic aminoalkenes. Key factors governing the reaction efficiency were determined and we were able to address the significantly more challenging intermolecular hydroamination by utilizing two rare earth metal-based catalyst families featuring sterically tunable C_1 - and C_2 -symmetric diolate ligand frameworks. The first example of an asymmetric intermolecular hydroamination of a simple alkene was demonstrated and enantioselectivities of up to 61% ee and 73% de were achieved in this novel catalytic process. Steric features of the voluminous silyl groups were shown to be detrimental for

both catalyst stability and catalytic performance. A novel NOBIN-based C_1 -symmetric diolate ligand family was introduced and it was utilized for preparation of rare earth and group 4 metal diolates. Novel NOBIN-based complexes were active catalysts in hydroamination/cyclization reaching selectivities of up to 92% ee. We have also addressed the problem of limited substrate scope of group 4 metal-based hydroamination catalysts by introducing novel zirconium bis(amidate) complexes which perform hydroamination/cyclization of challenging substrates, including aminoheptenes, under mild reaction conditions. In addition to our studies of a hydroamination reaction we have also addressed a complementary transformation which involves a C–H addition of an amine to an unactivated alkene and is known as a hydroaminoalkylation reaction. We have developed highly active and enantioselective (up to 98% ee) group 5 metal-based catalysts for this transformation using 3,3'-disilylated binaphtholate ligands and for the first time studied the kinetics and mechanism of the catalytic hydroaminoalkylation. The reaction was found to proceed via fast reversible non-dissociative metallaaziridine formation, followed by a fast alkene insertion and rate-determining amine exchange.

ACKNOWLEDGEMENTS

I would like to thank my research advisor, Dr. Kai Hultzsich, for his support, expertise and seemingly endless patience, which he was demonstrating during several exciting and productive years in Erlangen and New Jersey. I can only hope that Kai enjoyed our collaboration over this time as much as I did.

I would also like to thank Professor Alan Goldman, Professor Daniel Seidel and Professor Frieder Jäkle for joining my thesis committee and providing a very instructive feedback over the course of my work.

I am grateful to Dr. Tom Emge (Rutgers) and Dr. Frank Hampel (Erlangen) for the X-ray crystallographic measurements. I want to thank Professor Daniel Seidel, Eric Klauber, Nisha Mittal and Deepankar Das for kindly providing some of the chiral HPLC data.

Selected proligands, metal complexes and aminoalkene substrates mentioned in this work have been kindly provided by the current and former members of Hultzsich research group: Hiep Nguyen, Stephan Audörsch, Hyeunjoo Lee and Xiaoming Zhang.

I am indebted to several Hultzsich group veteran members, for their personal and professional contributions, in particular to Denis Gribkov, Patricia Horrillo and Boyan Lazarov. My thanks and best wishes also go to Boyan, Hiep, Lisa and John who are the current core of the Hultzsich research team.

Gratefully acknowledged are the key sources of joy and inspiration which included but were not limited to, Evelyn Waugh, Modest Mussorgsky and the New Jersey Devils.

Last but not least, I am and will always be thankful to my family and friends.

Table of Contents

Abstract of the Dissertation	ii
Acknowledgements.....	iv
Table of Contents	v
List of Tables	ix
List of Schemes.....	xii
List of Figures	xvi
List of abbreviations and symbols	xxii
I. Chapter 1. Asymmetric Hydroamination of Alkenes: Recent Developments and Major Challenges	1
I.1 Introduction: Synthesis of Amines via Hydroamination	1
I.2 Intramolecular Asymmetric Hydroamination of Simple Aminoalkenes	2
I.2.1 Rare Earth Metal-Based Catalysts	2
I.2.2 Alkali Metal-Based Catalysts	16
I.2.3 Alkaline Earth Metal-Based Catalysts.....	19
I.2.4 Group 4 Metal-Based Catalysts	20
I.2.5 Late Transition Metal Catalysts.....	26
I.2.6 Organocatalytic Asymmetric Hydroamination.....	31
I.2.7 Kinetic Resolution via Asymmetric Hydroamination	32
I.3 Intermolecular Hydroamination	35
I.3.1 Early Transition and Main Group Metal Catalysts.....	36
I.3.2 Late Transition Metal Catalysts.....	39
I.3.3 Enzymatic Asymmetric Hydroamination	48

I.4 Conclusions and Outlook.....	49
I.5 References	50
II Chapter 2. Kinetic Resolution of Aminoalkenes via Asymmetric Hydroamination: A Mechanistic Study.....	58
II.1 Introduction	58
II.2 Results and Discussion.....	59
II.2.1 Kinetic Resolution of α -Substituted Aminopentenes	59
II.2.2 Stereomodel for the Kinetic Resolution of Aminopentenes.....	70
II.2.3 Substrates other than α -substituted aminopentenes.....	72
II.3 Summary	78
II.4 Experimental	80
II.5 References	92
III Chapter 3. Asymmetric Intermolecular Hydroamination of Unactivated Alkenes with Simple Amines Catalyzed by Rare Earth Metal Binaphtholates	94
III.1 Introduction.....	94
III.2 Results and Discussion	94
III.2.1 Preliminary Studies on Intermolecular Hydroamination	94
III.2.2 Binaphtholate Catalyst Evaluation.....	103
III.2.3 Substrate Scope of Intermolecular Hydroamination.....	110
III.2.4 Mechanistic Observations	114
III.3 Conclusions and Outlook.....	120
III.4 Experimental	121
III.5 References.....	144

IV Chapter 4. Asymmetric Hydroamination of Alkenes Catalyzed by C1-Symmetric Rare Earth Metal and Zirconium Diolates.....	146
IV.1 Introduction.....	146
IV.2 Results and Discussion	149
IV.2.1 Ligand Design and Preparation	149
IV.2.2 Complex Synthesis	152
IV.2.3 Catalytic Intramolecular Hydroamination	154
IV.2.4 Intermolecular Asymmetric Hydroamination.....	160
IV.3 Conclusions.....	164
IV.4 Experimental.....	165
IV.5 References.....	196
V Chapter 5. Group 4 Metal Bis(Amidate)s in Asymmetric Hydroamination/Cyclization of Aminoalkenes	198
V.1 Introduction.....	198
V.2 Results and Discussion	200
V.2.1 Complex Synthesis.....	200
V.2.2 Catalytic Hydroamination	205
V.3 Conclusions.....	215
V.4 Experimental	217
V.5 References	244
VI Chapter 6. Asymmetric Intermolecular Hydroaminoalkylation of Unactivated Alkenes Catalyzed by Group 5 Metal Binaphtholates	247
VI.1 Introduction.....	247

VI.2 Results and Discussion	253
VI.2.1 Complex Synthesis	253
VI.2.2 Substrate Scope of Catalytic Hydroaminoalkylation.....	257
VI.2.3 Isotope Labeling Studies.....	262
VI.2.4 Empirical Rate Laws.....	272
VI.2.5 Kinetic Isotope Effects	276
VI.2.6 Mechanistic Model for Asymmetric Hydroaminoalkylation.....	277
VI.3 Group 5 Metal Binaphtholates in Catalytic Asymmetric Hydroamination .	289
VI.4 Conclusions.....	292
VI.5 Experimental.....	294
VI.6 References.....	332
Appendix A. Structures of complexes	336
Appendix B. Structures of aminoalkenes and corresponding hydroamination/cyclization products	338
Curriculum Vitae	339

Lists of Tables

Table I-1. Chiral lanthanocene-catalyzed asymmetric aminoalkene hydroamination/cyclization.....	7
Table I-2. Catalytic hydroamination-cyclization of 18 using diamidobinaphthyl ate-complexes.	12
Table I-3. Catalytic hydroamination-cyclization using diamidobinaphthyl ate-complexes formed in situ from proligand 20	13
Table I-4. Alkaline earth metal-catalyzed asymmetric hydroamination of aminopentenes.....	20
Table I-5. Asymmetric hydroamination of aminoalkenes catalyzed by zirconium complexes.	25
Table I-6. Rhodium-catalyzed enantioselective hydroamination-cyclization of aminopentenes.....	31
Table I-7. Catalytic kinetic resolution of chiral aminopentenes.	33
Table II-1. Kinetic resolution parameters of α -substituted aminopentenes	60
Table II-2. Preparation of highly enantioenriched α -substituted aminopentenes via kinetic resolution.....	67
Table II-3. Kinetic resolution parameters of α -substituted aminopentenes determined with 24a-Y	67
Table II-4. Kinetic resolution of 64 using binaphtholate catalysts 24-Ln at 25 °C.	73
Table II-5. Kinetic resolution parameters for 64 using 24a-Y	74
Table II-6. Attempted NMR-scale kinetic resolution of 66 at 30 °C.....	76

Table II-7. Kinetic resolution of aminohexene 71 using binaphtholate catalysts (<i>R</i>)- 24a and (<i>R</i>)- 24b at 80 °C.	78
Table II-8. Crystallographic data for (<i>R</i>)-Mosher amide of (<i>S</i>)- 64	90
Table III-1. Temperature dependence of the K^{dorm} value for the hydroamination of 6 with (<i>R</i>)- 24a-Y	102
Table III-2. Rare earth metal binaphtholates 24a-i in intermolecular hydroamination.	103
Table III-3. Intermolecular hydroamination of 1-heptene catalyzed by 80-Ln ...	108
Table III-4. Asymmetric intermolecular hydroamination catalyzed by 24a-Y . ..	111
Table IV-1. Catalyst evaluation for hydroamination/cyclization of 105	155
Table IV-2. Hydroamination/cyclization of various aminoalkenes catalyzed by 103c-Lu	157
Table IV-3. Catalytic kinetic resolution of chiral aminopentenes.	158
Table IV-4. Hydroamination/cyclization of aminopentenes, catalyzed by 104-M	159
Table IV-5. Intermolecular hydroamination of terminal alkenes catalyzed by 103-Ln	161
Table IV-6. Lanthanum-catalyzed intermolecular hydroamination of terminal alkenes.....	163
Table V-1. Asymmetric hydroamination-cyclization of aminoalkenes, catalyzed by 111	207
Table V-2. Diastereoselective hydroamination/cyclization of α -substituted aminopentenes.....	210

Table V-3. Asymmetric hydroamination/cyclization of aminoalkenes, catalyzed by (<i>R,R</i>)- 112d-Zr	214
Table V-4. Crystallographic data for (<i>R</i>)- 111d-Zr	238
Table V-5. Selected bond lengths [Å] and angles [°] for (<i>R</i>)- 111d-Zr -	239
Table V-6. Crystallographic data for (<i>R</i>)- 111ca-Zr	241
Table V-7. Bond lengths [Å] and angles [°] in (<i>R</i>)- 111ca-Zr	242
Table VI-1. Synthesis of group 5 metal binaphtholate complexes 127-M	254
Table VI-2. Selected Bond lengths [Å] and angles [°] in 127l-M (M = Ta, Nb).255	
Table VI-3. Catalytic asymmetric hydroaminoalkylation of 1-octene with N-methylaniline using binaphtholate tantalum and niobium Complexes	258
Table VI-4. Substrate scope in the intermolecular asymmetric hydroaminoalkylation catalyzed by 127j-M (M = Ta, Nb).	259
Table VI-5. Nonlinear fit to the models of various detalization levels.....	284
Table VI-6. Kinetic parameters for the reaction of 128a-d with 1-octene	285
Table VI-7. Kinetic parameters for the reaction of 128a-d with vinylcyclohexane.	287
Table VI-8. Catalytic asymmetric hydroamination/cyclization of aminoalkenes using binaphtholate tantalum and niobium complexes.	290
Table VI-9. Comparison of the “interrupted” and “continuous” reaction modes.321	
Table VI-10. Crystal structure and refinement data for 127l-Nb and 127l-Ta ...330	

List of Schemes

Scheme I-1. Proposed mechanism for the hydroamination/cyclization of aminoalkenes using alkali, alkaline earth and rare earth metal-based catalysts.	3
Scheme I-2. Concerted protonolysis/insertion via amine-assisted alkene insertion in hydroamination/cyclization	4
Scheme I-3. Proposed stereomodels for the lanthanocene-catalyzed hydroamination-cyclization of pent-4-enylamine (6).	8
Scheme I-4. Amine-induced epimerization of chiral lanthanocene complexes.....	8
Scheme I-5. Improved enantioselectivities in the hydroamination/cyclization of aminohexenes using a chiral octahydrofluorenyl ytrocene catalyst.	9
Scheme I-6. Bisoxazolinato rare earth metal catalysts in the hydroamination/cyclization of aminoalkenes.	10
Scheme I-7. Catalytic hydroamination/cyclization of aminoalkenes using chiral aminothiophenolate yttrium complexes.....	14
Scheme I-8. Catalytic hydroamination/cyclization of aminoalkenes using 3,3'-bis(trisarylsilyl)-substituted binaphtholate rare earth metal complexes 24	15
Scheme I-9. Hydroamination-cyclization of gem-disubstituted aminopentenes catalyzed by 27	16
Scheme I-10. Lithium-catalyzed asymmetric hydroamination-cyclization of aminoalkenes.....	17
Scheme I-11. Kinetic versus thermodynamic control in the lithium-catalyzed cyclization of aminostilbenes.....	18

Scheme I-12. Proposed mechanism for the hydroamination/cyclization of primary aminoalkenes involving group 4 metal imido species.	22
Scheme I-13. Hydroamination/cyclization of secondary aminoalkenes using a cationic chiral zirconium catalyst system.	24
Scheme I-14. Proposed mechanism for the gold-catalyzed dynamic kinetic resolution of aminoallenes.	35
Scheme I-15. Rare earth metal-catalyzed anti-Markovnikov hydroamination of vinyl arenes.	38
Scheme I-16. Gold-catalyzed asymmetric hydroamination of alkenes with cyclic ureas.	40
Scheme I-17. Proposed mechanism for the palladium-catalyzed hydroamination of vinyl arenes.	42
Scheme I-18. Preferential external attack of the aniline nucleophile leads to inversion of stereochemistry at the benzyl palladium intermediate.	43
Scheme I-19. Proposed mechanism for iridium-catalyzed hydroamination of norbornene via amine activation.	45
Scheme I-20. Stereoselective synthesis of cyclopentylamines via asymmetric hydroamination of norbornadiene.	46
Scheme I-21. Palladium-catalyzed asymmetric hydroamination of cyclohexadiene.	48
Scheme I-22. Enzymatic hydroamination of styrene derivatives.	49
Scheme II-1. Kinetic model of the resolution process.	63

Scheme II-2. Stereomodel for the kinetic resolution of α -substituted aminopentenes.	71
Scheme II-3. Proposed transition states in the kinetic resolution of 64	75
Scheme III-1. Additional amine binding to the metal center in generic intramolecular (A) and intermolecular (B) hydroamination.	96
Scheme III-2. Hydroamination/bicyclization of aminodiene 74 catalyzed by 73 . 97	
Scheme III-3. Synthesis and stability of precatalysts 24-Y	106
Scheme III-4. Synthesis of binaphtholates 80-Ln	108
Scheme III-5. Stereoselective addition of (<i>R</i>)- 90 to 1-heptene using (<i>S</i>)- 24a-Y and (<i>R</i>)- 24a-Y	112
Scheme III-6. Sequential inter-intramolecular hydroamination catalyzed by (<i>R</i>)- 24a-Y	113
Scheme III-7. Catalytically relevant forms of 24-Ln at various conditions.	118
Scheme III-8. Proposed mechanism for the deuterium scrambling.....	119
Scheme IV-1. Shifting the equilibrium between the “dormant” and active species by introducing an electron-donating site to the diolate backbone.	148
Scheme IV-2. Synthesis of 3-silylated NOBIN derivatives 98a-b	150
Scheme IV-3. Preparation of proligands 102a-g	151
Scheme IV-4. Preparation of rare earth metal diolates 103-Ln	152
Scheme IV-5. Preparation of group 4 metal diolates 104-M	154
Scheme IV-6. In situ preparation of lanthanum diolates from 102	162
Scheme V-1. Preparation of binaphthalenedicarboxamide ligands 110	200
Scheme V-2. Synthesis of zirconium bis(amidates) 111-Zr	202

Scheme VI-1. Inter- and intramolecular hydroaminoalkylation.	247
Scheme VI-2. Intermolecular hydroaminoalkylation of a vinyl arene.	249
Scheme VI-3. Regiodivergent hydroaminoalkylation catalyzed by 120 and 121	250
Scheme VI-4. Mechanism of intermolecular hydroaminoalkylation.....	251
Scheme VI-5. Hydroaminoalkylation of <i>N</i> -benzylmethylamine.	261
Scheme VI-6. Deuterium scrambling with 127j-Ta and possible mechanistic explanation.....	263
Scheme VI-7. Deuterium scrambling with 127j-Ta in the absence of alkene.....	264
Scheme VI-8. Isotopic labeling with 127j-Nb	265
Scheme VI-9. Mechanistic proposal for the intramolecular proton delivery.....	266
Scheme VI-10. Probing outer sphere protonolysis (step 3).	268
Scheme VI-11. Secondary alkyl C–H activation with 127j-Ta	269
Scheme VI-12. Hydroaminoalkylation of norbornene with 128a and 128a-d₃ ...	270
Scheme VI-13. Reversible insertion in norbornene hydroaminoalkylation.....	271
Scheme VI-14. Possible scenario for a concerted insertion-protonolysis in norbornene hydroaminoalkylation.	272
Scheme VI-15. Equilibrium between catalytic active five-coordinate species A and its “dormant” amine adduct AL	276
Scheme VI-16. Proposed mechanism for the intermolecular hydroaminoalkylation.	278

List of Figures

Figure I-1. Chiral lanthanocene precatalysts for asymmetric hydroamination.....	5
Figure I-2. Chiral alkaline earth metal catalysts.	19
Figure I-3. Selected group 4 metal catalysts for asymmetric hydroamination of primary aminoalkenes	24
Figure I-4. Mechanism of late transition metal-catalyzed hydroamination..	28
Figure I-5. Proposed stereomodel for kinetic resolution of chiral aminopentenes with an equatorial approach of the olefin.	34
Figure II-1. Rare earth metal 3,3'-bis(triarysilyl)binaphtholates.....	59
Figure II-2. Resolution factors for substrates 45a-g , determined with 24a-Ln and 24b-Ln	62
Figure I- 3. Plot of $\ln[(1-C)(1+ee)]$ vs $\ln[(1-C)(1-ee)]$ for the kinetic resolution of 45e using (<i>R</i>)- 24a-Y as a catalyst at various temperatures.....	65
Figure II-4. Time dependence of substrate consumption in the hydroamination/cyclization of (<i>R</i>)- 45e with (<i>S</i>)- 24a-Y (matching pair) in C ₆ D ₆	66
Figure II-5. Time dependence of substrate consumption in the hydroamination/cyclization of (<i>R</i>)- 3e with (<i>R</i>)- 24a-Y (mismatching pair) in C ₆ D ₆	66
Figure II-6. Eyring plot for the hydroamination/cyclization of (<i>R</i>)- 45e using (<i>S</i>)- 24a-Y and (<i>R</i>)- 24a-Y	70
Figure II-7. Time dependence of substrate consumption in the cyclohydroamination of 69 with (<i>R</i>)- 24a-Y in C ₆ D ₆	78
Figure II-8. ORTEP diagram for (<i>R</i>)-Mosher amide of (<i>S</i>)- 64	91

Figure III-1. Rare earth metal 3,3'-bis(triarysilyl)binaphtholates 24-Ln	95
Figure III-2. Kinetic profile for the hydroamination/cyclization of 74 with 73 at 40 °C in C ₆ D ₆	98
Figure III-3. Kinetic profile for the cyclization of 74 with (<i>R</i>)- 24a-Y at 30 °C in C ₆ D ₆	99
Figure III-4. Kinetic profile for the cyclization of 74 with (<i>R</i>)- 24a-Y in the presence of <i>n</i> -PrNH ₂ at 40 °C in C ₆ D ₆	101
Figure III-5. Diastereoselective hydroamination/cyclization of primary and secondary aminopentenes.	114
Figure III-6. Exponential amine consumption in the addition of benzylamine to 4-phenyl-1-butene in the presence of (<i>R</i>)- 24a-Y at 150 °C in C ₆ D ₆	115
Figure III-7. Observed pseudo-first order rate constant vs. alkene concentration for the reaction of benzylamine with 4-phenyl-1-butene in the presence of (<i>R</i>)- 24a-Y at 150 °C in C ₆ D ₆	116
Figure III-8. Dependency of <i>k</i> _{obs} on the concentration of (<i>R</i>)- 24a-Y in the addition of benzylamine to 4-phenyl-1-butene at 150 °C in C ₆ D ₆	116
Figure III 9. Observed pseudo-first order rate constant vs. amine concentration for the reaction of benzylamine with 4-phenyl-1-butene in the presence of (<i>R</i>)- 24a-Y at 150 °C in C ₆ D ₆	117
Figure IV-1. Rare earth metal catalysts (<i>R</i>)- 24-Ln and (<i>R</i>)- 21	147
Figure IV-2. Generic NOBIN-derived rare earth metal diolate complex.	149
Figure IV-3. Selectivity profiles for the cyclization of aminoalkene 105 catalyzed by 103-Y (red bars) and 103-Lu (green bars).....	156

Figure IV-4. Selectivity profile for the hydroamination/cyclization of 105 catalyzed by 104-Zr	160
Figure V-1. Schafer's and Scott's zirconium bis(amidate) catalyst for asymmetric hydroamination/cyclization of aminoalkenes.	199
Figure V-2. Crystal structures for (<i>R</i>)- 111d-Zr (left) (<i>R</i>)- 111ca-Zr (right).	203
Figure V-3. ¹ H NMR spectra in C ₆ D ₆ showing: a) pure aminopentene 6 , b) catalytic cyclization of 6 with catalyst (<i>S</i>)- 111c-Zr (2 mol%) at 110 °C and 51% conversion (spectrum taken at 25 °C); c) 7 after vacuum transfer (>98% conversion)...	209
Figure V-4. First-order kinetic plots for the cyclization of 18 in the presence of (<i>R</i>)- 111d-Zr in toluene- <i>d</i> ₈ at 90 °C.	212
Figure V-5. Observed first order rate constant for the cyclization of 18 in toluene- <i>d</i> ₈ at 90 °C vs. concentration of catalyst ((<i>R</i>)- 111d-Zr).	212
Figure V-6. Cyclization of 18 in the presence of <i>rac</i> - 111c-Zr and (<i>S</i>)- 111c-Zr in toluene- <i>d</i> ₈ at 90 °C.....	213
Figure V-7. Cyclization of 18 and 18-d ₂ in the presence of (<i>R</i>)- 111d-Zr in toluene- <i>d</i> ₈ at 90 °C.....	213
Figure V-8. Zi's zirconium tetrakis(κ ² -)amidate 119	214
Figure V-9. ORTEP diagram for (<i>R</i>)- 111d-Zr	238
Figure V-10. ORTEP diagram for (<i>R</i>)- 111ca-Zr	241
Figure VI-1. Selected group 4 and group 5 metal hydroaminoalkylation catalysts.	248
Figure VI-2. ORTEP diagram of the molecular structure of pentacoordinate complexes 127l-Nb (127l-Ta is isostructural to 127l-Nb).	255

Figure VI-3. ^1H NMR spectra of 127m-Ta in toluene- d_8 at various temperatures.	256
Figure VI-4. Dependence of observed first-order reaction constant on catalyst concentration for the reaction of 1-octene with PMPNHMe (128d) in the presence of (<i>R</i>)- 127j-Nb in C_6D_6 at 150 °C..	272
Figure VI-5. Dependence of pseudo first-order rate constant on alkene concentration for the reaction of 1-octene and vinylcyclohexane with PMPNHMe (128d) (0.29 M) in the presence of (<i>R</i>)- 127j-Nb in C_6D_6 at 150 °C..	273
Figure VI-6. First-order kinetic plots for the reaction of 1-octene with 4- $\text{FC}_6\text{H}_4\text{NHMe}$ (128b) in the presence of (<i>R</i>)- 127j-Nb in C_6D_6 at 150 °C.	275
Figure VI-7. First-order kinetic plots for the reaction of 1-octene with PhNHMe (128a) and its deuterated analogues in the presence of (<i>R</i>)- 127j-Nb in C_6D_6 at 150 °C.	277
Figure VI-8. Experimental reaction progress data (dots) for the reaction of 1-octene with 128b in the presence of (<i>R</i>)- 127j-Nb (0.017 M) in C_6D_6 at 150 °C vs. the simulated reaction curves (lines).	284
Figure VI-9. Hammett plot for turnover constant k_4 for the reaction of 128a-d with 1-octene.....	286
Figure VI-10. Experimental reaction progress data (dots) for the reaction of vinylcyclohexane with PMPNHCH ₃ (128d) in the presence of (<i>R</i>)- 127j-Nb in C_6D_6 at 150 °C versus the simulated reaction curves (lines).	288

Figure VI-11. First order dependence of observed first-order reaction constant on catalyst concentration for the reaction of 1-octene with PMPNHMe (128d) (0.20 M) in the presence of (<i>R</i>)- 127j-Nb in C ₆ D ₆ at 150 °C.....	322
Figure VI-12. Zero order dependence of the first-order rate constant on the alkene concentration for the reaction of 1-octene with PMPNHMe (128d) in the presence of (<i>R</i>)- 127j-Nb in C ₆ D ₆ at 150 °C.	323
Figure VI-13. First order logarithmic plots for the reaction of 1-octene (0.613 M) with PhNHMe (128a) in the presence of (<i>R</i>)- 127j-Nb in C ₆ D ₆ at 150 °C.	323
Figure VI-14. Experimental reaction progress data (dots) for the reaction of 1-octene with PhNHMe (128a) in the presence of (<i>R</i>)- 127j-Nb in C ₆ D ₆ at 150 °C vs. the simulated reaction curves (lines)	324
Figure VI-15. Experimental reaction progress data (dots) for the reaction of 1-octene with PMPNHMe (128d) in the presence of (<i>R</i>)- 127j-Nb in C ₆ D ₆ at 150 °C vs. the simulated reaction curves (lines).	324
Figure VI-16. Experimental reaction progress data (dots) for the reaction of 1-octene with <i>p</i> -ClC ₆ H ₄ NHMe (128c) in the presence of (<i>R</i>)- 127j-Nb in C ₆ D ₆ at 150 °C vs. the simulated reaction curves (lines).....	325
Figure VI-17. Experimental reaction progress data (dots) for the reaction of 1-octene with <i>p</i> -FC ₆ H ₄ NHMe (128b) in the presence of (<i>R</i>)- 127j-Nb in C ₆ D ₆ at 150 °C vs. the simulated reaction curves (lines).....	325
Figure VI-18. Experimental reaction progress data (dots) for the reaction of 1-octene (0.613 M) with PhNHCD ₃ (128a-CD₃) in the presence of (<i>R</i>)- 127j-Nb in C ₆ D ₆ at 150 °C vs. the simulated reaction curves (lines).....	326

Figure VI-19. Experimental reaction progress data (dots) for the reaction of 1-octene with PhNDMe (128a-ND) in the presence of (<i>R</i>)- 127j-Nb (0.020 M) in C ₆ D ₆ at 150 °C vs. the simulated reaction curves (lines).....	326
Figure VI-20. Experimental reaction progress data (dots) for the reaction of vinylcyclohexane with PhNHMe (128a) in the presence of (<i>R</i>)- 127j-Nb in C ₆ D ₆ at 150 °C vs. the simulated reaction curves (lines).....	327
Figure VI-21. Experimental reaction progress data (dots) for the reaction of vinylcyclohexane with <i>p</i> -FC ₆ H ₄ NHCH ₃ (128b) in the presence of (<i>R</i>)- 127j-Nb in C ₆ D ₆ at 150 °C vs. the simulated reaction curves (lines).....	327
Figure VI-22. Experimental reaction progress data (dots) for the reaction of vinylcyclohexane with <i>p</i> -ClC ₆ H ₄ NHCH ₃ (128c) in the presence of (<i>R</i>)- 127j-Nb in C ₆ D ₆ at 150 °C vs. the simulated reaction curves (lines).....	328
Figure VI-23. Experimental reaction progress data (dots) for the reaction of vinylcyclohexane with PMPNHCH ₃ (128d) in the presence of (<i>R</i>)- 127j-Nb in C ₆ D ₆ at 150 °C vs. the simulated reaction curves (lines).....	328
Figure VI-24. Experimental reaction progress data (dots) for the reaction of vinylcyclohexane with PMPNHCD ₃ (128d-CD₃) in the presence of (<i>R</i>)- 127j-Nb in C ₆ D ₆ at 150 °C vs. the simulated reaction curves (lines).....	329
Figure VI-25. ORTEP diagram of the molecular structure of the isostructural complexes 127l-M (M = Nb, Ta).....	331

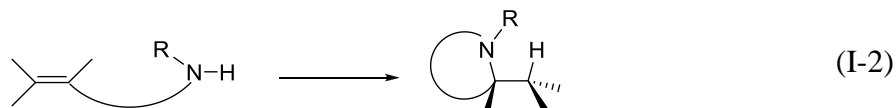
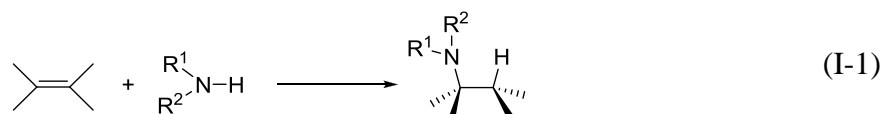
List of Abbreviations and Symbols

Å	Angstrom
BINAP	2,2-Bis(diphenylphosphino)-1,1'-bibaphthyl
BINCA	1,1'-Binaphthalene-2,2'-dicarboxylic acid
BINOL	1,1'-Binaphthalene-2,2'-diol
Bn	Benzyl
br	Broad
<i>n</i> -Bu	<i>n</i> -Butyl
<i>t</i> -Bu	<i>tert</i> -Butyl
d	Doublet
DEP	2,6-Diethylphenyl
DMF	<i>N,N</i> -Dimethylformamide
Et	Ethyl
HMPA	Hexamethylphosphoramide
Ln	Rare earth metal: Sc, Y, La–Lu
m	Multiplet
Me	Methyl
NOBIN	2-amino-2'-hydroxy-1,1'-binaphthyl
Ph	Phenyl
<i>i</i> -Pr	<i>iso</i> -Propyl
<i>n</i> -Pr	<i>n</i> -Propyl
q	Quartet
quint	Quintet
s	Singlet
sept	Septet
sext	Sextet
t	Triplet
THF	Tetrahydrofuran
<i>t_R</i>	Retention time
vt	Virtual (apparent) triplet
δ	<i>Delta</i> , chemical shift
κ	<i>Kappa</i> , denticity
η	<i>Eta</i> , hapticity

I Chapter 1. Asymmetric Hydroamination of Alkenes: Recent Developments and Major Challenges

I.1 Introduction: Synthesis of Amines via Hydroamination

The addition of an amine N–H bond across an unsaturated carbon-carbon linkage – the so-called hydroamination, allows a facile and highly atom-economical access to industrially relevant nitrogen containing basic and fine chemicals as well as naturally occurring alkaloid skeletons.¹⁻³ Significant research efforts have led to the development of efficient catalyst systems for inter- and intramolecular hydroamination reactions (Eqs. I-1 and I-2). Many catalytic systems based on transition metals (groups 3–5 and 8–10, as well as lanthanides and actinides) and main group metals (alkali and alkaline earth metals), as well as Brønsted acids, have been developed over the last six decades, especially the last two decades has seen significant progress. However, the majority of these catalyst systems are confined to a limited set of substrates, e.g. requiring activated multiple C–C bonds, such as 1,3-dienes, vinyl arenes, allenes, or ring-strained olefins.



The direct addition of amines to alkenes is thermodynamically feasible ($\Delta G^\circ \approx -14.7 \text{ kJ mol}^{-1}$ for the addition of ammonia to ethylene)^{4,5} with a slightly exothermic to thermoneutral reaction enthalpy. However, this seemingly simple reaction is hampered by a high activation barrier ($>200 \text{ kJ mol}^{-1}$) caused by a repulsion between

the nitrogen lone pair of the approaching amine and the π -bond of the electron rich olefin.⁶ The activation barrier cannot be overcome by increasing the reaction temperature because the negative reaction entropy shifts the equilibrium towards the starting materials. Therefore, amines add commonly only to activated, electron deficient alkenes (e.g. vinyl ethers or *aza*-Michael acceptors).^{7,8}

Because of its potential relevance for the synthesis of pharmaceuticals and biological-active molecules, most of which are chiral, the development of chiral catalysts for stereoselective hydroamination (including kinetic resolution of chiral amines) has drawn increasing attention over the last decade.⁹⁻¹⁴

In this chapter we will review most relevant examples of asymmetric alkene hydroamination and discuss the current state of the field and point out major challenges. Due to the space limitations and large amount of published data, only key examples will be shown, and only mechanistically important achiral systems will be referenced.

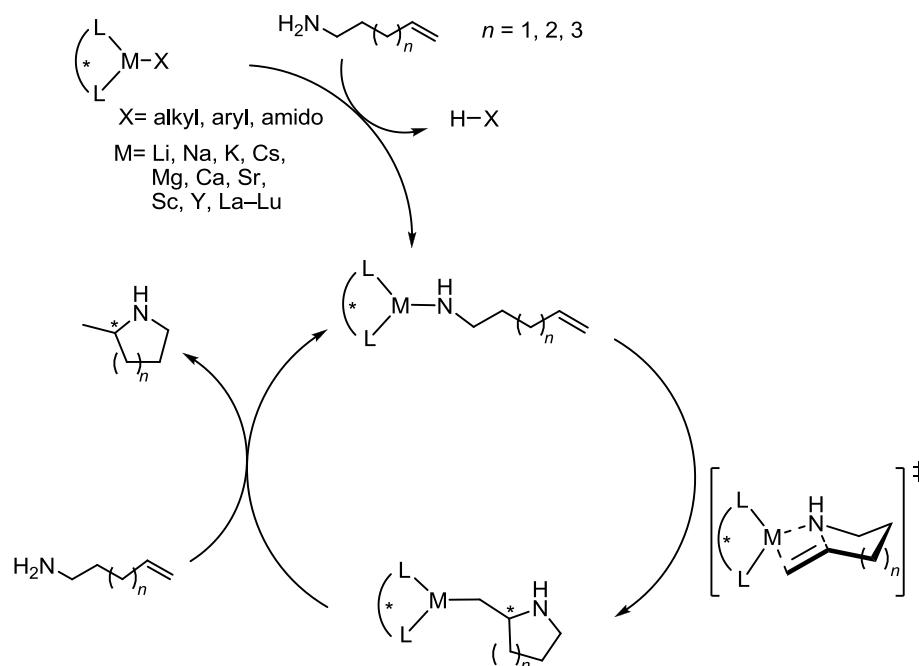
I.2 Intramolecular Asymmetric Hydroamination of Simple Aminoalkenes

I.2.1 Rare Earth Metal-Based Catalysts

Among hydroamination catalyst systems developed so far, organo rare earth metal complexes have been found to be the most versatile and most active catalysts for the hydroamination of non-activated alkenes, allenes, 1,3-dienes and alkynes.¹⁵ However, intermolecular hydroamination reactions with these catalysts are problematic, and most rare earth metal-catalyzed reactions have been performed in an intramolecular fashion producing predominantly pyrrolidine and piperidine derivatives.

The mechanism of the hydroamination/cyclization^{16,17} proceeds through a metal amido species, which is formed upon protonolysis of a metal amido, alkyl or aryl bond in the precatalyst (Scheme I-1), followed by insertion of the olefin into the metal amido bond with a seven-membered chair-like transition state (for $n = 1$). The roughly thermoneutral insertion step¹⁷ is usually rate determining, giving rise of a zero order rate dependence on substrate concentration and first order rate dependence on catalyst concentration. The resulting metal alkyl species undergoes fast protonolysis with a second amine molecule, regenerating the metal amido species and releasing the heterocyclic product.

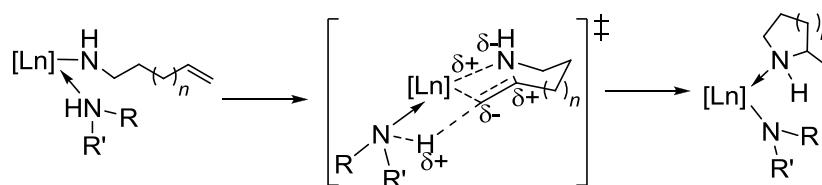
Scheme I-1. Proposed mechanism for the hydroamination/cyclization of aminoalkenes using alkali, alkaline earth and rare earth metal-based catalysts.



Although the protonolysis step is considered to be fast, a strong primary kinetic isotope effect^{16,18} as well as an effect of the isotope substitution on stereoselectivity^{16,19} have been observed, which is indicative of a significant N-H bond disruption in the

transition state of the rate-determining alkene insertion step, at least for certain substrate-catalyst combinations. A plausible explanation involves partial proton transfer from a coordinated amine to the α -carbon in the 4-membered insertion step (Scheme I-2).

Scheme I-2. Concerted protonolysis/insertion *via* amine-assisted alkene insertion in hydroamination/cyclization ($RR'NH$ = aminoalkene substrate or hydroamination product).



However, some experimental data, in particular the observation of sequential hydroamination/bicyclization sequences catalyzed by organo rare earth metal²⁰⁻²³ and organolithium²⁴ species is in conflict with this scenario, as the sequential reaction requires a finite lifetime for the rare earth-metal-alkyl intermediate. Therefore, the intermediacy of the metal-alkyl species and its potential lifetime is unclear at present and is probably strongly depending on catalyst and substrate structure. Unfortunately, involvement of concerted insertion/protonolysis pathway in a catalytical cycle has only been addressed computationally for aminoallenes²⁵ and aminodienes.²⁶ Although classical stepwise insertion/protonolysis was found more energetically accessible, a concerted process is not prohibitively high in energy and might also contribute depending on the spatial demands around the rare earth metal center.

While the insertion/protonolysis mechanism discussed above was established for rare earth metal complexes, alkali and alkaline earth metal-based systems are apparently

operating in agreement with the same or a similar mechanism. The rate-limiting step of the process might be different, as it was recently shown by DFT calculation that certain organomagnesium catalysts are operating via fast reversible alkene insertion and slow, rate-limiting protonolysis.²⁷

Chiral rare earth metal-based catalysts for the asymmetric hydroamination/cyclization of aminoalkenes were first introduced in 1992 by Marks and co-workers.^{28,29} The C_1 -symmetric chiral *ansa*-lanthanocene complexes **1–3** with (+)-neomenthyl, (–)-menthyl or (–)-phenylmenthyl substituents attached to one of the cyclopentadienyl ligands (Figure I-1) exist in two diastereomeric forms, depending on which diastereotopic face of the cyclopentadienyl ligand coordinates to the metal center. Generally, one of the two diastereomers predominates in solution and most of the complexes can be obtained diastereomerically pure by fractional crystallization.

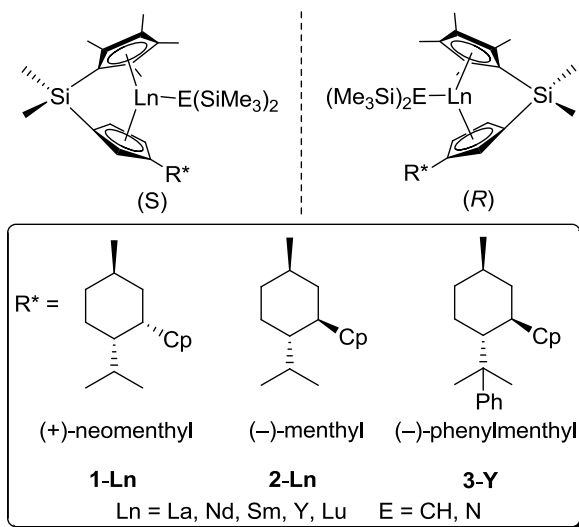
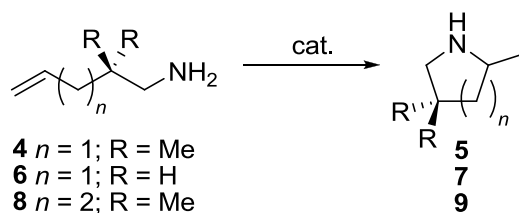


Figure I-1. Chiral lanthanocene precatalysts for asymmetric hydroamination.

The lanthanocene catalysts display high catalytic activity, which is proportional to the ionic radius of the rare earth metal (Table I-1). The rate of cyclization depends on the ring-size of the azacyclic product ($5 > 6 \gg 7$) and the presence of rate enhancing *gem*-

dialkyl substituents.³⁰ The proposed stereomodel for aminopentene substrates (Scheme I-3)²⁹ predicts preferred formation of the (*S*) pyrrolidine enantiomer due to unfavorable steric interactions between an axial substituent of the substrate with the substituents on the cyclopentadienyl ligands of the (*S*) lanthanocene diastereomer in the transition state of the cyclization. Hence, dominance of one of the two catalyst epimers is essential to achieve high enantioselectivities.

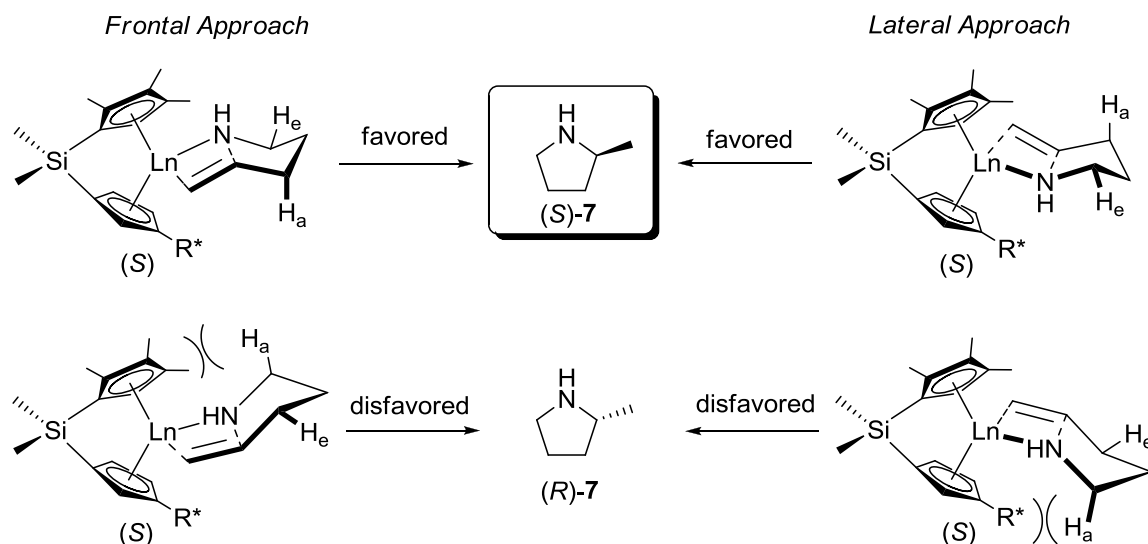
Unfortunately, the complexes underwent facile epimerization under the conditions of catalytic hydroamination *via* reversible protolytic cleavage of the metal cyclopentadienyl bond (Scheme I-4).^{29,31-33} Thus, the product enantioselectivity was limited by the catalyst's epimeric ratio in solution and the absolute configuration of the hydroamination product was independent of the diastereomeric purity of the precatalyst. Complexes with a (+)-neomenthyl substituent on the cyclopentadienyl ligand generally produced the (*R*)-(-)-pyrrolidines, whereas (-)-menthyl and (-)-phenylmenthyl substituted complexes yielded the (*S*)-(+)-pyrrolidines, which is in agreement with the proposed stereomodel and solution studies on the equilibrium epimer ratios in the presence of simple aliphatic amines.

Table I-1. Chiral lanthanocene-catalyzed asymmetric aminoalkenehydroamination/cyclization.²⁹

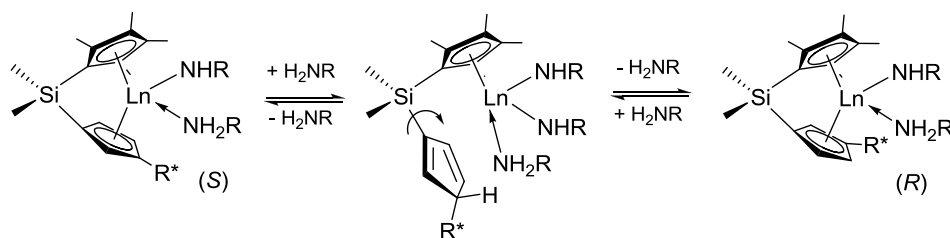
Cat.	Substrate	<i>T</i> , °C	<i>N_t</i> , ^a h ⁻¹	%ee (config)
(<i>R</i>)- 1-Sm	4	−30		64 (<i>R</i>)
(<i>R,S</i>)- 1-Y	4	25	38	36 (<i>R</i>)
(<i>R</i>)- 1-Y	4	25	21	40 (<i>R</i>)
(<i>S</i>)- 2-Sm	4	25	84	53 (<i>S</i>)
(<i>S</i>)- 2-Sm	4	−30		74 (<i>S</i>)
(<i>R</i>)- 3-Y	4	25	8	56 (<i>S</i>)
(60/40) (<i>R,S</i>)- 3-Y	4	25		54 (<i>S</i>)
(<i>S</i>)- 1-Sm	4	25	33	55 (<i>R</i>)
(<i>R</i>)- 1-Sm	6	25	62	52 (<i>R</i>)
(<i>S</i>)- 2-Sm	6	0		72 (<i>S</i>)
(<i>R</i>)- 3-Y	6	25		64 (<i>S</i>)
(<i>R</i>)- 1-Sm	6	25		17 (<i>R</i>)
(<i>R</i>)- 2-Sm	8	25	2	15 (<i>R</i>)

^a *N_t* = turn over number per hour

Scheme I-3. Proposed stereomodels for the lanthanocene-catalyzed hydroamination-cyclization of pent-4-enylamine (**6**).²⁹

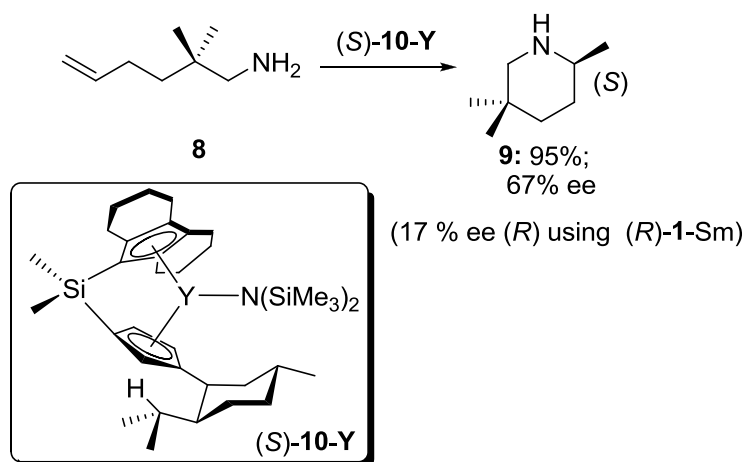


Scheme I-4. Amine-induced epimerization of chiral lanthanocene complexes.

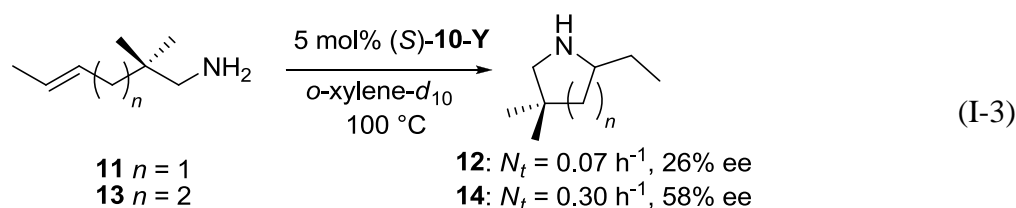


The highest enantioselectivities of up to 74% ee were achieved with the (–)-menthyl-substituted samarium complex (*S*)-**2-Sm** in the formation of pyrrolidine products, whereas formation of piperidines suffered from significantly diminished selectivities. The extended “wingspan” of the octahydrofluorenyl ligand in complex **10** was supposed to provide an increased enantiofacial discrimination for prochiral substrates, but only isolated examples of improved selectivities were observed (Scheme I-5).³¹

Scheme I-5. Improved enantioselectivities in the hydroamination/cyclization of aminohexenes using a chiral octahydrofluorenyl ytrocene catalyst.³¹



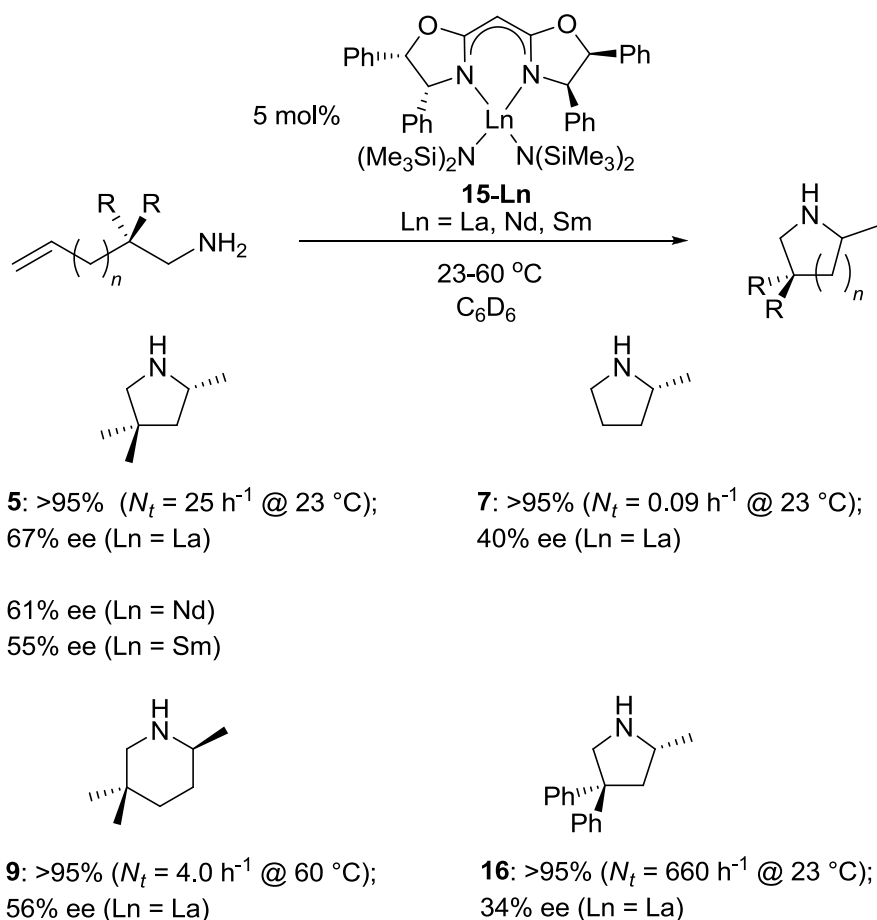
Internal 1,1- or 1,2-disubstituted olefins **11** and **13** are much less reactive for hydroamination and require significantly harsher reaction conditions.^{32,34-37} The formation of pyrrolidines and piperidines often proceeds at comparable rates (Eq. I-3), contrasting the general trend of significant faster five-membered ring formation observed with terminal aminoalkenes.³² Despite these harsh reaction conditions, moderate enantioselectivities of up to 58% ee were observed at 100 °C (up to 68% at 60 °C).



Significant progress in this area has been made since 2003 utilizing non-cyclopentadienyl-based ligand sets,^{18,19,33,38-63} thus, avoiding configurational instability issues of the chiral lanthanocene complexes. However, while enantioselectivities have improved rather significantly, only few catalyst systems^{18,19} display the same high catalytic activity as the lanthanocene catalysts.

A variety of bisoxazolinato rare earth metal complexes have been studied with regard to their hydroamination/cyclization catalytic activity (Scheme I-6).³⁹ The precatalysts could be conveniently generated in situ from $[\text{Ln}\{\text{N}(\text{SiMe}_3)_2\}_3]$ ($\text{Ln} = \text{La}, \text{Nd}, \text{Sm}, \text{Y}, \text{Lu}$) and the corresponding bisoxazoline, resulting in minimal reactivity loss, but with similar enantioselectivity, in comparison to the isolated precatalysts. The ligand accelerated catalyst system showed the highest rates for a 1:1 metal to ligand ratio.

Scheme I-6. Bisoxazolinato rare earth metal catalysts in the hydroamination/cyclization of aminoalkenes.³⁹

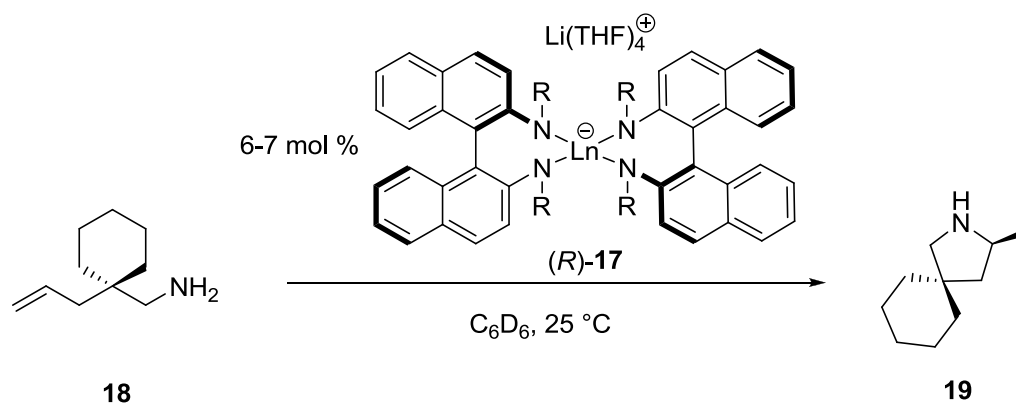


The ate-complexes $[\text{Li}(\text{THF})_4][\text{Ln}\{(R)-1,1'\text{-}\{\text{C}_{10}\text{H}_6\text{N}(\text{R})\}_2\}_2]$ ((*R*)-**17**; $\text{Ln} = \text{Sm}, \text{Yb}, \text{Y}$; $\text{R} = \text{alkyl}$)^{50,53,54,56,57,64-66} are unusual hydroamination catalysts as they lack an

obvious leaving amido or alkyl group that is replaced during the initiation step by the substrate. It is very likely that at least one of the amido groups is protonated during the catalytic cycle, analogous to the mechanism proposed for Michael additions and aldol reactions catalyzed by rare earth metal alkali metal-BINOL heterobimetallic complexes,^{67,68} and the observation of similar selectivities for rare earth metal complexes containing only one diamidobinaphthyl seem to support this proposal.^{12,49,52}

The best catalytic results for the ate-system were obtained using a small rare earth metal (Yb) and a large cyclopentyl-substituent on the diamidobinaphthyl amido-ligand (Table I-2), though the moderate catalytic activity required the presence of *gem*-dialkyl substituents in the aminoalkene substrates. The low reactivity of **17** should mainly be attributed to the rather electron rich diamidobinaphthyl ligand framework, as indicated by comparison to other diamidobinaphthyl^{12,55,65} or diamidobiphenyl,^{43,45} catalyst systems, rather than the unusual mode of catalyst activation.

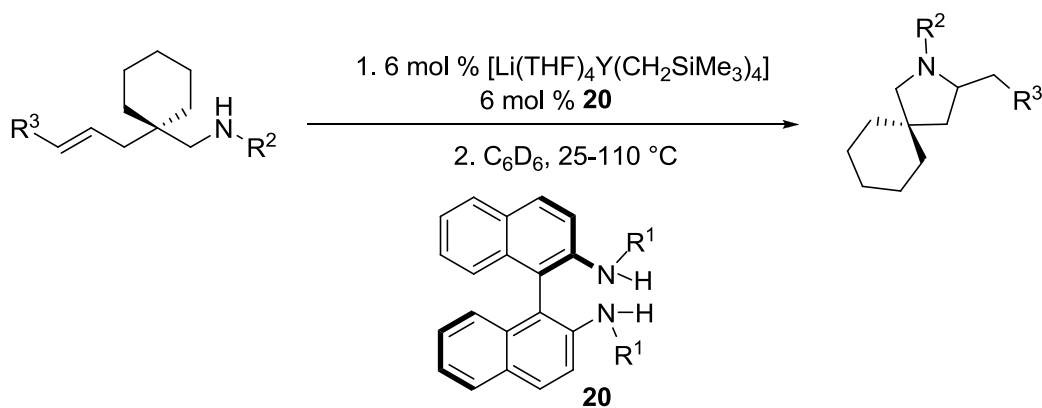
Table I-2. Catalytic hydroamination/cyclization **18** using diamidobinaphthyl ate-complexes.



R	Ln	t, h	% ee	conv., %	Ref.
<i>i</i> Pr	Y	20	67	100	65
Cy	Yb	18	65	94	66
C ₅ H ₉	Yb	20	87	90	64

Yttrium ate complexes containing only one diamidobinaphthyl fragment were developed by the same group^{48,51} and are applicable to a broader substrate scope than **17-Ln**. These catalysts are formed *in situ* from a readily available diaminobinaphthyl proligand **20** and yttrium ate-precursor and they have been successfully employed for the cyclohydroamination of 1,2-disubstituted alkenyl amines as well as secondary aminoalkenes (Table I-3). Only gem-disubstituted aminoalkenes were reported to be active in hydroamination-cyclization.

Table I-3. Catalytic hydroamination/cyclization using diamidobinaphthyl ate-complexes formed *in situ* from proligand **20**.

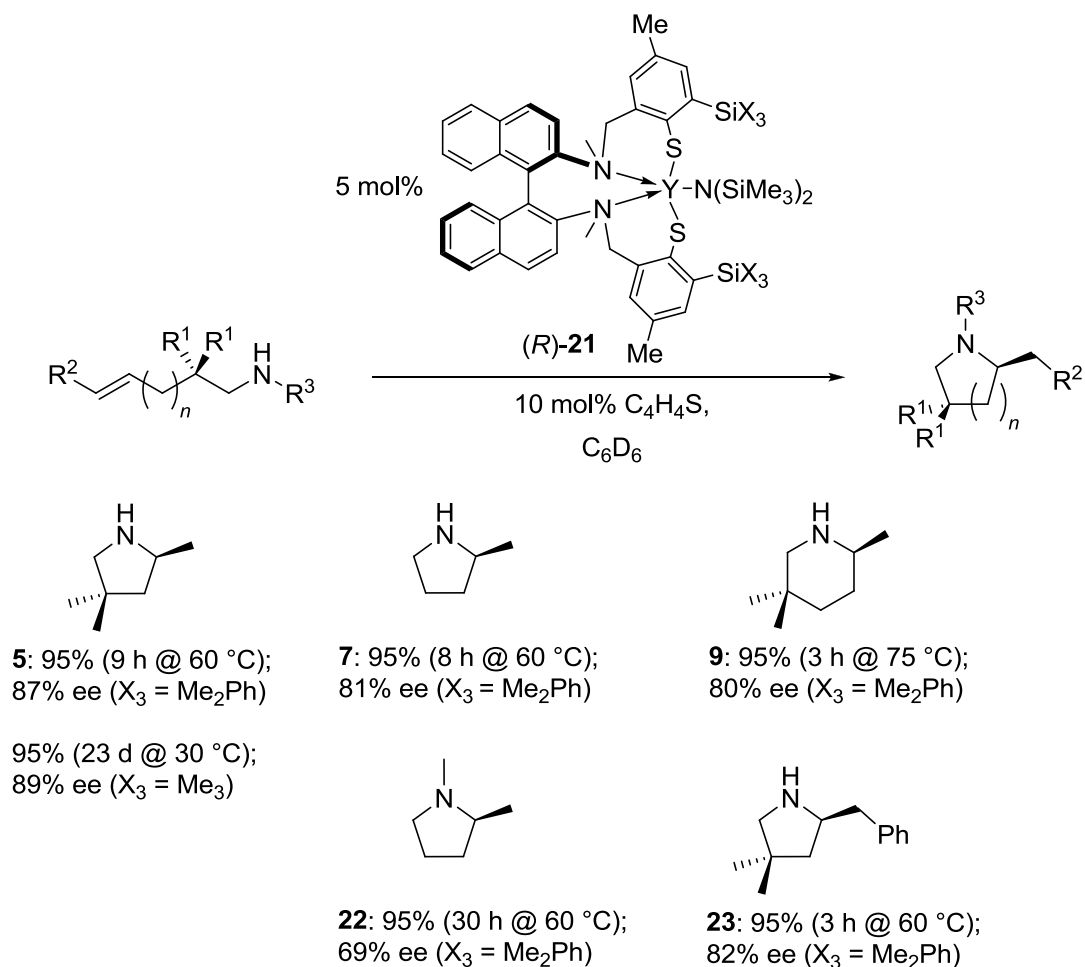


R^1	R^2	R^3	T, °C	t, h	% ee ^a	conv., %	Ref.
C_5H_9	Me	H	25	0.17	72	95	48
C_5H_9	H	Me	70	18	65	58	51
9-AnthrylCH ₂	H	Me	110	20	87	96	51

^aAbsolute configuration was not reported.

Good to high enantioselectivities for a wide range of aminoalkene substrates, including internal olefins or secondary amines, were achieved using the aminothiophenolate catalyst system (*R*)-**21** (Scheme I-7), which was also obtained *in situ*.⁵⁸ Variation of the steric demand of the silyl substituent attached to the thiophenolate moiety allowed facile fine-tuning of the enantiomeric excess, resulting in increasing selectivity with increasing steric hindrance. While the larger bite angle of the amino(thio)phenolate ligand is believed to improve enantiofacial differentiation through a better “reach around” of the chiral ligand around the metal center⁴⁵ the multidentate nature of the ligand also electronically saturates the metal center, resulting in diminished catalytic performance. Enantiomeric excess of up to 89% could be achieved at 30 °C, though reactions at this temperature required a long period of time to reach completion.

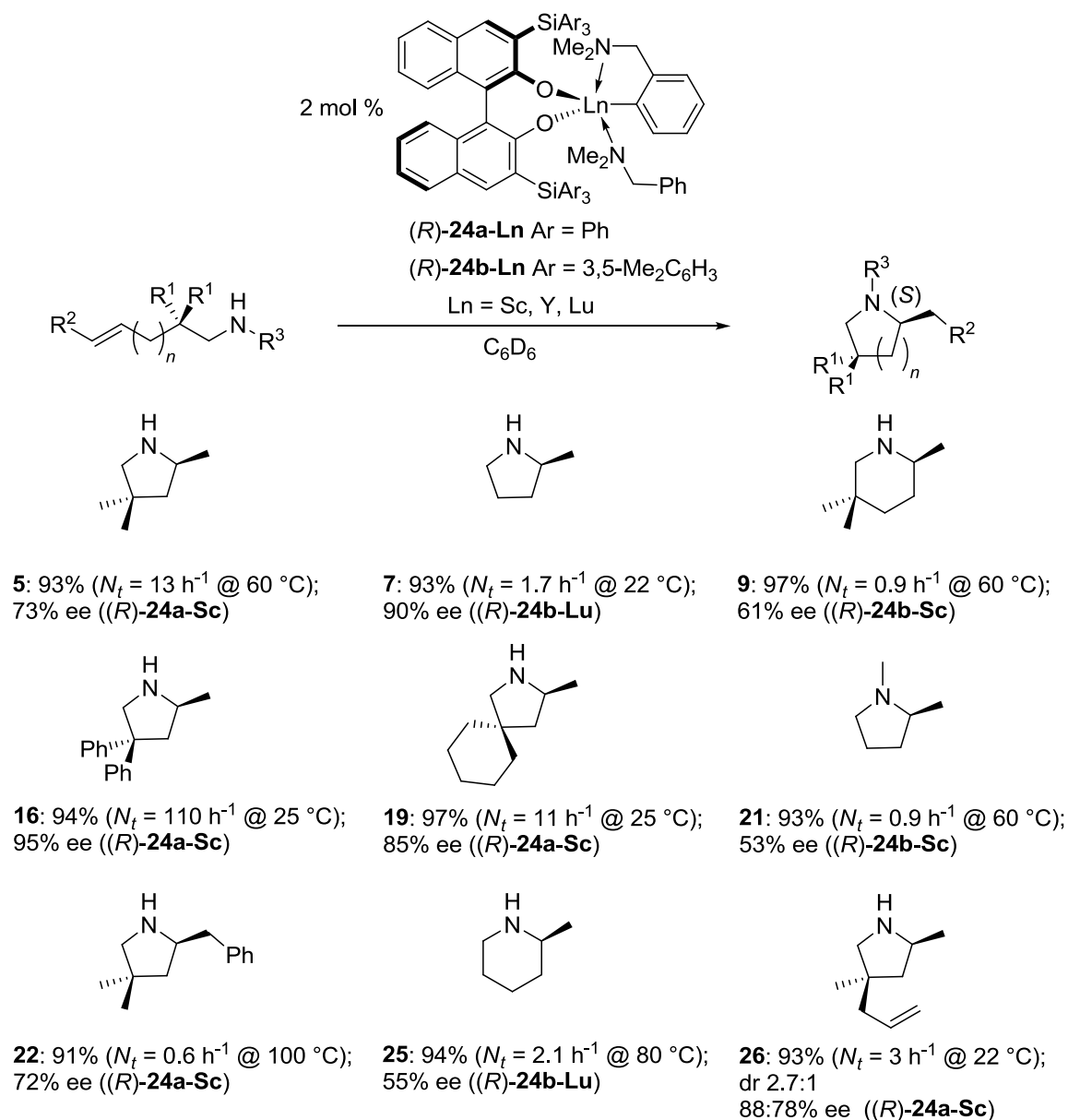
Scheme I-7. Catalytic hydroamination/cyclization of aminoalkenes using chiral aminothiophenolate yttrium complexes.⁵⁸



Significantly higher catalytic activities are achievable, if more electron deficient ligand sets are employed. 3,3'-Disubstituted binaphtholate aryl complexes **(R)-24-Ln**, (Ln = Sc, Y, Lu) with sterically demanding tris(aryl)silyl substituents in the 3 and 3' position, showed not only superior catalytic activity at room temperature, comparable in magnitude to lanthanocene catalysts, but also achieved up to 95% ee in hydroamination/cyclization reactions of aminoalkenes, among the highest enantioselectivities observed so far (Scheme I-8).¹⁸ The sterically demanding tris(aryl)silyl substituents in the diolate complexes play a pivotal role not only in

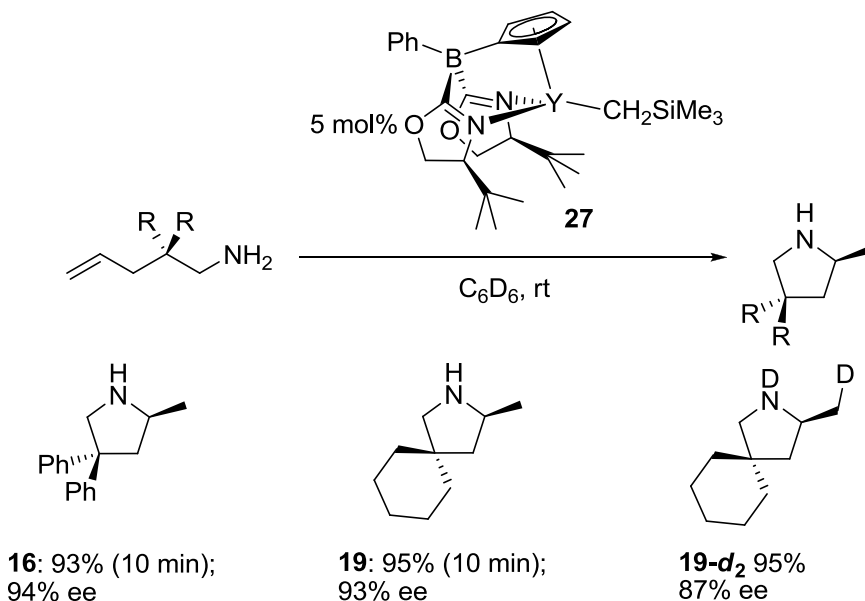
achieving high enantioselective, but they are also crucial to prevent undesired complex aggregation^{41,42} and reduce detrimental amine binding of the substrate and product to the catalytic active metal centers.¹⁸

Scheme I-8. Catalytic hydroamination/cyclization of aminoalkenes using 3,3'-bis(trisarylsilyl)-substituted binaphtholate rare earth metal complexes **24**.¹⁸



Catalysts **24**, first reported by Hultzsche et al. in 2004^{18,40} remained the only post-metallocene catalyst with a reactivity compared to that of lanthanocene hydroamination catalysts for nearly a decade. Recently, Sadow and coworkers have reported zwitterionic oxazolinylborato yttrium complex **27**, which displayed comparable reactivity in hydroamination-cyclization along with excellent enantioselectivity.¹⁹ Unfortunately, **27** seems to be confined to gem-disubstituted aminoalkenes (Scheme I-9). Isotopic perturbation of enantioselectivity was interpreted by the authors as an indication of a concerted insertion-protonolysis (Scheme I-2) and the possibility of reversible insertion/slow protonolysis sequence has not been considered.

Scheme I-9. Hydroamination-cyclization of gem-disubstituted aminopentenes catalyzed by **27**.¹⁹



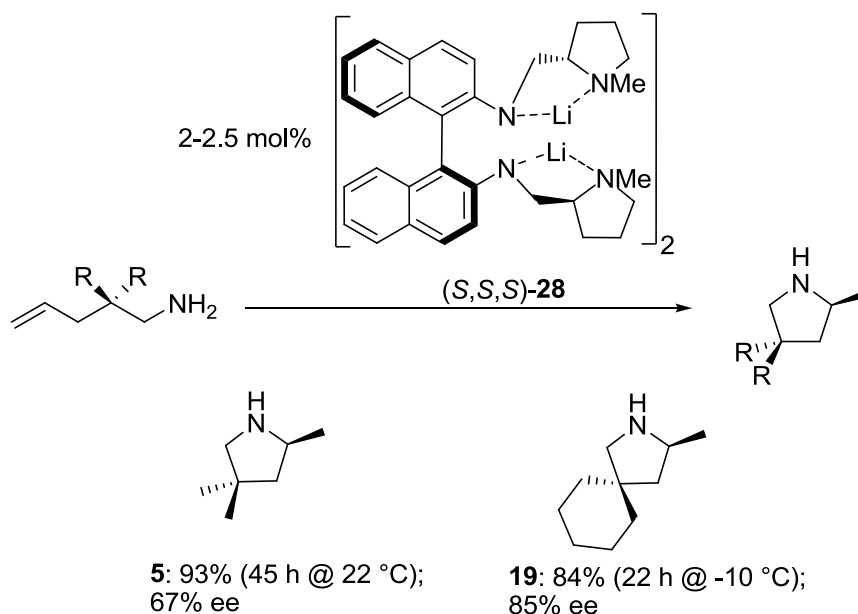
I.2.2 Alkali Metal-Based Catalysts

While hydroamination catalysts based on rare earth and early transition metals have been studied intensively over the last two decades, only a limited number of reports on alkali metal-based hydroamination catalysts have emerged, although the first reports

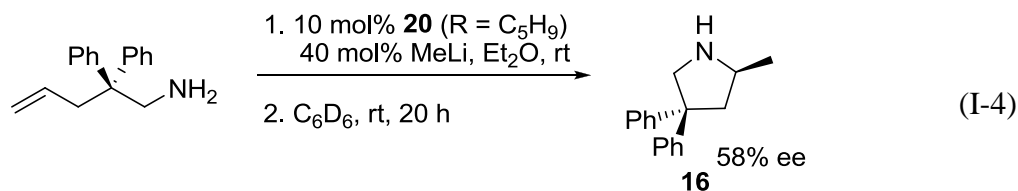
date back almost 60 years.⁶⁹ In particular the application of chiral alkali metal complexes in asymmetric hydroamination of non-activated aminoalkenes has drawn little attention to date.⁷⁰⁻⁷²

The proline derived diamidobinaphthyl dilithium salt (*S,S,S*)-**28**, which is dimeric in the solid state and can be prepared via deprotonation of the corresponding tetraamine with *n*-BuLi, represents the first example of a chiral main group metal-based catalyst for asymmetric intramolecular hydroamination reactions of aminoalkenes.⁷⁰ The unique reactivity of (*S,S,S*)-**28**, which allowed reactions at or below ambient temperatures with product enantioselectivities of up to 85% ee (Scheme I-10)⁷³ is believed to derive from the close proximity of the two lithium centers chelated by the proline substituents, because more simple lithium amides required significantly higher reaction temperatures and gave inferior selectivities.

Scheme I-10. Lithium-catalyzed asymmetric hydroamination-cyclization of aminoalkenes.^{70,73}

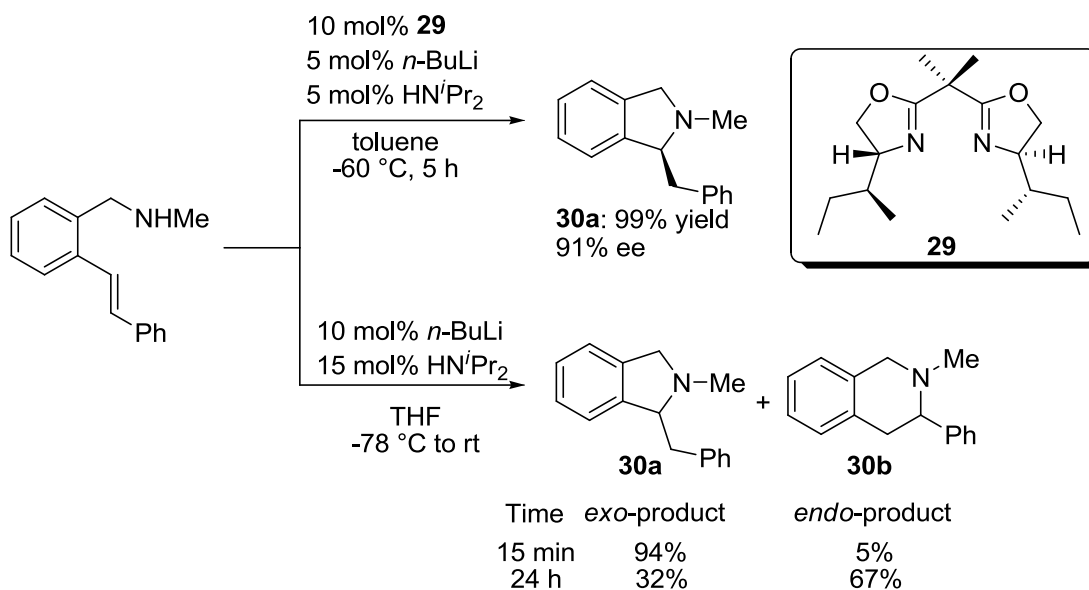


More recently, the less elaborate diaminobinaphthyl precursor **20** ($R = C_5H_9$) was shown to catalyze asymmetric hydroamination/cyclization after *in situ* lithiation (Eq. I-4).⁷²



The asymmetric hydroamination/cyclization of amino-substituted stilbenes was studied utilizing chiral bisoxazoline lithium catalysts.⁷¹ Enantioselectivities reaching as high as 91% ee were achieved (Scheme I-11). The reactions were performed in toluene at $-60\text{ }^{\circ}\text{C}$ to give the *exo*-cyclization product **30a** under kinetic control. However, the hydroamination/cyclization reaction in THF solution is reversible, producing the thermodynamically favored *endo*-cyclization product **30b**.

Scheme I-11. Kinetic versus thermodynamic control in the lithium-catalyzed cyclization of aminostilbenes.⁷¹



I.2.3 Alkaline Earth Metal-Based Catalysts

For chiral alkaline earth metal hydroamination catalysts (Figure I-2) one of the greatest challenges has been the development of a chiral catalyst system that can resist facile ligand redistribution via Schlenk equilibrium leading to achiral catalytically active species. Until very recent reports⁷⁴ most catalysts failed to reach even moderate enantioselectivities in aminoalkene hydroamination-cyclization (Table I-4).

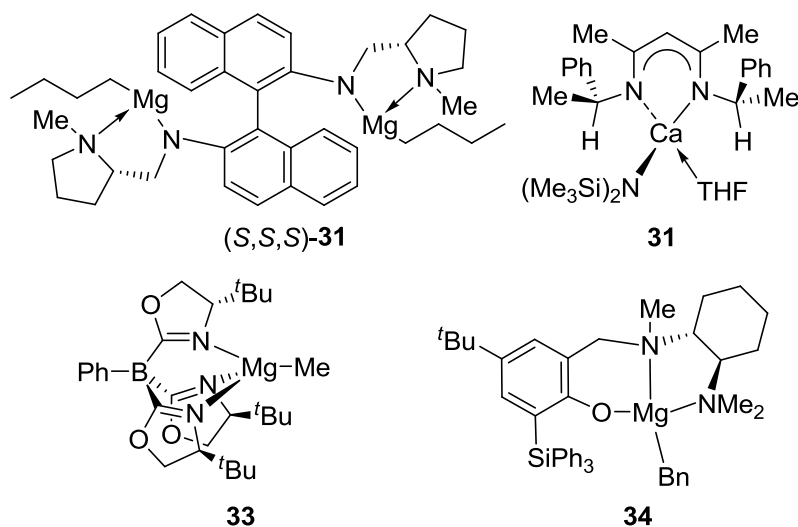
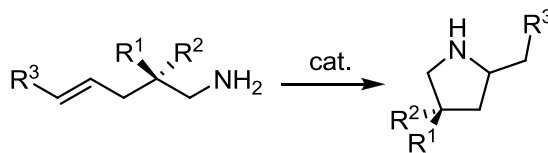


Figure I-2. Chiral alkaline earth metal catalysts.

The bis(amido) magnesium complex (S,S,S) -**31**⁷⁵ as well as the chiral diketiminato calcium compound **32**,⁷⁶ showed very low selectivity for the intramolecular hydroamination, apparently as a result of facile ligand redistribution reactions (Table I-4, entries 1 and 2). Although the tris(oxazoliny)borate **33** was reported to be stable to ligand redistribution, only low selectivities of up to 36% ee were obtained (Table I-4, entry 4).⁷⁷ In a marked contrast, the chiral magnesium (amino)phenolate **34**, recently developed in the Hultsch group⁷⁴ displayed selectivities of up to 93% ee as well as reactivity superior to that of the achiral⁷⁸ analog (Table I-4, entries 5–7). This promising

example illustrates that reactivity and selectivity levels of organolanthanide catalysts can also be achieved with alkaline earth metal-based catalysts.

Table I-4. Alkaline earth metal-catalyzed asymmetric hydroamination of aminopentenes.



Entry	R ¹ , R ²	R ³	cat.	[cat.]/[s], <i>T</i> , °C	<i>t</i> , h	Yield,	%ee	Ref.	
				mol%		%	(config)		
1	Me, Me	H	31	5	100	22	99	4 (<i>S</i>)	75
2	Ph, Ph	H	32	10	20	1	98	10 (<i>R</i>)	76
3	Me, Me	H	33	10	80	120	80	27 (<i>R</i>)	77
4	-(CH ₂) ₅ -	H	33	10	60	26	93	36 (<i>R</i>)	77
5	Me, Me	H	34	5	22	10	97	79 (<i>S</i>)	74
6	-(CH ₂) ₅ -	H	34	2	22	4.5	99	85 (<i>S</i>)	74
7	Ph, Ph	Ph	34	2	−20	12 h	98	93 (<i>S</i>)	74

I.2.4 Group 4 Metal-Based Catalysts

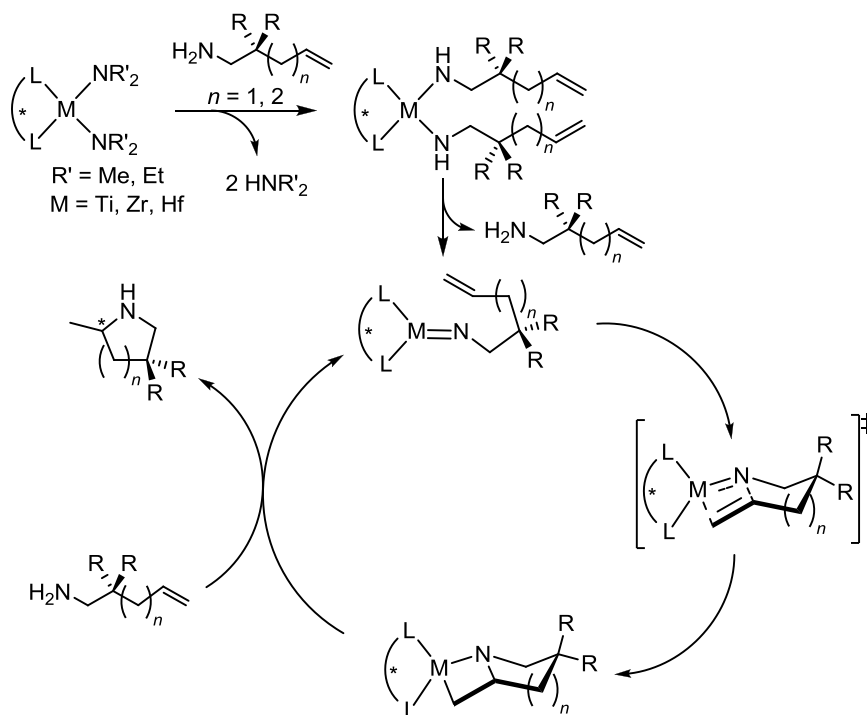
The chemistry of organometallic group 4 metal compounds is well developed thanks to their importance in polyolefin synthesis. Hence, their application in catalytic asymmetric hydroamination reactions is highly desirable. Group 4 metal complexes are commonly less sensitive and easier to prepare than rare earth metal complexes. Most important of all, many potential precatalysts or catalyst precursors are commercially available.

While most group 4 metal catalyst systems exhibit inferior reactivity and substrate scope in comparison to most rare earth metal- and alkaline earth metal-based catalyst systems, requiring high catalyst loadings and elevated reaction temperatures, recent

breakthrough discoveries on zwitterionic zirconium catalysts^{79,80} are promising to close the gap between these systems. Still, in most instances *gem*-dialkyl activation³⁰ of the aminoalkene substrate is required for catalytic turnover, therefore, suggesting that asymmetric intermolecular alkene hydroamination is still a remote goal.

The mechanism of alkene hydroamination is much less well understood than the mechanism for alkyne and allene hydroamination as the latter was the subject of detailed kinetic and mechanistic⁸¹⁻⁸⁶ as well as computational studies^{87,88}. The catalytically active species is believed to be a metal imido complex, which undergoes a reversible, rate-determining [2+2]-cycloaddition with a unsaturated carbon-carbon moiety, to yield an azametallacycle species. Subsequent protonolysis leads to the imine hydroamination product. Although no direct experimental^{89,90} or theoretical⁹¹ evidence was obtained, the same mechanism was proposed for the intramolecular hydroamination of aminoalkenes (Scheme I-12). The fact that *secondary* amines do not undergo reaction with most group 4 metal catalysts was interpreted in terms of prohibited formation of the imido-species, thus being supportive to the imido-mechanism.^{89,90,92,93}

Scheme I-12. Proposed mechanism for the hydroamination/cyclization of primary aminoalkenes involving group 4 metal imido species.



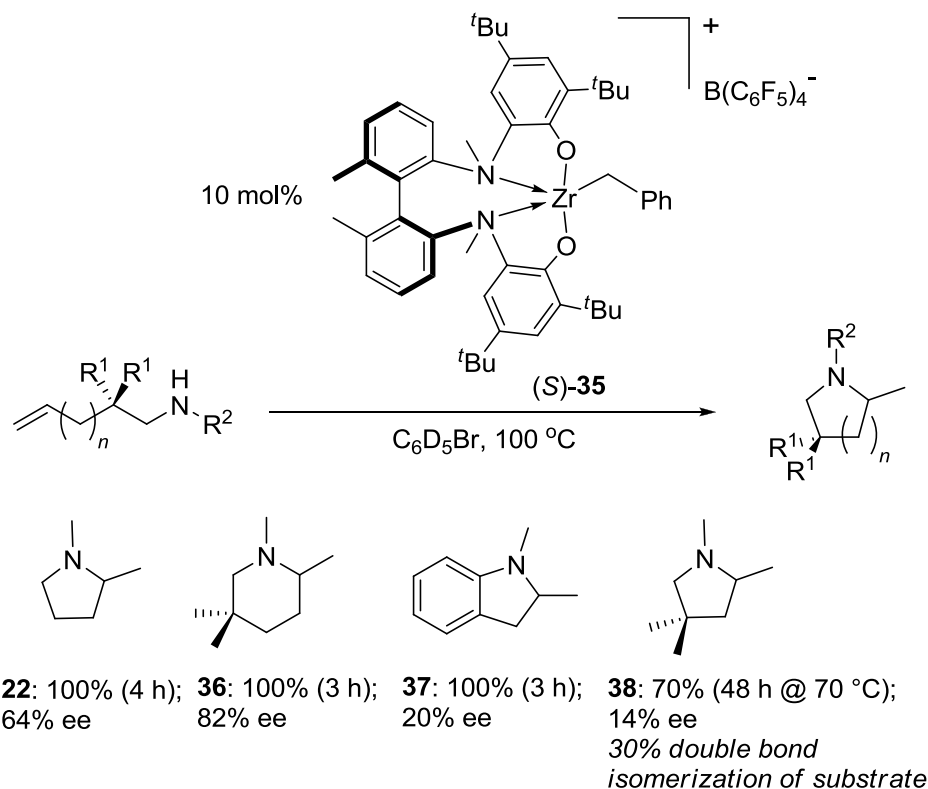
More recently, neutral zirconium-based catalysts capable to perform reactions with both primary and secondary amines in intra-⁹⁴⁻⁹⁶ and intermolecular^{96,97} reactions were reported. The imido-mechanism is obviously impossible, and an insertion mechanism, similar to the lanthanide-like mechanism shown in Scheme I-1 was proposed.⁹⁴ The isolation of an insertion intermediate in an intermolecular alkyne hydroamination reaction is compelling evidence in favor of the insertion mechanism.⁹⁷

Pronounced kinetic isotope effects, observed for group 4 metal-catalyzed reactions were interpreted in terms of either rate-determining metal imide formation⁹⁸ or concerted insertion/protonolysis⁸⁰ similar to that shown in Scheme I-2. A large isotopic perturbation of stereoselectivity, proving N–H bond breakage during N–C bond

formation⁸⁰ is supportive to the second argument; however, it is not yet clear whether such phenomena are common for all group 4 metal catalysts.

The first chiral group 4 metal catalyst system for asymmetric hydroamination/cyclization of aminoalkenes was based on the cationic aminophenolate complex (*S*)-**35**.⁹⁹ Secondary aminoalkenes reacted readily to yield hydroamination products with enantioselectivities of up to 82% ee (Scheme I-13). For catalyst solubility reasons, reactions were commonly performed at 100 °C in bromobenzene using 10 mol % catalyst loading. The mechanism of this cationic system is thought to proceed similar to the σ -bond metathesis mechanism of rare earth metal-based catalyst systems (Scheme I-1) which is in agreement with DFT calculations.¹⁰⁰ Primary aminoalkenes did not react, which was thought to be caused by facile α -deprotonation of the catalytic active cation metal-amido species leading to an unreactive metal-imido species.^{99,101,102} More recently, achiral cationic systems capable of cyclizing both secondary and primary aminoalkene have been developed, suggesting that the formation of a metal-imido species is not necessarily prohibitive to achieve a catalytic turnover.¹⁰³ The cationic catalyst systems are also prone to double bond isomerization via N–H activation that can significantly reduce product enantioselectivity and yield.^{99,101,104}

Scheme I-13. Hydroamination/cyclization of secondary aminoalkenes using a cationic chiral zirconium catalyst system.⁹⁹



In contrast to cationic group 4 metal hydroamination catalysts, their neutral counterparts (Figure I-3) will generally react only with primary aminoalkenes and reaction temperatures are typically higher (110–135 °C).

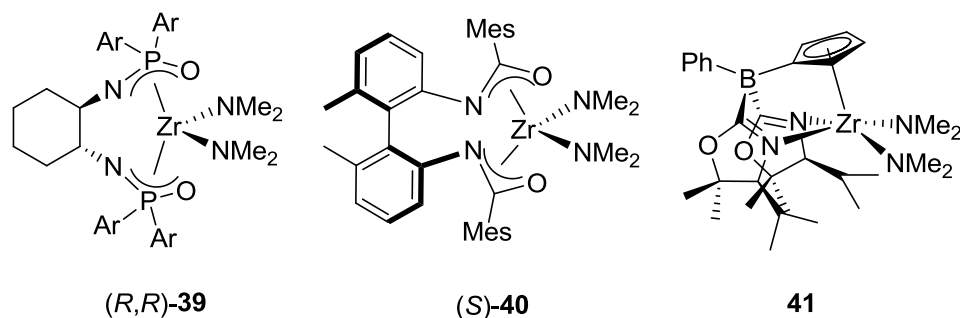
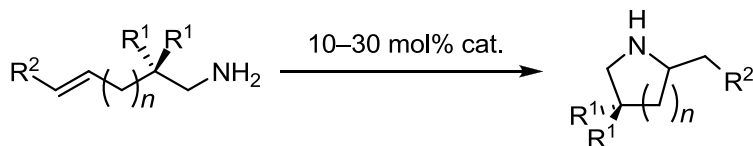


Figure I-3. Selected group 4 metal catalysts for asymmetric hydroamination of primary aminoalkenes (Mes = 2,4,6-Me₃C₆H₂; Ar = 3,5-Me₂C₆H₃).^{80,92,93,105}

Table I-5. Asymmetric hydroamination of aminoalkenes catalyzed by zirconium complexes.



Entry	cat.	<i>n</i>	R ¹	R ²	<i>T</i> , °C	<i>t</i> , h	Yield, %	% ee (config.)	Ref.
4	39	1	Me	H	115	24	95 ^a	80 (<i>S</i>)	92
5	39	1	H	H	135	72	33 ^a	62	92
6	39	1	Me	Ph	135	24	93 ^a	62	92
7	39	2	Me	H	85	24	99 ^a	51	92
8	40	1	Me	H	110	3	80	93 (<i>R</i>)	93,105,106
9	40	1	-(CH ₂) ₅ -	H	110	3	96	82 (<i>R</i>)	93,105,106
10	40	1	Allyl	H	110	4.5	88	74 (<i>R</i>)	93,105,106
11	40	1	Ph	H	110	1.3	93	74 (<i>S</i>)	93,105,106
12	40	2	Me	H	110	3	n.r.	21	93,105
14	41	1	Me	H	rt	7	89	89 (<i>R</i>)	80
15	41	1	-(CH ₂) ₅ -	H	23	1.25	88	90 (<i>R</i>)	80
16	41	1	-(CH ₂) ₅ -	H	23	n.r.	n.r.	97 (<i>R</i>) ^b	80
17	41	1	Ph	H	-30 ^c	120	>95	98 (<i>R</i>)	80
18	41	2	Ph	H	rt	30	65	46 (<i>R</i>)	80

^a Isolated as *N*-trifluoroacetamide. ^b Reaction of the *N*-deuterated substrate. ^c reaction in THF-*d*₈. n.r. = not reported.

The chiral bis(phosphinic amido) zirconium complex (*R,R*)-**39** exhibits superior reactivity and enantioselectivity for the cyclization of primary aminoalkenes in comparison to a wide range of diamido, diolate, and aminoalcoholate titanium, zirconium, and hafnium complexes.⁹² The cyclization of aminopentenes proceed with enantioselectivities as high as 80% ee, but formation of piperidines (Table I-5, entry 7) is

somewhat less selective. Unfortunately, mechanistic studies indicate that this catalyst system undergoes slow ligand redistribution reactions, leading to chiral catalytically inactive as well as achiral catalytically active species.

Higher enantioselectivities of up to 93% ee were achieved using the chiral bis(amidate) zirconium complex (*S*)-**40** (Mes = 2,4,6-Me₃C₆H₂),^{93,105-108} but again the high selectivities are limited to the formation of pyrrolidines, and unlike **39**, only *gem*-disubstituted substrates were reactive.

A notable breakthrough in both catalytic activity and selectivity was achieved with introduction of chiral zwitterionic zirconium cyclopentadienyl-bis(oxazolidinyl)borate **41**,⁸⁰ allowing reactions to be performed at temperatures as low as -30 °C. Hydroamination is highly stereoselective, achieving up to 98% ee for aminopentenes but is less selective not for aminohexenes (Table I-5, entries 14–18). The catalysts exhibit a significant primary kinetic isotope effect and an isotopic perturbation of enantioselectivity resulting in higher enantioselectivities for the *N*-deuterated substrates (Table I-5, entry 15 vs. entry 16). However, despite an incredible reactivity improvement, **40** is also confined to *gem*-dialkyl-activated substrates and failed to cyclize the unsubstituted aminopentene, which reacts only sluggishly even at 110 °C. Other challenging substrates for group 4 metal catalysts are aminoheptenes, as aminohexenes and aminoheptenes are frequently observed to undergo hydroaminoalkylation (via α -C–H activation) instead of hydroamination (via N–H activation).¹⁰⁹

I.2.5 Late Transition Metal Catalysts

High electro- and oxophilicity of early transition metal catalysts results in high basicity, moisture- and air-sensitivity and poor functional group tolerance which is a

significant drawback of these catalysts. In contrast, late transition metal catalysts have a potential to overcome these limitations. However, so far only a limited number of predominantly achiral catalyst systems are known to catalyze the hydroamination/cyclization of basic *N*-unprotected primary¹¹⁰⁻¹¹⁶ and secondary^{113-115,117-121} aminoalkenes as well as of *N*-protected substrates such as sulfonamides,¹²²⁻¹²⁴ carbamates,¹²⁵⁻¹²⁸ amides,^{122,125,129} and ureas.¹³⁰

The mechanism of late transition metal-catalyzed hydroaminations have been studied less intensively and they are much less understood compared to early transition and rare earth metal-catalyzed hydroaminations. However, it was established that late transition metal-catalyzed hydroaminations may proceed via different mechanisms depending on the substrate and the catalyst employed. Two general possible pathways for the intramolecular hydroamination of aminoalkenes with late transition metal catalysts are shown in Figure I-4. The amine activation (pathway **A**) includes oxidative addition of an amino group, followed by insertion of the unsaturated carbon-carbon bond into the metal-amide bond, and then reductive elimination. It is well documented that the iridium-catalyzed hydroamination of strained alkenes, such as norbornene, with anilines proceeds via pathway **A**.¹³¹⁻¹³³ Although amines other than anilines, such as ammonia, were also reported to undergo N–H oxidative addition to iridium¹³⁴⁻¹³⁶ and ruthenium¹³⁷ metal centers, no related catalytic systems were reported. The *syn*-insertion of an olefin into a late transition metal amide bond is also a feasible process, although this mode of insertion is unlikely to participate in known hydroamination processes.¹³⁸⁻¹⁴¹ DFT calculations suggest that pathway **A** is less favored than pathway **B** for hydroamination of alkenes with ammonia catalyzed by group 9 and 10 metal complexes.¹⁴² Interestingly, the

iridium-catalyzed hydroamination of aliphatic aminoalkenes was also proposed to proceed via pathway **B** as supported by DFT calculations.¹¹⁵

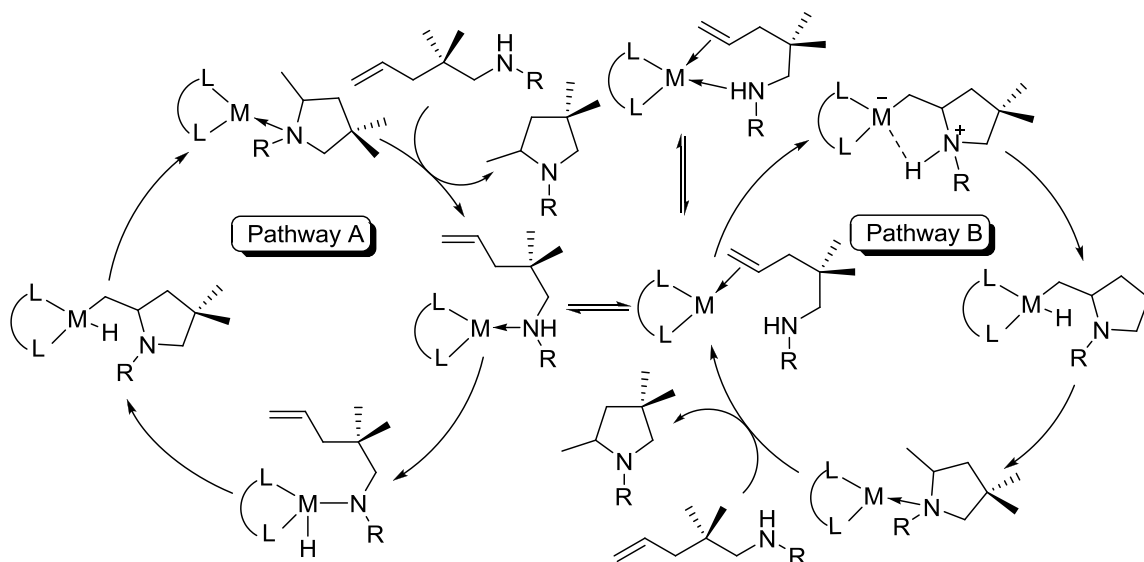


Figure I-4. Mechanism of late transition metal-catalyzed hydroamination. Pathway **A**: via amine activation. Pathway **B**: via alkene activation.

Key steps of pathway **B** include nucleophilic attack of the amine on the metal-coordinated olefin, leading to a zwitterionic intermediate. Proton transfer from nitrogen to the metal produces a β -aminoalkyl metal species, which then undergoes reductive elimination cleaving the metal-carbon bond. The direct protonolysis of the metal-carbon bond in the zwitterionic ammonium intermediate is also principally possible, but this step is in general less kinetically favorable than the stepwise process via reductive elimination. DFT calculations of the iridium-catalyzed intramolecular hydroamination suggest that this irreversible metal-carbon bond cleavage is rate-limiting, which is in line with the observed large negative activation entropy.¹¹⁵ It should be noted that coordination of the alkenyl moiety of the substrate to the metal center may be disfavored by a competitive coordination of the amino group, which does not directly lead to the

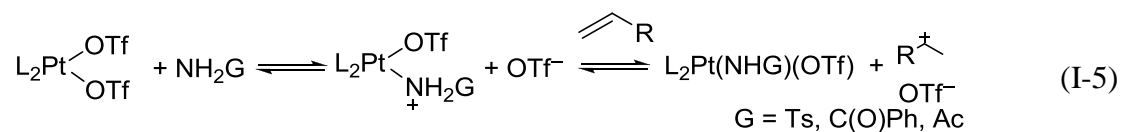
product formation according to pathway **B**. This explains why primary aminoalkenes are significantly less reactive than more sterically encumbered (and thus less prone to coordinate through nitrogen) secondary aminoalkenes for most late transition metal-based systems. Another important observation is that not all late transition metal-catalyzed systems are limited in turnover by the protonolysis step, as some examples of “fast” protonolysis in a POP-rhodium catalyst system are known.¹¹⁶

The same catalytic cycle was also proposed for hydroaminations with *N*-protected amines or less nucleophilic amines such as anilines. Mechanistic studies suggest that the protonolysis of the metal-carbon bond is the rate-determining step in the PNP-palladium-catalyzed intramolecular hydroamination of alkenyl carbamates and carboxamides.¹²⁸

Computational studies of the platinum-catalyzed addition of aniline to ethylene showed a high barrier for oxidative amine addition and revealed a nucleophilic attack on the coordinated ethylene as the rate-determining step.^{143,144}

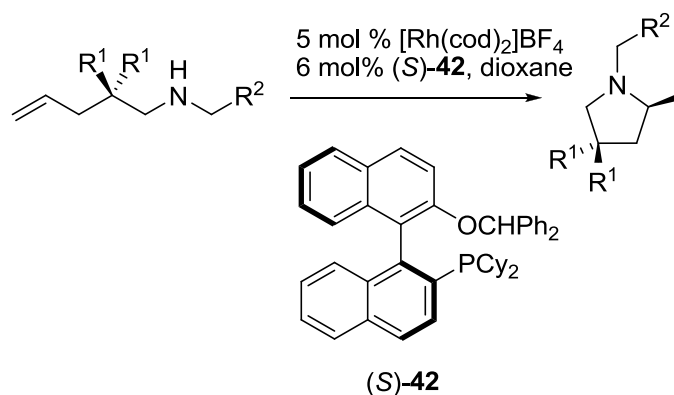
N-protected alkenyl hydrazides were shown to undergo intramolecular hydroamination via N–H-activation/olefin insertion rather than through nucleophilic attack on the coordinated alkene, which is one of the few examples of catalytic late transition metal-based systems operating via path **A**.¹⁴⁵

It should be noted that in certain cases the role of the metal catalyst may be limited to the generation of an acid via ligand exchange with the *N*-protected amine followed by protolytic dissociation. This activates the alkene to nucleophilic transformations, since the addition of *N*-protected amines to alkenes is also efficiently catalyzed with Brønsted acids such as TfOH (Eq. I-5).¹⁴⁶⁻¹⁴⁸



Most efforts in late transition metal catalyzed-intramolecular alkene hydroamination were centered on achiral systems, and only recently, a chiral Rhodium-based catalyst system¹⁴⁹ modeled after an achiral system¹¹³ has been introduced. The catalyst system using the cyclohexyl-modified MOP ligand **42** cyclizes *N*-benzyl-substituted aminopentenes in high yield under relatively mild reaction conditions and enantioselectivities of up to 91% ee (Table I-6). The nature of the protecting group can have a pronounced influence on product enantioselectivities, e.g. higher enantioselectivities are obtained in some cases when using the sterically more bulky *N*-(2-methyl)benzyl group. Unprotected primary aminoalkenes generally show poorer reactivity. The cyclization of aminohexene derivatives proceeds also with significantly diminished yield and enantioselectivity.

Table I-6. Rhodium-catalyzed enantioselective hydroamination/cyclization of aminopentenes.¹⁴⁹



Entry	R ¹ , R ¹	R ²	T, °C	<i>t</i> , h	Yield, %	% ee
1	H, H	Ph	70	20 ^a	48	90
2	Me, Me	2-CH ₃ C ₆ H ₄	70	20	75	62
3	-(CH ₂) ₅ -	2-CH ₃ C ₆ H ₄	70	20	80	63
4	Ph, Ph	2-CH ₃ C ₆ H ₄	70	15	92	84
5	Ph, Ph	2-CH ₃ C ₆ H ₄	50	24	91	88

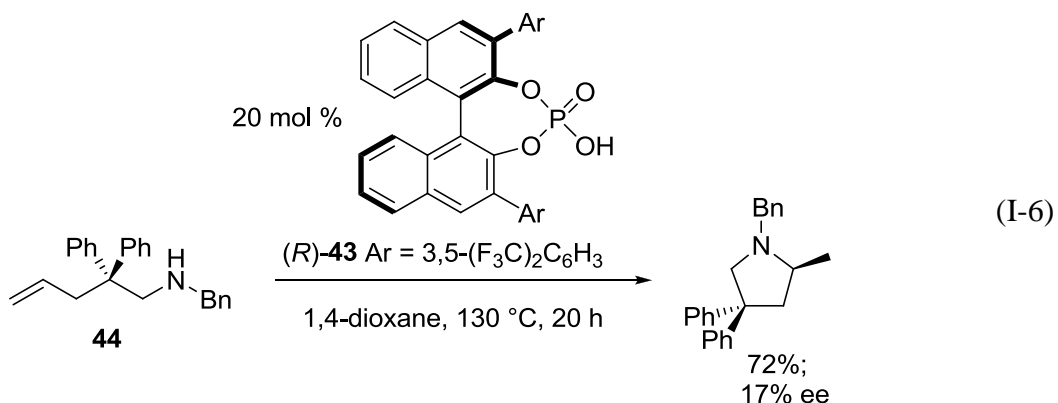
^a 10 mol % [Rh(COD)₂]₂BF₄, 12 mol % (S)-**42**

I.2.6 Organocatalytic Asymmetric Hydroamination

In the last decade, the field of asymmetric organocatalysis has seen significant progress. In particular, the application of Brønsted acids in metal-free enantioselective catalysis is rapidly increasing.¹⁵⁰⁻¹⁵² Several research groups have recently demonstrated that strong Brønsted acids can be used in both *intra*-¹⁵³⁻¹⁵⁵ and *intermolecular*¹⁵⁶⁻¹⁵⁹ hydroamination reactions, although most reactions are limited to weakly basic anilines and *N*-protected amines (sulfonamides, carbamates, etc.).

The first example of catalytic asymmetric metal-free hydroamination using the chiral phosphoric acid (*R*)-**43** was disclosed by Ackermann and coworkers (Eq.

I-6).¹⁶⁰ Although both selectivity and catalytic activity for the hydroamination of the secondary aminopentene **44** are rather low, the method itself remains very promising.



Toste et al. has utilized similar approach employing chiral (thio)phosphoric acids for highly enantioselective cyclohydroamination of *N*-protected dienes,¹⁶¹ however efficient organocatalytic efficient protocols for alkene hydroaminations are yet to be developed.

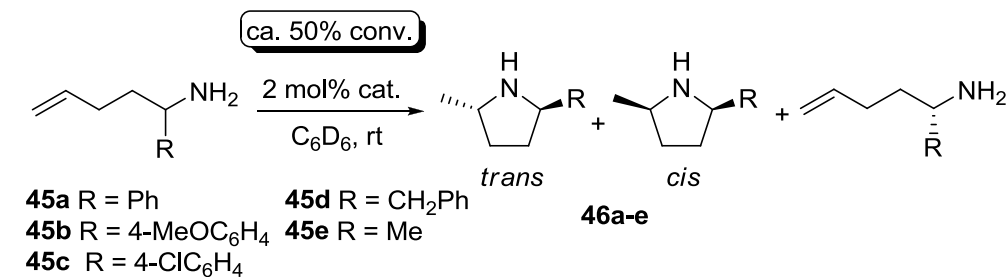
I.2.7 Kinetic Resolution via Asymmetric Hydroamination

Kinetic Resolution of Aminoalkenes

Kinetic resolution of racemic chiral amines is one of the promising directions for the further development of asymmetric hydroamination. Recently, our group has developed kinetic resolution of chiral aminoalkenes which has been achieved utilizing the binaphtholate complexes (*R*)-**24-Ln** (Table I-7).^{18,40} Various chiral aminopentenones were kinetically resolved with resolution factors *f* (defined as $f = K^{dias} \times k_{fast}/k_{slow}$; where K^{dias} is the Curtin-Hammett equilibrium constant between the two diastereomeric substrate/catalyst-complexes and k_{fast}/k_{slow} being the ratio between the faster and the slower reaction rate constant) as high as 19 and enantiomeric excess for recovered starting material reaching $\geq 80\%$ ee at conversions close to 50%. The 2,5-disubstituted

pyrrolidines were obtained in good to excellent *trans* diastereoselectivity, depending on the steric hindrance of the α -substituent. Preparative kinetic resolution of **45e** using 1 mol % (*R*)-**24a-Lu** gave enantiopure (*S*)-**45e** ($\geq 99\%$ ee) in 33% re-isolated yield at 64% conversion.¹⁸

Table I-7. Catalytic kinetic resolution of chiral aminopentenes.¹⁸



Entry	Substrate	Cat.	<i>t</i> , h	Conv., %	trans:cis	% ee of <i>f</i> recov. 45 .	
1	45a	(<i>R</i>)- 24a-Lu	15 ^a	52	$\geq 50:1$	83	19
2	45b	(<i>R</i>)- 24a-Y	8 ^a	50	$\geq 50:1$	78	19
3	45c	(<i>R</i>)- 24a-Y	18 ^a	50	$\geq 50:1$	71	12
4	45d	(<i>R</i>)- 24a-Y	9	50	20:1	42	3.6
5	45e	(<i>R</i>)- 24b-Y	26	52	13:1	80	16

^a At 40 °C.

The preferred formation of (2*S*,5*S*)-**46e** using (*R*)-binaphtholate complexes can be attributed to impeded cyclization of (*R*)-**45e** due to unfavorable steric interactions of the vinylic methylene protons with a trisarylsilyl substituent in the chair-like transition state (Figure I-5). Fast exchange between matching and mismatching aminoalkene prior to cyclization is imperative for an effective kinetic resolution process. Kinetic analysis of the kinetic resolution process has revealed that the Curtin-Hammett-equilibrium favors the matching substrate/catalyst combination in aminopentene substrate **45a** containing α -

aryl substituent¹⁸ and the reason of poor resolution factor in the case of alkyl-substituted substrates remained unclear.

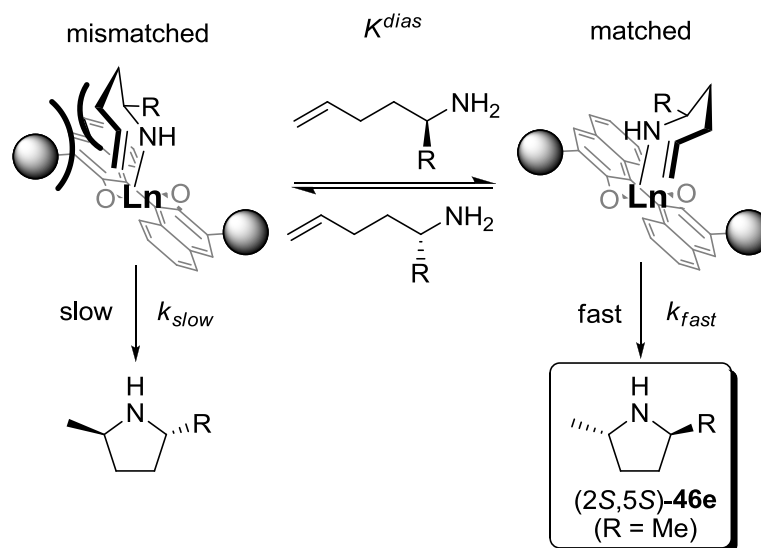
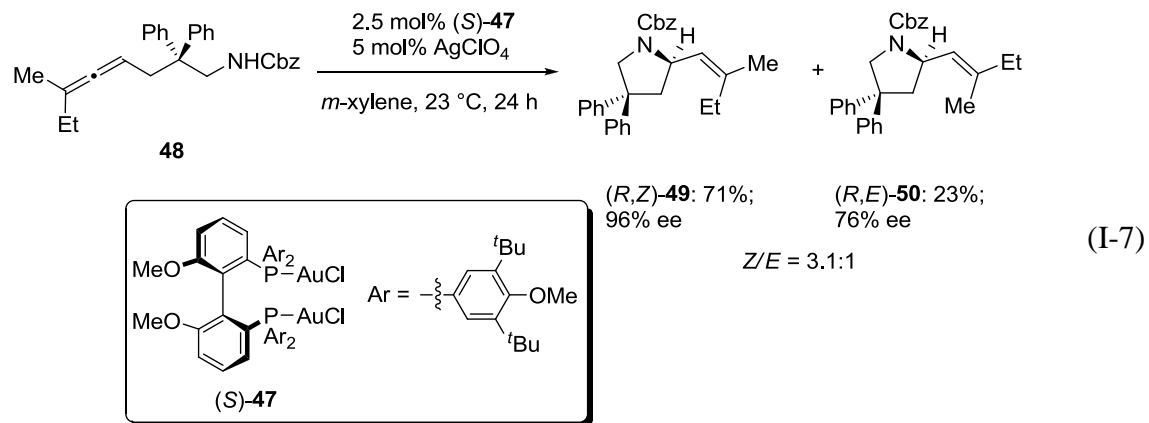


Figure I-5. Proposed stereomodel for kinetic resolution of chiral aminopentenes with an equatorial approach of the olefin.

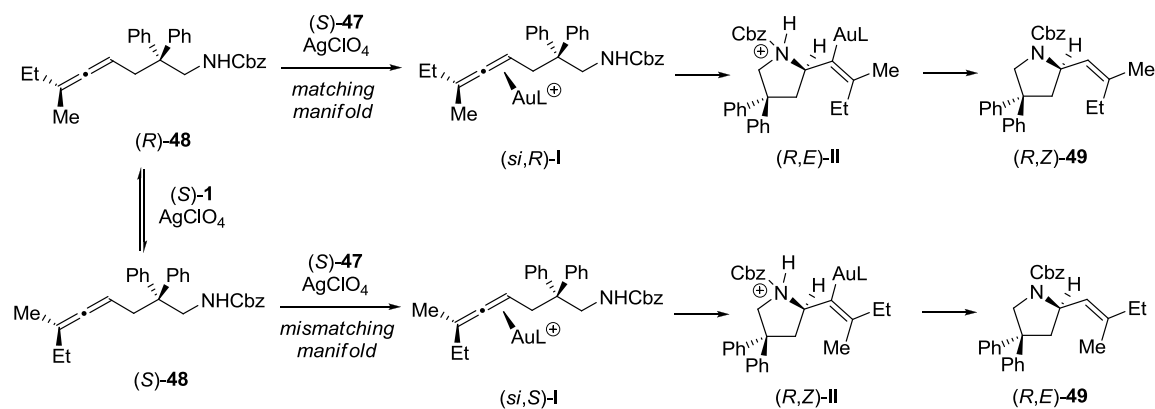
Dynamic Kinetic Resolution of N-Protected Aminoallenes

Cationic gold(I) complexes are well known to racemize allenes,¹⁶² which can be exploited in the facile dynamic kinetic resolution of axially chiral *N*-(γ -allenyl) carbamates with trisubstituted allenyl groups.¹⁶³ A mixture of the dinuclear gold(I) phosphine complex (*S*)-**47** and AgClO_4 catalyzed the cyclization of the Cbz-protected aminoallene **48** to yield predominantly the (*Z*)-vinylpyrrolidine (*R,Z*)-**49** with excellent enantioselectivity (Eq. I-7). Initial mechanistic studies suggest that the (*E*)-vinylpyrrolidine (*R,E*)-**50** is formed in the mismatched reaction manifold (Scheme I-14). In the matching manifold, the cationic gold(I)-species is believed to coordinate preferentially to the *si* face of the allene substrate ((*si,R*)-**I**). Subsequent attack of the tethered nucleophilic carbamate nitrogen leads to the σ -alkenyl-gold complex (*R,E*)-**II**.

Finally, protonolysis of the Au–C bond proceeds with retention of configuration, releasing the (*R,Z*)-vinylpyrrolidine product.



Scheme I-14. Proposed mechanism for the gold-catalyzed dynamic kinetic resolution of aminoallenes.



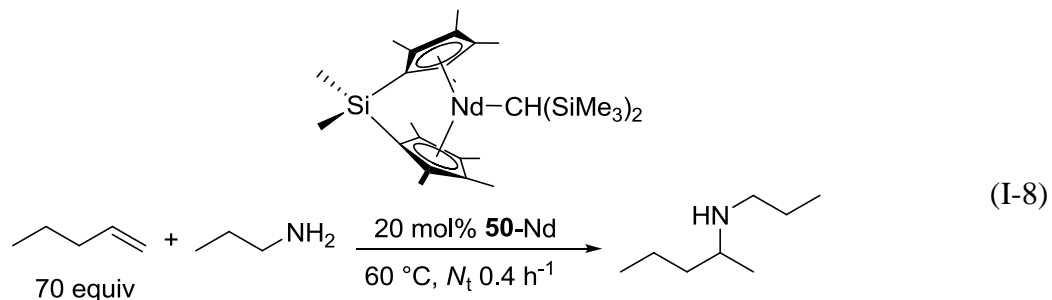
I.3 Intermolecular Hydroamination

Despite the incredible growth of a number of publications on hydroamination observed over last decade,² examples of intermolecular hydroamination of unactivated alkenes are very rare. In particular, the asymmetric hydroamination remains very challenging. Below we will fully cover known examples of asymmetric hydroamination

of alkenes published to date. Unfortunately, all these examples include either activated alkenes, such as diene, styrene or norbornene, or they are employing *N*-protected amines. Although asymmetric hydroamination of *unactivated* alkenes with *simple* amines was not known prior to the present work, we will mention some non-asymmetric reactions which might be relevant to further development of stereoselective methods.

I.3.1 Early Transition and Main Group Metal Catalysts

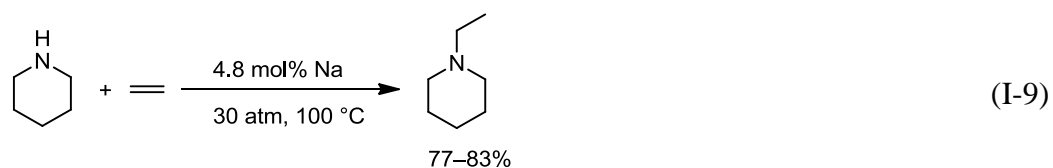
While the *intramolecular* hydroamination of aminoalkenes is catalyzed efficiently by a variety of early transition or main group metal catalyst systems, the *intermolecular* hydroamination of alkenes is significantly more challenging. Unfavorable factors are not only the negative reaction entropy, but also the competition between strongly coordinating amines and weakly binding alkenes. For rare-earth-metal-based catalysts only a limited number of reports utilizing either lanthanocene,^{20,164} phenylene-bridged binuclear half-sandwich,¹⁶⁵ or binaphtholate¹⁸ complexes have been documented in the literature. The Markovnikov-addition to an unactivated alkene requires large excess of the alkene in order to overcome the competition between strongly binding amines and weakly binding alkenes, even if the sterically open *ansa*-lanthanocene $\text{Me}_2\text{Si}(\text{C}_5\text{Me}_4)_2\text{NdCH}(\text{SiMe}_3)_2$ (**50-Nd**) is employed (Eq. I-8).¹⁶⁴



The intermolecular hydroamination of unactivated alkenes with alkali metal catalysts has been known for a long time and a comprehensive review is available.⁶⁹

Reactions of ethylene with ammonia or primary amines catalyzed by elemental lithium,¹⁶⁶ sodium,¹⁶⁷⁻¹⁷⁰ potassium,¹⁶⁷ alkali metal hydrides¹⁶⁷ and amides^{171,172} typically require high reaction temperatures (250–500 °C) and pressures (up to 1000 bar) and result in mixtures of mono-, di- and triethylamine in moderate yields.

Reactions of secondary alkenes are more practical (Eq. I-9)¹⁷³ as they allow selective formation of tertiary ethylamines employing alkali metals in their elemental form,^{170,173} as alkali metal amides,¹⁷⁴⁻¹⁷⁸ which can also be generated in situ from the corresponding metal alkyls, or as metal hydrides.¹⁷⁷



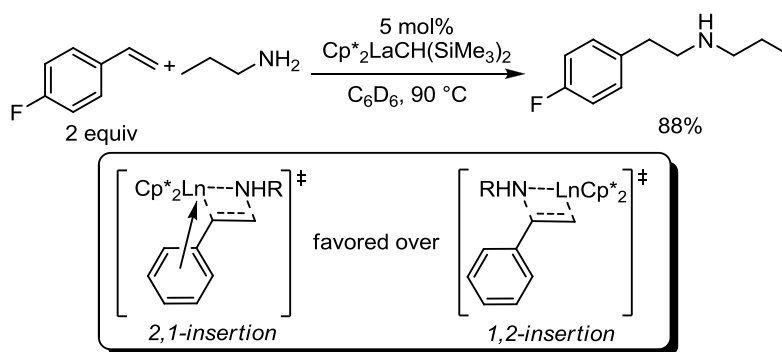
Alkali-metal-catalyzed hydroamination of unactivated higher alkenes is significantly less feasible.^{174,178}

The double bond in vinyl arenes is activated as a result of its conjugation to the aromatic ring system. Hence, vinyl arenes generally react more smoothly in hydroamination reactions in comparison to simple, unactivated alkenes, especially in intermolecular processes.

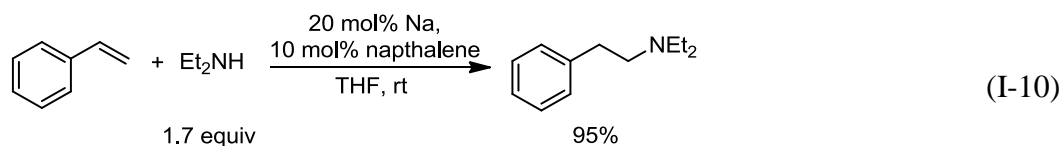
Contrary to simple aliphatic-substituted alkenes, the metal-catalyzed hydroamination of vinyl arenes proceeds usually with high *anti*-Markovnikov selectivity to give β-phenethylamine derivatives (Scheme I-15). This reversal of regioselectivity may be explained with the alkene insertion step proceeding through the sterically more encumbered transition state which is favored due to attractive metal–arene interactions and resonance stabilization of the benzyl carbanion. The same selectivity pattern is

observed for alkali¹⁷⁹ and alkaline earth^{74,180,181} metal catalysts and is also explained by metal-aryl interactions as shown by DFT-calculations.¹⁷⁹

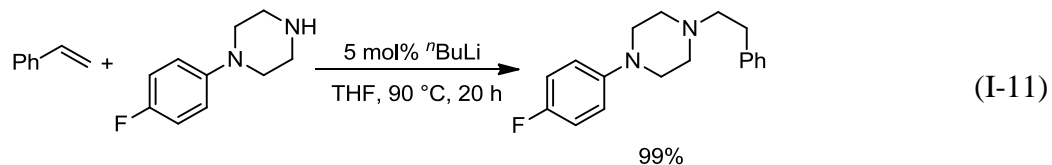
Scheme I-15. Rare earth metal-catalyzed *anti*-Markovnikov hydroamination of vinyl arenes.²⁰



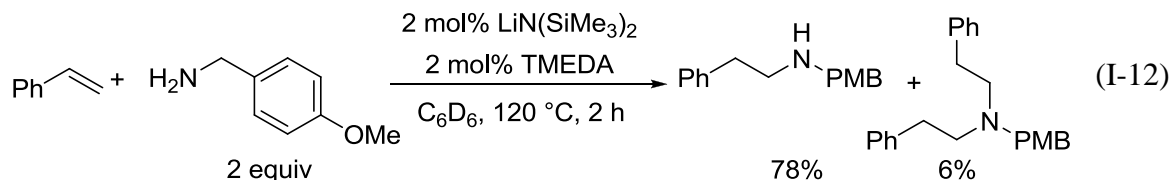
Due to the high reactivity of vinyl arenes, a broader range of catalysts is available, including very robust and readily accessible compounds. Sodium metal readily catalyzes the hydroamination of styrene with secondary¹⁸²⁻¹⁸⁶ or primary^{187,188} aliphatic amines at ambient or slightly elevated temperatures. The *anti*-Markovnikov addition of the amine moiety is favored (Eq. I-10)¹⁸⁵



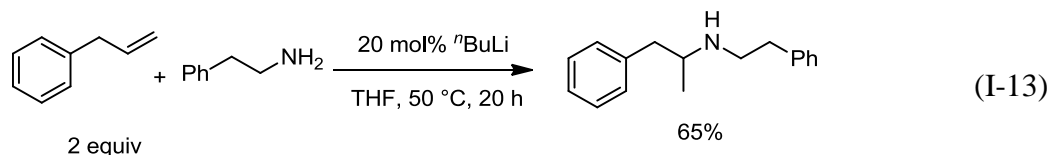
Lithium alkyls can also be used as homogeneous base-type catalysts for *anti*-Markovnikov addition of primary^{189,190} and secondary^{189,191,192} amines to vinyl arenes. The reactions typically proceed in good to excellent yields to give β -phenethylamine derivatives (Eq. I-11)¹⁹¹ Unfortunately, ammonia does not exhibit the same reactivity as primary and secondary amines.



The simple lithium amide LiHMDS catalyzes the addition of aliphatic and (notably) aromatic amines to vinyl arenes.¹⁷⁹ The catalytic activity is increased by addition of TMEDA and the reaction can be carried out in bulk without additional solvent. More reactive primary aliphatic amines also form a bis-hydroamination product, although the formation of the latter may be suppressed by using an excess of amine (Eq. I-12). Less reactive aromatic amines and α - and β -substituted styrenes give the mono-hydroamination adduct selectively.¹⁷⁹ Other readily available alkali-metal-based catalysts include NaH¹⁹², *t*-BuOK,^{190,193,194} and CsOH.¹⁹⁵



Although alkali metal amides cannot catalyze intermolecular hydroamination of higher unactivated alkenes, allylbenzene derivatives react smoothly via base-catalyzed isomerization into β -methyl styrene derivatives, which are active enough to form hydroamination product (Eq. I-13).¹⁹⁶

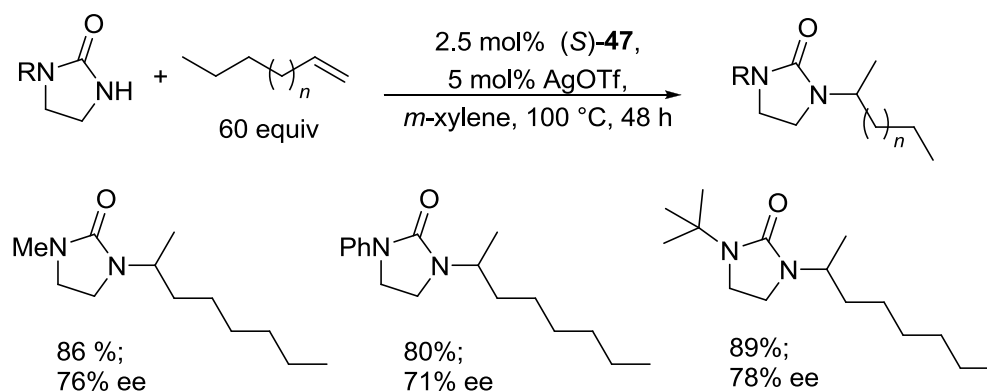


I.3.2 Late Transition Metal Catalysts

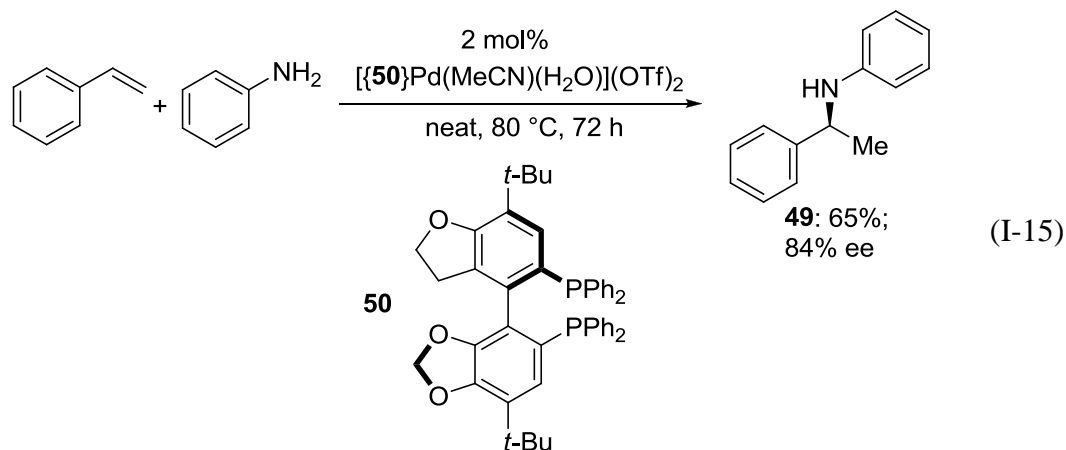
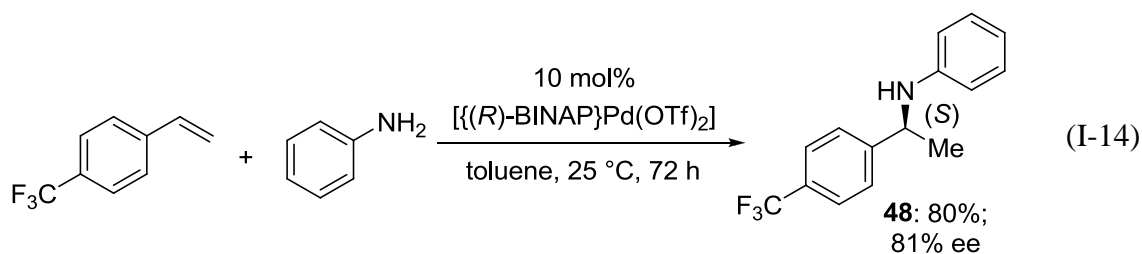
Although several significant contributions to the field of intermolecular hydroamination of simple alkenes have been made within the last decade, the asymmetric

hydroamination of *non-activated* alkenes with *unprotected* amines has yet to be elaborated and the first asymmetric intermolecular hydroamination of terminal, non-activated alkenes with cyclic ureas has been reported only recently (Scheme I-16).¹⁹⁷ The Markovnikov addition proceeded with up to 78% ee utilizing the axial chiral MeOBIPHEP-ligated bis(gold(I))-catalyst system (*S*)-**47**. Unfortunately, the reaction required a large excess of the alkene substrate and lower alkene loadings led to diminished enantioselectivities.

Scheme I-16. Gold-catalyzed asymmetric hydroamination of alkenes with cyclic ureas.¹⁹⁷

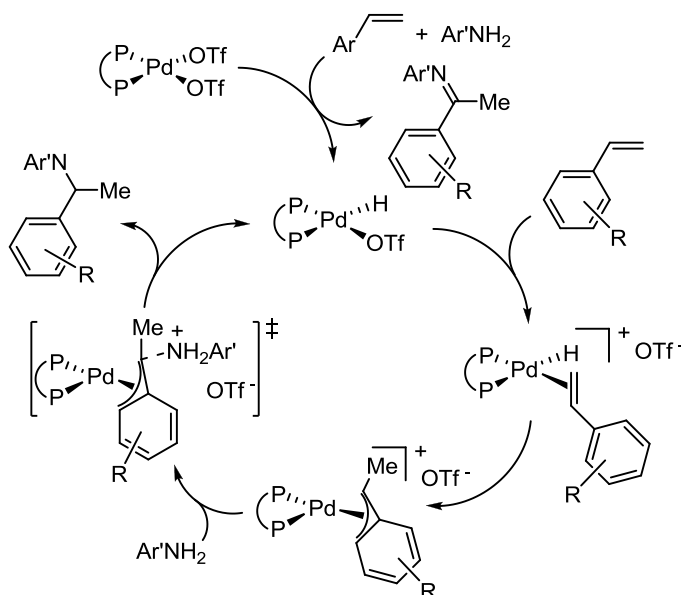


Since more reactive alkenes, such as vinyl arenes or sterically strained polycycles, react more readily in the hydroamination reaction, several asymmetric hydroamination reactions utilizing these substrates have been disclosed. Weakly basic anilines can react with vinyl arenes to give the Markovnikov addition products **48** and **49** with good yields and enantioselectivities in the presence of palladium complex with chiral diphosphine ligands such as BINAP(Eq. I-14)^{198,199} or *t*-BuSEGPPOS **50** (Eq. I-15).²⁰⁰



The proposed mechanism for this process involves an insertion of the vinyl arene into a palladium hydride species, followed by a nucleophilic attack of the amine on the resulting η^3 -benzylic palladium intermediate (Scheme I-17).²⁰¹⁻²⁰³ The high Markovnikov regioselectivity results from the electronically favored secondary insertion of the vinyl arene in the palladium hydride bond. Similar mechanistic models have been suggested for the late transition metal catalyzed hydroamination of allenes,²⁰⁴⁻²⁰⁶ and dienes.^{203,207-209} Generally, the η^3 -allyl species were identified as the resting state of the catalyst during the hydroamination reaction, indicating that nucleophilic attack is rate determining.^{201,209}

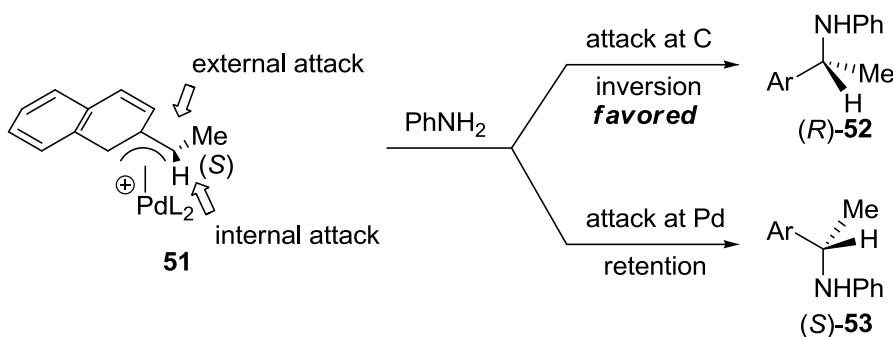
Scheme I-17. Proposed mechanism for the palladium-catalyzed hydroamination of vinyl arenes.



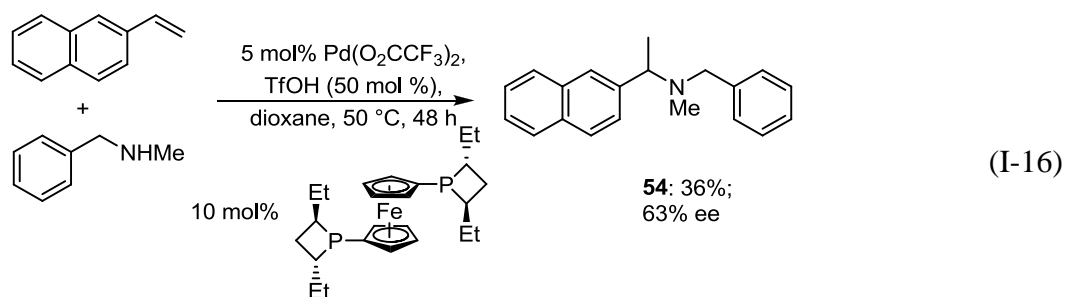
Two mechanistically plausible scenarios for the nucleophilic attack on the η^3 -benzyl palladium species seem feasible. Formation of the C–N bond could occur either via external attack of the amine via inversion of configuration at the carbon stereocenter, or alternatively the amine could coordinate to palladium followed by an internal attack on the η^3 -benzyl ligand. Mechanistic investigations²⁰¹ using stoichiometric amounts of the enantio- and diastereomerically pure η^3 -benzyl palladium complex $[(R)\text{-Tol-BINAP}]\{\eta^3\text{-1-(2-naphthyl)ethyl}\}\text{Pd}(\text{OTf})$ (**51**) revealed that the reaction with aniline produced predominantly (*R*)-*N*-1-(2-naphthyl)ethylaniline ((*R*)-**52**), consistent with external nucleophilic attack (Scheme I-18).²⁰¹ However, it was noted that the catalytic reaction of $[(R)\text{-Tol-BINAP}]\text{Pd}(\text{OTf})_2$ with vinyl arenes and amines produced preferentially the opposite enantiomeric (*S*)-amine hydroamination product; indicating, in analogy to asymmetric rhodium-catalyzed hydrogenation,²¹⁰ that the minor diastereomer

of the catalytic active benzyl palladium species was responsible for the majority of product formed in the catalytic process.

Scheme I-18. Preferential external attack of the aniline nucleophile leads to inversion of stereochemistry at the benzyl palladium intermediate.

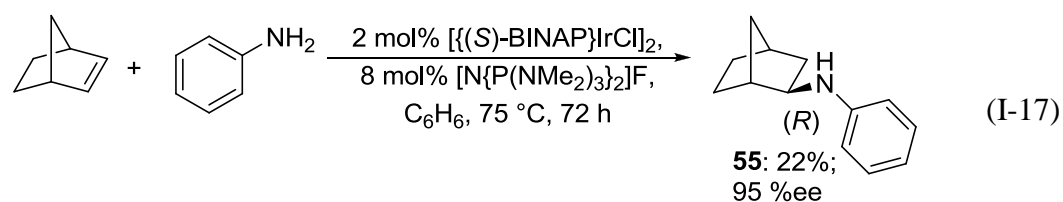


The range of amines involved may be expanded to more basic alkylamines (Eq. I-16).²⁰² Compound **54** was obtained in moderate yield and enantioselectivity utilizing the (*R,R*)-Et-FerroTANE ligand. Note that almost stoichiometric amounts of a strong Brønsted acid are required to afford the Markovnikov hydroamination product of the vinyl arene. The necessary intermediacy of η^3 -benzyl palladium makes the possible development of palladium-catalyzed intermolecular hydroamination of simple alkenes rather unlikely.



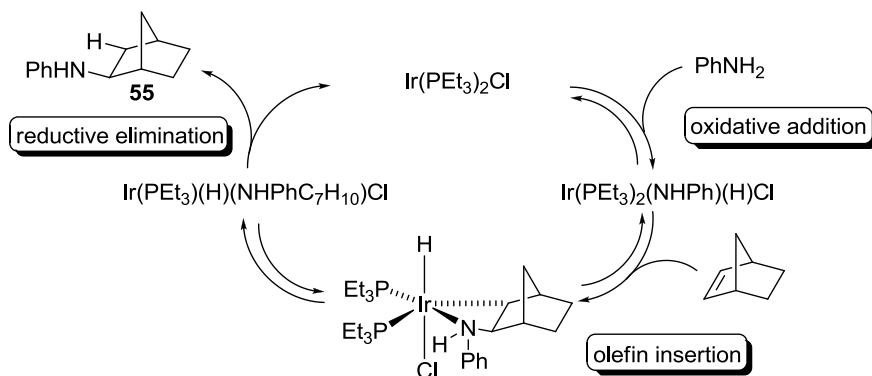
Enhanced reactivity of strained polycyclic olefins such as norbornene has made them attractive model compounds for intermolecular hydroamination. In most cases the reaction employs a late transition metal-based catalyst and requires elevated temperatures

and extended reaction times. The first chiral iridium-based catalyst system was reported by Togni in 1997 (Eq. I-17).¹³² The activity and enantioselectivity of this catalyst system was significantly enhanced by addition of Schwesinger's "naked" fluoride $[\text{N}\{\text{P}(\text{NMe}_2)_3\}_2]\text{F}$. In some cases the addition of fluoride also resulted in a reversal of absolute product configuration. However, the reason for the strong fluoride effect remains unclear, but it has been suggested that hydrogen bridging of the fluoride could play a role.



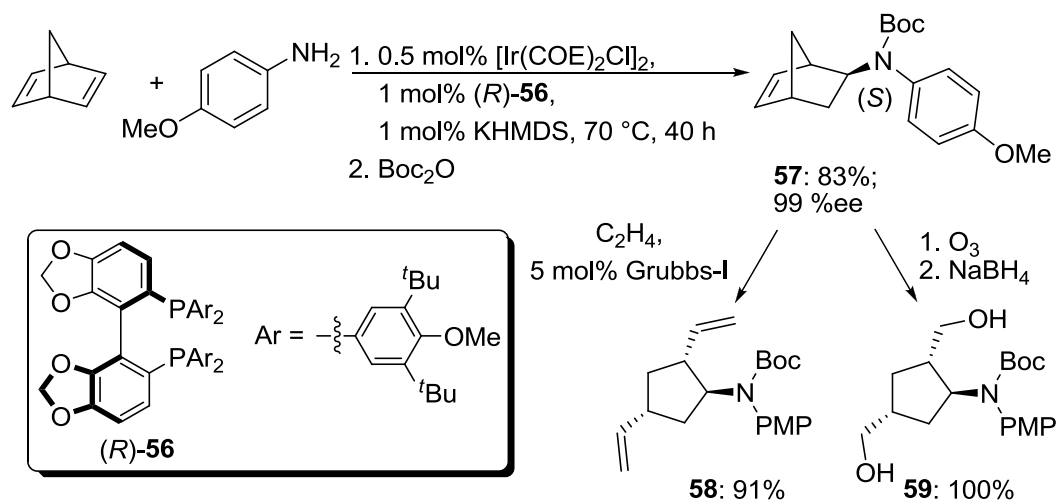
Earlier mechanistic studies by Milstein on an achiral Ir-catalyst system indicated that the iridium-catalyzed norbornene hydroamination involves amine activation as a key step in the catalytic cycle,¹³¹ rather than *alkene* activation which is observed for most other late transition metal catalyzed hydroamination reactions.²¹¹ Thus, the iridium-catalyzed hydroamination of norbornene with aniline is initiated by an oxidative addition of aniline to the metal center, followed by insertion of the strained olefin into the iridium-amido bond (Scheme I-19). Subsequent reductive elimination completes the catalytic cycle and gives the hydroamination product **55**.

Scheme I-19. Proposed mechanism for iridium-catalyzed hydroamination of norbornene via amine activation.

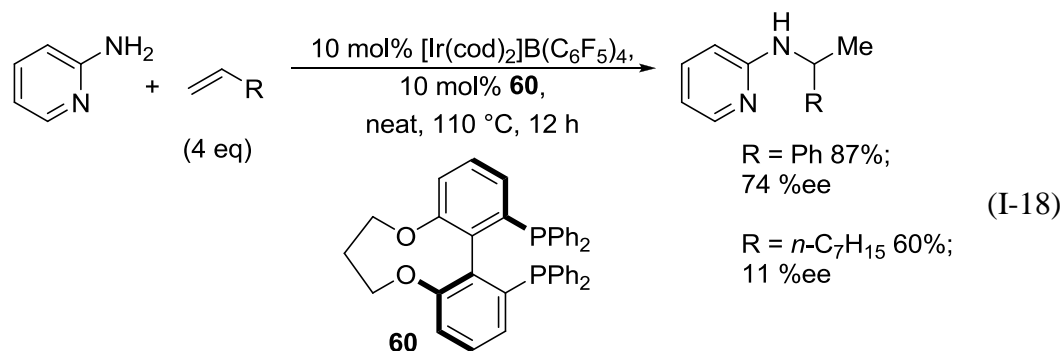


This chemistry was extended to a number of bicyclic alkenes and dienes utilizing various chelating axially chiral bisphosphine iridium-catalyst (Scheme I-20).¹³³ Further synthetic transformations of the chiral hydroamination product **57** provide access to functionally substituted chiral cyclopentylamines with multiple stereocenters, such as **58** and **59**. It should be noted that alkylamines, such as octylamine or *N*-methyl aniline, and sterically encumbered aniline derivatives, such as *o*-toluidine or *o*-anisidine did not undergo hydroamination reactions under these conditions.

Scheme I-20. Stereoselective synthesis of cyclopentylamines via asymmetric hydroamination of norbornadiene.

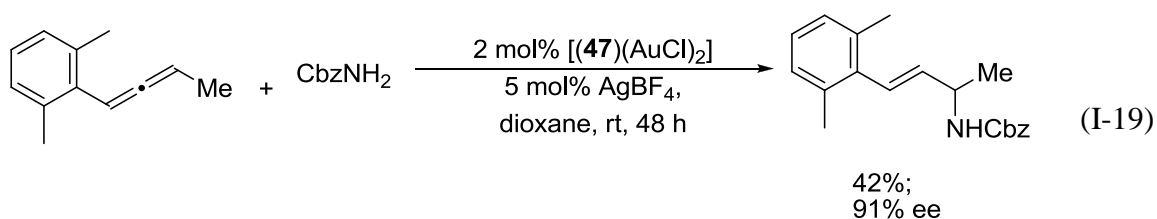


Although it seems that iridium-catalyzed hydroamination with anilines is restricted to norbornene, it was recently found that 2-aminopyridines can react with styrenes and even simple α -olefins under similar conditions. Moderate to high ee values were achieved in the presence of $\text{C}_3\text{-TUNEPHOS}$ **60** (Eq. I-18).²¹²

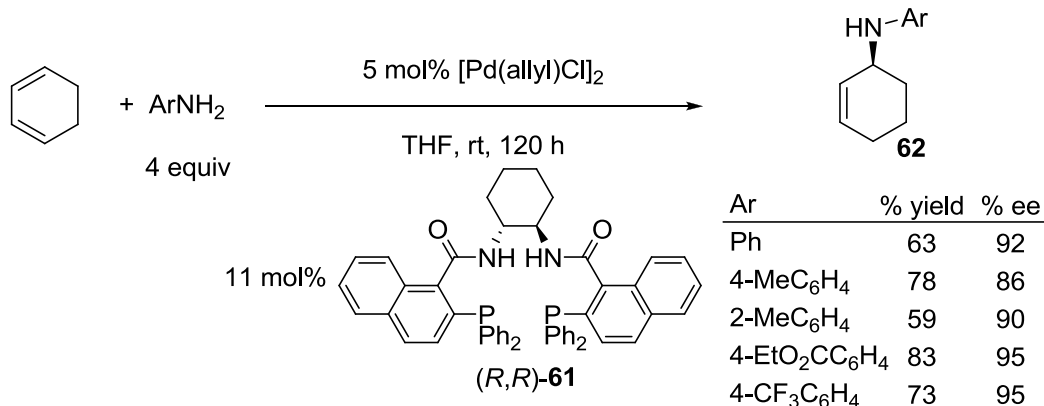


Conjugated and cumulated dienes can be considered a terminal case of an activated alkene. Intermolecular hydroamination of this substrate classes is much more feasible than that of unactivated alkenes.

Gold-catalyzed asymmetric intermolecular hydroamination of 1,3-disubstituted allenes with carbamates was recently reported by Widenhoefer.²¹³ In the case of 1-aryl-3-methyl substituted allenes, enantioselectivities up to 91% can be achieved in the presence of the biphosphine ligand (*S*)-**47** (Eq. I-19).²¹³ Note that reaction conditions are significantly milder than in the case of related gold-catalyzed hydroamination of alkenes with ureas (Scheme I-16) and no large excess of alkene is necessary due to high π -basicity of allene moiety.

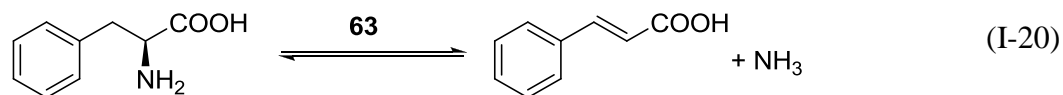


Hydroamination of 1,3-conjugated dienes has been studied in great detail in part due to their enhanced reactivity compared to other unsaturated substrates.²¹⁴ Initial attempts towards asymmetric intermolecular hydroamination of 1,3-dienes were disclosed as early as in 1980.²¹⁵ However, high levels of stereo- and chemoselectivity have so far been achieved for cyclic dienes only. The palladium-catalyzed asymmetric hydroamination of cyclohexadiene with arylamines utilizing a variant of Trost's ligand (*R,R*)-**61** proceeds to yield cyclic allylamines **62** with high enantioselectivities under mild conditions (Scheme I-21).²⁰⁷ The mechanism is believed to follow a similar pathway as proposed for palladium-catalyzed hydroamination of vinyl arenes (Scheme I-17).²⁰³

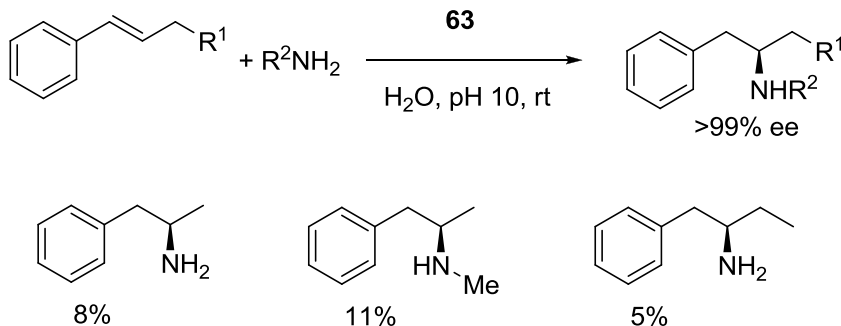
Scheme I-21. Palladium-catalyzed asymmetric hydroamination of cyclohexadiene.²⁰⁷

I.3.3 Enzymatic Asymmetric Hydroamination

The last decade has been marked by a constantly growing presence of biocatalysis in stereoselective synthetic methodology.²¹⁶ Phenylalanine ammonia lyase (PAL) **63** is an enzyme known to mediate the deamination of phenylalanine into *E*-cinnamic acid and ammonia (Eq. I-20).²¹⁷



Recently, researchers from BASF have reported very promising results for the hydroamination of styrene derivatives catalyzed by **63** from the parsley plant *Petroselinum Crispum* (Scheme I-22).²¹⁸ Although the method is currently limited to *E*- β -methylstyrene derivatives and very few amines are reactive, the approach can certainly become a solid foundation for future advances in the area.

Scheme I-22. Enzymatic hydroamination of styrene derivatives.

I.4 Conclusions and Outlook

The stereoselective hydroamination of alkenes has seen significant development over the last decade. Unfortunately, the overwhelming majority of research efforts were dedicated to intramolecular reactions. High levels of activity and stereoselectivity were achieved for hydroamination/cyclization of aminoalkenes; however, stereoselective *intermolecular* hydroamination remains an elusive goal. The few known examples of early transition (lanthanides in particular) metal-catalyzed non-asymmetric intermolecular hydroamination suggest that there is room for further development. On the other hand, late transition metal catalysts, which enjoy potential broader availability and practicality, were already demonstrated to catalyze stereoselective intermolecular reactions with activated substrates. It seems unlikely though, that these systems can be applied to unactivated alkenes and amines due to obvious mechanistic restrictions. Nevertheless, recent advances in intramolecular hydroamination of simple aminoalkenes catalyzed by late transition metals suggest that there is still room for further development.

I.5 References

- (1) Müller, T. E.; Beller, M. *Chem. Rev.* **1998**, *98*, 675-703.
- (2) Müller, T. E.; Hultsch, K. C.; Yus, M.; Foubelo, F.; Tada, M. *Chem. Rev.* **2008**, *108*, 3795-3892.
- (3) Brunet, J. J.; Neibecker, D. In *Catalytic Heterofunctionalization from Hydroamination to Hydrozirconation*; Togni, A., Grützmaier, H., Eds.; VCH: Weinheim, 2001, p 91-141.
- (4) Steinborn, D.; Taube, R. *Z. Chem.* **1986**, *26*, 349-59.
- (5) Taube, R. In *Applied Homogeneous Catalysis*; Cornils, B., Herrmann, W. A., Eds.; VCH: Weinheim, 2002; Vol. 2, p 513-524.
- (6) Sitha, S.; Jewell, L. L. *Tetrahedron* **2011**, *66*, 3030-3036.
- (7) Hii, K. K. *Pure Appl. Chem.* **2006**, *78*, 341-349.
- (8) Xu, L.-W.; Xia, C.-G. *Eur. J. Org. Chem.* **2005**, 633-639.
- (9) Roesky, P. W.; Müller, T. E. *Angew. Chem. Int. Ed.* **2003**, *42*, 2708-2710.
- (10) Hultsch, K. C. *Adv. Synth. Catal.* **2005**, *347*, 367-391.
- (11) Hultsch, K. C. *Org. Biomol. Chem.* **2005**, *3*, 1819-1824.
- (12) Aillaud, I.; Collin, J.; Hannedouche, J.; Schulz, E. *Dalton Trans.* **2007**, 5105-5118.
- (13) Reznichenko, A. L.; Hultsch, K. C. In *Chiral Amine Synthesis: Methods, Developments and Applications*; 1st ed.; Nugent, T., Ed.; Wiley-VCH: 2010, p 341-376.
- (14) Reznichenko, A. L.; Hultsch, K. C. In *Science of Synthesis, Stereoselective Synthesis*; De Vries, J. G., Molander, G. A., Evans, P. A., Eds.; Thieme: 2010; Vol. 1, p 689-729.
- (15) Hong, S.; Marks, T. J. *Acc. Chem. Res.* **2004**, *37*, 673-686.
- (16) Gagné, M. R.; Stern, C. L.; Marks, T. J. *J. Am. Chem. Soc.* **1992**, *114*, 275-294.
- (17) Motta, A.; Lanza, G.; Fragalà, I. L.; Marks, T. J. *Organometallics* **2004**, *23*, 4097-4104.
- (18) Gribkov, D. V.; Hultsch, K. C.; Hampel, F. *J. Am. Chem. Soc.* **2006**, *128*, 3748-3759.
- (19) Manna, K.; Kruse, M. L.; Sadow, A. D. *ACS Catal.* **2011**, *1*, 1637-1642.
- (20) Ryu, J.-S.; Li, G. Y.; Marks, T. J. *J. Am. Chem. Soc.* **2003**, *125*, 12584-12605.
- (21) Molander, G. A.; Pack, S. K. *Tetrahedron* **2003**, *59*, 10581-10591.
- (22) Molander, G. A.; Pack, S. K. *J. Org. Chem.* **2003**, *68*, 9214-9220.
- (23) Li, Y.; Marks, T. J. *J. Am. Chem. Soc.* **1998**, *120*, 1757-1771.
- (24) Tsuchida, S.; Kaneshige, A.; Ogata, T.; Baba, H.; Yamamoto, Y.; Tomioka, K. *Org. Lett.* **2008**, *10*, 3635-3638.
- (25) Tobisch, S. *Dalton Trans.* **2011**, *40*, 249-261.
- (26) Tobisch, S. *Chem. Eur. J.* **2010**, *16*, 13814-13824.
- (27) Tobisch, S. *Chem. Eur. J.* **2011**, *17*, 14974-14986.
- (28) Gagné, M. R.; Brard, L.; Conticello, V. P.; Giardello, M. A.; Stern, C. L.; Marks, T. J. *Organometallics* **1992**, *11*, 2003-2005.

- (29) Giardello, M. A.; Conticello, V. P.; Brard, L.; Gagné, M. R.; Marks, T. J. *J. Am. Chem. Soc.* **1994**, *116*, 10241-10254.
- (30) Jung, M. E.; Piizzi, G. *Chem. Rev.* **2005**, *105*, 1735-1766.
- (31) Douglass, M. R.; Ogasawara, M.; Hong, S.; Metz, M. V.; Marks, T. J. *Organometallics* **2002**, *21*, 283-292.
- (32) Ryu, J.-S.; Marks, T. J.; McDonald, F. E. *J. Org. Chem.* **2004**, *69*, 1038-1052.
- (33) Vitanova, D. V.; Hampel, F.; Hultzs, K. C. *J. Organomet. Chem.* **2007**, *692*, 4690-4701.
- (34) Molander, G. A.; Dowdy, E. D. *J. Org. Chem.* **1998**, *63*, 8983-8988.
- (35) Molander, G. A.; Dowdy, E. D. *J. Org. Chem.* **1999**, *64*, 6515-6517.
- (36) Ryu, J.-S.; Marks, T. J.; McDonald, F. E. *Org. Lett.* **2001**, *3*, 3091-3094.
- (37) Kim, Y. K.; Livinghouse, T. *Angew. Chem. Int. Ed.* **2002**, *41*, 3645.
- (38) Yu, X.; Marks, T. J. *Organometallics* **2007**, *26*, 365-376.
- (39) Hong, S.; Tian, S.; Metz, M. V.; Marks, T. J. *J. Am. Chem. Soc.* **2003**, *125*, 14768-14783.
- (40) Gribkov, D. V.; Hultzs, K. C. *Chem. Commun.* **2004**, 730-731.
- (41) Gribkov, D. V.; Hampel, F.; Hultzs, K. C. *Eur. J. Inorg. Chem.* **2004**, 4091-4101.
- (42) Gribkov, D. V.; Hultzs, K. C.; Hampel, F. *Chem. Eur. J.* **2003**, *9*, 4796-4810.
- (43) O'Shaughnessy, P. N.; Gillespie, K. M.; Knight, P. D.; Munslow, I.; Scott, P. *Dalton Trans.* **2004**, 2251-2256.
- (44) O'Shaughnessy, P. N.; Scott, P. *Tetrahedron: Asymmetry* **2003**, *14*, 1979-1983.
- (45) O'Shaughnessy, P. N.; Knight, P. D.; Morton, C.; Gillespie, K. M.; Scott, P. *Chem. Commun.* **2003**, 1770-1771.
- (46) Heck, R.; Schulz, E.; Collin, J.; Carpentier, J.-F. *J. Mol. Cat. A* **2007**, *268*, 163-168.
- (47) Benndorf, P.; Jenter, J.; Zielke, L.; Roesky, P. W. *Chem. Commun.* **2011**, *47*, 2574-2576.
- (48) Queffelec, C.; Boeda, F.; Pouilhes, A.; Meddour, A.; Kouklovsky, C.; Hannedouche, J.; Collin, J.; Schulz, E. *ChemCatChem* **2011**, *3*, 122-126.
- (49) Hannedouche, J.; Collin, J.; Trifonov, A.; Schulz, E. *J. Organomet. Chem.* **2011**, *696*, 255-262.
- (50) Chapurina, Y.; Ibrahim, H.; Guillot, R.; Kolodziej, E.; Collin, J.; Trifonov, A.; Schulz, E.; Hannedouche, J. *J. Org. Chem.* **2011**, *76*, 10163-10172.
- (51) Chapurina, Y.; Hannedouche, J.; Collin, J.; Guillot, R.; Schulz, E.; Trifonov, A. *Chem. Commun.* **2010**, *46*, 6918-6920.
- (52) Aillaud, I.; Collin, J.; Hannedouche, J.; Schulz, E.; Trifonov, A. *Tetrahedron Lett.* **2010**, *51*, 4742-4745.
- (53) Hannedouche, J.; Aillaud, I.; Collin, J.; Schulz, E.; Trifonov, A. *Chem. Commun.* **2008**, 3552-3554.
- (54) Aillaud, I.; Wright, K.; Collin, J.; Schulz, E.; Mazaleyrat, J.-P. *Tetrahedron: Asymmetry* **2008**, *19*, 82-92.

- (55) Aillaud, I.; Lyubov, D.; Collin, J.; Guillot, R.; Hannedouche, J.; Schulz, E.; Trifonov, A. *Organometallics* **2008**, *27*, 5929-5936.
- (56) Collin, J.; Daran, J.-D.; Jacquet, O.; Schulz, E.; Trifonov, A. *Chem. Eur. J.* **2005**, *11*, 3455-3462.
- (57) Collin, J.; Daran, J.-D.; Schulz, E.; Trifonov, A. *Chem. Commun.* **2003**, 3048-3049.
- (58) Kim, J. Y.; Livinghouse, T. *Org. Lett.* **2005**, *7*, 1737-1739.
- (59) Meyer, N.; Zulys, A.; Roesky, P. W. *Organometallics* **2006**, *25*, 4179-4182.
- (60) Wang, Q.; Zhang, F.; Song, H.; Zi, G. *J. Organomet. Chem.* **2011**, *696*, 2186-2192.
- (61) Wang, Q.; Xiang, L.; Song, H.; Zi, G. *J. Organomet. Chem.* **2009**, *694*, 691-696.
- (62) Zi, G.; Xiang, L.; Song, H. *Organometallics* **2008**, *27*, 1242-1246.
- (63) Xiang, L.; Wang, Q.; Song, H.; Zi, G. *Organometallics* **2007**, *26*, 5323-5329.
- (64) Aillaud, I.; Collin, J.; Duhayon, C.; Guillot, R.; Lyubov, D.; Schulz, E.; Trifonov, A. *Chem. Eur. J.* **2008**, *14*, 2189-2200.
- (65) Riegert, D.; Collin, J.; Daran, J.-D.; Fillebeen, T.; Schulz, E.; Lyubov, D.; Fukin, G.; Trifonov, A. *Eur. J. Inorg. Chem.* **2007**, 1159-1168.
- (66) Riegert, D.; Collin, J.; Meddour, A.; Schulz, E.; Trifonov, A. *J. Org. Chem.* **2006**, *71*, 2514-2517.
- (67) Shibasaki, M.; Yoshikawa, N. *Chem. Rev.* **2002**, *102*, 2187-2209.
- (68) Yamagiwa, N.; Matsunaga, S.; Shibasaki, M. *Angew. Chem. Int. Ed.* **2004**, *43*, 4493-4497.
- (69) Seayad, J.; Tillack, A.; Hartung, C. G.; Beller, M. *Adv. Synth. Catal.* **2002**, *344*, 795.
- (70) Horrillo Martínez, P.; Hultsch, K. C.; Hampel, F. *Chem. Commun.* **2006**, 2221-2223.
- (71) Ogata, T.; Ujihara, A.; Tsuchida, S.; Shimizu, T.; Kaneshige, A.; Tomioka, K. *Tetrahedron Lett.* **2007**, *48*, 6648-6650.
- (72) Deschamp, J.; Collin, J.; Hannedouche, J.; Schulz, E. *Eur. J. Org. Chem.* **2011**, *2011*, 3329-3338.
- (73) Horrillo-Martínez, P., PhD thesis, Universität Erlangen-Nürnberg, 2008.
- (74) Zhang, X.; Emge, T. J.; Hultsch, K. C. *Angew. Chem. Int. Ed.* **2012**, *51*, 394-398.
- (75) Horrillo-Martínez, P.; Hultsch, K. C. *Tetrahedron Letters* **2009**, *50*, 2054-2056.
- (76) Buch, F.; Harder, S. *Z. Naturforsch., B: Chem.* **2008**, *63*, 169-177.
- (77) Neal, S. R.; Ellern, A.; Sadow, A. D. *J. Organomet. Chem.* **2011**, *696*, 228-234.
- (78) Zhang, X.; Emge, T. J.; Hultsch, K. C. *Organometallics* **2010**, *29*, 5871-5877.
- (79) Manna, K.; Ellern, A.; Sadow, A. D. *Chem. Commun.* **2010**, *46*, 339-341.
- (80) Manna, K.; Xu, S.; Sadow, A. D. *Angew. Chem. Int. Ed.* **2011**, *50*, 1865-1868.

- (81) Walsh, P. J.; Baranger, A. M.; Bergman, R. G. *J. Am. Chem. Soc.* **1992**, *114*, 1708-1719.
- (82) Baranger, A. M.; Walsh, P. J.; Bergman, R. G. *J. Am. Chem. Soc.* **1993**, *115*, 2753-2763.
- (83) Walsh, P. J.; Hollander, F. J.; Bergman, R. G. *Organometallics* **1993**, *12*, 3705-3723.
- (84) Lee, S. Y.; Bergman, R. G. *Tetrahedron* **1995**, *51*, 4255-4276.
- (85) Polse, J. L.; Andersen, R. A.; Bergman, R. G. *J. Am. Chem. Soc.* **1998**, *120*, 13405-13414.
- (86) Pohlki, F.; Doye, S. *Angew. Chem. Int. Ed.* **2001**, *40*, 2305-2308.
- (87) Straub, B. F.; Bergman, R. G. *Angew. Chem. Int. Ed.* **2001**, *40*, 4632-4635.
- (88) Tobisch, S. *Chem. Eur. J.* **2007**, *13*, 4884-4894.
- (89) Kim, H.; Lee, P. H.; Livinghouse, T. *Chem. Commun.* **2005**, 5205-5207.
- (90) Bexrud, J. A.; Beard, J. D.; Leitch, D. C.; Schafer, L. L. *Org. Lett.* **2005**, *7*, 1959-1962.
- (91) Müller, C.; Koch, R.; Doye, S. *Chem. Eur. J.* **2008**, *14*, 10430-10436.
- (92) Watson, D. A.; Chiu, M.; Bergman, R. G. *Organometallics* **2006**, *25*, 4731-4733.
- (93) Wood, M. C.; Leitch, D. C.; Yeung, C. S.; Kozak, J. A.; Schafer, L. L. *Angew. Chem. Int. Ed.* **2007**, *46*, 354-358.
- (94) Stubbert, B. D.; Marks, T. J. *J. Am. Chem. Soc.* **2007**, *129*, 6149-6167.
- (95) Majumder, S.; Odom, A. L. *Organometallics* **2008**, *27*, 1174-1177.
- (96) Leitch, D. C.; Payne, P. R.; Dunbar, C. R.; Schafer, L. L. *J. Am. Chem. Soc.* **2009**, *131*, 18246-18247.
- (97) Leitch, D.; Turner, C.; Schafer, L. *Angew. Chem. Int. Ed.* **2010**, *49*, 6382-6386.
- (98) Allan, L. E. N.; Clarkson, G. J.; Fox, D. J.; Gott, A. L.; Scott, P. *J. Am. Chem. Soc.* **2010**, *132*, 15308-15320.
- (99) Knight, P. D.; Munslow, I.; O'Shaughnessy, P. N.; Scott, P. *Chem. Commun.* **2004**, 894-895.
- (100) Tobisch, S. *Dalton Trans.* **2006**, 4277-4285.
- (101) Gribkov, D. V.; Hultsch, K. C. *Angew. Chem. Int. Ed.* **2004**, *44*, 5542-5546.
- (102) Kissounko, D. A.; Epshteyn, A.; Fettingner, J. C.; Sita, L. R. *Organometallics* **2006**, *25*, 1076-1078.
- (103) Wang, X.; Chen, Z.; Sun, X.-L.; Tang, Y.; Xie, Z. *Org. Lett.* **2011**, *13*, 4758-4761.
- (104) Gribkov, D. V., PhD thesis, Universität Erlangen-Nürnberg, 2005.
- (105) Wood, M. C.; Leitch, D. C.; Yeung, C. S.; Kozak, J. A.; Schafer, L. L. *Angew. Chem., Int. Ed.* **2009**, *48*, 6937.
- (106) Wood, M. C.; Leitch, D. C.; Yeung, C. S.; Kozak, J. A.; Schafer, L. L. *Angew. Chem. Int. Ed.* **2010**, *49*, 6475-6475.
- (107) Gott, A. L.; Clarke, A. J.; Clarkson, G. J.; Scott, P. *Organometallics* **2007**, *26*, 1729-1737.

- (108) Zi, G.; Zhang, F.; Xiang, L.; Chen, Y.; Fang, W.; Song, H. *Dalton Trans.* **2010**, 39, 4048-4061.
- (109) Roesky, P. W. *Angew. Chem., Int. Ed.* **2009**, 48, 4892-4894.
- (110) Ambuehl, J.; Pregosin, P. S.; Venanzi, L. M.; Ughetto, G.; Zambonelli, L. *J. Organomet. Chem.* **1978**, 160, 329-35.
- (111) Ambuehl, J.; Pregosin, P. S.; Venanzi, L. M.; Consiglio, G.; Bachechi, F.; Zambonelli, L. *J. Organomet. Chem.* **1979**, 181, 255-69.
- (112) Bender, C. F.; Widenhoefer, R. A. *Chem. Commun.* **2008**, 2741-2743.
- (113) Liu, Z.; Hartwig, J. F. *J. Am. Chem. Soc.* **2008**, 130, 1570-1571.
- (114) Ohmiya, H.; Moriya, T.; Sawamura, M. *Organic Letters* **2009**, 11, 2145-2147.
- (115) Hesp, K. D.; Tobisch, S.; Stradiotto, M. *J. Am. Chem. Soc.* **2009**, 132, 413-426.
- (116) Julian, L. D.; Hartwig, J. F. *J. Am. Chem. Soc.* **2010**, 132, 13813-13822.
- (117) Bender, C. F.; Widenhoefer, R. A. *J. Am. Chem. Soc.* **2005**, 127, 1070-1071.
- (118) Bender, C. F.; Hudson, W. B.; Widenhoefer, R. A. *Organometallics* **2008**, 27, 2356-2358.
- (119) Bauer, E. B.; Andavan, G. T. S.; Hollis, T. K.; Rubio, R. J.; Cho, J.; Kuchenbeiser, G. R.; Helgert, T. R.; Letko, C. S.; Tham, F. S. *Org. Lett.* **2008**, 10, 1175-1178.
- (120) Lavery, C. B.; Ferguson, M. J.; Stradiotto, M. *Organometallics* **2010**, 29, 6125-6128.
- (121) Liu, Z.; Yamamichi, H.; Madrahimov, S. T.; Hartwig, J. F. *J. Am. Chem. Soc.* **2011**, 133, 2772-2782.
- (122) Liu, X.-Y.; Li, C.-H.; Che, C.-M. *Org. Lett.* **2006**, 8, 2707-2710.
- (123) Zhang, J.; Yang, C.-G.; He, C. *J. Am. Chem. Soc.* **2006**, 128, 1798-1799.
- (124) Komeyama, K.; Morimoto, T.; Takaki, K. *Angew. Chem., Int. Ed.* **2006**, 45, 2938-2941.
- (125) Michael, F. E.; Cochran, B. M. *J. Am. Chem. Soc.* **2006**, 128, 4246-4247.
- (126) Han, X.; Widenhoefer, R. A. *Angew. Chem., Int. Ed.* **2006**, 45, 1747-1749.
- (127) Cochran, B. M.; Michael, F. E. *Org. Lett.* **2008**, 10, 329-332.
- (128) Cochran, B. M.; Michael, F. E. *J. Am. Chem. Soc.* **2008**, 130, 2786-2792.
- (129) Bender, C. F.; Widenhoefer, R. A. *Chem. Commun.* **2006**, 4143-4144.
- (130) Bender, C. F.; Widenhoefer, R. A. *Org. Lett.* **2006**, 8, 5303-5305.
- (131) Casalnuovo, A. L.; Calabrese, J. C.; Milstein, D. *J. Am. Chem. Soc.* **1988**, 110, 6738-6744.
- (132) Dorta, R.; Egli, P.; Zürcher, F.; Togni, A. *J. Am. Chem. Soc.* **1997**, 119, 10857-10858.
- (133) Zhou, J.; Hartwig, J. F. *J. Am. Chem. Soc.* **2008**, 12220-12221.
- (134) Casalnuovo, A. L.; Calabrese, J. C.; Milstein, D. *Inorg. Chem.* **1987**, 26, 971-973.
- (135) Zhao, J.; Goldman, A. S.; Hartwig, J. F. *Science* **2005**, 307, 1080-1082.
- (136) Morgan, E.; MacLean, D. F.; McDonald, R.; Turculet, L. *J. Am. Chem. Soc.* **2009**, 131, 14234-14236.

- (137) Khaskin, E.; Iron, M. A.; Shimon, L. J. W.; Zhang, J.; Milstein, D. *J. Am. Chem. Soc.* **2010**, *132*, 8542-8543.
- (138) Hanley, P. S.; Hartwig, J. F. *J. Am. Chem. Soc.* **2011**, *133*, 15661-15673.
- (139) Hanley, P. S.; Markovic, D.; Hartwig, J. F. *J. Am. Chem. Soc.* **2010**, *132*, 6302-6303.
- (140) Neukom, J. D.; Perch, N. S.; Wolfe, J. P. *J. Am. Chem. Soc.* **2010**, *132*, 6276-6277.
- (141) Neukom, J. D.; Perch, N. S.; Wolfe, J. P. *Organometallics* **2011**, *30*, 1269-1277.
- (142) Senn, H. M.; Blöchl, P. E.; Togni, A. *J. Am. Chem. Soc.* **2000**, *122*, 4098-4107.
- (143) Dub, P. A.; Poli, R. *J. Mol. Catal. A: Chem.* **2010**, *324*, 89-96.
- (144) Dub, P. A.; Poli, R. *J. Am. Chem. Soc.* **2010**, *132*, 13799-13812.
- (145) Hoover, J. M.; DiPasquale, A.; Mayer, J. M.; Michael, F. E. *J. Am. Chem. Soc.* **2010**, *132*, 5043-5053.
- (146) Karshtedt, D.; Bell, A. T.; Tilley, T. D. *J. Am. Chem. Soc.* **2005**, *127*, 12640-12646.
- (147) McBee, J. L.; Bell, A. T.; Tilley, T. D. *J. Am. Chem. Soc.* **2008**, *130*, 16562-16571.
- (148) Taylor, J. G.; Adrio, L. A.; Hii, K. K. *Dalton Trans.* **2010**, *39*, 1171-1175.
- (149) Shen, X.; Buchwald, S. L. *Angew. Chem. Int. Ed.* **2010**, *49*, 564-567.
- (150) Dalko, P. I.; Moisan, L. *Angew. Chem. Int. Ed.* **2004**, *43*, 5138-5175.
- (151) Seayad, J.; List, B. *Org. Biomol. Chem.* **2005**, *3*, 719-724.
- (152) Akiyama, T. *Chem. Rev.* **2007**, *107*, 5744-5758.
- (153) Schlummer, B.; Hartwig, J. F. *Org. Lett.* **2002**, *4*, 1471-1474.
- (154) Haskins, C. M.; Knight, D. W. *Chem. Commun.* **2002**, 2724-2725.
- (155) Ackermann, L.; Kaspar, L. T.; Althammer, A. *Org. Biomol. Chem.* **2007**, *5*, 1975-1978.
- (156) Anderson, L. L.; Arnold, J.; Bergman, R. G. *J. Am. Chem. Soc.* **2005**, *127*, 14542-14543.
- (157) Rosenfeld, D. C.; Shekhar, S.; Takemiya, A.; Utsunomiya, M.; Hartwig, J. F. *Org. Lett.* **2006**, *8*, 4179-4182.
- (158) Marcsekova, K.; Doye, S. *Synthesis* **2007**, 145-154.
- (159) Yang, L.; Xu, L.-W.; Xia, C.-G. *Tetrahedron Lett.* **2008**, *49*, 2882-2885.
- (160) Ackermann, L.; Althammer, A. *Synlett* **2008**, 995-998.
- (161) Shapiro, N. D.; Rauniyar, V.; Hamilton, G. L.; Wu, J.; Toste, F. D. *Nature* **2011**, *470*, 245-249.
- (162) Sherry, B. D.; Toste, F. D. *J. Am. Chem. Soc.* **2004**, *126*, 15978-15979.
- (163) Zhang, Z.; Bender, C. F.; Widenhoefer, R. A. *J. Am. Chem. Soc.* **2007**, *129*, 14148-14149.
- (164) Li, Y.; Marks, T. J. *Organometallics* **1996**, *15*, 3770-3772.
- (165) Yuen, H. F.; Marks, T. J. *Organometallics* **2009**, *28*, 2423-2440.
- (166) Howk, B. W.; Little, E. L.; Scott, S. L.; Whitman, G. M. *J. Am. Chem. Soc.* **1954**, *76*, 1899-1902.
- (167) Whitman, G. M.; (E. I. du Pont de Nemours & Co., Inc.). US 2501556, 1950.

- (168) Gresham, W. F.; Brooks, R. E.; Bruner, W. M.; (E. I. du Pont de Nemours & Co.). US 2501509, 1950.
- (169) Stroh, R.; Ebersberger, J.; Haberland, H.; Hahn, W. *Angew. Chem.* **1957**, 69, 124-131.
- (170) Closson, R. D.; Napolitano, J. P.; Ecke, G. G.; Kolka, A. J. *J. Org. Chem.* **1957**, 22, 646-649.
- (171) Pez, G. P.; (Allied Chemical Corp., USA). US 4302603, 1981.
- (172) Pez, G. P.; (Allied Chemical Corp., USA). US 4336162, 1982.
- (173) Wollensak, J.; Closson, R. D. *Org. Synth.* **1963**, 43, 45-8.
- (174) Lehmkuhl, H.; Reinehr, D. *J. Organometal. Chem.* **1973**, 55, 215-20.
- (175) Pez, G. P.; Galle, J. E. *Pure Appl. Chem.* **1985**, 57, 1917-26.
- (176) Steinborn, D.; Thies, B.; Wagner, I.; Taube, R. *Z. Chem.* **1989**, 29, 333-4.
- (177) Boehling, R.; Steinbrenner, U.; Funke, F.; Dier, R.; (BASF Aktiengesellschaft, Germany). WO 03/042156, 2003.
- (178) Khedkar, V.; Tillack, A.; Benisch, C.; Melder, J.-P.; Beller, M. *J. Mol. Catal. A: Chem.* **2005**, 241, 175-183.
- (179) Horrillo-Martínez, P.; Hultzs, K. C.; Gil, A.; Branchadell, V. *Eur. J. Org. Chem.* **2007**, 3311-3325.
- (180) Barrett, A. G. M.; Brinkmann, C.; Crimmin, M. R.; Hill, M. S.; Hunt, P.; Procopiou, P. A. *J. Am. Chem. Soc.* **2009**, 131, 12906-12907.
- (181) Brinkmann, C.; Barrett, A. G. M.; Hill, M. S.; Procopiou, P. A. *J. Am. Chem. Soc.* **2012**, 134, 2193-2207.
- (182) Danforth, J. D.; (Universal Oil Products Co.). US 2449644, 1948.
- (183) Herbert, B. *Liebig Ann.* **1950**, 566, 210-244.
- (184) Razdan, R. K. *J. Chem. Soc. D* **1969**, 770 - 771.
- (185) Fujita, T.; Suga, K.; Watanabe, S. *Aust. J. Chem.* **1974**, 27, 531-5.
- (186) Fujita, T.; Suga, K.; Watanabe, S. *Chem. Ind. (London)* **1973**, 231-232.
- (187) Wegler, R.; Pieper, G. *Chem. Ber.* **1950**, 83, 1-6.
- (188) Asahara, T.; Senn, M.; Tanabe, S.; Den, N. *Bull. Chem. Soc. Jpn.* **1969**, 42, 1996-2005.
- (189) Schlott, R. J.; Falk, J. C.; Narducy, K. W. *J. Org. Chem.* **1972**, 37, 4243-4245.
- (190) Beller, M.; Breindl, C.; Riermeier, T. H.; Tillack, A. *J. Org. Chem.* **2001**, 66, 1403-1412.
- (191) Beller, M.; Breindl, C. *Tetrahedron* **1998**, 54, 6359-6368.
- (192) Kumar, K.; Michalik, D.; Castro, I. G.; Tillack, A.; Zapf, A.; Arlt, M.; Heinrich, T.; Boettcher, H.; Beller, M. *Chem. Eur. J.* **2004**, 10, 746-757.
- (193) Beller, M.; Breindl, C.; Riermeier, T. H.; Eichberger, M.; Trauthwein, H. *Angew. Chem. Int. Ed.* **1998**, 37, 3389-3391.
- (194) Seijas, J. A.; Vazquez-Tato, M. P.; Martinez, M. M. *Synlett* **2001**, 875-877.
- (195) Tzalis, D.; Koradin, C.; Knochel, P. *Tetrahedron Lett.* **1999**, 40, 6193-6195.
- (196) Hartung, C. G.; Breindl, C.; Tillack, A.; Beller, M. *Tetrahedron* **2000**, 56, 5157-5162.

- (197) Zhang, Z.; Lee, S. D.; Widenhoefer, R. A. *J. Am. Chem. Soc.* **2009**, *131*, 5372-5373.
- (198) Kawatsura, M.; Hartwig, J. F. *J. Am. Chem. Soc.* **2000**, *122*, 9546-9547.
- (199) Li, K.; Horton, P. N.; Hursthouse, M. B.; Hii, K. K. *J. Organomet. Chem.* **2003**, *665*, 250-257.
- (200) Hu, A.; Ogasawara, M.; Sakamoto, T.; Okada, A.; Nakajima, K.; Takahashi, T.; Lin, W. *Adv. Synth. Catal.* **2006**, *348*, 2051-2056.
- (201) Nettekoven, U.; Hartwig, J. F. *J. Am. Chem. Soc.* **2002**, *124*, 1166-1167.
- (202) Utsunomiya, M.; Hartwig, J. F. *J. Am. Chem. Soc.* **2003**, *125*, 14286-14287.
- (203) Johns, A. M.; Utsunomiya, M.; Incarvito, C. D.; Hartwig, J. F. *J. Am. Chem. Soc.* **2006**, *128*, 1828-1839.
- (204) Besson, L.; Gore, J.; Cases, B. *Tetrahedron Lett.* **1995**, *36*, 3857-3860.
- (205) Al-Masum, M.; Meguro, M.; Yamamoto, Y. *Tetrahedron Lett.* **1997**, *38*, 6071-6074.
- (206) Meguro, M.; Yamamoto, Y. *Tetrahedron Lett.* **1998**, *39*, 5421-5424.
- (207) Löber, O.; Kawatsura, M.; Hartwig, J. F. *J. Am. Chem. Soc.* **2001**, *123*, 4366-4367.
- (208) Minami, T.; Okamoto, H.; Ikeda, S.; Tanaka, R.; Ozawa, F.; Yoshifuji, M. *Angew. Chem. Int. Ed.* **2001**, *40*, 4501-4503.
- (209) Pawlas, J.; Nakao, Y.; Kawatsura, M.; Hartwig, J. F. *J. Am. Chem. Soc.* **2002**, *124*, 3669-3679.
- (210) Landis, C. R.; Halpern, J. *J. Am. Chem. Soc.* **1987**, *109*, 1746-1754.
- (211) Beller, M.; Breindl, C.; Eichberger, M.; Hartung, C. G.; Seayad, J.; Thiel, O. R.; Tillack, A.; Trauthwein, H. *Synlett* **2002**, 1579-1594.
- (212) Pan, S.; Endo, K.; Shibata, T. *Org. Lett.* **2012**, *14*, 780-783.
- (213) Butler, K. L.; Tragni, M.; Widenhoefer, R. A. *Angew. Chem. Int. Ed.* **2012**, *51*, 5175-5178.
- (214) Dzhemilev, U. M.; Tolstikov, G. A.; Khusnutdinov, R. I. *Russ. J. Org. Chem.* **2009**, *45*, 957-987.
- (215) Dzhemilev, U. M.; Fakhretdinov, R. N.; Telin, A. G.; Tolstikov, G. A.; Panasenkov, A. A.; Vasil'eva, E. V. *Russ. Chem. Bull.* **1980**, *29*, 1943-1948.
- (216) Gröger, H. In *Catalytic Asymmetric Synthesis*; 3 ed.; Ojima, I., Ed.; Wiley: 2010, p 269-341.
- (217) Hyun, M. W.; Yun, Y. H.; Kim, J. Y.; Kim, S. H. *Mycobiology* **2011**, *39*, 257-265.
- (218) Hauer, B.; Schneider, N.; Drew, D.; Ditrich, K.; Turner, N.; Nestl, B. M.; (BASF Aktiengesellschaft, Germany). WO2011/012632, 2011.

II Chapter 2. Kinetic Resolution of Aminoalkenes via Asymmetric Hydroamination: A Mechanistic Study

II.1 Introduction

The importance of nitrogen-containing organic compounds in biological systems and industrially relevant basic and fine chemicals has sparked significant research efforts to develop efficient synthetic protocols.^{1,2} One of the simplest approaches, the hydroamination reaction, has found significant attention only in recent years with the development of more efficient transition metal based catalyst systems.^{3,4} In particular the generation of new stereogenic centers constitutes an attractive application of the hydroamination process, but the development of chiral catalysts for the asymmetric hydroamination of alkenes (AHA) has remained challenging.⁵⁻⁷

Investigations in the Hultsch research group have been focused on the development of chiral biphenolate and binaphtholate⁸⁻¹¹ rare earth metal hydroamination catalysts and in particular complexes **24-Ln** (Ln = Sc, Y, Lu) based on sterically demanding 3,3'-bis(trisarylsilyl)-substituted binaphtholate ligands¹¹ (Figure II-1) have proven to be highly active and enantioselective, achieving up to 95% ee in hydroamination/cyclization of aminoalkenes. Furthermore, **24-Ln** were also efficient in the catalytic kinetic resolution of chiral aminoalkenes via hydroamination/cyclization (Eq. II-1) and, therefore, emerged as an atom-efficient alternative to other available methods of kinetic resolution of chiral amines which was previously performed in a dynamic¹²⁻¹⁶ and non-dynamic¹⁷⁻²⁰ fashion.

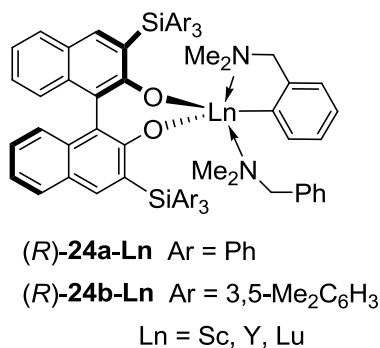
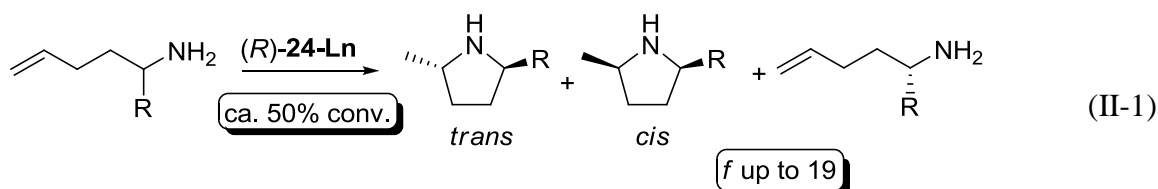


Figure II-1. Rare earth metal 3,3'-bis(triarylsilyl)binaphtholates.



Kinetic resolution of chiral α -substituted aminoalkenes containing aryl substituents proceeded smoothly with high diastereoselectivity (*trans*:*cis* up to 50:1) and high resolution factors (f up to 19) using chiral binaphtholate complexes (*R*)-**24-Ln** (Eq. II-1). Unfortunately, kinetic resolution of chiral α -substituted aminoalkenes containing aliphatic substituents proceeded with deteriorating efficiency, but increasing *trans*:*cis* diastereoselectivity, with increasing steric demand of the alkyl substituent.

In this chapter we present a detailed kinetic study of this kinetic resolution process, which sheds some light on the mechanism of this catalytic asymmetric hydroamination and the mode of operation of the chiral binaphtholate catalysts.

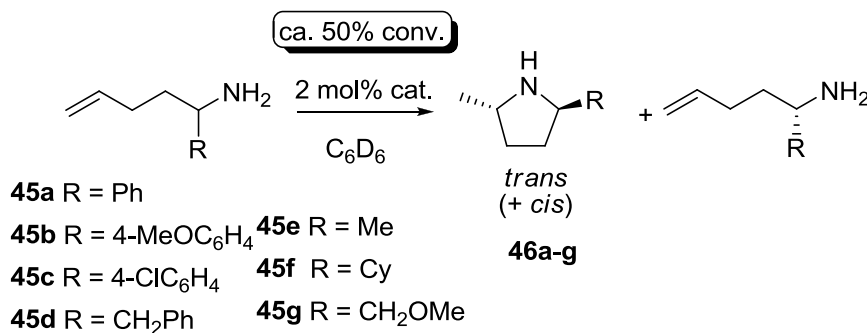
II.2 Results and Discussion

II.2.1 Kinetic Resolution of α -Substituted Aminopentenes

In extension of previous studies in the Hultsch group,^{10,11} we surveyed a broader set of α -substituted aminoalkenes with 6 different binaphtholate rare earth metal

complexes **24-Ln** (Table II-1, Figure II-2). As noted previously, the highest resolution factors were observed for the α -aryl-substituted aminoalkenes **45a-c**, with **24a-Lu** being most efficient for **45a**.¹¹ In contrast to general trends in (non kinetic resolution type) asymmetric hydroamination reactions, the efficiency in kinetic resolution often increases with the ionic radius size of the rare earth metal. For example, the triphenylsilyl-substituted binaphtholate yttrium complex **24a-Y** was superior for the 4-methoxyphenyl-substituted aminopentene **45b** (Table II-1, entry 5), whereas the sterically more congested tris(3,5-xylyl)silyl-substituted binaphtholate yttrium complex **24b-Y** was most efficient for the electron-withdrawing 4-chlorophenyl-substituted aminopentene **45c** (Table II-1, entry 14).

Table II-1. Kinetic resolution parameters of α -substituted aminopenes.^a



Entry	Subst.	Cat.	t, h	T, °C	Conv., %	%ee of recovered 45	<i>f</i>
1	45a	24a-Y	95	22	50	74	15 ^b
2	45a	24a-Lu	15	40	52	83	19 ^b
3	45a	24b-Y	18	40	52	63	7 ^b
4	45a	24b-Lu	40	22	52	59	6 ^b
5	45b	24a-Y	8	40	50	78	19 ^b

6	45b	24a-Lu	26	40	47	70	18
7	45b	24a-Sc	35	50	55	69	7
8	45b	24b-Y	14	40	34	40	12
9	45b	24b-Lu	24	40	52	70	11
10	45b	24b-Sc	22	50	51	54	6
11	45c	24a-Y	18	40	50	71	12 ^b
12	45c	24a-Lu	17	40	55	77	10
13	45c	24a-Sc	22	50	60	81	8
14	45c	24b-Y	10	40	51	80	19
15	45c	24b-Lu	21	40	50	68	11
16	45c	24b-Sc	24	50	49	68	12
17	45d	24a-Y	9	22	50	42	3.6 ^b
18	45d	24a-Lu	26	22	50	32	2.6
19	45d	24a-Sc	40	40	64	60	3.5
20	45d	24b-Y	27	22	52	38	2.9 ^b
21	45d	24b-Lu	13	22	70	42	2.0
22	45d	24b-Sc	33	40	55	47	3.5
23	45e	24a-Y	25.5	22	53	72	9.5 ^b
24	45e	24a-Lu	42	22	55	73	8.4 ^b
25	45e	24a-Sc	94	40	51	73	12 ^b
26	45e	24b-Y	26	22	52	80	16 ^b
27	45e	22b-Lu	24.5	22	51	75	14 ^b
28	45e	24b-Sc	94	40	50	73	14 ^b
29	45f	24a-Y	8	22	56	49	3.5
30	45f	24a-Lu	23	22	47	51	6.0
31	45f	24a-Sc	34	40	75	67	2.9
32	45f	24b-Y	46	22	59	54	3.6
33	45f	24b-Lu	47	22	46	44	4.7
34	45f	24b-Sc	49	40	47	32	2.8
35	45g	24a-Y	85	40	50	33	2.7

36	45g	24a-Lu	120	40	59	9	1.2
37	45g	24b-Y	180	40	45	20	2.0
38	45g	24b-Lu	94	40	56	9	1.2

^a Reaction conditions: 2 mo 1% cat., C₆D₆Aratm, 0.5–1 M substrate. ^b Data from ref. 11.

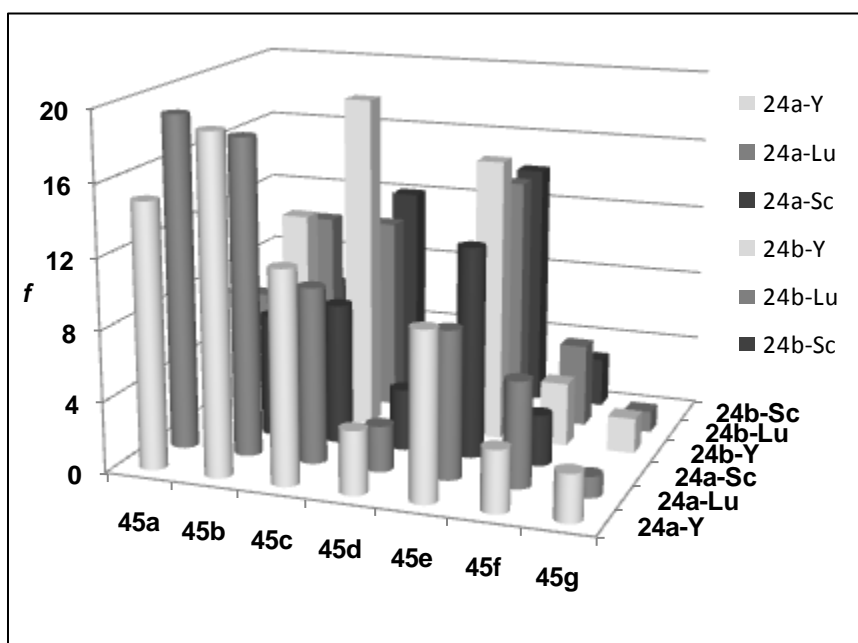


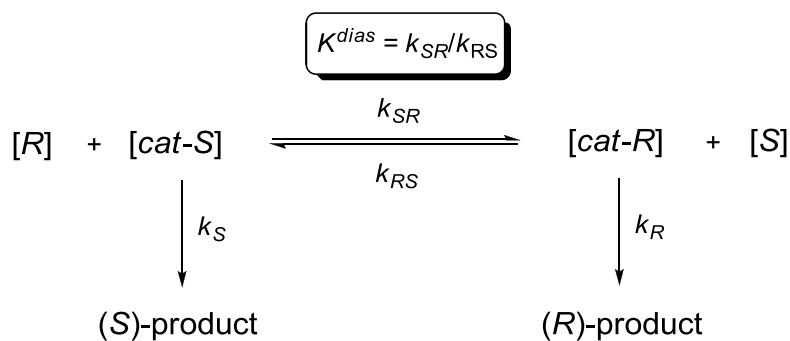
Figure II-2. Resolution factors for substrates **45a-g**, determined with **24a-Ln** (cylinders) and **24b-Ln** (boxes).

For α -alkyl-substituted aminoalkenes, high selectivities are only observed for the sterically least demanding substrate **45e** using the sterically more demanding tris(3,5-xylyl)silyl-substituted catalyst **24b** in general and the yttrium complex **24b-Y** in particular. Sterically more demanding α -alkyl substrates, such as the benzyl-substituted **45d** and the cyclohexyl-substituted **45f** exhibit significantly diminished resolution factors. Both scandium and yttrium complexes show slightly higher kinetic resolution efficiency for **45d**, while the opposite observation (highest selectivity for **24a-Lu**, Table

II-1, entry 30) is true for **45f**. The cyclization of the MOM-substituted aminoalkene **45g** is significantly retarded, obviously due to the chelating nature of the pending ether functionality. In contrast to our anticipation, the chelating donor group did not improve the kinetic resolution efficiency, with essential no kinetic discrimination of the two substrate enantiomers for lutetium catalysts and only slightly better efficiencies for yttrium catalysts. Again, the highest selectivity was observed for **24a-Y** (Table II-1, entry 35).

According to the general model for the kinetic resolution of racemic aminoalkenes via catalytic hydroamination (Scheme II-1),¹¹ the total amount of the catalyst [**Ln**] is distributed between two substrate/catalyst complexes [**cat-S**] and [**cat-R**] (Eq. II-2), which readily interconvert with an equilibrium constant K^{dias} (Eq. II-3). Each of the complexes reacts with a corresponding rate constant (k_R and k_S) to give the corresponding hydroamination products. Previous NMR spectroscopic investigations of **24a-Y** and **24b-Y** have revealed that the rate of interconversion between the two diastereomeric substrate/catalyst complexes is rapid even at low temperatures and significantly higher than both rates of cyclization.¹¹

Scheme II-1. Kinetic model of the resolution process.



$$[Ln] = [cat-S] + [cat-R] \quad (II-2)$$

$$K^{dias} = \frac{k_{SR}}{k_{RS}} = \frac{[cat-R][S]}{[cat-S][R]} \quad (II-3)$$

The resolution factor f depends on 3 independent parameters: the equilibrium constant K^{dias} and the cyclization rate constants of both substrate/catalyst complexes. For the sake of simplicity k_R/k_S represents k_{fast}/k_{slow} for all substrates, which may be determined independently. Thus for f (Eq. II-4):

$$f = K^{dias} \frac{k_R}{k_S} \quad (II-4)$$

For pseudo-first-order reactions (zero-order in aminoalkene over broad concentration range) (Eqs. II-5 and II-6):

$$-\frac{d[R]}{dt} = k_R[cat-R] \quad (II-5)$$

$$-\frac{d[S]}{dt} = k_S[cat-S] \quad (II-6)$$

Combining Eqs. II-3, II-5 and II-6, a differential equation II-7 can be obtained:

$$\frac{d[R]}{[R]} = K^{dias} \frac{k_R}{k_S} \frac{d[S]}{[S]} \quad (II-7)$$

Integrating Eq. II-7 and using Eq. II-4 gives an expression for a resolution factor as a function of isomer composition (Eq. II-8):

$$f = K^{dias} \frac{k_R}{k_S} = \frac{\ln([R]/[R]_0)}{\ln([S]/[S]_0)} \quad (II-8)$$

Equation (II-8) can be derived to a more practical expression which would operate easily experimentally observed parameters. Assuming that the reaction starts at the racemic mixture ($[R]_0 = [S]_0 = 0.5$) and that the (*R*)-enantiomer is consumed faster, the

dependence of each enantiomer concentration on conversion C and enantiomeric excess ee :

$$[R] = \frac{[(1-C)(1-ee)]}{2} \quad (\text{II-9})$$

$$[S] = \frac{[(1-C)(1+ee)]}{2} \quad (\text{II-10})$$

Considering Eqs. II-9 and II-10, equation II-8 can be rewritten:

$$f = K^{dias} \frac{k_R}{k_S} = \frac{\ln[(1-C)(1-ee)]}{\ln[(1-C)(1+ee)]} \quad (\text{II-11})$$

According to (Eq. II-11), a plot of $\ln[(1-C)(1-ee)]$ versus $\ln[(1-C)(1+ee)]$ provides the resolution factor f (Figure II-1), while kinetic measurements using an enantiopure substrate and either the (*R*)- or (*S*)-catalyst gives access to the zero-order reaction rate constants k_R and k_S for the matching (Figure II-4) and mismatching (Figure II-5) substrate/catalyst combination.

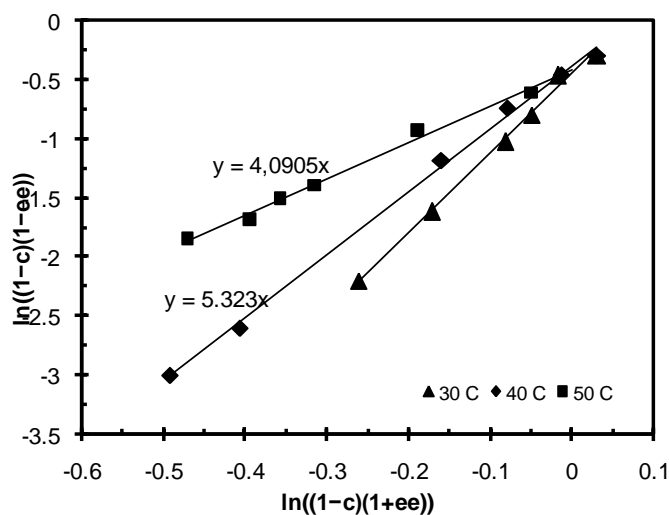


Figure II-3. Plot of $\ln[(1-C)(1+ee)]$ vs $\ln[(1-C)(1-ee)]$ for the kinetic resolution of **45e** using (*R*)-**24a-Y** as a catalyst at various temperatures.

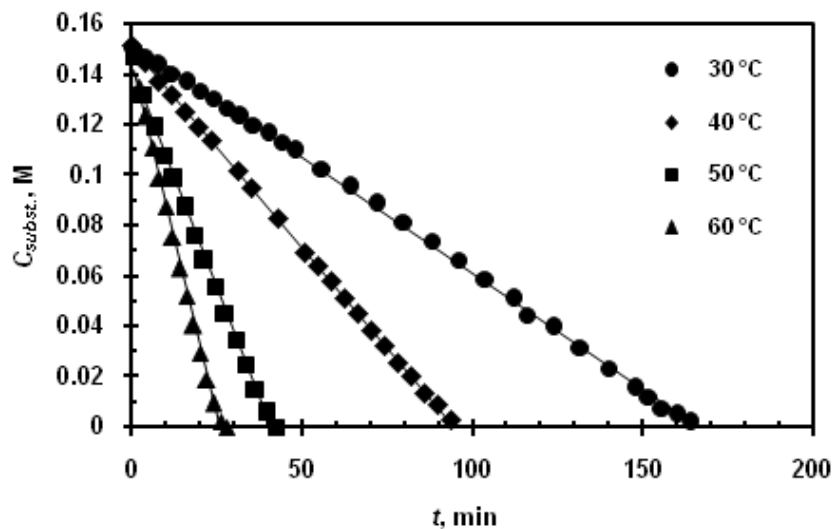


Figure II-4. Time dependence of substrate consumption in the hydroamination/cyclization of (*R*)-**45e** ($[\mathbf{45e}]_0 = 0.152\text{ M}$) with (*S*)-**24a-Y** ($[cat.] = 0.00228\text{ M}$), (matching pair) in C_6D_6 .

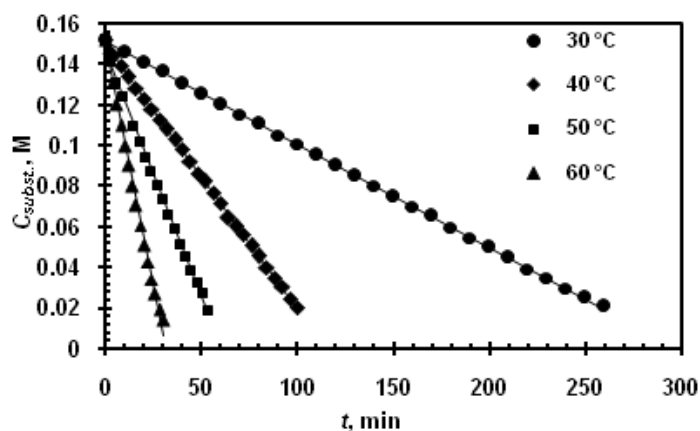


Figure II-5. Time dependence of substrate consumption in the hydroamination/cyclization of (*R*)-**45e** ($[\mathbf{45e}]_0 = 0.152\text{ M}$), with (*R*)-**24a-Y** ($[cat.] = 0.00833\text{ M}$) (mismatching pair) in C_6D_6 .

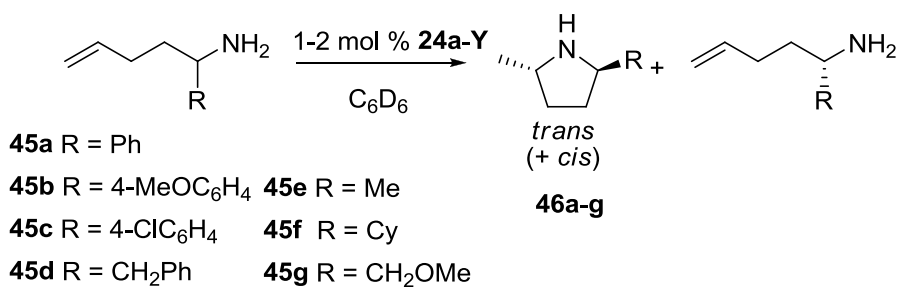
Enantiopure substrates were obtained either via large-scale kinetic resolution (**45a-45f**, Table II-2) using the best resolution catalysts for each particular substrate or via

fractional crystallization of the ammonium salt with (*R*)-(-)-mandelic acid (**45g**). The kinetic data and resolution parameters obtained for substrates **45a-45g** using (*R*)-**24a-Y** and (*S*)-**24a-Y** are summarized in Table II-3.

Table II-2. Preparation of highly enantioenriched α -substituted aminopentenes via kinetic resolution.

Subst.	Cat.	T, °C	<i>f</i>	Conv., %	Yield of recovered 45 , %	% ee of recovered 45
45a-d₂	(<i>R</i>)- 24a-Lu	40	19	61	34	98
45b	(<i>R</i>)- 24a-Lu	40	18	60	36	98
45c	(<i>R</i>)- 24b-Y	40	19	61	30	97
45d	(<i>R</i>)- 24a-Sc	25	5	83	12	> 98
45e	(<i>R</i>)- 24b-Y	25	15	64	30	97
45f	(<i>R</i>)- 24a-Lu	25	6	84	9	98

Table II-3. Kinetic resolution parameters of α -substituted aminopentenes determined with **24a-Y**.



Entry	Subst.	T, °C	<i>f</i>	$k_{fast}, 10^{-3} \cdot s^{-1}$ ^a	k_{fast}/k_{slow} ^b	K^{dias}	trans:cis (fast/slow) ^c
1	45a	50	12.8	5.45	6.6	1.9	>50:1/9.2:1 ^d
2	45a	60	11.5	11.3	7.1	1.6	>50:1/8.8:1 ^d

3	45a-d₂	50	11.0	1.42	5.3	2.1	>50:1/15:1
4	45a-d₂	60	9.1	2.10	4.9	1.9	>50:1/15:1
5	45b	40	18.1	0.81	9.5	1.9	>50:1/>50:1
6	45c	40	13.2	4.5	4.2	3.1	>50:1/>50:1
7	45d	30	2.6	2.5	9.6	0.27	>30:1/>30:1
8	45e	30	6.4	8.5	7.6	0.84	>30:1/2.8:1
9	45e	40	5.2	14.0	7.1	0.73	>30:1/2.2:1
10	45e	50	4.1	30.4	7.0	0.59	>30:1/2.1:1
11	45f	30	2.7	8.5	8.5	0.32	9:1/1.4:1
12	45g	50	4.1	2.2	3.2	1.28	6:1/2:1
13	45g	60	6.6	5.1	3.4	1.93	5:1/1.8:1

^a $k_{fast} = k_R$ for **45a-45d**, **45f**, and **45g**; $k_{fast} = k_S$ for **45e**. ^b $k_{fast}/k_{slow} = k_R/k_S$ for **45a-45d**, **45f**, and **45g**; $k_{fast}/k_{slow} = k_S/k_R$ for **45e**. ^c Determined via integration of CHN proton signals of pyrrolidines in the ¹H NMR spectra after full conversion. ^d Kinetic data from ref 11.

In agreement to the previous finding for the phenyl-substituted substrate **45a**,¹¹ the aryl-substituted substrates **45b** and **45c** both exhibit an equilibrium constant K^{dias} in favor of the matching substrate/catalyst-complex ($K^{dias} > 1$). Thus, K^{dias} and the k_R/k_S ratio both favor the resolution process. Also, cyclization of **45b** and **45c** proceeded with the same high diastereoselectivities as for **45a**.

The cyclization of the *N*-deuterated aminoalkene **45a-d₂** proceeded with a significant primary kinetic isotope effect (KIE, $k_H/k_D = 3.8$ at 50 °C and 5.4 at 60 °C), which is in agreement to previous findings on the hydroamination/cyclization of achiral aminopentenes.^{11,21} Although no N–H bond breaking is involved in the rate-determining olefin insertion step according to the generally accepted mechanism for the hydroamination/cyclization of aminoalkenes,²¹ it has been proposed that partial proton transfer from a coordinated amine may stabilize the 4-membered ring olefin insertion

transition state.²¹ Despite this pronounced KIE, the rates of both reaction channels are affected to a similar extent and the resulting resolution parameters seem to be similar to those of the non-deuterated substrate **45a**. However, a mismatching substrate-catalyst combination for **45a-d₂** gave slightly higher diastereoselectivity, which can serve as an argument of a N–H (or N–D, respectively) bond participation in the C–N bond formation process.^{21,22}

Compared to the aryl-substituted aminoalkenes **45a-45c**, the alkyl- and benzyl-substituted aminopentenenes **45d-45f** behaved quite differently. Here, the Curtin-Hammett pre-equilibrium favored the mismatching substrate/catalyst-complex ($K^{\text{dias}} < 1$), thus, effectively reducing the efficiency of the kinetic resolution process. A notable exception is the MOM-substituted substrate **45g**, which displayed a preference for the matching substrate/catalyst-complex, possibly as a result of the coordinating donor substituent. Diastereoselectivities were lower for substrates **45e-45g** than for **45a-45d** and the mismatching substrate/catalyst combination exhibited significantly reduced diastereoselectivities. Interestingly, the benzyl-substituted aminoalkene **45d** combines properties of both substrate families, a Curtin-Hammett pre-equilibrium in favor of the mismatching substrate/catalyst-complex, while achieving high *trans/cis*-diastereoselectivities.

While the equilibrium constant is strongly affected by the α -substituent, the relative reaction rate k_R/k_S remains in the range of 7–10 for all substrates, except for **45c** and **45g**.

The activation parameters for the matching ($\Delta H^\ddagger = 47.3(3.5) \text{ kJ mol}^{-1}$, $\Delta S^\ddagger = -128(11) \text{ J K}^{-1} \text{ mol}^{-1}$) and mismatching ($\Delta H^\ddagger = 54.9(3.1) \text{ kJ mol}^{-1}$, $\Delta S^\ddagger = -121(9) \text{ J K}^{-1}$)

$^1\text{mol}^{-1}$) substrate/catalyst combination for the cyclization of **45e** were obtained from the Eyring plot for k_{fast} and k_{slow} (Figure II-6). The data compare well with the parameters obtained previously for **45a** (matching: $\Delta H^\ddagger = 52.2(2.8) \text{ kJ mol}^{-1}$, $\Delta S^\ddagger = -127(8) \text{ J K}^{-1} \text{ mol}^{-1}$; mismatching: $\Delta H^\ddagger = 57.7(1.3) \text{ kJ mol}^{-1}$, $\Delta S^\ddagger = -126(4) \text{ J K}^{-1} \text{ mol}^{-1}$).¹¹ The negative activation entropy is a strong indicator for a highly organized transition state.^{11,21}

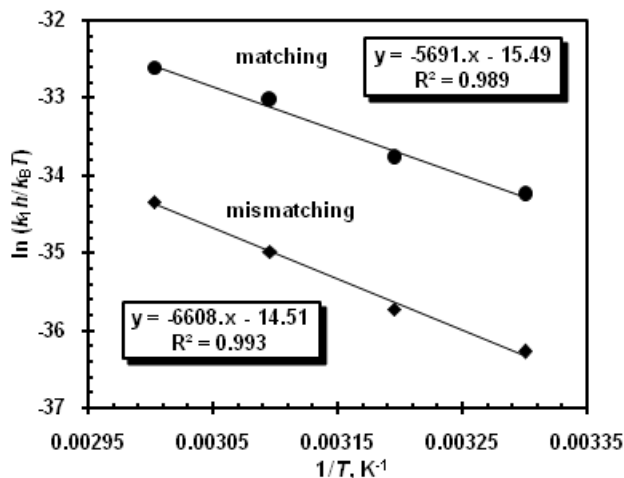


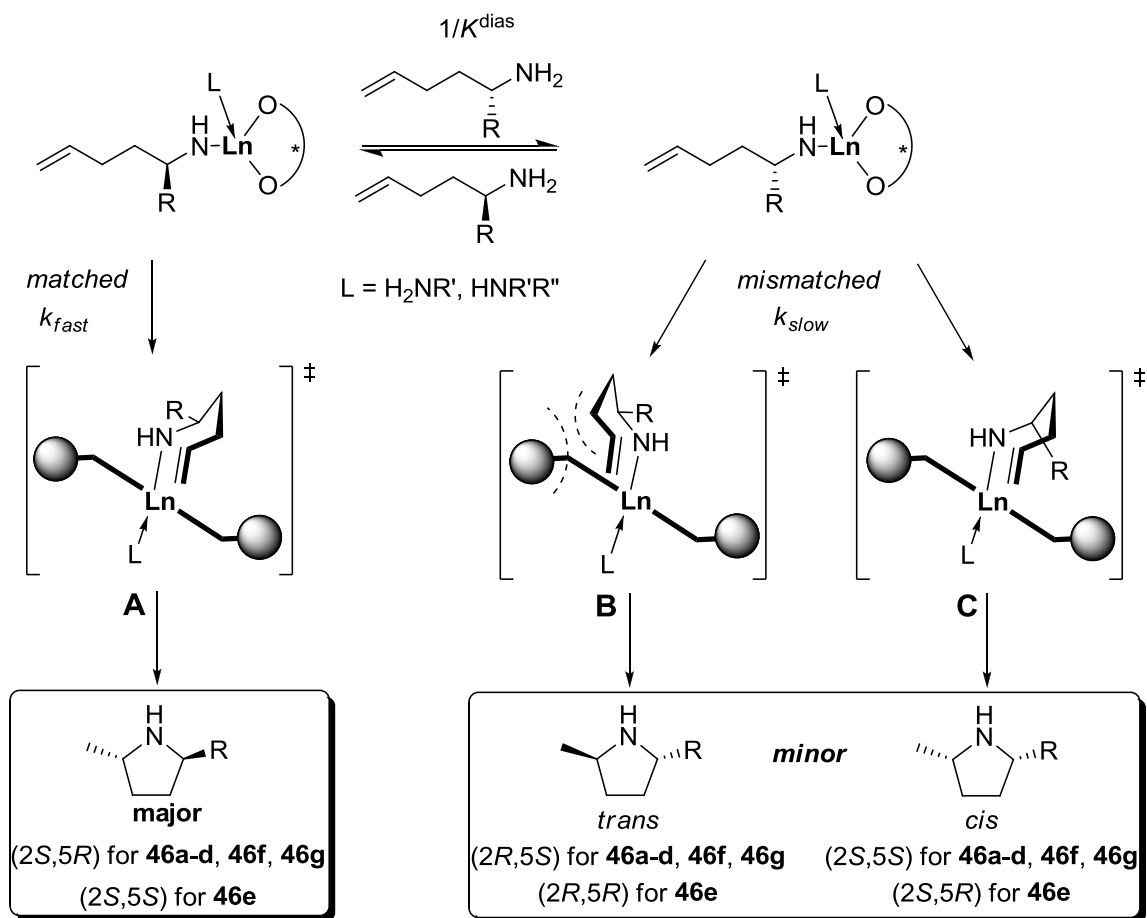
Figure II-6. Eyring plot for the hydroamination/cyclization of (*R*)-**45e** using (*S*)-**24a-Y** (●) and (*R*)-**24a-Y** (◆).

II.2.2 Stereomodel for the Kinetic Resolution of Aminopentenes

X-Ray crystallographic and optical rotational evidence show that the (*R*)-binaphtholate catalysts **23** react faster with (*R*)-**45a-45d**, respectively with (*S*)-**45e**. A comparison of the ^{19}F NMR spectra of the Mosher amides also indicates that (*R*)-**45f** and (*R*)-**45g** are the matching substrates for these catalysts. A general stereomodel for the binaphtholate rare earth metal-catalyzed kinetic resolution of α -substituted aminoalkenes via intramolecular hydroamination in agreement with these findings has been proposed (Scheme II-2).¹¹ According to this model, the rare earth metal amide preferentially

approaches the alkene moiety from the *re* face (Scheme II-2, **A**), whereas the approach from the *si* face of the alkene is hampered due to unfavorable repulsive interactions between the substrate alkyl chain and the sterically demanding trisarylsilyl substituent of the (*R*)-binaphtholate ligand (Scheme II-2, **B**). Each of the two diastereomeric substrate/catalyst complexes has two possible cyclization pathways.

Scheme II-2. Stereomodel for the kinetic resolution of α -substituted aminopentenes. For the matching substrate only the pathway leading to the preferred *trans*-isomer is shown.



The high *trans*-diastereoselectivities observed for aryl-substituted aminopentenes suggest that these substrates preferably cyclize through a transition state with an

equatorial orientation of the aryl substituent in both substrate/catalyst complexes. This may be explained either by a potential coordinative interaction of the phenyl ring with the metal²³ or a π -interaction with a naphthyl ring of the binaphtholate ligand, thus providing additional stabilization to the complex with equatorial aryl-substituent. Furthermore, this weak attractive interaction of the aryl substituent in **45a-45c** may explain the slight preference for the matching substrate/catalyst complex over the mismatching substrate/catalyst complex ($K^{\text{dias}} > 1$) and similar donor metal interactions can be proposed for the methylether-substituted **45g**. Interestingly, the equilibrium constant K^{dias} for **45g** increases with increasing temperature, whereas the aryl-substituted **45a** displays the opposite behavior.

The decreased *trans/cis* diastereoselectivity observed for the mismatched substrate/catalyst combination for **45a**, **45e** and **45f** can be rationalized with an alternative approach of the metal amide bond to the *re* face of the alkene moiety, in which the α -substituent rests in an axial position (Scheme II-2, C). Interestingly, substrates **45b**, **45c** and **45d** exhibit the same high level of *trans*-diastereoselectivity, suggesting that unfavorable steric interactions of these larger, more extended α -substituents with the tris(aryl)silyl substituent of the binaphtholate ligand preclude that reaction pathway C becomes an alternative to pathway B.

II.2.3 Substrates Other than α -Substituted Aminopentenenes

In order to investigate the general influence of the position of the substituent in the substrate on the resolution process, we investigated the kinetic resolution of the β -phenyl-substituted aminopentene **64** (Table II-4).

Table II-4. Kinetic resolution of **64** ($[subst.]_0 = 2.0$ M) using 2 mol % binaphtholate catalysts **24-Ln** at 25 °C.

$\text{64} \xrightarrow[25\text{ }^\circ\text{C}]{\text{2 mol\% (R)-cat., C}_6\text{D}_6} \text{trans-(2R,4S)-65} + \text{cis-(2S,4S)-65} + \text{(R)-64}$

Cat.	Conv., % ^a	trans/cis ^b	% ee of recovered 64 ^c	<i>f</i>
24a-Y	53	1:1.3	17	1.6
24a-Lu	51	1:1.3	26	2.1
24a-Sc	54	1:1.3	34	2.5
24b-Y	47	1:1.2	17	1.8
24b-Lu	55	1:1.2	31	2.2
24b-Sc	50	1:1.2	11	1.4

^a Determined by ¹H NMR spectroscopy using ferrocene as an internal standard.

^b Determined by ¹H NMR spectroscopy. ^c Determined by ¹⁹F NMR spectroscopy of the corresponding Mosher amide.

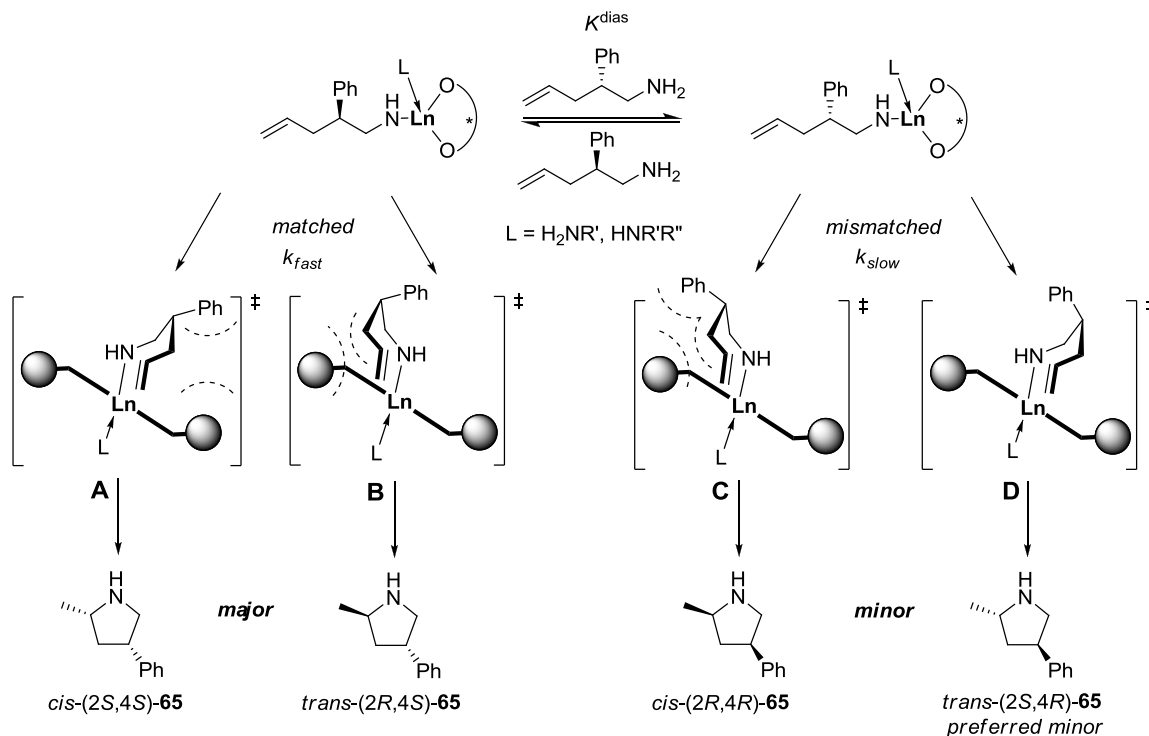
Although the preparative-scale kinetic resolution of **64** could not be achieved due to the low resolution factors, we succeeded to isolate enantiopure (*S*)-**64** after repeated crystallization of the corresponding (*R*)-mandelate. The absolute configuration was established by X-ray crystallographic analysis of the corresponding Mosher amide.¹⁹F NMR spectroscopic analysis of the Mosher amide of **64** recovered from the kinetic resolution reaction using complexes (*R*)-**24a** and (*R*)-**24b** was thus identified to be the (*R*)-enantiomer, indicating that (*S*)-**64** reacts faster with the (*R*)-binaphtholate catalysts. With (*S*)-**64** in hand, we began to study the kinetics and diastereoselectivity of the matching and mismatching substrate/catalyst pairs (Table II-5) using **24a-Y** as catalyst.

Table II-5. Kinetic resolution parameters for **64** using **24a-Y**.

$T, ^\circ\text{C}$	f	$k_{fast},$ $10^{-3} \cdot \text{s}^{-1a}$	k_{fast}/k_{slow}	K^{dias}	$trans:cis$ (matching/ mismatching)
30	1.5	0.58	1.64	0.92	1:1.3/6:1
40	1.5	1.32	1.73	0.87	1:1.4/7:1
50	1.4	3.00	1.48	0.95	1:1.4/7:1

^a The rates for the matching and mismatching substrate/catalyst combination were determined with (S)-**64** using either (R)-**24a-Y** (matching combination) or (S)-**24a-Y** (mismatching combination).

Table II-5 illustrates that in contrast to **45a-45g** kinetic resolution of **64** proceeded with very low reaction rate difference k_{fast}/k_{slow} between the matching and mismatching substrate/catalyst pair. Furthermore, with $K^{dias} \approx 0.9$, the mismatching substrate/catalyst complex is only slightly favored in the Curtin-Hammett pre-equilibrium. Overall, the more remote placement of the phenyl substituent in the β -position to the amino group significantly diminishes its influence on the kinetic resolution. However, it is noteworthy that the *trans/cis*-diastereomeric ratio shifts dramatically going from the matching to the mismatching substrate/catalyst pair. The matching substrate/catalyst combination indicates a slight preference for formation of the *cis*-pyrrolidine diastereomer, which is in agreement with a preferred equatorial orientation of the phenyl substituent in the approach of the metal amide to the *re* face of the alkene moiety (Scheme II-3, **A**).

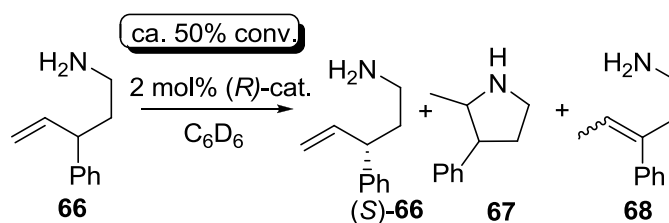
Scheme II-3. Proposed transition states in the kinetic resolution of **64**.

The strong preference for the *trans*-pyrrolidine product in case of the mismatching substrate/catalyst combination may be explained with an additional steric interaction of the equatorial phenyl-substituent with the trisarylsilyl binaphtholate ligand in the approach of the metal amide bond to the *si* face of the alkene leading to the *cis*-pyrrolidine (Scheme II-3, **C**), while the approach to the *re* face (Scheme II-3, **D**) leading to the *trans*-pyrrolidine puts the phenyl substituent in an axial position without disadvantageous steric interactions with the binaphtholate ligand. Thus, in contrast to the case of **45a-45c**, there is no tendency to keep the phenyl ring in an equatorial position.

We then directed our attention to the kinetic resolution of 3-phenylpent-4-en-1-amine (**66**), which features a phenyl substituent in the γ -position relative to the amino group, respectively, in allylic position to the alkene moiety. We anticipated that the closer proximity to the alkene might increase the influence on the outcome of the kinetic

resolution. Unfortunately, the kinetic resolution of **66** led to partial double bond isomerization. The side reaction can be explained with the increased reactivity of the benzylic position for the C–H activation leading to a stabilized η^3 -allyl intermediate. This is the first example of alkene isomerization with either **24a** or **24b**. Nevertheless, enantioenriched (*S*)-**66** was recovered from the reaction mixture at ca. 50% conversion (Table II-6).

Table II-6. Attempted NMR-scale kinetic resolution of **66** at 30 °C.



Cat.	Conv., %	67:68	% <i>ee</i> of recovered 66 ^a	<i>f</i>
24a-Y	47	7:1	39	3.7
24b-Y	51	6:1	65	8.2

^a Determined by chiral HPLC of the 2-naphthoyl amide of **66** recovered from the reaction mixture.

Since the enantioenrichment of **66** may result from kinetic resolution both via hydroamination or isomerization (transformation to **67** or **68**, respectively), the obtained resolution factor value cannot be interpreted unambiguously. We proposed that the aliphatic analogue of **66** lacking the reactive benzylic proton (**69**), would be less prone to side-reactions. Indeed, when γ -methylaminopentene **69** was subjected to **24**, the cyclization proceeded cleanly (Eq. II-12). Unfortunately, due to the remote position of the relatively small methyl substituent with respect to the amino group, we were unable

to determine the enantiomeric excess of **69**. However, a strong deviation from the zero-order kinetics is suggesting that **69** can be resolved kinetically (Figure II-7).

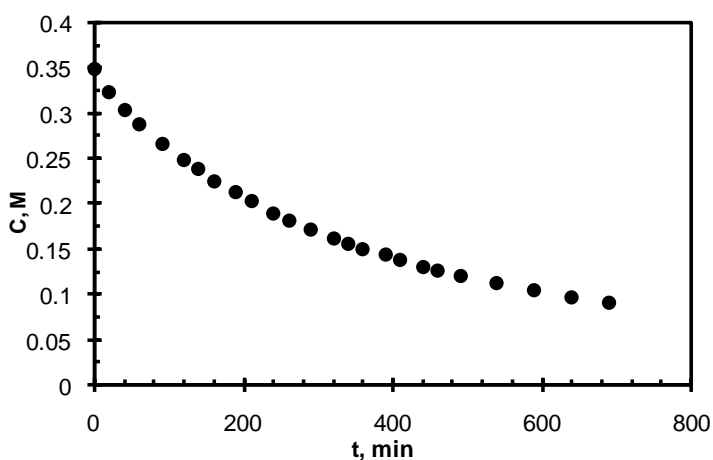
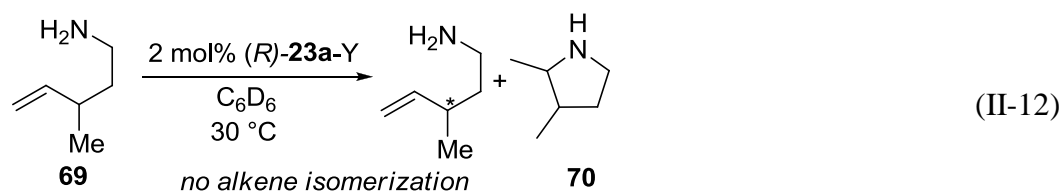


Figure II-7. Time dependence of substrate consumption in the hydroamination of **69**

($[\mathbf{69}]_0 = 0.35 \text{ M}$) with (*R*)-**24a-Y** ($[cat.] = 0.0012 \text{ M}$) in C_6D_6 at 30°C .

Previously, our group has reported the kinetic resolution of hept-6-en-2-amine with a moderate resolution factor of 3.3 using (*R*)-**24b-Y** at 80°C .¹¹ We hoped that better resolution factors may be achieved in the kinetic resolution of the aryl-substituted aminohexene **71**, but, unfortunately, the resolution factor was limited below 3 for this substrate (Table II-7), which was insufficient for a preparative-scale kinetic resolution.

Table II-7. Kinetic resolution of aminohexene **71** ($[subst.]_0 = 2.0$ M) using binaphtholate catalysts (*R*)-**24a** and (*R*)-**24b** at 80 °C.

ca. 50% conv.

2 mol% (*R*)-cat.

C_6D_6

80 °C

71 → **(S)-71** + **72**

Cat.	Conv., % ^a	<i>trans/cis</i> ^b	% ee of 71 recovered ^c	<i>f</i>
24a-Y	45	1:3	11	1.5
24a-Lu	51	1:6	26	2.1
24a-Sc	47	1:7	18	1.5
24b-Y	72	1:2.5	11	1.3
24b-Lu	55	1:5	31	2.2
24b-Sc	60	1:4	47	2.9

^a Determined by 1H NMR spectroscopy based on an internal standard. ^b Determined by 1H NMR spectroscopy. ^c Determined by ^{19}F NMR spectroscopy of the corresponding Mosher amide.

II.3 Summary

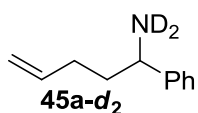
The kinetic resolution of chiral aminoalkenes via hydroamination/cyclization was studied using 3,3'-bis(trisarylsilyl)-substituted binaphtholate rare earth metal complexes. While the resolution of 1-aryl aminopentenes proceeds with high efficiency and high *trans*-diastereoselectivity, the resolution process of 1-alkyl aminopentenes suffers from decreasing resolution efficiency with increasing steric demand of the aliphatic substituent. Kinetic studies of the matching and mismatching substrate/catalyst pair using enantiopure substrates and either the (*R*)- or (*S*)-binaphtholate catalysts revealed that the difference in resolution efficiency stems from a shift of the Curtin-Hammett pre-

equilibrium. While 1-aryl aminopentenes favor the matching substrate/catalyst complex, preference for the mismatching substrate/catalyst complex for 1-alkyl aminopentenes diminishes resolution efficiency, whereas the relative cyclization rate for the two diastereomeric substrate/catalyst complexes remains in a typical range of 6–10:1. Plausible attractive π -interactions between the aryl substituent and either the metal center or the aromatic system of the bis(trisarylsilyl)-substituted binaphtholate ligand may explain increased stability of the matching substrate/catalyst complex. Incidentally, also the MOM-substituted aminopentene **45g** exhibits a strong preference of the matching substrate/catalyst complex, possibly due to the chelating nature of the MOM-substituent. The proximity of the stereocenter to the amino group in the aminoalkene substrate is crucial to achieve good kinetic resolution efficiency. The more remote β -phenyl substituent in 2-phenyl-pent-4-en-1-amine (**65**) results in diminished discrimination of the substrate enantiomers with respect to the relative rate of cyclization of the two substrate/catalyst complexes and a Curtin-Hammett pre-equilibrium close to unity.

Since the poor resolution factors for alkyl-substituted aminopentenes result from an unfavorable position of the Curtin-Hammett pre-equilibrium, it may be envisioned that modification of the catalyst backbone, such as introducing additional bulky alkyl groups might improve the overall resolution efficiency.

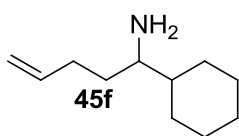
II.4 Experimental

General Considerations. All reactions with air- or moisture sensitive materials were performed in oven (120 °C) and flame-dried glassware under an inert atmosphere of argon, employing standard Schlenk and glovebox techniques. Hexanes and THF were sparged with argon for 1 h and then passed through a column with activated alumina prior to use. Benzene and C₆D₆ were vacuum transferred from sodium/benzophenone ketyl. Amines were distilled twice from finely powdered CaH₂. Complexes **24a-Ln** and **24b-Ln** (Ln=Sc, Y, Lu),¹¹ substrates **45a-45d**,¹¹ **45e**,²⁴ **64**,²⁴ **66**²⁵ and crotyl vinyl ether²⁶ were prepared according to previously described procedures. (*R*)-(+)- α -Methoxy- α -trifluoro-methylphenylacetic acid (Mosher acid) was transformed to its acid chloride using oxalyl chloride/DMF in hexanes.²⁷ The enantiomeric excesses of **45a-g**, **64** and **71** was measured by ¹⁹F NMR spectroscopy of the corresponding Mosher amides as reported previously.¹¹ The enantiomeric excess of **66** was measured by chiral HPLC of the corresponding 2-naphthoyl amide on a Chiralcel OD column, eluent hexane/IPA=90/10, flow rate 1 mL/min, rt 39.0 min (major isomer obtained from *R*-catalyst); 41.2 min (minor isomer). The absolute configuration of enantioenriched **66** was established by comparison of the optical rotation sign of the *N*-benzoyl derivative with literature data.²⁸



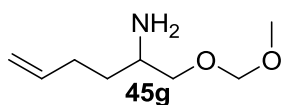
1-Phenylpent-4-en-1-amine-*d*₂ (45a-d**₂).** A mixture of **45a** (1.60 g, 9.9 mmol), hexanes (5 mL) and D₂O (2 mL) was stirred in a sealed flask at 60 °C overnight. After cooling to a room temperature, the aqueous layer was separated and discarded. The procedure was repeated twice with fresh 2 mL aliquots of D₂O. The organic layer was dried over molecular sieves and the solvent removed in

vacuo. The residue was distilled twice from CaH_2 at reduced pressure to give 1.20 g (74%) of *N*-deuterated amine as a colorless liquid (bp 120 °C, 1 mmHg) with >95% of isotopic substitution according to ^1H NMR spectroscopy. Mosher Adduct ^{19}F NMR, (C_6D_6 , 60 °C): $\delta = -69.35$ (*R*), -69.47 (*S*).



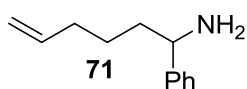
1-Cyclohexylpent-4-en-1-amine (45f). To a solution of cyclohexanecarboxylic acid chloride (5.84 g, 39.8 mmol) in THF (100 mL) was added copper(I) iodide (200 mg, 1.05 mmol). The resulting suspension was cooled to -30°C and a solution of but-3-ene magnesium bromide prepared from 4-bromobut-1-ene (5.40 g, 40.0 mmol), and magnesium turnings (0.96 g, 39.5 mmol) in THF (100 mL) was added dropwise over 1 h, while the temperature was maintained below -20°C . The mixture was stirred at the same temperature for 2 hrs and was then allowed to warm to room temperature. The solvent was removed in vacuo, the residue was dissolved in CH_2Cl_2 (70 mL) and 1 M HCl (50 mL). The organic layer was separated, filtered to remove precipitated copper salts, washed with 10% NaHCO_3 and dried over Na_2SO_4 . The solvent was removed by rotary evaporation and the residue was dissolved in abs. MeOH. Ammonium acetate (15 g, 200 mmol) and NaBH_3CN (1.0 g, 15 mmol) were added in one portion at room temperature. The mixture was stirred at room temperature for 1 day. Concentrated HCl was added carefully until pH <2, and the solvent was removed in vacuo. The residue was taken up in water (150 mL) and extracted once with ether (20 mL). The aqueous solution was brought to pH >12 with solid KOH and extracted with ether (3×20 mL). The combined extracts were dried over KOH and evaporated in vacuo. The residue was treated with finely powdered CaH_2 for 2 h and was then distilled twice from CaH_2 at reduced pressure to give 4.20 g (62%) of **45f** as

a colorless liquid, bp 120 °C at 1 mmHg. ^1H NMR (400 MHz, CDCl_3): δ = 5.76 (m, 1H, =CH), 5.01–4.87 (m, 2H, =CH₂), 2.44 (m, 1H, CHNH₂), 2.14–2.02 (m, 2H), 1.72–1.51 (m, 6H), 1.28–0.83 (m, 9 H); $^{13}\text{C}\{^1\text{H}\}$ NMR (75.5 MHz, CDCl_3): δ = 138.8 (=CH), 114.3 (=CH₂), 55.5, 43.9, 34.0, 30.8, 29.6, 27.8, 26.6, 26.5, 26.4. HRMS (m/z) [M]⁺ calcd for $\text{C}_{11}\text{H}_{22}\text{N}$ [$\text{M}-\text{H}$]⁺ 168.1752, found 168.1747. Mosher adduct ^{19}F NMR (CDCl_3 , 25 °C): δ = –69.08 (*R*), –69.25 (*S*).



1-(Methoxymethyl)pent-4-enylamine (45g). To a solution of but-3-ene magnesium bromide prepared from 4-bromobut-1-ene (13.5 g, 0.10 mol), and magnesium turnings (2.43 g, 0.10 mol) in THF (100 mL) was added dropwise methoxyacetonitrile (7.11 g 0.10 mol) over 15 min at room temperature. The dark-red reaction mixture was stirred under reflux for 2 h. The mixture was then cooled down and quenched with 100 mL of saturated ammonium chloride solution. The product was extracted with ether (2 × 70 mL). The combined organic layers were washed with water, brine and dried over Na_2SO_4 . The solvent was evaporated in vacuo and the residue was dissolved in MeOH (200 mL). Ammonium acetate (61 g, 0.80 mol) and NaBH_3CN (3.76 g, 60 mmol) were added in one portion at room temperature. The mixture was stirred at room temperature for 1 day. Concentrated HCl was added carefully until pH <2, and the solvent was removed in vacuo. The residue was taken up in water (15 mL) and extracted with ether (20 mL). The aqueous solution was brought to pH >12 with solid KOH and extracted with ether (3 × 20 mL). The combined extracts were dried over KOH and evaporated in vacuo. The residue was treated with finely powdered calcium hydride for 2 h and was then distilled twice from CaH_2 at reduced pressure to give 4.50 g (35%) of **45g** as a colorless liquid, bp 95–104 °C at 200

mmHg. ^1H NMR (300 MHz, CDCl_3): δ = 5.78 (m, 1H, =CH), 5.04–4.91 (m, 2H, =CH₂), 3.34–3.30 (m, 4H, CH₃, OCH₂), 3.12 (m, 1H, OCH₂) 2.93 (m, 1H, CHN), 2.20–2.02 (m, 2H), 1.25 (br s, 2H, NH₂); ^{13}C NMR (100 MHz, CDCl_3): δ = 138.4 (=CH), 114.6 (=CH₂), 78.2, 58.9, 50.3, 33.4, 30.3. Mosher adduct ^{19}F NMR (C_6D_6 , 70 °C): δ –69.41 (*S*), –69.48 (*R*).

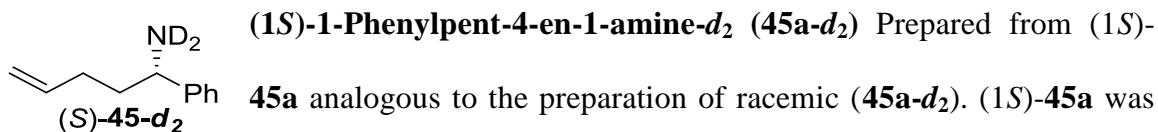


1-Phenyl-hex-5-en-1-amine (71). To a solution of benzoyl chloride (4.20 g, 30 mmol) in THF (700 mL) was added copper(I) iodide (0.19 g, 1.0 mmol). The resulting suspension was cooled to –30 °C and a solution of pent-4-ene magnesium bromide prepared from 5-bromopent-1-ene (4.47 g, 30 mmol), and magnesium turnings (0.72 g, 30 mmol) in THF (50 mL) was added dropwise over 1 h, while the temperature was maintained below –20 °C. The mixture was stirred at the same temperature for 2 h and was then allowed to reach room temperature. The solvent was removed in vacuo and the residue was taken up in dichloromethane (70 mL) and 1 M HCl (50 mL). The organic layer was separated, filtered to remove precipitated copper salts, washed with 10% NaHCO_3 and dried over Na_2SO_4 . The solvent was removed by rotary evaporation and residue was dissolved in abs. MeOH (100 mL). Ammonium acetate (15 g, 200 mmol) and NaBH_3CN (2.0 g, 30 mmol) were added in one portion at room temperature. The mixture was stirred at room temperature for 1 day. Concentrated HCl was added carefully until pH <2, and the solvent was removed in vacuo. The residue was taken up in water (150 mL) and extracted once with ether (30 mL). The aqueous solution was brought to pH >12 with solid KOH and extracted with ether (3 × 30 mL). The combined extracts were dried over KOH and evaporated in vacuo. The residue was treated with finely powdered CaH_2 for 2 h and was then distilled twice

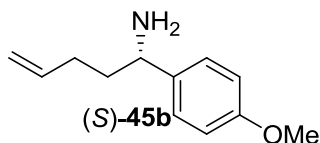
from CaH_2 at reduced pressure to yield 3.70 g (70%) of **71** as a colorless liquid, bp 95–99 °C at 0.5 mmHg. ^1H NMR (400 MHz, CDCl_3): δ = 7.36–7.25 (m, 5H), 5.78 (m, 1H, =CH), 5.03–4.94 (m, 2H, =CH₂), 3.93 (t, $^3J_{\text{H,H}}$ = 10.3 Hz, 1H, CH), 2.11 (m, 2H, CH₂), 1.70 (m, 2H, CH₂), 1.52–1.45 (m, 4H); $^{13}\text{C}\{^1\text{H}\}$ NMR (75.5 MHz, CDCl_3): δ = 146.7 (aryl), 138.6 (=CH), 128.4, 126.9, 126.3 (aryl), 114.6 (=CH₂), 56.2, 39.1, 33.7, 25.8. Mosher adduct ^{19}F NMR (CDCl_3 , 25 °C): δ = –69.29 (*R*), –69.40 (*S*).

General procedure for analytical kinetic resolution. In the glovebox, a screw cap NMR tube was charged with the catalyst (20 μmol), C_6D_6 (0.5 mL), the substrate (1.00 mmol), and ferrocene (2 μmol) as internal standard. The NMR tube was heated in a thermostated oil bath where required. The conversion was then monitored by NMR spectroscopy and the reactions were stopped after an appropriate conversion had been reached. Separation of the product pyrrolidine and the aminoalkene was achieved by aqueous extraction of the secondary ammonium acetate from the primary amine benzaldimine.¹¹

General procedure for preparative-scale kinetic resolution. In the glovebox, a flask was charged with the catalyst (0.1 mmol), C_6H_6 (10 mL), and substrate (15.00 mmol). The conversion and enantiomeric excess of the starting material was then monitored by NMR spectroscopy and the reactions were stopped after minimum 98% *ee* had been reached. After the standard benzaldimine work-up procedure,¹¹ chiral amines were purified by vacuum distillation from CaH_2 .

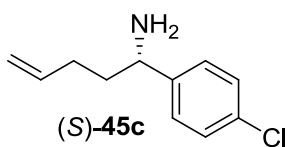


resolved from **45a** using (*R*)-**24a-Lu** as described previously.¹¹



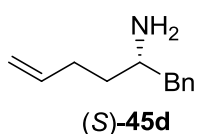
(1S)-1-(4-Methoxyphenyl)-pent-4-en-1-amine ((S)-45b).

Resolved from **45b** by (*R*)-**24a-Y** ($f = 18$), yield 36%, colorless liquid, bp 105 °C at 0.2 mm Hg. Spectroscopic properties are in agreement with literature data.¹¹



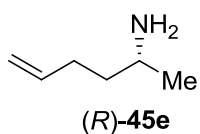
(1S)-1-(4-Chlorophenyl)-pent-4-en-1-amine ((S)-45c).

Resolved from **45c** by (*R*)-**24b-Y** ($f = 19$), yield 30%, colorless liquid, bp 100-110 °C at 0.2 mmHg. Spectroscopic properties are in agreement with literature data.¹¹



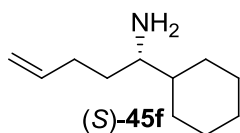
(2S)-1-Phenylhex-5-en-2-amine ((S)-45d). Resolved from **45d** by

(*R*)-**24a-Sc** ($f = 5$), yield 12%, colorless liquid, bp 103 °C at 0.2 mm Hg. Spectroscopic properties are in agreement with literature data.¹¹



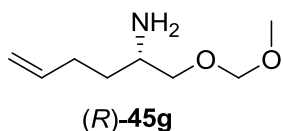
(2R)-Hex-5-en-2-amine ((R)-45e). Resolved from **45e** by (*R*)-**24b-Y**

($f = 15$), yield 30%, colorless liquid, bp 114 °C at 760 mm Hg. $[\alpha]_D^{20} = -5.6$ ($c = 0.5$ in MeOH). Spectroscopic properties are in agreement with literature data.²⁴

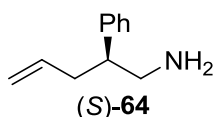


(1S)-1-(Cyclohexyl)-hex-5-en-1-amine ((S)-45f). Resolved from

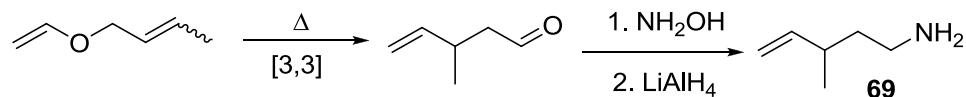
45f ($f = 6$) using (*R*)-**24a-Lu**, yield 9%, colorless liquid, bp 80 °C at 0.2 mmHg. Spectroscopic properties are identical to those of racemic **45f**.



(1R)-1-(Methoxymethyl)pent-4-en-1-amine ((R)-45g). A hot solution of **45g** (3.48 g, 27 mmol) and (*R*)-(-)-mandelic acid (4.12 g, 34 mmol) in isopropanol (40 mL) was allowed to cool slowly to 0 °C. The precipitated salt was filtered off after 12 h, dried on air and recrystallized again. After 12 crystallizations, more than 92% of *ee* was achieved, according to ^{19}F NMR of Mosher amide. The salt was treated with 10% NaOH (20 mL) and the amine was extracted with ether (2 × 40 mL). The combined extracts were dried over KOH and the ether was evaporated. The residue was distilled twice from CaH_2 under reduced pressure to give 0.45 g (12%) of (*R*)-**45g** as a colorless liquid, bp 94–102 °C at 200 mm Hg. Spectroscopic properties are identical to those of racemic **45g**.



(2S)-2-Phenyl-pent-4-en-1-amine ((S)-64). A hot solution of racemic **64** (5.44 g, 34 mmol) and (*R*)-(-)-mandelic acid (5.19 g, 34 mmol) in ethanol (40 mL) was allowed to cool slowly to 0 °C. The precipitated salt was filtered off, dried in air and crystallized again. After 13 crystallizations, an enantiomeric excess $\geq 98\%$ was reached according to ^{19}F NMR spectroscopy of the Mosher amide. The salt was treated with 20% NaOH (20 mL) and the amine was extracted with Et_2O (2 × 40 mL). The combined extracts were dried over KOH and the ether was evaporated *in vacuo*. The resulting residue was distilled twice from CaH_2 under reduced pressure (bp 102 °C at 0.1 mmHg) to give 0.75 g (13%) of (*S*)-**64** as a colorless liquid. Spectroscopic data are in agreement with the data reported in the literature.²⁴ Mosher adduct ^{19}F NMR (CDCl_3 , 40 °C): δ -69.58 (*R*), -69.63 (*S*).

3-Methylpent-4-enylamine (69)

3-Methylpent-4-enaloxime. A Teflon-valve equipped flask was charged with 7.0 g (51 mmol) of crotyl vinyl ether, sealed and kept at 150–155 °C for 4 h. After cooling to room temperature, the rearranged product was carefully added to a solution of 4.76 g (69 mmol) of hydroxylamine hydrochloride in water (10 mL). A solution of K₂CO₃ (4.27 g, 31 mmol) in water (7 mL) was added dropwise. The emulsion was stirred at room temperature. for 1 h, organic layer was separated, and aqueous layer was extracted twice with 20 mL of ether. The combined organic layer was dried (MgSO₄) and distilled at reduced pressure to give 2.8 g of the target oxime as a 1:1 mixture of Z/E isomers. Yield 40%, colorless liquid, bp 120 °C, 100 mm. ¹H NMR (300 MHz, CDCl₃): δ = 8.8 and 8.4 (each br s 1H, OH), 7.39 (t, ³J_(H,H) 6.3 Hz, 1H, CH=N, isomer 1), 6.71 (t, ³J_(H,H) = 5.1 Hz, 1H, CH=N, isomer 2), other signals are overlapped and cannot be separated: 5.72 (m, 1H, =CH), 5.05–4.96 (m, 2H =CH₂), 2.40–2.34 (m, 2H, CH₂), 2.26–2.22 (m, 1H, CH), 1.07–1.02 (m, 3H, CH₃); ¹³C{¹H} NMR (75.5 MHz, CDCl₃): δ = 151.33, 151.06 (CH=N); 142.72, 142.55 (=CH), 113.75, 113.67 (=CH₂), 36.0, 31.3 (CH₂), 35.70, 35. 11 (CH), 19.97, 19.65 (CH₃).

3-Methylpent-4-enylamine (69). To a stirred suspension of 1.2 g (31 mmol) of LiAlH₄ in 20 ml of ether a solution of 3-methylpent-4-enaloxime (2.8 g, 20 mmol) in ether (10 ml) was added dropwise at 0 °C. The mixture was stirred overnight at room

temperature, cooled back to 0 °C and carefully quenched with sequential addition of water (1.2 mL), 15 % NaOH (1.2 mL) and water again (4 mL). The white precipitate was filtered off and washed with ether (3 × 20mL). The filtrate was dried (NaOH) and distilled. After 2 distillations from CaH₂, 2.0 g of the target aminoalkene **69** were obtained. Yield 72%, colorless liquid, bp 115 °C, 760 mm Hg. ¹H NMR (300 MHz, CDCl₃): δ = 5.65 (m, 1H, =CH), 4.94–4.84 (m, 2H, =CH₂), 2.65 (t, ³J_(H,H) = 7.6 Hz, 2H, CH₂N), 2.22–2.13 (m, 1H, CH), 1.44–1.36 (m, 4H), 0.98 (d, ³J_(H,H) = 7.6 Hz, 3H, CH₃); ¹³C{¹H} NMR (75.5 MHz, CDCl₃): δ 144.3 (=CH), 112.7 (=CH₂), 40.5, 40.1, 35.6, 20.3 (CH₃). The spectroscopic data is in agreement with previously published data.²⁵

General procedure for the determination of enantiomeric excess via Mosher amides. The amine (0.08–0.1 mmol) was dissolved in CDCl₃ or C₆D₆ (0.5 mL) in a NMR tube. DIPEA (2.5 equiv with respect to the amine) and (*S*)-Mosher acid chloride (1.5 equiv with respect to the amine) were added. Enantiomeric excess was then determined by ¹⁹F NMR spectroscopy at 60–100 °C.

Typical Kinetic procedure

In a glovebox, a screw cap NMR tube was charged with aliquots of standard solutions of **24a-Y** (50 μL, 0.105M in C₆D₆) and substrate (100 μL, 1.62 M in C₆D₆), and then C₆D₆ (350 μL) was added for a total volume of 600 μL. Ferrocene (5–8 mg) was added and the NMR tube was sealed and removed from the glovebox. The mixture was then placed into a thermostated NMR probe and the reaction progress was monitored periodically in pre-programmed intervals by observing the disappearance of olefinic signals in ¹H NMR spectra compared to the signal of ferrocene as an internal standard.

Crystallography. X-ray quality crystals of (*R*)-Mosher amide of (*S*)-**64** and (*R*)-mandelate of (*R*)-**45g**^{*} were obtained by recrystallization from ether/hexanes and isopropanol solution at room temperature, respectively. Data were collected on a Nonius Kappa CCD Diffractometer at 173(2) K, wavelength 0.71073 Å and are summarized in Table II-8. Cell parameters were obtained from 2579 ((*S*)-**64-Mos**), reflections within the range $1.7 < \theta < 27.5^\circ$. Lorentz, polarization, and empirical absorption corrections were applied. The space group was determined from systematic absences. The structure was solved by direct methods (SHELXS program).²⁹ All positional and atomic displacement parameters (ADP) were refined with all reflections data by full-matrix least squares on F^2 using SHELXL.²⁹ Non-hydrogen atoms were refined anisotropically. Hydrogen atoms were constrained to idealized positions using a riding model. The absolute structure was refined using the Flack parameter.³⁰ The drawing of the molecule (Figure II-8) was realized with the help of ORTEP-3.³¹

* A preliminary-grade X-ray crystallographic analysis of the ammonium salt of (*R*)-**45g** with (*R*)-(-)-mandelic acid confirmed the assigned absolute configuration relative to the known configuration of mandelic acid. A poor quality of the crystal did not allow to unambiguously determine the absolute configuration of the salt and use the data for publication.

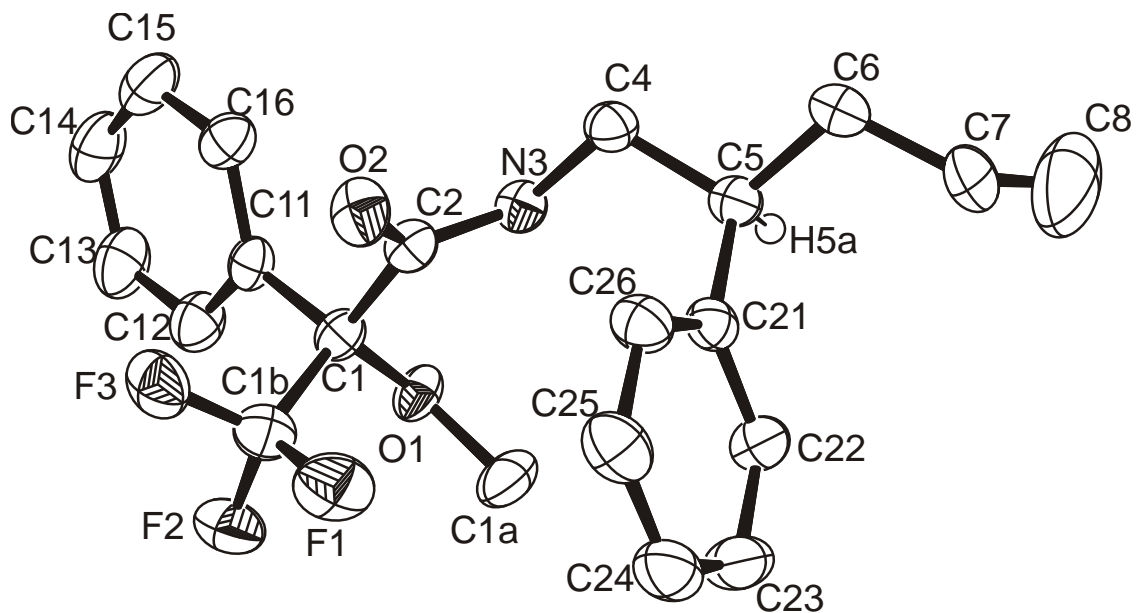


Figure II-8. ORTEP diagram for (*R*)-Mosher amide of (*S*)-**64**. Thermal ellipsoids are shown at 50% probability level, hydrogen atoms except H5a are omitted for clarity.

Table II-8. Crystallographic data for (*R*)-Mosher amide of (*S*)-**64**.

Parameter	Value
Empirical formula	C ₂₁ H ₂₂ F ₃ NO ₂
Formula weight	377.40
Crystal system	Orthorhombic
Space group	P2 ₁ 2 ₁ 2 ₁
Unit cell dimensions	$a = 8.4708(1) \text{ \AA}$, $\alpha = 90^\circ$ $b = 9.6130(1) \text{ \AA}$, $\beta = 90^\circ$ $c = 23.8477(4) \text{ \AA}$, $\gamma = 90^\circ$
Volume	1941.91(4) \AA^3
Z	4
Density (calculated)	1.291 Mg/m ³
Absorption coefficient	0.102 mm ⁻¹
F(000)	792
Crystal size	0.35 × 0.15 × 0.10 mm ³

Θ range for data collection	1.71 to 27.50°
Index ranges	$-10 \leq h \leq 10, -12 \leq k \leq 12, -30 \leq l \leq 30$
Reflections collected	4459
Independent reflections	4459 [R(int) = 0.0000]
Completeness to θ	100.0%
Absorption correction	Empirical
Max. and min. transmission	0.9899 and 0.9652
Data / restraints / parameters	4459 / 0 / 245
Goodness-of-fit on F^2	1.063
Final R indices [$I > 2\sigma(I)$]	R1 = 0.0498, wR2 = 0.1350
R indices (all data)	R1 = 0.0654, wR2 = 0.1480
Absolute structure parameter	-0.7(8)
Largest diff. peak and hole	0.816 and -0.351 e.Å ⁻³

II.5 References

- (1) Ricci, A. *Modern Amination Methods* Wiley-VCH: Weinheim, 2000.
- (2) Ricci, A. *Amino Group Chemistry: From Synthesis to the Life Sciences*; Wiley-VCH: Weinheim, 2008.
- (3) Müller, T. E.; Hultzs, K. C.; Yus, M.; Foubelo, F.; Tada, M. *Chem. Rev.* **2008**, *108*, 3795-3892.
- (4) Müller, T. E.; Beller, M. *Chem. Rev.* **1998**, *98*, 675-703.
- (5) Reznichenko, A. L.; Hultzs, K. C. In *Science of Synthesis, Stereoselective Synthesis*; De Vries, J. G., Molander, G. A., Evans, P. A., Eds.; Thieme: 2010; Vol. 1, p 689-729.
- (6) Reznichenko, A. L.; Hultzs, K. C. In *Chiral Amine Synthesis: Methods, Developments and Applications*; 1st ed.; Nugent, T., Ed.; Wiley-VCH: 2010, p 341-376.
- (7) Hultzs, K. C. *Adv. Synth. Catal.* **2005**, *347*, 367-391.
- (8) Gribkov, D. V.; Hultzs, K. C.; Hampel, F. *Chem. Eur. J.* **2003**, *9*, 4796-4810.
- (9) Gribkov, D. V.; Hampel, F.; Hultzs, K. C. *Eur. J. Inorg. Chem.* **2004**, 4091-4101.
- (10) Gribkov, D. V.; Hultzs, K. C. *Chem. Commun.* **2004**, 730-731.
- (11) Gribkov, D. V.; Hultzs, K. C.; Hampel, F. *J. Am. Chem. Soc.* **2006**, *128*, 3748-3759.
- (12) Dunsmore, C. J.; Carr, R.; Fleming, T.; Turner, N. J. *J. Am. Chem. Soc.* **2006**, *128*, 2224-2225.
- (13) Parvulescu, A. N.; Jacobs, P. A.; De Vos, D. E. *Chem. Eur. J.* **2007**, *13*, 2034-2043.
- (14) Hoben, C. E.; Kanupp, L.; Bäckvall, J.-E. *Tetrahedron Lett.* **2008**, *49*, 977-979.
- (15) Parvulescu, A. N.; Jacobs, P. A.; De Vos, D. E. *Adv. Synth. Catal.* **2008**, *350*, 113-121.
- (16) Truppo, M. D.; Turner, N. J.; Rozzell, J. D. *Chem. Commun.* **2009**, 2127-2129.
- (17) Arai, S.; Bellemin-Laponnaz, S.; Fu, G. C. *Angew. Chem. Int. Ed.* **2001**, *40*, 234-236.
- (18) van Rantwijk, F.; Sheldon, R. A. *Tetrahedron* **2004**, *60*, 501-519.
- (19) Ismail, H.; Lau, R. M.; van Rantwijk, F.; Sheldon, R. A. *Adv. Synth. Catal.* **2008**, *350*, 1511-1516.
- (20) De, C. K.; Klauber, E. G.; Seidel, D. *J. Am. Chem. Soc.* **2009**, *131*, 17060-17061.
- (21) Gagné, M. R.; Stern, C. L.; Marks, T. J. *J. Am. Chem. Soc.* **1992**, *114*, 275-294.
- (22) Manna, K.; Kruse, M. L.; Sadow, A. D. *ACS Catal.* **2011**, *1*, 1637-1642.
- (23) Bochkarev, M. N. *Chem. Rev.* **2002**, *102*, 2089-2118.
- (24) Kim, J. Y.; Livinghouse, T. *Org. Lett.* **2005**, *7*, 4391-4393.
- (25) Yang, Q.; Ney, J. E.; Wolfe, J. P. *Org. Lett.* **2005**, *7*, 2575-2578.

- (26) Laurent, A.; Mison, P.; Nafti, A.; Pellissier, N. *Tetrahedron Lett.* **1982**, 23, 655-658.
- (27) Smith, P. M.; Thomas, E. J. *J. Chem. Soc., Perkin Trans. 1* **1998**, 3541-3556.
- (28) Gao, M.; Wang, D.-X.; Zheng, Q.-Y.; Wang, M.-X. *J. Org. Chem.* **2006**, 71, 9532-9535.
- (29) Sheldrick, G. *Acta Crystallogr.* **2008**, A64, 112-122.
- (30) Flack, H. *Acta Cryst.* **1983**, A39, 876-881.
- (31) Farrugia, L. J. *J. Appl. Cryst.* **1997**, 30, 565.

III Chapter 3. Asymmetric Intermolecular Hydroamination of Unactivated Alkenes with Simple Amines Catalyzed by Rare Earth Metal Binaphtholates

III.1 Introduction

Asymmetric intermolecular hydroamination of unactivated alkenes with simple amines is arguably the most challenging transformation in hydroamination catalysis¹⁻³ (see also Chapter 1). Prior to our work, only the stereoselective hydroamination of unactivated alkenes with ureas has been reported, which is a “hydroureation” rather than a hydroamination in a formal sense.⁴ Moreover, the existing achiral examples of intermolecular hydroamination of unactivated alkenes with unbiased simple amines are scarce and most of them are not general (see section I.3). Hence, the development of catalysts for a stereoselective intermolecular hydroamination remains an important goal.

In this chapter we will present our studies on intermolecular asymmetric hydroamination catalyzed by rare earth metal binaphtholates.

III.2 Results and Discussion

III.2.1 Preliminary Studies on Intermolecular Hydroamination

As it was mentioned in Chapters 1 and 2, rare earth metal binaphtholates **24-Ln** developed in the Hultsch group are the most active and one of the most stereoselective catalysts available for the intramolecular hydroamination/cyclization of aminoalkenes, including the kinetic resolution of racemic aminoalkenes.⁵⁻⁷

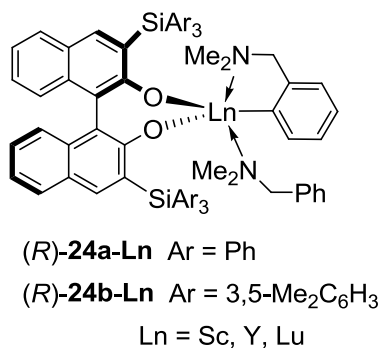
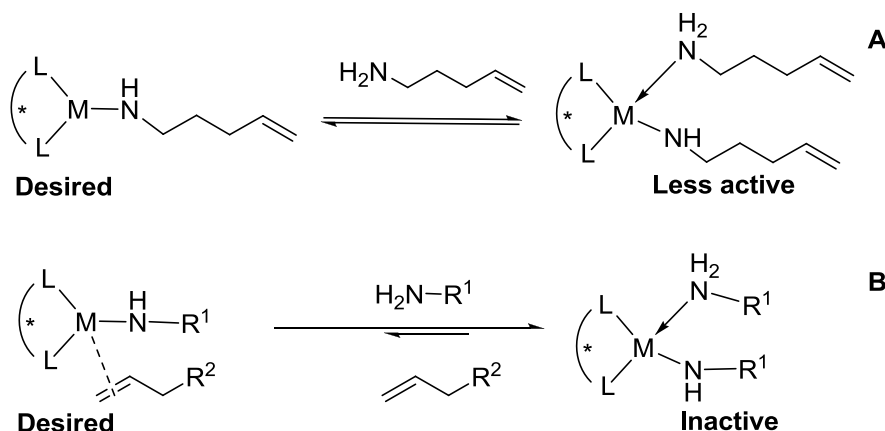


Figure III-1. Rare earth metal 3,3'-bis(triarysilyl)binaphtholates **24-Ln**.

Prior to our work, the only hydroamination catalyst which excelled in intramolecular reactions and which was potent enough in intermolecular hydroamination of unactivated alkenes was the open *ansa*-lanthanocene Me₂Si(C₅Me₄)₂NdCH(SiMe₃)₂ (**50-Nd**) developed in the Marks group (Eq. I-8).⁸ It should be noted that this achiral catalytic system required tremendous excess (>70 equiv.) of the weakly-binding alkene in order to overcome the disfavoring competition from the strong-binding amine. Previous studies with **24-Ln** demonstrated that in analogy to the highly Lewis-acidic and azaphilic lanthanocene catalysts⁹ the binaphtholates **24-Ln** also tend to suffer from excessive amine binding in hydroamination/cyclization reactions.⁶ There is no doubt that this undesired phenomenon is still acceptable in the intramolecular reactions; however, it is less tolerable in the more challenging intermolecular hydroamination which lacks the tether between two crucial substrates of a different binding power (Scheme III-1, **B**).

Scheme III-1. Additional amine binding to the metal center in generic intramolecular (**A**) and intermolecular (**B**) hydroamination.

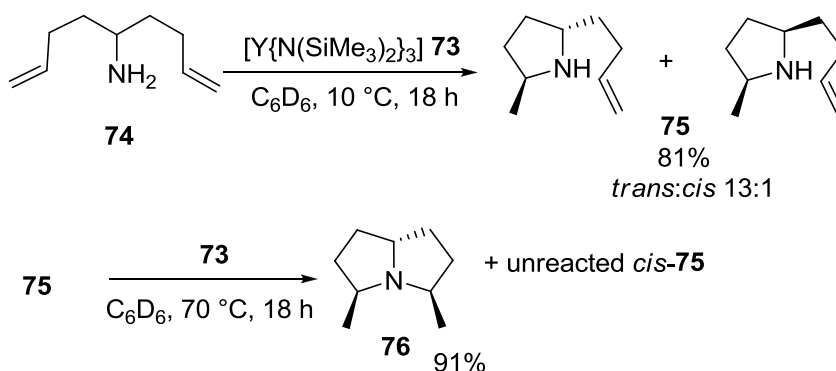


Another important problem of early transition metal-catalyzed hydroamination is the chemoselectivity. Indeed, most intermolecular reactions involving primary amines and ammonia lead to mixtures of primary, secondary and tertiary amines (see section I.3.1). Some additional experiments binaphtholate catalysts **24-Ln** suggested that this system can overcome the aforementioned restrictions and provided some more general leads for the catalyst design in intermolecular hydroamination.

We first directed our attention to the sequential hydroamination/cyclization of the primary amino diene **74** (Scheme III-2). The transformation was first studied by Livinghouse,¹⁰ and it was found that the simple yttrium trisamide **73** catalyzes at room temperature the intramolecular hydroamination to give pyrrolidine **75** as a mixture of *trans*:*cis* isomers with a 13:1 ratio. Under more forcing reaction conditions, *trans*-**75** cyclized cleanly into the bicyclic product **76**, while *cis*-**75** remained unchanged due to the relative stereochemistry disfavoring the second cyclization. Sequential hydroamination/cyclization of **74** can serve as a formal functional model for the

intermolecular hydroamination of alkene with a primary amine. As **74** represents the primary amine, the hydroamination product **75** can be related to a product of the intermolecular hydroamination, which then may or may not participate in a second hydroamination step with another alkene molecule, ultimately producing a tertiary amine.

Scheme III-2. Hydroamination/bicyclization of aminodiene **74** catalyzed by **73**.¹⁰



In the absence of any reported kinetic data, we repeated this study from Livinghouse. As shown in Figure III-2, both transformations from **74** to **75** and from **75** to **76** can proceed at 40 °C in the presence of the yttrium trisamide **73**. However, the second transformation is significantly slower and takes much longer to reach appreciable conversion. This order of reactivity primary > secondary aminoalkene, is rather common in catalytic hydroamination/cyclization (See section I.2) and results from diminished insertive reactivity of a more bulky metal-amido species.

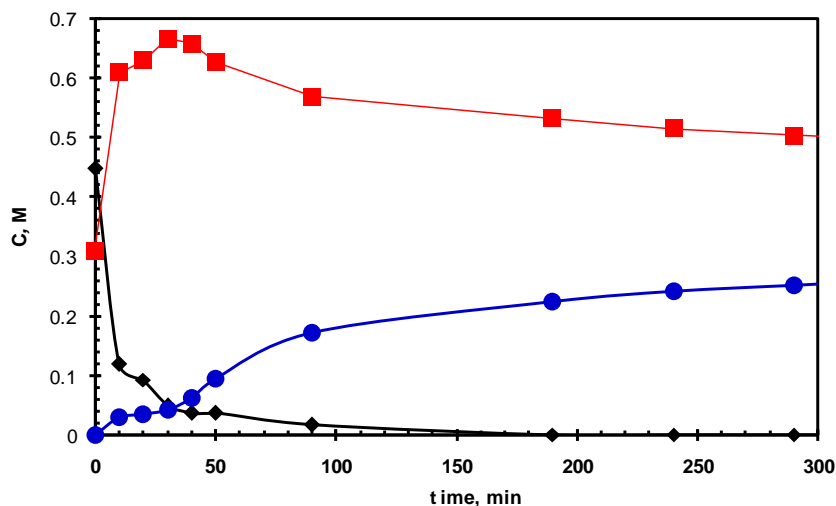


Figure III-2. Kinetic profile for the hydroamination/cyclization of **74** ($[\mathbf{74}]_0 = 0.67$ M) with **73** (0.02 M, 3 mol %) at 40 °C in C_6D_6 . Concentration data is shown for **74** (◆), *trans*-**75** (■) and **76** (●).

This observation also implies that if this reactivity order will be translated to the intermolecular reactions, the desired direction of the reaction can easily be programmed by the careful choice of reaction conditions. For example, Livinghouse et al. took advantage of this approach in intramolecular transformation by running the reaction below the room temperature in order to obtain pyrrolidine **75** cleanly (Scheme III-2).

It should be noted that although these conclusions seem to be trivial and intuitively simple they should be used carefully when comparing simple trisamides catalyst **73** and binaphtholate catalysts **24-Ln**, because the latter compound features significantly more electron-deficient and sterically protected metal center, which is responsible for its superior reactivity. Indeed, when the cyclization of **74** was carried out in the presence of **24a-Y**, a strikingly different kinetic pattern was observed (Figure III-3).

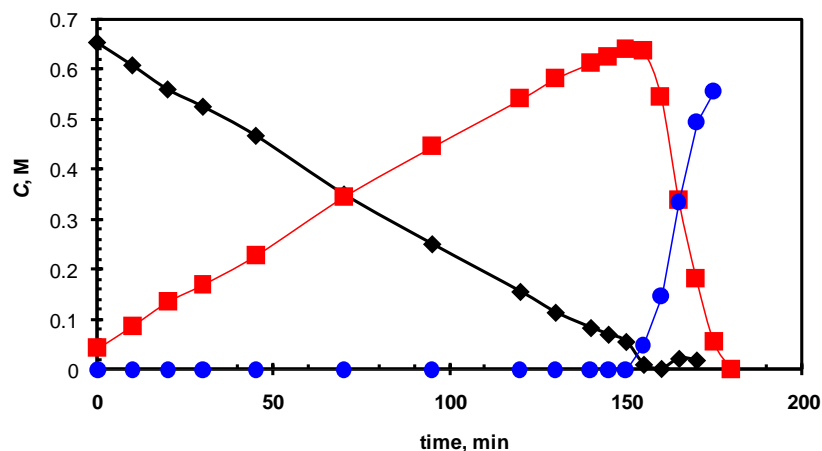


Figure III-3. Kinetic profile for the cyclization of **74** ($[\mathbf{74}]_0 = 0.67$ M) with (*R*)-**24a-Y** (0.01 M, 1.5 mol %) at 30 °C in C_6D_6 . Concentration data shown for **74** (◆), *trans*-**75** (■) and **76** (●).

While the superior reactivity of **24-Y** resulting in shorter reaction time at lower temperature and catalyst loading was expected, the relative rate of monocyclization and bicyclization was surprisingly altered (Figure III-3). Although the second cyclization step proceeded much faster than the first one (25 min versus 150 min at 30 °C), the bicyclization took place only *after* the first step was completed. As long as aminodiene **74** was detected in the mixture, no formation of bicycle **76** was observed. This observation suggests that the notion that the hydroamination of the secondary amine is faster compared to the hydroamination of the primary aminoalkene **74** is an oversimplification. Indeed, if the secondary amine **75** would be 6 times more reactive than **74**, then no trace of **75** should be detectable in the mixture over the course of reaction. This implies that the first (slow) hydroamination of the primary amine **74** and the second (fast) hydroamination of the secondary amine **75** should be differentiated not according to the reactivity of the *substrate* but instead according to the reactivity of the

catalyst. One might argue that the catalyst derived from the precatalyst **24a-Y** is the same in both reactions; however, this does not seem to be the case if some important details are considered. Indeed, as shown on the Scheme III-1, equilibrium **A**, the catalytically active species is in a constant equilibrium with the “dormant” species containing an additional amine ligand. Although it might be oversimplification to see the “dormant” species as catalytically inactive⁶ it is justified to assume that shifting equilibrium **A** to the right diminishes the net catalytic activity. While equilibrium **A** on Scheme III-1 is shown to involve an aminoalkene substrate, it can also involve the hydroamination product or any other Lewis base present in the reaction mixture. Thus it is reasonable to propose that for sterically unprotected yttrium trisamide **73**, both **74** and **75** can bind to the metal center with comparable equilibrium constants. As a result, the catalyst remains more or less in the same state over the course of both reactions, and the hydroamination of the secondary amine **75** is *slower* due to the less reactive *substrate*. On the other hand, the sterically more protected **24a-Y** should display preferential binding of the primary amine **74** whereas more hindered **75** will not bind as efficiently. As a result, equilibrium on Scheme III-1 shifts in favor of the lower coordinate species when **74** is consumed, and the hydroamination of the secondary amine **75** is *faster* due to the more reactive *catalyst*.

In order to test this hypothesis, we tried to reproduce the reaction with addition of 10 equiv (relative to catalyst) of *n*-propylamine as a mimic of **74** that does not get consumed in the reaction. No acceleration effect was observed, and the behavior was similar to that of the trisamide (Figure III-4).

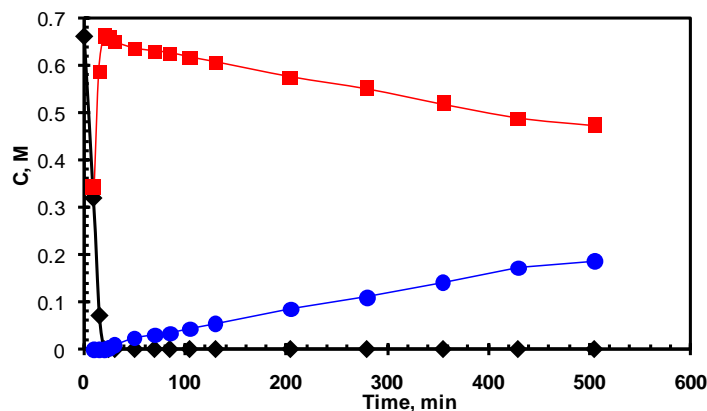


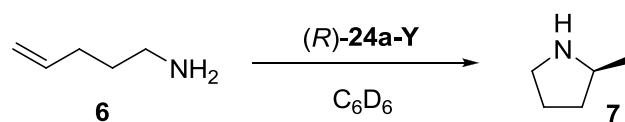
Figure III-4. Kinetic profile for the cyclization of **74** ($[\mathbf{74}]_0 = 0.67$ M) with (*R*)-**24a-Y** (0.02 M, 3 mol %) in the presence of *n*-PrNH₂ (0.2 M) at 40 °C in C₆D₆. Concentration data shown for **74** (◆), **75** (■) and **76** (●).

These studies on the hydroamination/cyclization of diene **74** catalyzed by **24-Y** and trisamide **73** allowed us to several important conclusions. First, we saw that the chemoselectivity of the reaction can be driven by both substrate and catalyst activity. If the catalyst is maintaining the same level of activity, reactions of primary and secondary amines are very different in relative feasibility, thus, leaving room for development of chemoselective transformations. More important, the control of the aggregation state of the catalyst is an invaluable tool in reaching significantly higher reactivity in the hydroamination reaction. Although the demonstrated example illustrates this approach using a tunable substrate, it seems reasonable to propose that the same effect can be reached by adjusting the steric properties of the catalyst. In addition, it is obvious that the formation of “dormant” species can also be suppressed by factors other than sterics, such as the electronic properties of the ligand and the temperature. While the electronic properties of the catalyst family **24-Ln** cannot be tuned without introducing significant

changes to the ligand core, the temperature factor is more readily accessible. As it was demonstrated previously, the temperature dependence of K^{dorm} (the equilibrium constant for the equation **A** on Scheme III-1) is expected to resemble that of a complex association constant, i.e. decrease with increasing temperature.⁶ As shown in Table III-1, while the dormant species is dominant near room temperature, the “naked” and, therefore, more reactive species constitutes almost entire amount of catalytic species at higher temperatures. Certainly, the obvious drawbacks of high temperatures, such as catalyst decomposition and poor selectivity, should be considered when employing this approach to limit amine binding.

To conclude, we envisioned that the control of the catalyst aggregations state which may be facilitated via tuning of the steric environment of the catalyst and substrate, as well as by the electronic demands of the ligand and reaction temperature is a key to enhanced reactivity in intra- and intermolecular hydroamination.

Table III-1. Temperature dependence of the K^{dorm} value for the hydroamination of **6** with (*R*)-**24a-Y**.



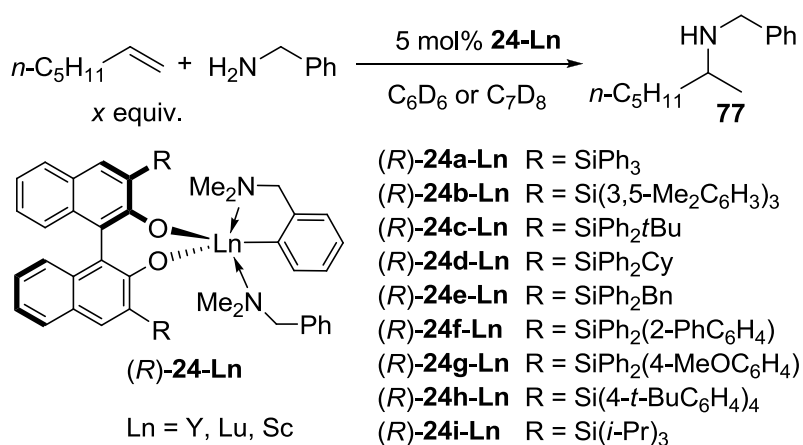
T, °C	K^{dorm}
40	2.5 ^a
60	0.89 ^a
100	0.15 ^b
150	0.02 ^b

^a From ref. 6. ^b Extrapolation.

III.2.2 Binaphtholate Catalyst Evaluation

We have chosen a reaction between readily available benzylamine and 1-heptene as a model process. Rare earth metal binaphtholates **24a-Ln** and **24b-Ln**, as well as a more representative library of novel binaphtholate complexes **24c-i** were screened (Table III-2).

Table III-2. Rare earth metal binaphtholates **24a-i** in intermolecular hydroamination.^a



Entry	cat.	x	T, °C	t , h	% conv. ^b (% yield) ^c	% ee ^d (config.)
1	$(R)\text{-}\mathbf{24a-Y}$	15	150	36	90 (65)	58 (<i>R</i>)
2	$(R)\text{-}\mathbf{24a-Y}$	12	150	48	-- (78) ^e	58 (<i>R</i>) ^f
3	$(R)\text{-}\mathbf{24a-Y}$	7	150	48	85 (57)	57 (<i>R</i>)
4	$(R)\text{-}\mathbf{24a-Y}^g$	50	150	18	95 (68)	54 (<i>R</i>)
5	$(S)\text{-}\mathbf{24a-Y}$	15	170	18	95	55 (<i>S</i>)
6	$(R)\text{-}\mathbf{24a-Lu}$	15	150	30	95 (62)	40 (<i>R</i>)
7	$(R)\text{-}\mathbf{24a-Sc}$	15	170	24	--(0)	--
8	$(R)\text{-}\mathbf{24b-Y}$	15	150	24	90 (61)	44 (<i>R</i>)
9	$(R)\text{-}\mathbf{24c-Y}$	15	150	48	85 (59)	46 (<i>R</i>)
10	$(R)\text{-}\mathbf{24d-Y}$	15	150	17	90	47 (<i>R</i>)

11	(<i>R</i>)- 24e-Y	15	150	24	95(64)	47 (<i>R</i>)
12	(<i>R</i>)- 24f-Y	15	150	96	95(69)	50 (<i>R</i>)
13	(<i>R</i>)- 24g-Y	15	150	12	45	60 (<i>R</i>)
14	(<i>R</i>)- 24h-Y	15	150	11	95(72)	58 (<i>R</i>)
15	(<i>R</i>)- 24i-Y	15	150	72	60 (44)	38 (<i>R</i>)

[a] General reaction conditions: 3.0 mmol 1-heptene, 0.2 mmol amine, 10 μ mol cat. (0.1 mL of a 0.1 M cat. solution in C₆D₆ or toluene-*d*₈). ^b The conv. of amine was determined via ¹H NMR spectroscopic analysis. ^c Isolated yield after column chromatography. ^d Determined by ¹⁹F NMR spectroscopy of the Mosher amide after removal of the *N*-benzyl group. ^e Preparative scale reaction using 12.0 mmol 1-heptene, 1.0 mmol benzylamine. ^f Confirmed by chiral HPLC of the corresponding *N*-benzamide. ^g 8 mol% cat.

The triphenylsilyl-substituted binaphtholate yttrium complex (*R*)-**24a-Y** yielded exclusively the Markovnikov hydroamination product **77** and achieved the highest enantiomeric excess of 58% (Table III-2, entry 1). The reaction was carried out with a 15-fold excess of alkene, which was used in order to accelerate the reaction. Lower alkene:amine ratios led to longer reaction times and lower conversion (Table III-2, entry 3), while a larger excess of alkene led to a slight acceleration of the reaction (Table III-2, entry 4). The enantiomeric excess did not show any significant dependence on the alkene:amine ratio. According to ¹⁹F NMR spectroscopic data of the Mosher amide of the *N*-debenzylated primary amine,¹¹ the absolute configuration of **77** derived from (*R*)-**24a-Ln** was found to be (*R*), which is the opposite selectivity to that observed for the intramolecular hydroamination of aminopentenes with these catalysts.⁶

The reaction can be run at even more forcing conditions, e. g. at 170 °C and, remarkably, only a slight erosion of enantioselectivity is observed (Table III-2, entry 5). The smaller ionic radius of lutetium in (*R*)-**24a-Lu** results in lower selectivity, while the

activity remains comparable to yttrium, however (*R*)-**24a-Sc** did not display any catalytic activity at all (Table III-2, entries 6 and 7).

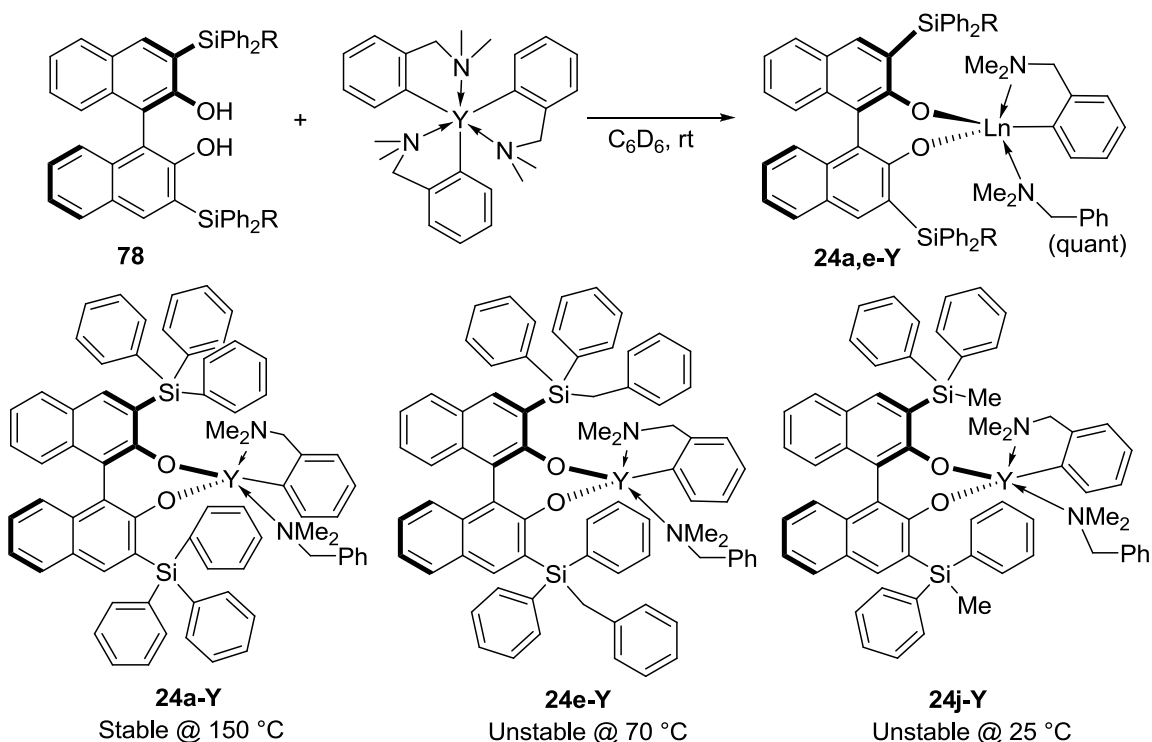
The sterically more shielded tris(xylyl)silyl-substituted binaphtholate complex (*R*)-**24b-Y** and the novel complexes **24c-g** featuring a silyl group with a SiPh₂R substitution pattern, did not show significantly improved results compared to **24a-Y**. The highest enantioselectivity of 60% ee was obtained for *p*-methoxyphenyl(diphenyl)silyl substituted **24g-Y**. Unfortunately, this catalyst showed significant decomposition at 150 °C and, therefore, reaction could not be completed. The steric influence on the reaction rate was manifested by the slowest reaction in the case of the bulky (*o*-biphenyl)diphenylsilyl-substituted **24f-Y**, which was the least active catalyst in this series.

The novel tris(aryl)silyl- or tris(alkyl)silyl-substituted binaphtholates **24h** and **24i** also displayed a strong dependence of the reaction outcome on the ligand sterics. The aryl-substituted complex **24h-Y** was the most potent catalyst of the series, unfortunately it was less selective than **24a-Y**. Catalyst **24i-Y**, lacking the aryl groups on the silyl moiety, showed very low activity and the lowest enantioselectivity.

While the binaphthol proligands **78** along with the organolanthanide precursors of the type [Ln(*o*-C₆H₄CH₂NMe₂)₃] have been shown to be very convenient starting materials for the rapid and clean preparation of highly active compounds **24-Ln** (Scheme III-3),¹² this synthetic approach is not universal. First, it was shown that for many metallocene¹³ and post-metallocene⁶ systems the catalytic activity in hydroamination/cyclization increases with increasing ionic radius of the rare earth metal. Thus, lanthanum and neodymium complexes usually enjoy higher activities than their

yttrium and lutetium counterparts.¹⁴ Unfortunately, the lanthanum member of the $[\text{Ln}(o\text{-C}_6\text{H}_4\text{CH}_2\text{NMe}_2)_3]$ precursor family is not known and therefore lanthanum binaphtholates are not accessible via this route.

Scheme III-3. Synthesis and stability of precatalysts **24-Y**.

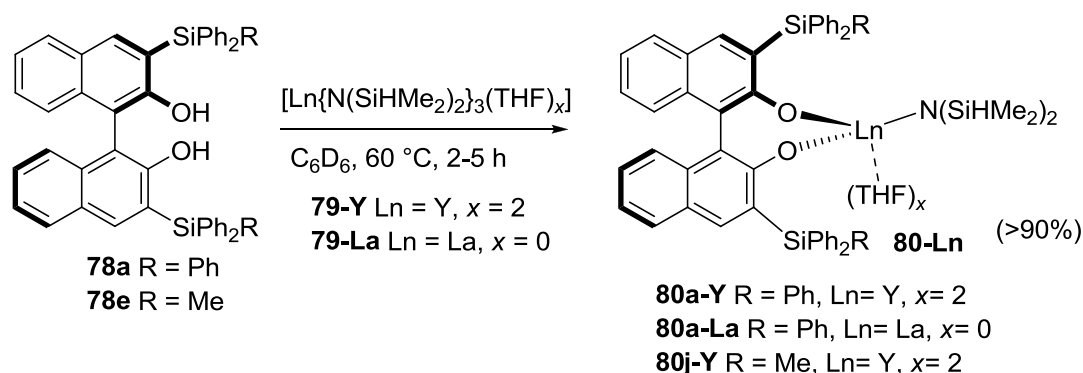
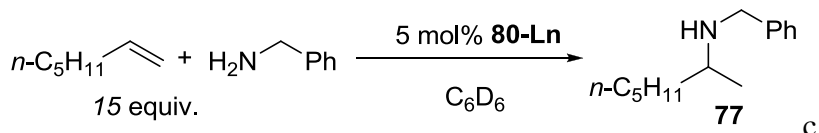


In addition, only a limited number of yttrium precatalysts of type **24-Y** are accessible. The stability of the corresponding binaphtholate aryl complexes correlates with the steric features of the ligand. While the previously known⁶ triphenylsilyl-substituted complex **24a-Y** does not show any decomposition after 1 hour at 150 °C, its benzyl(diphenyl)silyl analogue **24e-Y** was found to decompose rapidly at 70 °C. Note that this thermal instability corresponds only to the precatalyst. However, upon cleavage of the aryl group by an amine a stable amido species is formed which can smoothly operate in the catalytic cycle (Table III-2, entry 11). The preparation of the least bulky

24j-Y was unsuccessful because this species decomposes within minutes at room temperature. This data suggests that complexes **24-Ln** are the *kinetic*, but not the *thermodynamic* products of the reaction of **78** with $[\text{Ln}(o\text{-C}_6\text{H}_4\text{CH}_2\text{NMe}_2)_3]$. Steric protection is necessary for the kinetic stabilization of the monometallic well-defined species **24-Ln**. In our series the lowest acceptable degree of steric protection is represented by **24e-Y**.

In order to evaluate broader variety of binaphtholate ligands and rare earth metals in the intermolecular hydroamination, we directed our attention to the rare earth metal precursors $[\text{Ln}\{\text{N}(\text{SiHMe}_2)_2\}_3(\text{THF})_x]$ **79**, which were already used previously in our group as precursors for various rare earth metal complexes.¹²

The synthesis of the corresponding binaphtholate complexes **80a-Y**, **80j-Y** and **80a-La** was carried out as shown in Scheme III-4. The amine elimination required elevated temperatures and extended reaction time due to lower basicity of the bis(dimethylsilyl)amide compared to the aryl ligand in complexes $[\text{Ln}(o\text{-C}_6\text{H}_4\text{CH}_2\text{NMe}_2)_3]$. Compounds **80-Ln** were obtained with purity exceeding 90% according to the NMR spectroscopic data of the reaction mixtures, and were further tested in catalytic experiments without additional purification. Notably, neither of the complexes **80-Ln** showed any noticeable decomposition even at 150 °C, thus suggesting that the precatalyst instability problem was successfully addressed.

Scheme III-4. Synthesis of binaphtholates **80-Ln**.**Table III-3.** Intermolecular hydroamination of 1-heptene catalyzed by **80-Ln**.

Entry	cat.	T, °C	t, h	% conv. ^a (% yield) ^b	% ee ^c (config.)
1	(<i>R</i>)- 80j-Y	180	48	0 (–)	–
2	(<i>R</i>)- 80a-Y	170	120	90 (65)	54 (<i>R</i>)
3	(<i>R</i>)- 80a-La	180	48	0 (–)	–

^a By ¹H NMR spectroscopic analysis. ^b Isolated yield after column chromatography.

^c Determined by ¹⁹F NMR spectroscopy of the Mosher amide after removal of the *N*-benzyl group.

As shown in Table III-3, the yttrium binaphtholate catalyst **80j-Y**, bearing the methyl(diphenyl)silyl groups, that was inaccessible via the traditional route to the complexes **24-Y**, was completely catalytically inactive. This result should be interpreted carefully, as both binaphtholate ligand backbone and leaving group of the precatalyst were modified in **80j-Y** compared to the parent complex **24a-Y**, which is catalytically

active. Indeed, it has been known for almost a decade¹² that the low acidity of aryl or alkyl C–H bonds makes the corresponding alkyl or aryl rare earth metal complexes the preferred precatalysts in hydroamination, because the catalyst activation (Scheme I–1) is smooth and irreversible. In contrast, the less basic and more sterically encumbered disilazides $N(\text{SiXMe}_2)_2$ ($X = \text{H, Me}$) are less prone to be substituted by a catalytically relevant amine and are highly competitive in its binding to the metal center. Thus, the absence of reactivity of **80j-Y** can be attributed to the poor leaving group alone. However, the same poor leaving group, when used in the triphenylsilyl-substituted species **80a-Y** does not prevent the reaction from occurring. Although the reactivity is significantly diminished compared to **24a-Y**, the enantioselectivity remains nearly the same. This suggests that the leaving group itself does not play any significant role during the catalytic cycle, but it diminishes the concentration of the catalytically relevant species. Thus, the dramatic loss of catalytic activity when a triphenylsilyl group (**24a-Y**) is replaced by a methyl(diphenyl)silyl group (**80j-Y**) should be interpreted as a result of the lack of sufficient steric bulk in complex **80j-Y**. As the olefin insertion step in the rare earth metal-catalyzed hydroamination is generally more feasible for the more sterically accessible metal center,¹⁴ it can be speculated that our observations should result from an unfavored position of the dormant-active species equilibrium (Scheme III-1). This hypothesis is in agreement with the lack of catalytic activity of **80a-La** because the triphenylsilyl group meets the necessary minimal steric protection criteria for the mid-sized yttrium and lutetium, but is insufficient for the larger lanthanum. This implies that binaphtholate ligands bearing more bulky substituents than **78a** can be applied for the lanthanum binaphtholate catalyzed hydroamination.

Presently, the combination of high selectivity and good activity of **24a-Y** along with its readily availability makes it the catalyst of choice for further studies of the intermolecular hydroamination.

III.2.3 Substrate Scope of Intermolecular Hydroamination

Analogous to 1-heptene, linear and branched 1-alkenes are converted to their respective *N*-benzyl-alkan-2-amines **81–85** with good activity (Table III-4, entries 1–5) and exclusive Markovnikov selectivity using **24a-Y**. However, branching in the allylic position of the alkene, for example in vinyl cyclohexane (Table III-4, entry 6) leads to significantly diminished reactivity. The highest reactivity was observed for 4-phenyl-1-butene, which permitted to use a lower alkene:amine ratio of 10:1. All reactions with **24a-Y** produced similar selectivities in the range of 51–61% ee. Reactions with cyclopentylamine proceed with comparable enantioselectivity, but diminished activity (Table III-4, entries 8, 9). Similar observations were made for *para*-methoxy benzylamine (Table III-4, entry 10), in which the reduced reactivity can be attributed to a possible deactivation of the catalyst by the methoxy group, as well as for the *ortho*-methylbenzylamine (Table III-4, entry 7) featuring additional steric bulk in the aryl ring.

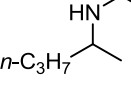
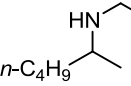
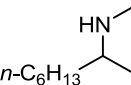
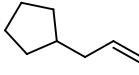
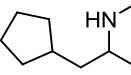
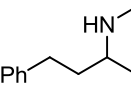
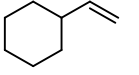
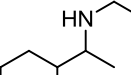
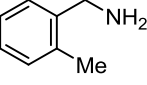
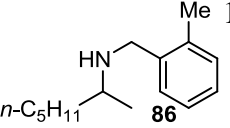
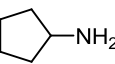
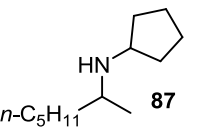
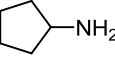
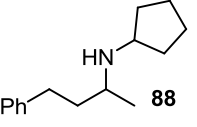
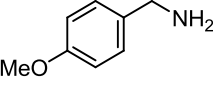
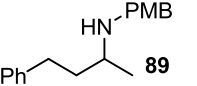
Disubstituted alkenes, such as cyclohexene and α -methylstyrene, did not react even at more forcing conditions, marking the limitation of the current reaction scope to unbranched terminal alkenes. Neither simple secondary amines, such as diethylamine or piperidine, nor any of the hydroamination products showed any traces of conversion to the corresponding tertiary amines. Therefore, the reaction is chemoselective to the

monoalkylation of primary amines. Electron-deficient arylamines (anilines) or bulky primary alkylamines (*tert*-butylamine and neopentylamine) were unreactive as well.

Table III-4. Asymmetric Intermolecular Hydroamination Catalyzed by **24a-Y**.

$$\text{R}^1\text{CH=CH}_2 + \text{R}^2\text{NH}_2 \xrightarrow[\text{C}_6\text{D}_6, 150\text{ }^\circ\text{C}]{5\text{ mol\% (R)-24a-Y}} \text{R}^2\text{CH}_2\text{CH(R}^1\text{)NH-R}^2$$

x eq.

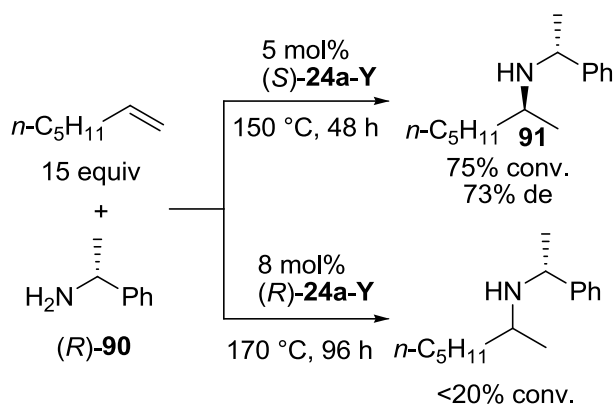
Entry	Alkene	Amine	Product	<i>x</i>	<i>t</i> , h	% Conv. ^a (% yield) ^b	% ee
1	<i>n</i> -C ₃ H ₇ CH=CH ₂	PhCH ₂ NH ₂	 81	14	72	90 (70)	61 ^c
2	<i>n</i> -C ₄ H ₉ CH=CH ₂	PhCH ₂ NH ₂	 82	13	72	90 (54)	61 ^{c,d}
3	<i>n</i> -C ₆ H ₁₃ CH=CH ₂	PhCH ₂ NH ₂	 83	15	40	97 (72)	57 ^c
4		PhCH ₂ NH ₂	 84	15	19	95 (59)	51 ^{c,d}
5	PhCH ₂ CH ₂ CH=CH ₂	PhCH ₂ NH ₂	 85	10	11	100 (72)	56 ^{c,e}
6		PhCH ₂ NH ₂	 86	12	96 ^f	25	--
7	<i>n</i> -C ₅ H ₁₁ CH=CH ₂		 87	15	80	75(63)	45
8	<i>n</i> -C ₅ H ₁₁ CH=CH ₂		 88	15	60	95 (61)	61 ^g
9	PhCH ₂ CH ₂ CH=CH ₂		 89	9	39	90 (68)	54 ^g
10	PhCH ₂ CH ₂ CH=CH ₂		 90	10	48	85 (67)	56 ^g

^b By ¹H NMR spectroscopy. ^c Isolated yield after column chromatography. ^d Determined by ¹⁹F NMR spectroscopy of the Mosher amide after removal of the benzyl group via hydrogenation. ^e (*S*)-isomer of **24a-Y** was used. ^f Determined by chiral HPLC of the *N*-

benzamide.^f 8 mol% *rac*-**24a-Y**, 170 °C. ^g Determined via ¹H NMR spectroscopy of the *O*-acetyl mandelic acid salt.

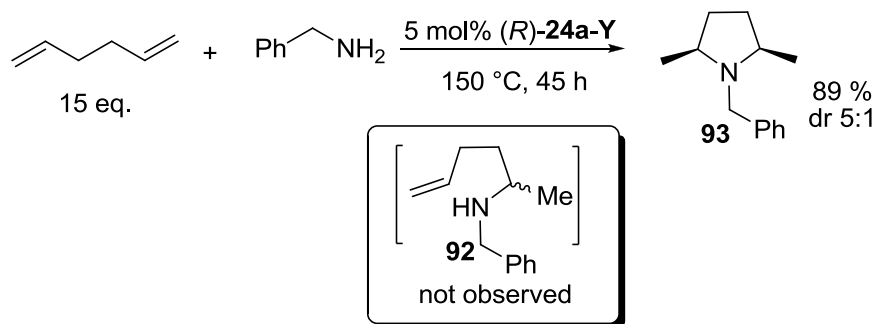
As demonstrated by work of our group^{5,6} (see also Chapter 2) and others,¹⁵ the kinetic resolution of racemic amines is a promising new direction in asymmetric hydroamination. So far, only intramolecular examples have been reported. Thus we attempted to utilize intermolecular hydroamination to resolve 1-phenylethanamine **90**. The reaction of 1-heptene with the enantiomerically pure (*R*)-**90** using (*S*)-**24a-Y** produces the hydroamination product **91** in 54% yield (75% conversion) and a diastereomeric excess of 73%, while the reaction of the apparent mismatching catalyst (*R*)-**24a-Y** led only to traces of the hydroamination product even at elevated reaction temperatures and longer reaction times (Scheme III-5). The high degree of kinetic discrimination of the matching versus the mismatching substrate-catalyst combination suggests that the intermolecular asymmetric hydroamination can become a useful tool for the kinetic resolution of racemic amines.

Scheme III-5. Stereoselective addition of (*R*)-**90** to 1-heptene using (*S*)-**24a-Y** and (*R*)-**24a-Y**.



As was noted previously, the transformation of a secondary to a tertiary amine was not achieved in the intermolecular hydroamination catalyzed by **24a-Y**. However, a tandem process involving two sequential hydroamination reactions of both primary and secondary amines can be realized if a non-conjugated diene substrate is used instead of a simple alkene. The reaction of α,ω -hexadiene with benzylamine proceeded smoothly to the *N*-benzylpyrrolidine derivative **93** with good *cis:trans* diastereoselectivity (Scheme III-6). The intermediate aminoalkene **92** was not observed over the course of reaction which is not surprising due to the significant higher rate of the intramolecular versus intermolecular alkene hydroamination. Note that in contrast to the *trans*-selective cyclization of primary aminoalkene **45e** catalyzed by **24a**^{5,6} (see also Chapter 2), the *cis*-diastereomer was favored in case of the secondary aminoalkene **92** which is also in agreement with previous findings for a cationic zirconium catalyst system.¹⁶ The plausible cyclization transition states are shown in Figure III-5. The chair-like transition state leading to the *trans*-isomer of the primary aminoalkene **45e** is less encumbered due to reduced 1,3-diaxial interactions, whereas *gauche* interactions of the *N*-substituent make the *cis*-pyrrolidine **93** the preferred product in case of the secondary aminoalkene **92**.

Scheme III-6. Sequential inter-intramolecular hydroamination catalyzed by **24a-Y**.



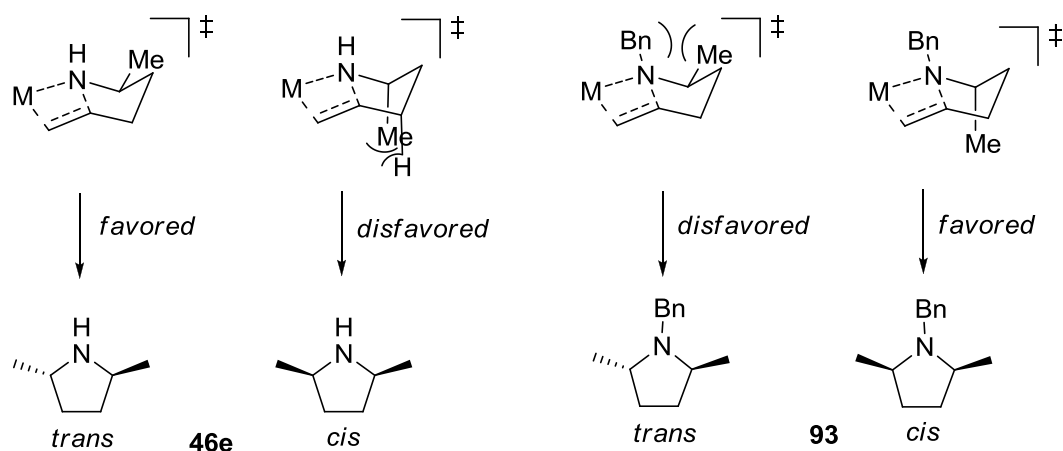
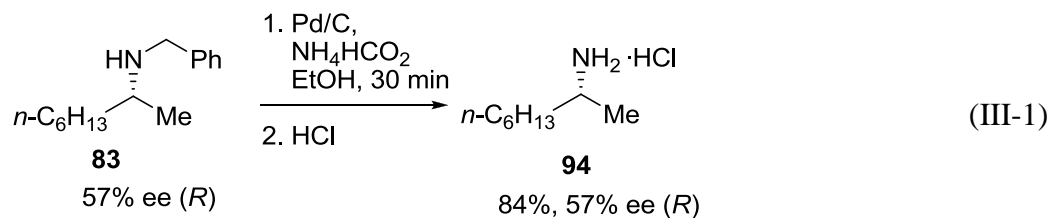


Figure III-5. Diastereoselective hydroamination/cyclization of primary and secondary aminopentenes.

It should also be noted that although primary amines cannot be obtained directly via asymmetric hydroamination catalyzed by **24-Y**, removal of the *N*-benzyl group via transfer hydrogenation yields primary amines such as **94** in good yields without racemization (Eq. III-1). Thus, benzylamine can serve as an ammonia equivalent in hydroamination catalysis.



III.2.4 Mechanistic Observations

The reaction of benzylamine with 4-phenylbutene has been chosen for kinetic studies. We have found that in the presence of an excess of alkene, the reaction is first

order with respect to amine (Figure III-6), alkene (Figure III-7), and catalyst concentration (Figure III-8).

These data suggest a participation of the amine in the catalytic steps leading from the resting state of the catalyst to the presumably rate-determining alkene insertion step. Although kinetic data for these types of reactions are scarce, it should be noted that a zero order rate dependence on the amine concentration was observed in the rare-earth metal-catalyzed intermolecular hydroamination of alkynes¹⁷ and the base-catalyzed hydroamination of ethylene with diethylamine.¹⁸

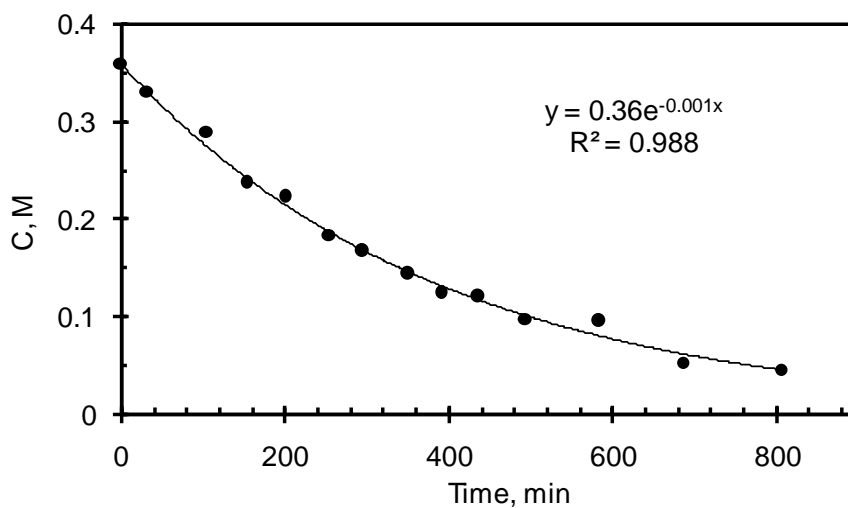


Figure III-6. Exponential amine consumption in the addition of benzylamine [$C_0 = 0.36$ M] to 4-phenyl-1-butene [$C_0 = 2.1$ M] in the presence of (*R*)-**24a-Y** [$C_0 = 0.015$ M] at 150 °C in C_6D_6 .

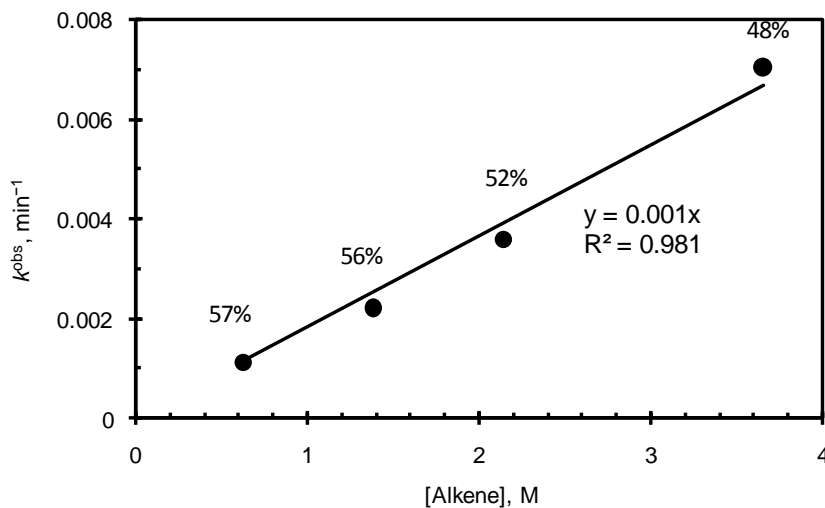


Figure III-7. Observed pseudo-first order rate constant vs. alkene concentration for the reaction of benzylamine [$C_0 = 0.17$ M] with 4-phenyl-1-butene in the presence of (*R*)-**24a-Y** [$C_0 = 0.032$ M] at 150 °C in C_6D_6 . Enantiomeric excess values for the isolated product **85** are shown as well.

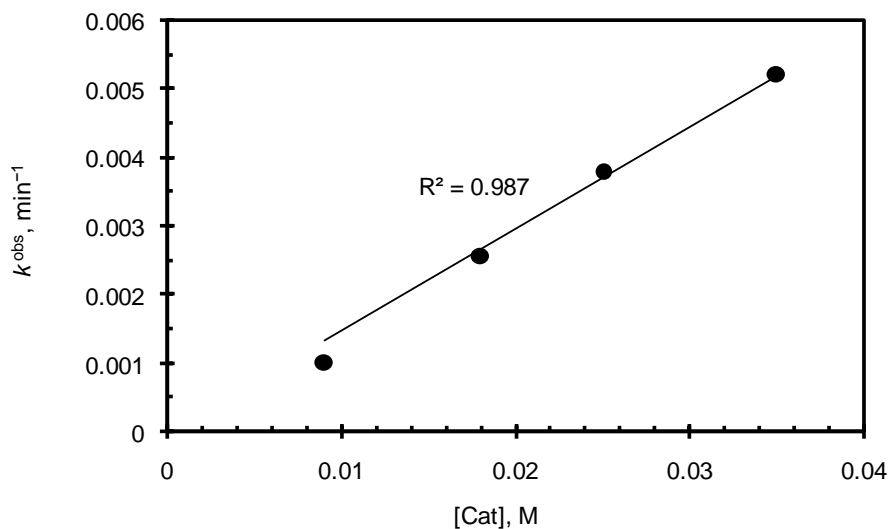


Figure III-8. Dependency of k_{obs} on the concentration of (*R*)-**24a-Y** in the addition of benzylamine [$C_0 = 0.17$ M] to 4-phenyl-1-butene [$C_0 = 1.53$ M] at 150 °C in C_6D_6 .

Another important observation is the strong inhibitive effect of the amine, as the observed first-order constant decreases significantly with increasing amine concentration (Figure III-9). This observation may seem to be in conflict with the predicted value of the amine binding (Scheme III-1) constant K^{dorm} , which should be negligible at 150 °C as shown in Table III-1. It should be kept in mind though, that the value of K^{dorm} determined for the intramolecular hydroamination at the room temperature and above describes the equilibrium between bis (amino)amide **C** and a lower coordinate and more reactive mono(amino)amide **B** (

Scheme III-7). It is very likely that at elevated temperature the “naked” amide **A** becomes the catalytically relevant species, which is in equilibrium with species **B**, and the contribution of **C** should be small according to Table III-1.

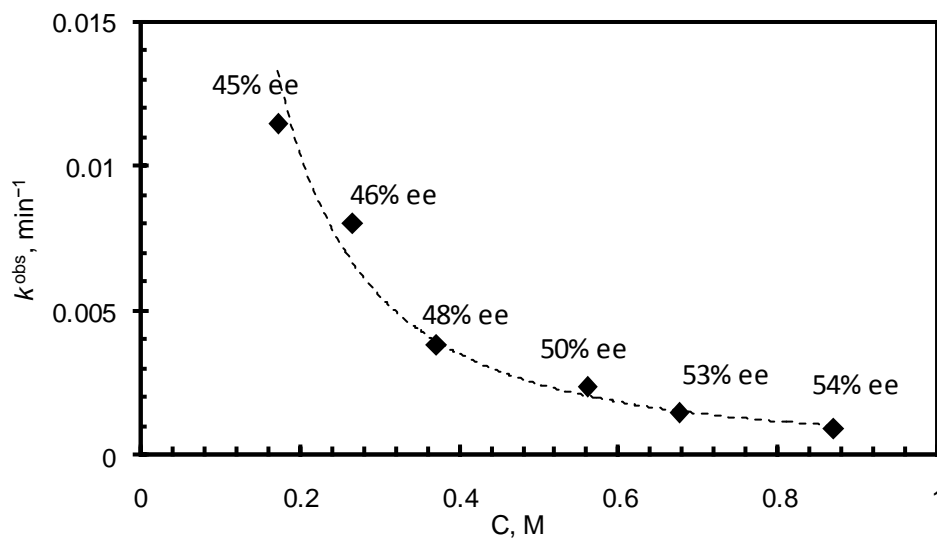
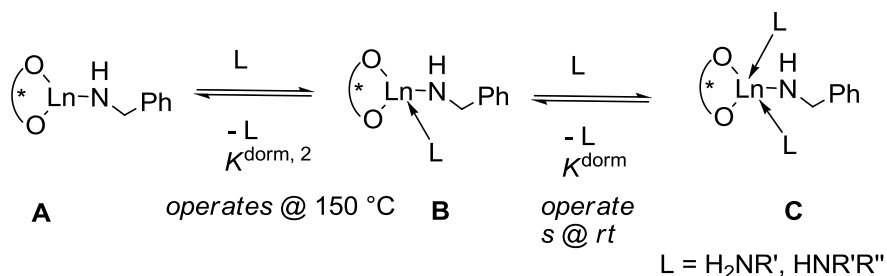


Figure III-9. Observed pseudo-first order rate constant vs. amine concentration for the reaction of benzylamine [$C_0 = 0.17\text{--}0.85 \text{ M}$] with 4-phenyl-1-butene [$C_0 = 2.1 \text{ M}$] in the

presence of (*R*)-**24a-Y** [$C_0 = 0.032$ M] at 150 °C in C_6D_6 . The line is drawn as a guide for an eye. Enantiomeric excess values for the isolated product **85** are shown as well.

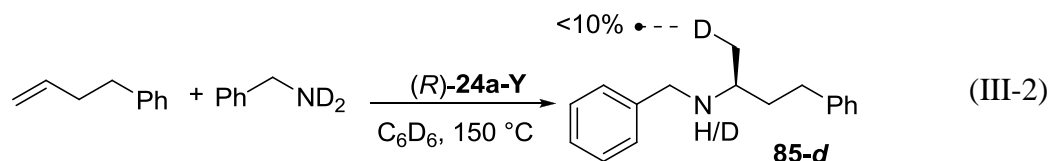
Scheme III-7. Catalytically relevant forms of **24-Ln** at various conditions.



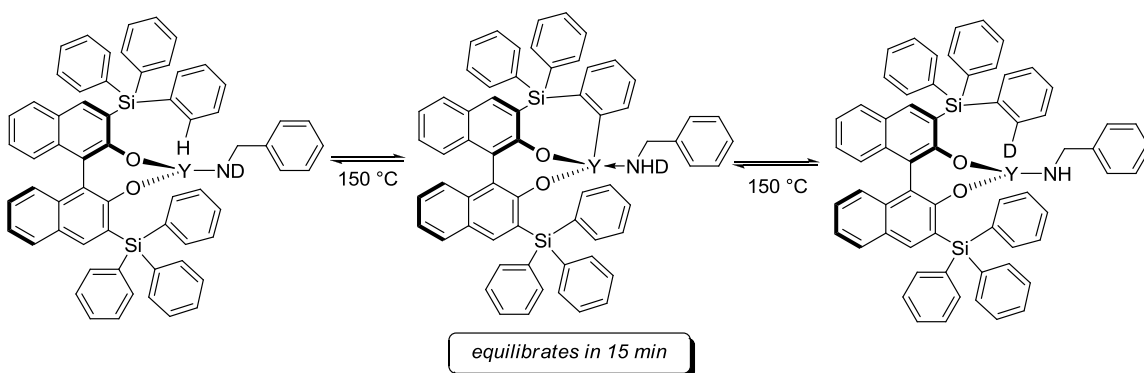
It is also important to note that the stereoselectivity of the hydroamination reaction seems to be dependent on the total amine concentration. The enantiomeric excess of **85** increases from 45 to 54% ee with a 5-fold increase of amine concentration (Figure III-9). This observation suggests that two catalytic pathways involving both species **A** (high reactivity, lower selectivity) and **B** (low reactivity, higher selectivity) are co-existing in the “net” catalytic hydroamination reaction. Similar observation has been previously made for species **B** and **C** for the intramolecular hydroamination at lower temperatures.⁶ Unfortunately, the relatively low reactivity and significant error in the determination of concentrations and conversions from the broad NMR spectra did not provide sufficient accuracy to determine of $K^{\text{dorm}, 2}$ and turnover rate constants.

An unexpected result occurred when *N,N*-dideutero-benzylamine was reacted with 4-phenylbutene in the presence of **24a-Y** (Eq. III-2). The isolated product **85-d** contained less than 10% of deuterium in the methyl group, and a large amount of deuterium was found in the re-isolated proligand **78a**. Isotope exchange apparently involved activation of the ligand aryl C–H bond. Incorporation of deuterium from the *N*-

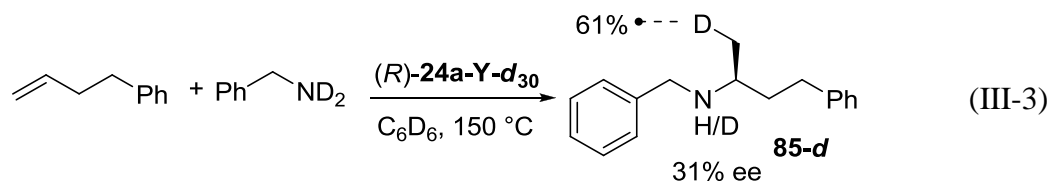
deuterated amine into the *ortho*-position of the triphenylsilyl groups was observed within minutes at 150 °C in the absence of an alkene as well. Therefore, this process is unlikely catalytically relevant (Scheme III-8).



Scheme III-8. Proposed mechanism for the deuterium scrambling.



We attempted to suppress the deuterium leakage by introducing the complex (*R*)-**24a-Y-d₃₀** with perdeuterated triphenylsilyl groups. This catalyst yielded (*R*)-**85-d** with increased, but still incomplete, deuteration of the methyl group, possibly due to the C–H activation of *N,N*-dimethylbenzylamine present in the reaction mixture. Remarkable observations were the primary kinetic isotope effect $k^{\text{obs}}(\text{NH}_2)/k^{\text{obs}}(\text{ND}_2) = 2.1$ and a significant perturbation of enantioselectivity, as **85-d** was obtained in 31% ee (Eq. III-3) versus 56% ee for **85** (Table III-4, entry 5).



These observations, along with the kinetic data, suggest that the reaction is proceeding via a proton-assisted concerted insertion-protonolysis pathway similar to transition state depicted in Scheme I-2.^{13,19} The stereo- and rate-determining steps both seem to involve the C–H bond formation. It should also be noted that the protonolysis of the metal-alkyl bond may involve either the N–H bond of an amine or the aryl C–H bond of the ligand as these two pathways cannot be discriminated unambiguously with the available data.

III.3 Conclusions and Outlook

Rare earth metal binaphtholate catalysts **24-Ln** were demonstrated to catalyze the intermolecular asymmetric hydroamination of unactivated alkenes with simple primary amines which is a first ever example of this challenging transformation. The reaction requires high temperatures (typically 150 °C) and high alkene concentrations (10–15-fold excess) to proceed. It yields the corresponding Markovnikov addition products with moderate enantiomeric excess (50–61% ee). A readily available library of tunable binaphtholate ligands allowed the determination of the necessary minimum of steric protection, which is a pre-requisite of an efficient hydroamination reaction. Coordination of the amine molecules to the Lewis acidic rare earth metal center plays a pivotal role in the catalytic performance and can be controlled by steric features of the amine, the catalyst, as well as by the reaction temperature. Mechanistic observations suggest a protonolysis-assisted rate-limiting alkene insertion, and at least two competitive catalytic pathways marked by different catalytic efficiency and selectivity are coexisting in the catalytic system. While the substrate scope remains rather narrow, the protocol can be

applied to sequential inter-intramolecular reactions as well as to the kinetic resolution of racemic amines.

Further studies with a focus on enhancing the catalytic activity by at least 1-2 orders of magnitude should follow the work presented here. Currently, the low reactivity does not allow us to perform more advanced kinetic and mechanistic studies, which should become available with more reactive systems. The observed dramatic reactivity changes driven by seemingly delicate steric manipulations are encouraging that this goal is attainable.

III.4 Experimental

General considerations. All reactions with air- or moisture sensitive materials were performed in oven (120 °C) and flame-dried glassware under an inert atmosphere of argon, employing standard Schlenk and glovebox techniques. Hexanes, pentane and THF were sparged with argon for 1 h and then passed through a column with activated alumina prior to use. Alkenes, benzene and C₆D₆ were vacuum transferred from sodium/benzophenone ketyl. Amines were distilled twice from finely powdered CaH₂.

¹H, ²H{¹H}, ¹³C{¹H} and ¹⁹F NMR spectra were recorded on Varian (300, 400, 500 MHz) spectrometers at 25 °C unless stated otherwise. Chemical shifts are reported in ppm downfield from tetramethylsilane with the signal of the deuterated (¹³C, ²H) or undeuterated (¹H) portion of the solvent as internal standard. Mass spectra were recorded on a Finnigan LCQ-DUO mass spectrometer. HPLC analysis was carried out on an Agilent 1200 series instrument with multiple wavelength detector using Chiralcel OD-H, OJ-H, and Chiralpak AS-H columns (25 × □4.6 mm). Silica gel (230–400 mesh, Sorbent

Technologies) and alumina (80–200 mesh, EMD) were used for column chromatography. Elemental analyses were performed by Robertson Microlit Laboratories, Inc., Ledgewood, NJ.

(*S*)-Mosher acid was transformed into the corresponding (*R*)-Mosher acid chloride according to a literature protocol.²⁰ Aminodiene substrate 5-amino-nona-1,8-diene (**74**) was prepared as described previously.²¹

Ligand Synthesis

(*R*)-2,2'-Bis(methoxymethoxy)-1,1'-binaphthyl,²² (*R*)-3,3'-dibromo-2,2'-dihydroxy-1,1'-binaphthyl, (*R*)-3,3'-bis(triphenylsilyl)-2,2'-dihydroxy-1,1'-binaphthyl (**78a**), (*R*)-3,3'-bis[*tert*-butyl(diphenyl)silyl]-1,1'-binaphthalene-2,2'-diol (**78c**),²³ chloro-(cyclohexyl)diphenylsilane²⁴ and chloro(4-methoxyphenyl)-diphenylsilane²⁵ were synthesized according to literature procedures. Proligand **78e** was prepared as described in Chapter 6.

(1,1'-Biphen-2-yl)diphenylchlorosilane. To a solution of 2-bromobiphenyl (4.17 g, 18.0 mmol) in Et₂O (50 mL) *t*-BuLi (1.6 M in pentane, 23 mL, 36.8 mmol) was added dropwise at –80°C. After 15 min at this temperature, dichlorodiphenylsilane (3.8 mL, 4.55 g, 18.0 mmol) was added dropwise. The resulting mixture was allowed to warm to room temperature and stirred overnight. The solvent was removed in vacuo and the residue was extracted with warm toluene (2 × 20 mL). The combined extracts were concentrated to ca 5 mL volume, and were treated with pentane (10 mL) to induce precipitation. After filtration, 3.50 g (51% yield) of the target product were obtained in

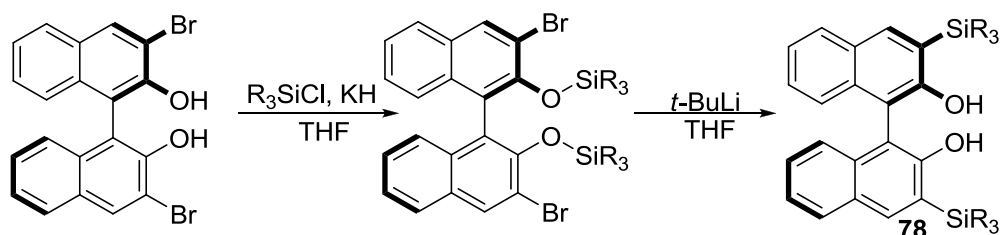
the form of small white crystals. ^1H NMR (400 MHz, CDCl_3): δ = 7.77 (d, $^3J(\text{H,H})$ = 7.6 Hz), 7.54–7.45 (m, 4H), 7.42–7.35 (m, 3H), 7.31–7.25 (m, 5H), 7.11–7.04 (m, 1H), 7.03–6.97 (m, 3H, aryl-H); $^{13}\text{C}\{^1\text{H}\}$ NMR (CDCl_3 , 75 MHz): δ = 150.2, 142.5, 137.3, 134.8, 134.1, 131.2, 130.6, 130.5, 130.0, 129.5, 127.8, 127.4, 127.0, 126.4 (aryl).

Bromobenzene- d_5 .²⁶ To a mixture of C_6D_6 (100.0 g, 1.19 mol) and anhydrous AlCl_3 (5 mg) was added dropwise bromine (61.0 mL, 90 g, 1.19 mol) while maintaining room temperature by means of a large water bath. The rate of addition was maintained low so that each drop of bromine was added to an already colorless reaction mixture. Hydrogen bromide was trapped in a large beaker with water. After the addition was complete, the mixture was washed with sodium bicarbonate (100 mL) and dried (Na_2SO_4). Fractional distillation from CaH_2 with a 15 cm Vigreux column yielded 85.0 g (44%) of the target compound as a colorless liquid, bp 14–45 °C (760 mm Hg). $^2\text{H}\{^1\text{H}\}$ NMR (76.7 MHz, CDCl_3): δ = 7.64 (br s, 2D), 7.42 (br s, 1D), 7.34 (br s, 2D); $^{13}\text{C}\{^1\text{H}\}$ NMR (125 MHz, CDCl_3): δ = 131.1 (t, $^1J(\text{C,D})$ = 24.9 Hz), 129.5 (t, $^1J(\text{C,D})$ = 23.8 Hz), 126.3 (t, $^1J(\text{C,D})$ = 24.9 Hz), 122.2 (s, CBr).

Triphenylchlorosilane- d_{15} . A solution of phenyl- d_5 magnesium bromide (15.2 mmol), prepared from magnesium turnings (4.8 g, 20 mmol) and $\text{C}_6\text{D}_5\text{Br}$ (24.7 g, 15 mmol) in THF (150 mL) was added dropwise at -10°C to a solution of SiCl_4 (0.58 mL, 5 mmol) in THF (50 mL) over 30 min. The resulting suspension was heated to a reflux, and stirred under reflux for 3 h. It was cooled to room temperature and concentrated *in vacuo*. The residue was dissolved in CH_2Cl_2 (100 mL) and filtered through a short pad of celite.

The filtrate was concentrated *in vacuo* to yield 8.4 g (49%) of product as a white solid. $^2\text{H}\{^1\text{H}\}$ NMR (76.7 MHz, $\text{CHCl}_3 + 20 \mu\text{L CDCl}_3$): $\delta = 7.80$ (br s, 6D), 7.60 (br s, 3D), 7.54 (br s, 6D); $^{13}\text{C}\{^1\text{H}\}$ NMR (125 MHz, CDCl_3): $\delta = 134.7$ (t, $^1J(\text{C,D}) = 24.7$ Hz) , 132.6 (s, CSi), 130.2 (t, $^1J(\text{C,D}) = 24.3$ Hz), 127.6 (t, $^1J(\text{C,D}) = 24.7$ Hz).

General procedure for preparation of (*R*)-78f,g and 78a-*d*₃₀.



To a solution of (*R*)-3,3'-dibromo-2,2'-dihydroxy-1,1'-binaphthyl (400 mg, 0.90 mmol) in THF (20 mL) was added KH (80 mg, 2.0 mmol) under stirring. The mixture was stirred at room temperature for 30 minutes and then the corresponding chlorosilane (1.85 mmol) was added. The mixture was stirred overnight at room temperature, cooled down to -78°C and a *t*-butyl lithium solution (2.5 mL, 3.7 mmol, 1.5 M in pentane) was added dropwise. The yellow solution was stirred for 5 min at -78°C and was then allowed to reach room temperature slowly, after which it was stirred for an additional hour. The reaction was quenched with saturated aqueous NH_4Cl (50 mL) and the product was extracted with Et_2O (3×20 mL). The combined organic layers were dried (Na_2SO_4) and concentrated. The product was purified using column chromatography on silica (hexanes/ CH_2Cl_2 70:30), to afford the pure diol proligand.

(*R*)-3,3'-Bis[benzyl(diphenyl)silyl]-2,2'-dihydroxy-1,1'-binaphthyl ((*R*)-78e).

White powder (350 mg, 47% overall yield); mp $129\text{--}132^\circ\text{C}$. ^1H NMR (400 MHz, C_6D_6):

δ = 8.11 (s, 2H), 7.7–7.59 (m, 8H), 7.38–7.32 (d, $^3J(\text{H,H}) = 7.9$ Hz, 2H), 7.31–6.90 (m, 28H), 4.83 (s, 2H, OH), 3.22 (d, $^2J(\text{H,H}) = 13.8$ Hz, 2H, CH₂), 3.16 (d, $^2J(\text{H,H}) = 13.8$ Hz, 2H, CH₂); $^{13}\text{C}\{^1\text{H}\}$ NMR (125 MHz, C₆D₆): δ = 157.2 (CO), 142.0, 139.3, 136.4, 136.35, 135.3, 135.06, 135.01, 129.82, 129.78, 129.6, 129.4, 128.5, 128.43, 128.38, 128.29, 128.14, 128.08, 124.9, 124.18, 124.14, 110.6 (aryl), 23.9 (CH₂). Anal. Calcd for C₅₈H₄₆O₂Si₂: C, 83.81; H, 5.58; Found: C, 83.71; H, 5.33.

(*R*)-3,3'-Bis[1,1'-biphenyl-2yl(diphenyl)silyl]-2,2'-dihydroxy-1,1'-binaphthyl

((*R*)-78f). White powder, 489 mg, 57% overall yield. ^1H NMR (400 MHz, C₆D₆): δ = 8.13 (s, 2H), 7.87–7.79 (m, 8H), 7.40 (d, $^3J(\text{H,H}) = 7.4$ Hz, 2H), 7.34–6.91 (m, 28H), 6.55 (t, $^3J(\text{H,H}) = 7.4$ Hz, 4H), 6.35 (t, $^3J(\text{H,H}) = 7.4$ Hz, 2H), 4.65 (s, 2H, OH); $^{13}\text{C}\{^1\text{H}\}$ NMR (100 MHz, C₆D₆): δ = 156.6 (CO), 150.5, 143.8, 141.2, 138.2, 137.5, 137.3, 136.6, 136.1, 134.5, 133.4, 130.9, 129.9, 129.7, 129.4, 129.2, 128.5, 128.1, 127.9, 127.4, 126.9, 126.5, 125.1, 124.1, 123.9, 110.4 (aryl).

(*R*)-3,3'-bis[4-Methoxyphenyl(diphenyl)silyl]-2,2'-dihydroxy-1,1'-binaphthyl

((*R*)-78g). White powder, 535 mg, 69% overall yield. ^1H NMR (400 MHz, C₆D₆): δ = 7.97 (s, 2H), 7.76 (d, $^3J(\text{H,H}) = 7.8$ Hz, 2H), 7.69 (d, $^3J(\text{H,H}) = 7.1$ Hz, 8H), 7.63 (d, $^3J(\text{H,H}) = 8.6$ Hz, 4H), 7.48–7.29 (m, 18H), 6.96 (d, $^3J(\text{H,H}) = 8.2$ Hz, 4H), 5.37 (s, 2H, OH), 3.85 (s, 6H, OCH₃); $^{13}\text{C}\{^1\text{H}\}$ NMR (100 MHz, C₆D₆): δ = 160.8, 156.5 (CO), 142.0, 137.9, 136.2, 134.7, 134.6, 129.4, 129.2, 129.0, 128.1, 127.8, 124.8, 123.93, 123.91, 123.8, 113.6, 110.7 (aryl), 55.0 (MeO).

(*R*)-3,3'-Bis[triphenylsilyl-*d*₁₅]-2,2'-dihydroxy-1,1'-binaphthyl ((*R*)-78a-*d*₃₀).

White powder, 457 mg, 61% overall yield. ¹H NMR (300 MHz, CDCl₃): δ = 8.11 (s, 2H), 7.7–7.59 (m, 8H), 7.38–7.32 (d, ³*J*(H,H) = 7.9 Hz, 2H), 7.31–6.90 (m, 28H), 4.83 (s, 2H, OH), 3.22 (d, ²*J*(H,H) = 13.8 Hz, 2H, CH₂), 3.16 (d, ²*J*(H,H) = 13.8 Hz, 2H, CH₂); ¹³C{¹H} NMR (125 MHz, CDCl₃): δ = 156.5 (CO), 142.1, 135.9 (t, ¹*J*(C,D) = 23.9 Hz), 134.7, 134.0, 129.2, 129.04, 128.99 (br t, ¹*J*(C,D) = 24 Hz), 128.2, 127.3 (t, ¹*J*(C,D) = 23.7 Hz), 123.9, 123.8, 123.7, 110.6 (aryl).

(*R*)-3,3'-Bis[cyclohexyl(diphenyl)silyl]-1,1'-binaphthalene-2,2'-diol ((*R*)-78d).*

To a solution of (*R*)-3,3'-dibromo-1,1'-binaphthalene-2,2'-diol (1.00 g, 2.25 mmol) in DMF (10 mL) was added imidazole (0.92 g, 13.5 mmol) and chloro(cyclohexyl)diphenylsilane (2.17 g, 7.2 mmol). The resulting mixture was stirred at 70 °C overnight. The reaction was quenched by addition of saturated aqueous NaHCO₃ (15 mL). The product was extracted with dichloromethane (3 × 30 mL). The combined organic layers were washed with water (3 × 10 mL), dried (Na₂SO₄), and concentrated in vacuo. Flash chromatography on a short silica pad (hexanes/CH₂Cl₂ 80:20) afforded crude bis(silylether) as a white solid (1.10 g, 50 %) which was subjected to the next reaction without further purification. The crude bis(silylether) was dissolved in THF (30 mL), and a *t*-butyllithium solution (2.9 mL, 4.64 mmol, 1.6 M in pentane) was added dropwise at –60 °C. The yellow solution was stirred for 5 min at –60 °C and was then allowed to reach room temperature slowly, after which it was stirred for an additional

* The procedure was developed by Hiep Nguyen in the Hultsch group.

hour. The reaction was quenched with saturated aqueous NH_4Cl (50 mL) and the product was extracted with Et_2O (3×20 mL). The combined organic layers were dried (Na_2SO_4), concentrated and the product was purified using column chromatography on silica (hexanes/ CH_2Cl_2 80:20), to afford the pure product as a white powder (0.71 g, 45 % overall yield); mp 26–65°C; ^1H NMR (500 MHz, C_6D_6): δ = 8.20 (s, 2H), 7.85–7.77 (m, 8H), 7.46–7.42 (m, 2H), 7.35–7.26 (m, 12H), 7.15–7.08 (m, 2H), 7.06–6.98 (m, 4H, aryl-H), 4.59 (s, 2H, OH), 2.09–2.02 (m, 4H, CH_2), 1.95–1.89 (m, 2H, CH_2), 1.77–1.71 (m, 6H, CH_2), 1.44–1.34 (m, 8H, CH_2), 1.25–1.16 (m, 2H, CH, Cy); $^{13}\text{C}\{^1\text{H}\}$ NMR (125 MHz, C_6D_6): δ = 157.3 (CO), 141.4, 136.5, 135.2, 135.1, 135.0, 129.9, 124.2, 124.0, 110.3 (aryl), 29.2 (CH_2), 29.1 (CH_2), 28.84 (CH_2), 28.78 (CH_2), 27.4 (CH_2), 24.7 (CH, Cy). Anal. Calcd for $\text{C}_{56}\text{H}_{54}\text{O}_2\text{Si}_2$: C, 82.51; H, 6.68; N, 7.93. Found: C, 82.31; H, 6.69.

(*R*)-3,3'-Bis[methyl(diphenyl)silyl]-2,2'-dihydroxy-1,1'-binaphthyl ((*R*)-78j).

To a solution of (*R*)-2,2'-bis(methoxymethoxy)-1,1'-binaphthyl (2.34 g, 6.25 mmol) in Et_2O (100 mL) was added *n*-butyl lithium (8.0 mL, 12.8 mmol, 1.6 M solution in hexanes) under stirring. The mixture was stirred at room temperature for 4 h and was then cooled to -78°C . Then HMPA (2.3 mL, 13 mmol), THF (50 mL) and methyldiphenylchlorosilane (2.7 mL, 12.8 mmol) were added in this order. The mixture was then allowed to warm slowly to room temperature, after which it was stirred for an additional 2 h. The reaction was quenched with saturated aqueous NH_4Cl (100 mL) and the organic layer was collected. The aqueous layer was extracted with Et_2O (50 mL). The combined organic layers were concentrated without drying. The residue was dissolved in CHCl_3 (30 mL) and then EtOH (30 mL) and 12 N HCl (5 mL) were added. The resulting

homogeneous solution was refluxed overnight, cooled down and concentrated. The residue was partitioned between water (100 mL) and CH₂Cl₂ (50 mL). The organic layer was collected and the residue was extracted with CH₂Cl₂ (50 mL). The combined organic layers were dried (Na₂SO₄) and concentrated. The product was purified using column chromatography on silica (hexanes/CH₂Cl₂ 70:30), to afford the pure diol proligand as a white powder (2.59 g, 61% overall yield); mp 122–124°C. ¹H NMR (500 MHz, CDCl₃): δ = 7.90 (s, 2H), 7.75–7.72 (m, 2H), 7.62–7.59 (m, 8H), 7.43–7.34 (m, 12 H, aryl-H), 7.32–7.28 (m, 4H), 7.18–7.16 (m, 2H, aryl-H), 5.19 (s, 2H, OH), 0.98 (s, 6H, CH₃); ¹³C{¹H} NMR (125 MHz, CDCl₃): δ = 156.9 (CO), 140.8, 136.43, 136.41, 135.3, 135.2, 134.7, 129.4, 129.34, 129.32, 129.0, 128.0, 127.9, 127.8, 125.5, 124.0, 123.8, 110.4 (aryl), –2.9 (CH₃). Anal. Calcd for C₄₆H₃₈O₂Si₂: C, 81.37; H, 5.64; Found: C, 81.34; H, 5.75.

Complex Synthesis

Rare earth metal precursors [Ln(*o*-C₆H₄CH₂NMe₂)₃] (Ln= Y, Lu, Sc),²⁷ [La{CH(C₆H₅)NMe₂}₃],²⁸ [Y{N(SiHMe₂)₂}₃(THF)₂]²⁹ and [La{N(SiHMe₂)₂}₃]³⁰ were synthesized according to the published protocols. Complexes **24a-Y**, **24b-Y**, **24a-Sc**, **24a-Lu**⁶ and **80a-Y**⁶ were prepared as reported previously. Complexes **24h-Y** and **24i-Y** were prepared by Hiep Nguyen and Hyeunjoo Lee in the Hultsch group and the synthesis will be reported elsewhere in due course.

Complex Syntheses – General Procedure for the NMR-Scale Preparation. To a mixture of diol proligand **78** (0.05 mmol) and the rare earth metal precursor (0.05 mmol) was added C₆D₆ (490 mg, 500 μL). The mixture was shaken vigorously and then

left for 5 minutes at room or slightly elevated temperature. Clean quantitative conversion to the diolate complex was confirmed by NMR spectroscopy. Aliquots of the resulting complex solution were used directly for the catalytic experiments.

(*R*)-[Y{BINOL-TBDPS}(*o*-C₆H₄CH₂NMe₂)(Me₂NCH₂Ph)] ((*R*)-24c-Y**).** To a mixture of (*R*)-**78c** (45.6 mg, 0.06 mmol) and [Y(*o*-C₆H₄CH₂NMe₂)₃] (29.3 mg, 0.06 mmol) was added toluene-*d*₈ (0.55 mL). The mixture was kept at room temperature for 1 h. ¹H and ¹³C NMR spectra showed clean formation of (*R*)-**24c-Y**, which was used directly for catalytic experiments. ¹H NMR (500 MHz, toluene-*d*₈, 0 °C): δ = 8.55 (s, 1H; aryl-H), 8.52 (s, 1H), 8.07 (d, ³*J*(H,H) = 8.1 Hz, 2H), 7.95 (m, 1H), 7.93 (m, 1H), 7.89–7.84 (m, 4H), 7.57 (d, ³*J*(H,H) = 6.9 Hz, 1H), 7.55 (d, ³*J*(H,H) = 8.1 Hz, 1H), 7.49–7.46 (m, 1H), 7.34–6.94 (m, 21H, including 5H from free PhCH₂NMe₂), 6.77 (d, ³*J*(H,H) = 7.6 Hz, 1H), 6.62 (d, ³*J*(H,H) = 6.9 Hz, 2H, aryl-H), 3.33 (d, ²*J*(H,H) = 13.9 Hz, 1H, *o*-C₆H₄CH₂NMe₂), 3.09 (br s, 2H, PhCH₂NMe₂), 2.52 (d, ²*J*(H,H) = 13.2 Hz, 1H, *o*-C₆H₄CH₂NMe₂), 1.44 (s, 9H, *t*-Bu), 1.41 (s, 3H, *o*-C₆H₄CH₂NMe₂), 1.39 (s, 9H, *t*-Bu), 1.29 (s, 3H, PhCH₂NMe₂), 1.24 (s, 3H, PhCH₂NMe₂), 1.19 (s, 3H, *o*-C₆H₄CH₂NMe₂); ¹³C{¹H} NMR (125 MHz, toluene-*d*₈, 0 °C): δ = 181.9 (d, ¹*J*(Y,C) = 52.6 Hz), 163.4 (CO), 162.8 (CO), 148.3, 141.4, 141.2, 139.3, 138.9, 138.3, 137.18, 137.15, 136.83, 136.75, 136.71, 136.68, 136.5, 131.9, 130.0, 129.7, 129.3, 129.24, 129.23, 128.82, 128.76, 128.6, 128.4, 128.3, 128.2, 128.1, 127.7, 127.5, 127.4, 127.2, 126.0, 125.8, 125.6, 125.5, 122.6, 122.4, 117.18, 117.15 (aryl), 68.0 (*o*-C₆H₄CH₂NMe₂), 58.0 (C₆H₅CH₂NMe₂), 46.8 (N(CH₃)₂), 44.2 (N(CH₃)₂), 40.4 (C₆H₅CH₂NMe₂), 40.3 (C₆H₅CH₂NMe₂), 29.7 (C(CH₃)₃), 29.4 (C(CH₃)₃), 19.7 (C(CH₃)₃), 19.6 (C(CH₃)₃).

(*R*)-[Y{BINOL-SiPh₂Cy}(*o*-C₆H₄CH₂NMe₂)(Me₂NCH₂Ph)] ((*R*)-24d-Y). To a mixture of (*R*)-78d (48.9 mg, 0.06 mmol) and [Y(*o*-C₆H₄CH₂NMe₂)₃] (29.3 mg, 0.06 mmol) was added C₆D₆ (0.55 mL). The mixture was kept at room temperature for 1 h. ¹H and ¹³C NMR spectra showed clean formation of (*R*)-24d-Y, which was used directly for catalytic experiments. ¹H NMR (500 MHz, C₆D₆): δ = 8.48 (s, 1H), 8.47 (s, 1H), 7.95–7.91 (m, 2H), 7.85–7.82 (m, 6H), 7.72–7.68 (m, 1H), 7.65 (d, ³J(H,H) = 6.9 Hz, 1H), 7.60 (d, ³J(H,H) = 8.0 Hz, 1H), 7.55 (m, 2H), 7.34–6.94 (m, 22H, including 5H from free PhCH₂NMe₂), 6.80 (d, ³J(H,H) = 7.3 Hz, 1H), 6.67 (m, 2H; aryl-H), 3.13 (d, ²J(H,H) = 13.9 Hz, 1H, *o*-C₆H₄CH₂NMe₂), 2.99 (d, ²J(H,H) = 13.2 Hz, 1H, PhCH₂NMe₂), 2.93 (d, ²J(H,H) = 13.2 Hz, 1H, PhCH₂NMe₂), 2.33 (d, ²J(H,H) = 13.9 Hz, 1H, *o*-C₆H₄CH₂NMe₂), 2.20–2.12 (m, 8H), 1.70–0.60 (m, 10H), 1.40–0.26 (m, 14H), 1.05–0.97 (m, 8H); ¹³C NMR (125 MHz, C₆D₆): δ = 181.5 (d, ¹J(Y,C) = 46.5 Hz), 163.5 (CO), 162.5 (CO), 148.8, 140.1, 140.0, 139.2, 139.1, 138.3, 136.9, 136.7, 136.2, 135.72, 135.67, 135.57, 135.46, 131.8, 130.3, 129.3, 129.2, 129.1, 128.8, 128.7, 128.51, 128.45, 128.38, 128.29, 127.9, 127.17, 126.0, 125.8, 125.6, 125.5, 124.8, 122.54, 122.48, 116.9, 116.9 (aryl), 67.6 (CH₂), 57.9 (CH₂ of coordinated amine), 46.1 (N(CH₃)₂), 43.6 (N(CH₃)₂), 40.5 (C₆H₅CH₂NMe₂), 40.2 (C₆H₅CH₂NMe₂), 29.0 (CH₂), 28.9 (CH₂), 28.8 (CH₂), 28.6 (CH₂), 28.5 (CH₂), 27.9 (CH₂), 27.8 (CH₂), 27.21 (CH₂), 27.20 (CH₂, Cy), 23.7 (CH), 23.4 (CH, Cy).

(R)-[Y(Binol-SiBnPh₂)(*o*-C₆H₄CH₂NMe₂)]·(Me₂NCH₂Ph) ((R)-24e-Y).^{*} To a mixture of **(R)-78e** (53.3 mg, 64.1 μmol) and [Y(*o*-C₆H₄CH₂NMe₂)₃] (31.5 mg, 64.1 μmol) C₆D₆ (0.60 mL) C₆D₆ was added and the mixture was sealed and shaken vigorously in the screw cap NMR tube. ¹H and ¹³C NMR showed clean formation of **(R)-24e-Y**, which was used directly for catalytic experiments. ¹H NMR (400 MHz, C₆D₆): δ = 8.41 (s, 1H), 8.38 (s, 1H), 7.90–7.50 (m, 11H), 7.40–6.70 (m, 41H, aryl-H), 3.81 (d, ²J(H,H) = 12.9 Hz, 1H, CH₂Si), 3.73 (d, ²J(H,H) = 13.3 Hz, 1H, CH₂Si), 3.26 (br s, 5H, CH₂, PhCH₂NMe₂ and CH₂Si), 3.01 (d, ²J(H,H) = 13.1 Hz, 1H, CH₂), 2.85 (d, ²J(H,H) = 13.3 Hz, 1H, CH₂), 2.82 (d, ²J(H,H) = 13.3 Hz, 1H, CH₂), 2.47 (d, ²J(H,H) = 14.1 Hz, 1H, CH₂), 2.09 (s, 10H, N(CH₃)₂), 1.85 (s, 3H, C₆H₄CH₂NMe₂), 1.35 (s, 5H), 1.22 (s, 3H, NCH₃, *o*-C₆H₄CH₂NMe₂); ¹³C{¹H} NMR (100 MHz, C₆D₆): δ = 181.3 (d, ¹J(C,Y) = 52.4 Hz), 163.9, 162.2, 148.7, 140.7, 140.4, 140.0, 139.5, 139.4, 139.2, 138.3, 136.9, 136.8, 136.5, 136.1, 135.8, 135.6, 135.2, 129.8, 129.6, 129.5, 129.4, 129.3, 129.1, 128.9, 128.8, 128.63, 128.59, 128.54, 128.48, 128.3, 128.2, 128.1, 127.8, 127.5, 127.4, 127.3, 127.0, 126.19, 126.15, 126.07, 125.6, 124.84, 124.82, 124.6, 122.6, 122.5, 118.0, 116.5 (aryl), 67.4 (CH₂), 64.5 (C₆H₄CH₂NMe₂), 58.4 (PhCH₂NMe₂), 45.8 (N(CH₃)₂), 45.3 (N(CH₃)₂), 44.5 (N(CH₃)₂), 40.6 (N(CH₃)₂), 24.0 (SiCH₂).

(R)-[Y{BINOL-SiPh₂(*o*-biphenyl)}(*o*-C₆H₄CH₂NMe₂)(Me₂NCH₂Ph)] ((R)-24f-Y). To a mixture of **(R)-78f** (30.5 mg, 0.032 mmol) and [Y(*o*-C₆H₄CH₂NMe₂)₃] (15.7 mg, 0.032 mmol) was added C₆D₆ (0.50 mL). The mixture was kept at room temperature for

^{*} The synthesis was performed by Stephan Audörsch in the Hultzsich group.

0.5 h. ^1H and ^{13}C NMR spectra showed clean formation of (*R*)-**78f**-Y, which was used directly for catalytic experiments. ^1H NMR (400 MHz, C_6D_6 , 7 °C): δ = 8.36 (s, 1H), 8.35 (s, 1H), 8.26 (d, $^3J(\text{H,H})$ = 7.0 Hz, 1H), 8.14 (d, $^3J(\text{H,H})$ = 7.4 Hz, 2H), 7.94 (m, 2H), 7.82 (d, $^3J(\text{H,H})$ = 7.4 Hz, 2H), 7.77–7.73 (m, 3H), 7.59 (d, $^3J(\text{H,H})$ = 6.3 Hz, 1H), 7.52 (d, $^3J(\text{H,H})$ = 7.8 Hz, 1H), 7.47 (d, $^3J(\text{H,H})$ = 7.8 Hz, 1H), 7.46–6.75 (m, 42H, Aryl-H), 3.01 (s, 2H), 2.93 (d, $^2J(\text{H,H})$ = 14.1 Hz, 1H, *o*- $\text{C}_6\text{H}_4\text{CH}_2\text{NMe}_2$), 2.62 (d, $^2J(\text{H,H})$ = 14.1 Hz, 1H, *o*- $\text{C}_6\text{H}_4\text{CH}_2\text{NMe}_2$), 1.59 (s, 3H, *o*- $\text{C}_6\text{H}_4\text{CH}_2\text{NMe}_2$), 1.17 (br s, 6H, $\text{PhCH}_2\text{NMe}_2$), 1.14 (s, 3H, *o*- $\text{C}_6\text{H}_4\text{CH}_2\text{NMe}_2$); $^{13}\text{C}\{^1\text{H}\}$ NMR (100 MHz, C_6D_6 , 7 °C): δ = 181.9 (d, $^1J(\text{Y,C})$ = 52.3 Hz), 163.3, 162.4, 150.4, 150.3, 148.7, 144.7, 144.4, 141.6, 141.1, 140.0, 139.3, 139.2, 138.7, 137.5, 137.3, 137.04, 136.99, 136.8, 136.7, 136.6, 136.24, 136.20, 136.16, 134.8, 134.0, 131.9, 131.8, 130.9, 130.1, 129.8, 129.1, 128.5, 127.5, 127.2, 126.8, 126.7, 125.9, 125.6, 122.3, 117.4, 116.6 (aryl), 67.5 (*o*- $\text{C}_6\text{H}_4\text{CH}_2\text{NMe}_2$), 57.8 ($\text{C}_6\text{H}_5\text{CH}_2\text{NMe}_2$), 45.7 ($\text{N}(\text{CH}_3)_2$), 44.8 ($\text{N}(\text{CH}_3)_2$), 40.5 ($\text{C}_6\text{H}_5\text{CH}_2\text{NMe}_2$), 40.1 ($\text{C}_6\text{H}_5\text{CH}_2\text{NMe}_2$).

(*R*)-[Y{BINOL-SiPh₂C₆H₄OMe}(*o*-C₆H₄CH₂NMe₂)(Me₂NCH₂Ph)] ((*R*)-24g**-Y).** To a mixture of (*R*)-**78g** (33.0 mg, 0.039 mmol) and [Y(*o*-C₆H₄CH₂NMe₂)₃] (19.3 mg, 0.039 mmol) was added toluene-*d*₈ (0.55 mL). The mixture was kept at room temperature for 0.5 h. ^1H and ^{13}C NMR spectra showed clean formation of (*R*)-**24g**-Y, which was used directly for catalytic experiments. ^1H NMR (400 MHz, toluene-*d*₈, 0 °C): δ = 8.44 (s, 1H), 8.40 (s, 1H), 8.00–7.89 (m, 8H), 7.82 (d, $^3J(\text{H,H})$ = 8.1 Hz, 2H), 7.54–7.49 (m, 2H), 7.41 (d, $^3J(\text{H,H})$ = 7.8 Hz, 2H), 7.26–6.85 (m, 36H), 6.67 (d, $^3J(\text{H,H})$ = 7.8 Hz, 2H), 6.61–6.55 (m, 6H, aryl-H), 3.16 (m, 10H), 3.08 (d, $^2J(\text{H,H})$ = 13.3 Hz, 1H, *o*-

$\text{C}_6\text{H}_4\text{CH}_2\text{NMe}_2$), 2.43 (d, $^2J(\text{H,H}) = 13.3$ Hz, 1H, $o\text{-C}_6\text{H}_4\text{CH}_2\text{NMe}_2$), 1.47 (s, 3H, $o\text{-C}_6\text{H}_4\text{CH}_2\text{NMe}_2$), 1.31 (s, 3H, $\text{PhCH}_2\text{NMe}_2$), 1.25 (s, 3H, $\text{PhCH}_2\text{NMe}_2$), 1.17 (s, 3H, $o\text{-C}_6\text{H}_4\text{CH}_2\text{NMe}_2$); $^{13}\text{C}\{^1\text{H}\}$ NMR (100 MHz, toluene- d_8 , 0 °C): $\delta = 182.0$ (d, $^1J(\text{Y,C}) = 53.0$ Hz), 163.0, 162.7, 161.0, 160.9, 148.5, 141.5, 139.9, 139.4, 139.3, 138.6, 138.6, 138.43, 138.36, 137.2, 137.0, 136.89, 136.85, 136.77, 136.50, 136.46, 136.4, 136.2, 131.9, 131.8, 116.5, 114.2, 114.1, 114.0, 113.9 (aryl), 68.0 ($o\text{-C}_6\text{H}_4\text{CH}_2\text{NMe}_2$), 58.0 ($\text{C}_6\text{H}_5\text{CH}_2\text{NMe}_2$), 54.3, 46.5 ($\text{N}(\text{CH}_3)_2$), 44.1 ($\text{N}(\text{CH}_3)_2$), 40.4 ($\text{C}_6\text{H}_5\text{CH}_2\text{NMe}_2$), 40.3 ($\text{C}_6\text{H}_5\text{CH}_2\text{NMe}_2$).

General Procedure for the NMR-Scale Preparation of compounds 80j-Y and 80a-La. To a mixture of diol proligand **78** (0.05 mmol) and the rare earth metal trisamide precursor **79** (0.05 mmol) was added C_6D_6 (490 mg, 500 μL). The mixture was shaken vigorously and then heated to 60 °C until no further changes were detected. Approximately 85–90% conversion to the diolate complexes **80-Ln** was confirmed by ^1H NMR spectroscopy. The solution was then subjected to a freeze-drying procedure in order to remove $\text{HN}(\text{SiHMe}_2)_2$, and the residue was re-dissolved in C_6D_6 . Aliquots of the resulting complex solution were used directly for the catalytic experiments.

(R)-[La{BINOL-SiPh₃}N(SiHMe₂)₂] ((R)-80a-La). To a mixture of (*R*)-**78a** (19.5 mg, 0.024 mmol) and $[\text{La}\{\text{N}(\text{SiHMe}_2)_2\}_3]$ (13.0 mg, 0.024 mmol) was added C_6D_6 (0.55 mL). The mixture was kept at 60 °C for 4 h. ^1H and ^{13}C NMR spectra showed 95% conversion to (*R*)-**80a-La**, which was used directly for catalytic experiments after freeze-drying and re-dissolving in C_6D_6 . ^1H NMR (500 MHz, C_6D_6): $\delta = 8.14$ (s, 2H), 7.82 (d,

$^3J(\text{H,H}) = 6.6$ Hz, 12H), 7.58–7.52 (m, 4H), 7.12–6.92 (m, 22H, aryl-H), 3.79 (sept, $^3J(\text{H,H}) = 2.9$ Hz, 2H, SiH), -0.09 (d, $^3J(\text{H,H}) = 2.9$ Hz, 6H, CH_3SiH), -0.29 (d, $^3J(\text{H,H}) = 2.9$ Hz, 6H, CH_3SiH); $^{13}\text{C}\{^1\text{H}\}$ NMR (125 MHz, C_6D_6): $\delta = 165.7$ (CO), 139.4, 138.4, 137.1, 129.7, 129.1, 128.9, 128.7, 128.3, 127.9, 126.8, 126.2, 121.7 (aryl), 2.0 (SiCH_3), 1.9 (SiCH_3).

(*R*)-[Y{BINOL-SiPh₂Me}(N(SiHMe₂)₂)(THF)₂] ((*R*)-80j-Y). To a mixture of (*R*)-78j (25.9 mg, 0.038 mmol) and [Y(N(SiHMe₂)₂)₃(THF)₂] (24.0 mg, 0.038 mmol) was added C_6D_6 (0.55 mL). The mixture was kept at 60 °C for 4 h. The ^1H NMR spectrum showed 80% conversion to (*R*)-80j-Y, which was used directly for catalytic experiments after freeze-drying and re-dissolving in C_6D_6 . ^1H NMR (300 MHz, C_6D_6): 7.99 (s, 2H), 7.85–7.82 (m, 6H), 7.40–6.88 (m, 20H, aryl-H), 4.92 (sept, $^3J(\text{H,H}) = 2.9$ Hz, 2H, SiH), 3.37 (br m, 4H, THF), 3.18 (br m, 4H, THF), 1.27 (s, 6H, $2\text{CH}_3\text{SiPh}_2$), 0.88 (br m, 8H THF), 0.28 (d, $^3J(\text{H,H}) = 2.7$ Hz, 6H, CH_3SiH), 0.14 (d, $^3J(\text{H,H}) = 2.7$ Hz, 6H, CH_3SiH).

General procedure for intermolecular hydroamination reactions. In the glovebox, a screw cap NMR tube was charged with an appropriate amine (0.2 mmol), alkene (3 mmol) and a solution of catalyst (0.1 M in C_6D_6 or toluene-*d*₈, 0.1 mL, 10.0 μmol , 5 mol%). The tube was then sealed, removed from the glovebox and placed into the thermostated oil bath. Flame-sealed NMR tubes were used for more volatile substrates, such as 1-hexene or 1-pentene. The progress of the reaction was monitored by

^1H NMR spectroscopy. After completion of the reaction, the mixture was concentrated in vacuo and purified by column chromatography on a 3 cm height pad of silica or alumina.

Determination of enantiomeric excess through diastereomeric salt formation (Method A).

The isolated hydroamination product (25 μmol) and (*R*)-*O*-acetylmandelic acid (5.8 mg, 30 μmol) were dissolved in CDCl_3 or CD_3CN (0.6 mL). The solution was allowed to stay 30 minutes at room temperature, and then the ^1H NMR spectrum was recorded. Integration of CH_3CHNH signals of the diastereomeric salts afforded the enantiomeric excess value for the hydroamination product.

Determination of enantiomeric excess via debenzylation/Mosher amide formation sequence (Method B).

The isolated *N*-benzyl hydroamination product (0.03 mmol) was dissolved in absolute ethanol (2 mL). Ammonium formate (32 mg, 0.5 mmol) and 10% palladium on charcoal (11 mg, 0.01 mmol) were added, and the mixture was stirred under reflux for 30 min. The precipitate was filtered off, and the filtrate was treated with 1M HCl (2 mL). The volatiles were removed *in vacuo*, the residue was dissolved in water (5 mL) and then water was removed under reduced pressure. The residue was then dissolved in CDCl_3 or C_6D_6 (0.6 mL) and filtered through a short pad of celite into the NMR tube containing Mosher chloride (10 mg, 0.04 mmol) and DIPEA (26 mg, 0.2 mmol). A ^{19}F NMR spectrum was then taken to determine the enantiomeric excess. The absolute configuration of heptan-2-amine was determined using literature data.¹¹ The enantiomeric excess for *N*-benzyl-4-phenylbutan-2-amine determined using method **B** was identical to that obtained via methods **A** and **C**.

Determination of enantiomeric excess via chiral HPLC (Method C).

N-benzoylation of isolated hydroamination product. The hydroamination product (0.1 mmol) was dissolved in CH₂Cl₂ (1 mL) and then DIPEA (26 mg, 0.2 mmol) and benzoyl chloride (21 mg, 0.15 mmol) were added. The mixture was stirred at room temperature for 3 h. Volatiles were removed *in vacuo* and the residue was partitioned between Et₂O (2 mL) and 2M NaOH (2 mL). The resulting emulsion was stirred for 2 h and then the organic layer was separated, washed with brine (1 mL), dried (Na₂SO₄), and concentrated. The residue was purified by flash chromatography on silica (CH₂Cl₂), if necessary, or was directly subjected to a chiral HPLC analysis.

N-(1-Methylhexyl)benzamide. Prepared from **77**. Colorless oil. ¹H NMR (400 MHz, CDCl₃, 65 °C): δ = 7.52–7.16 (m, 10H, aryl-H), 4.87 (d, ²J(H,H) = 15.2 Hz, 1H, CHN), 4.45 (d, ²J(H,H) = 15.2 Hz, 1H, CHN), 3.94 (br s, 1H, CHN), 1.56 (br s, 1H), 1.31–1.05 (br s, 10H), 0.82 (m, 4H); ¹³C NMR could not be acquired as signals are very broad and obscure due to rotamer interconversion at 25–80 °C. HPLC (AS-H, hexane/2-propanol 90:10, 1 mL/min): *t*_R 23.3 min (*R*-isomer), 22.3 min (*S*-isomer).

N-(1-Methyl-3-phenylpropyl)benzamide. Prepared from **85**. Colorless oil. ¹H NMR (400 MHz, CDCl₃, 65 °C): δ = 8.10 (d, ³J(H,H) = 7.8 Hz, 1H), 7.60–6.96 (m, 14H, aryl-H), 4.71 (br s, 1H, CHN), 4.58 (d, ²J(H,H) = 14.5 Hz, 1H, CHN), 2.49 (br s, 2H), 1.99 (br s, 1H), 1.17 (br s, 1H), 1.19 (d, ³J(H,H) = 6.3 Hz, 3H, CH₃); ¹³C NMR could not be acquired as signals are very broad and obscure due to rotamer interconversion at 25–80

°C. HPLC (AS-H, hexane/2-propanol 90:10, 1 mL/min): t_R 25.5 min (*R*-isomer), 45.5 min (*S*-isomer).

(*R*)-*N*-Benzylheptan-2-amine (77).³¹ Prepared from 1-heptene and benzylamine according to Table III-2, entry 1. Purified by column chromatography on alumina (hexanes/EtOAc 100:0.6). Yield 24.8 mg, 65%; colorless oil, 58% ee. ¹H NMR (400 MHz, CDCl₃): δ = 7.33–7.30 (m, 4H) 7.25–7.21 (m, 1H, aryl-H), 3.82 (d, ²*J*(H,H) = 13.0 Hz, 1H, PhCH₂NH), 3.73 (d, ²*J*(H,H) = 13.0 Hz, 1H, PhCH₂NH), 2.68 (sext, ³*J*(H,H) = 6.2 Hz, 1H, CHNH), 1.50–1.41 (m, 1H, CH₂) 1.34–1.23 (m, 8H, CH₂ and NH), 1.07 (d, ³*J*(H,H) = 6.2 Hz, 3H, CH₃CHNH), 0.89 (t, ³*J*(H,H) = 6.9 Hz, 3H, CH₃CH₂); ¹³C{¹H} NMR (100 MHz, CDCl₃): δ = 140.9 (*C*_{ipso}), 128.4, 128.1, 126.8 (aryl), 52.5 (CH(CH₃)NH), 51.4 (CH₂NH), 37.1 (CH₂), 32.1 (CH₂), 25.7 (CH₂), 22.7 (CH₂), 20.3 (CH₃CHNH), 14.1 (CH₃CH₂). ¹⁹F NMR of Mosher amide of heptan-2-amine (470 MHz, C₆D₆, 60 °C): δ = –69.35 (*S*-isomer, minor), –69.42 (*R*-isomer, major).

(*R*)-*N*-Benzylpentan-2-amine (81).³² Prepared from 1-pentene and benzylamine according to Table III-4, entry 1. Purified by column chromatography on alumina (pentane/EtOAc 100:0.6). Yield 22.8 mg, 70%; colorless oil, 61% ee. ¹H NMR (500 MHz, CDCl₃): δ = 7.36–7.30 (m, 4H), 7.25–7.21 (m, 1H, aryl-H), 3.82 (d, ²*J*(H,H) = 13.0 Hz, 1H, PhCH₂NH), 3.73 (d, ²*J*(H,H) = 13.0 Hz, 1H, PhCH₂NH), 2.69 (sext, ³*J*(H,H) = 6.3 Hz, 1H, CHNH), 1.51–1.43 (m, 2H, CH₂ and NH), 1.37–1.28 (m, 3H, CH₂), 1.07 (d, ³*J*(H,H) = 6.1 Hz; 3H, CH₃CHNH), 0.89 (t, ³*J*(H,H) = 6.9 Hz; 3H, CH₃CH₂); ¹³C{¹H} NMR (125 MHz, CDCl₃): δ = 140.9 (*C*_{ipso}), 128.4, 128.1, 126.8 (aryl), 52.3 (CH(CH₃)NH), 51.4 (CH₂NH), 39.4 (CH₂), 20.3 (CH₂), 19.2 (CH₃CHNH)

14.3 (CH₃CH₂). ¹⁹F NMR of Mosher amide of pentan-2-amine (470 MHz, CDCl₃, 60 °C): δ = −69.43 (*S*-isomer, minor), −69.53 (*R*-isomer, major).

(*S*)-*N*-Benzylhexan-2-amine (82).³³ Prepared from 1-hexene and benzylamine according to Table III-4, entry 2. Purified by column chromatography on alumina (pentane/EtOAc 100:0.6). Yield 19.2 mg, 54%; colorless oil, 61% ee. ¹H NMR (500 MHz, CDCl₃): δ = 7.32–7.30 (m, 4H) 7.25–7.21 (m, 1H, aryl-H), 3.82 (d, ²*J*(H,H) = 13.0 Hz, 1H, PhCH₂NH), 3.73 (d, ²*J*(H,H) = 13.0 Hz, 1H, PhCH₂NH), 2.68 (sext, ³*J*(H,H) = 6.3 Hz, 1H, CHNH), 1.65–1.46 (m, 2H, CH₂ and NH), 1.36–1.26 (m, 5H, CH₂), 1.08 (d, ³*J*(H,H) = 6.4 Hz, 3H, CH₃CHNH), 0.89 (t, ³*J*(H,H) = 6.9 Hz, 3H, CH₃CH₂); ¹³C{¹H} NMR (125 MHz, CDCl₃): δ = 140.6 (C_{ipso}), 128.4, 128.2, 126.9 (aryl), 52.5 (CH(CH₃)NH), 51.3 (CH₂NH), 36.7 (CH₂), 28.2 (CH₂), 22.9 (CH₂), 20.2 (CH₃CHNH), 14.1 (CH₃CH₂). ¹⁹F NMR of Mosher amide of hexan-2-amine (470 MHz, CDCl₃, 65 °C): δ = −69.39 (*S*-isomer, major), −69.47 (*R*-isomer, minor).

(*R*)-*N*-Benzyl-octan-2-amine (83).³⁴ Prepared from 1-hexene and benzylamine according to Table III-4, entry 3. Purified by column chromatography on alumina (hexanes/EtOAc 100:0.4). Yield 29.5 mg, 72%; colorless oil, 57% ee. ¹H NMR (500 MHz, CDCl₃): δ = 7.33–7.30 (m, 4H), 7.25–7.21 (m, 1H, aryl-H), 3.82 (d, ²*J*(H,H) = 13.0 Hz, 1H, PhCH₂NH), 3.73 (d, ²*J*(H,H) = 13.0 Hz, 1H, PhCH₂NH), 2.68 (sext, ³*J*(H,H) = 6.3 Hz, 1H, CHNH), 1.50–1.46 (m, 2H, CH₂ and NH), 1.33–1.25 (m, 9H, CH₂), 1.07 (d, ³*J*(H,H) = 6.4 Hz, 3H, CH₃CHNH), 0.87 (t, ³*J*(H,H) = 6.8 Hz, 3H, CH₃CH₂); ¹³C{¹H} NMR (125 MHz, CDCl₃): δ = 140.9 (C_{ipso}), 128.4, 128.1, 126.8 (aryl), 52.5 (CH(CH₃)NH), 51.4 (CH₂NH), 37.1 (CH₂), 31.9 (CH₂), 29.5 (CH₂), 26.0

(CH₂), 22.6 (CH₂), 20.3 (CH₃CHNH) 14.1 (CH₃CH₂). ¹⁹F NMR of Mosher amide of octan-2-amine (470 MHz, C₆D₆, 60 °C): δ = −69.25 (*S*-isomer, minor), −69.32 (*R*-isomer, major).

(*S*)-*N*-Benzyl-1-cyclopentylpropan-2-amine (84).³⁵ Prepared from allylcyclopentane and benzylamine according to Table III-4, entry 4. Purified by column chromatography on alumina (hexanes/EtOAc 100:0.6). Yield 24.0 mg, 59%; colorless oil, 51% ee. ¹H NMR (400 MHz, CDCl₃): δ = 7.34–7.29 (m, 4H), 7.26–7.21 (m, 1H, aryl-H), 3.83 (d, ²*J*(H,H) = 12.9 Hz, 1H, PhCH₂NH), 3.72 (d, ²*J*(H,H) = 12.9 Hz, 1H, PhCH₂NH), 2.69 (sext, ³*J*(H,H) = 6.4 Hz, 1H, CHNH), 1.88–1.78 (m, 1H), 1.77–1.67 (m, 2H), 1.63–1.54 (m, 2H), 1.53–1.43 (m, 4H), 1.36–1.25 (m, 1H), 1.20 (br s, 1H, NH), 1.08 (d, ³*J*(H,H) = 6.3 Hz, 3H, CH₃CHNH), 1.06–1.00 (m, 1H); ¹³C{¹H} NMR (100 MHz, CDCl₃): δ = 140.9 (*C*_{ipso}), 128.4, 128.1, 126.8 (aryl), 51.8 (CH(CH₃)NH), 51.4 (CH₂NH), 43.9 (CH₂), 37.1 (CH), 33.1 (CH₂), 32.8 (CH₂), 25.1 (CH₂), 25.0 (CH₂), 20.7 (CH₃). ¹⁹F NMR of Mosher amide of 1-cyclopentylpropan-2-amine (470 MHz, C₆D₆, 60 °C): δ = −69.25 (*S*-isomer, major), −69.30 (*R*-isomer, minor).

(*S*)-*N*-Benzyl-4-phenylbutan-2-amine (85).³¹ Prepared from 4-phenyl-1-butene and benzylamine according to Table III-4, entry 5. Purified by column chromatography on silica (CH₂Cl₂/7 M NH₃ in MeOH 100:1). Yield 32.4 mg, 72%; colorless oil, 56% ee. ¹H NMR (500 MHz, CDCl₃): δ = 7.34–7.22 (m, 7H), 7.19–7.16 (m, 3H, aryl-H), 3.82 (d, ²*J*(H,H) = 13.0 Hz, 1H, PhCH₂NH), 3.73 (d, ²*J*(H,H) = 12.9 Hz, 1H, PhCH₂NH), 2.69 (sext, ³*J*(H,H) = 6.3 Hz, 1H, CHNH), 2.70–2.61 (m, 2H), 1.85–1.78 (m, 1H), 1.71–1.64 (m, 1H), 1.49 (br s, 1H, NH), 1.14 (d, ³*J*(H,H) = 6.4 Hz, 3H, CH₃CHNH); ¹³C{¹H} NMR

(125 MHz, CDCl₃): δ = 142.5 (*C*_{ipso}), 140.8 (*C*_{ipso}), 128.35, 128.32, 128.30, 128.1, 126.8, 125.7 (aryl) 52.0 (CH(CH₃)NH), 51.3 (CH₂NH), 38.7 (CH₂), 32.3 (CH₂), 20.4 (CH₃).

(*R*)-*N*-(2-Methylbenzyl)heptan-2-amine (86). Prepared from 1-heptene and *o*-methylbenzylamine according to Table III-4, entry 7. Purified by column chromatography on alumina (hexanes/EtOAc 100:0.6). Yield 25.6 mg, 63%; colorless oil, 45% ee. ¹H NMR (400 MHz, CDCl₃): δ = 7.30–7.27 (m, 1H), 7.20–7.05 (m, 3H, aryl-H), 3.79 (d, ²*J*(H,H) = 12.9 Hz, 1H, ArCH₂NH), 3.70 (d, ²*J*(H,H) = 12.9 Hz, 1H, ArCH₂NH), 2.69 (sext, ³*J*(H,H) = 6.7 Hz, 1H, CHNH), 2.35 (s, 3H, CH₃C₆H₄), 1.51–1.41 (m, 1H; CH₂) 1.34–1.23 (m, 8H, CH₂ and NH), 1.10 (d, ³*J*(H,H) = 6.3 Hz, 3H, CH₃CHNH), 0.88 (t, ³*J*(H,H) = 6.6 Hz, 3H, CH₃CH₂); ¹³C{¹H} NMR (100 MHz, CDCl₃): δ = 138.8, 136.2 (*C*_{ipso}), 130.2, 128.5, 126.9, 125.9 (aryl), 53.2 (CH(CH₃)NH), 49.2 (CH₂NH), 37.1 (CH₂), 32.1 (CH₂), 25.7 (CH₂), 22.7 (CH₂), 20.4 (CH₃CHNH), 18.9 (CH₃C₆H₃), 14.1 (CH₃CH₂). ¹⁹F NMR of Mosher amide of heptan-2-amine (470 MHz, C₆D₆, 60 °C): δ = –69.35 (*S*-isomer, minor), –69.42 (*R*-isomer, major).

(*S*)-*N*-(Heptan-2-yl)cyclopentanamine (87). Prepared from 1-heptene and cyclopentanamine according to Table III-4, entry 8. Purified by column chromatography on alumina (hexanes/EtOAc 100:0.4). Yield 22.3 mg, 61%; colorless oil, 61% ee. ¹H NMR (500 MHz, CDCl₃): δ = 3.14 (quint, ³*J*(H,H) = 7.1 Hz, 1H, (CH₂)₄CHNH), 2.64 (sext, ³*J*(H,H) = 6.2 Hz, 1H, CHNH), 1.90–1.80 (m, 2H), 1.68–1.62 (m, 2H), 1.55–1.47 (m, 2H), 1.43–1.37 (m, 1H), 1.32–1.20 (m, 10H), 1.01 (d, ³*J*(H,H) = 6.3 Hz, 3H, CH₃CHNH), 0.89 (t, ³*J*(H,H) = 7.0 Hz, 3H, CH₃CH₂); ¹³C{¹H} NMR (125 MHz, CDCl₃): δ = 57.0 ((CH₂)₄CHN), 51.4 (CH(CH₃)NH), 37.5 (CH₂), 33.9 (CH₂), 33.4 (CH₂), 32.1

(CH₂), 25.8 (CH₂), 23.86 (CH₂), 23.85 (CH₂), 22.9 (CH₂), 20.8 (CH₃CHNH), 14.1 (CH₃CH₂); MS (ESI): m/z 184 [M + H]⁺.

(S)-N-(4-Phenylbutan-2-yl)cyclopentanamine (88). Prepared from 4-phenyl-1-butene and cyclopentanamine according to Table III-4, entry 9. Purified by column chromatography on silica (CH₂Cl₂/7 M NH₃ in MeOH 100:1). Yield 29.5 mg, 68%; colorless oil, 54% ee. ¹H NMR (400 MHz, CDCl₃): δ = 7.29–7.25 (m, 3H), 7.19–7.15 (m, 2H, aryl-H), 3.15 (quint, ³J(H,H) = 7.0 Hz, 1H, (CH₂)₄CHNH), 2.71 (sext, ³J(H,H) = 6.3 Hz, 1H, CHNH), 2.67–2.58 (m, 2H), 1.88–1.72 (m, 3H), 1.70–1.61 (m, 3H), 1.56–1.45 (m, 2H), 1.28–1.18 (m, 3H), 1.09 (d, ³J(H,H) = 6.3 Hz, 3H, CH₃CHNH); ¹³C{¹H} NMR (100 MHz, CDCl₃): δ = 142.5 (C_{ipso}), 129.31, 129.29, 128.31, 125.7 (aryl), 56.9 ((CH₂)₄CHNH), 51.0 (CH(CH₃)NH), 39.0 (CH₂), 33.9 (CH₂), 33.4 (CH₂), 32.4 (CH₂), 23.86 (CH₂), 23.84 (CH₂), 20.8 (CH₃); MS (ESI): m/z 218 [M + H]⁺.

(S)-N-(p-Methoxybenzyl)-4-phenylbutan-2-amine (89).³⁶ Prepared from 4-phenyl-1-butene and *p*-methoxy benzylamine according to Table III-4, entry 10. Purified by column chromatography on silica (CH₂Cl₂/7 M NH₃ in MeOH 100:1). Yield 36.0 mg, 67%; colorless oil, 56% ee. ¹H NMR (400 MHz, CDCl₃): δ = 7.29–7.15 (m, 7H), 6.85 (d, ³J(H,H) = 8.6 Hz, 2H, aryl-H), 3.79 (s, 3H, CH₃O), 3.76 (d, ²J(H,H) = 12.5 Hz, 1H, ArCH₂NH), 3.66 (d, ²J(H,H) = 12.5 Hz, 1H, ArCH₂NH), 2.72 (sext, ³J(H,H) = 6.3 Hz, 1H, CHNH), 2.68–2.59 (m, 2H), 1.84–1.76 (m, 1H), 1.70–1.61 (m, 1H), 1.43 (br s, 1H, NH), 1.13 (d, ³J(H,H) = 6.3 Hz, 3H, CH₃CHNH); ¹³C{¹H} NMR (100 MHz, CDCl₃): δ = 158.5 (CH₃OC), 142.5 (C_{quart}), 132.9 (C_{quart}), 129.3, 128.33, 128.31, 125.7, 113.8 (aryl), 55.3 (CH₃O), 51.9 (CH(CH₃)NH), 50.7 (CH₂NH), 38.7 (CH₂), 32.3 (CH₂), 20.4 (CH₃).

^{19}F NMR of Mosher amide of 4-phenylbutan-2-amine (470 MHz, C_6D_6 , 60 °C): δ = -69.22 (*S*-isomer, major), -69.35 (*R*-isomer, minor).

(*S*)-*N*-((*R*)-1-Phenylethyl)heptan-2-amine (91).³⁷ Prepared from 1-heptene (294 mg, 3.0 mmol) and (*R*)-1-phenylethanamine **90** (24.2 mg, 0.20 mmol) using (*S*)-**24a**-Y according to Scheme III-5. Purified by column chromatography on alumina (Hexanes/EtOAc 100:0.6). Yield 21.8 mg, 50%; colorless oil, 73% de. ^1H NMR (500 MHz, CDCl_3 ,) signals of major (*S,R*) isomer: δ = 7.34–7.30 (m, 4H) 7.25–7.22 (m, 1H, aryl-H), 3.91 (q, $^3J(\text{H,H})$ = 6.6 Hz, 1H, $\text{PhCH}(\text{CH}_3)\text{NH}$), 2.39 (sext, $^3J(\text{H,H})$ = 6.1 Hz, 1H, CHNH) 1.35 (d, $^3J(\text{H,H})$ = 6.6 Hz, 3H, $\text{PhCH}(\text{CH}_3)\text{NH}$), 1.35–1.15 (m, 9H, CH_2 and NH), 1.01 (d, $^3J(\text{H,H})$ = 6.1 Hz; 3H, CH_3CHNH), 0.86 (t, $^3J(\text{H,H})$ = 7.1 Hz, 3H, CH_3CH_2); signals of minor (*R,R*) isomer: δ = 2.54–2.49 (m, 1H, CHNH), 0.96 (d, $^3J(\text{H,H})$ = 6.4 Hz, 3H, CH_3CHNH), 0.89 (t, $^3J(\text{H,H})$ = 6.8 Hz, 3H, CH_3CH_2), other signals are overlapping with the signals of the major isomer; $^{13}\text{C}\{^1\text{H}\}$ NMR (125 MHz, CDCl_3) signals of major isomer: δ = 146.0 (C_{ipso}), 128.3, 126.7, 126.5 (aryl), 54.8 ($\text{PhCH}(\text{CH}_3)\text{NH}$), 49.6 (CHNH), 38.1 (CH_2), 31.9 (CH_2), 25.7 (CH_2), 25.1 (CH_3), 22.6 (CH_2), 20.0 ($\text{PhCH}(\text{CH}_3)\text{NH}$), 14.0 (CH_3CH_2). ^{19}F NMR of Mosher amide of heptan-2-amine (470 MHz, C_6D_6 , 60 °C): δ -69.35 (*S*-isomer, major), -69.42 (*R*-isomer, minor).

***N*-Benzyl-2,5-dimethylpyrrolidine (93).**³⁸ Prepared from 1,5-hexadiene (246 mg, 3.0 mmol) and benzylamine (21.4 mg, 0.20 mmol) according to Scheme III-6. Purified by column chromatography on alumina (hexanes). Colorless oil, yield 32.8 mg, 87%; mixture of *cis:trans* isomers 5:1. ^1H NMR (400 MHz, CDCl_3) signals of the *cis*-isomer: δ = 7.41–7.19 (m, 5H, aryl-H), 3.74 (s, 2H, $\text{C}_6\text{H}_5\text{CH}_2$), 2.59 (m, 2H), 1.77 (m,

2H), 1.35 (m, 2H), 1.05 (d, $^3J(\text{H,H}) = 6.3$ Hz, 6H, 2 CH₃); signals of the *trans*-isomer: $\delta =$ 3.83 (d, $^2J(\text{H,H}) = 13.7$ Hz, 1H, PhCH₂NH), 3.51 (d, $^2J(\text{H,H}) = 13.7$ Hz, 1H, PhCH₂NH), 3.00 (m, 2H), 0.97 (d, $^3J(\text{H,H}) = 6.2$ Hz, 6H, 2 CH₃), other signals are overlapped with the signals of *cis*-isomer; $^{13}\text{C}\{^1\text{H}\}$ NMR (100 MHz, CDCl₃) signals of *cis*-isomer: $\delta =$ 139.3, (C_{ipso}), 129.3, 127.9, 126.6 (aryl), 59.5 (CH(CH₃)NH), 55.1 (CH₂NH), 31.3 (CH₂), 20.6 (CH₂).

(*R*)-Octan-2-amine hydrochloride (94).³⁹ (*R*)-*N*-benzyloctan-2-amine **83** (19.0 mg, 87 μmol) was dissolved in ethanol (2 mL), and ammonium formate (64 mg, 1.0 mmol) and 10% palladium on charcoal (22 mg, 20 μmol) were added, and the mixture was stirred under reflux for 30 min. The precipitate was filtered off, and the filtrate was treated with 1M HCl (2 mL). The volatiles were removed *in vacuo*, the residue was dissolved in water (5 mL) and then water was removed under reduced pressure. The residue was then treated with CHCl₃ (5 mL), the precipitate was filtered off and the filtrate was concentrated *in vacuo* to yield 12.0 mg (73 μmol , 84% yield) of the target compound as an off-white waxy solid. ^1H NMR (400 MHz, CDCl₃): $\delta =$ 8.31 (br s, 3H, NH₃), 3.30 (m, 1H, CHNH), 1.84–1.74 (m, 1H, CH₂), 1.65–1.55 (m, 1H, CH₂), 1.45–1.20 (m, 11H, CH₃CHNH and CH₂), 0.86 (t, $^3J(\text{H,H}) = 6.3\text{Hz}$, 3H, CH₃CH₂); $^{13}\text{C}\{^1\text{H}\}$ NMR (100 MHz, CDCl₃): $\delta =$ 48.5 (CH(CH₃)NH), 34.9 (CH₂), 31.5 (CH₂), 28.8 (CH₂), 25.5 (CH₂), 22.5 (CH₂), 18.7 (CH₃CHNH), 14.0 (CH₃CH₂).

III.5 References

- (1) Müller, T. E.; Hultzs, K. C.; Yus, M.; Foubelo, F.; Tada, M. *Chem. Rev.* **2008**, *108*, 3795-3892.
- (2) Reznichenko, A. L.; Hultzs, K. C. In *Chiral Amine Synthesis: Methods, Developments and Applications*; 1st ed.; Nugent, T., Ed.; Wiley-VCH: 2010, p 341-376.
- (3) Reznichenko, A. L.; Hultzs, K. C. In *Science of Synthesis, Stereoselective Synthesis*; De Vries, J. G., Molander, G. A., Evans, P. A., Eds.; Thieme: 2010; Vol. 1, p 689-729.
- (4) Zhang, Z.; Lee, S. D.; Widenhoefer, R. A. *J. Am. Chem. Soc.* **2009**, *131*, 5372-5373.
- (5) Reznichenko, A. L.; Hampel, F.; Hultzs, K. C. *Chem. Eur. J.* **2009**, *15*, 12819-12827.
- (6) Gribkov, D. V.; Hultzs, K. C.; Hampel, F. *J. Am. Chem. Soc.* **2006**, *128*, 3748-3759.
- (7) Gribkov, D. V.; Hultzs, K. C. *Chem. Commun.* **2004**, 730-731.
- (8) Li, Y.; Marks, T. J. *Organometallics* **1996**, *15*, 3770-3772.
- (9) Giardello, M. A.; Conticello, V. P.; Brard, L.; Gagné, M. R.; Marks, T. J. *J. Am. Chem. Soc.* **1994**, *116*, 10241-10254.
- (10) Kim, Y. K.; Livinghouse, T.; Bercaw, J. E. *Tetrahedron Lett.* **2001**, *42*, 2933-2935.
- (11) Sullivan, G. R.; Dale, J. A.; Mosher, H. S. *J. Org. Chem.* **1973**, *38*, 2143-2147.
- (12) Hultzs, K. C.; Gribkov, D. V.; Hampel, F. *J. Organomet. Chem.* **2005**, *690*, 4441-4452.
- (13) Gagné, M. R.; Stern, C. L.; Marks, T. J. *J. Am. Chem. Soc.* **1992**, *114*, 275-294.
- (14) Reznichenko, A. L.; Hultzs, K. C. *Struct. Bond.* **2010**, *137*, 1-48.
- (15) Zhang, Z.; Bender, C. F.; Widenhoefer, R. A. *J. Am. Chem. Soc.* **2007**, *129*, 14148-14149.
- (16) Gribkov, D. V.; Hultzs, K. C. *Angew. Chem. Int. Ed.* **2004**, *44*, 5542-5546.
- (17) Ryu, J.-S.; Li, G. Y.; Marks, T. J. *J. Am. Chem. Soc.* **2003**, *125*, 12584-12605.
- (18) Khedkar, V.; Tillack, A.; Benisch, C.; Melder, J.-P.; Beller, M. *J. Mol. Catal. A: Chem.* **2005**, *241*, 175-183.
- (19) Manna, K.; Kruse, M. L.; Sadow, A. D. *ACS Catal.* **2011**, *1*, 1637-1642.
- (20) Smith, P. M.; Thomas, E. J. *J. Chem. Soc., Perkin Trans. 1* **1998**, 3541-3556.
- (21) Kim, J. Y.; Livinghouse, T. *Org. Lett.* **2005**, *7*, 4391-4393.
- (22) Totland, K. M.; Boyd, T. J.; Lavoie, G. G.; Davis, W. M.; Schrock, R. R. *Macromolecules* **1996**, *29*, 6114-6125.
- (23) Maruoka, K.; Ito, T.; Araki, Y.; Shirasaka, T.; Yamamoto, H. *Bull. Chem. Soc. Jpn.* **1988**, *61*, 2975-2976.

- (24) Nadvornik, M.; Handlir, K.; Holecek, J.; Klikorka, J.; Lycka, A. Z. *Chem.* **1980**, *20*, 343.
- (25) Gilman, H.; Dunn, G. E. *J. Am. Chem. Soc.* **1951**, *73*, 3404-3407.
- (26) Kozhushkov, S. I.; Yufit, D. S.; Ackermann, L. *Org. Lett.* **2008**, *10*, 3409-3412.
- (27) Gribkov, D. V., PhD thesis, Universität Erlangen-Nürnberg, 2005.
- (28) Behrle, A. C.; Schmidt, J. A. R. *Organometallics* **2011**, *30*, 3915-3918.
- (29) Anwander, R.; Runte, O.; Eppinger, J.; Gerstberger, G.; Herdtweck, E.; Spiegler, M. *Dalton Trans.* **1998**, 847-858.
- (30) Yuen, H. F.; Marks, T. J. *Organometallics* **2009**, *28*, 2423-2440.
- (31) Peterson, M.; Bowman, A.; Morgan, S. *Synth. Commun.* **2002**, *32*, 443-448.
- (32) Yu, Z.; Alesso, S.; Pears, D.; Worthington, P. A.; Luke, R. W. A.; Bradley, M. J. *Chem. Soc., Perkin Trans. I* **2001**, 1947-1952.
- (33) Andres, C.; Nieto, J.; Pedrosa, R.; Villamanan, N. *J. Org. Chem.* **1996**, *61*, 4130-4135.
- (34) Lopez, R. M.; Fu, G. C. *Tetrahedron* **1997**, *53*, 16349-16354.
- (35) Khedkar, V.; Tillack, A.; Beller, M. *Org. Lett.* **2003**, *5*, 4767-4770.
- (36) Sugiura, M.; Kumahara, M.; Nakajima, M. *Chem. Commun.* **2009**, 3585-3587.
- (37) Alvaro, G.; Savoia, D.; Valentinetti, M. R. *Tetrahedron* **1996**, *52*, 12571-12586.
- (38) Quinet, C.; Jourdain, P.; Hermans, C.; Ates, A.; Lucas, I.; Markó, I. E. *Tetrahedron* **2008**, *64*, 1077-1087.
- (39) Nugent, T. C.; El-Shazly, M.; Wakchaure, V. N. *J. Org. Chem.* **2008**, *73*, 1297-1305.

IV Chapter 4. Asymmetric Hydroamination of Alkenes Catalyzed by C_1 -Symmetric Rare Earth Metal and Zirconium Diolates

IV.1 Introduction

In context of development of efficient synthetic protocols^{1,2} towards various amines, the hydroamination reaction, which is arguably one the simplest approaches, has found significant attention.^{3,4} An area of particular interest has been the generation of new stereogenic centers during the C–N bond forming process, but the development of chiral catalysts for the asymmetric hydroamination of alkenes (AHA) has remained mostly challenging (see also Chapter 1).⁵⁻⁷

Organo rare earth metal complexes were already shown to excel in a plethora of catalytic transformations⁸ and the hydroamination of alkenes is possibly the most exciting application of organo rare earth metal complexes (see section I.2.1). Thus, rare earth metal binaphtholate complexes **24-Ln** (Figure IV-1) are the most active and among the most stereoselective catalysts for aminoalkene hydroamination/cyclization^{9,10} and kinetic resolution of racemic aminoalkenes^{9,11} (see also Chapter 2). Furthermore, complexes **24-Ln** are the only catalysts to date which are able to perform stereocontrolled *intermolecular* hydroamination of unactivated alkenes with simple amines¹² (see also Chapter 3). Although the latter transformation catalyzed by **24-Ln** shows the general feasibility of the approach itself, it still requires rather forcing reaction conditions and suffers from moderate selectivity and a need to employ a large excess of alkene (see Chapter 3). It may be envisioned that at least some of these drawbacks result from the high Lewis acidity of the electron-deficient binaphtholate complex **24-Ln** that leads to a

stronger binding of exogenous amine molecules to the metal center and results in diminished catalytic activity¹³ (see also Chapter 3).

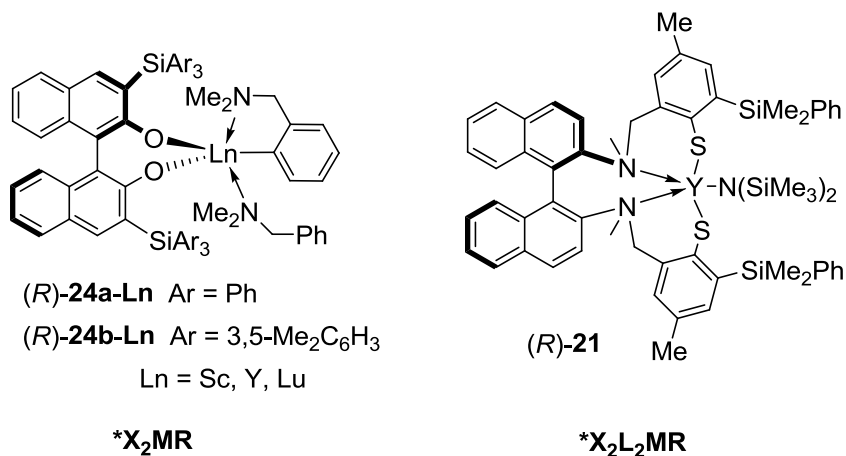


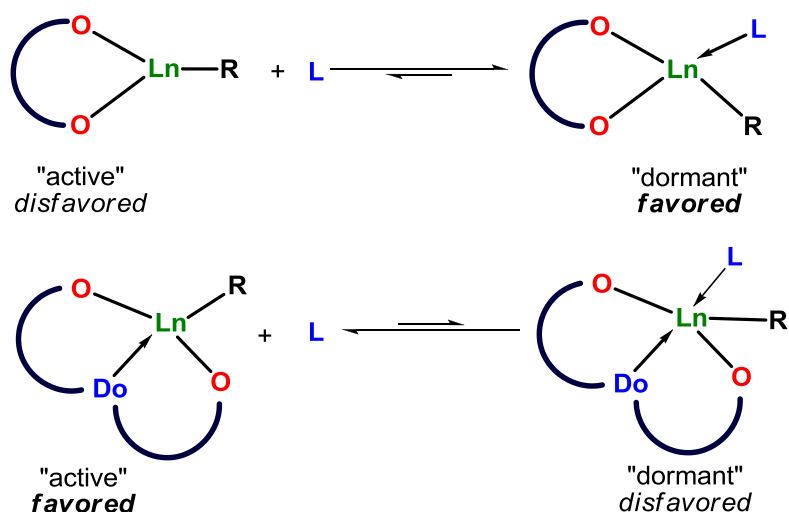
Figure IV-1. Rare earth metal catalysts **(R)-24-Ln** and **(R)-21**.

We have demonstrated in Chapter 3 that the undesired amine binding can be reduced by elevation of the reaction temperature as well as by controlling the steric features of the ligand backbone. In fact, an interplay of these two factors resulted in the high catalytic activity of a number of complexes from that series. We conceived that the formation of an amine-bound “dormant” species can also be reduced by introducing an additional L-type donor site to the chiral diolate backbone (Scheme IV-1).

It should also be noted that employing tridentate diolate ligand systems can also potentially lead to better enantioselectivity control. On the other hand, an additional donor site introduced in proximity to the metal center reduces its electrophilicity and can therefore result in decreased reactivity in alkene insertion reactions. An interplay of these two factors, as well as the steric features of the novel diolate ligand can be detrimental in both catalytic performance and stereoselectivity and should be carefully considered. For example, aminothiophenolate catalyst system **(R)-21**, featuring tetradentate chiral ligand

of the L_2X_2 type (Figure IV-1) was significantly less reactive, but also in some cases more selective than catalyst (*R*)-**24-Y** in the hydroamination/cyclization of aminopentenes (see section I.2.1).¹⁴ We proposed that the “intermediate” ligand of the LX_2 type can still benefit from additional ligand denticity and yet allow the appreciable level of the reactivity comparable to that of (*R*)-**24-Y**.

Scheme IV-1. Shifting the equilibrium between the “dormant” and active species by introducing an electron-donating site to the diolate backbone.



In this chapter we will describe our studies on the synthesis of novel chiral C_1 -symmetric rare earth and group 4 metal (amino)diolate complexes and their application in asymmetric intra- and intermolecular hydroamination of unactivated alkenes with simple amines.

IV.2 Results and Discussion

IV.2.1 Ligand Design and Preparation

We chose chiral C_1 -symmetric NOBIN-derived diolate complexes (Figure IV-2) as model system for the novel diolate ligand concept shown in Scheme IV-1.

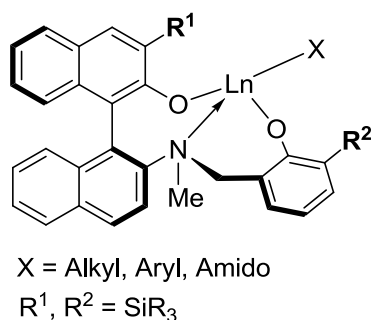


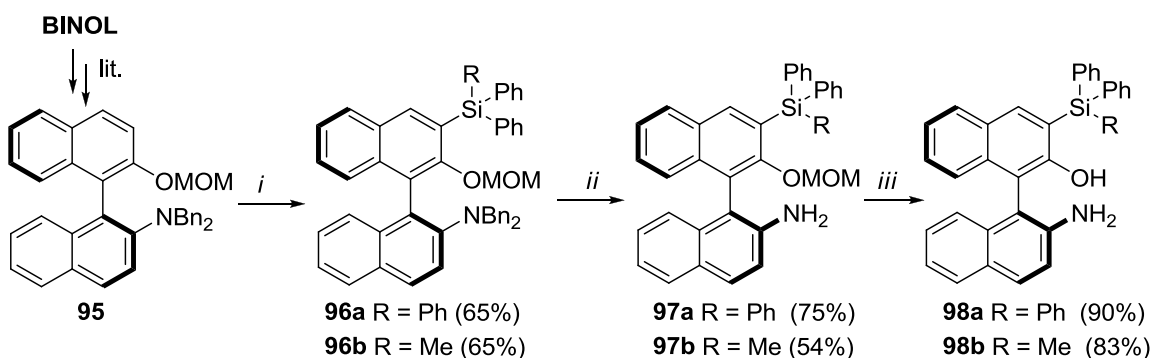
Figure IV-2. Generic NOBIN-derived rare earth metal diolate complex.

The importance of introducing sterically demanding substituents in the *ortho*-position of the diolate moiety in order to improve catalytic reactivity in the hydroamination catalysis has already been demonstrated for a group of rare earth metal diolate complexes.¹⁵ Thus, the ability to easily tune these substituents can be important to adapt the catalyst design successfully. Based on our previous experience with tris(alkyl)silyl- and tris(aryl)silyl-substituents which are readily introduced to the ligand framework and are available in a variety of degrees of steric bulk^{12,16,17} (see also Chapters 3 and 6), we chose silyl substituents for the “tunable” sites R¹ and R² (Figure IV-2).

The silylated NOBIN **98** was chosen as a key precursor for the diol proligand preparation. **98** was synthesized in 3 steps from the *O,N*-bis-protected NOBIN derivative **95** according to Scheme IV-2. Multigram-scale preparation of compound **95** starting from readily available BINOL in 4 steps is a well-documented literature procedure, which

represents one of the most concise routes to chiral NOBIN ligands.^{18,19} Removal of the MOM-group from **97a** (Scheme IV-2, step iii) required protection of the amino-group which was otherwise hampering the acid-catalyzed hydrolysis of the acetal, at least in conditions compatible with acid-sensitive silyl groups.* Upon MOM cleavage, the trifluoroacetyl group was easily removed with NaBH₄ to give the silylated NOBIN **98**.

Scheme IV-2. Synthesis of 3-silylated NOBIN derivatives **98a-b**.



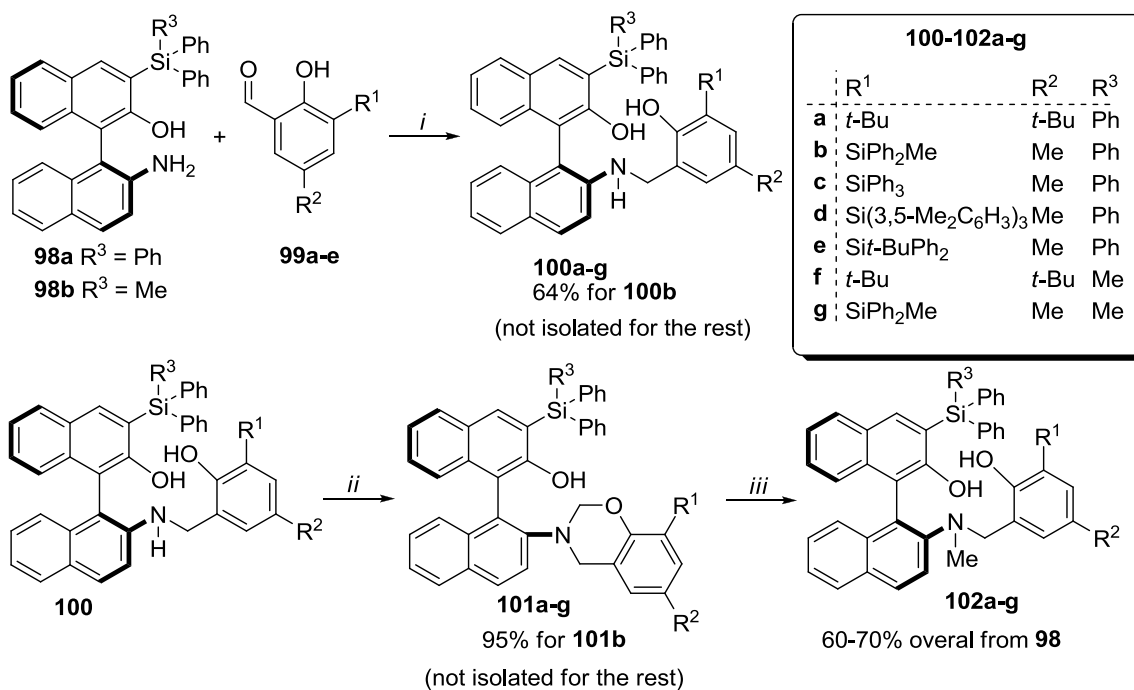
Reaction conditions: ⁱ 1. *n*-BuLi, Et₂O, 0 °C, 5 h. 2. THF, HMPA, RPh₂SiCl, -30 to 25 °C. ⁱⁱ NH₄HCOO, EtOH, reflux. ⁱⁱⁱ 1. (CF₃CO)₂O, Et₃N, DCM. 2. HCl, dioxane, 60 °C. 3. NaBH₄, EtOH, reflux.

With amines **98** in hand, we applied the typical “salen” coupling methodology using variously substituted salicylaldehydes **99** (Scheme IV-3). Schiff base formation followed by reduction yielded secondary amines of the “salan” type (**100**). Attempted reductive amination of amines **100** with formaldehyde led to an unexpected result, as a redox-neutral cyclization to cyclic amins **101** proceeded cleanly instead of formation of

* Non-silylated MOM-protected NOBIN was hydrolyzed by H₂SO₄ (conc.) in refluxing methanol in ref. 17. However, compounds **97** showed loss of silyl groups instead of MOM cleavage at these or similar conditions.

the anticipated *N*-methyl derivative **102**. The latter, however, were obtained via reduction of *N,O*-acetals **101** with lithium aluminum hydride (Scheme IV-3, step iii).

Scheme IV-3. Preparation of proligands **102a-g**.



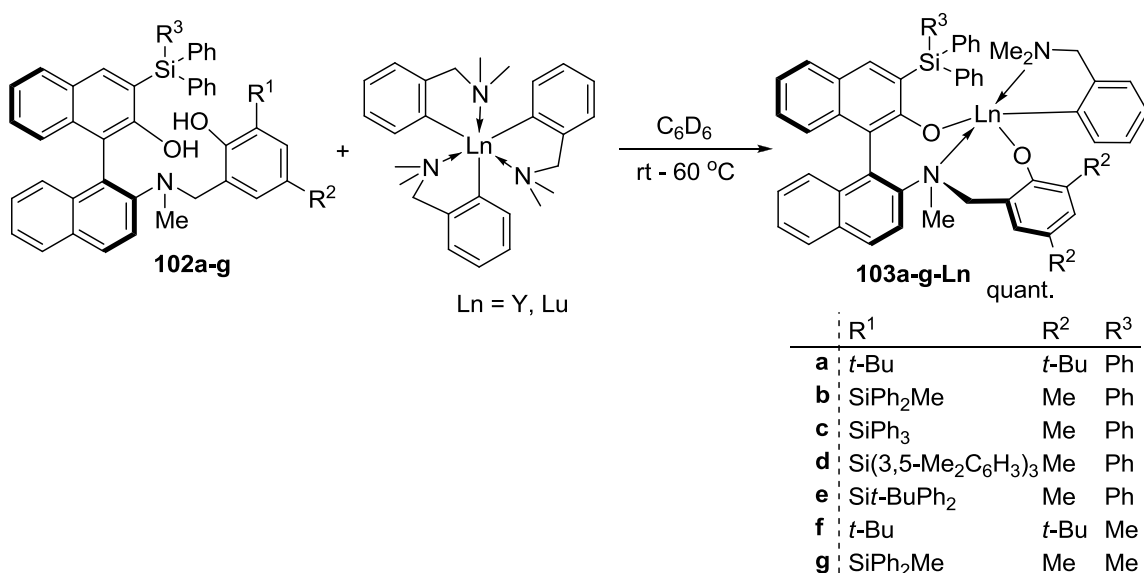
Reaction conditions: ⁱ 1. TsOH, toluene, 90 °C, 24 h. 2. LiAlH₄, Et₂O, 25 °C, 10 min. ⁱⁱ NaBH(AcO)₃, CH₂O, THF, 25 °C, 10 min. ⁱⁱⁱ LiAlH₄, Et₂O, 25 °C, 10 min.

A number of NOBIN-based diol proligands **102**, such as 3-triphenylsilyl-substituted NOBIN derived **102a-e** and 3-(diphenylmethylsilyl)-substituted NOBIN derived **102f-g** were obtained using this methodology.

IV.2.2 Complex Synthesis

Having diol proligands **102a-g** prepared, we proceeded with the synthesis of rare earth metal diolate complexes using tris(aryl) rare earth metal precursors $[\text{Ln}(\text{o-C}_6\text{H}_4\text{CH}_2\text{NMe}_2)_3]$ ($\text{Ln} = \text{Y}, \text{Lu}$) (Scheme IV-4).

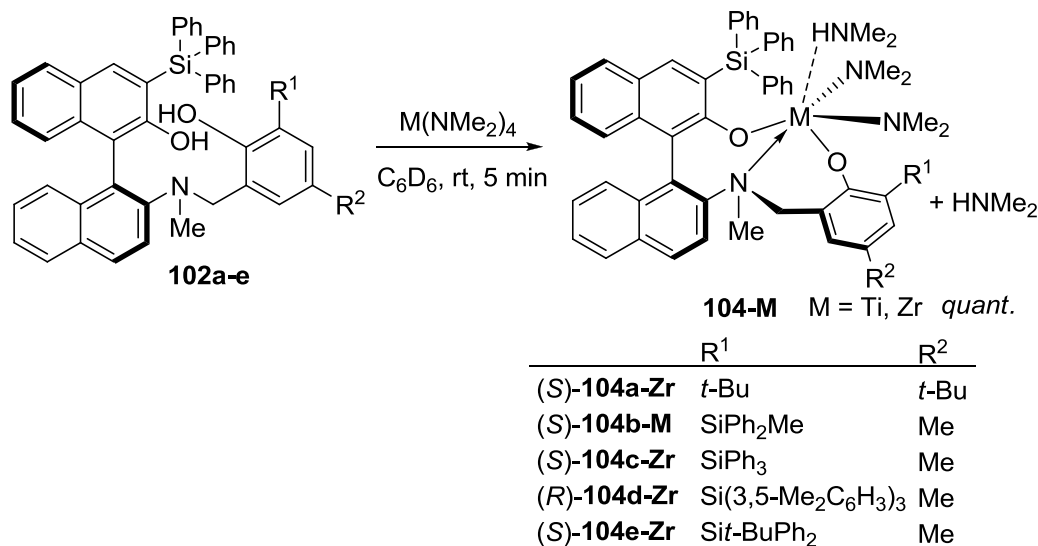
Scheme IV-4. Preparation of rare earth metal diolates **103-Ln**.



The arene elimination proceeded smoothly at room temperature or slightly elevated temperature, and complexes **103-Y** were obtained for the whole family of proligands **102** along with lutetium compounds **103a-e-Lu**. It is noteworthy that according to the ^1H and ^{13}C NMR spectra of the crude reaction mixtures, compounds **103-Ln** do not contain a coordinated molecule of *N,N*-dimethylbenzylamine, which is a characteristic feature of the binaphtholate complexes **24-Ln**.¹⁰ This observation is indicative of diminished Lewis acidity of **103-Ln** compared to **24-Ln** and may also result from increased steric protection of a tridentate ligand framework. Another important observation was the steric versatility of the diolate complexes accessed via the route

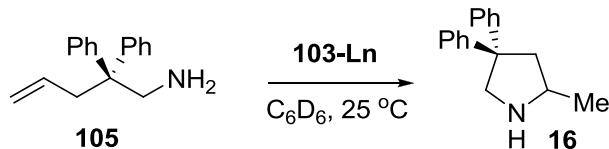
shown in Scheme IV-4. Along with compound **103c-Y**, which resembles the parent triphenylsilyl binaphtholate complex **24a-Y**, compound **103f-Y** features a methyl(diphenyl)silyl and a *tert*-butyl substituents, both of which are too “small” to form a corresponding stable binaphtholate precatalyst (see Chapter 3). It may be speculated that the broader range of tolerated steric bulk results from the increased ligand denticity and bite angle. Complexes **103-Ln** were typically prepared in situ and catalytically tested without isolation. However, the complexes can also be isolated by freeze-drying as powders containing small amount of residual free *N,N*-dimethylbenzylamine. Catalysts **103-Ln** did not show any noticeable decomposition after heating to 150 °C for 1 hour in solution, but the isolated solid catalysts were found to decompose above 60 °C. Unfortunately, no X-ray quality crystals were obtained from **103-Ln** despite significant efforts.

The constantly growing research efforts towards the development of group 4 metal-based hydroamination catalysts (see Section I.2.4 and Chapter 3) have encouraged us to utilize our new ligand set for the synthesis of corresponding zirconium and titanium complexes. As expected, amine elimination reaction of proligands **102a-e** with commercially available precursors $M(NMe_2)_4$ ($M = Zr, Ti$) lead cleanly to the complexes **104a-e-Zr** and **104b-Ti** (Scheme IV-5). According to the 1H and ^{13}C NMR spectra of the crude reaction mixtures, compounds **104-M** contain a coordinated molecule of dimethylamine, however upon freeze-drying the coordinated amine was easily removed from **104b-Ti**. Catalysts **104-M** were prepared in situ and were tested without isolation.

Scheme IV-5. Preparation of group 4 metal diolates **104-M**.

IV.2.3 Catalytic Intramolecular Hydroamination

For the initial evaluation of the catalytic activity of compounds **103-Ln** we chose aminopentene substrate **105**. Triphenylsilyl-substituted complexes **103a-e** showed high turnover frequencies for the cyclization of aminopentene **105** (Table IV-1, entries 1–9). The activity is on the same magnitude as that of **24-Ln**.¹⁰ No significant influence of the silyl substituent on the phenolate moiety on the catalytic efficiency was observed and the catalysts reached turnover frequencies in the range of 100–400 h⁻¹. However, the sterically less encumbered methyl(diphenylsilyl)-substituted diolates **103f-Y** and **103g-Y** displayed somewhat lower reactivity (Table IV-1, entries 10, 11).

Table IV-1. Catalyst evaluation for hydroamination/cyclization of **105**.

Entry	Catalyst	Cat./Sub. mol %	Time, min ^a	TOF, h ^{-1b}	% ee (config.) ^c
1	(<i>S</i>)- 103a-Y	1	30	200	17 (<i>S</i>)
2	(<i>S</i>)- 103a-Lu	2	30	100	48 (<i>S</i>)
3	(<i>S</i>)- 103b-Y	2	15	230	6 (<i>S</i>)
4	(<i>S</i>)- 103c-Y	2.2	6	400	27 (<i>S</i>)
5	(<i>S</i>)- 103c-Lu	1.4	15	200	92 (<i>S</i>) ^d
6	(<i>R</i>)- 103d-Y	2	20	150	8 (<i>R</i>)
7	(<i>R</i>)- 103d-Lu	1	40	150	4 (<i>R</i>)
8	(<i>S</i>)- 103e-Y	2	15	200	48 (<i>S</i>)
9	(<i>S</i>)- 103e-Lu	2	30	100	77 (<i>S</i>)
10	(<i>S</i>)- 103f-Y	2	60	50	48 (<i>R</i>)
11	(<i>S</i>)- 103g-Y	2	75	40	13 (<i>S</i>)

^a Time for >95% conversion. ^b Overall turnover frequency. ^c Determined by ¹⁹F NMR of the corresponding Mosher amide. ^d Determined by chiral HPLC of the corresponding *N*-benzamide.

The stereoselectivity of the hydroamination/cyclization has a nonlinear dependence of the steric bulk of the substituent on the phenolate moiety of the complex (Figure IV-3). A moderate stereoselectivity is observed for the tertiary butyl-substituted **103a-Y** (Table IV-1, entry 1); however, the slightly bulkier Ph₂SiMe-substituted **103b-Y** was less selective while a further increase in steric bulk in complexes **103c-Y** and **103e-Y** resulted in a higher selectivity. The highest enantioselectivity of 92% ee was observed for the smaller lutetium metal in complex **103c-Lu** (Table IV-1, entry 5).

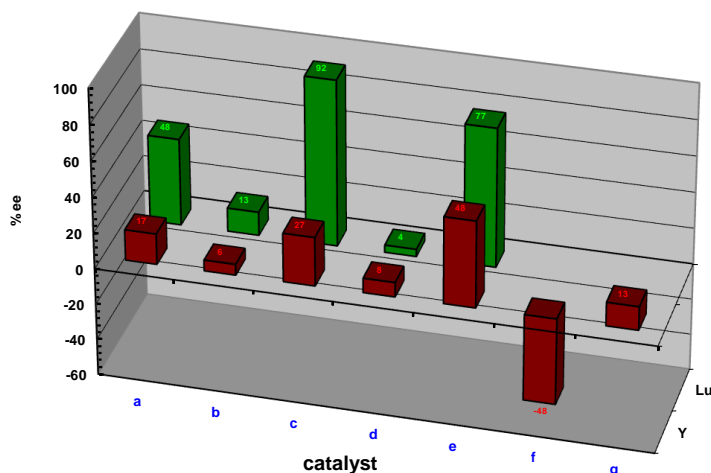
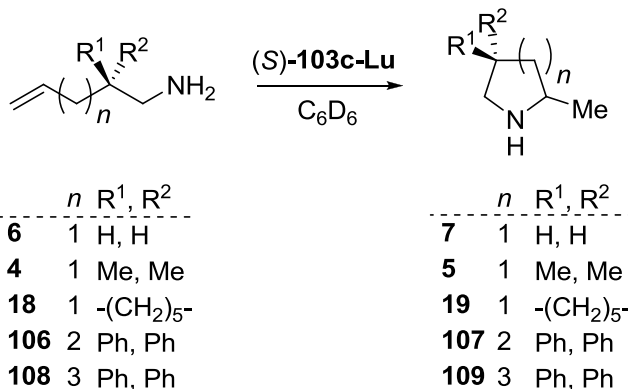


Figure IV-3. Selectivity profiles for the cyclization of aminoalkene **105** catalyzed by **103-Y** (red bars) and **103-Lu** (green bars).

In order to have a deeper insight into the catalytic properties of novel catalysts, we investigated hydroamination/cyclization of a broader range of aminoalkenes, catalyzed by (*S*)-**103c-Lu** (Table IV-2).

Hydroamination/cyclization of various aminoalkenes into pyrrolidine, piperidine and azepane derivatives was also smoothly catalyzed by **103c-Lu** and moderate enantiomeric excesses were observed in most cases (Table IV-2). Interestingly, the enantioselectivity of 73% ee observed for piperidine **106** is one of the highest values reached to date in the hydroamination of aminohexenes (Table IV-2, entry 4). While hydroamination/cyclization of activated substrates (**105**, **4**, **18**) catalyzed by **103c-Lu** was only slightly less efficient than that catalyzed by **24-Ln**, a significantly more diminished reactivity of the former is clearly manifested by the example in entry 1. While compounds **24-Ln** were able to cyclize the unbiased aminopentene **6** lacking additional substituents at room temperature, compound **103c-Lu** was reactive only at 80 °C.

Table IV-2. Hydroamination/cyclization of various aminoalkenes catalyzed by **103c-Lu**.

Entry	Substrate	Cat./Sub., mol %	T, °C	Time, h ^a	TOF, h ^{-1b}	%ee (Config.)
1	6	4	80	1.6	15	59 (<i>S</i>)
2	4	1.4	40	7	13	62 (<i>S</i>)
3	18	1.4	25	0.6	200	52 (<i>S</i>)
4	106	2	25	2.7	20	73
5	108	4	90	51	0.5	27

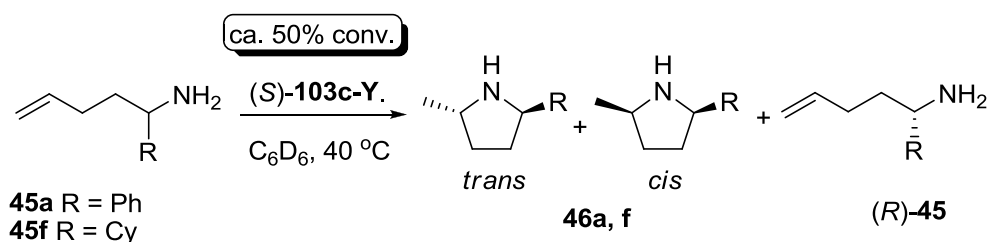
^a Time to >95% conversion. ^b Overall turnover frequency.

Catalysts **103-Ln** can also be applied to the kinetic resolution of chiral racemic aminoalkenes^{10,11} (see also Chapter 2). Aryl- and alkyl-substituted aminopentenes **45** were resolved by (*S*)-**103c-Y**, albeit with moderate resolution factors (Table IV-3). Higher reactivity and better resolution efficiency were previously observed for both **45a** and **45f** with binaphtholate catalysts **24-Ln** (see Chapter 2). In line with the reversal of enantioselectivity in hydroamination/cyclization compared to **24-Ln**, an opposite enantiomer (*R*-) of **45** was obtained in enantioenriched form with catalyst (*S*)-**103c-Y**.

To conclude, novel catalysts **103-Ln** displayed slightly diminished performance in hydroamination/cyclization of aminoalkenes compared to **24-Ln**. As expected, the

reaction selectivity depends dramatically on the steric features of the tunable silyl groups of the catalyst. Introduction of the additional donor site to the diolate ligand framework has led to a noticeable depletion of the catalytic reactivity. However, the cyclization of unbiased aminopentene **6** is encouraging that intermolecular hydroamination catalyzed by **103-Ln** is attainable.

Table IV-3. Catalytic kinetic resolution of chiral aminopentenes.

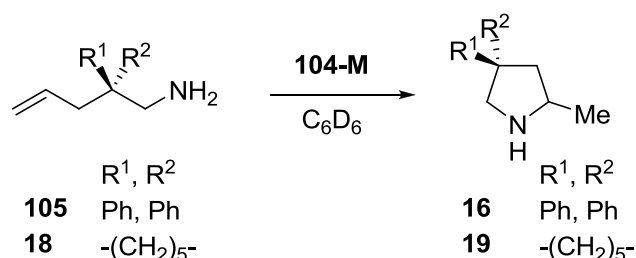


Entry	Substrate	<i>t</i> , h	Conv., %	<i>trans</i> : <i>cis</i>	% ee of <i>f</i>	recov. 45
1	45a	19	55	≥ 50:1	62	5.9
2	45f	20	54	9:1	46	3.4

The novel group 4 metal diolates **104-M** also displayed some catalytic reactivity in the hydroamination/cyclization of aminopentenes. (Table IV-4). In agreement with most observations for aminoalkene cyclizations,³ titanium complex **104b-Ti** displayed significantly lower reactivity than its zirconium analog **104b-Zr** and failed to cyclize the otherwise very active substrate **105** (Table IV-4, entries 1, 2). The catalytic activity depends on the steric features of the substituent in the phenolate moiety with the least bulky *t*-butyl group giving highest reactivity for **104a-Zr**. Notably, compounds **104b-Zr** and **104d-Zr** yielded the pyrrolidine **16** of the configuration opposite to that produced by

the rest of the series (Figure IV-4). Sterically demanding substituents, such as *t*-BuPh₂Si or Ph₃Si, provide the highest enantioselectivities (up to 67 % ee for **16**). Overall, the catalytic activity of the novel zirconium complexes lies within the typical range for most traditional neutral group 4 catalytic systems (see Section I.2.4 and Chapter 5) and high temperatures are required even for the hydroamination/cyclization of *gem*-disubstituted²⁰ aminopentenes.

Table IV-4. Hydroamination/cyclization of aminopentenes, catalyzed by **104-M**.



Entry	Substrate	Catalyst	Cat./Sub. mol %	T, °C	Time, h ^a	% ee (config.)
1	105	(<i>S</i>)- 104b-Ti	5	130	120 ^b	--
2	105	(<i>S</i>)- 104a-Zr	4.5	100	5	46 (<i>R</i>)
3	105	(<i>S</i>)- 104b-Zr	5	100	7	27(<i>S</i>)
4	105	(<i>S</i>)- 104c-Zr	5	100	10	57 (<i>R</i>)
5	105	(<i>R</i>)- 104d-Zr	5	130	13	29 (<i>R</i>)
6	105	(<i>S</i>)- 104e-Zr	4	100	14	67 (<i>R</i>)
7	18	(<i>S</i>)- 104e-Zr	4	100	36	34 (<i>R</i>)

^a Time given for >95% conversion unless stated otherwise. ^b <5% conversion.

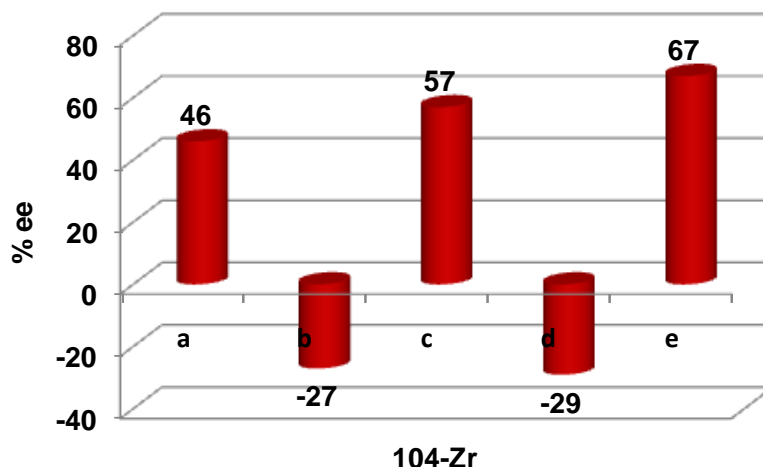


Figure IV-4. Selectivity profile for the hydroamination/cyclization of **105** catalyzed by **104-Zr**.

IV.2.4 Intermolecular Asymmetric Hydroamination

Although the intramolecular hydroamination reactions showed diminished reactivity of **103-Ln** compared to **24-Ln**, we proceeded with the evaluation of novel diolate catalysts in the intermolecular asymmetric hydroamination of terminal alkenes with benzylamine (Table IV-5).

Again, compounds **103-Ln** were significantly less reactive, and the reactivity drops dramatically with increasing of the steric bulk of the ligand. Thus, no reactivity was observed for sterically encumbered di-(trisaryl)silyl-substituted compounds **103c-Y** and **103d-Y** which have silyl substitution pattern similar to that of **24a-Y** and **24b-Y**, respectively. For the triphenylsilyl-substituted NOBIN complexes, only least encumbered (in the phenolate moiety) **103a-Ln** and **103b-Ln** were catalytically active, although still significantly less efficient than **24a-Ln** (see Chapter 3). However, the methyl(diphenyl)silyl-substituted (on naphtholate moiety) complexes **103f-Y** and **103g-Y**

displayed higher reactivity which might be compared to that of **24-Ln** (Table IV-5, entries 6, 10, 11). Unfortunately, the selectivity drops significantly when the steric bulk is decreased, and only 40% ee was achieved for amine **77** using **103b-Y**. Once again, the steric bulk of complexes **103-Ln** has a significant influence on the catalytic activity. The modified ligand backbone in complexes **103-Ln** allows and favors the application of the mid-sized *tert*-butyl and methyl(diphenyl)silyl substituents, neither of which was acceptable for the parent C_2 -symmetric binaphtholate system in complexes **24-Ln**.

Table IV-5. Intermolecular hydroamination of terminal alkenes catalyzed by **103-Ln**.

$\text{R-CH=CH}_2 + \text{H}_2\text{N-CH}_2\text{-Ph} \xrightarrow[\text{C}_6\text{D}_6]{5 \text{ mol\% } \mathbf{103-Ln}}$

$x \text{ equiv.}$

$\text{77 R} = n\text{-C}_5\text{H}_{11}$
 $\text{85 R} = \text{PhCH}_2\text{CH}_2$

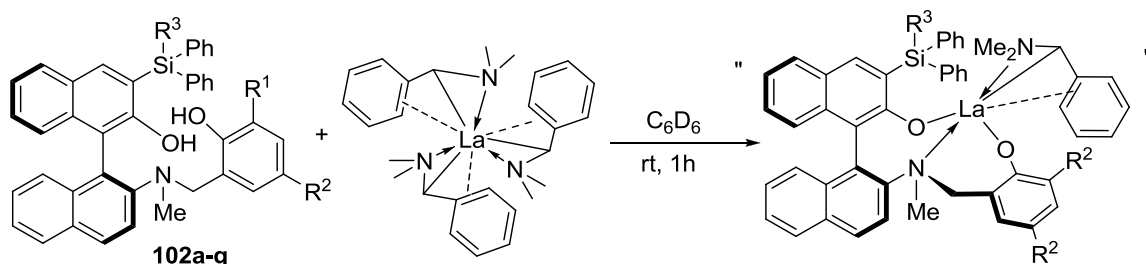
Entry	R	cat.	<i>x</i>	T, °C	<i>t</i> , h	% conv. ^a (% yield) ^b	% ee ^c (confi)
1	<i>n</i> -C ₅ H ₁₁	(<i>S</i>)- 103a-Y	15	150	96	85 (62)	32 (<i>R</i>)
2	<i>n</i> -C ₅ H ₁₁	(<i>S</i>)- 103a-Lu	15	150	96	75 (62)	7 (<i>R</i>)
3	<i>n</i> -C ₅ H ₁₁	(<i>S</i>)- 103b-Lu	15	150	140	70 (51)	40 (<i>S</i>)
4	<i>n</i> -C ₅ H ₁₁	(<i>S</i>)- 103c-Y	15	170	120	trace	--
5	<i>n</i> -C ₅ H ₁₁	(<i>S</i>)- 103d-Y	15	170	120	trace	--
6	<i>n</i> -C ₅ H ₁₁	(<i>S</i>)- 103g-Y	15	170	90	70(53)	4 (<i>S</i>)
7	PhCH ₂ CH ₂	(<i>S</i>)- 103a-Y	10	150	76	80 (67)	17 (<i>R</i>)
8	PhCH ₂ CH ₂	(<i>S</i>)- 103a-Lu	10	150	96	75 (61)	9 (<i>R</i>)
9	PhCH ₂ CH ₂	(<i>S</i>)- 103b-Lu	10	150	96	75 (59)	33 (<i>S</i>)
10	PhCH ₂ CH ₂	(<i>S</i>)- 103f-Y	10	150	50	80 (63)	20 (<i>R</i>)
11	PhCH ₂ CH ₂	(<i>S</i>)- 103g-Y	10	150	48	85 (66)	5 (<i>R</i>)

^a By ¹H NMR spectroscopic analysis. ^b Isolated yield after column chromatography.

^c Determined by chiral HPLC of the corresponding *N*-benzamide.

As was demonstrated in Chapter 3, larger rare earth metals such as lanthanum might require a ligand with a larger bite-angle to be active in the intermolecular hydroamination. We were unable to unambiguously detect any well-defined La complex species after the reaction of **102** with lanthanum trisamides $[\text{La}\{\text{N}(\text{SiMe}_3)_2\}_3]$. The crude reaction mixtures were found to contain multiple species and were catalytically inactive in the intermolecular hydroamination. To our surprise, when the novel tris(aminoalkyl) lanthanum precursor $[\text{La}\{\text{CH}(\text{C}_6\text{H}_5)\text{NMe}_2\}_3]^{21}$ was treated with **102**, the resulting mixtures remarkably displayed some catalytic activity in the intermolecular hydroamination (Table IV-6). ^1H NMR signals of the crude reaction mixtures (Scheme IV-6) were extremely broad even at $-80\text{ }^\circ\text{C}$ presumably due the fluxional character of the (dimethylamino)benzyl lanthanum moiety.²¹

Scheme IV-6. In situ preparation of lanthanum diolates from **102**.



It appears that the larger lanthanum indeed demands different level of steric protection for the catalytic activity in intermolecular hydroamination. While the triphenylsilyl-substituted yttrium complexes **103c-Y** and **103d-Y** were catalytically inactive, the corresponding lanthanum diolates derived from proligands **102c** and **102d** were the only catalytically active lanthanum species. The same trend is observed for the

bidentate binaphthol proligands **78**. The lanthanum complex formed from triphenylsilyl-substituted proligand **78a** was unreactive (Table IV-6, entry 5), which is in agreement with results obtained for complex **80a-La** (see Chapter 3). However, the more sterically encumbered binaphthol proligands **78d** and **78i** resulted in the catalytically active complexes. Overall, the larger lanthanum metal did not result in any significant improvements in catalytic intermolecular hydroamination, which stands in stark contrast to the general trend in intramolecular hydroamination.⁸

Table IV-6. Lanthanum-catalyzed intermolecular hydroamination of terminal alkenes.

$\text{Ph-CH}_2\text{-CH=CH}_2 + \text{H}_2\text{N-CH}_2\text{-Ph} \xrightarrow[\text{C}_6\text{D}_6]{\text{5 mol\% [La\{CH(Ph)NMe}_2\}_3]} \text{Ph-CH}_2\text{-CH}_2\text{-CH(Ph)-CH}_2\text{-NH-CH}_2\text{-Ph}$

10 equiv. **85**

Entry	Ligand	T, °C	t, h	% conv. ^a (% yield) ^b	% ee ^c (config.)
1	(<i>S</i>)- 102a	170	48	Trace	--
2	(<i>S</i>)- 102c	150	96	85 (61)	37 (<i>R</i>)
3	(<i>R</i>)- 102d	150	120	90 (66)	28 (<i>S</i>)
4	(<i>S</i>)- 102g	170	48	Trace	--
5	(<i>R</i>)- 78a	170	48	0	--
6	(<i>R</i>)- 78d	150	96	90 (69)	37 (<i>R</i>)
7	(<i>R</i>)- 78i	150	90	75 (59)	14 (<i>R</i>)

^a By ¹H NMR spectroscopic analysis. ^b Isolated yield after column chromatography. ^c Determined by chiral HPLC of the corresponding *N*-benzamide.

Presently, novel *C*₁-symmetric rare earth metal diolates **103-Ln** did not result in any improvements in either selectivity or catalytic reactivity in asymmetric

intermolecular hydroamination compared to binaphtholates **24-Ln**. In fact, the reactivity was remarkably lowered, presumably due to the presence of an additional donor site in the ligand backbone. The extended range of the ligand steric features tolerated by the precatalyst allowed us to observe the highest and the lowest acceptable level of steric bulk required for the catalytic reactivity for mid-sized (Lu, Y) and large (La) rare earth metals.

IV.3 Conclusions

A new family of C_1 -symmetric NOBIN-based diolate ligands **102** with multiple tunable sites were developed and synthesized. The corresponding diolate complexes of the rare earth metals featuring various degree of steric protection were synthesized and were shown to be catalytically active in intra- and intermolecular hydroamination of unactivated alkenes. The hydroamination of aminopentenes and aminohexenes proceeded with enantioselectivities of up to 92 and 73% ee, respectively. The enantioselectivity of hydroamination/cyclization as well as the reactivity in the intermolecular hydroamination are critically dependent on the steric features of the ligand framework. In addition, several lanthanum-based hydroamination catalysts were prepared *in situ* and were applied to the intermolecular hydroamination as well. Overall, the novel catalytic system was found to be slightly less reactive and selective than the rare earth metal binaphtholate catalysts **24-Ln**.

IV.4 Experimental

General considerations. All reactions with air- or moisture sensitive materials were performed in oven (120 °C) and flame-dried glassware under an inert atmosphere of argon, employing standard Schlenk and glovebox techniques. Hexanes, pentane and THF were sparged with argon for 1 h and then passed through a column with activated alumina prior to use. Alkenes, benzene and C₆D₆ were vacuum transferred from sodium/benzophenone ketyl. Amines and aminoalkenes were distilled twice from finely powdered CaH₂.

¹H, ¹³C{¹H} and ¹⁹F NMR spectra were recorded on Varian (300, 400, 500 MHz) spectrometers at 25 °C unless stated otherwise. Chemical shifts are reported in ppm downfield from tetramethylsilane with the signal of the deuterated (¹³C) or undeuterated (¹H) portion of the solvent as internal standard. Mass spectra were recorded on a Finnigan LCQ-DUO mass spectrometer. HPLC analysis was carried out on an Agilent 1200 series instrument with multiple wavelength detector using Chiralcel OD-H and Chiralpak AS-H columns (25 × 4.6 mm). Silica gel (230–400 mesh, Sorbent Technologies) and alumina (80–200 mesh, EMD) were used for column chromatography.

(*S*)-Mosher acid was transformed into the corresponding (*R*)-Mosher acid chloride according to a literature protocol.²²

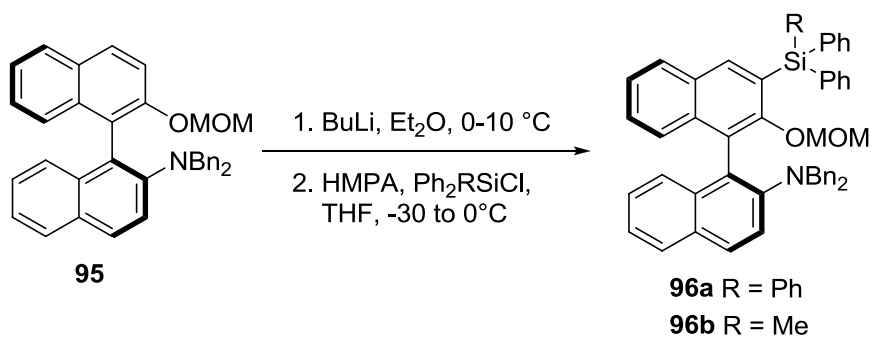
The aminoalkene substrates pent-3-enylamine (**6**),²³ 2,2-diphenylpent-4-enyl amine (**105**),²⁴ 2,2-dimethyl-pent-4-enyl amine (**4**),²⁵ (1-allylcyclohexyl)methylamine (**18**),²⁶ 2,2-diphenylhex-5-enyl amine (**106**)²⁷ and 2,2-diphenylhept-6-enyl amine (**108**),²⁸ 1-phenylpent-4-enylamine (**84a**)¹⁰ and 1-cyclohexylpent-4-enylamine (**84f**)¹¹ were synthesized according to literature protocols.

The hydroamination products 2-methylpyrrolidine (**7**),²⁹ 2,4,4-trimethylpyrrolidine (**5**),²³ 3-methyl-2-azaspiro[4,5]decane (**19**),³⁰ 2-methyl-4,4-diphenylpyrrolidine (**16**),²⁴ 2-methyl-5,5-diphenylpiperidine (**107**)²⁴, 2-methyl-6,6-diphenylazepane (**109**)³¹ 2-methyl-5-phenylpyrrolidine (**46a**)⁹ and 2-cyclohexyl-5-methylpyrrolidine (**46f**)³² are known compounds and were identified by comparison to the literature NMR spectroscopic data. The absolute configuration of the hydroamination products was determined by comparison of the ¹⁹F NMR spectroscopic data with the assignments reported previously.¹⁰

Ligand Synthesis

2,6-Dibromo-4-methylphenol,³³ *N,N*-dibenzyl-*N*-[2'-(methoxymethoxy)-1,1'-binaphthalen-2-yl]amine (**95**),¹⁸ 3,5-di-*tert*-butylsalicylaldehyde (**99a**)³⁴ and silyl-substituted aldehydes (**99b-c**)³⁵ were prepared according to literature protocols.

Silylation of protected NOBIN **95**.



To a stirred solution of **95** (4.58 g, 9.0 mmol) in Et₂O (80 mL) *n*-BuLi (2.5 M in hexanes, 4.7 mL, 11.7 mmol) was added dropwise at 0 °C. The mixture was stirred at this temperature for 5 h then 2 h at room temperature and cooled down to −30 °C. THF (50 mL), a solution of chlorotriphenylsilane (3.45 g, 11.7 mmol) in THF (10 mL) and HMPA

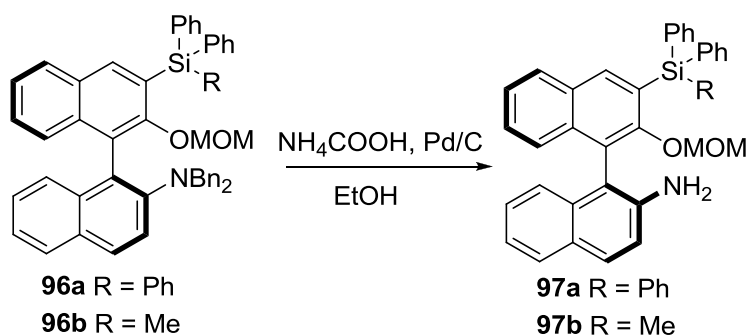
(2.1 mL, 12 mmol) were added to the solution in that order. The dark-brown solution was allowed to reach room temperature slowly and was stirred overnight. The mixture was quenched with saturated ammonium chloride solution (100 mL) and the product was extracted with dichloromethane (2×50 mL). Combined organic extracts were dried (Na_2SO_4) and concentrated. The residue was purified by column chromatography.

***N,N*-Dibenzyl-*N*-[2'-(methoxymethoxy)-3'-(triphenylsilyl)-1,1'-binaphthalen-2-yl]amine (96a).** Purified by column chromatography on silica (hexanes/toluene = 1:1) to give 4.51 g (65%) of **96a** as a white solid. ^1H NMR (500 MHz, CDCl_3): δ = 7.88 (s, 1H), 7.71 (d, $^3J(\text{H,H})$ = 8.8 Hz, 1H), 7.68 (d, $^3J(\text{H,H})$ = 7.8 Hz, 1H), 7.63 (d, $^3J(\text{H,H})$ = 8.3 Hz, 1H), 7.57 (d, $^3J(\text{H,H})$ = 7.8 Hz, 6H, SiPh_3), 7.30–7.10 (m, 16H), 7.05 (vt, $^3J(\text{H,H})$ = 8.1, 7.1 Hz, 1H), 7.00–6.89 (m, 7H), 6.85–6.80 (m, 4H, aryl-H), 3.94 (m, 5H, $2\text{CH}_2\text{Ph}$, CH_2O), 3.65 (d, 1H, $^2J(\text{H,H})$ = 5.1 Hz, CH_2O), 2.04 (s, 3H, CH_3); $^{13}\text{C}\{^1\text{H}\}$ NMR (CDCl_3 , 125 MHz): δ = 157.4, 148.7, 141.2, 138.4, 136.5, 135.9, 135.09, 135.06, 130.3, 130.1, 129.3, 126.0, 125.1, 124.5, 124.1, 122.8 (aryl), 97.4 (CH_2O), 56.6 (CH_3), 55.8 (CH_2Ph).

***N,N*-Dibenzyl-*N*-[2'-(methoxymethoxy)-3'-[methyl(diphenyl)silyl]-1,1'-binaphthalen-2-yl]amine (96b).** Purified by column chromatography on silica (hexanes/DCM = 5:3) to give 4.13 g (65%) of **96b** as a white solid. ^1H NMR (500 MHz, CDCl_3): δ = 7.86 (s, 1H), 7.83 (d, $^3J(\text{H,H})$ = 8.8 Hz, 1H), 7.79 (d, $^3J(\text{H,H})$ = 8.1 Hz, 1H), 7.73 (d, $^3J(\text{H,H})$ = 8.3 Hz, 1H), 7.61 (d, $^3J(\text{H,H})$ = 7.3 Hz, 2H), 7.55 (d, $^3J(\text{H,H})$ = 7.3 Hz, 2H), 7.44–7.29 (m, 9H), 7.21–7.10 (m, 9H), 7.00 (d, $^3J(\text{H,H})$ = 8.6 Hz, 1H), 6.92 (dd, $^3J(\text{H,H})$ = 7.6 Hz, $^4J(\text{H,H})$ = 2.0 Hz, 4H, aryl-H), 4.05 (d, $^2J(\text{H,H})$ = 14.4 Hz, 2H,

PhCH₂N), 3.99 (d, ²J(H,H) = 4.7 Hz, 1H, CH₂O), 3.95 (d, ²J(H,H) = 4.7 Hz, 1H, CH₂O), 3.89 (d, ²J(H,H) = 14.4 Hz, 2H, PhCH₂N), 2.33 (s, 3H, CH₃O), 0.96 (s, 3H, SiCH₃); ¹³C{¹H} NMR (125 MHz, CDCl₃): δ = 157.2 (CO), 148.9, 139.9, 138.5, 137.3, 136.7, 145.6, 135.5, 135.1, 135.0, 130.9, 130.4, 130.2, 129.3, 129.2, 128.9, 128.5, 128.3, 127.9, 127.82, 127.78, 127.7, 127.6, 127.1, 126.6, 126.3, 126.2, 126.1, 125.5, 124.5, 124.2, 122.7 (aryl), 97.8 (CH₂O), 56.6 (CH₃O), 56.0 (CH₂Ph), -3.0 (SiCH₃).

Debenzylation of amine **96**.



To a stirred suspension of **96** (4.6 mmol) in absolute ethanol (150 mL), were added ammonium formate (5.0 g, 80 mmol) and 10% Pd on charcoal (1.2 g, 0.23 mmol) and the mixture was refluxed for 2 days [**CAUTION**: condensation of ammonium salts in reflux condenser may result in isolated overpressured system]. The mixture was cooled, filtered through celite and the filtrate was concentrated *in vacuo* and treated with 2% KOH solution (100 mL). The product was extracted with dichloromethane (2 × 100 mL). The combined organic extracts were dried (Na₂SO₄) and the solvent was evaporated. The residue was purified by flash chromatography.

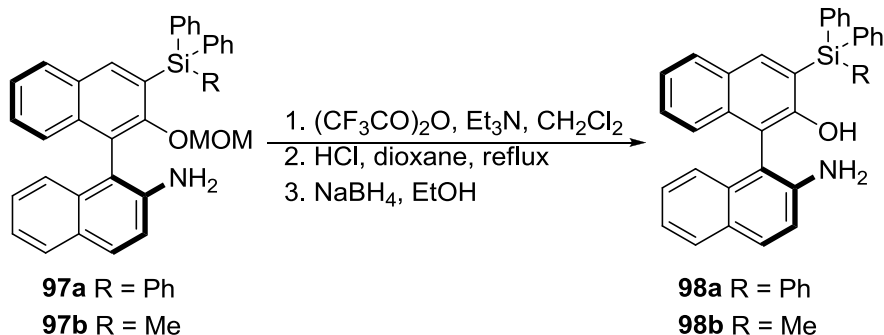
2'-(Methoxymethoxy)-3'-(triphenylsilyl)-1,1'-binaphthalen-2-amine (97a).

Purified on short silica column (hexanes/DCM = 1:1) to give 2.01 g (75%) of **97a** as a white solid. ^1H NMR (400 MHz, CDCl_3): δ = 7.95 (s, 1H), 7.77 (d, $^3J(\text{H,H})$ = 8.6 Hz, 1H), 7.78–7.73 (m, 2H), 7.67 (d, $^3J(\text{H,H})$ = 7.8 Hz, 6H), 7.43–7.30 (m, 12H), 7.26–7.16 (m, 3H), 7.07 (d, $^3J(\text{H,H})$ = 8.6 Hz, 1H, aryl-H), 3.91 (d, 1H, $^2J(\text{H,H})$ = 5.1 Hz, CH_2O), 3.87 (d, 1H, $^2J(\text{H,H})$ = 5.1 Hz, CH_2O), 3.7 (br s, 2H, NH_2), 2.20 (s, 3H, CH_3); $^{13}\text{C}\{^1\text{H}\}$ NMR (100 MHz, CDCl_3): δ = 158.0, 142.6, 141.1, 136.5, 135.0, 134.9, 134.3, 130.6, 129.49, 129.45, 124.4, 122.2, 121.7, 118.0, 114.0, 97.4, 55.6. MS (ESI): m/z 587.9 [$\text{M} + \text{H}$] $^+$.

2'-(Methoxymethoxy)-3'-[methyl(diphenyl)silyl]-1,1'-binaphthalen-2-amine

(97b). Purified on short silica column (hexanes/DCM = 1:1) to give 1.32 g (54%) of **97b** as a white solid. ^1H NMR (400 MHz, CDCl_3): δ = 7.86 (s, 1H), 7.77–7.71 (m, 2H), 7.62–7.58 (m, 3H), 7.41–7.31 (m, 6H), 7.22–7.18 (m, 2H), 7.08–7.04 (m, 2H, aryl-H), 4.19 (d, 1H, $^2J(\text{H,H})$ = 4.7 Hz, CH_2O), 4.12 (d, 1H, $^2J(\text{H,H})$ = 4.7 Hz, CH_2O), 3.7 (br s, 2H, NH_2), 2.44 (s, 3H, CH_3O), 1.01 (s, 3H, CH_3Si); $^{13}\text{C}\{^1\text{H}\}$ NMR (100 MHz, CDCl_3): δ = 158.2, 142.6, 141.1, 135.3, 134.0, 134.9, 134.3, 130.6, 129.49, 129.45, 124.4, 122.2, 121.7, 118.0, 114.0, 97.4, 55.9, –3.0 (CH_3Si). MS (ESI): m/z 526.2 [$\text{M} + \text{H}$] $^+$.

Deprotection of acetal **97**.



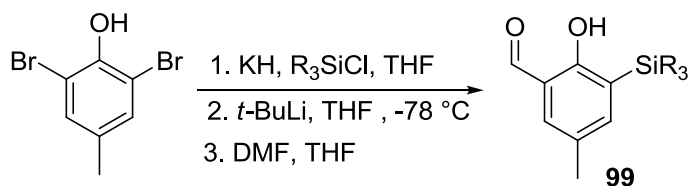
To a stirred solution of **97** (3.4 mmol) and Et₃N (0.71 mL, 5.0 mmol) in dichloromethane (20 mL) was added trifluoroacetic anhydride (0.53 mL, 4.0 mmol) dropwise at 0 °C. The mixture was stirred at room temperature for 2 min, washed with 1 M HCl (5 mL) and concentrated *in vacuo*. The residue was dissolved in dioxane (10 mL) and 12 M HCl (1 mL) was added. The mixture was stirred overnight at 65 °C. The mixture was neutralized with a saturated NaHCO₃ solution and the product was extracted with ethyl acetate (2 × 75 mL). The combined organic extracts were dried (Na₂SO₄) and the solvent was evaporated. The residue was dissolved in ethanol (10 mL) and treated with NaBH₄ (0.34 g, 10 mmol). The mixture was stirred at room temperature overnight and was quenched by addition of 2% KOH solution (50 mL). The product was extracted with dichloromethane (2 × 50 mL). The combined organic extracts were dried (Na₂SO₄), passed through a short silica plug and the solvent was evaporated to give **98**.

2'-Amino-3-(triphenylsilyl)-1,1'-binaphthalen-2-ol (98a). White solid, yield 90%. ¹H NMR (400 MHz, CDCl₃): δ = 7.90 (s, 1H), 7.79 (d, ³J(H,H) = 9.0 Hz, 1H), 7.78–7.72 (m, 2H), 7.67 (d, ³J(H,H) = 8.2 Hz, 6H), 7.43–7.34 (m, 8H), 7.30–7.19 (m, 6H), 7.14–7.11 (m, 1H), 7.09 (d, ³J(H,H) = 9.0 Hz, 1H, aryl-H), 5.29 (s, 1H, OH), 3.76

(br s, 2H, NH₂); ¹³C{¹H} NMR (100 MHz, CDCl₃): δ = 155.6, 143.7, 141.2, 136.3, 134.6, 134.0, 130.5, 129.4, 129.2, 123.5, 123.4, 122.7, 118.1, 113.7, 108.6.

2'-Amino-3-[methyl(diphenyl)silyl]-1,1'-binaphthalen-2-ol (98b). Off-white solid, yield 83%. ¹H NMR (400 MHz, CDCl₃): δ = 7.83 (s, 1H), 7.80 (d, ³J(H,H) = 8.6 Hz, 1H), 7.78–7.73 (m, 2H), 7.59 (d, ³J(H,H) = 8.2 Hz, 4H), 7.43–7.31 (m, 6H), 7.30–7.15 (m, 6H), 7.10 (d, ³J(H,H) = 8.6 Hz, 1H), 7.06 (m, 1H, aryl-H), 5.25 (s, 1H, OH), 3.74 (br s, 2H, NH₂), 0.96 (s, 3H, SiCH₃); ¹³C{¹H} NMR (100 MHz, CDCl₃): δ = 155.6, 143.7, 141.2, 136.3, 134.6, 134.0, 130.5, 129.4, 129.2, 123.5, 123.4, 122.7, 118.1, 113.7, 107.6, –2.7 (Si CH₃).

General procedure for synthesis of aldehydes 99d and 99e (adopted from ref. 35)



To a solution of the 2,6-dibromo-4-methylphenol (5 mmol) in THF (25 mL) was added slowly KH (400 mg, 10.0 mmol) at 0 °C. After stirring for 30 min, an appropriate chlorosilane (5 mmol) was added in one portion. The reaction mixture was heated to reflux for 16–48 h (monitored by TLC). The solvent was then removed in vacuo and the residue diluted with hexanes (100 mL) and water (50 mL). The layers were separated and the organic layer was washed with aqueous HCl (0.2N, 30 mL), water (30 mL), and brine (30 mL). The solution was then dried (Na₂SO₄) and concentrated in vacuo. The crude silyl ethers were used directly in the next step without further purification.

A solution of silyl ether (1.50 mmol) in Et₂O (3.0 mL) was cooled to -78°C and then *t*-BuLi (1.7 M in pentane, 3.53 mL, 6.00 mmol) was added dropwise. The dark red reaction mixture was stirred for 1.5 h while warming to 0°C . The mixture was then cooled to -78°C and DMF (0.465 mL, 6.00 mmol) was added in one portion. The reaction mixture was allowed to warm to 0°C and then quenched with saturated aq. NH₄Cl (5.0 mL) and diluted with EtOAc (75 mL). The layers were separated and the organic layer was washed with H₂O (2×15 mL), brine (25 mL), dried (Na₂SO₄), and concentrated *in vacuo* to afford the crude salicylaldehyde **99**. Flash chromatography (silica gel, EtOAc/hexanes, DCM/hexanes or benzene/hexanes) afforded the pure salicylaldehyde **99**.

2-Hydroxy-5-methyl-3-[tris(3,5-dimethylphenyl)silyl]benzaldehyde (99d).

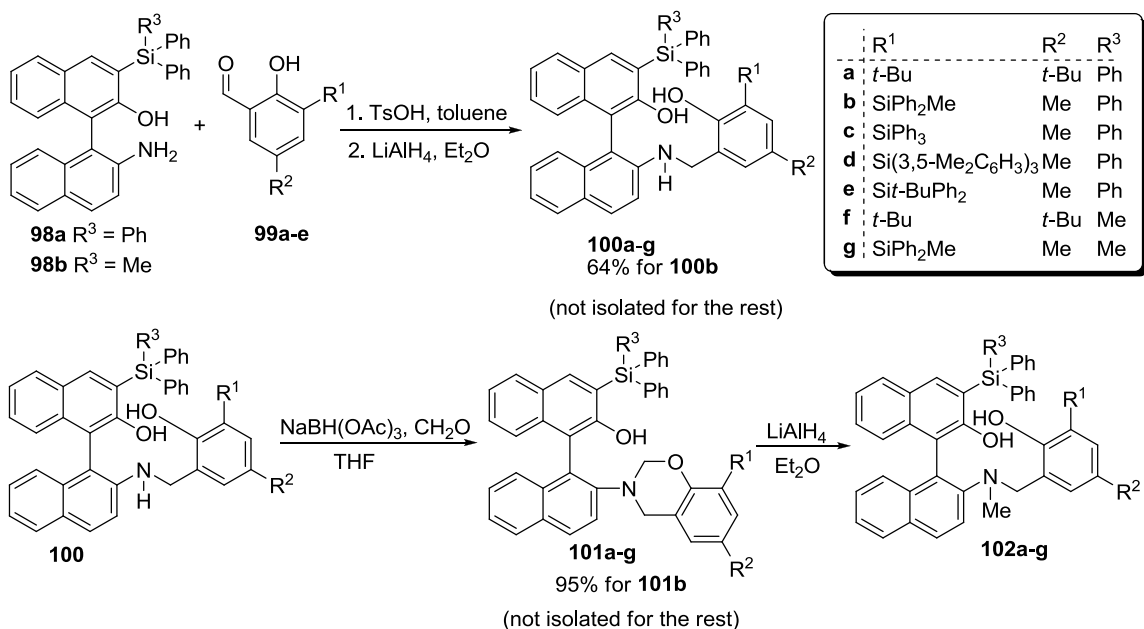
White solid, purified by flash chromatography on silica (hexanes/DCM=3:1). Yield 48 %. ¹H NMR (500 MHz, C₆D₆): δ = 11.81 (s, 1H, CHO), 9.21 (s, 1H, OH), 7.70–7.68 (m, 7H), 6.91 (s, 3H), 6.62 (s, 1H), 2.10 (s, 18 H, 6 CH₃), 1.86 (s, 3H, CH₃); ¹³C{¹H} NMR (125 MHz, C₆D₆): δ = 196.5 (CHO), 165.3 (CO), 147.1, 137.2, 135.9, 134.9, 134.7, 131.7, 128.6, 124.8, 120.1, 21.4 (CH₃), 20.1 (CH₃).

3-[*tert*-Butyl(diphenyl)silyl]-2-hydroxy-5-methylbenzaldehyde (99e).

White solid, purified by flash chromatography on silica (hexanes/toluene=2:1-1:1). Yield 80 %. ¹H NMR (400 MHz, CDCl₃): δ = 11.43 (s, 1H, CHO), 9.89 (s, 1H, OH), 7.56–7.54 (m, 4H), 7.44–7.34 (m, 7H), 7.20 (s, 1H), 2.21 (s, 3H, CH₃), 1.21 (s, 9H, *t*-Bu); ¹³C{¹H} NMR (100 MHz, CDCl₃): δ = 196.5 (CHO), 165.3 (CO), 147.1, 137.2, 135.9, 134.9, 134.7, 131.7, 128.6, 124.8, 120.1, 21.4 (CH₃), 20.1 (CH₃).

NMR (75 MHz, CDCl₃): δ = 196.7 (CHO), 164.4 (CO), 147.7, 136.1, 135.5, 134.8, 129.1, 128.6, 127.6, 124.0, 119.5, 29.6 (3 CH₃), 20.4 (CH₃), 18.5 (C(CH₃)₃)

Preparation of diol proligands **102**



To a suspension of aminophenol **98** (300 mg, 0.55 mmol) and aldehyde **99** (0.60 mmol) in toluene (10 mL) was added TsOH·H₂O and the mixture was stirred at 100 °C for 2 days. The solvent was evaporated and the residue was purified by flash chromatography on a short silica pad (hexanes/EtOAc 10:1). The eluate was evaporated and the residue was immediately subjected to the reduction as follows. The yellow Schiff base was dissolved in Et₂O (15 mL) and LiAlH₄ (100 mg, 3.1 mmol) was added in one portion. The originally yellow solution turned green immediately upon addition of the hydride. The mixture was stirred at room temperature for additional 10 min (TLC), quenched with 2% KOH (10 mL) and extracted with ethyl acetate (2 × 20 mL). The combined organic extracts were dried (Na₂SO₄) and the solvent was evaporated to yield crude secondary amine **100**. Compound **100b** was characterized by NMR spectroscopy,

other secondary amines were used further without characterization. The salane compound **100** was dissolved in THF (10 mL) and formaline (30% solution, 0.36 mL, 4 mmol) and $\text{NaBH}(\text{OAc})_3$ (420 mg, 2.0 mmol) were added in one portion at rt. The mixture was stirred for 20 min (monitored by TLC), then quenched with 2% KOH (20 mL) and extracted with Et_2O (2×50 mL). The combined organic layers were dried (Na_2SO_4) and passed through a short alumina plug. Compound **101b** was characterized by NMR, and all other amins were used further without characterization. To a stirred eluate containing cyclic amination intermediate **101**, LiAlH_4 (40 mg, 1 mmol) was added in one portion at room temperature. The mixture was stirred for 10 min, then quenched with 2% KOH (50 mL) and extracted with Et_2O (3×40 mL). The combined organic layers were passed through a short alumina plug and concentrated. The residue was dissolved in benzene (5 mL), frozen, and then subjected to a freeze-drying procedure to yield the proligand **102**.

2'-({2-Hydroxy-5-methyl-3-[methyl(diphenyl)silyl]benzyl}amino)-3-

(triphenyl-silyl)-1,1'-binaphthalen-2-ol (100b). Obtained via general procedure from **98a** and **99b**. White solid, yield 64%. ^1H NMR (500 MHz, C_6D_6): δ = 8.23 (s, 1H), 7.86–7.84 (m, 6H) 7.65 (m, 2H), 7.61–7.57 (m, 3H), 7.49 (d, $^3J(\text{H,H})$ = 9.1 Hz, 1H), 7.39 (d, $^3J(\text{H,H})$ = 7.6 Hz, 1H), 7.27–7.20 (m, 11H), 7.14–7.06 (m, 11H), 7.02–6.98 (m, 2H), 6.75 (s, 1H), 3.82 (vt, $^3J(\text{H,H})$ = 4.7, 3.7 Hz, 1H, NH), 3.64 (dd, $^2J(\text{H,H})$ = 15.7 Hz, $^3J(\text{H,H})$ = 3.7 Hz, 1H, CH_2), 3.59 (dd, $^2J(\text{H,H})$ = 15.7 Hz, $^3J(\text{H,H})$ = 4.7 Hz, 1H, CH_2), 2.03 (s, 3H, CH_3C), 0.93 (s, 3H, CH_3Si); $^{13}\text{C}\{^1\text{H}\}$ NMR (125 MHz, C_6D_6): δ = 159.9, 156.4 (CO), 145.2, 142.0, 137.18, 137.17, 137.1, 136.9, 135.62, 135.60, 135.31, 135.1, 134.0, 131.0,

130.9, 129.9, 129.7, 129.46, 129.44, 129.1, 128.6, 128.5, 128.08, 128.06, 124.5, 124.3, 124.2, 124.1, 123.8, 122.8, 122.7, 116.2, 113.5, 112.9 (aryl), 48.1 (CH₂), 20.6 (CH₃C), -2.6 (CH₃Si).

2'-[6-Methyl-8-[methyl(diphenyl)silyl]-2*H*-1,3-benzoxazin-3(4*H*)-yl]-3-

(triphenylsilyl)-1,1'-binaphthalen-2-ol (101b) To a stirred solution of **101a** (340 mg, 0.4 mmol) and formaline (0.36 mL, 4 mmol) in THF (10 mL) was added NaBH(OAc)₃ (420 mg, 2 mmol) in one portion at room temperature. The mixture was stirred for 10 min, then quenched with 2% KOH (10 mL) and extracted with Et₂O (2 × 50 mL). Combined organic layers were passed through a short alumina plug and evaporated to give 300 mg (96%) of the cyclic amination **101b** as an off-white solid which quickly oxidizes on air. ¹H NMR (400 MHz, C₆D₆): δ = 8.15 (s, 1H), 7.82 (d, ³*J*(H,H) = 7.0 Hz, 6H), 7.63–7.59 (m, 6H), 7.39–7.35 (m, 2H), 7.30 (d, ³*J*(H,H) = 8.6 Hz, 1H), 7.22–7.05 (m, 13H), 7.11–7.05 (m, 4H), 6.98–6.92 (m, 4H), 6.23 (s, 1H, aryl-H), 5.07 (s, 1H, OH), 4.60 (d, ²*J*(H,H) = 10.6 Hz, 1H, OCH₂), 4.35 (d, ²*J*(H,H) = 10.6 Hz, 1H, OCH₂), 3.82 (d, ²*J*(H,H) = 16.8 Hz, 1H, CH₂), 3.82 (d, ²*J*(H,H) = 16.8 Hz, 1H, CH₂), 3.76 (d, ²*J*(H,H) = 16.8 Hz, 1H, CH₂), 1.89 (s, 3H, CH₃C), 0.91 (s, 3H, CH₃Si); ¹³C{¹H} NMR (100 MHz, C₆D₆): δ = 157.2, 155.2 (CO), 147.8, 141.3, 137.32, 137.28, 136.9, 136.4, 135.68, 135.67, 135.5, 135.4, 134.1, 131.6, 130.6, 129.9, 129.8, 129.64, 129.58, 129.35, 129.32, 129.29, 128.5, 128.1, 128.0, 127.9, 127.2, 125.7, 125.2, 125.0, 124.8, 123.7, 123.66, 123.62, 122.92, 121.78, 120.2, 117.2 (aryl), 79.8 (OCH₂), 51.6 (NCH₂), 20.5 (CH₃C), -2.6 (CH₃Si).

2'-[(3,5-Di-*tert*-butyl-2-hydroxybenzyl)(methylamino)]-3-(triphenylsilyl)-1,1'-binaphthalen-2-ol (102a). Prepared from **98a** and **99a**. White solid, yield 79 %. ^1H NMR (500 MHz, C_6D_6): δ = 8.74 (s, 1H), 8.21 (s, 1H), 7.82 (d, $^3J(\text{H,H})$ = 7.6 Hz, 6H), 7.78 (d, $^3J(\text{H,H})$ = 8.8 Hz, 1H), 7.72 (d, $^3J(\text{H,H})$ = 8.3 Hz, 1H), 7.54 (d, $^3J(\text{H,H})$ = 7.8 Hz, 1H), 7.49 (d, $^3J(\text{H,H})$ = 8.6 Hz, 1H), 7.40 (m, 1H), 7.35 (d, $^3J(\text{H,H})$ = 8.8 Hz, 1H), 7.25 (vt, $^3J(\text{H,H})$ = 7.6, 7.3 Hz, 1H), 7.20 (t, $^3J(\text{H,H})$ = 7.8 Hz, 3H), 7.09 (t, $^3J(\text{H,H})$ = 7.6 Hz, 3H), 7.05–7.00 (m, 3H), 6.93 (s, 1H, aryl-H), 4.29 (s, 1H, OH), 3.92 (d, $^2J(\text{H,H})$ = 13.2 Hz, 1H, CH_2), 3.58 (d, $^2J(\text{H,H})$ = 13.2 Hz, 1H, CH_2), 2.31 (s, 3H, CH_3), 1.40 (s, 9 H, $\text{C}(\text{CH}_3)_3$), 1.33 (s, 9H, $\text{C}(\text{CH}_3)_3$); $^{13}\text{C}\{^1\text{H}\}$ NMR (125 MHz, C_6D_6): δ = 155.4, 154.5, 151.0, 142.1, 140.4, 136.9, 135.9, 135.6, 135.1, 133.9, 132.8, 130.7, 130.6, 129.6, 129.3, 128.5, 128.3, 128.1, 127.9, 127.5, 126.5, 126.4, 123.9, 123.8, 123.7, 123.3, 121.3, 120.3, 115.9 (aryl-C), 63.6 (CH_2), 40.4 (CH_3), 35.0 ($\text{C}(\text{CH}_3)_3$), 34.3 ($\text{C}(\text{CH}_3)_3$), 32.0 ($\text{C}(\text{CH}_3)_3$), 29.7 $\text{C}(\text{CH}_3)_3$.

2'-[2-Hydroxy-5-methyl-3-[methyl(diphenyl)silyl]benzyl](methylamino)-3-(triphenylsilyl)-1,1'-binaphthalen-2-ol (102b). Prepared from **101b**. White solid, yield 97%. ^1H NMR (500 MHz, C_6D_6): δ = 8.24 (s, 1H), 8.14 (s, 1H), 7.84 (d, $^3J(\text{H,H})$ = 6.8 Hz, 6H), 7.75 (d, $^3J(\text{H,H})$ = 9.1 Hz, 1H), 7.70 (d, $^3J(\text{H,H})$ = 7.8 Hz, 1H), 7.61–7.56 (m, 2H), 7.48 (d, $^3J(\text{H,H})$ = 6.4 Hz, 2H), 7.44 (m, $^3J(\text{H,H})$ = 8.7 Hz, 1H), 7.31–7.28 (m, 2H), 7.24 (t, $^3J(\text{H,H})$ = 7.6 Hz, 6H), 7.18–7.08 (m, 11H), 7.03–6.93 (m, 3H), 6.73 (s, 1H, aryl-H), 4.26 (s, 1H, OH), 3.87 (d, $^2J(\text{H,H})$ = 13.2 Hz, 1H, CH_2), 3.61 (d, $^2J(\text{H,H})$ = 13.2 Hz, 1H, CH_2), 2.24 (s, 3H, CH_3N), 2.06 (s, 3H, CH_3C), 0.78 (s, 3H, CH_3Si); $^{13}\text{C}\{^1\text{H}\}$ NMR (125 MHz, C_6D_6): δ = 160.84, 155.2 (CO), 150.9, 142.1, 137.73, 137.65, 137.63, 136.9,

135.7, 135.5, 135.2, 135.1, 133.8, 132.6, 132.1, 130.7, 130.2, 129.6, 129.4, 129.1, 128.9, 128.5, 128.1, 127.93, 127.89, 127.77, 127.6, 127.5, 127.3, 126.3, 126.1, 123.8, 123.6, 123.4, 122.2, 120.1, 115.8 (aryl), 62.0 (CH₂), 40.7 (CH₃N), 20.6 (CH₃C), -2.3 (CH₃Si).

2'-[[2-Hydroxy-5-methyl-3-(triphenylsilyl)benzyl](methylamino)-3-(triphenylsilyl)-1,1'-binaphthalen-2-ol (102c). Prepared from **98a** and **99c**. White solid, yield 72 %. ¹H NMR (400 MHz, C₆D₆): δ = 8.06 (s, 1H), 7.82 (s, 1H), 7.77 (d, ³J(H,H) = 7.0 Hz, 6H), 7.67 (d, ³J(H,H) = 9.0 Hz, 1H), 7.63 (d, ³J(H,H) = 8.2 Hz, 1H), 7.57 (d, ³J(H,H) = 7.4 Hz, 6H), 7.36 (d, ³J(H,H) = 8.6 Hz, 1H), 7.22–6.93 (m, 23H), 6.74–6.70 (m, 2H, aryl-H), 4.25 (s, 1H, OH), 3.84 (d, ²J(H,H) = 12.9 Hz, 1H, CH₂), 3.58 (d, ²J(H,H) = 12.9 Hz, 1H, CH₂), 2.15 (s, 3H, CH₃N), 1.99 (s, 3 H, CH₃C); ¹³C{¹H} NMR (100 MHz, C₆D₆): δ = 160.4, 155.0 (CO), 150.8, 142.1, 138.8, 136.9, 136.8, 135.7, 135.3, 134.6, 133.7, 132.8, 132.2, 130.5, 130.0, 129.6, 129.3, 129.2, 128.1, 127.8, 127.5, 126.1, 126.0, 125.7, 124.0, 123.3, 122.8, 121.1, 120.9, 120.8, 115.9 (aryl-C), 60.9 (CH₂), 40.5 (CH₃N), 20.6 (CH₃C).

2'-[[2-Hydroxy-5-methyl-3-[tris(3,5-dimethylphenyl)silyl]benzyl](methylamino)-3-(triphenylsilyl)-1,1'-binaphthalen-2-ol (102d). Prepared from **98a** and **99d**. White solid, yield 82 %. ¹H NMR (400 MHz, C₆D₆): δ = 8.12 (s, 1H), 7.80 (d, ³J(H,H) = 7.8 Hz, 6H), 7.64 (d, ³J(H,H) = 8.2 Hz, 1H), 7.63 (d, ³J(H,H) = 9.0 Hz, 1H), 7.59 (m, 1H), 7.57 (s, 6H), 7.39–7.36 (m, 3 H), 7.26 (d, ³J(H,H) = 9.3 Hz, 1H), 7.22–7.16 (m, 9 H), 7.09 (d, ³J(H,H) = 8.6 Hz, 1H), 7.02 (t, ³J(H,H) = 7.7 Hz, 1H), 6.97 (vt, ³J(H,H) = 8.1, 6.9 Hz, 1H), 6.90 (d, ³J(H,H) = 7.7 Hz, 1H), 6.87 (s, 3H), 6.63 (s, 1H, aryl-H),

4.79 (s, 1H, OH), 3.93 (d, $^2J(\text{H,H}) = 13.7$ Hz, 1H, CH₂), 3.90 (d, $^2J(\text{H,H}) = 13.7$ Hz, 1H, CH₂), 2.43 (s, 3H, CH₃N), 2.09 (s, 18H, 6 CH₃C), 1.95 (s, 3H, CH₃C); $^{13}\text{C}\{^1\text{H}\}$ NMR (100 MHz, C₆D₆): $\delta = 160.0, 155.4, 150.6, 141.5, 138.7, 137.0, 136.9, 135.5, 135.4, 135.3, 134.6, 134.1, 133.3, 131.7, 131.5, 130.4, 129.7, 129.6, 129.2, 128.8, 128.5, 128.0, 127.3, 125.58, 125.55, 124.4, 124.2, 123.8, 123.7, 122.7, 122.1, 121.4, 116.9$ (aryl-C), 58.5 (CH₂), 40.4 (CH₃N), 21.5 (CH₃C), 20.6 (CH₃C).

2'-[3-[*tert*-Butyl(diphenyl)silyl]-2-hydroxy-5-methylbenzyl](methylamino)-3-(triphenylsilyl)-1,1'-binaphthalen-2-ol (102e). Prepared from **98a** and **99e**. White solid, yield 85 %. ^1H NMR (400 MHz, C₆D₆): $\delta = 8.13$ (br s, 1H), 8.02 (s, 1H), 7.76 (d, $^3J(\text{H,H}) = 7.1$ Hz, 6H), 7.71 (d, $^3J(\text{H,H}) = 9.0$ Hz, 1H), 7.65 (d, $^3J(\text{H,H}) = 8.2$ Hz, 1H), 7.61 (d, $^3J(\text{H,H}) = 6.7$ Hz, 2H), 7.52 (d, $^3J(\text{H,H}) = 7.1$ Hz, 2H), 7.33 (d, $^3J(\text{H,H}) = 8.6$ Hz, 1H), 7.29 (d, $^3J(\text{H,H}) = 9.0$ Hz, 1H), 7.21–6.95 (m, 21H), 6.83 (vt, $^3J(\text{H,H}) = 6.7, 7.8$ Hz, 1 H), 6.70 (s, 1H, aryl-H), 4.19 (s, 1H, OH), 3.98 (d, $^2J(\text{H,H}) = 13.3$ Hz, 1H, CH₂), 3.56 (d, $^2J(\text{H,H}) = 13.3$ Hz, 1H, CH₂), 2.29 (s, 3H), 1.97 (s, 3H), 1.10 (s, 9H, C(CH₃)₃); $^{13}\text{C}\{^1\text{H}\}$ NMR (100 MHz, C₆D₆): $\delta = 160.1, 155.1, 150.9, 142.3, 139.9, 136.9, 136.75, 136.72, 136.3, 135.2, 134.8, 133.7, 132.6, 132.3, 130.7, 129.6, 128.9, 128.8, 128.5, 128.1, 127.9, 127.7, 127.5, 127.0, 126.3, 126.0, 124.0, 123.4, 123.2, 121.6, 121.0, 120.5, 115.8$ (aryl-C), 62.1 (CH₂), 40.6 (CH₃N), 30.3, 20.6, 18.8.

2'-[(3,5-Di-*tert*-Butyl-2-hydroxybenzyl)(methylamino)-3-(triphenylsilyl)-1,1'-binaphthalen-2-ol (102f) Prepared from **98b** and **99a**. White solid, yield 71 %. ^1H NMR (500 MHz, C₆D₆): $\delta = 8.64$ (s, 1H), 8.15 (s, 1H), 7.77 (d, $^3J(\text{H,H}) = 8.6$ Hz, 6H),

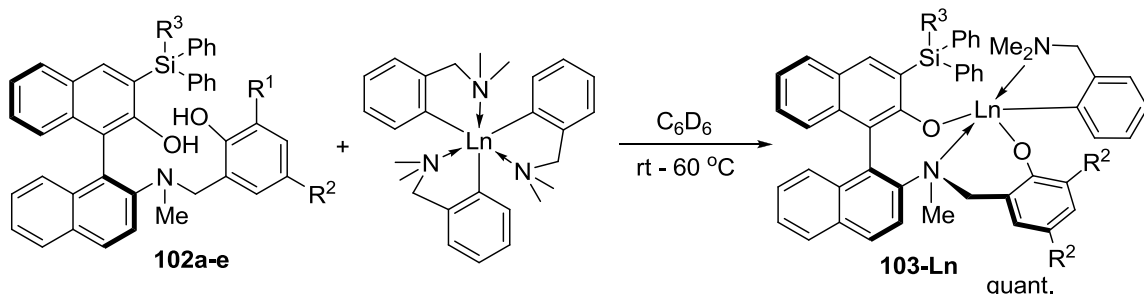
7.71–7.67 (m, 5H), 7.58 (d, $^3J(\text{H,H}) = 8.2$ Hz, 1H), 7.43 (d, $^3J(\text{H,H}) = 8.2$ Hz, 1H), 7.39 (d, $^4J(\text{H,H}) = 2.4$ Hz, 1H), 7.34 (d, $^3J(\text{H,H}) = 8.4$ Hz, 1H), 7.22–7.14 (m, 7H), 7.07–7.03 (m, 2H), 7.02–7.99 (m, 4H), 6.96 (m, 1H), 6.90 (d, $^4J(\text{H,H}) = 2.4$ Hz, 1H, aryl-H), 4.29 (s, 1H, OH), 3.85 (d, $^2J(\text{H,H}) = 13.3$ Hz, 1H, CH₂), 3.66 (d, $^2J(\text{H,H}) = 13.3$ Hz, 1H, CH₂), 2.27 (s, 3H, CH₃), 1.37 (s, 9 H, C(CH₃)₃), 1.36 (s, 9H, C(CH₃)₃), 1.05 (s, 3H, CH₃Si); $^{13}\text{C}\{^1\text{H}\}$ NMR (100 MHz, C₆D₆): $\delta = 155.5, 154.4$ (CO), 151.0, 140.8, 140.7, 140.4, 137.1, 136.8, 135.9, 135.8, 135.7, 135.5, 135.4, 134.0, 132.7, 130.9, 130.7, 130.4, 129.4, 129.3, 126.5, 125.3, 123.9, 123.7, 123.4, 123.2, 121.4, 121.3, 120.3, 115.3 (aryl), 63.3 (CH₂), 40.4 (NCH₃), 35.0 (C(CH₃)₃), 34.3 (C(CH₃)₃), 32.1 (C(CH₃)₃), 29.8 C(CH₃)₃, –2.9 (CH₃Si).

2'-[2-Hydroxy-5-methyl-3-[methyl(diphenyl)silyl]benzyl](methylamino)-3-[methyl(diphenyl)silyl]-1,1'-binaphthalen-2-ol (102g). Prepared from **98b** and **99b**. White solid, yield 93%. ^1H NMR (500 MHz, C₆D₆): $\delta = 8.17$ (s, 1H), 8.03 (s, 1H), 7.75 (d, $^3J(\text{H,H}) = 8.6$ Hz, 1H), 7.68 (m, 5H), 7.60 (m, 1H), 7.49 (d, $^3J(\text{H,H}) = 7.1$, Hz, 1H), 7.39 (d, $^3J(\text{H,H}) = 7.8$, Hz, 1H), 7.31 (d, $^3J(\text{H,H}) = 8.6$, Hz, 1H), 7.24–7.08 (m, 15H), 6.98 (m, 4H), 6.70 (s, 1H, aryl-H), 4.31 (s, 1H, OH), 3.82 (d, $^2J(\text{H,H}) = 13.2$ Hz, 1H, CH₂), 3.67 (d, $^2J(\text{H,H}) = 13.2$ Hz, 1H, CH₂), 2.23 (s, 3H, CH₃N), 2.04 (s, 3H, CH₃C), 1.00 (s, 3H, CH₃Si), 0.85 (s, 3H, CH₃Si); $^{13}\text{C}\{^1\text{H}\}$ NMR (C₆D₆, 125 MHz) δ : 160.84, 155.4 (CO), 150.9, 140.7, 137.74, 137.66, 137.2, 136.8, 135.8, 135.7, 135.6, 135.0, 133.9, 132.5, 132.2, 130.8, 130.0, 129.44, 129.38, 128.9, 128.5, 127.1, 126.3, 126.2, 124.9, 123.7, 122.1, 121.2, 120.1, 115.2 (Aryl-C), 61.8 (CH₂), 40.8 (CH₃N), 20.5 (CH₃C), –2.3 (CH₃Si), –2.7 (CH₃Si).

Complex Synthesis

Rare earth metal precursors $\text{Ln}(o\text{-C}_6\text{H}_4\text{CH}_2\text{NMe}_2)_3$ ($\text{Ln} = \text{Y}, \text{Lu}$),¹³ and $\text{La}[\text{CH}(\text{C}_6\text{H}_5)\text{NMe}_2]_3$ ²¹ were synthesized according to the published protocols.

General Procedure for the NMR-Scale Preparation of **103-Ln**.



To a mixture of diol proligand **102** (0.05 mmol) and the rare earth metal precursor (0.05 mmol) was added C_6D_6 (490 mg, 500 μL). The mixture was shaken vigorously and then left for 5 minutes at room temperature or slightly elevated temperature. Clean quantitative conversion to the diolate complex **103-Ln** was confirmed by NMR spectroscopy. Aliquots of the resulting complex solution were used directly for the catalytic experiments.

(S)-[Y{NOBIN-TPS/*t*-Bu}(*o*-C₆H₄CH₂NMe₂)] ((S)-103a-Y). To a mixture of (*S*)-**102a** (28.4 mg, 0.036 mmol) and $[\text{Y}(o\text{-C}_6\text{H}_4\text{CH}_2\text{NMe}_2)_3]$ (18.0 mg, 0.036 mmol) was added C_6D_6 (0.55 mL). The mixture was kept at room temperature for 2 h. ^1H and ^{13}C NMR spectra showed clean formation of (*S*)-**103a-Y**, which was used directly for catalytic experiments. ^1H NMR (500 MHz, C_6D_6): $\delta = 7.99$ (d, $^3J(\text{H,H}) = 9.0$ Hz, 1H), 7.88 (s, 1H), 7.74 (d, $^3J(\text{H,H}) = 7.8$ Hz, 6H), 7.68 (d, $^3J(\text{H,H}) = 8.2$ Hz, 1H), 7.65 (d, $^3J(\text{H,H}) = 9.3$ Hz, 1H), 7.62 (d, $^3J(\text{H,H}) = 8.1$ Hz, 1H), 7.51 (s, 1H), 7.32–7.26 (m, 7H),

7.13–6.79 (m, 20H, aryl), 4.48 (d, $^2J(\text{H,H}) = 12.2$ Hz, 1H, CH_2N), 3.60 (d, $^2J(\text{H,H}) = 12.2$ Hz, 1H, CH_2N), 3.53 (d, $^2J(\text{H,H}) = 13.7$ Hz, 1H, $o\text{-C}_6\text{H}_4\text{CH}_2\text{NMe}_2$), 3.25 (s, 4H, $2\text{C}_6\text{H}_5\text{NCH}_2\text{NMe}_2$), 2.98 (d, $^2J(\text{H,H}) = 13.7$ Hz, 1H, $o\text{-C}_6\text{H}_4\text{CH}_2\text{NMe}_2$), 2.47 (s, 3H, NCH_3), 2.06 (s, 12 H, $2\text{C}_6\text{H}_5\text{CH}_2\text{NMe}_2$), 1.75 (br s, 3H, $o\text{-C}_6\text{H}_4\text{CH}_2\text{NMe}_2$), 1.44 (s, 9 H, $\text{C}(\text{CH}_3)_3$), 1.41 (s, 9H, $\text{C}(\text{CH}_3)_3$), 1.01 (s, 3H, $o\text{-C}_6\text{H}_4\text{CH}_2\text{NMe}_2$); $^{13}\text{C}\{^1\text{H}\}$ NMR (100 MHz, C_6D_6): $\delta = 179.7$ (d, $^1J(\text{C,Y}) = 62$ Hz, C-Y), 164.4 (CO), 161.1 (CO), 146.1, 142.9, 142.3, 140.0, 138.3, 138.2, 137.8, 136.8, 136.6, 136.1, 135.7, 132.1, 131.3, 130.9, 129.6, 129.1, 128.9, 128.5, 128.3, 127.6, 127.5, 127.4, 127.2, 127.0, 126.4, 126.3, 126.2, 125.4, 125.0, 124.9, 124.4, 123.7, 121.8, 120.0, 118.2 (aryl), 67.0 (CH_2N), 64.5 ($\text{C}_6\text{H}_5\text{CH}_2\text{NMe}_2$), 59.1 (CH_2N), 45.4 ($\text{C}_6\text{H}_5\text{CH}_2\text{NMe}_2$), 44.5 ($\text{N}(\text{CH}_3)_2$), 43.2 ($\text{N}(\text{CH}_3)_2$), 38.5 (CH_3N), 35.4 ($\text{C}(\text{CH}_3)_3$), 34.3 ($\text{C}(\text{CH}_3)_3$), 32.2 ($\text{C}(\text{CH}_3)_3$), 30.1 ($\text{C}(\text{CH}_3)_3$).

(*S*)-[Lu{NOBIN-TPS/*t*-Bu}(*o*-C₆H₄CH₂NMe₂)] ((*S*)-103a-Lu**).** To a mixture of (*S*)-**102a** (23.6 mg, 0.038 mmol) and [Lu(*o*-C₆H₄CH₂NMe₂)₃] (22.0 mg, 0.038 mmol) was added C₆D₆ (0.55 mL). The mixture was kept at room temperature for 30 min. ^1H and ^{13}C NMR showed clean formation of (*S*)-**103a-Lu**, which was used directly for catalytic experiments. ^1H NMR (500 MHz, C_6D_6 , 60 °C): $\delta = 7.98$ (d, $^3J(\text{H,H}) = 9.0$ Hz, 1H), 7.92 (s, 1H), 7.76 (d, $^3J(\text{H,H}) = 7.8$ Hz, 6H), 7.66 (d, $^3J(\text{H,H}) = 9.0$ Hz, 1H), 7.62 (d, $^3J(\text{H,H}) = 8.8$ Hz, 1H), 7.55 (d, $^4J(\text{H,H}) = 2.2$ Hz, 1H), 7.32–7.26 (m, 6H), 7.19–6.90 (m, 20H, aryl-H), 6.86–6.78 (m, 3H), 6.64 (d, $^3J(\text{H,H}) = 7.3$ Hz, 1H), 6.48 (d, $^3J(\text{H,H}) = 7.3$ Hz, 1H), 4.57 (d, $^2J(\text{H,H}) = 12.2$ Hz, 1H, CH_2N), 3.69 (d, $^2J(\text{H,H}) = 12.2$ Hz, 1H, CH_2N), 3.62 (d, $^2J(\text{H,H}) = 13.7$ Hz, 1H, $o\text{-C}_6\text{H}_4\text{CH}_2\text{NMe}_2$), 3.24 (s, 4H, $2\text{C}_6\text{H}_5\text{NCH}_2\text{NMe}_2$), 2.88 (d, $^2J(\text{H,H}) = 13.7$ Hz, 1H, $o\text{-C}_6\text{H}_4\text{CH}_2\text{NMe}_2$), 2.44 (s, 3H, NCH_3), 2.06 (s, 12 H, $2\text{C}_6\text{H}_5\text{CH}_2\text{NMe}_2$), 1.75 (s, 3H, $o\text{-C}_6\text{H}_4\text{CH}_2\text{NMe}_2$), 1.46 (s, 9 H, $\text{C}(\text{CH}_3)_3$), 1.42 (s, 9H,

$\text{C}(\text{CH}_3)_3$), 1.31 (s, 3H, *o*- $\text{C}_6\text{H}_4\text{CH}_2\text{NMe}_2$); $^{13}\text{C}\{^1\text{H}\}$ NMR (125 MHz, C_6D_6): δ = 187.5 (C-Lu), 165.0 (CO), 161.5 (CO), 146.2, 143.0, 140.0, 139.7, 138.3, 137.8, 136.8, 136.7, 136.2, 132.1, 130.6, 129.6, 129.1, 128.93, 128.87, 128.5, 128.4, 128.3, 127.9, 127.7, 127.4, 120.1, 118.3 (Aryl-C), 66.2 (CH_2N), 64.5 ($\text{C}_6\text{H}_5\text{CH}_2\text{NMe}_2$), 59.2 (CH_2N), 45.4 ($\text{C}_6\text{H}_5\text{CH}_2\text{NMe}_2$), 44.8 ($\text{N}(\text{CH}_3)_2$), 43.6 ($\text{N}(\text{CH}_3)_2$), 38.6 (CH_3N), 35.3 ($\text{C}(\text{CH}_3)_3$), 34.2 ($\text{C}(\text{CH}_3)_3$), 32.2 ($\text{C}(\text{CH}_3)_3$), 30.7 ($\text{C}(\text{CH}_3)_3$).

(*S*)-[Y{NOBIN-TPS/SiPh₂Me}(*o*- $\text{C}_6\text{H}_4\text{CH}_2\text{NMe}_2$)] ((*S*)-103b-Y**).** To a mixture of (*S*)-**102b** (29.0 mg, 0.033 mmol) and $[\text{Y}(\textit{o}\text{-C}_6\text{H}_4\text{CH}_2\text{NMe}_2)_3]$ (16.3 mg, 0.033 mmol) was added C_6D_6 (0.55 mL). The mixture was kept at room temperature for 30 min. ^1H and ^{13}C NMR spectra showed clean formation of (*S*)-**103b-Y**, which was used directly for catalytic experiments. ^1H NMR (500 MHz, C_6D_6 , 60 °C): δ = 7.94 (d, $^3J(\text{H,H})$ = 9.0 Hz, 1H), 7.76 (d, $^3J(\text{H,H})$ = 7.8 Hz, 6H), 7.53–6.57 (m, 40H), 6.54 (m, 2H, aryl-H), 4.47 (d, $^2J(\text{H,H})$ = 12.2 Hz, 1H, CH_2N), 3.78 (d, $^2J(\text{H,H})$ = 12.2 Hz, 1H, CH_2N), 2.70 (d, $^2J(\text{H,H})$ = 13.7 Hz, 1H, *o*- $\text{C}_6\text{H}_4\text{CH}_2\text{NMe}_2$), 2.47 (s, 3H, NCH_3), 2.32 (d, $^2J(\text{H,H})$ = 13.7 Hz, 1H, *o*- $\text{C}_6\text{H}_4\text{CH}_2\text{NMe}_2$), 1.22 (s, 3H, *o*- $\text{C}_6\text{H}_4\text{CH}_2\text{NMe}_2$), 1.04 (s, 3H, *o*- $\text{C}_6\text{H}_4\text{CH}_2\text{NMe}_2$), 0.78 (s, 3H, SiCH_3); $^{13}\text{C}\{^1\text{H}\}$ NMR (100 MHz, C_6D_6): δ = 179.4 (d, $^1J(\text{C,Y})$ = 61 Hz, C-Y), 168.4 (CO), 164.6 (CO), 146.5, 143.0, 140.4, 140.0, 139.0, 138.1, 137.72, 137.67, 137.03, 136.98, 136.9, 136.8, 136.7, 136.1, 136.0, 135.6, 135.4, 135.3, 132.0, 131.0, 129.81, 129.76, 129.3, 129.1, 129.04, 129.01, 128.54, 128.50, 128.45, 128.4, 128.1, 127.6, 127.4, 127.2, 126.5, 126.4, 126.0, 125.3, 125.2, 124.8, 124.6, 122.7, 121.8, 121.31, 120.0, 118.2 (aryl), 65.9 (CH_2N), 64.5 ($\text{C}_6\text{H}_5\text{CH}_2\text{NMe}_2$), 58.7 (CH_2N), 45.4

(C₆H₅CH₂NMe₂), 44.0 (N(CH₃)₂), 42.6 (N(CH₃)₂), 38.7 (CH₃N), 20.5 (CH₃C), -1.0 (CH₃Si).

(S)-[Y{NOBIN-TPS/TPS}(*o*-C₆H₄CH₂NMe₂)] ((S)-103c-Y). To a mixture of (S)-102c (23.4 mg, 0.025 mmol) and [Y(*o*-C₆H₄CH₂NMe₂)₃] (12.3 mg, 0.025 mmol) was added C₆D₆ (0.55 mL). The mixture was kept at room temperature for 30 min. ¹H and ¹³C NMR spectra showed clean formation of (S)-103c-Y, which was used directly for catalytic experiments. ¹H NMR (500 MHz, C₆D₆, 65 °C): δ = 7.98 (s, 1H), 7.86 (d, ³J(H,H) = 9.3 Hz, 1H), 7.72 (d, ³J(H,H) = 7.8 Hz, 6H), 7.69 (m, 2H), 7.60 (d, ³J(H,H) = 7.8 Hz, 6H), 7.58 (m, 2H), 7.37 (d, ³J(H,H) = 8.8 Hz, 2H), 7.27 (d, ³J(H,H) = 7.1 Hz, 12H), 7.20 (m, 1H), 7.15–6.85 (m, 25H), 6.77 (m, 2H), 6.71 (m, 1H), 6.86–6.78 (m, 3H), 6.57 (d, ³J(H,H) = 8.3 Hz, 1H), 6.47 (d, ³J(H,H) = 7.3 Hz, 1H, aryl), 4.42 (d, ²J(H,H) = 12.7 Hz, 1H, CH₂N), 4.26 (d, ²J(H,H) = 12.7 Hz, 1H, CH₂N), 3.24 (s, 4H, 2C₆H₅NCH₂NMe₂), 2.75 (d, ²J(H,H) = 13.9 Hz, 1H, *o*-C₆H₄CH₂NMe₂), 2.66 (s, 3H, NCH₃), 2.49 (d, J = 13.7 Hz, 1H, *o*-C₆H₄CH₂NMe₂), 2.07 (3H, CH₃C), 2.06 (s, 12 H, 2C₆H₅CH₂NMe₂), 0.86 (br s, 6H, *o*-C₆H₄CH₂NMe₂); ¹³C{¹H} NMR (125 MHz, C₆D₆): δ = 179.9 (d, ¹J(C,Y) = 60 Hz, C-Y), 168.3 (CO), 164.9 (CO), 146.6, 143.0, 141.0, 140.0, 138.4, 137.6, 136.93, 136.87, 136.81, 136.75, 135.6, 135.4, 131.8, 130.8, 130.7, 129.7, 129.3, 129.1, 128.5, 128.3, 128.1, 127.9, 127.5, 127.4, 127.2, 126.7, 126.5, 125.9, 125.5, 125.2, 125.7, 124.6, 123.7, 121.9, 120.4, 120.3, 118.1 (aryl), 66.5 (CH₂N), 64.5 (C₆H₅CH₂NMe₂), 58.9 (CH₂N), 45.4 (C₆H₅CH₂NMe₂), 43.0 (N(CH₃)₂), 42.9 (N(CH₃)₂), 39.4 (CH₃N), 20.6 (CH₃C).

(S)-[Lu{NOBIN-TPS/TPS}(*o*-C₆H₄CH₂NMe₂)] ((S)-103c-Lu). To a mixture of (S)-**102c** (23.4 mg, 0.025 mmol) and [Lu(*o*-C₆H₄CH₂NMe₂)₃] (14.3 mg, 0.025 mmol) was added C₆D₆ (0.55 mL). The mixture was kept at room temperature for 30 min. ¹H and ¹³C NMR spectra showed clean formation of (S)-**103c-Lu**, which was used directly for catalytic experiments. ¹H NMR (400 MHz, C₆D₆): δ = 8.04 (s, 1H), 7.92–7.88 (m, 2H), 7.74 (d, ³J(H,H) = 8.0 Hz, 6H), 7.66–7.59 (m, 10H), 7.31–6.77 (m, 31H), 6.60 (d, ³J(H,H) = 7.9 Hz, 2H), 6.48–6.46 (m, 2H), 4.50 (d, ²J(H,H) = 12.5 Hz, 1H, CH₂), 4.19 (d, ²J(H,H) = 12.5 Hz, 1H, CH₂), 3.22 (s, 4 H, 2C₆H₅CH₂NMe₂), 2.91 (d, ²J(H,H) = 14.1 Hz, 1H, CH₂), 2.72 (s, 3H), 2.46 (d, ²J(H,H) = 14.1 Hz, 1H, CH₂), 2.09 (s, 3H), 2.02 (s, 12H, 2C₆H₅CH₂NMe₂), 1.32 (s, 3H, NMe₂), 0.99 (s, 3H, NMe₂); ¹³C {¹H}NMR (125 MHz, C₆D₆): δ = 187.5 (C-Lu), 167.4, 165.2, 147.2, 147.0, 143.2, 142.5, 141.0, 139.9, 139.9, 139.8, 139.3, 137.81, 136.76, 136.5, 132.0, 129.5, 129.2, 129.0, 128.9, 128.3, 127.3, 127.0, 127.3, 126.8, 126.1, 125.6, 125.3, 125.1, 124.9, 124.7, 122.8, 120.9, 120.2, 118.0 (aryl), 69.5, 65.3, 64.4, 46.1, 45.3, 43.0, 20.42 (CH₃C).

(S)-[Y{NOBIN-TPS/TPDMS}(*o*-C₆H₄CH₂NMe₂)] ((S)-103d-Y). To a mixture of (S)-**102d** (30.8 mg, 0.030 mmol) and [Y(*o*-C₆H₄CH₂NMe₂)₃] (14.8 mg, 0.030 mmol) was added C₆D₆ (0.55 mL). The mixture was kept at 60 °C for 3 h. ¹H and ¹³C NMR spectra showed clean formation of (S)-**103d-Y**, which was used directly for catalytic experiments. ¹H NMR (400 MHz, C₆D₆): δ = 8.03 (s, 1H), 8.01 (d, ³J(H,H) = 9.0 Hz, 1H), 7.77 (d, ³J(H,H) = 9.3 Hz, 1H), 7.69 (d, ³J(H,H) = 8.0 Hz, 6H), 7.65 (d, ³J(H,H) = 8.3 Hz, 1H), 7.55 (s, 6H), 7.53 (m, 1H), 7.39 (br s, 1H), 7.35 (d, ³J(H,H) = 7.8 Hz, 1H), 7.31 (d, ³J(H,H) = 7.8 Hz, 3H), 7.19–7.01 (m, 14H), 6.90–6.75 (m, 13H), 6.72 (d, ³J(H,H)

= 7.6 Hz, 1H), 6.67 (d, $^3J(\text{H,H}) = 8.3$ Hz, 1H, aryl-H), 5.16 (d, $^2J(\text{H,H}) = 13.0$ Hz, 1H, CH_2N), 4.08 (d, $^2J(\text{H,H}) = 13.0$ Hz, 1H, CH_2N), 3.37 (d, $^2J(\text{H,H}) = 13.7$ Hz, 1H, *o*- $\text{C}_6\text{H}_4\text{CH}_2\text{NMe}_2$), 3.23 (s, 4H, $2\text{C}_6\text{H}_5\text{NCH}_2\text{NMe}_2$), 2.84 (s, 3H, NCH_3), 2.29 (d, $^2J(\text{H,H}) = 13.7$ Hz, 1H, *o*- $\text{C}_6\text{H}_4\text{CH}_2\text{NMe}_2$), 2.08 (3H, CH_3C), 2.06 (s, 12 H, $2\text{C}_6\text{H}_5\text{CH}_2\text{NMe}_2$), 1.97 (s, 18H, 6 CH_3C), 1.15 (s, 3H, *o*- $\text{C}_6\text{H}_4\text{CH}_2\text{NMe}_2$), 0.45 (s, 3H, *o*- $\text{C}_6\text{H}_4\text{CH}_2\text{NMe}_2$); $^{13}\text{C}\{^1\text{H}\}$ NMR (125 MHz, C_6D_6): $\delta = 179.5$ (d, $^1J(\text{C,Y}) = 61$ Hz, C-Y), 168.1 (CO), 164.0 (CO), 146.9, 143.3, 143.0, 141.4, 140.0, 139.0, 138.0, 137.3, 137.2, 136.7, 136.6, 135.7, 135.6, 134.8, 132.4, 131.4, 130.4, 129.4, 129.1, 128.9, 128.53, 128.46, 128.3, 128.2, 127.9, 127.2, 126.7, 126.4, 126.3, 125.7, 125.4, 125.3, 124.8, 123.6, 122.0, 121.4, 120.0, 117.1 (aryl), 66.8 (CH_2N), 64.5 ($\text{C}_6\text{H}_5\text{CH}_2\text{NMe}_2$), 58.4 (CH_2N), 45.4 ($\text{C}_6\text{H}_5\text{CH}_2\text{NMe}_2$), 42.7 ($\text{N}(\text{CH}_3)_2$), 42.5 ($\text{N}(\text{CH}_3)_2$), 40.2 (CH_3N), 21.4 (6 CH_3C), 20.6 (CH_3C).

(*S*)-[Lu{NOBIN-TPS/TPDMS}(*o*- $\text{C}_6\text{H}_4\text{CH}_2\text{NMe}_2$)] ((*S*)-103d-Lu). To a mixture of (*S*)-**102d** (30.8 mg, 0.030 mmol) and $[\text{Lu}(\textit{o}\text{-C}_6\text{H}_4\text{CH}_2\text{NMe}_2)_3]$ (16.0 mg, 0.030 mmol) was added C_6D_6 (0.55 mL). The mixture was kept at room temperature for 1 h. ^1H and ^{13}C NMR spectra showed clean formation of (*S*)-**103d-Lu**, which was used directly for catalytic experiments. ^1H NMR (500 MHz, C_6D_6): $\delta = 8.07$ (s, 1H), 8.06 (m, 1H), 7.76 (d, $^3J(\text{H,H}) = 9.1$ Hz, 1H), 7.71 (d, $^3J(\text{H,H}) = 7.3$ Hz, 6H), 7.62 (d, $^3J(\text{H,H}) = 8.3$ Hz, 1H), 7.57 (s, 6H), 7.44 (m, 1H), 7.32 (d, $^3J(\text{H,H}) = 8.1$ Hz, 6H), 7.21–7.01 (m, 15H), 6.90–6.75 (m, 14H), 6.64 (d, $^3J(\text{H,H}) = 8.3$ Hz, 1H, aryl-H), 5.20 (br s, 1H, CH_2N), 3.93 (br s, 1H, CH_2N), 3.55 (br s, 1H, *o*- $\text{C}_6\text{H}_4\text{CH}_2\text{NMe}_2$), 3.22 (s, 4H, $2\text{C}_6\text{H}_5\text{NCH}_2\text{NMe}_2$), 2.88 (s, 3H, NCH_3), 2.19 (d, $^2J(\text{H,H}) = 14.7$ Hz, 1H, *o*- $\text{C}_6\text{H}_4\text{CH}_2\text{NMe}_2$), 2.08 (3H, CH_3C), 2.04 (s, 12 H, $2\text{C}_6\text{H}_5\text{CH}_2\text{NMe}_2$), 1.97 (s, 18H, 6 CH_3C), 1.23 (s, 3H, *o*- $\text{C}_6\text{H}_4\text{CH}_2\text{NMe}_2$), 0.35 (s, 3H, *o*- $\text{C}_6\text{H}_4\text{CH}_2\text{NMe}_2$); $^{13}\text{C}\{^1\text{H}\}$ NMR (125 MHz, C_6D_6): $\delta = 187.2$ (C-Lu), 168.5 (CO),

164.5 (CO), 147.1, 143.1, 142.9, 141.5, 140.3, 140.0, 137.9, 137.2, 136.8, 136.5, 135.9, 135.6, 134.8, 132.4, 131.5, 130.2, 129.4, 129.1, 128.8, 128.54, 128.47, 128.3, 127.7, 127.6, 127.2, 126.9, 125.7, 124.9, 122.0, 120.0 (aryl-C), 65.8 (CH₂N), 64.5 (C₆H₅CH₂NMe₂), 58.1 (CH₂N), 45.4 (C₆H₅CH₂NMe₂), 42.8 (N(CH₃)₂), 42.5 (N(CH₃)₂), 40.3 (CH₃N), 21.4 (6CH₃C), 20.6 (CH₃C).

(S)-[Y{NOBIN-TPS/TBDPS}(*o*-C₆H₄CH₂NMe₂)] ((S)-103e-Y). To a mixture of (S)-**102e** (27.5 mg, 0.030 mmol) and [Y(*o*-C₆H₄CH₂NMe₂)₃] (14.8 mg, 0.030 mmol) was added C₆D₆ (0.55 mL). The mixture was kept at 60 °C for 1 h. The ¹H and ¹³C NMR spectra showed clean formation of (S)-**103e-Y**, which was used directly for catalytic experiments. ¹H NMR (C₆D₆, 500 MHz): δ = 8.00 (s, 1H), 7.74 (d, ³J(H,H) = 7.9 Hz, 6H), 7.65–7.63 (m, 3H) 7.53 (d, ³J(H,H) = 7.6 Hz, 3H), 7.42 (d, ³J(H,H) = 8.6 Hz, 2H), 7.31 (d, ³J(H,H) = 7.3 Hz, 4H), 7.23 (d, ³J(H,H) = 6.6 Hz, 1 H), 7.17–7.12 (m, 6H), 7.09–6.90 (m, 20H), 6.87 (d, ³J(H,H) = 6.8.3 Hz, 1H), 6.85–6.81 (m, 2H), 6.78 (br s, 1H), 6.62 (d, ³J(H,H) = 8.3 Hz, 1H), 6.50 (d, ³J(H,H) = 7.3 Hz, 1H, aryl-H), 4.25 (br s 2H, CH₂), 3.22 (s, 4H), 2.50 (br s, 2H), 2.48 (s, 3H), 2.20 (s, 3H), 2.03 (s, 12 H, NMe₂), 1.12 (s, 9H, *t*-Bu), 0.99 (s, 3H, NMe₂), 0.81 (s, 3H, NMe₂); ¹³C{¹H} NMR (125 MHz, C₆D₆): δ = 180.3 (d, ¹J(C,Y) = 59 Hz, C-Y), 168.0, 166.1, 146.3, 143.0, 140.2, 140.0, 138.9, 137.3, 137.2, 136.85, 136.81, 136.79, 136.3, 134.9, 131.2, 131.1, 129.7, 129.1, 129.0, 128.6, 128.53, 128.45, 128.4, 128.29, 128.26, 127.9, 127.4, 127.2, 126.9, 126.3, 125.7, 124.8, 124.7, 124.4, 124.3, 121.8, 120.7, 120.5, 118.6 (Aryl-C), 66.5 (CH₂N), 64.5, 58.6 (CH₃N), 45.4, 43.5, 43.1, 38.9, 29.8 ((CH₃)₃C), 20.7(CH₃Ar), 19.3 ((CH₃)₃C).

(S)-[Lu{NOBIN-TPS/TBDPS}(*o*-C₆H₄CH₂NMe₂)] ((S)-103e-Lu). To a mixture of (S)-**102e** (27.5 mg, 0.030 mmol) and [Lu(*o*-C₆H₄CH₂NMe₂)₃] (17.8 mg, 0.030 mmol) was added C₆D₆ (0.55 mL). The mixture was kept at 60 °C for 30 min. ¹H NMR (500 MHz, C₆D₆): δ = 8.00 (s, 1H), 7.75 (d, ³J(H,H) = 9.3 Hz, 6H), 7.67–7.64 (m, 3H), 7.60 (d, ³J(H,H) = 9.0 Hz, 1H), 7.53–7.40 (m, 4H), 7.31–7.25 (m, 5H), 7.17–6.99 (m, 22H), 6.83–6.76 (m, 5H), 6.56 (d, ³J(H,H) = 7.3 Hz, 1H), 6.43 (br s, 1H), 4.3 (br s 2H, CH₂), 3.22 (s, 4H, HBDMA), 2.64 (br s, 2H), 2.22 (s, 3H), 2.05 (s, 12 H, NMe₂), 1.09 (s, 9H, *t*-Bu), 1.05 (s, 3H, NMe₂), 0.78 (s, 3H, NMe₂); ¹³C{¹H} NMR (125 MHz, C₆D₆): δ = 187.6 (C-Lu), 168.2, 165.4, 146.8, 143.3, 140.3, 140.0, 139.7, 137.9, 137.2, 137.0, 136.8, 136.3, 131.9, 129.7, 129.1, 129.0, 128.9, 128.7, 128.53, 128.46, 128.3, 127.6, 127.39, 127.36, 127.2, 126.6, 126.0, 125.7, 125.1, 125.0, 124.8, 121.9, 121.0, 120.4, 118.3 (aryl), 68.2 (CH₂N), 65.5 (C₆H₅CH₂NMe₂), 45.4 (C₆H₅CH₂NMe₂), 43.9, 43.3, 29.8, 20.7 (C(CH₃)₃), 19.3 (*t*-Bu).

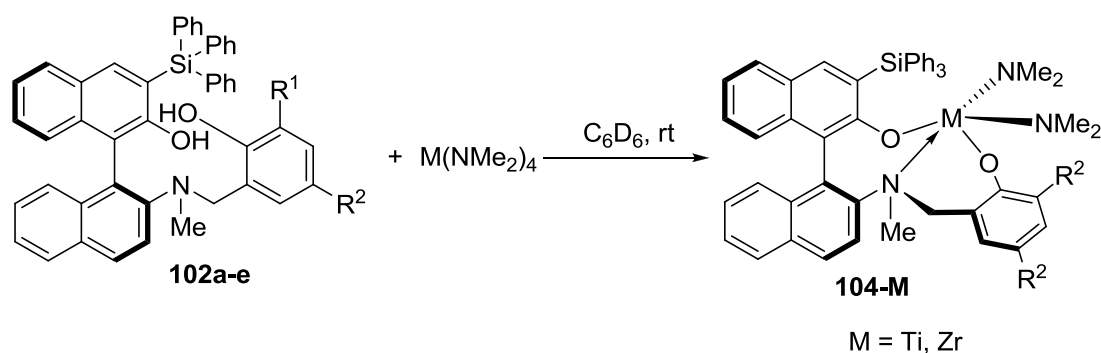
(S)-[Y{NOBIN-SiPh₂Me/*t*-Bu}(*o*-C₆H₄CH₂NMe₂)] ((S)-103f-Y). To a mixture of (S)-**102f** (26.5 mg, 0.037 mmol) and [Y(*o*-C₆H₄CH₂NMe₂)₃] (18.2 mg, 0.037 mmol) was added C₆D₆ (0.55 mL). The mixture was kept at room temperature for 3 h. ¹H and ¹³C NMR spectra showed clean formation of (S)-**103f-Y**, which was used directly for catalytic experiments. ¹H NMR (500 MHz, C₆D₆, 65 °C): δ = 8.03 (d, ³J(H,H) = 9.1 Hz, 1H), 7.87 (s, 1H), 7.69–7.60 (m, 6H), 7.53 (d, ⁴J(H,H) = 2.4 Hz, 1H), 7.43 (d, ³J(H,H) = 8.6 Hz, 1H), 7.34–6.98 (m, 26H), 6.91 (d, ⁴J(H,H) = 2.4 Hz, 1H), 6.84 (m, 2H), 6.6 (d, ³J(H,H) = 7.3 Hz, 1H), 6.44 (m, 1H Aryl-H), 4.46 (d, ²J(H,H) = 12.5 Hz, 1H, CH₂N), 3.83 (d, ²J(H,H) = 13.9 Hz, 1H, *o*-C₆H₄CH₂NMe₂), 3.69 (d, ²J(H,H) = 12.5 Hz, 1H,

CH_2N), 3.25 (s, 4H, $2\text{C}_6\text{H}_5\text{NCH}_2\text{NMe}_2$), 2.92 (d, $^2J(\text{H,H}) = 13.9$ Hz, 1H, $o\text{-C}_6\text{H}_4\text{CH}_2\text{NMe}_2$), 2.23 (br s, 2.23 (br s, 3H, $o\text{-C}_6\text{H}_4\text{CH}_2\text{NMe}_2$), 2.16 (br s, 3H, NCH_3), 1.58 (s, 9 H, $\text{C}(\text{CH}_3)_3$), 1.40 (s, 9H, $\text{C}(\text{CH}_3)_3$), 0.98 (s, 3H, CH_3Si); $^{13}\text{C}\{^1\text{H}\}$ NMR (100 MHz, C_6D_6): $\delta = 179.9$ (d, $^1J(\text{C,Y}) = 57$ Hz, C-Y), 164.5 (CO), 161.0 (CO), 146.2, 141.7, 141.6, 140.0, 138.9, 138.4, 138.2, 137.6, 136.0, 135.7, 132.1, 131.9, 131.0, 129.6, 129.2, 129.1, 128.9, 127.2, 127.0, 126.6, 126.2, 125.6, 124.9, 124.7, 124.4, 123.7, 121.7, 120.3, 117.1 (aryl), 67.3 (CH_2N), 64.5 ($\text{C}_6\text{H}_5\text{CH}_2\text{NMe}_2$), 58.3 (CH_2N), 45.4 ($\text{C}_6\text{H}_5\text{CH}_2\text{NMe}_2$), 42.9 ($\text{N}(\text{CH}_3)_2$), 38.8 (CH_3N), 35.4($\text{C}(\text{CH}_3)_3$), 34.2 ($\text{C}(\text{CH}_3)_3$), 32.2 ($\text{C}(\text{CH}_3)_3$), 30.3 ($\text{C}(\text{CH}_3)_3$), -1.7 (CH_3Si).

(*S*)-[Y{NOBIN- SiPh₂Me/SiPh₂Me}(*o*-C₆H₄CH₂NMe₂)] ((*S*)-103g-Y**).** To a mixture of (*S*)-**102g** (38.9 mg, 0.048 mmol) and [Y(*o*-C₆H₄CH₂NMe₂)₃] (23.7 mg, 0.048 mmol) was added C_6D_6 (0.55 mL). The mixture was kept at 50 °C for 40 min. ^1H and ^{13}C NMR spectra showed clean formation of (*S*)-**103g-Y**, which was used directly for catalytic experiments. ^1H NMR (500 MHz, C_6D_6 , 65 °C): $\delta = 8.03$ (d, $^3J(\text{H,H}) = 9.0$ Hz, 1H), 7.93 (s, 1H), 7.14–7.70 (m, 6H), 7.65 (m, 4H), 7.58 (d, $^3J(\text{H,H}) = 6.6$ Hz, 1H), 7.51 (m, 1H), 7.42–7.38 (m, 3H), 7.31–6.99 (m, 30H), 6.88 (m, 2H), 6.83 (d, $^4J(\text{H,H}) = 2.2$ Hz, 1H), 6.62 (d, $^3J(\text{H,H}) = 7.3$ Hz, 1H), 6.47 (m, 1H, aryl-H), 4.62(d, $^2J(\text{H,H}) = 12.7$ Hz, 1H, CH_2N), 3.78 (d, $^2J(\text{H,H}) = 12.7$ Hz, 1H, CH_2N), 3.11 (d, $^2J(\text{H,H}) = 13.9$ Hz, 1H, $o\text{-C}_6\text{H}_4\text{CH}_2\text{NMe}_2$), 2.52 (d, $^2J(\text{H,H}) = 13.9$ Hz, 1H, $o\text{-C}_6\text{H}_4\text{CH}_2\text{NMe}_2$), 2.35 (s, 3H, NCH_3), 2.08 (s, 3H, $o\text{-C}_6\text{H}_4\text{CH}_2\text{NMe}_2$), 1.55 (s, 3H, $o\text{-C}_6\text{H}_4\text{CH}_2\text{NMe}_2$), 1.09 (s, 3H, CH_3Si), 1.07 (s, 3H, CH_3Si); $^{13}\text{C}\{^1\text{H}\}$ NMR (125 MHz, C_6D_6): $\delta = 179.4$ (d, $^1J(\text{C,Y}) = 61$ Hz, C-Y), 168.2 (CO), 164.4 (CO), 146.5, 141.7, 141.6, 140.2, 140.0, 138.8, 138.6, 138.2, 137.8,

137.4, 137.3, 136.1, 136.0, 135.9, 135.7, 135.6, 135.3, 135.2, 132.1, 131.0, 129.8, 129.6, 129.3, 129.2, 129.1, 128.9, 128.5, 128.3, 127.7, 127.3, 127.2, 125.5, 125.4, 124.8, 124.7, 122.6, 121.9, 121.7, 120.1, 117.1 (aryl), 66.3 (CH₂N), 64.5 (C₆H₅CH₂NMe₂), 57.9 (CH₂N), 45.4 (C₆H₅CH₂NMe₂), 42.4 (N(CH₃)₂), 39.0 (CH₃N), 20.5 (CH₃C), -0.8 (CH₃Si), -2.1 (CH₃Si).

NMR-scale preparation of **104-M** (M = Ti, Zr)



A screw cap NMR tube was charged with equimolar (0.045 mmol) amounts of the bisamide proligand **102** and the corresponding group 4 metal tetrakis(dimethylamide) and then C₆D₆ (0.6 mL) was added. The NMR tube was sealed, removed from the glovebox and the NMR spectra were recorded. Complexes were isolated as solids using a freeze-drying technique. Standard solutions of isolated complexes and complexes prepared *in situ* were used for catalytic experiments.

(S)-[Ti{NOBIN-TPS/SiPh₂Me}(NMe₂)₂] ((S)-104b-Ti**).** Yellow solid after freeze-drying in vacuo. ¹H NMR (300 MHz, C₆D₆): δ = 8.14 (s, 1H), 8.02 (d, ³J(H,H) = 7.3 Hz, 6H), 7.90 (d, ³J(H,H) = 8.8 Hz, 1H), 7.83 (d, ³J(H,H) = 7.9 Hz, 1H), 7.60–7.67 (m, 2H), 7.52–6.90 (m, 18H), 6.77 (m, 3H), 6.57 (d, ³J(H,H) = 10.0 Hz, 1H), 6.51 (d,

$^3J(\text{H,H}) = 7.6 \text{ Hz}$, 1H), 5.55 (d, $^2J(\text{H,H}) = 15.9 \text{ Hz}$, 1H, CH_2), 3.13 (d, $^2J(\text{H,H}) = 15.9 \text{ Hz}$, 1H, CH_2), 3.24 (s, 3H, NCH_3), 2.31 (s, 3H), 2.15 (br s, 6 H), 0.51 (s, 3H, SiCH_3); $^{13}\text{C}\{^1\text{H}\}$ NMR (125 MHz, C_6D_6): $\delta = 165.2, 164.5, 144.5, 143.1, 138.5, 137.8, 137.2, 137.1, 136.9, 136.2, 135.6, 135.1, 131.8, 130.7, 129.7, 129.1, 128.7, 127.4, 126.6, 126.33, 126.25, 125.7, 125.4, 125.3, 122.5, 121.9, 119.8, 119.7, 65.6, 47.2, 38.8, 37.9, 20.8, -1.71$.

(S)-[Zr{NOBIN-TPS/*t*-Bu}(NMe₂)₂] ((S)-104a-Zr). Prepared in situ only, yellowish solution in C_6D_6 . ^1H NMR (400 MHz, C_6D_6): $\delta = 8.01$ (s, 1H), 7.86 (d, $^3J(\text{H,H}) = 7.6 \text{ Hz}$, 6H), 7.69 (vt, $^3J(\text{H,H}) = 9.7 \text{ Hz}$, $^3J(\text{H,H}) = 10.0 \text{ Hz}$, 2H), 7.57 (s, 1H), 7.34–7.31 (m, 3H), 7.19–7.08 (m, 8H), 7.03 (s, 1 H), 6.94–6.85 (m, 5H), 4.45 (d, $^2J(\text{H,H}) = 12.0 \text{ Hz}$, 1H, CH_2), 3.92 (d, $^2J(\text{H,H}) = 12.0 \text{ Hz}$, 1H, CH_2), 2.47 (s, 3H, NCH_3), 2.22–2.16 (m, 27H), 1.45 (s, 9H, *t*-Bu), 1.42 (s, 9H, *t*-Bu); $^{13}\text{C}\{^1\text{H}\}$ NMR (100 MHz, C_6D_6): $\delta = 162.7, 158.0, 148.9, 142.2, 140.8, 137.2, 137.0, 136.8, 135.9, 131.1, 129.7, 129.2, 128.9, 128.2, 127.52, 127.46, 127.2, 126.9, 126.3, 126.1, 126.0, 124.95, 124.93, 124.0, 122.8, 121.7, 118.8, 60.2(\text{CH}_2\text{N}), 43.0(\text{CH}_3\text{NCH}_2), 40.8 (\text{NMe}_2), 38.93 (\text{NMe}_2), 38.92 (\text{HNMe}_2), 35.2, 34.4, 32.0, 30.6$.

(S)-[Zr{NOBIN-TPS/SiPh₂Me}(NMe₂)₂] ((S)-104b-Zr). Prepared in situ only, colorless solution in C_6D_6 . Prepared in situ only, colorless solution in C_6D_6 . ^1H NMR (400 MHz, C_6D_6): $\delta = 8.06$ (s, 1H), 7.86–7.84 (m, 6H), 7.66 (d, $^3J(\text{H,H}) = 9.4 \text{ Hz}$, 1H), 7.68 (s, 1H), 7.56–7.53 (m, 2H), 7.50–7.47 (m, 2H), 7.84–7.28 (m, 2H), 7.25–6.89 (m, 18H), 6.82 (m, 1H), 4.64 (d, $^2J(\text{H,H}) = 13.7 \text{ Hz}$, 1H, CH_2), 3.85 (d, $^2J(\text{H,H}) = 12.0 \text{ Hz}$,

1H, CH₂), 2.51 (s, 3H, NCH₃), 2.13 (s, 12H, HNMe₂), 2.01 (s, 3H, CH₃C) 1.98 (s, 6H, NMe₂), 1.68 (s, 6H, NMe₂), 0.71 (s, 3H, CH₃Si). ¹³C{¹H} NMR (100 MHz, C₆D₆): δ = 165.1, 163.5, 150.6, 141.6, 138.9, 138.4, 137.8, 136.8, 123.6, 136.5, 135.8, 135.6, 135.4, 135.0, 131.0, 129.7, 129.6, 129.3, 129.2, 129.0, 128.9, 128.2, 127.9, 127.2, 126.8, 126.5, 126.0, 125.7, 125.3, 124.6, 124.5, 123.5, 123.0, 122.5, 121.0, 58.2 (CH₂), 41.7 (NCH₃), 40.0 (NMe₂), 39.7 (NMe₂), 38.9 (HNMe₂), 20.6 (CCH₃), -2.8 (SiCH₃).

(S)-[Zr{NOBIN-TPS/TPS}(NMe₂)₂] ((S)-104c-Zr). Prepared in situ only, yellow solution in C₆D₆. ¹H NMR (500 MHz, C₆D₆): δ = 8.11 (s, 1H), 7.87–7.84 (m, 6H), 7.72 (d, ³J(H,H) = 9.1 Hz, 1H), 7.69 (d, ³J(H,H) = 7.8 Hz, 1H), 7.62 (d, ³J(H,H) = 7.8 Hz, 6H), 7.38–7.35 (m, 3H), 7.32 (s, 1 H), 7.19–7.07 (m, 25H), 6.98–6.94 (m, 4 H), 6.83 (d, ³J(H,H) = 8.6 Hz, 1H), 4.77 (d, ²J(H,H) = 13.9 Hz, 1H, CH₂), 3.85 (d, ²J(H,H) = 13.9 Hz, 1H, CH₂), 2.58 (s, 3H, NCH₃), 2.10 (m, 15H), 1.70 (s, 6H, NMe₂), 1.65 (s, 6H, NMe₂); ¹³C{¹H} NMR (125 MHz, C₆D₆): δ = 165.2, 163.4, 149.8, 141.6, 140.0, 136.8, 136.7, 136.5, 136.3, 135.6, 135.1, 131.2, 129.5, 129.4, 129.3, 129.2, 128.9, 128.5, 128.3, 128.1, 127.9, 127.3, 126.80, 126.79, 126.7, 125.8, 125.18, 125.16, 124.7, 123.0, 122.7, 121.8, 59.0 (CH₂), 41.1(CH₃N), 40.7 (NMe₂), 40.4 (NMe₂), 38.9, 20.7 (CH₃C).

(R)-[Zr{NOBIN-TPS/TPDMS}(NMe₂)₂] ((R)-104d-Zr). Prepared in situ only, colorless solution in C₆D₆. ¹H NMR (400 MHz, C₆D₆): δ = 8.15 (s, 1H), 7.82–7.80 (m, 6H), 7.63 (d, ³J(H,H) = 9.0 Hz, 1H), 7.58 (d, ³J(H,H) = 8.2 Hz, 1H), 7.52 (d, ³J(H,H) = 9.4 Hz, 1H), 7.46 (s, 6H), 7.37 (m, 1 H), 7.16–7.05 (m, 12H), 6.92–6.84 (m, 5 H), 6.77 (s, 3H), 4.32 (d, ²J(H,H) = 12.5 Hz, 1H, CH₂), 4.16 (d, ²J(H,H) = 12.5 Hz, 1H, CH₂), 2.53 (s,

3H, NCH₃), 2.06–1.90 (m, 45 H); ¹³C{¹H} NMR (100 MHz, C₆D₆): δ = 165.3, 163.6, 150.0, 141.7, 140.6, 140.5, 137.2, 137.0, 136.89, 136.84, 136.82, 136.76, 136.5, 136.0, 134.7, 134.6, 131.2, 131.1, 129.4, 129.2, 128.9, 127.6, 127.3, 126.7, 125.8, 125.3, 124.5, 122.9, 122.7, 122.3, 120.3, 59.7 (CH₂), 41.2, 41.13, 41.07, 40.8, 38.9, 21.48, 20.72.

(S)-[Zr{NOBIN-TPS/SiPh₂Me}(NMe₂)₂] ((S)-104e-Zr). Prepared in situ only, yellow solution in C₆D₆. ¹H NMR (300 MHz, C₆D₆): δ = 8.08 (s, 1H), 7.88–7.85 (m, 6H), 7.72–7.63 (m, 7H), 7.54–7.53 (m, 1H), 7.37–7.29 (m, 4H), 7.18–7.07 (m, 13H), 6.96–6.83 (m, 6 H, aryl-H), 4.61 (d, ²J(H,H)=13.5 Hz, 1H, CH₂), 3.98 (d, ²J(H,H)=13.5 Hz, 1H, CH₂), 2.54 (s, 3H, NCH₃), 2.15 (s, 3H, CH₃), 2.13 (s, 12H, HNMe₂), 1.80 (s, 6H, NMe₂), 1.77 (s, 6H, NMe₂), 1.22 (s, 9H, C(CH₃)₃); ¹³C{¹H} NMR (C₆D₆, 100 MHz) δ: 165.4, 163.7, 150.0, 141.7, 140.5, 137.2, 136.81, 136.77, 136.7, 136.63, 136.61, 135.7, 134.9, 131.0, 129.7, 129.6, 129.2, 128.9, 127.3, 126.7, 126.9, 125.8, 125.4, 125.3, 124.6, 122.9, 122.6, 121.9, 121.0, 58.9 (CH₂), 41.3, 40.4, 40.3, 38.9, 29.7, 20.7, 18.9.

General procedure for intermolecular hydroamination reactions. In the glovebox, a screw cap NMR tube was charged with an appropriate amine (0.2 mmol), alkene (3 mmol) and a solution of catalyst (0.1 M in C₆D₆, 0.1 mL, 10.0 μmol, 5 mol%). The tube was then sealed, removed from the glovebox and placed into the thermostated oil bath. The progress of the reaction was monitored by ¹H NMR spectroscopy. After completion of the reaction, the mixture was concentrated in vacuo and purified by column chromatography on a 3 cm height pad of silica or alumina.

Determination of enantiomeric excess via debenzylation/Mosher amide formation sequence (Method A).

Isolated *N*-benzyl hydroamination product (0.03 mmol) was dissolved in absolute ethanol (2 mL). Ammonium formate (32 mg, 0.5 mmol) and 10% palladium on charcoal (11 mg, 0.01 mmol) were added, and the mixture was stirred under reflux for 30 min. The precipitate was filtered off, and the filtrate was treated with 1M HCl (2 mL). The volatiles were removed *in vacuo*, the residue was dissolved in water (5 mL) and then water was removed under reduced pressure. The residue was then dissolved in CDCl₃ or C₆D₆ (0.6 mL) and filtered through a short pad of celite into the NMR tube containing Mosher chloride (10 mg, 0.04 mmol) and DIPEA (26 mg, 0.2 mmol). A ¹⁹F NMR spectrum was then taken to determine the enantiomeric excess. The absolute configuration of heptan-2-amine was determined using literature data.³⁶ The enantiomeric excess for *N*-benzyl-4-phenylbutan-2-amine determined using method A was identical to that obtained via methods B.

Determination of enantiomeric excess via chiral HPLC (Method B).

***N*-benzoylation of isolated hydroamination product.** The hydroamination product (0.1 mmol) was dissolved in CH₂Cl₂ (1 mL) and then DIPEA (26 mg, 0.2 mmol) and benzoyl chloride (21 mg, 0.15 mmol) were added. The mixture was stirred at room temperature for 3 h. Volatiles were removed *in vacuo* and the residue was partitioned between Et₂O (2 mL) and 2M NaOH (2 mL). The resulting emulsion was stirred for 2 h and then the organic layer was separated, washed with brine (1 mL), dried (Na₂SO₄), and concentrated. The residue was purified by flash chromatography on silica (CH₂Cl₂), if necessary, or was directly subjected to a chiral HPLC analysis.

***N*-(1-Methylhexyl)benzamide.** Prepared from **77**. Colorless oil. ^1H NMR (400 MHz, CDCl_3 , 65 °C): δ = 7.52–7.16 (m, 10H, aryl-H), 4.87 (d, $^2J(\text{H,H})$ = 15.2 Hz, 1H, CHN), 4.45 (d, $^2J(\text{H,H})$ = 15.2 Hz, 1H, CHN), 3.94 (br s, 1H, CHN), 1.56 (br s, 1H), 1.31–1.05 (br s, 10H), 0.82 (m, 4H); ^{13}C NMR could not be acquired as signals are very broad and obscure due to rotamer interconversion. HPLC (AS-H, hexane/2-propanol 90:10, 1 mL/min): t_{R} 23.3 min (*R*-isomer), 22.3 min (*S*-isomer).

***N*-(1-Methyl-3-phenylpropyl)benzamide.** Prepared from **85**. Colorless oil. ^1H NMR (400 MHz, CDCl_3 , 65 °C): δ = 8.10 (d, $^3J(\text{H,H})$ = 7.8 Hz, 1H), 7.60–6.96 (m, 14H, aryl-H), 4.71 (br s, 1H, CHN), 4.58 (d, $^2J(\text{H,H})$ = 14.5 Hz, 1H, CHN), 2.49 (br s, 2H), 1.99 (br s, 1H), 1.17 (br s, 1H), 1.19 (d, $^3J(\text{H,H})$ = 12.3 Hz, 3H, CH_3); ^{13}C NMR could not be acquired as signals are very broad and obscure due to rotamer interconversion. HPLC (AS-H, hexane/2-propanol 90:10, 1 mL/min): t_{R} 25.5 min (*R*-isomer), 45.5 min (*S*-isomer).

(*R*)-*N*-Benzylheptan-2-amine (77**).**³⁷ Prepared from 1-heptene and benzylamine according to Table IV-5, entry 3. Purified by column chromatography on alumina (hexanes/EtOAc 100:0.6). Yield 65%; colorless oil, 40% ee. ^1H NMR (400 MHz, CDCl_3): δ = 7.33–7.30 (m, 4H, aryl-H) 7.25–7.21 (m, 1H, aryl-H), 3.82 (d, $^2J(\text{H,H})$ = 13.0 Hz, 1H, PhCH_2NH), 3.73 (d, $^2J(\text{H,H})$ = 13.0 Hz, 1H, PhCH_2NH), 2.68 (sext, $^3J(\text{H,H})$ = 6.2 Hz, 1H, CHNH), 1.50–1.41 (m, 1H, CH_2) 1.34–1.23 (m, 8H, CH_2 and NH), 1.07 (d, $^3J(\text{H,H})$ = 6.2 Hz, 3H, CH_3CHNH), 0.89 (t, $^3J(\text{H,H})$ = 6.9 Hz, 3H, CH_3CH_2);

$^{13}\text{C}\{^1\text{H}\}$ NMR (100 MHz, CDCl_3): δ = 140.9 (C_{ipso}), 128.4, 128.1, 126.8 (aryl), 52.5 ($\text{CH}(\text{CH}_3)\text{NH}$), 51.4 (CH_2NH), 37.1 (CH_2), 32.1 (CH_2), 25.7 (CH_2), 22.7 (CH_2), 20.3 (CH_3CHNH), 14.1 (CH_3CH_2).

(S)-N-Benzyl-4-phenylbutan-2-amine (85).³⁷ Prepared from 4-phenyl-1-butene and benzylamine according to Table IV-6, entry 2. Purified by column chromatography on silica ($\text{CH}_2\text{Cl}_2/7\text{ M NH}_3$ in MeOH 100:1). Yield 72%; colorless oil, 56% ee. ^1H NMR (500 MHz, CDCl_3): δ = 7.34–7.22 (m, 7H), 7.19–7.16 (m, 3H, aryl-H), 3.82 (d, $^2J(\text{H,H})$ = 13.0 Hz, 1H, PhCH_2NH), 3.73 (d, $^2J(\text{H,H})$ = 12.9 Hz, 1H, PhCH_2NH), 2.69 (sext, $^3J(\text{H,H})$ = 6.3 Hz, 1H, CHNH), 2.70–2.61 (m, 2H), 1.85–1.78 (m, 1H), 1.71–1.64 (m, 1H), 1.49 (br s, 1H, NH), 1.14 (d, $^3J(\text{H,H})$ = 6.4 Hz, 3H, CH_3CHNH); $^{13}\text{C}\{^1\text{H}\}$ NMR (125 MHz, CDCl_3): δ = 142.5 (C_{quart}), 140.8 (C_{quart}), 128.35, 128.32, 128.30, 128.1, 126.8, 125.7 (aryl), 52.0 ($\text{CH}(\text{CH}_3)\text{NH}$), 51.3 (CH_2NH), 38.7 (CH_2), 32.3 (CH_2), 20.4 (CH_3).

IV.5 References

- (1) Ricci, A. *Modern Amination Methods* Wiley-VCH: Weinheim, 2000.
- (2) Ricci, A. *Amino Group Chemistry: From Synthesis to the Life Sciences*; Wiley-VCH: Weinheim, 2008.
- (3) Müller, C.; Saak, W.; Doye, S. *Eur. J. Org. Chem.* **2008**, 2731-2739.
- (4) Müller, T. E.; Beller, M. *Chem. Rev.* **1998**, 98, 675-703.
- (5) Reznichenko, A. L.; Hultzs, K. C. In *Chiral Amine Synthesis: Methods, Developments and Applications*; 1st ed.; Nugent, T., Ed.; Wiley-VCH: 2010, p 341-376.
- (6) Reznichenko, A. L.; Hultzs, K. C. In *Science of Synthesis, Stereoselective Synthesis*; De Vries, J. G., Molander, G. A., Evans, P. A., Eds.; Thieme: 2010; Vol. 1, p 689-729.
- (7) Hultzs, K. C. *Adv. Synth. Catal.* **2005**, 347, 367-391.
- (8) Reznichenko, A. L.; Hultzs, K. C. *Struct. Bond.* **2010**, 137, 1-48.
- (9) Gribkov, D. V.; Hultzs, K. C. *Chem. Commun.* **2004**, 730-731.
- (10) Gribkov, D. V.; Hultzs, K. C.; Hampel, F. *J. Am. Chem. Soc.* **2006**, 128, 3748-3759.
- (11) Reznichenko, A. L.; Hampel, F.; Hultzs, K. C. *Chem. Eur. J.* **2009**, 15, 12819-12827.
- (12) Reznichenko, A. L.; Nguyen, H. N.; Hultzs, K. C. *Angew. Chem., Int. Ed.* **2010**, 49, 8984-8987.
- (13) Gribkov, D. V., PhD thesis, Universität Erlangen-Nürnberg, 2005.
- (14) Kim, J. Y.; Livinghouse, T. *Org. Lett.* **2005**, 7, 1737-1739.
- (15) Hultzs, K. C.; Gribkov, D. V.; Hampel, F. *J. Organomet. Chem.* **2005**, 690, 4441-4452.
- (16) Reznichenko, A. L.; Emge, T. J.; Audörsch, S.; Klauber, E. G.; Hultzs, K. C.; Schmidt, B. *Organometallics* **2011**, 30, 921-924.
- (17) Reznichenko, A. L.; Hultzs, K. C. *J. Am. Chem. Soc.* **2012**, 134, 3300-3311.
- (18) Ooi, T.; Ohmatsu, K.; Maruoka, K. *J. Am. Chem. Soc.* **2007**, 129, 2410-2411.
- (19) Säliger, D.; Brückner, R. *Synlett* **2009**, 109-111.
- (20) Jung, M. E.; Piizzi, G. *Chem. Rev.* **2005**, 105, 1735-1766.
- (21) Behrle, A. C.; Schmidt, J. A. R. *Organometallics* **2011**, 30, 3915-3918.
- (22) Smith, P. M.; Thomas, E. J. *J. Chem. Soc., Perkin Trans. 1* **1998**, 3541-3556.
- (23) Gagné, M. R.; Stern, C. L.; Marks, T. J. *J. Am. Chem. Soc.* **1992**, 114, 275-294.
- (24) Hong, S.; Tian, S.; Metz, M. V.; Marks, T. J. *J. Am. Chem. Soc.* **2003**, 125, 14768-14783.
- (25) Tamaru, Y.; Hojo, M.; Higashimura, H.; Yoshida, Z. *J. Am. Chem. Soc.* **1998**, 120, 3994-4002.
- (26) Bender, C. F.; Widenhoefer, R. A. *J. Am. Chem. Soc.* **2005**, 127, 1070-1071.

- (27) Kondo, T.; Okada, T.; Mitsudo, T.-a. *J. Am. Chem. Soc.* **2002**, *124*, 186-187.
- (28) Bexrud, J. A.; Beard, J. D.; Leitch, D. C.; Schafer, L. L. *Org. Lett.* **2005**, *7*, 1959-1962.
- (29) Quinet, C.; Jourdain, P.; Hermans, C.; Ates, A.; Lucas, I.; Markó, I. E. *Tetrahedron* **2008**, *64*, 1077-1087.
- (30) Collin, J.; Daran, J.-D.; Jacquet, O.; Schulz, E.; Trifonov, A. *Chem. Eur. J.* **2005**, *11*, 3455-3462.
- (31) Bexrud, J. A.; Eisenberger, P.; Leitch, D. C.; Payne, P. R.; Schafer, L. L. *J. Am. Chem. Soc.* **2009**, *131*, 2116-2118.
- (32) Reznichenko, A. L.; Hultzs, K. C. *Organometallics* **2010**, *29*, 24-27.
- (33) Sankaranarayanan, A.; Chandalia, S. B. *Org. Proc. Res. Dev.* **2006**, *10*, 487-492.
- (34) Larrow, J. F.; Jacobsen, E. N. *Org. Synth.* **1998**, *75*, 1.
- (35) Thadani, A. N.; Huang, Y.; Rawal, V. H. *Org. Lett.* **2007**, *9*, 3873-3876.
- (36) Sullivan, G. R.; Dale, J. A.; Mosher, H. S. *J. Org. Chem.* **1973**, *38*, 2143-2147.
- (37) Peterson, M.; Bowman, A.; Morgan, S. *Synth. Commun.* **2002**, *32*, 443-448.

V Chapter 5. Group 4 Metal Bis(Amidate)s in Asymmetric Hydroamination/Cyclization of Aminoalkenes

V.1 Introduction

The importance of nitrogen containing compounds in biological systems and industrially relevant basic and fine chemicals has sparked significant research efforts to develop efficient synthetic protocols.^{1,2} The hydroamination reaction, which is arguably one of the simplest approaches, has found significant attention only in recent years with the development of more efficient transition metal based catalyst systems.^{3,4} As a broadly applicable, efficient and selective hydroamination catalyst is yet to be developed, thorough and systematic investigations of novel catalytic systems are required for the further progress of the field. An area of particular interest has been the generation of new stereogenic centers during the hydroamination process, but the development of chiral catalysts for the asymmetric hydroamination of alkenes (AHA) has remained challenging.⁵⁻⁷

Group 4 metal-based catalyst systems have been studied intensively in the hydroamination of alkynes and allenes,^{3,8,9} while reactions involving unactivated alkenes have emerged only in recent years.¹⁰⁻²² Schafer and coworkers²³ have developed amidate titanium and zirconium hydroamination catalysts that exhibit promising hydroamination activity, including cyclization of primary aminoalkenes. Chiral variants of these catalysts developed in Schafer's¹³ and Scott's¹⁸ group have displayed enantioselectivities of up to 93% ee in the hydroamination/cyclization of aminopentenes. As of 2009, the zirconium bis(amidate) catalyst **I** (Figure V-1) was the most selective and one of the most active group 4 metal catalysts.

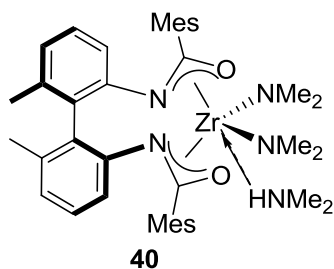


Figure V-1. Schafer's and Scott's zirconium bis(amidate) catalyst for asymmetric hydroamination/cyclization of aminoalkenes.

While being the champion of group 4 metal hydroamination catalysts, **40** possesses several important drawbacks such as very low reactivity and limited substrate scope. Alkene hydroamination with group 4 metal-based catalysts requires significantly harsher reaction conditions (100–150 °C) and higher catalyst loadings (typically 5–20 mol%) in comparison to rare earth metal-based catalysts.^{24–27} Catalyst **40**, like many other neutral group 4 metal catalyst systems with a very few exceptions^{15,19,20} has been limited to *gem*-dialkyl-activated aminopentenes or aminoheptenes. Cyclization of aminoheptenes with group 4 metal catalysts led to the unexpected formation of the hydroaminoalkylation product rather than the anticipated 7-membered ring hydroamination product.^{14,28,29}

We envisioned that the reactivity of bis(amidate) **40** can be significantly enhanced by tuning the electronic properties of the amidate ligand as well as by controlling the steric demands of the amidate backbone governed by alternative connectivity in the amide backbone. In this chapter we will describe our studies on the synthesis of novel bis(amidate) ligands based on binaphthalenedicarboxylic acid (BINCA) and their application to group 4 metal-catalyzed asymmetric hydroamination.

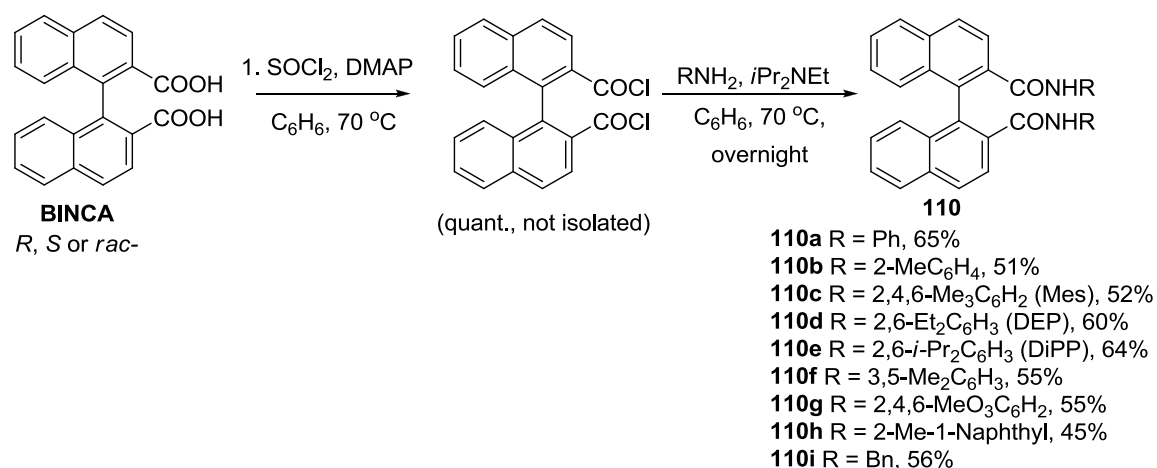
V.2 Results and Discussion

V.2.1 Complex Synthesis

We selected binaphthalenedicarboxylic acid (BINCA) as a key starting material for the preparation of novel bis(amidate) ligands, based on its readily availability and excellent configurational stability.³⁰ To our surprise, no bis(amidate) BINCA-based ligands have been reported so far and the related ligands with a biphenyl backbone were reported only almost simultaneously with³¹ or soon after³² the publication of our studies.³³ For our initial study we selected several aromatic and aliphatic amines with varying steric demand to synthesize corresponding zirconium bis(amidate) complexes.

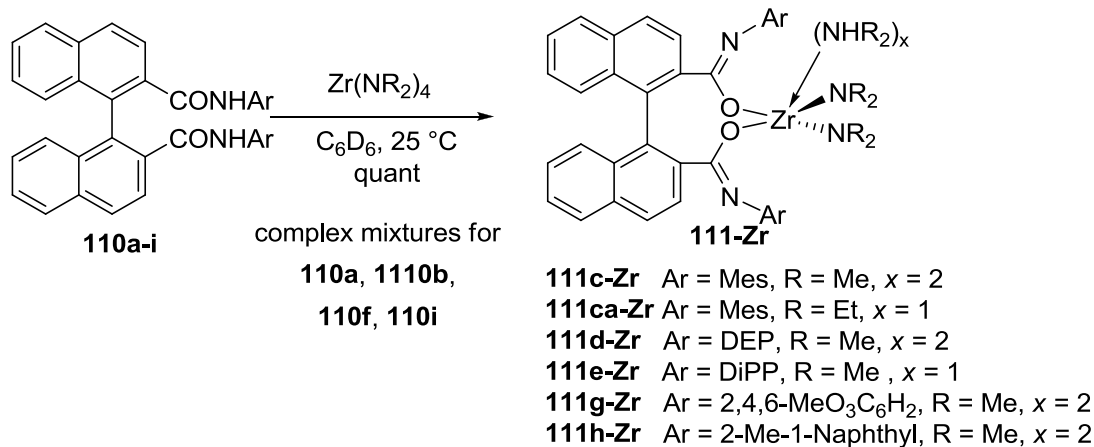
The synthesis of the desired bis(amide) proligands **110a-f** proceeded in a convenient two-step, one-pot sequence (Scheme V-1) in moderate yields. The BINCA acid chloride was not isolated; however, it may easily be stored indefinitely at anhydrous conditions, thus making the ligand preparation even easier.

Scheme V-1. Preparation of binaphthalenedicarboxamide ligands **110**.



With a family of proligands **110a-i** in hand, we proceeded with the synthesis of the corresponding bis(amidates) **111-Zr**. The outcome of a NMR-scale amine elimination reaction with simple zirconium tetrakis(amides) showed notable discrepancy between two groups of proligands. Aryl-substituted amides **110c-e**, **110g** and **110h** bearing an ortho-disubstituted arene moiety yielded well-defined C_2 -symmetric species **111-Zr**, which can be formulated as the amine adduct $(\mathbf{110})\text{Zr}(\text{NR}_2)_2(\text{NHR})_2$ (Scheme V-2) in quantitative yield. The less sterically demanding proligands **110a**, **110b**, **110f** and **110i** produced complex mixtures when reacted with either $\text{Zr}(\text{NMe}_2)_4$ or $\text{Zr}(\text{NEt}_2)_4$ under a variety of conditions and, most notably, the corresponding species **111-Zr** were not detected. Thus, in analogy to the case of rare earth metal biphenolate and binaphtholate complexes,³⁴ a certain degree of steric bulk is required for a successful monometallic complex formation. Although we could not isolate and characterize any species from the unsuccessful reactions it can be speculated that the formation of bi- or polymetallic species with a bridging bis(amidate) ligand might take place in the absence of a sterically protecting ligand backbone. Indeed, this hypothesis was later experimentally confirmed for related complexes by Schafer et al.³²

Complexes **111-Zr** were isolated either as mono(amine) adduct (complexes **111e-Zr** and **111ca-Zr**) and bis(amine) adducts (complexes **111c-Zr**, **111d-Zr** and **111h-Zr**) based on NMR spectroscopy. However, elemental analyses indicated the absence of coordinating amines, which were presumably lost during the storage or transportation to the analytical facility. Extended evacuation at 30–50 °C results in complete loss of dimethylamine for **111-Zr**.

Scheme V-2. Synthesis of zirconium bis(amidates) **111-Zr**.

The observation of a single carbonyl signal for **111d-h** in the ^{13}C NMR spectrum at around 161 ppm is indicative of a κ^1 -binding mode of the amidate ligand.¹⁸ This observation is remarkably contrasting **40** which was found to be featuring a κ^2 binding of both amidate ligands.^{13,18} The reaction of the least sterically demanding ligand **110c** led an unsymmetric species **111c-Zr** and **111ca-Zr** with two carbonyl signals at 160.8 and 178.6 ppm, which is indicative of a co-existence of two different binding modes (κ^1 / κ^2) of the two amidate moieties in solution.

Crystal structure determination of **111d-Zr** confirmed the κ^1 – binding mode of the amidate ligand and showed a C_2 -symmetric octahedral environment at the zirconium center including two dimethylamino ligands (Figure V-2). Interestingly, compound **111ca-Zr** also crystallized as a κ^1, κ^1 -bis(amidate) complex of trigonal bipyramidal geometry and a single diethylamino ligand (Figure V-2).

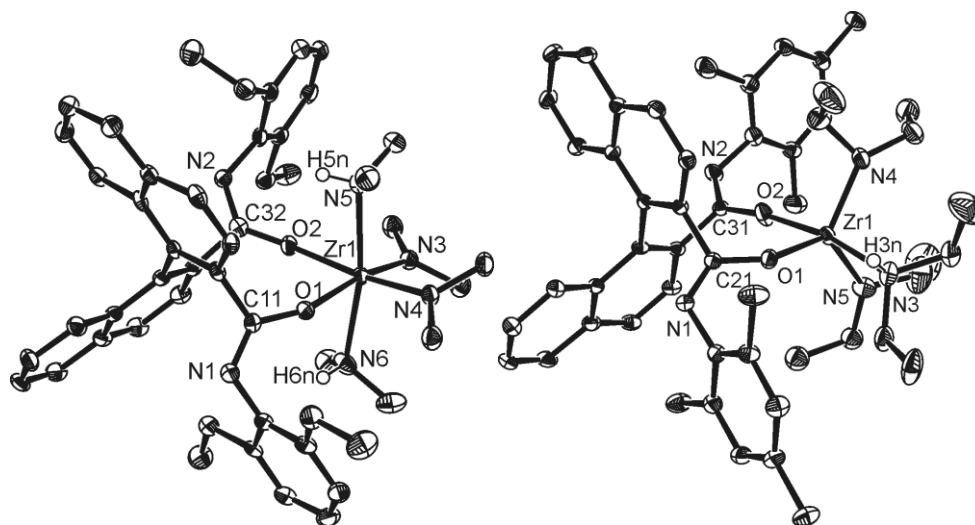


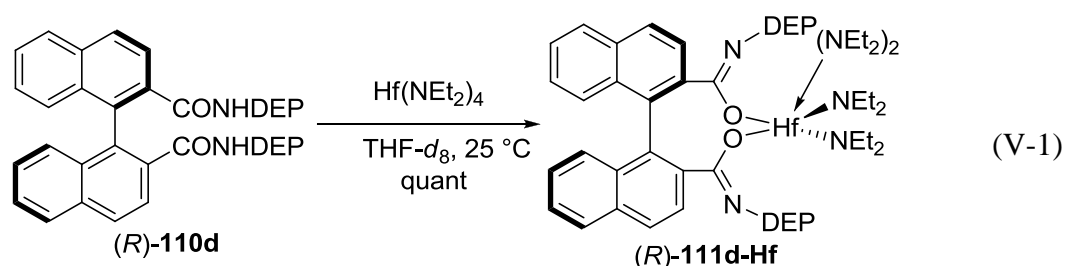
Figure V-2. Crystal structures for (*R*)-**111d-Zr** (left) (*R*)-**111ca-Zr** (right). Thermal ellipsoids shown with a 50% probability level. Hydrogen atoms, except for those attached to nitrogen atoms, are omitted for clarity.

Several important structural consequences arise from switching from the κ^2, κ^2 -bis(amidate) **40** to κ^1, κ^1 -binding mode observed for bis(amidate) **111-Zr**. As the tetradentate amidate ligand is converted to a bidentate one, the biaryl backbone becomes more “open” and the biaryl dihedral angle increases from 68.3(0.6)° in **40** to 76.1(0.5)° in **111d-Zr** and 88.3(0.5)° in **111ca-Zr**, which might result in both better accessibility of the metal center (higher reactivity) but also in lower stereinduction as the chiral pocket becomes more loose. The nitrogen atom of the amidate moiety is not involved in bonding with zirconium and the bulky aryl substituent is placed relatively remote from the reaction site, which might impact the stereodiscrimination as well. The metal center in **111-Zr** is clearly less electronically saturated from the interaction with the amidate ligand. This is illustrated by significantly shorter metal-amino ligand bonds (2.371(2) Å in **111d-Zr** and 2.416(2) Å in **111ca-Zr** vs 2.536(6) Å in **40**¹³) suggesting the higher

Lewis basicity of **111-Zr** compared to **40**. The metal-amido bond lengths seem to be less dependent on the amidate structure: 2.032(3) Å in **2b-Zr** and 2.071(2) Å in **2aa-Zr** vs 2.066(4) Å in **40**.

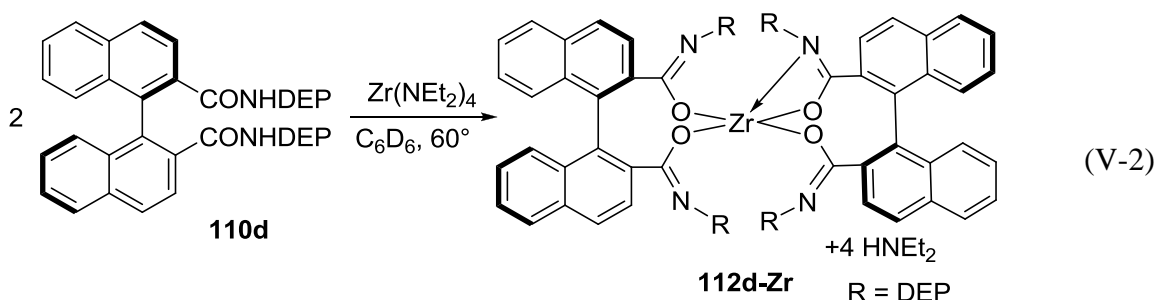
The precatalysts **111-Zr** may be isolated by removal of the solvent *in vacuo* with retention of two equivalents of dimethylamine. The isolated catalysts exhibited the same reactivity independently of being isolated or generated *in situ* (See V.2.2). Thus, for convenience the catalysts were generally prepared *in situ* and used in a standard solution.

We attempted to use the developed methodology to access other group 4 metal complexes **111**. The reaction of the proligands **110c-e** and **110h** as well as of less bulky **110** with $\text{Ti}(\text{NMe}_2)_4$ or $\text{Ti}(\text{NEt}_2)_4$ lead to a mixture of products under a variety of conditions, and a corresponding species **111-Ti** could not be observed. While the reaction of **110** with $\text{Hf}(\text{NEt}_2)_4$ in C_6D_6 or C_7D_8 also did not result in formation of **111**, we were able to prepare **111d-Hf** by carrying the reaction in $\text{THF-}d_8$ (Eq. V-1). Compound **111d-Hf** displayed κ^1, κ^1 -binding mode in solution according to the ^{13}C NMR spectroscopic data.



Recently, Zi and coworkers have prepared a tetrakis(amidate) analogue of **40** by reacting the Schafer type ligand with zirconium amide precursor in a 2:1 molar ratio.³⁵ Although this compound did not show any catalytic activity in aminoalkene

hydroamination, we envisioned that modified amidate proligands **110** may produce a different outcome. When proligand **110d** was treated with 0.5 eq. $\text{Zr}(\text{NEt}_2)_4$ at slightly elevated temperature in C_6D_6 , clean formation of the new C_1 -symmetric amidate species **112d-Zr** was detected (Eq. V-2). All 4 amidate ligand fragments are non-equivalent. Three amidate groups are bound in a κ^1 -mode (CO signal at 160–159 ppm in the ^{13}C NMR spectrum), whereas one remaining amidate is bound in a κ^2 -mode. Unfortunately, we were unable to obtain X-Ray quality crystals of **112d-Zr**.

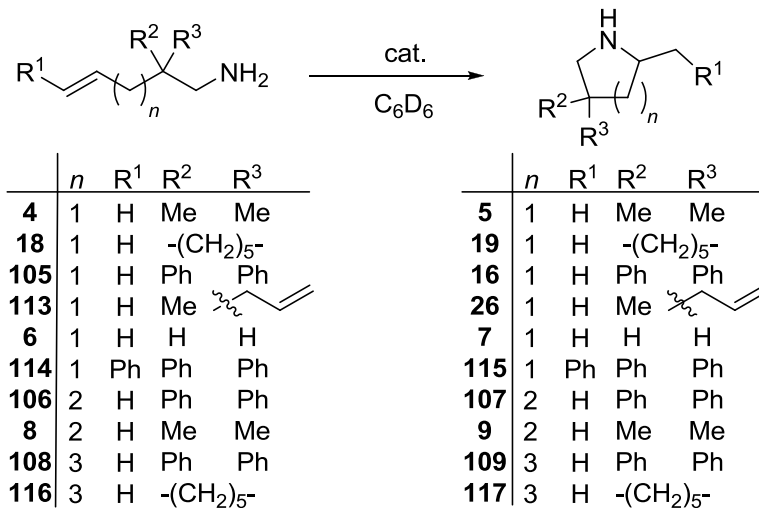


V.2.2 Catalytic Hydroamination

A screening of the bis(amidate) complexes **111** in various catalytic hydroamination/cyclization reactions (Table V-1) revealed a remarkable increase in catalytic performance compared to previously studied group 4 alkene hydroamination catalyst systems (Table V-1). Most notably, reactions could be performed with catalyst loadings as low as 0.5 mol% (Table V-1, entry 12) and reaction temperatures as low as 70 °C (Table V-1, entry 4).

As anticipated, increasing the steric bulk of the *gem*-dialkyl-substituent in aminopentenes **4**, **18**, **105** and **113** resulted in higher rates of cyclization; allowing to perform cyclizations with low catalyst loadings and lower reaction temperatures. In the absence of any *gem*-dialkyl-substituent the cyclization of **6** required slightly higher reaction temperatures, higher catalyst loadings, and longer reaction times (Table V-1,

entry 16). However, there are only a limited set of group 4 metal catalysts capable to cyclize this substrate and they typically require harsher reaction conditions (≥ 10 mol% catalyst loading, ≥ 120 °C).^{15,19,20} Complexes **2** catalyze not only the cyclization of aminohexenes **8** and **106**, they also facilitate formation of the *azepanes* **109** and **117** (Table V-1, entries 20–22), which are the first examples for an enantioselective 7-membered aza-ring formation via catalytic hydroamination. This contrasts previous reported attempts of hydroamination/cyclization of aminoheptene derivatives that either gave no product^{14,36,37} or resulted in a hydroaminoalkylation process instead.^{28,29,38} The only previous example of hydroamination/cyclization of an aminoheptene with a group 4 metal catalyst has been reported recently by Schafer while studying the hydroaminoalkylation reaction. The achiral bis(amidate) zirconium catalyst required forcing reaction conditions (20 mol % cat., 145 °C, 115 h, 55% conv.).^{11,29} Notably, under the catalytic conditions employed in this study, we did not observe hydroaminoalkylation or olefin isomerization products in any of the catalytic reactions.

Table V-1. Asymmetric hydroamination-cyclization of aminoalkenes, catalyzed by **111**.^a

entry	subst.	cat. (mol %)	T, °C	Time, h ^b	% ee (config)
1	4	(<i>S</i>)- 111c-Zr (2)	100	26	23 (<i>R</i>)
2	4	(<i>R</i>)- 111d-Zr (2)	100	7	42 (<i>S</i>) ^c
3	4	(<i>S</i>)- 111e-Zr (5)	110	6	<5% (<i>R</i>)
4	18	(<i>S</i>)- 111c-Zr (6)	70	28	16 (<i>R</i>)
5	18	(<i>R</i>)- 111d-Zr (1)	90	12	26(<i>S</i>)
6	18	(<i>S</i>)- 111e-Zr (2)	110	3	11 (<i>S</i>)
7	18	(<i>S</i>)- 111g-Zr (4)	100	0.5	41 (<i>S</i>) ^d
8	105	(<i>S</i>)- 111c-Zr (4)	80	14	54 (<i>S</i>) ^e
9	105	(<i>R</i>)- 111d-Zr (1)	100	2.5	36 (<i>R</i>)
10	105	(<i>R</i>)- 111d-Hf (3)	100	3	43 (<i>R</i>) ^d
11	105	(<i>S</i>)- 111e-Zr (2)	100	1.5	39 (<i>S</i>)
12	105	(<i>rac</i>)- 111e-Zr (0.5)	100	6	--
13	105	(<i>R</i>)- 111h-Zr (1)	100	2	13 (<i>S</i>)
14	113	(<i>S</i>)- 111c-Zr (2)	90	13	60 / 0 ^f
15	113	(<i>R</i>)- 111d-Zr (2)	90	9	48 / 48 ^g
16	6	(<i>S</i>)- 111c-Zr (8)	120	39	7 (<i>R</i>)
17	114	(<i>S</i>)- 111c-Zr (6)	110	16	8
18	106	(<i>S</i>)- 111c-Zr (4)	100	3	33

19	8	(<i>S</i>)- 111c-Zr (2)	100	7	7
20	108	(<i>S</i>)- 111c-Zr (8)	120	51	60
21	108	(<i>R</i>)- 111h-Zr (1)	120	35	61
22	116	(<i>S</i>)- 111c-Zr (10)	120	40	11

^a Reaction conditions: C₆D₆, Ar atm. ^b Time for >95% conv. based on ¹H NMR spectroscopy using ferrocene as internal standard. ^c 84% isolated yield. ^d less than 50% conversion. ^e Run with isolated catalysts, identical results with catalyst prepared *in situ*, 85% isolated yield. ^f dr = 1.6:1. ^g dr = 1.8:1.

All hydroamination reactions proceeded cleanly to high (>95%) conversions without any noticeable formation of side-products (see Figure V-3), with an exception of reactions catalyzed by **111d-Hf** (Table V-1, entry 10) and **111g-Zr** (Table V-1, entry 7), which did not exceed 50% conversion even after prolonged heating. We propose that this might be due to poor stability of the corresponding complexes. Indeed, when the precatalysts **111g-Zr** and **111d-Hf** were kept in C₆D₆ at 100 °C for a period of 1 h, a significant decomposition was observed in both cases. No apparent decomposition was observed for other precatalysts **111** after extended heating to 150 °C in C₆D₆.

It seems reasonable to assume that the significant higher reactivity of complexes **111** in comparison to previously studied group 4 metal alkene hydroamination catalysts (including amidate complexes such as **40**) may be attributed to the κ^1 binding mode of the amidate moieties leading to a more electron deficient, thus more reactive metal center. On the other hand, this κ^1 binding mode puts the stereodirecting *N*-aryl substituents in a more remote position, pointing away from the metal center. Coincidentally, the highest enantioselectivity achieved with a related tantalum κ^1 -bis(amidate) in the catalytic hydroaminoalkylation of norbornene was also 61% ee.³¹ Therefore, it is not too astonishing that the enantioselectivities achieved with complexes

111 do not compare well with the best selectivities reported to date for group 4 metal-catalyzed alkene hydroamination reactions.^{13,18,19,39-41} Nevertheless, it seems remarkable that the highest selectivity of 61% ee was observed in the formation of the azepane **117** using catalyst **111h-Zr**. Generally, the sterically less demanding mesityl substituent in **111c** resulted in higher enantioselectivities, which may be rationalized by a mixed κ^1/κ^2 -binding mode of the two amidate moieties in this complex.

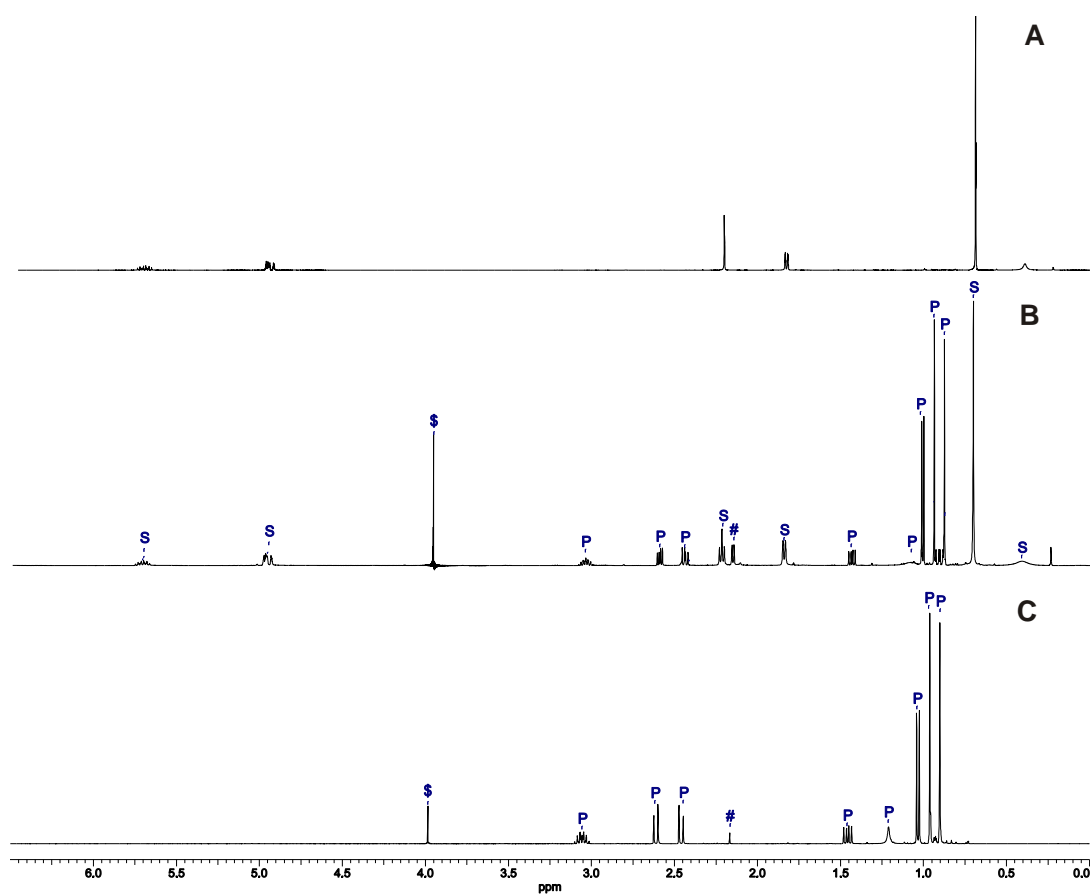
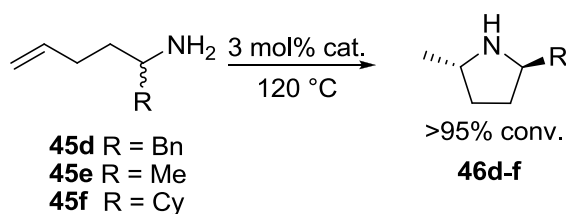


Figure V-3. ^1H NMR spectra in C_6D_6 showing: a) pure aminopentene **6**, b) catalytic cyclization of **6** with catalyst (*S*)-**111c-Zr** (2 mol%) at 110 °C and 51% conversion (spectrum taken at 25 °C); c) **7** after vacuum transfer (>98% conversion). (S = aminoalkene **6**, P = pyrrolidine **7**, \$ = ferrocene; # = dimethylamine).

The scope of the reaction is not limited to terminal olefins, but also the internal olefin **3f** was cyclized efficiently. Cyclization of α -alkyl-substituted aminopentenes proceeded with high *trans/cis* diastereoselectivities (Table V-2), but no kinetic resolution⁴² (see also Chapter 2) of the starting material was observed, as the starting material remained racemic at conversions as high as 86%. Although it is conceivable that the zirconium catalysts may racemize the substrate,⁴³ the cyclization of enantiomerically pure **9a** did not show any sign of racemization of the starting material.

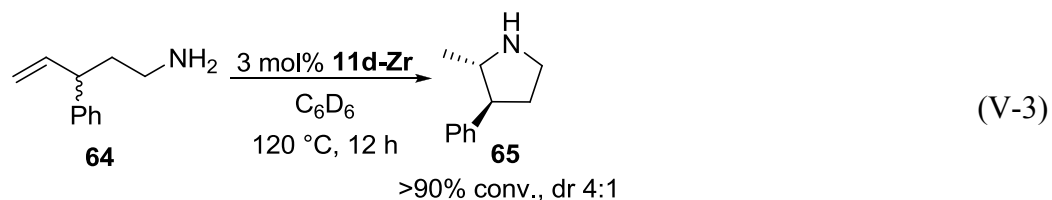
Table V-2. Diastereoselective hydroamination/cyclization of α -substituted aminopentenes.



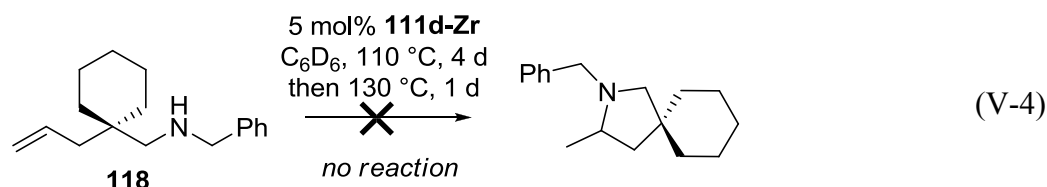
subst.	cat.	<i>t</i> , h	<i>trans:cis</i>	yield, % ^a
45d	111d-Zr	25	>30:1	95
45e	111d-Zr	20	15:1	94
45f	111c-Zr	12	>30:1	88 ^b

^a NMR yield based on ¹H NMR spectroscopy using ferrocene as internal standard. ^b Isolated yield.

Cyclization of **64** (Eq. V-3) proceeded chemoselectively without any substrate isomerization, remarkably contrasting our observations with binaphtholate rare earth metal complexes that are highly resistant to olefin isomerizations otherwise⁴² (see also Chapter 2).



However, no reaction was observed for the *N*-benzyl aminopentene derivative **118** even under more forcing reaction conditions (Eq. V-4), which is in agreement to most²⁰ previous studies on neutral group 4 metal based catalysts.^{12,15,17}



This finding has been previously interpreted as an indicator for a [2+2]-cycloaddition mechanism analogous to group 4 metal-catalyzed alkyne and allene hydroaminations (see section II.1.2) as the secondary amine does not allow formation of a metal imido species required in this mechanism.^{12,15,17}

Kinetic studies indicate that the reaction is first order in aminoalkene substrate and **111-Zr** (Figure V-4 and Figure V-5), which is in agreement to some studies,^{14,19} while others have observed a zero order rate dependence on substrate concentration^{16,17,44} or a mixed-order saturation kinetics.⁴¹ Certainly, the reaction order in substrate depends on the underlying reaction mechanism and the structure of the catalytic active species. To that end, it is interesting to note that enantiopure and racemic catalysts **111-Zr** exhibited the same rate of cyclization (Figure V-6), which is highly indicative (in conjunction with the first order rate dependence on catalyst concentration) that the resting state of the catalyst in this process is a monometallic species.

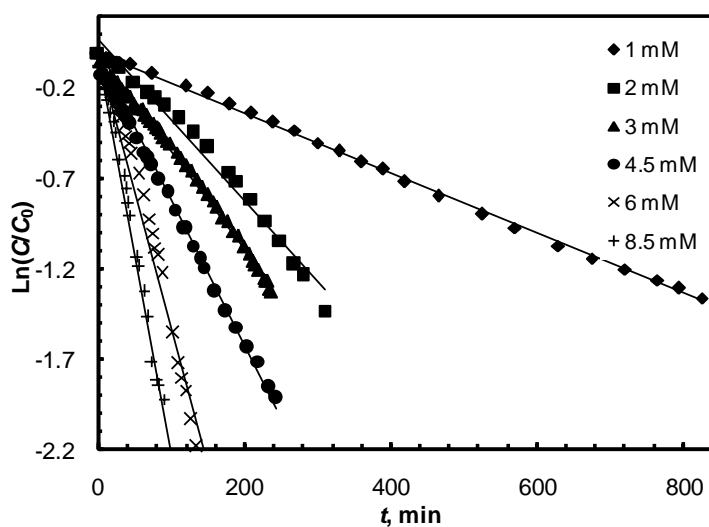


Figure V-4. First-order kinetic plots for the cyclization of **18** ($[C]_0 = 0.10\text{M}$) in the presence of (*R*)-**111d-Zr** (1–8.5 mM) in toluene- d_8 at 90 °C.

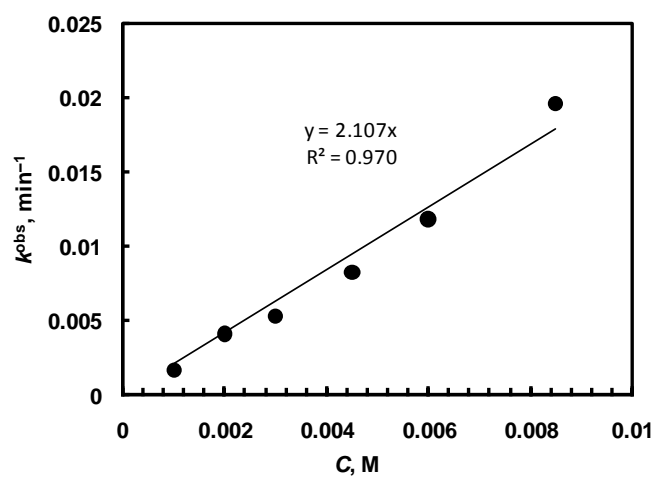


Figure V-5. Observed first order rate constant for the cyclization of **18** ($C_0 = 0.102\text{M}$) in toluene- d_8 at 90 °C vs. concentration of catalyst ((*R*)-**111d-Zr**).

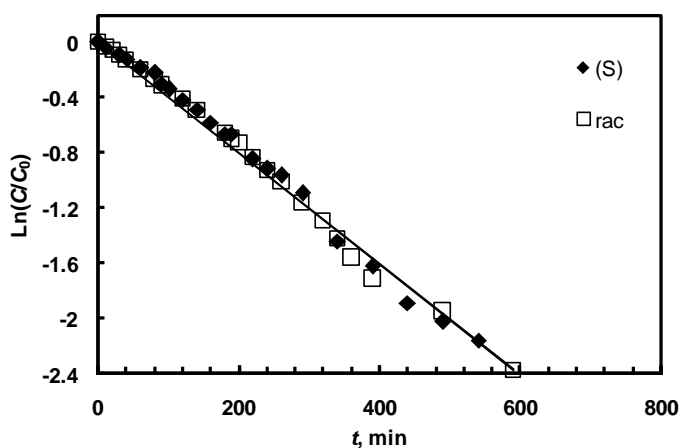


Figure V-6. Cyclization of **18** ($[C]_0 = 0.097\text{M}$) in the presence of *rac*-**111c-Zr** and (*S*)-**111c-Zr** (0.0039 M) in toluene- d_8 at 90 °C.

A strong primary kinetic isotope effect of 4.2 in the cyclization of **18** (Figure V-7) is in agreement to a previous study by Scott^{16,44} and the resulting pyrrolidine **19- d_2** shows deuteration exclusively at the α -methyl position (as well as at nitrogen). Notably, no isotopic perturbation of enantioselectivity was observed, in marked contrast to observations of Sadow et al.⁴¹

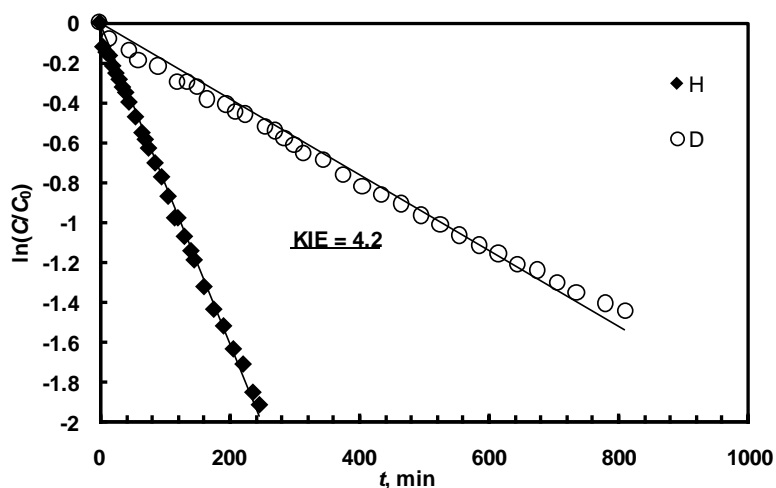


Figure V-7. Cyclization of **18** and **18- d_2** ($[C]_0 = 0.102\text{M}$) in the presence of (*R*)-**111d-Zr** (0.0045M) in toluene- d_8 at 90 °C.

Although the reactivity was lower than that of **111-Zr**, enantioselectivities of up to 85% ee were achieved. While some unorthodox hydroamination precatalysts lacking the obvious leaving group such as organolanthanide ate-complexes **17** are known (see Table I-2),⁴⁵ the reactivity of **112d-Zr** is quite remarkable in the context of ongoing discussions on the mechanism of group 4 metal-catalyzed hydroamination (see section I.2.4). Indeed, the imido-mechanism (see Scheme I-12) would require two protolytically cleavable X-type ligands in order to form the key metal-imido species.¹⁶ Also, proton-assisted concerted insertion-protonolysis, which has been advocated by Sadow et al. requires two amido ligands as well.⁴¹ However, due to the high acidity of the amide fragment, protonation of two amidate ligands with a simple amine seems unlikely. Furthermore, such protonation would likely to lead to a bis(amidate) **111-Zr**-like species. However, both lower reactivity and higher selectivity of the hydroamination with **112-Zr** suggest that the bis(amidate) **111-Zr** is not present in the mixture in catalytically relevant concentrations. This is further manifested by the absence of hydroamination reactivity of both **6** and **114** with **112d-Zr** even at 150 °C, while each of these reactions was shown to be catalyzed by **111-Zr** under significantly milder conditions (Table V-1).

V.3 Conclusions

Chiral bis(κ^1)-amidates of zirconium displayed enhanced level of reactivity in hydroamination/cyclization compared to the previous group 4 metal-based catalysts. The enhancement of reactivity was obtained by tuning the amidate ligand towards a less electron-saturating binding mode which resulted in a more electrophilic metal center. The reactivity improvement was not only of a quantitative character, allowing lower

temperatures and catalyst loadings, but also a qualitative difference was made by successful application to previously challenging substrates, such as aminoheptenes, and aminoalkenes lacking gem-dialkyl substitution. Within a year of our initial report,³³ group 4 metal catalysts with very high reactivity and selectivity; however, applicable only to gem-diactivated aminopentenes^{41,46} and also (achiral) catalysts capable of selective cyclization of aminoheptenes¹² were reported. However, catalysts **111-Zr** still remain the only hydroamination catalysts which can afford azepanes via stereoselective hydroamination/cyclization. Unique structure and reactivity of the tetrakis(amidate) **112-Zr** suggests that unorthodox ligand systems such as X₃- and X₄- type ligands can also be employed for group 4 metals in catalytic hydroamination.

V.4 Experimental

General considerations. All reactions with air- or moisture sensitive materials were performed in oven (120 °C) and flame-dried glassware under an inert atmosphere of dry nitrogen or argon, employing standard Schlenk and glovebox techniques. THF was sparged with argon for 1 h and then passed through a column with activated alumina prior to use. Benzene, benzene- d_6 , THF- d_8 , and toluene- d_8 were distilled from sodium/benzophenone ketyl. DMF and aminoalkenes were distilled from CaH_2 and stored under Ar over 4Å molecular sieves. All starting materials are commercially available and were used as received.

^1H , ^{13}C , and ^{19}F NMR spectra were recorded on Varian (300, 400, 500 MHz) spectrometers at 25 °C unless stated otherwise. Chemical shifts are reported in ppm downfield from tetramethylsilane with the undeuterated portion of the solvent as internal standard. Enantiomeric excess of the hydroamination products were determined by ^{19}F NMR of their Mosher amides at 60–100 °C (*vide infra*). HPLC analysis was carried out on an Agilent 1200 series instrument with multiple wavelength UV detector using Chiralcel OD-H and Chiralpak AS-H columns (25 × □4.6 mm). Silica gel (230–400 mesh, Sorbent Technologies) and alumina (80–200 mesh, EMD) were used for column chromatography. Silica-covered aluminum plates (60 F, EMD) were used for analytical TLC. Melting points were determined with a Buchi 535 digital melting point apparatus. Elemental analyses were performed by Robertson Microlit Laboratories, Inc., Madison, NJ.

$\text{Zr}(\text{NEt}_2)_4$ and $\text{Hf}(\text{NEt}_2)_4$ were synthesized according to the literature protocols.⁴⁷

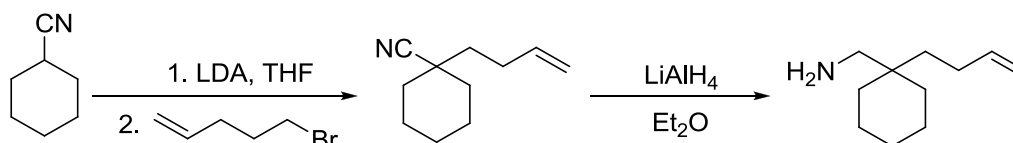
(*S*)-Mosher acid was converted into the corresponding (*R*)-Mosher acid chloride according to a literature procedure.⁴⁸

Aminoalkenes 2,2-dimethyl-pent-4-enyl amine (**4**),⁴⁹ (1-allylcyclohexyl)methylamine (**18**),⁵⁰ 2,2-diphenylpent-4-enyl amine (**105**),⁵¹ 2-allyl-2-methylpent-4-enyl amine (**113**),⁵² pent-4-enyl amine (**6**),²⁷ 2,2,5-triphenylpent-4-enyl amine (**114**),⁵³ 2,2-diphenylhex-5-enyl amine (**106**),⁵⁴ 2,2-dimethylhex-5-enyl amine (**8**),²⁶ 2,2-diphenylhept-6-enyl amine (**108**),³⁶ 1-benzylpent-4-enyl amine (**45d**),⁴² 1-methylpent-4-enyl amine (**45e**),⁵⁵ 1-cyclohexylpent-4-enyl amine (**45f**),⁴² 3-phenylpent-4-enyl amine (**64**)⁵⁶ and *N*[(1-allylcyclohexyl)-methyl]-*N*-benzylamine (**118**)⁵⁰ were synthesized according to the literature protocols.

Hydroamination products 2,4,4-trimethylpyrrolidine (**5**),²⁷ 3-methyl-2-azaspiro[4,5]decane (**19**),⁵⁷ 2-methyl-4,4-diphenylpyrrolidine (**16**),⁵¹ 4-allyl-2,4-dimethylpyrrolidine (**26**),⁵⁸ 2-methylpyrrolidine (**7**),²⁷ 2-benzyl-4,4-diphenylpyrrolidine (**115**),³⁶ 2-methyl-5,5-diphenylpiperidine (**107**),⁵⁹ 2,5,5-trimethylpiperidine (**9**),⁶⁰ 2-methyl-6,6-diphenylazepane (**109**),²⁹ 2-benzyl-5-methylpyrrolidine (**46d**),²⁶ 2,5-dimethylpyrrolidine (**46e**)⁶¹ and 2-methyl-3-phenylpyrrolidine (**65**)⁶² are known compounds and were identified by comparison to the literature NMR spectroscopic data.

Substrate synthesis

1-Pent-4-enylcyclohexyl)methylamine



1-Pent-4-enylcyclohexanecarbonitrile THF (150 mL) was cooled to $-30\text{ }^{\circ}\text{C}$ and *n*-BuLi (36 mL, 2.5 M in hexanes, 91 mmol) was added, followed by addition of diisopropylamine (13.3 mL, 9.60 g, 95 mmol) at $-30\text{ }^{\circ}\text{C}$. The resulting solution was allowed to warm to $-10\text{ }^{\circ}\text{C}$ and it was then cooled back to $-30\text{ }^{\circ}\text{C}$. Cyclohexanecarbonitrile (9.81g, 90 mmol) was added dropwise to this solution. The reaction mixture was stirred for 1 h at $-30\text{ }^{\circ}\text{C}$ and was then treated with a solution of 1-bromopent-5-ene (13.6 g, 91 mmol) in THF (20 mL). The reaction mixture was allowed to reach room temperature and was stirred at this temperature for additional 4 hours. Water (100 mL) and saturated NH_4Cl solution (100 mL) were added, the product was extracted with ether ($2\times 100\text{ mL}$). The combined organic layer was washed with brine, dried over Na_2SO_4 and concentrated by rotary evaporation. The crude material was distilled (bp $130\text{--}139\text{ }^{\circ}\text{C}$, 10 mm Hg) to give 12.35 g (77%) of a colorless oil. ^1H NMR (300 MHz, CDCl_3): δ = 5.76 (m, 1H, =CH), 5.02–4.93 (m, 2H, =CH₂), 2.10–2.01 (m, 2H), 1.97–1.93 (m, 3H), 1.72–1.47 (m, 10H), 1.24–1.13 (m, 3H); $^{13}\text{C}\{^1\text{H}\}$ NMR (75 MHz, CDCl_3): δ = 137.9 (=CH), 123.6 ($\text{C}\equiv\text{N}$), 115.1 (=CH₂), 39.9, 38.9, 35.7, 35.6, 33.6, 25.4, 23.5, 23.0.

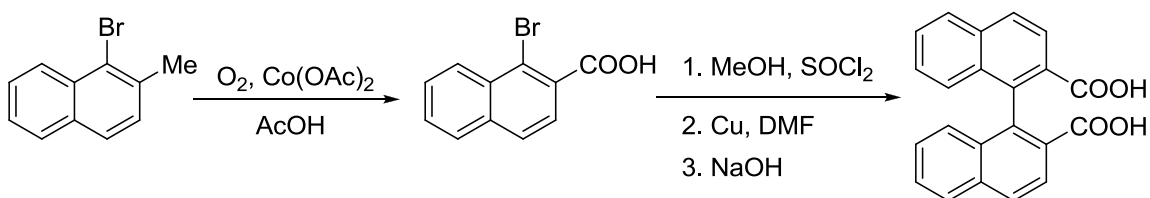
(1-Pent-4-enylcyclohexyl)methylamine (116). To a mixture of LiAlH_4 (3.93 g, 0.1 mol) and Et_2O (200 mL) was added a solution of 1-pent-4-enylcyclohexanecarbonitrile (12.35 g, 69 mmol) in Et_2O (40 mL) at $0\text{ }^{\circ}\text{C}$. The reaction mixture was stirred at room temperature for 6 h. Then the suspension was cooled to $0\text{ }^{\circ}\text{C}$ and treated carefully with water (4 mL), 15% NaOH (4 mL) and then again water (20 mL). The ether layer was decanted off from the white precipitate and the precipitate was refluxed with additional portion of Et_2O (100 mL). The combined organic layers were

dried (Na_2SO_4) overnight and were then concentrated by rotary evaporation. The residue was distilled from CaH_2 (145 °C, 10 mm) give 10.0 g (80 %) of the target amine as a colorless oil. ^1H NMR (500 MHz, CDCl_3): δ = 5.78 (m, 1H, =CH), 5.00–4.91 (m, 2H, =CH₂), 2.02–2.00 (m, 2H, CH_2NH_2), 1.39–1.37 (m, 4H), 1.30–1.18 (m, 9H), 0.86 (br s, 2H, NH_2); $^{13}\text{C}\{^1\text{H}\}$ NMR (125 MHz, CDCl_3): δ = 139.0 (=CH), 114.4 (=CH₂), 48.6, 36.3, 34.6, 34.2, 33.4, 26.5, 22.2, 21.5.

Ligand Synthesis

2,4,6-Trimethoxyaniline A mixture of 2,4,6-trimethoxynitrobenzene (1.50 g, 7.0 mmol), $\text{SnCl}_2 \cdot 2\text{H}_2\text{O}$ (4.4 g, 19 mmol), HCl (12 M, 5 mL) and ethanol (10 mL) was stirred overnight at room temperature and then 4 h at 50 °C (TLC-control). The mixture was poured into 10% ml of KOH (100 mL), cooled down and extracted with ether (2×30 mL). Combined organic layers were washed with water, then brine, dried (Na_2SO_4) and concentrated *in vacuo* to afford 1.01 g of the product as a brown oil (79% yield). ^1H NMR (CDCl_3 , 300 MHz): 6.16 (s, 2H), 3.82 (s, 6H, OMe), 3.75 (s, 3H, OMe), 3.49 (br s, 2H, NH_2); ^{13}C NMR (CDCl_3 , 75 MHz): δ = 152.5, 148.0, 118.9, 104.7, 91.3, 55.77, 55.72. NMR data is in agreement with the literature.⁶³

***rac*-1,1'-Binaphthalene-2,2'-dicarboxylic acid (BINCA)** (adopted from the literature).^{64,65}



1-Bromo-2-naphthoic acid. A mixture of 1-bromo-2-methylnaphthalene (25.0 g, 0.11 mol), ethylmethylketone (10 mL), $\text{Co}(\text{OAc})_2 \cdot (\text{H}_2\text{O})_4$ (5.60 g, 23 mmol) and glacial

acetic acid (150 mL) was stirred at 110–113 °C for 2 days, while oxygen was bubbled slowly through the solution. The reaction mixture was slowly changing its color from purple to dark brown. After achieving ca. 60% conversion by TLC the reaction appeared to stop and was quenched by pouring it on ice (500 g) to produce black viscous substance with an intensive unpleasant aldehyde-like odor. Solid NaCl (50 g) was added and the mixture was extracted with EtOAc (3 × 150 mL). The combined organic layer was washed with brine (100 mL), concentrated to 100 mL, diluted with toluene (200 mL) and then extracted with 2M NaOH (3 × 200 mL) after which organic layer may be discarded. The combined dark brown aqueous NaOH extract was refluxed with charcoal (50 g) for 4 h, cooled down and filtered. HCl (12 M) was added carefully to the yellowish filtrate under stirring until pH~0 to produce a white precipitate. After additional stirring for 30 min at room temperature, the solid was filtered off, washed with water until pH~7 and dried *in vacuo* to give 13.5 g (49% yield) of pure 1-bromo-naphtalene-2-carboxylic acid as a white solid, mp 190 °C. ¹H NMR (300 MHz, DMSO-*d*₆): δ = 13.6 (br s, 1H, COOH), 8.32 (d, ³*J*(H,H) = 9.1 Hz, 1H), 8.06–8.03 (m, 2H), 7.76–7.67 (m, 3H). The ¹H NMR spectrum is similar to a low resolution spectrum reported previously.⁶⁴

***rac*-BINCA.** The naphthoic acid obtained above (13.5 g, 53 mmol) was dissolved in MeOH (100 mL) and 1 drop of DMF was added. SOCl₂ (11 mL, 9.0 g, 154 mmol) was added dropwise under stirring. After the addition was complete, the mixture was stirred at reflux for 1 h (TLC-control) then cooled down and carefully poured into NaHCO₃ *sat.* (300 mL). Reaction product was extracted with ether (2 × 50 mL), and the combined organic layer was washed with brine (50 mL). The solution was then dried (Na₂SO₄) and

concentrated *in vacuo* to afford 14.0 g of methylnaphthoate as a brown liquid (53 mmol, 100% yield) which was used without further purification. The ester was dissolved in dry DMF (20 mL), and copper powder (5.4 g, 85 mmol) was added. The mixture was stirred at 120 °C for 4 h (checked by TLC). The mixture was cooled down, diluted with EtOAc (100 mL) and filtered through celite to remove copper salts. The organic layers were washed with NaHCO₃ *sat.* (2 × 50 mL) then brine, dried (Na₂SO₄) and concentrated. Flash column on 6 cm of silica (hexane/dichloromethane 1:1) afforded the BINCA-dimethyl diester (7.0 g, 71%) as a white solid. R_f 0.2 (hexanes/EtOAc 9:1). The solid was suspended in MeOH (30 mL), and NaOH (15%, 20 mL) was added. The mixture was stirred at reflux for 2 h, then diluted with water (150 mL) and extracted with ether (50 mL). The ether layer was discarded, and the aqueous layer was carefully brought to pH~0 with 12 M HCl to produce a white precipitate. After additional stirring for 30min at room temperature, the solid was filtered off, washed with water until pH~7 and dried *in vacuo* to give 6.40 g (98% yield) of pure BINCA as a white solid, mp 276–279 °C. ¹H NMR (500 MHz, DMSO-*d*₆): δ = 12.4 (br s, 2H, COOH), 8.09–8.03 (m, 6H), 7.54 (vt, ³J(H,H) = 6.9 Hz, 2H), 7.27 (vt, ³J(H,H) = 8.3 Hz, 2H), 7.54 (d, ³J(H,H) = 8.5 Hz, 2H); ¹³C{¹H} NMR (125 MHz, (DMSO-*d*₆): δ = 167.6 (COOH), 139.4, 134.3, 132.5, 128.1, 127.9, 127.5, 127.4, 126.6, 126.0. The NMR spectra are in agreement with literature data.⁶⁵

Resolution of BINCA (a modified literature⁶⁶ procedure).

To a solution of *rac*-BINCA (5.0 g, 14.6 mmol) in THF (100 mL) was added DCC (3.0 g, 14.6 mmol) and the mixture was refluxed for 2 h to form a white precipitate. (*R*)-1-phenylethylamine (2.11 g, 17.5 mmol), and triethylamine (2.0 mL, 14.6 mmol) were added at room temperature, and the mixture was refluxed overnight. The mixture

was concentrated *in vacuo* and the residue was quenched with 1N HCl (100 mL) and extracted with dichloromethane (100 mL). The extract was dried (Na_2SO_4) and evaporated, and the residue was crystallized from acetonitrile (80 mL, crystals collected at 10 °C) to give 2.10 g of a yellowish solid which was ca. 90% pure by NMR-spectroscopy,⁶⁶ but containing only 1 diastereomer of the target amide (*R,R*). The mother liquor was evaporated and recrystallized twice from 80 mL of 95% ethanol to give 2.1 g of the pure (*S,R*) diastereomer. Each diastereomer was refluxed with SOCl_2 (30 mL) for 4 h to afford black mixture, then SOCl_2 was distilled off *in vacuo* and the residue was treated with 40% KOH (30 mL) and refluxed for 1 day. The mixture was diluted with water (150 mL) and extracted with ether (50 mL). The organic layer was discarded and the aqueous layer was refluxed with charcoal (10 g) for 5 h, cooled down to room temperature and filtered. The filtrate was brought to pH~0 with HCl (12 M),* cooled to 0 °C and extracted with EtOAc (2 × 50 mL). The combined organic layers were washed with water until pH~7, then washed with brine, dried (Na_2SO_4) and concentrated to 10 mL volume. Hexane (20 mL) was then added to induce precipitation, and the volatiles were removed to afford the chiral BINCA as a fine snow-white microcrystalline powder with NMR spectra identical to that of *rac*-BINCA. 1.0 g of each *R*- and *S*-isomer were obtained (20% overall or 40% chemical yield each) according to this procedure. Small fractions (10 mg) were converted to dimethyl diesters by refluxing with 1 mL of SOCl_2 in MeOH (10 mL) for 4 h. The reaction mixtures were quenched with *sat.* NaHCO_3 and

* A significant amount of fine silica gel might appear at this point due to the flask corrosion during the previous step, making the extraction impossible. If the silica appears, EtOAc should be added and the mixture should be refluxed for 2 h resulting in an aggregation of silica which can then be easily filtered off.

extracted with ether (15 mL). The organic layer was dried (Na₂SO₄) and concentrated, and the residue was subjected to a HPLC analysis (OD-H column, Hexanes/*i*-PrOH 90:10, 1 mL/min).⁶⁷ (*R*)-BINCA was found to be 97% ee (*t_R* 7 min), and (*S*)-isomer was of 99% ee stereopurity (*t_R* 9 min).

Bis(carboxamido) ligands (General procedure)

To a suspension of BINCA (171 mg, 0.50 mmol) in benzene (1 mL) were added SOCl₂ (2 mL) and DMAP (1 crystal). The mixture was stirred at 70 °C overnight and the volatiles were removed *in vacuo*. Benzene (3 mL), DIPEA (0.5 mL, 3 mmol) and the appropriate aniline (2 mmol) were added and the mixture was stirred for 1 h at room temperature and then overnight at 70 °C until conversion was complete according to TLC. HCl (1N, 10 mL) was added and the product was extracted with dichloromethane (2 × 50 mL). The combined organic layers were washed with water, dried (Na₂SO₄) and concentrated. The residue was subjected to a column chromatography on silica.

***rac*-*N,N'*-diphenyl-1,1'-binaphthalene-2,2'-dicarboxamide (110a).** White solid, 65% yield, *R_f* = 0.2 (DCM/CH₃CN = 30:1). ¹H NMR (500 MHz, DMSO-*d*₆): δ = 10.98 (s, 2H, 2NH), 8.16 (d, ³*J*(H,H) = 8.6 Hz, 2H), 8.02 (d, ³*J*(H,H) = 8.1 Hz, 2H), 7.89 (d, ³*J*(H,H) = 8.3 Hz, 2H), 7.53 (vt, ³*J*(H,H) = 8.1 Hz, ³*J*(H,H) = 6.8 Hz, 2H), 7.36–7.31 (m, 6H), 7.18 (t, ³*J*(H,H) = 7.8 Hz, 4H), 7.13 (d, ³*J*(H,H) = 8.6 Hz, 2H), 6.98 (t, ³*J*(H,H) = 7.3 Hz, 2H). ¹³C{¹H} NMR (125 MHz, DMSO-*d*₆): δ = 168.3 (CO), 138.3, 134.8, 133.6, 132.5, 131.5, 128.8, 128.7, 128.2, 127.2, 126.0, 124.3, 123.9, 119.4.

(R)-N,N'-bis(2-methylphenyl)-1,1'-binaphthalene-2,2'-dicarboxamide (110b).

White solid, 51% yield, R_f = 0.2 (DCM/CH₃CN = 30:1). ¹H NMR (500 MHz, DMSO-*d*₆): δ = 10.40 (s, 2H, 2NH), 8.20 (d, ³*J*(H,H) = 8.6 Hz, 2H), 8.08 (d, ³*J*(H,H) = 8.3 Hz, 2H), 7.86 (d, ³*J*(H,H) = 8.6 Hz, 2H), 7.58 (vt, ³*J*(H,H) = 8.3 Hz, ³*J*(H,H) = 6.8 Hz, 2H), 7.39 (vt, ³*J*(H,H) = 8.3 Hz, ³*J*(H,H) = 7.1 Hz, 2H), 7.22 (d, ³*J*(H,H) = 8.6 Hz, 2H), 7.03–6.97 (m, 6H), 6.81–6.80 (m, 2H), 1.55 (s, 6H, 2CH₃). ¹³C{¹H} NMR (125 MHz, DMSO-*d*₆): δ = 168.4 (CO), 135.4, 135.1, 133.7, 132.58, 132.56, 131.7, 130.2, 128.6, 128.1, 127.14, 127.05, 126.2, 125.8, 125.1, 124.4, 17.1 (CH₃).

(S)-N,N'-Dimesityl-1,1'-binaphthalene-2,2'-dicarboxamide (110c).

White solid, 52% yield, R_f = 0.1 (DCM/CH₃CN = 30:1). Mp 259–262 °C. MS (ESI): *m/z* 577.2 [M + H]⁺. IR (film): ν 3420, 3220, 1638 cm⁻¹. ¹H NMR (300 MHz, DMSO-*d*₆): δ = 10.30 (s, 2H, NH), 8.21 (d, ³*J*(H,H) = 8.5 Hz, 2H), 8.09 (d, ³*J*(H,H) = 8.2 Hz, 2H), 7.83 (d, ³*J*(H,H) = 8.5 Hz, 2H), 7.57 (vt, ³*J*(H,H) = 8.0 Hz, ³*J*(H,H) = 7.3 Hz, 2H), 7.37 (t, ³*J*(H,H) = 7.6 Hz), 7.16 (d, ³*J*(H,H) = 8.5 Hz, 2H), 6.67 (s, 4H), 2.10 (s, 6H, CH₃), 1.43 (s, 12H, CH₃); ¹³C{¹H} NMR (100 MHz, DMSO-*d*₆): δ = 168.2 (CO), 135.5, 135.3, 134.4, 133.7, 132.5, 132.1, 131.6, 128.5, 128.1, 128.0, 127.1, 126.9, 126.3, 124.5, 20.3, 17.1. Anal. Calcd for C₄₀H₃₆N₂O₂: C, 83.30; H, 6.29; N, 4.86. Found: C, 82.50; H, 6.38; N, 4.60.

(S)-N,N'-Bis(2,6-diethylphenyl)-1,1'-binaphthalene-2,2'-dicarboxamide

(110d). White solid, 60% yield, R_f = 0.15 (DCM/CH₃CN = 30:1). Mp 286–289 °C (dec). MS (ESI): *m/z* 605.2 [M + H]⁺. IR (film): ν = 3440, 3220, 1636 cm⁻¹. ¹H NMR (300 MHz, DMSO-*d*₆, 60 °C): δ = 11.41 (br s, 2H, NH), 8.22 (d, ³*J*(H,H) = 8.5 Hz, 2H), 8.11 (d, ³*J*(H,H) = 8.2 Hz, 2H), 7.73 (d, ³*J*(H,H) = 8.2 Hz, 2H), 7.62 (t, ³*J*(H,H) = 7.4 Hz, 2H),

7.35 (t, $^3J(\text{H,H}) = 7.5$ Hz, 2H), 7.21–7.10 (m, 4H), 6.95 (d, $^3J(\text{H,H}) = 7.7$ Hz, 4H), 1.96 (br s, 8H, CH_2), 0.84 (t, $^3J(\text{H,H}) = 7.0$ Hz, 12H, CH_3); $^{13}\text{C}\{^1\text{H}\}$ NMR (75 MHz, $\text{DMSO-}d_6$, 60 °C): $\delta = 168.8$ (CO), 140.8, 135.2, 133.6, 132.7, 132.3, 132.1, 128.4, 127.8, 126.82, 126.77, 126.6, 126.1, 125.2, 124.1, 23.2, 13.6. Anal. Calcd for $\text{C}_{42}\text{H}_{40}\text{N}_2\text{O}_2$: C, 83.41; H, 6.67; N, 4.63. Found: C, 83.62; H, 6.88; N, 4.65.

(*R*)-*N,N'*-Bis(2,6-diisopropylphenyl)-1,1'-binaphthalene-2,2'-dicarboxamide

(110e). White solid, 64% yield, $R_f = 0.2$ (DCM/ $\text{CH}_3\text{CN} = 30:1$). Mp 302–306 °C (dec). MS (ESI): m/z 661.3 $[\text{M} + \text{H}]^+$. IR (film): $\nu = 3420, 3200, 1634$ cm^{-1} . ^1H NMR (300 MHz, $\text{DMSO-}d_6$): $\delta = 10.39$ (s, 2H, NH), 8.28 (d, $^3J(\text{H,H}) = 8.5$ Hz, 2H), 8.13 (d, $^3J(\text{H,H}) = 8.2$ Hz, 2H), 7.81 (d, $^3J(\text{H,H}) = 8.5$ Hz, 2H), 7.60 (t, $^3J(\text{H,H}) = 7.1$ Hz, 2H), 7.38 (t, $^3J(\text{H,H}) = 7.1$ Hz, 2H), 7.15–7.10 (m, 4H), 6.96 (d, $^3J(\text{H,H}) = 8.0$ Hz, 4H), 2.38–2.29 (m, 2H, CHCH_3), 2.24–2.13 (m, 2H, CHCH_3), 0.83 (d, $^3J(\text{H,H}) = 7.0$ Hz, 6H, CH_3), 0.72 (d, $^3J(\text{H,H}) = 7.0$ Hz, 6H, CH_3), 0.62 (d, $^3J(\text{H,H}) = 6.8$ Hz, 6H, CH_3), 0.58 (d, $^3J(\text{H,H}) = 6.8$ Hz, 6H, 2 CH_3); $^{13}\text{C}\{^1\text{H}\}$ NMR (75 MHz, $\text{DMSO-}d_6$): $\delta = 169.5$ (CO), 145.7, 135.5, 133.8, 132.2, 131.3, 128.8, 128.2, 127.5, 127.0, 126.3, 124.3, 122.8, 122.7, 27.8, 27.5, 23.5, 23.4, 22.94, 22.8. Anal. Calcd for $\text{C}_{40}\text{H}_{36}\text{N}_2\text{O}_2$: C, 83.60; H, 7.32; N, 4.24. Found: C, 83.86; H, 7.58; N, 4.18.

(*S*)-*N,N'*-bis(3,5-dimethylphenyl)-1,1'-binaphthalene-2,2'-dicarboxamide

(110f). White solid, 55% yield, $R_f = 0.3$ (hexane/EtOAc = 4:1). ^1H NMR (500MHz, $\text{DMSO-}d_6$): $\delta = 10.79$ (s, 2H, 2NH), 8.16 (d, $^3J(\text{H,H}) = 8.6$ Hz, 2H), 8.03 (d, $^3J(\text{H,H}) = 8.1$ Hz, 2H), 7.87 (d, $^3J(\text{H,H}) = 8.6$ Hz, 2H), 7.53 (vt, $^3J(\text{H,H}) = 7.6$ Hz, $^3J(\text{H,H}) = 7.3$ Hz,

2H), 7.34 (vt, $^3J(\text{H,H}) = 7.8$ Hz, $^3J(\text{H,H}) = 7.6$ Hz, 2H), 7.11 (d, $^3J(\text{H,H}) = 8.6$ Hz, 2H), 6.92 (s, 4H), 6.62 (s, 2H), 2.11 (s, 12H, 4CH₃). $^{13}\text{C}\{^1\text{H}\}$ NMR (125 MHz, DMSO-*d*₆): $\delta = 168.1$ (CO), 138.2, 137.6, 134.9, 133.6, 132.5, 131.5, 128.7, 128.1, 127.13, 127.11, 126.0, 125.4, 124.4, 117.2, 20.9.

(*S*)-*N,N'*-bis(2,4,6-trimethoxyphenyl)-1,1'-binaphthalene-2,2'-dicarboxamide

(110g). White solid, 55% yield, *R*_f = 0.4 (DCM/MeOH=25:1). ^1H NMR (300 MHz, DMSO-*d*₆): $\delta = 9.76$ (s, 2H, 2NH), 8.15 (d, $^3J(\text{H,H}) = 8.6$ Hz, 2H), 8.07 (d, $^3J(\text{H,H}) = 7.9$ Hz, 2H), 7.74 (d, $^3J(\text{H,H}) = 8.5$ Hz, 2H), 7.55 (vt, $^3J(\text{H,H}) = 7.7$ Hz, $^3J(\text{H,H}) = 7.3$ Hz, 2H), 7.30 (vt, $^3J(\text{H,H}) = 7.4$ Hz, $^3J(\text{H,H}) = 7.3$ Hz, 2H), 7.04 (d, $^3J(\text{H,H}) = 8.5$ Hz, 2H), 6.02 (s, 4H), 3.31 (s, 6H, 2 OCH₃), 3.21 (s, 12H, 4 OCH₃). $^{13}\text{C}\{^1\text{H}\}$ NMR (75 MHz, DMSO-*d*₆): $\delta = 168.6$ (CO), 159.3, 156.3, 135.2, 133.6, 133.0, 132.3, 127.9, 127.7, 126.6, 126.5, 124.7, 17.0, 90.8, 55.3, 55.2.

(*S*)-*N,N'*-bis(2-methyl-1-naphthyl)-1,1'-binaphthalene-2,2'-dicarboxamide

(110h). White solid, 45% yield, *R*_f = 0.2 (DCM/CH₃CN=25:1). ^1H NMR (400 MHz, DMSO-*d*₆, 90 °C): $\delta = 10.66$ (s, 2H, 2NH), 8.31 (d, $^3J(\text{H,H}) = 8.6$ Hz, 2H), 8.21 (d, $^3J(\text{H,H}) = 8.2$ Hz, 2H), 7.98 (d, $^3J(\text{H,H}) = 8.6$ Hz, 2H), 7.74 (d, $^3J(\text{H,H}) = 8.2$ Hz, 2H), 7.68 (, $^3J(\text{H,H}) = 7.8$ Hz, 2H), 7.64 (d, $^3J(\text{H,H}) = 8.6$ Hz, 2H), 7.49 (t, $^3J(\text{H,H}) = 7.8$ Hz, 2H), 7.37 (d, $J = 8.4$ Hz, 2H), 7.29 (t, $^3J(\text{H,H}) = 7.1$ Hz, 2H), 7.23 (d, $^3J(\text{H,H}) = 8.2$ Hz, 2H), 6.98 (t, $^3J(\text{H,H}) = 7.4$ Hz, 2H), 6.75 (br m, 2H), 1.81 (br s, 6H, 2 CH₃). ^{13}C NMR spectrum contained only very broad signals of low intensity even after prolonged acquisition.

(R)-N,N'-Dibenzyl-1,1'-binaphthalene-2,2'-dicarboxamide (110i). White solid, 56% yield, R_f = 0.15 (DCM/CH₃CN=100:1). ¹H NMR (300 MHz, DMSO-*d*₆): δ = 9.48 (s, 2H, 2NH), 8.16 (d, ³J(H,H) = 8.8 Hz, 2H), 8.11 (d, ³J(H,H) = 8.2 Hz, 2H), 7.57 (vt, ³J(H,H) = 7.9 Hz, ³J(H,H) = 7.1 Hz, 2H), 7.31 (vt, ³J(H,H) = 8.5 Hz, ³J(H,H) = 7.0 Hz, 2H), 7.05–7.02 (m, 4H), 6.92 (vt, ³J(H,H) = 7.9 Hz, ³J(H,H) = 7.4 Hz, 2H), 6.40 (d, ³J(H,H) = 7.6 Hz, 4H), 4.14 (d, ²J(H,H) = 15.8 Hz, 4H, 2 CH₂). ¹³C{¹H} NMR (75 MHz, DMSO-*d*₆): δ = 170.0 (CO), 138.8, 136.2, 134.4, 133.6, 133.0, 128.8, 128.34, 128.28, 127.4, 127.3, 127.1, 127.0, 124.7, 43.5.

Complex synthesis

A screw cap NMR tube was charged with equimolar amounts of the bisamide proligand **1** and the corresponding metal tetrakis(amide) (0.01–0.03 mmol) and then C₆D₆ or THF-*d*₈ (0.6 mL) was added. The NMR tube was sealed, removed from the glovebox and shaken vigorously until the insoluble proligand was fully dissolved. Then the NMR spectra were recorded. Complexes were isolated in quantitative yields as solids using a freeze-drying technique. Standard solutions of isolated complexes and complexes prepared *in situ* were used for catalytic experiments.

(S)-111c-Zr. White solid. ¹H NMR (300 MHz, C₆D₆): δ = 8.00 (d, ³J(H,H) = 8.5 Hz, 2H), 7.85 (d, ³J(H,H) = 8.2 Hz, 2H), 7.69 (d, ³J(H,H) = 8.2 Hz, 4H), 7.14 (vt, ³J(H,H) = 7.4 Hz, 2H), 6.99 (t, ³J(H,H) = 7.6 Hz, 2H), 6.78 (s, 2H), 6.53 (s, 2H), 2.54 (s, 12H), 2.43 (s, 6H), 2.12 (s, 6H), 1.87 (br s, 18H); ¹³C{¹H} NMR (100 MHz, C₆D₆): δ = 178.6

(CO), 161.0 (CO), 146.3, 143.5, 142.4, 139.4, 135.1, 134.6, 133.6, 133.5, 133.0, 132.2, 130.6, 130.0, 129.1, 127.6, 127.0, 126.4, 125.9, 43.9 (ZrNMe₂), 42.0 (HNMe₂), 39.2 (HNMe₂), 20.8 (CH₃), 19.3 (CH₃), 17.4 (CH₃). Anal. Calcd for C₄₄H₄₆N₄O₂Zr: C, 70.08; H, 6.15; N, 7.43. Found: C, 64.96; H, 6.31; N, 7.28.

(R)-111ca-Zr. Yellow solid. ¹H NMR (300 MHz, C₆D₆): δ = 8.00 (d, ³J(H,H) = 8.5 Hz, 2H), 7.85 (d, ³J(H,H) = 8.2 Hz, 2H), 7.69 (d, ³J(H,H) = 8.2 Hz, 4H), 7.14 (t, ³J(H,H) = 7.4 Hz, 2H), 6.99 (t, ³J(H,H) = 7.6 Hz, 2H), 6.78 (s, 2H), 6.53 (s, 2H), 2.54 (s, 12H), 2.43 (s, 6H), 2.12 (s, 6H), 1.87 (br s, 18H); ¹³C{¹H} NMR (75 MHz, C₆D₆): δ = 178.2 (CO), 159.9 (CO), 145.6, 138.6, 137.3, 134.4, 133.6, 1133.5, 129.8, 129.0, 128.8, 128.7, 128.4, 128.2, 128.0, 127.8, 127.5, 124.6 (Aryl), 43.4(ZrNEt₂), 41.5 (HNMe₂), 20.8, 20.6, 20.5, 20.3 20.0, 19.8, 19.0, 17.2, 14.9, 14.3.

(R)-111d-Zr. White microcrystalline solid. ¹H NMR (500 MHz, C₆D₆): δ = 8.04 (d, ³J(H,H) = 8.2 Hz, 2H), 7.85 (d, ³J(H,H) = 8.3 Hz, 2H), 7.67 (d, ³J(H,H) = 8.0 Hz, 2H), 7.59 (d, ³J(H,H) = 8.8 Hz, 2H), 7.13–7.01 (m, 2H), 7.93 (d, ³J(H,H) = 7.1 Hz, 2H), 6.92 (t, ³J(H,H) = 7.1 Hz, 2H), 6.86 (t, ³J(H,H) = 7.5 Hz, 2H), 6.80 (d, ³J(H,H) = 7.3 Hz, 2H), 3.13–3.06 (m, 2H, CH₂), 2.65–2.58 (m, 2H, CH₂), 2.43 (s, 12 H, ZrNMe₂), 1.73 (br s, 12H, HNMe₂), 1.40 (t, ³J(H,H) = 7.5 Hz, 6H, CH₃), 1.29–1.24 (m, 2H, CH₂), 1.15–1.1 (m, 2H, CH₂), 1.01 (br s, 2H, HNMe₂), 0.54 (t, ³J(H,H) = 7.4 Hz, 6H, CH₃); ¹³C{¹H} NMR (125 MHz, C₆D₆): δ = 160.6 (CO), 147.6, 138.8, 134.53, 134.50, 134.0, 133.8, 133.6, 128.8, 128.29, 128.27, 127.7, 127.1, 126.4, 125.9, 125.2, 125.0, 122.0, 41.8

(ZrNMe₂), 39.0 (HNMe₂), 26.1 (CH₂), 23.7 (CH₂), 14.2 (CH₃), 13.6 (CH₃). Anal. Calcd for C₄₆H₅₀N₄O₂Zr: C, 70.64; H, 6.44; N, 7.16. Found: C, 66.55; H, 6.38; N, 6.80.

(*R*)-**111d-Hf**. Colorless solution, prepared *in situ* only. ¹H NMR (500 MHz, THF-*d*₈, 60 °C): δ = 8.03 (d, ³*J*(H,H) = 8.3 Hz, 2H), 7.92 (d, ³*J*(H,H) = 8.6 Hz, 2H), 7.76 (br. m, 2H), 7.40 (vt, ³*J*(H,H) = 8.1; 6.9 Hz, 2H), 7.29 (d, ³*J*(H,H) = 7.8 Hz, 2H), 7.22–7.19 (m, 2H), 6.82 (d, ³*J*(H,H) = 6.6 Hz, 2H), 6.66–6.60 (m, 4H, aryl), 2.90–2.87 (m, 2H, CH₂), 2.79–2.70 (m, 8H, 4CH₂), 2.61–2.56 (m, 8H, 4CH₂), 2.53–2.45 (m, 2H, CH₂), 1.26 (t, ³*J*(H,H) = 7.3 Hz, 6H, 2CH₃), 1.09 (t, ³*J*(H,H) = 7.1 Hz, 12H, 4CH₃), 0.68 (t, ³*J*(H,H) = 7.1 Hz, 12H, 4CH₃), 0.83 (t, ³*J*(H,H) = 7.6 Hz, 6H, 2CH₃); ¹³C{¹H} NMR (125 MHz, THF-*d*₈): δ = 160.3 (CO), 147.6, 147.4, 139.2, 134.8, 134.6, 134.3, 133.9, 129.0, 128.8, 128.4, 127.2, 126.7, 125.1, 124.6, 122.1 (aryl), 44.9 (ZrN(CH₂CH₃)₂), 41.8 (HN(CH₂CH₃)₂), 26.2 (CH₃CH₂C), 23.5 (CH₃CH₂C), 15.9 (ZrN(CH₂CH₃)₂), 15.2 (HN(CH₂CH₃)₂), 14.1(CH₃CH₂C), 13.2 (CH₃CH₂C).

(*S*)-**111e-Zr**. Colorless solution, prepared *in situ*. ¹H NMR (400MHz, C₆D₆): δ = 8.15 (d, ³*J*(H,H) = 8.2 Hz, 2H), 7.85 (d, ³*J*(H,H) = 8.2 Hz, 2H), 7.62 (d, ³*J*(H,H) = 7.8 Hz, 2H), 7.51 (d, ³*J*(H,H) = 7.8 Hz, 2H), 7.11–7.07 (m, 2H), 7.05–7.02 (m, 2H), 6.94–6.87 (m, 6H), 3.52–3.45 (m, 2H), 2.33 (s, 12H, ZrNMe₂), 1.88–1.81 (m, 2H), 1.71 (s, 6H, HNMe₂), 1.69 (s, 6H, HNMe₂), 1.51 (d, ³*J*(H,H) = 6.7 Hz, 6H, CH₃), 1.32 (d, ³*J*(H,H) = 7.1 Hz, 6H, CH₃), 0.77 (br s, 2H, HNMe₂), 0.59 (d, ³*J*(H,H) = 6.7 Hz, 6H, CH₃), 0.42 (d, ³*J*(H,H) = 6.7 Hz, 6H, CH₃); ¹³C{¹H} NMR (100 MHz, C₆D₆): δ = 160.7 (CO), 146.4, 139.9, 138.6, 137.9, 134.2, 133.9, 133.8, 128.5, 128.4, 127.8, 127.3, 126.54, 126.50,

123.0, 122.5, 121.7, 41.5 (ZrNMe_2), 39.0 (HNMe_2), 29.4 (CHCH_3), 28.0 (CHCH_3), 24.4 (CH_3), 23.8 (CH_3), 22.6 (CH_3), 22.4 (CH_3).

(*S*)-**111e-Zr** (mono-amine adduct). White microcrystalline solid by freeze-drying of a solution containing (*S*)-**111e-Zr**. ^1H NMR (300 MHz, C_6D_6): δ = 8.18 (d, $^3J(\text{H,H})$ = 8.2 Hz, 2H), 7.90 (d, $^3J(\text{H,H})$ = 8.2 Hz, 2H), 7.66 (d, $^3J(\text{H,H})$ = 7.8 Hz, 2H), 7.58 (d, $^3J(\text{H,H})$ = 7.8 Hz, 2H), 7.15–7.05 (m, 4H), 7.00–6.90 (m, 6H), 3.57–3.48 (m, 2H), 2.33 (s, 12H, ZrNMe_2), 1.93–1.84 (m, 2H), 1.53 (d, $^3J(\text{H,H})$ = 6.7 Hz, 6H, CH_3), 1.41 (s, 6H, HNMe_2), 1.35 (d, $^3J(\text{H,H})$ = 6.7 Hz, 6H, CH_3), 1.04 (br s, 1H, HNMe_2), 0.61 (d, $^3J(\text{H,H})$ = 6.7 Hz, 6H, CH_3), 0.40 (d, $^3J(\text{H,H})$ = 6.7 Hz, 6H, CH_3). $^{13}\text{C}\{^1\text{H}\}$ NMR (125 MHz, C_6D_6): δ = 160.6 (CO), 146.2, 140.0, 138.4, 137.9, 134.2, 134.0, 133.9, 128.6, 128.5, 128.3, 127.9, 127.2, 126.6, 126.3, 123.3, 122.5, 121.7, 40.2 (ZrNMe_2), 38.6 (HNMe_2), 29.3 (2 CHCH_3), 27.8 (2 CHCH_3), 24.0 (2 CH_3), 23.7 (2 CH_3), 23.2 (2 CH_3), 22.7 (2 CH_3). Anal. Calcd for $\text{C}_{50}\text{H}_{58}\text{N}_4\text{O}_2\text{Zr}$: C, 71.64; H, 6.97; N, 6.68. Found: C, 68.00; H, 6.86; N, 6.01.

(*S*)-**111g-Zr**. White solid, colorless solution. ^1H NMR (500 MHz, C_6D_6): δ = 7.94 (d, $^3J(\text{H,H})$ = 8.6 Hz, 2H), 7.63 (d, $^3J(\text{H,H})$ = 8.6 Hz, 2H), 7.55 (d, $^3J(\text{H,H})$ = 8.1 Hz, 2H), 7.22–7.19 (m, 2H), 6.08–7.04 (m, 2H), 6.58–6.55 (m, 2H), 6.31 (d, $^3J(\text{H,H})$ = 8.6 Hz, 2H), 5.64 (d, $^3J(\text{H,H})$ = 2.4 Hz, 2H), 4.90 (d, $^3J(\text{H,H})$ = 2.4 Hz, 2H), 3.36 (s, 6H, OMe), 3.26 (s, 6H, OMe), 3.06 (s, 6H), 2.74 (s, 6H), 2.52–2.48 (m, 9H), 2.22–2.19 (br m, 9H). $^{13}\text{C}\{^1\text{H}\}$ NMR (125 MHz, C_6D_6): δ = 168.9 (CO), 155.7, 152.6, 149.7, 139.8, 133.3, 132.3, 131.0, 129.1, 128.7, 128.3, 126.7, 126.1, 125.1, 124.6, 120.3, 90.3, 90.1, 54.5, 54.3, 53.6, 45.11, 40.0, 39.1.

(*S*)-**111h-Zr**. White solid. ^1H NMR (300 MHz, C_6D_6): δ = 8.00 (d, $^3J(\text{H,H})$ = 8.5 Hz, 2H), 7.85 (d, $^3J(\text{H,H})$ = 8.2 Hz, 2H), 7.69 (d, $^3J(\text{H,H})$ = 8.2 Hz, 4H), 7.14 (t, $^3J(\text{H,H})$ = 7.4 Hz, 2H), 6.99 (t, $^3J(\text{H,H})$ = 7.6 Hz, 2H), 6.78 (s, 2H), 6.53 (s, 2H), 2.54 (s, 12H), 2.43 (s, 6H), 2.12 (s, 6H), 1.87 (br s, 18H); $^{13}\text{C}\{^1\text{H}\}$ NMR (100 MHz, C_6D_6): δ = 162.4 (CO), 145.8, 140.3, 134.7, 133.4, 133.3, 133.1, 129.6, 128.9, 128.5, 128.1, 127.51, 127.46, 126.8, 125.7, 124.4, 124.3, 123.4, 121.0 (aryl), 44.9 (ZrNMe_2), 38.7 (HNMe_2), 19.2 (CH_3).

(*R,R*)-**112d-Zr**. Colorless solution, prepared in situ only. ^1H NMR (500 MHz, C_6D_6 , 70 °C): δ = 7.99 (d, $^3J(\text{H,H})$ = 6.1 Hz, 1H), 7.88–7.37 (m, 13H), 7.34 (d, $^3J(\text{H,H})$ = 7.1 Hz, 1H), 7.19–6.62 (m, 14H), 6.81 (m, 1H), 6.68–6.61 (m, 3H), 6.50–6.43 (m, 4H), 6.29 (m, 1H), 6.12 (d, $^3J(\text{H,H})$ = 7.8 Hz, 1H), 5.20 (br s, 1H, aryl-H), 2.59 (m, 6H), 2.50 (q, J = 7.5 Hz, 16H, 8 CH_2 , 4 HNEt_2), 2.42 (br s, 6H), 2.28 (br s, 6H), 2.12 (br s, 6H), 2.03 (br s, 6H), 1.81 (br s, 6H), 1.17 (br s, 3H), 0.99 (t, $^3J(\text{H,H})$ = 7.5 Hz, 24H, 8 CH_3 , 4 HNEt_2); $^{13}\text{C}\{^1\text{H}\}$ NMR (125 MHz, C_6D_6 , 125 MHz): δ = 183.2, 158.8, 158.1, 157.3 (CO), 145.6, 143.9, 143.7, 138.9, 138.6, 137.1, 136.3, 135.4, 134.6, 134.4, 134.0, 133.6, 133.48, 133.45, 133.3, 133.2, 133.1, 133.0, 132.7, 131.9, 131.3, 131.2, 130.7, 130.5, 130.2, 129.9, 129.6, 129.2, 129.0, 128.9, 128.8, 128.7, 128.6, 128.5, 128.4, 128.34, 128.29, 128.1, 127.9, 127.7, 127.6, 127.5, 127.4, 127.3, 127.24, 127.17, 127.1, 127.0, 126.9, 126.0, 125.9, 124.7, 124.4 (aryl), 44.3 ($\text{HN}(\text{CH}_2\text{CH}_3)_2$), 21.7, 21.3, 20.9, 20.8, 20.6, 20.4, 19.8, 19.7, 19.6, 18.6, 15.7 ($\text{HN}(\text{CH}_2\text{CH}_3)_2$), 11.8 (CH_3), 11.3 (CH_3).

General procedure for NMR-scale catalytic hydroamination/cyclization reactions. In the glovebox, a screw cap NMR tube was charged with ferrocene (6.0 mg, 32.3 μmol), C_6D_6 (0.5 mL), and the substrate (0.30 mmol). Then a solution of the appropriate complex, either prepared *in situ* or isolated, in C_6D_6 (0.05 M) was added. The NMR tube was sealed, removed from the glovebox and placed in the thermostated oil bath or thermostated NMR probe and the conversion was monitored by NMR spectroscopy by following the disappearance of the olefinic signals of the substrate relative to the internal standard ferrocene. The reaction time was recorded when a conversion of at least 95% was achieved.

General procedure for preparation of Mosher amides. The amine (0.08–0.1 mmol) was dissolved in CDCl_3 , C_6D_6 , or toluene- d_8 (0.5 mL) in a NMR tube. Hünig's base (2.5 equiv. with respect to the amine) and (*R*)-Mosher chloride (1.5 eq. with respect to the amine) were added. Enantiomeric excess was then determined by ^{19}F NMR at 60–100 $^\circ\text{C}$.

General procedure for determination of enantiomeric excess through salt formation.²⁴ The cyclic amine was vacuum transferred from the NMR tube into a 25 mL round-bottom flask which contained (*R*)-(-)-*O*-acetylmandelic acid (1.05 eq). The resulting mixture was stirred at 22 $^\circ\text{C}$ for 2–3 h and the volatiles were removed *in vacuo*. The resulting diastereomeric salt was then dissolved in CDCl_3 and the enantiomeric excess was determined by ^1H NMR spectroscopy.

Preparative-scale hydroamination reactions

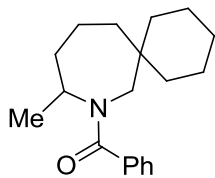
2,4,4-trimethylpyrrolidine hydrochloride (5·HCl).⁶⁸ In the glovebox, a flask was fitted with a stirring bar and was charged with **4** (45 mg, 0.40 mmol), toluene (1 mL) and (*R*)-**111d-Zr** (0.060 M in C₆D₆, 0.13 mL, 7.8 μmol, 2 mol%). The solution was then stirred at 100 °C for 7 h. All volatiles were then vacuum transferred, diluted with Et₂O (2 mL), and carefully treated with hydrochloric acid (1.59 mL, 0.5 M, 0.81 mmol) at 0 °C. After 30 min, the suspension was brought to room temperature and the solvent was removed *in vacuo*. The white precipitate was washed with diethyl ether (2 × 1 mL) and then dried in air to give 51 mg (84%) of **5·HCl** as a white powder in 42% ee according to ¹⁹F NMR spectroscopy of the Mosher amide. ¹H NMR (400 MHz, CDCl₃): δ = 9.87 (br s, 1H, NH₂Cl), 9.47 (br s, 1H, NH₂Cl), 3.88–3.85 (m, 1H, CH(CH₃)NH₂Cl), 3.12–3.10 (m, 1H, CH₂NH₂Cl), 2.99–2.97 (m, 1H, CH₂NH₂Cl), 1.87 (dd, 1H, ²J(H,H) = 12.9 Hz, ³J(H,H) = 6.5 Hz, CH₂CH(CH₃)NH₂Cl), 1.53 (dd, 1H, ²J(H,H) = 12.9 Hz, ³J(H,H) = 11.2 Hz, CH₂CH(CH₃)NH₂Cl), 1.48 (d, ³J(H,H) = 6.5 Hz, CH(CH₃)NH₂Cl), 1.16 (s, 3H, C(CH₃)₂), 1.11 (s, 3H, C(CH₃)₂); ¹³C{¹H} NMR (100 MHz, CDCl₃): δ = 56.3 (CH₂NH₂Cl), 55.3 (CH(CH₃)NH₂Cl), 46.9 (CH₂CH(CH₃)NH₂Cl), 38.7 (C(CH₃)₂), 27.22 (C(CH₃)₂), 27.19 (C(CH₃)₂), 18.0 (CH(CH₃)).

3-Methyl-2-aza-spiro[4.5]decane (19).⁵⁷ In the glovebox, a screw cap NMR tube was charged with **18** (75 mg, 0.49 mmol), C₆D₆ (0.4 mL), and (*S*)-**111c-Zr** (0.076M in C₆D₆, 0.13 mL, 9.8 μmol, 2 mol%). The NMR tube was sealed, removed from the glovebox and kept for 20 h at 80 °C. All volatiles were then transferred under high vacuum. The solvent was removed under reduced pressure to give 59 mg (79%) of **19** as a colorless liquid in 25% ee according to ¹⁹F NMR spectroscopy of the Mosher amide..

^1H NMR (400 MHz, C_6D_6): δ = 3.00 (m, 1H, $\text{CH}(\text{CH}_3)\text{NH}$), 2.73 (d, $^2J(\text{H,H})$ = 10.4 Hz, 1H, CH_2NH), 2.50 (d, $^2J(\text{H,H})$ = 10.4 Hz, 1H, CH_2NH), 1.55 (dd, $^2J(\text{H,H})$ = 12.3 Hz, $^3J(\text{H,H})$ = 6.6 Hz, 1H, $\text{CH}(\text{CH}_3)\text{CH}_2$), 1.29 (br m, 10H, CH_2), 1.06 (d, $^3J(\text{H,H})$ = 6.2 Hz, 3H, $\text{CH}(\text{CH}_3)\text{NH}$), 1.06 (br s, 1H, NH, obscured by other signal), 0.88 (dd, $^2J(\text{H,H})$ = 12.3 Hz, $^3J(\text{H,H})$ = 9.1 Hz, 1H, $\text{CH}(\text{CH}_3)\text{CH}_2$); $^{13}\text{C}\{^1\text{H}\}$ NMR (100 MHz, C_6D_6): δ = 59.7 (CH_2NH), 54.1 ($\text{CH}(\text{CH}_3)\text{NH}$), 47.8 ($\text{CH}_2\text{CH}(\text{CH}_3)\text{NH}$), 43.9, 39.0 (CH_2), 37.6 (CH_2), 26.5 (CH_2), 24.2 (CH_2), 24.1 (CH_2), 22.0 ($\text{CH}(\text{CH}_3)\text{NH}$).

2-Methyl-4,4-diphenylpyrrolidine (16).⁵¹ In the glovebox, a flask was fitted with a stirring bar and was charged with **105** (94 mg, 0.40 mmol), toluene (1 mL) and (*S*)-**111c-Zr** (0.11 mL 0.076M in C_6D_6 , 8.0 μmol , 2 mol%). The solution was then stirred at 80 °C overnight. The solution was diluted with Et_2O (10 mL), flushed through a short silica pad, concentrated and dissolved in hexanes (5 mL). The precipitate was filtered off, and the filtrate was washed with water (2 mL) and brine (2 mL). The organic layer was dried over Na_2SO_4 and concentrated *in vacuo* to give 80 mg of **16** (85%) as a colorless oil in 52% ee according to ^{19}F NMR spectroscopy of the Mosher amide. ^1H NMR (400 MHz, C_6D_6): δ = 7.22–7.20 (m, 2H), 7.14–7.08 (m, 6H), 7.04–7.00 (m, 2H, aryl-H), 3.51 (d, $^2J(\text{H,H})$ = 10.9 Hz, 1H, CH_2N), 3.34 (d, $^2J(\text{H,H})$ = 10.9 Hz, 1H, CH_2N), 3.16–3.11 (m, 1H, CHN), 2.39 (dd, $^2J(\text{H,H})$ = 12.4 Hz, $^3J(\text{H,H})$ = 6.3 Hz, 1H, CHCH_2), 1.80 (dd, $^2J(\text{H,H})$ = 12.3 Hz, $^3J(\text{H,H})$ = 9.2 Hz, 1H, CHCH_2), 1.27 (br s, 1H, NH), 1.01 (d, $^3J(\text{H,H})$ = 6.2 Hz, 3H, CH_3); $^{13}\text{C}\{^1\text{H}\}$ NMR (75.5 MHz, C_6D_6): δ = 148.8, 148.2, 128.4, 127.58, 127.51, 126.04, 126.00 (aryl), 58.7 (CH_2NH), 57.3 (CPh_2), 53.1 ($\text{CH}(\text{CH}_3)\text{NH}$), 47.6 (CH_2), 22.5 (CH_3).

9-Methyl-8-azaspiro[5,6]dodecane (117). In the glovebox, a screw cap NMR tube was charged with **116** (27.1 mg, 0.15 mmol), C₆D₆ (0.4 mL), and (*R*)-**111h-Zr** (0.01 M in C₆D₆, 150 μ L, 15 μ mol, 10 mol%). The NMR tube was sealed, removed from the glovebox and kept for 40 h at 120 °C. The reaction mixture was loaded on small amount of alumina and concentrated. Column chromatography on a short alumina plug (Hexanes-EtOAc 100:1) gave 16.1 mg (60%) of **117** as a colorless liquid. ¹H NMR (400 MHz, CDCl₃): δ = 2.84 (d, ²*J*(H,H) = 13.7 Hz, 1H, NCH₂), 2.71–2.63 (m, 1H, CH₃CH), 2.35 (d, ²*J*(H,H) = 13.7 Hz, 1H, NCH₂), 1.77–1.70 (m, 1H), 1.68–1.48 (m, 2H), 1.45–1.12 (m, 14H), 1.05 (d, ³*J*(H,H) = 6.3 Hz, 3H, CH₃); ¹³C{¹H} NMR (100 MHz, CDCl₃): δ = 58.7, 57.2, 40.5, 38.5, 37.6, 37.0, 36.0, 26.6, 23.7, 21.9, 21.8, 21.1.



***N*-Benzoyl-9-methyl-8-azaspiro[5,6]dodecane.** Azepane **117** (13.5 mg, 0.075 mmol) was dissolved in CH₂Cl₂ (1 mL) and then DIPEA (26 mg, 0.2 mmol) and benzoyl chloride (21 mg, 0.15 mmol) were added. The mixture was stirred at room temperature for 3 h. Volatiles were removed in vacuo and the residue was partitioned between Et₂O (2 mL) and 2M NaOH (2 mL). The resulting emulsion was stirred for 2 h and then the organic layer was separated, washed with brine (1 mL), dried (Na₂SO₄), and concentrated. The residue was purified by flash chromatography on silica (CH₂Cl₂) and subjected to a chiral HPLC analysis. Colorless oil. ¹H NMR (400 MHz, DMSO-*d*₆, 70 °C): δ = 7.44–7.39 (m, 3H), 7.32–7.30 (m, 2H, Aryl-H), 4.16 (br s, 1H, CHN), 3.80 (br s, 1H, CHN), 2.68 (br s, 1H, CHN), 1.91–1.84 (m, 1H), 1.80–1.85 (m, 1H), 1.62–1.55 (m, 1H), 1.50–1.18 (m, 11H), 1.08 (t, ²*J*(H,H) =

12.3 Hz, 1H), 0.94 (br s, 3H, CH₃); ¹³C{¹H} NMR (100 MHz, DMSO-*d*₆, 70 °C): δ = 171.1 (CO), 137.8 (Aryl), other signals are very broad and obscure due to rotamer interconversion. HPLC (AS-H, hexane/2-propanol 90:10, 0.5 mL/min): *t*_R 15.5 min (major), 18.9 min (minor); indicating 11% ee.

***trans*-2-Cyclohexyl-5-methylpyrrolidine (46f).** In the glovebox, a screw cap NMR tube was charged with **45f** (50 mg, 0.30 mmol), C₆D₆ (0.4 mL) and *rac*-**111c-Zr** (0.12 mL 0.076M in C₆D₆, 8.9 μmol, 3 mol%). The NMR tube was then sealed, removed from the glovebox and placed in the thermostated (120 °C) oil bath for 12 h. All volatiles were then transferred under high vacuum. The solvent was removed under reduced pressure to give 44 mg (88%) of **46f** as a colorless liquid with dr >30:1 according to ¹H NMR spectroscopy. MS (ESI): *m/z* 168.2 [M + H]⁺. ¹H NMR (500 MHz, C₆D₆): δ = 3.12–3.05 (m, 1H, CH(CH₃)NH), 2.82–2.78 (m, 1H, CH(Cy)NH), 1.92–1.89 (m, 1H), 1.78–1.61 (m, 7H), 1.30–1.06 (m, 7H), 0.98 (d ³*J*(H,H) = 6.3 Hz, 3H, CH₃), 0.98–0.90 (m, 3H), 0.69 (br s, 1H, NH); ¹³C{¹H} NMR (125 MHz, C₆D₆): δ = 63.6 (CyCHNH), 53.9 (CH₃CHNH), 44.8 (CHCH(Cy)NH), 35.4 (CH₂), 31.1 (CH₂), 31.0 (CH₂), 30.5 (CH₂), 27.1 (CH₂), 26.74 (CH₂), 26.67 (CH₂), 22.2 (CH(CH₃)NH).

Crystallography. X-ray quality crystals of (*R*)-**111d-Zr** and (*R*)-**111ca-Zr** were obtained by recrystallization from benzene at room temperature. Data were collected on a Bruker Apex-II CCD Diffractometer at 100(2) K, wavelength 0.71073 Å and are summarized in (Table V-4 and Table V-6). Lorentz, polarization, and empirical absorption corrections were applied. The space group was determined from systematic

absences. The structure was solved by direct methods (SHELXS program).⁶⁹ All positional and atomic displacement parameters (ADP) were refined with all reflections data by full-matrix least squares on F^2 using SHELXL.⁶⁹ Non-hydrogen atoms were refined anisotropically. Hydrogen atoms were constrained to idealized positions using a riding model. The absolute structure was refined using the Flack parameter.⁷⁰ The drawing of the molecules was realized with the help of WinOrtep.⁷¹

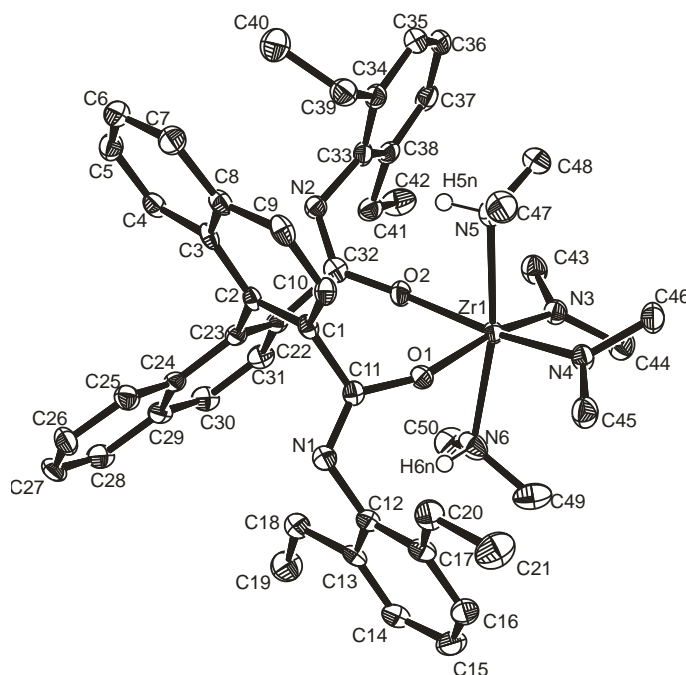


Figure V-9. ORTEP diagram for (*R*)-**111d-Zr**. Thermal ellipsoids are shown at the 50% probability level, hydrogen atoms, except H5n and H6n are omitted for clarity.

Table V-4. Crystallographic data for (*R*)-**111d-Zr**.

Parameter	Value
Empirical formula	$C_{50}H_{64}N_6O_2Zr$
Formula weight	872.29
Temperature	100(2) K
Wavelength	0.71073 Å

Crystal system	Orthorhombic
Space group	P2 ₁ 2 ₁ 2 ₁
Unit cell dimensions	$a = 11.9140(5) \text{ \AA}$, $\alpha = 90^\circ$ $b = 13.4359(5) \text{ \AA}$, $\beta = 90^\circ$ $c = 28.0449(12) \text{ \AA}$, $\gamma = 90^\circ$
Volume	4489.3(3) \AA^3
Z	4
Density (calculated)	1.291 Mg/m ³
Absorption coefficient	0.291 mm ⁻¹
F(000)	1848
Crystal size	0.20 × 0.10 × 0.02 mm ³
Θ range for data collection	1.68 to 28.28°.
Index ranges	-11 ≤ <i>h</i> ≤ 15, -17 ≤ <i>k</i> ≤ 17, -37 ≤ <i>l</i> ≤ 34
Reflections collected	21017
Independent reflections	10963 [R(int) = 0.0431]
Completeness to θ = 28.28°	99.8 %
Absorption correction	Semi-empirical from equivalents
Max. and min. transmission	0.994 and 0.944
Refinement method	Full-matrix least-squares on F ²
Data / restraints / parameters	10963 / 0 / 552
Goodness-of-fit on F ²	1.001
Final R indices [<i>I</i> > 2σ(<i>I</i>)]	R1 = 0.0445, wR2 = 0.0766
R indices (all data)	R1 = 0.0659, wR2 = 0.0831
Absolute structure parameter	0.00(2)
Largest diff. peak and hole	0.491 and -0.341 e. \AA^{-3}

Table V-5. Selected bond lengths [\AA] and angles [$^\circ$] for (*R*)-**111d-Zr**.

Zr1-N3	2.070(2)
Zr1-N4	2.072(2)

Zr1-O2	2.1128(18)
Zr1-O1	2.1174(18)
Zr1-N6	2.365(2)
Zr1-N5	2.377(2)
O1-C11	1.321(3)
O2-C32	1.315(3)
N1-C11	1.275(3)
N1-C12	1.411(4)
N2-C32	1.279(3)
N2-C33	1.416(4)
N3-Zr1-N4	92.79(9)
N3-Zr1-O2	94.00(8)
N4-Zr1-O2	168.30(9)
N3-Zr1-O1	167.82(9)
N4-Zr1-O1	89.21(8)
O2-Zr1-O1	86.15(7)
N3-Zr1-N6	87.85(10)
N4-Zr1-N6	98.59(9)
O2-Zr1-N6	91.18(8)
O1-Zr1-N6	79.97(9)
N3-Zr1-N5	98.61(10)
N4-Zr1-N5	89.17(9)
O2-Zr1-N5	80.41(8)
O1-Zr1-N5	93.44(9)
N6-Zr1-N5	169.69(9)
C11-O1-Zr1	151.56(16)
C32-O2-Zr1	153.03(19)
C11-N1-C12	119.2(2)
C32-N2-C33	122.4(2)
Binaphthyl dihedral	76.1

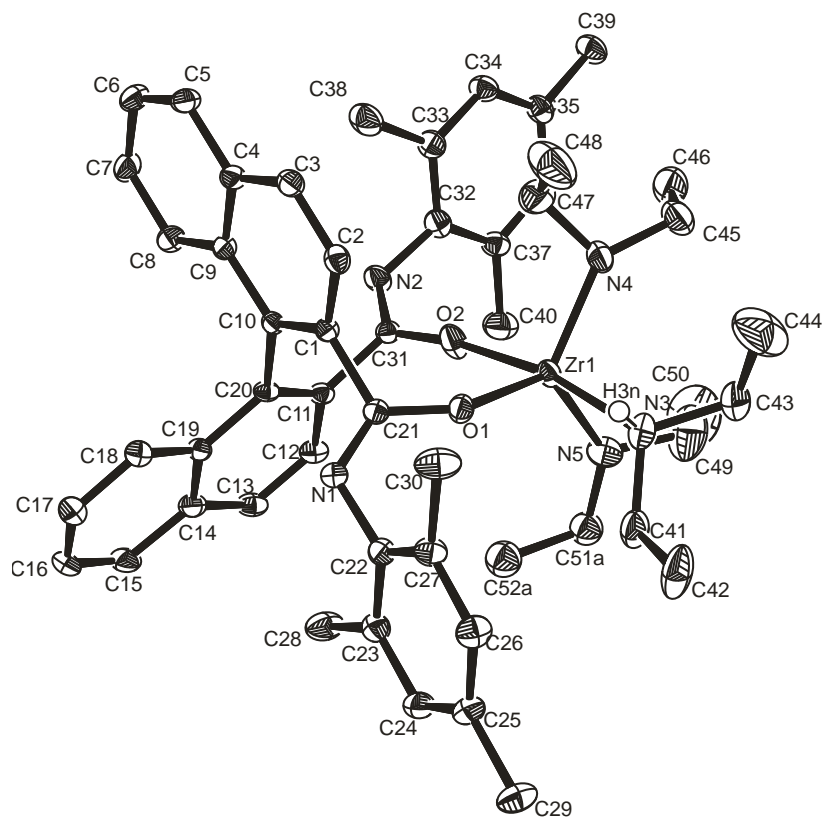


Figure V-10. ORTEP diagram for (*R*)-**111ca-Zr**. Thermal ellipsoids are shown at the 50% probability level, hydrogen atoms, except H3n are omitted for clarity.

Table V-6. Crystallographic data for (*R*)-**111ca-Zr**.

Parameter	Value
Empirical formula	C ₅₂ H ₆₅ N ₅ O ₂ Zr
Formula weight	883.31
Temperature	100(2) K
Wavelength	0.71073 Å
Crystal system	Monoclinic
Space group	P2 ₁
Unit cell dimensions	$a = 12.1764(8)$ Å, $\alpha = 90^\circ$.

	$b = 17.9217(13) \text{ \AA}, \beta = 119.406(1)^\circ.$
	$c = 12.2932(8) \text{ \AA}, \gamma = 90^\circ.$
Volume	$2337.0(3) \text{ \AA}^3$
Z	2
Density (calculated)	1.255 Mg/m^3
Absorption coefficient	0.280 mm^{-1}
F(000)	936
Crystal size	$0.24 \times 0.12 \times 0.10 \text{ mm}^3$
Θ range for data collection	1.90 to 32.02° .
Index ranges	$-17 \leq h \leq 18, -24 \leq k \leq 26, -18 \leq l \leq 18$
Reflections collected	24762
Independent reflections	14879 [R(int) = 0.0233]
Completeness to $\theta = 32.02^\circ$	98.5 %
Absorption correction	Semi-empirical from equivalents
Max. and min. transmission	0.972 and 0.935
Refinement method	Full-matrix least-squares on F^2
Data / restraints / parameters	14879 / 882 / 556
Goodness-of-fit on F^2	1.002
Final R indices [$I > 2\sigma(I)$]	R1 = 0.0469, wR2 = 0.1191
R indices (all data)	R1 = 0.0499, wR2 = 0.1209
Absolute structure parameter	0.02(2)
Largest diff. peak and hole	1.239 and $-0.707 \text{ e.\AA}^{-3}$

Table V-7. Selected bond lengths [\AA] and angles [$^\circ$] in (*R*)-**111ca-Zr**.

Zr1-N4	2.027(2)
Zr1-O2	2.0284(18)
Zr1-N5	2.037(3)
Zr1-O1	2.0552(16)

Zr1-N3	2.416(2)
O1-C21	1.328(3)
O2-C31	1.309(3)
N1-C21	1.268(3)
N1-C22	1.426(3)
N2-C31	1.266(3)
N2-C32	1.419(3)
N3-C41	1.497(4)
N3-C43	1.506(4)
N3-H3N	0.78(4)
N4-Zr1-O2	98.60(9)
N4-Zr1-N5	118.87(10)
O2-Zr1-N5	97.11(10)
N4-Zr1-O1	113.86(9)
O2-Zr1-O1	88.66(7)
N5-Zr1-O1	125.22(9)
N4-Zr1-N3	90.20(9)
O2-Zr1-N3	165.65(8)
N5-Zr1-N3	88.42(9)
O1-Zr1-N3	77.38(7)
C21-O1-Zr1	143.51(14)
C31-O2-Zr1	170.51(17)
Binaphthyl dihedral	88.3

V.5 References

- (1) Ricci, A. *Modern Amination Methods* Wiley-VCH: Weinheim, 2000.
- (2) Ricci, A. *Amino Group Chemistry: From Synthesis to the Life Sciences*; Wiley-VCH: Weinheim, 2008.
- (3) Müller, T. E.; Hultzs, K. C.; Yus, M.; Foubelo, F.; Tada, M. *Chem. Rev.* **2008**, *108*, 3795-3892.
- (4) Müller, T. E.; Beller, M. *Chem. Rev.* **1998**, *98*, 675-703.
- (5) Reznichenko, A. L.; Hultzs, K. C. In *Chiral Amine Synthesis: Methods, Developments and Applications*; 1st ed.; Nugent, T., Ed.; Wiley-VCH: 2010, p 341-376.
- (6) Reznichenko, A. L.; Hultzs, K. C. In *Science of Synthesis, Stereoselective Synthesis*; De Vries, J. G., Molander, G. A., Evans, P. A., Eds.; Thieme: 2010; Vol. 1, p 689-729.
- (7) Hultzs, K. C. *Adv. Synth. Catal.* **2005**, *347*, 367-391.
- (8) Severin, R.; Doye, S. *Chem. Soc. Rev.* **2007**, *36*, 1407-1420.
- (9) Pohlki, F.; Doye, S. *Chem. Soc. Rev.* **2003**, *32*, 104-114.
- (10) Manna, K.; Ellern, A.; Sadow, A. D. *Chem. Commun.* **2010**, *46*, 339-341.
- (11) Bexrud, J. A.; Schafer, L. L. *Dalton Trans.* **2010**, *39*, 361-363.
- (12) Leitch, D. C.; Payne, P. R.; Dunbar, C. R.; Schafer, L. L. *J. Am. Chem. Soc.* **2009**, *131*, 18246-18247.
- (13) Wood, M. C.; Leitch, D. C.; Yeung, C. S.; Kozak, J. A.; Schafer, L. L. *Angew. Chem. Int. Ed.* **2007**, *46*, 354-358.
- (14) Müller, C.; Saak, W.; Doye, S. *Eur. J. Org. Chem.* **2008**, 2731-2739.
- (15) Majumder, S.; Odom, A. L. *Organometallics* **2008**, *27*, 1174-1177.
- (16) Allan, L. E. N.; Clarkson, G. J.; Fox, D. J.; Gott, A. L.; Scott, P. *J. Am. Chem. Soc.* **2010**, *132*, 15308-15320.
- (17) Stubbert, B. D.; Marks, T. J. *J. Am. Chem. Soc.* **2007**, *129*, 6149-6167.
- (18) Gott, A. L.; Clarke, A. J.; Clarkson, G. J.; Scott, P. *Organometallics* **2007**, *26*, 1729-1737.
- (19) Watson, D. A.; Chiu, M.; Bergman, R. G. *Organometallics* **2006**, *25*, 4731-4733.
- (20) Kim, H.; Lee, P. H.; Livinghouse, T. *Chem. Commun.* **2005**, 5205-5207.
- (21) Knight, P. D.; Munslow, I.; O'Shaughnessy, P. N.; Scott, P. *Chem. Commun.* **2004**, 894-895.
- (22) Gribkov, D. V.; Hultzs, K. C. *Angew. Chem. Int. Ed.* **2004**, *44*, 5542-5546.
- (23) Eisenberger, P.; Schafer, L. L. *Pure Appl. Chem.* **2010**, *82*, 1503-1515.
- (24) Hong, S.; Marks, T. J. *Acc. Chem. Res.* **2004**, *37*, 673-686.
- (25) Giardello, M. A.; Conticello, V. P.; Brard, L.; Gagné, M. R.; Marks, T. J. *J. Am. Chem. Soc.* **1994**, *116*, 10241-10254.
- (26) Gribkov, D. V.; Hultzs, K. C.; Hampel, F. *J. Am. Chem. Soc.* **2006**, *128*, 3748-3759.
- (27) Gagné, M. R.; Stern, C. L.; Marks, T. J. *J. Am. Chem. Soc.* **1992**, *114*, 275-294.

- (28) Kubiak, R.; Prochnow, I.; Doye, S. *Angew. Chem. Int. Ed.* **2009**, *48*, 1153-1156.
- (29) Bexrud, J. A.; Eisenberger, P.; Leitch, D. C.; Payne, P. R.; Schafer, L. L. *J. Am. Chem. Soc.* **2009**, *131*, 2116-2118.
- (30) Oi, S.; Matsuzaka, Y.; Yamashita, J.; Miyano, S. *Bull. Chem. Soc. Jpn.* **1989**, *62*, 956-957.
- (31) Eisenberger, P.; Ayinla, R. O.; Lauzon, J. M. P.; Schafer, L. L. *Angew. Chem. Int. Ed.* **2009**, *48*, 8361-8365.
- (32) Ayinla, R. O.; Gibson, T.; Schafer, L. L. *J. Organomet. Chem.* **2011**, *696*, 50-60.
- (33) Reznichenko, A. L.; Hultsch, K. C. *Organometallics* **2010**, *29*, 24-27.
- (34) Hultsch, K. C.; Gribkov, D. V.; Hampel, F. *J. Organomet. Chem.* **2005**, *690*, 4441-4452.
- (35) Zi, G.; Zhang, F.; Xiang, L.; Chen, Y.; Fang, W.; Song, H. *Dalton Trans.* **2010**, *39*, 4048-4061.
- (36) Bexrud, J. A.; Beard, J. D.; Leitch, D. C.; Schafer, L. L. *Org. Lett.* **2005**, *7*, 1959-1962.
- (37) Müller, C.; Loos, C.; Schulenberg, N.; Doye, S. *Eur. J. Org. Chem.* **2006**, 2499-2503.
- (38) Prochnow, I.; Kubiak, R.; Frey, O. N.; Beckhaus, R.; Doye, S. *ChemCatChem* **2009**, *1*, 162-172.
- (39) Wood, M. C.; Leitch, D. C.; Yeung, C. S.; Kozak, J. A.; Schafer, L. L. *Angew. Chem. Int. Ed.* **2010**, *49*, 6475-6475.
- (40) Wood, M. C.; Leitch, D. C.; Yeung, C. S.; Kozak, J. A.; Schafer, L. L. *Angew. Chem., Int. Ed.* **2009**, *48*, 6937.
- (41) Manna, K.; Xu, S.; Sadow, A. D. *Angew. Chem. Int. Ed.* **2011**, *50*, 1865-1868.
- (42) Reznichenko, A. L.; Hampel, F.; Hultsch, K. C. *Chem. Eur. J.* **2009**, *15*, 12819-12827.
- (43) Pohlki, F.; Bytschkov, I.; Siebeneicher, H.; Heutling, A.; König, W. A.; Doye, S. *Eur. J. Org. Chem.* **2004**, 1967-1972.
- (44) Gott, A. L.; Clarke, A. J.; Clarkson, G. J.; Scott, P. *Chem. Commun.* **2008**, 1422-1424.
- (45) Hannedouche, J.; Collin, J.; Trifonov, A.; Schulz, E. *J. Organomet. Chem.* **2011**, *696*, 255-262.
- (46) Manna, K.; Kruse, M. L.; Sadow, A. D. *ACS Catal.* **2011**, *1*, 1637-1642.
- (47) Bradley, D. C.; Gitlitz, M. H. *J. Chem. Soc. A* **1969**, 980-984.
- (48) Smith, P. M.; Thomas, E. J. *J. Chem. Soc., Perkin Trans. 1* **1998**, 3541-3556.
- (49) Tamaru, Y.; Hojo, M.; Higashimura, H.; Yoshida, Z. *J. Am. Chem. Soc.* **1998**, *110*, 3994-4002.
- (50) Bender, C. F.; Widenhoefer, R. A. *J. Am. Chem. Soc.* **2005**, *127*, 1070-1071.
- (51) Hong, S.; Tian, S.; Metz, M. V.; Marks, T. J. *J. Am. Chem. Soc.* **2003**, *125*, 14768-14783.

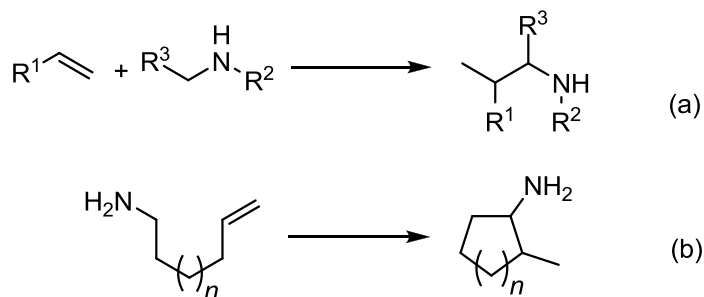
- (52) Gribkov, D. V.; Hultzs, K. C.; Hampel, F. *Chem. Eur. J.* **2003**, *9*, 4796-4810.
- (53) Black, D. S. C.; Doyle, J. E. *Austr. J. Chem.* **1978**, *31*, 2247-2257.
- (54) Kondo, T.; Okada, T.; Mitsudo, T.-a. *J. Am. Chem. Soc.* **2002**, *124*, 186-187.
- (55) Kim, J. Y.; Livinghouse, T. *Org. Lett.* **2005**, *7*, 4391-4393.
- (56) Yang, Q.; Ney, J. E.; Wolfe, J. P. *Org. Lett.* **2005**, *7*, 2575-2578.
- (57) Collin, J.; Daran, J.-D.; Jacquet, O.; Schulz, E.; Trifonov, A. *Chem. Eur. J.* **2005**, *11*, 3455-3462.
- (58) Hultzs, K. C.; Hampel, F.; Wagner, T. *Organometallics* **2004**, *23*, 2601-2612.
- (59) Crimmin, M. R.; Casely, I. J.; Hill, M. S. *J. Am. Chem. Soc.* **2005**, *127*, 2042-2043.
- (60) Lauterwasser, F.; Hayes, P. G.; Braese, S.; Piers, W. E.; Schafer, L. L. *Organometallics* **2004**, *23*, 2234-2237.
- (61) Katritzky, A. R.; Cui, X.-L.; Yang, B.; Steel, P. J. *J. Org. Chem.* **1999**, *64*, 1979-1985.
- (62) Meyers, A. I.; Snyder, L. *J. Org. Chem.* **1992**, *57*, 3814-3819.
- (63) Kamer, P. C. J.; Nolte, R. J. M.; Drenth, W. *J. Am. Chem. Soc.* **1988**, *110*, 6818-6825.
- (64) Hellwinkel, D.; Bohnet, S. *Chem. Ber.* **1987**, *120*, 1151-1173.
- (65) Seki, M.; Yamada, S.-I.; Kuroda, T.; Imashiro, R.; Shimizu, T. *Synthesis* **2000**, 1677-1680.
- (66) Kanoh, S.; Hongoh, Y.; Motoi, M.; Suda, H. *Bull. Chem. Soc. Jpn.* **1988**, *61*, 1032-1034.
- (67) Nelson, T. D.; Meyers, A. I. *J. Org. Chem.* **1994**, *59*, 2655-2658.
- (68) Kim, J. Y.; Livinghouse, T. *Org. Lett.* **2005**, *7*, 1737-1739.
- (69) Sheldrick, G. *Acta Crystallogr.* **2008**, *A64*, 112-122.
- (70) Flack, H. *Acta Cryst.* **1983**, *A39*, 876-881.
- (71) Farrugia, L. J. *J. Appl. Cryst.* **1997**, *30*, 565.

VI Chapter 6. Asymmetric Intermolecular Hydroaminoalkylation of Unactivated Alkenes Catalyzed by Group 5 Metal Binaphtholates

VI.1 Introduction

The hydroaminoalkylation is an emerging atom-efficient direct alkene-to-amine transformation complementary to hydroamination reaction. It has the potential to become a versatile synthetic approach to various important amines^{1,2} using both intra- and intermolecular variant of the reaction (Scheme VI-1).

Scheme VI-1. Inter- and intramolecular hydroaminoalkylation.



While initial observations of catalytic hydroaminoalkylation were published more than 30 years ago,^{3,4} this reaction has become a subject of intensive research efforts only recently.^{1,2} Although few examples of main group metal-catalyzed α -C-H addition of amines to alkenes are known,⁵ the majority of hydroaminoalkylation catalysts reported to date are based on d^0 group 4⁶⁻¹¹ and group 5¹²⁻¹⁶ metal complexes (Figure VI-1).

In line with earlier observations,^{3,4} Herzon and Hartwig have demonstrated that the homoleptic tantalum amide **119**¹² and the heteroleptic chloro bisamide **120**¹³ are active catalysts for the intermolecular hydroaminoalkylation of unactivated olefins with secondary amines (Scheme VI-1, reaction a), with the latter catalyst being more reactive and applicable to a broader range of substrates, including dialkylamines (reaction a,

$R^3=H$, Alk, $R^2=Alk$) as amide **119** was only effective for the activation of more reactive arylalkylamines. Branched addition products were obtained exclusively and it was found that polysubstituted olefins are significantly less prone to undergo hydroaminoalkylation.

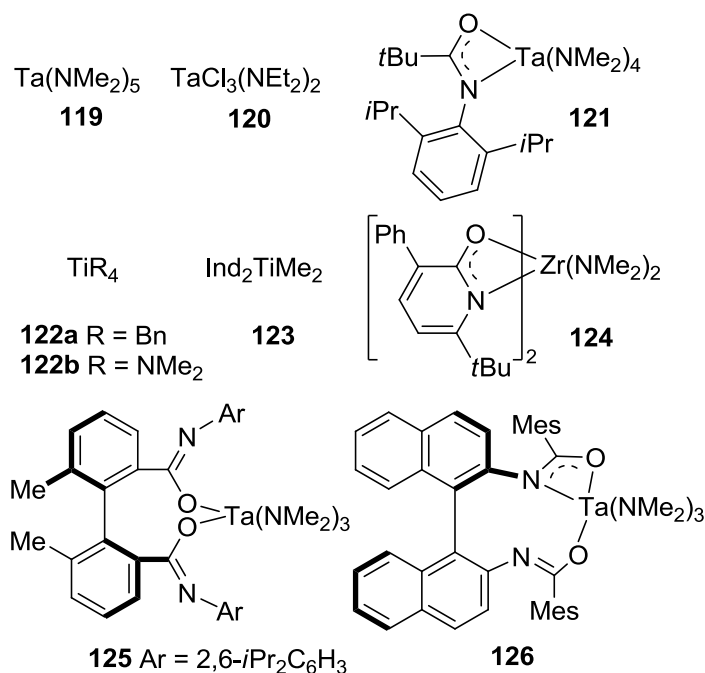


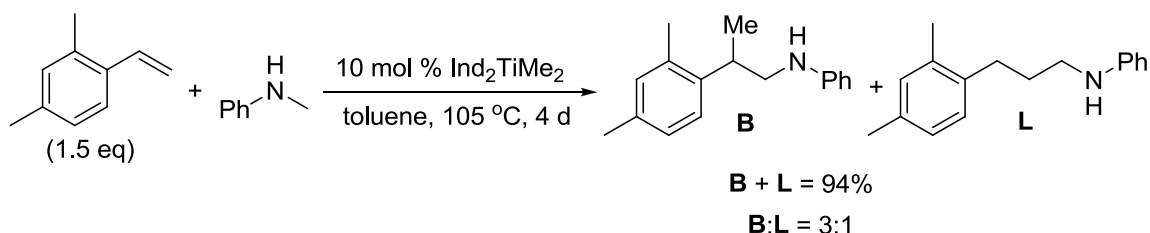
Figure VI-1. Selected group 4 and group 5 metal hydroaminoalkylation catalysts.

More recently, Schafer and coworkers have developed a family of various amidate tantalum catalysts, such as **121** and similar structures.¹⁴ Tantalum amidates displayed reactivities similar to that of **119** and **120**. The observation of hydroaminoalkylation as a side reaction of hydroamination (Scheme VI-1, reaction b, $n = 1, 2$)⁶ has sparked the development of group 4 metal hydroaminoalkylation catalysts. The homoleptic tetrabenzyl titanium **122a,b**^{7,8} or bis(indenyl) complex **123**¹⁰ were shown to catalyze intra- and intermolecular hydroaminoalkylations, although the latter reaction was found to be feasible only in the case of alkylarylamines (reaction a, $R^3 = H$, Alk, $R^2 = Ar$). Another notable feature of group 4 catalysts is the reactivity of *primary* amines which

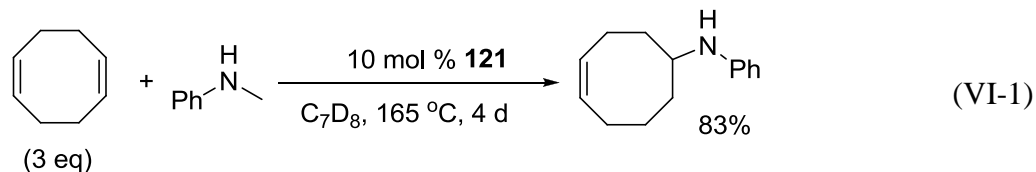
could only be achieved in the intramolecular (b) process and no reports on group 5 metal-catalyzed additions of primary amines to alkenes are known so far.

The intermolecular hydroaminoalkylation of terminal alkenes with secondary amines proceeds with excellent branched:linear selectivities exceeding 99:1 in most cases. A notable and somewhat expected exception is the case of vinyl arenes which were reported to produce large quantities (up to 25%) of the linear isomer (Scheme VI-2).¹⁰

Scheme VI-2. Intermolecular hydroaminoalkylation of a vinyl arene.



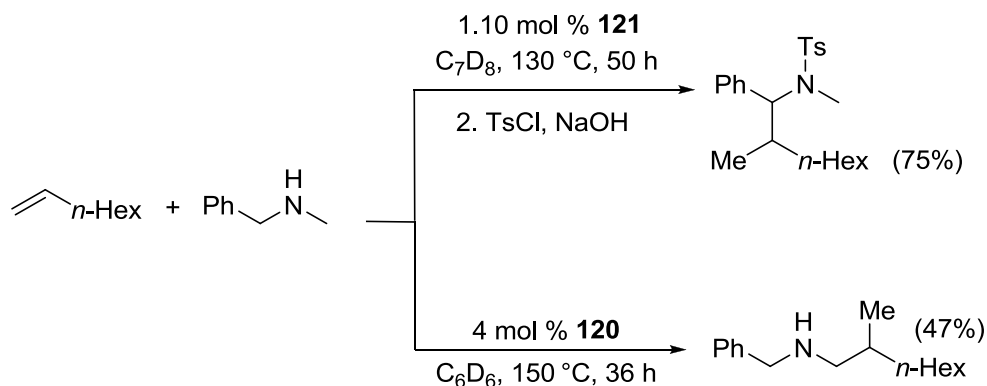
Even 1,2-disubstituted alkenes represent challenging substrates in the intermolecular hydroaminoalkylation. While the highly strained and therefore highly activated norbornene has reactivity of the same magnitude as terminal alkenes with most known catalysts,^{10,12} 1,2-disubstituted alkenes were only reported to undergo hydroaminoalkylation in the presence of **121** (Eq. V-1).



When a non-symmetric secondary dialkylamine is employed in hydroaminoalkylation reaction, two possible products resulting from activation of the two different alkyl groups can be formed. The vast majority of known group 4 and 5 catalysts reported to date displayed a pronounced preference for the activation of the less

substituted alkyl group (i.e. methyl over methylene). The activation of a tertiary alkyl C–H bond in the hydroaminoalkylation is unknown. Remarkably, catalyst **121** displayed a very different behavior, yielding the sterically more encumbered reaction product (Scheme VI-3).¹⁴

Scheme VI-3. Regiodivergent hydroaminoalkylation catalyzed by **120**¹³ and **121**.¹⁴



Catalysts for intermolecular hydroaminoalkylation have been developed employing κ^1 -¹⁴ and κ^1 -/ κ^2 -amidate^{15,16} frameworks. In line with the selectivity trends previously reported for the asymmetric hydroamination with related zirconium amidate complexes¹⁷⁻²⁰ (see also Chapter 5), the sterically more hindered chelating κ^2 -amidates **126** displayed higher enantioselectivities (up to 93% ee for norbornene).¹⁵ However, in contrast to the reactivity trends observed in intramolecular hydroaminations, the sterically and electronically more saturated complex **126** was reported to be more active than the sterically more accessible and electronically unsaturated complex **125**.

Reports on relative activity of different group 5 metals have been controversial. While early studies showed that Nb(NMe₂)₅ was displaying slightly higher reactivity than its tantalum counterpart **119**,³ it was claimed that the niobium analogue of the bis(amidate) complex **126** was completely catalytically inactive.¹⁵

catalyzed by **119**,¹² whereas step 1 is virtually irreversible in the case of catalyst **120**¹³ as indicated by isotopic labeling studies. The same studies implicate that steps 2 and 3 should be fast, as the catalyst has no metal-carbon bond in its resting state. The preferred reactivity of the methyl over a methylene group in case of **120** was explained by a more feasible aziridine formation involving more the accessible C–H bond;¹³ however, no explanation for the opposite behavior of **121** (Scheme VI-3) was provided.¹⁴

Recently, Doye and coworkers reported that the intramolecular hydroaminoalkylation of primary aminoalkenes catalyzed by $\text{Ti}(\text{NMe}_2)_4$ (**122b**) involves a rate-limiting C–H activation step, as indicated by a pronounced kinetic isotope effect.¹¹ The lack of a sterically demanding spectator ligand in **122b** resulted in catalyst aggregation and a complex kinetic behavior at higher catalyst concentrations.¹¹

In summary, several research groups have demonstrated that the hydroaminoalkylation is a promising method for direct, atom-economic alkene-to-amine transformation. In particular, the number of known substrates and catalysts for the intermolecular hydroaminoalkylation exceeds the number of examples for the intermolecular hydroamination reaction, which provides an excellent opportunity for the further development. An obvious gap in the understanding of the mechanistic details of this process needs to be addressed in order to surpass current limitations, such as narrow substrate scope and low catalytic activity and the need of harsh reaction conditions. In addition, the asymmetric hydroaminoalkylation yielding chiral amines is still in its infancy and stereoselectivities are, with a few exceptions, only moderate.

VI.2 Results and Discussion

Based on our previous experience with 3,3'-silylated rare earth metal binaphtholate catalysts **24-Ln** in intermolecular alkene hydroamination²² (see also Chapter 3) we envisioned that these easily accessible and readily sterically tunable ligands with proven thermal stability and a robust character can be employed in hydroaminoalkylation as well. We proposed that group 5 metal binaphtholates could serve as efficient and tunable catalyst for the enantioselective intermolecular hydroaminoalkylation and would allow us to fill some gaps in our understanding of the reaction mechanism.

VI.2.1 Complex Synthesis

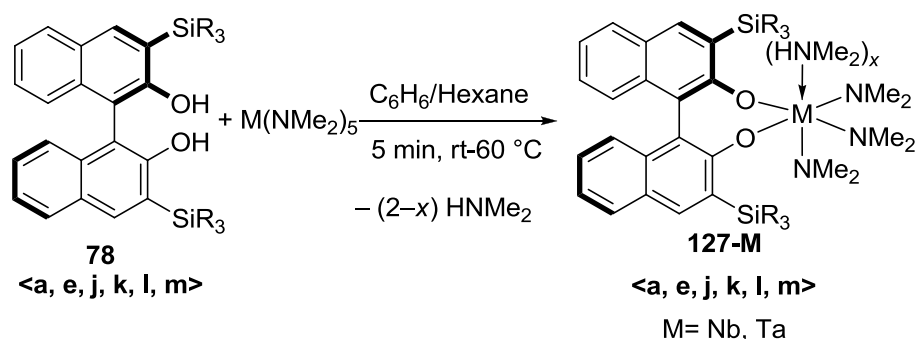
Encouraged by an early report of Rothwell,^{23,24} that several 3,3'-disilylated tantalum binaphtholate complexes are accessible via an amine elimination reaction between Ta(NMe₂)₅ and the corresponding diol proligands, we took the same synthetic approach to access a library of sterically diverse tantalum and niobium binaphtholates.

A series of enantiomerically pure complexes (*R*)-**127-M** (M = Nb, Ta) was prepared successfully via amine elimination (Table VI-1). While the reactions are quantitative according to NMR spectroscopic analysis, the isolated yields after recrystallization of the niobium complexes are often lower in comparison to their tantalum counterparts due to their slightly higher solubility.

The complexes generally retain one equivalent of dimethylamine according to NMR spectroscopy and the coordinated base could not be removed even after extended heating in vacuum. This observation is in agreement with the findings by Rothwell and coworkers who had reported compounds **127a-Ta**, **127j-Ta** and **127m-Ta** previously

(including the X-ray crystal structure of the octahedral **127j-Ta** and **127m-Ta**).²⁴ However, the *tert*-butyldimethylsilyl-substituted complexes **127l-Nb** and **127l-Ta** crystallized in the base-free form and the X-Ray crystallographic analysis of the isostructural complexes confirmed a slightly distorted trigonal-bipyramidal geometry around the metal (Figure VI-2, Table VI-2). Compounds **127k-M** displayed an intermediate stability for the hexacoordinate adduct which was unstable after prolonged stay at room temperature for **127k-Nb** and under gentle heating for **127k-Ta**.

Table VI-1. Synthesis of group 5 metal binaphtholate complexes **127-M**.



Ligand	R ₃ Si	Product	Yield, <i>x</i>		Yield, <i>x</i>	
			M = Ta, %		M = Nb, %	
78a	Ph ₃ Si	127a-M	100 ^a	1	56	1
78e	Ph ₂ BnSi	127l-M	86	1	74	1
78j	Ph ₂ MeSi	127j-M	76	1	77	1
78k	<i>i</i> -Pr ₂ MeSi	127k-M	49	1	39	0
78l	<i>t</i> -BuMe ₂ Si	127l-M	64	0	75	0
78m	Me ₃ Si	127m-M	89	1	66	1

^a Complex was prepared on NMR scale *in situ* only.

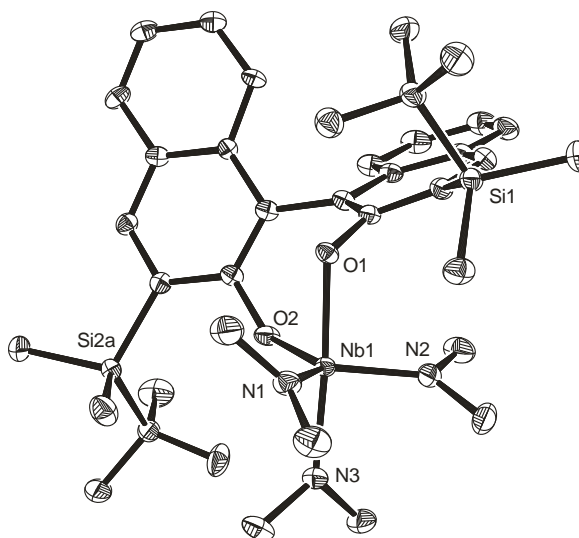


Figure VI-2. ORTEP diagram of the molecular structure of pentacoordinate complexes **127l-Nb** (**127l-Ta** is isostructural to **127l-Nb**). Thermal ellipsoids are shown at the 50% probability level. Hydrogen atoms as well as one position of the disordered naphthyl ring and the disordered silane group are omitted for clarity.

Table VI-2. Selected Bond lengths [\AA] and angles [$^\circ$] in **127l-M** (M = Ta, Nb).

	127l-Nb	127l-Ta
M-N1	1.9528(13)	1.9591(15)
M-N2	1.9351(12)	1.9354(15)
M-N3	2.0380(12)	2.0303(14)
M-O1	2.0916(9)	2.0763(12)
M-O2	1.9594(9)	1.9478(11)
O1-M-O2	85.43(4)	85.10(5)
O1-M-N1	84.88(4)	84.75(5)
O1-M-N2	96.27(5)	96.09(5)
O1-M-N3	172.32(5)	172.27(5)
O127-M-N1	125.79(5)	125.36(6)
O127-M-N2	114.08(5)	114.80(6)

O127-M-N3	97.77(4)	97.46(5)
N1-M-N2	119.95(6)	119.61(6)
N1-M-N3	87.60(5)	87.83(6)
N127-M-N3	88.82(5)	89.48(6)
M-O1-C1	112.89(8)	113.61(9)
M-O2-C17a	135.92(13)	136.58(11)
Binaphthyl dihedral	68.5(2)	68.1(2)

All complexes **127-M** were characterized by NMR as pseudo- C_2 -symmetric species in solution with all 3 amido-groups being NMR-equivalent. This observation is likely due to the fluxional character of the complexes and indeed low temperature ^1H NMR study of **127m-Ta** revealed a C_1 symmetric species with non-equivalent amido groups and naphthalene rings at $-70\text{ }^\circ\text{C}$ (Figure VI-3).

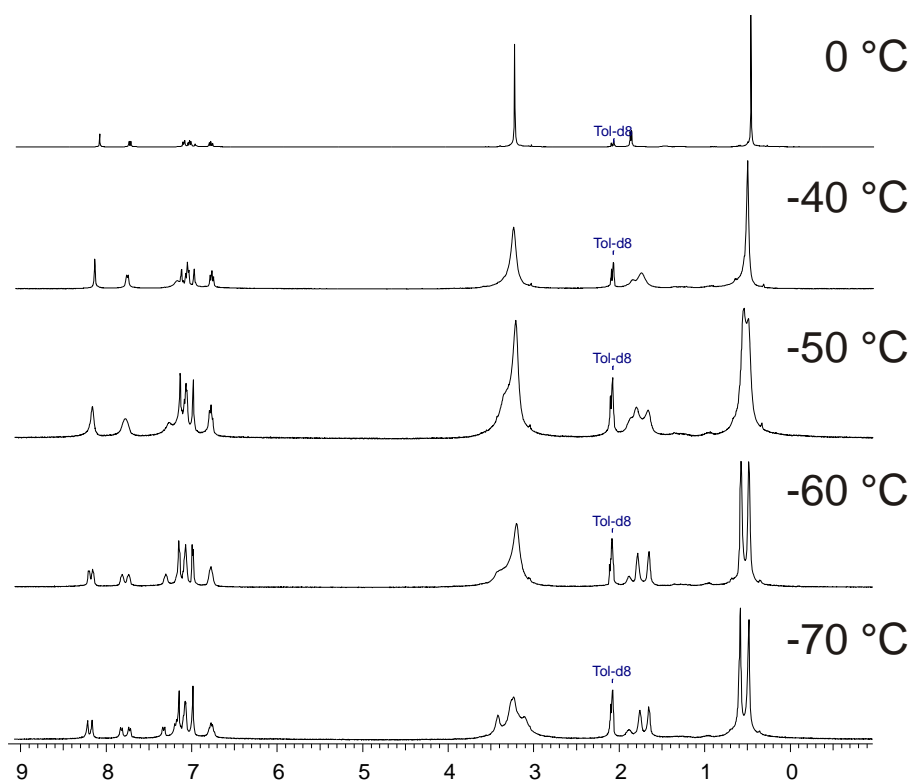


Figure VI-3. ^1H NMR spectra of **127m-Ta** in toluene- d_8 at various temperatures.

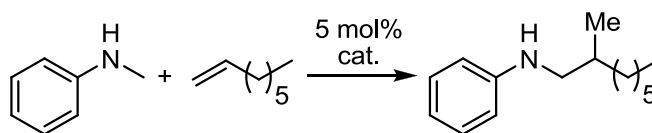
VI.2.2 Substrate Scope of Catalytic Hydroaminoalkylation

For our initial tests on catalytic hydroaminoalkylation we chose 1-octene and *N*-methylaniline as model substrates (Table VI-3). The catalytic activity of catalysts **127-M** significantly decreased with increasing steric bulk of the silyl substituents, with the most encumbered catalysts **127a** and **127e** producing only trace amounts of product even at 170 °C (Table VI-3, entries 1–4). Under our standard conditions at 150 °C, the methyldiphenylsilyl-substituted complexes **127j-Nb** and **127j-Ta** exhibited the highest selectivity (Table VI-3, entries 7 and 10), whereas the slightly more demanding methyldiisopropylsilyl-substituted complexes **127k-Nb** and **127k-Ta** displayed slightly lower selectivities than **127j-M** (Table VI-3, entries 5 and 6). The sterically least demanding trimethylsilyl-substituted **127m-M** displayed the highest activity, but also the lowest selectivity in this series. All catalytic reactions were marked by an exclusive (>99:1) formation of the branched addition product.

The niobium complexes were generally more active than their tantalum analogues, but the enantioselectivities were quite comparable in most cases. The discrepancy of reactivity of the tantalum and niobium complexes is even more pronounced at lower temperatures, as the tantalum complexes gave poor reactivity below 140 °C, while the niobium catalyst **127j-Nb** was reactive even at 100 °C to give the highest selectivity of 81% ee for this model reaction (Table VI-3, entry 12). Notably, **127j-Nb** appears to be more active at 100 °C than the chiral catalyst **125** at 130 °C.¹⁴

It should also be noted that complexes prepared *in situ* showed identical reactivity and selectivity as analytically pure samples isolated after recrystallization (Table VI-3, entries 7 and 8).

Table VI-3. Catalytic asymmetric hydroaminoalkylation of 1-octene with *N*-methylaniline using binaphtholate tantalum and niobium Complexes.^a



entry	cat.	<i>T</i> , °C; <i>t</i> , h	% yield ^b	% ee ^c
1	127a-Ta	170; 48	trace	nd
2	127a-Nb	170; 48	trace	nd
3	127e-Ta	170; 48	trace	nd
4	127e-Nb	170; 48	trace	nd
5	127k-Ta	150; 31	89	65
6	127k-Nb	140; 20	93	60
7	127j-Ta	150; 14	88	72
8	127j-Ta^d	150; 14	91	72
9	127j-Ta	130; 65	89	73
10	127j-Nb	150; 7	85	72
11	127j-Nb	130; 58	91	79
12	127j-Nb	100; 105	92	81
13	127l-Ta	150; 12	79	49
14	127l-Nb	150; 8	72	61
15	127m-Ta	150; 5	87	34
16	127m-Nb	150; 3	91	54

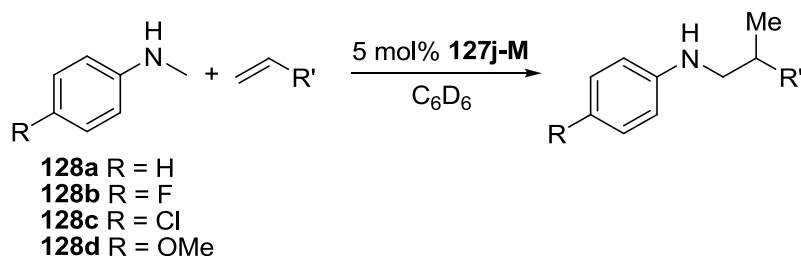
^a Conditions: *N*-methylaniline (0.2 mmol), 1-octene (0.4 mmol), cat. (0.01 mmol, 5 mol%), C₆D₆ (0.3 mL), 150 °C, Ar atm. ^b Isolated yield of *N*-benzamide. ^c Determined by chiral HPLC of *N*-benzamide. ^d **127k-Ta** was prepared in situ and was directly used for the catalytic experiment. nd = not determined.

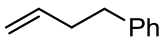
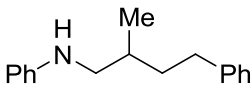
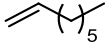
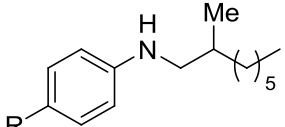
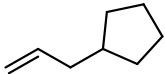
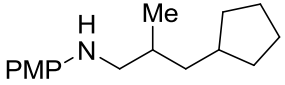
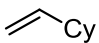
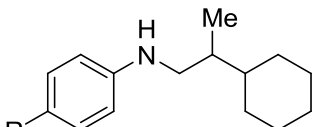
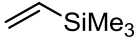
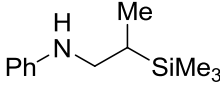
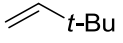
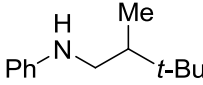

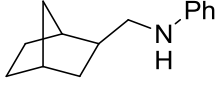
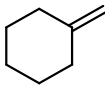
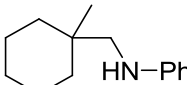
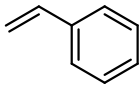
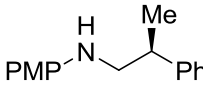
We decided to use the most selective catalyst **127j-M** for our further studies on the scope of the hydroaminoalkylation reaction at 100 °C (optimal enantioselectivity) and 150 °C (optimal reaction time).

Reaction Scope in Amine. As shown in (Table VI-4), various *N*-methylanilines **128** bearing both electron-withdrawing and electron-donating substituents exhibit similar reactivities and selectivities in reactions involving terminal olefins. The niobium complex **127j-Nb** displayed systematically higher reactivity in comparison to its tantalum analogue **127j-Ta**. The unsymmetric dialkylamine *N*-benzylmethylamine (Scheme VI-5) was less reactive than arylalkylamines. Here the difference in reactivity of niobium and tantalum was even more pronounced, with the niobium complex reacting at 150 °C, while tantalum required a significantly higher reaction temperature of 180 °C.

The reactions of *N*-methylaniline derivatives **128** provide enantioselectivities in a relatively narrow range of 66–80% ee at 140 °C, while the reaction of *N*-benzylmethylamine was significantly less selective. None of the reactions produced any detectable amount of the linear addition product; however, the reaction of *N*-benzylmethylamine produced the regioisomer **138b** originating from activation of the benzylic position as a minor byproduct (Scheme VI-5). The regioselective formation of **138a** is in agreement with observations for **120**¹³ but is in remarkable contrast to selectivities found for the amidate **121**.¹⁴

Table VI-4. Substrate scope in the intermolecular asymmetric hydroaminoalkylation catalyzed by **127j-M** (M = Ta, Nb).^a

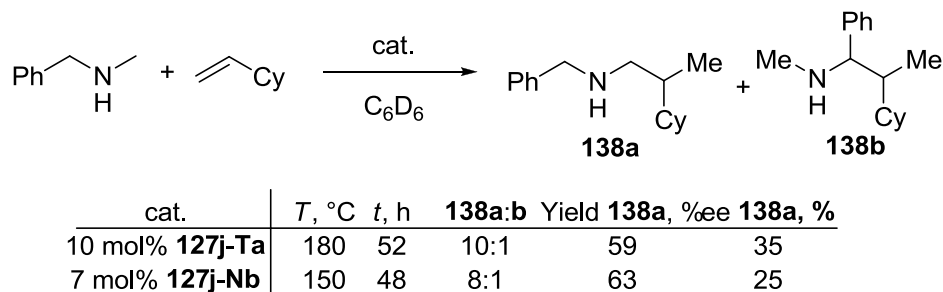


Entry	128	Alkene	Product	M	T, °C; t, h	Yield, %	ee, % ^b
1	a			Ta	140; 24	79	67
2	a		129	Nb	140; 12	71	70
3	a			Nb	140; 7	85	73
4	a		130a-d	Nb	100; 105	92	81
5	b			Nb	140; 7	95	66
6	b			Nb	100; 69	89	82
7	c			Nb	140; 6	90	67
8	d			Nb	140; 5	89	74
9	d			Nb	140; 13	88	71
10	d		131	Nb	100; 38	89	81
11	a			Nb	140; 9	89	80
12	a		132a-d	Nb	100; 60	92	91
13	b			Nb	140; 8	93	73 ^c
14	c			Nb	140; 8	82	71 ^d
15	d			Nb	140; 5	87	75 ^d
16	a			Nb	140; 9	93	92
17	a		133	Nb	100; 48	82	98
18	a			Nb	150; 72	70	82
			134				
19	a			Ta	140; 40	65	61
20	a		135	Nb	140; 12	61	59
21	a			Nb	140; 48	72	--
			136				
22	d			Nb	100; 48	73	71 ^d
			137				

^a Reaction conditions: amine (0.2 mmol), alkene (0.4 mmol), **127j-M** (0.01 mmol, 5 mol %), C₆D₆, Ar atm. ^b Determined by chiral HPLC of the corresponding *N*-benzamide. ^c Determined by ¹H NMR spectroscopy of (*S*)-Mosher amide. ^d Determined by chiral HPLC.

The sluggish reactivity of a secondary alkylamino group is further manifested by the absence of product formation in the reaction of 1-octene with *N*-ethylaniline, pyrrolidine and tetrahydroisoquinoline at 150–180 °C. It should be noted that these and similar amines lacking an *N*-methyl group did react with the tantalum amidate catalyst **121**¹⁴ and Ind₂TiMe₂ **123**.¹⁰ While multiple mechanistic scenarios may account for the enhanced regioselectivity of catalysts **127j-Ta** and **127j-Nb**, it is notable that their preference of activating the *N*-methyl group is greater than that of other known group 4 and group 5 metal catalysts.

Scheme VI-5. Hydroaminoalkylation of *N*-benzylmethylamine.



Scope in alkene. Linear, α - and β -branched terminal olefins exhibit comparable reactivities in hydroaminoalkylations (Table VI-4, entries 1–20), which seems to be remarkable in comparison to a significant diminished reactivity of α -branched terminal olefins observed in the intermolecular hydroamination²² (see also Chapters 3 and 4). Higher enantioselectivities were observed for sterically more demanding alkenes (Table VI-4, entries 2, 3, 11, and 16) as well at lower reaction temperatures (Table VI-4, entries 4, 6, 10, 12, and 17). Unactivated 1,2-disubstituted alkenes, such as cyclohexene, were unreactive; however, the more activated norbornene provided the corresponding product

135, though only in moderate yield due to formation of poly(norbornene) as a side reaction. Methylene cyclohexane exhibited lower reactivity because of the gem-disubstituted double bond. Other 1,1-disubstituted alkenes, such as α -methylstyrene, were unreactive. Notably, all reactions proceeded with excellent branched to linear regioselectivity exceeding 50:1. This also includes the reaction of **128d** with styrene at 100 °C, which produced the branched product (*S*)-(-)-**137** with >50:1 regioselectivity in 71% ee when using (*R*)-**127j-Nb** (Table VI-4, entry 22). The highest enantioselectivity of 98% ee was observed in the reaction of *N*-methylaniline (**128a**) with trimethyl(vinyl)silane at 100 °C (Table VI-4, entry 17). *tert*-Butylethylene showed the lowest reactivity among terminal alkenes, yielding the hydroaminoalkylation product **133** only after prolonged heating at 150 °C with **127j-Nb**. It is remarkable that neither **119** nor **120** was reactive for that substrate even at 180 °C, further manifesting the superior reactivity of **127-Nb**.

In summary, catalyst **127j-Nb** was demonstrated to be highly a regioselective and the most reactive and enantioselective catalyst for the asymmetric intermolecular hydroaminoalkylation. With a few exceptions, the catalyst is applicable only to terminal alkenes, and is unreactive for secondary alkyl amino groups. Having shown the scope and limitation of our binaphtholate catalysts, we proceeded to the kinetic and mechanistic studies of the hydroaminoalkylation reaction.

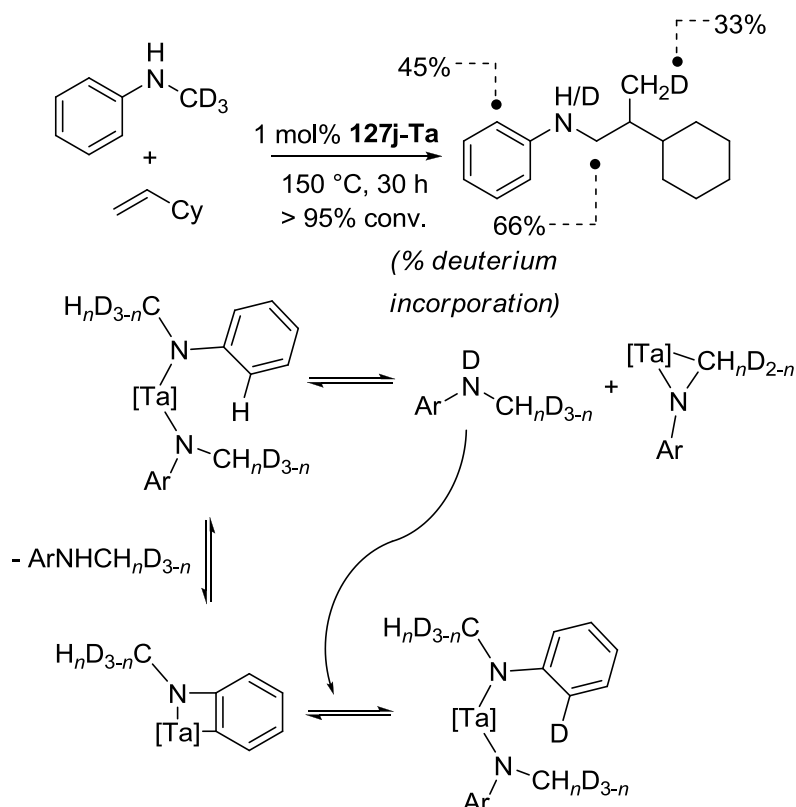
VI.2.3 Isotope Labeling Studies

As noted in the Introduction, the data on the mechanism of hydroaminoalkylation reaction (Scheme VI-4) is very limited. However, several important findings were

obtained through the isotopic labeling studies in intermolecular (**119**¹² and **120**¹³) and intramolecular (**122**)¹¹ hydroaminoalkylations. We took similar approach in order to gain further insight into the mechanism of the reaction catalyzed by **127-M**.

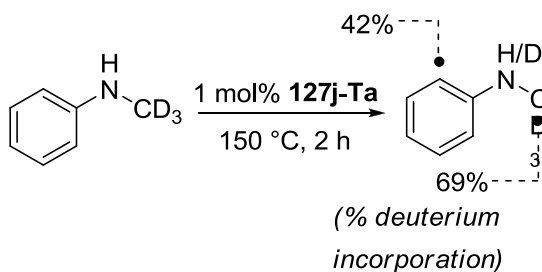
Reaction of *N*-(methyl-*d*₃)-aniline with vinylcyclohexane catalyzed by **127j-Ta** led to a product with largely depleted deuterium content at the methylene group and significant deuterium incorporation into the ortho-positions of the aryl ring (Scheme VI-6). This leakage of deuterium from the methylene group was interpreted as an indicator of a reversible metallaaziridine formation (Scheme VI-4, step 1),¹³ whereas the incorporation of deuterium into the aryl ring should result from the intramolecular C–H activation via cyclometallation (Scheme VI-6).¹²

Scheme VI-6. Deuterium scrambling with **127j-Ta** and possible mechanistic explanation.

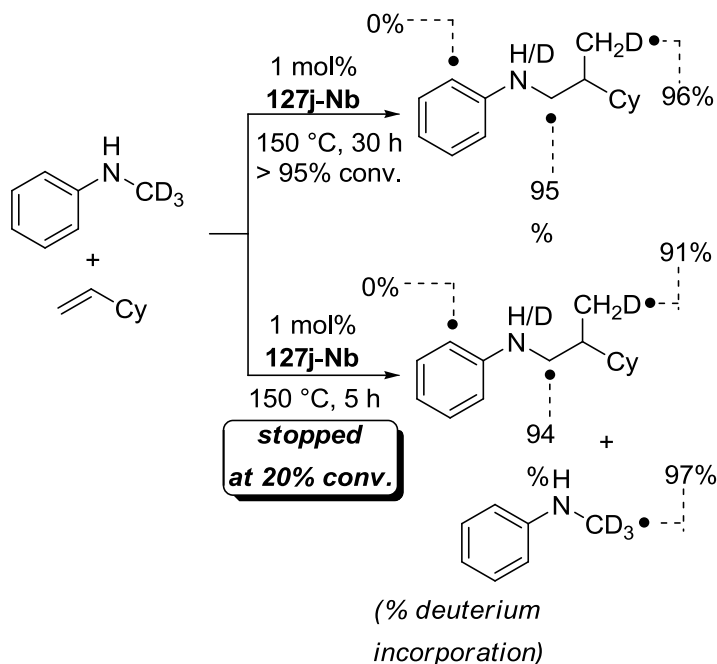


An important feature is the low incorporation of deuterium into the methyl group compared to that of the ortho-position of the aryl ring. Although 1.67 equiv deuterium are released from the original CD₃ group, only 33% of the methyl groups in the product are labeled (= 11% total deuteration of CH₃), suggesting that the protonation Scheme VI-4, step 3) proceeds predominantly with an *N*-proteo amine rather than an *N*-deutero amine, which is in agreement with observations for **119**¹² and **122b**.¹¹ The reaction of *N*-(methyl-*d*₃)-aniline with a catalytic amount of **127j-Ta** (1 mol%) in the absence of alkene (Scheme VI-7) resulted in a similar incorporation of deuterium into the ortho-position of the aniline (42% deuterium after 2 hours at 150 °C), indicating that the reversible cyclometallation is likely preceding the insertion Scheme VI-4, step 2) and is not necessarily part of the catalytic cycle.

Scheme VI-7. Deuterium scrambling with **127j-Ta** in the absence of alkene.



A strikingly different outcome was observed when **127j-Nb** was used instead of **127j-Ta**. In this case, the reaction of *N*-(methyl-*d*₃)-aniline with vinylcyclohexane proceeded with almost complete retention of deuterium in the methylene group and no ortho-metallation of the aniline aromatic ring was observed (Scheme VI-8).

Scheme VI-8. Isotopic labeling with **127j-Nb**.

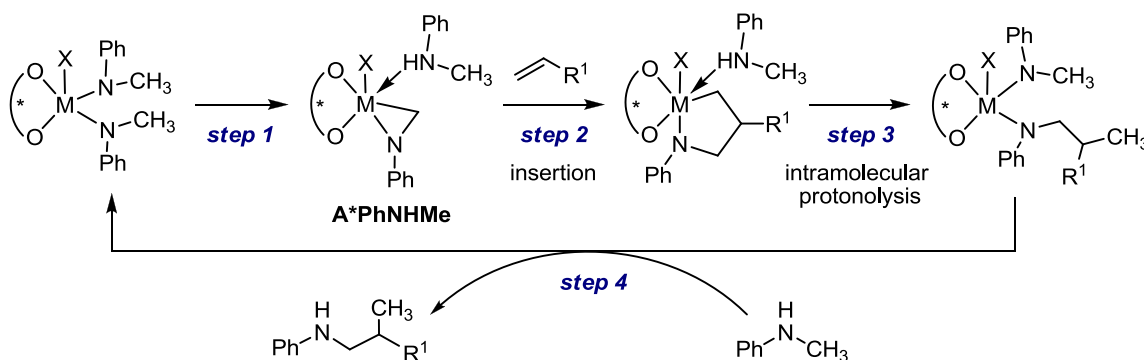
Thus, it seems that the lower reactivity of tantalum compared to niobium can be attributed in part to the formation of a cyclometalated species that removes the catalyst from its active state.

The absence of *ortho*-metallation for the niobium catalyst supports the hypothesis that this process is non-productive in character. The retention of deuterium in the methylene group is similar to that observed with **120**,¹³ which was interpreted as a result of irreversible C–H activation (Scheme VI-4, step 1) followed by rapid olefin insertion (Scheme VI-4, step 2). However, one feature of the reaction catalyzed by **127j-Nb** is unprecedented, which is almost complete (96%) deuteration of the methyl group of the product, while the reaction with catalyst **120** resulted in only 30% deuteration in our hands. Even more strikingly, when the reaction was stopped at ~20% conversion and starting material and product were recovered, high deuterium incorporation into the

methyl group of the product (91%) along with almost complete retention of deuterium in the starting material (97%) was observed (Scheme VI-8).

Unfortunately, direct quantitative determination of the extend of deuteration of the amine NH group is complicated due to broad and overlapping signals in the reaction mixture and loss of the amine deuterium during work-up. However, complete retention of deuterium in the molecule of the starting material suggests that most of the N–H groups are still undeuterated at low conversion. The high degree of monodeuteration of the methyl group in the product indicates that protonolysis of the azametallacyclopentane intermediate (Scheme VI-4, step 3) occurs almost exclusively with an *N*-deutero amine. Thus, the deuterium from the *N*-(methyl-*d*₃)-aniline starting material is transferred with high selectivity to the methyl group in the product. Although direct catalytic protonolysis of the metal-alkyl bond with another C–H bond via σ -bond metathesis is known,²⁵⁻²⁹ the non-dissociative formation of the metallazaaziridine **A*PhNHMe** (Scheme VI-9, step 1) with retention of the coordinated amine molecule during the insertion (Scheme VI-9, step 2) seems to be a more realistic mechanistic scenario. The subsequent protonolysis (Scheme VI-9, step 3) proceeds in an intramolecular fashion without participation of an external amine.

Scheme VI-9. Mechanistic proposal for the intramolecular proton delivery.



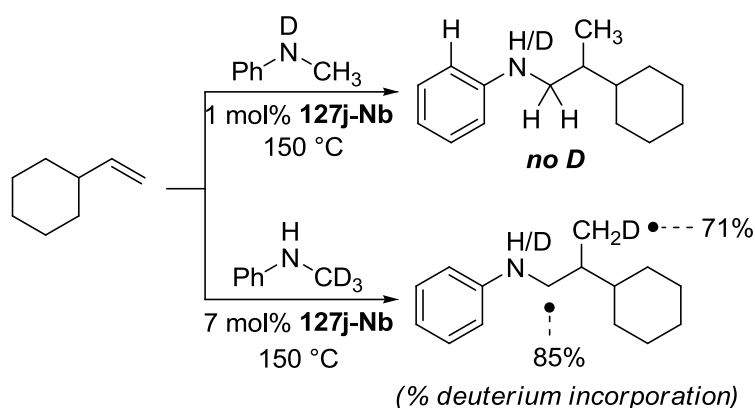
Several important consequences arise from the mechanism depicted in Scheme VI-9. First, the lack of deuterium scrambling from the methylene position cannot serve as a proof¹³ of an irreversible character of step 1. In fact, since a non-dissociative metallaaziridine formation can be reversed in a fully degenerate process, reversible metallaaziridine formation will still result in retention of deuterium. Indeed, prolonged heating of **127j-M** (M = Ta, Nb) in the presence or absence of a slight excess of **128a** (0–10 equiv) to 100–130 °C did not result in conversion to – or even observation of – the metallaaziridine **A*PhNHMe** according to ¹H NMR spectroscopy. However, the catalytic reactions proceeded smoothly in the presence of an alkene, which is another indicator that step 1 is reversible and the equilibrium is shifted towards the bisamide species. Second, the presence of a coordinated amine during the insertion step 2 can result in a concerted protonolysis-assisted insertion, so that steps 2 and 3 could merge into a single, concerted reaction step. This process would be reminiscent to a number of early transition metal hydroamination catalysts that have been proposed to operate via a protonolysis-assisted alkene insertion into a metal-nitrogen bond.³⁰⁻³⁸

Quenching of a reaction mixture of **128a** and 1-octene, containing 25 mol% **127j-M** (M = Ta, Nb) at ca. 40% conversion with 12M DCl/D₂O did not result in any noticeable deuterium incorporation into the methyl group of either product **130a** or starting material **128a**, further suggesting that the concentration of metallaaziridine and metal-alkyl species remains low over the course of the reaction.

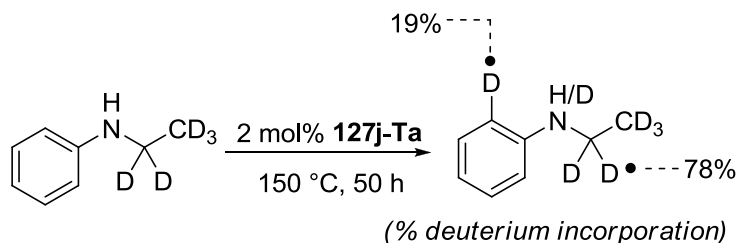
The incomplete (< 98%) deuteration of the product methyl group (Scheme VI-8) could arise from partial intermolecular protonation of the metal-carbon bond by an external amine. However, no measurable deuterium incorporation was observed in the

reaction of *N*-deutero-*N*-methyl-aniline with vinylcyclohexane using 1 mol% **127j-Nb** (Scheme VI-10). On the other hand, the same reaction with *N*-(methyl-*d*₃)-aniline using 7 mol% **127j-Nb** led to a diminished deuteration of the methyl group (71%) and depletion of deuterium from the methylene group (85%). These observations suggest that the residual protonation results from C–H activation of the dimethylamido groups of the precatalyst rather than from outer-sphere protonolysis.

Scheme VI-10. Probing outer sphere protonolysis (step 3).



As mentioned previously, a notable feature of catalysts **1** is a pronounced preference for activation of primary over secondary C–H bonds resulting in a lack of reactivity towards substrates without an *N*-methyl group. Previously, an isotopic labeling study with **120** suggested that hampered C–H activation limited the hydroaminoalkylation of secondary C–H bonds.¹³ In our case, although no hydroaminoalkylation product was formed with *N*-ethyl-aniline using either **127j-Ta** or **127j-Nb**, *N*-(ethyl-*d*₅)-aniline displayed some deuterium scrambling after 50 hours at 150 °C in the presence of **127j-Ta** (Scheme VI-11).

Scheme VI-11. Secondary alkyl C–H activation with **127j-Ta**.

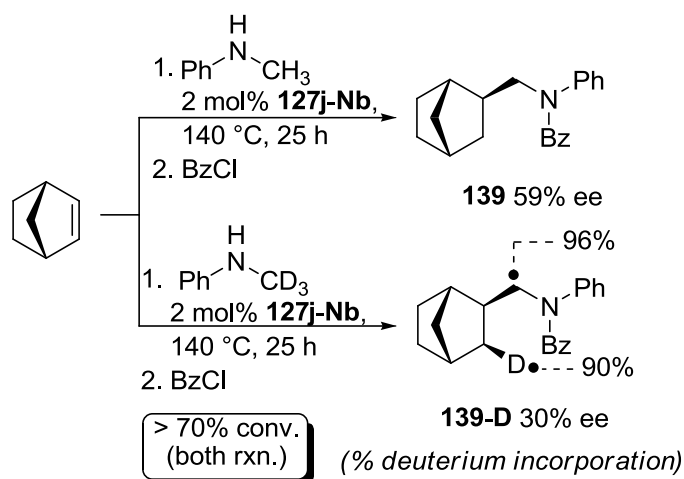
Despite the rate of deuterium exchange being considerably slower than in case of *N*-(methyl-*d*₃)-aniline, it seems that C–H activation of a secondary C–H bond is not prohibited. The lack of reactivity of methylene C–H bonds should therefore result from hampered alkene insertion (Scheme VI-9, step 2) rather than hampered C–H activation (Scheme VI-9, step 1).

The stereochemistry of olefin insertion into a metal-ligand bond can provide invaluable information on the details of the reaction mechanism. For example, the stereochemistry of the inter-^{39,40} and intramolecular⁴¹⁻⁴³ olefin insertion into a palladium-amide bond as well as the intramolecular gold-⁴⁴ and Brønsted acid-catalyzed⁴⁵ cyclization of alkenyl sulfonamides has been investigated in the context of the hydroamination reaction.

We have performed the reaction of norbornene with *N*-(methyl-*d*₃)-aniline in the presence of **127j-Nb** (Scheme VI-12). Consistent with our previous findings, high retention of deuterium in the methylene position along with high deuteration of the cyclic methylene group were observed. The delivery of deuterium to the ring proceeded exclusively to the exo-position thus yielding the *syn*-insertion isomer of **135** (isolated as benzamide **139-D**). These results are in agreement with observations of Milstein et al. on iridium-catalyzed hydroamination of norbornene with aniline.⁴⁶ Most interestingly, the

deuterated benzamide **139-D** was formed with significant lower enantioselectivity (30% ee) in comparison to the undeuterated congener **139** (59% ee).

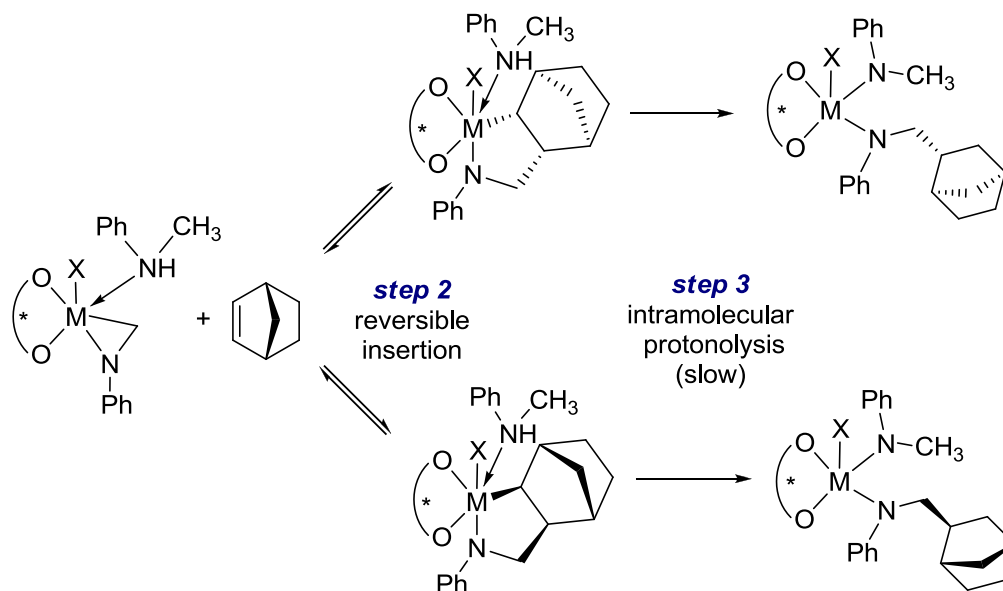
Scheme VI-12. Hydroaminoalkylation of norbornene with **128a** and **128a-d₃**.



While the *syn*-addition to the olefin is consistent with the inner-sphere olefin insertion mechanism and, therefore, is an expected result, the significant perturbation of enantioselectivity in the formation of **139-D** caused by the isotopic substitution is striking. As the stereodetermining step itself (insertion, Scheme VI-9, step 2) does not directly involve the cleavage or formation of a C–H bond as the protonolysis (Scheme VI-9, step 3) does, the perturbation of enantioselectivity suggests that step 2 is reversible,^{47–49} and is faster than intramolecular protonolysis (Scheme VI-13). The fact that this phenomenon is observed in the case of norbornene is likely due to the fact that the intramolecular protonolysis (Scheme VI-13, step 3) involves proton transfer to a more sterically hindered methine carbon as opposed to the methylene group in the case of α -olefins. Indeed, no perturbation of enantioselectivity was observed in the case of α -olefins: 73% ee vs. 73% ee for **130a-D** and **130a** and 79.5% ee vs. 80% ee for **132a-D**

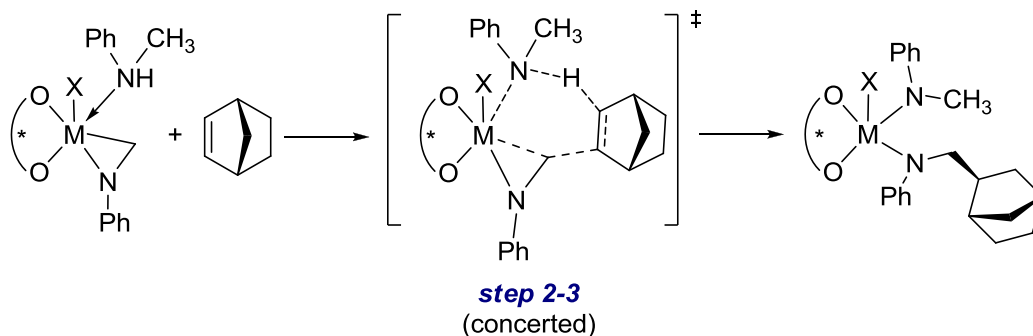
and **132a**, respectively, thus strongly suggesting an effectively irreversible insertion (Scheme VI-13, step 2) and fast intramolecular protonolysis (Scheme VI-13, step 3).

Scheme VI-13. Reversible insertion in norbornene hydroaminoalkylation.



An alternative explanation for the observed perturbation of enantioselectivity would involve a concerted insertion-protonolysis step with participation of a coordinated amine, which is both stereodetermining and involves the conversion of an N-H bond into a C-H bond (Scheme VI-14). This scenario was used to explain the isotopic perturbation of enantioselectivity in the zirconium-catalyzed intramolecular hydroamination of aminoalkenes.^{33,37} However, this proposal does not explain the unique behavior of norbornene with respect to the perturbation of enantioselectivity as found in this study. Furthermore, the concerted insertion-protonolysis sequence recently proposed for a magnesium hydroamination catalyst system³² was soon afterwards shown to proceed via fast reversible insertion and rate-determining protonolysis according to DFT calculations.⁵⁰

Scheme VI-14. Possible scenario for a concerted insertion-protonolysis in norbornene hydroaminoalkylation.



VI.2.4 Empirical Rate Laws

In order to determine the empirical rate laws, a kinetic investigation of the hydroaminoalkylation of *N*-methyl-anilines **128a–d** with 1-octene and vinylcyclohexane using **127j-Nb** was performed. The reaction displays a relatively well-behaved first order kinetic pattern in amine over the course of 2–3 half-lives in the presence of an excess of alkene. The observed first-order rate constant is linearly dependent on the catalyst concentration **127j-Nb** (Figure VI-4), therefore, indicating a first order dependence in **2** and **127j-Nb**.

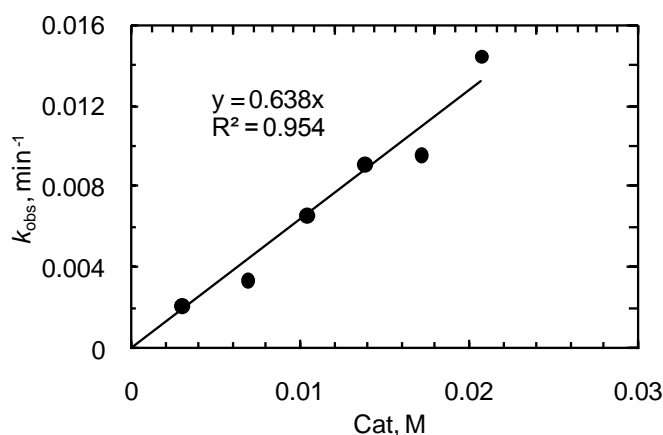


Figure VI-4. Dependence of observed first-order reaction constant on catalyst concentration for the reaction of 1-octene (0.613 M) with PMPNHMe (**128d**) (0.20 M) in

the presence of (*R*)-**127j-Nb** (0.003–0.022M) in C₆D₆ at 150 °C. The line represents the least-square fit to the data points.

Although a first order rate dependence on catalyst concentration is in good agreement with a well-defined monometallic species participating in the catalytic reaction, it should be noted that a nonlinear saturation behavior was recently reported for the intramolecular aminoalkene hydroaminoalkylation catalyzed by **122b**.¹¹

An attempt to determine the reaction order in alkene showed a pronounced discrepancy between non-hindered (1-octene) and hindered (vinylcyclohexane) alkenes (Figure VI-5).

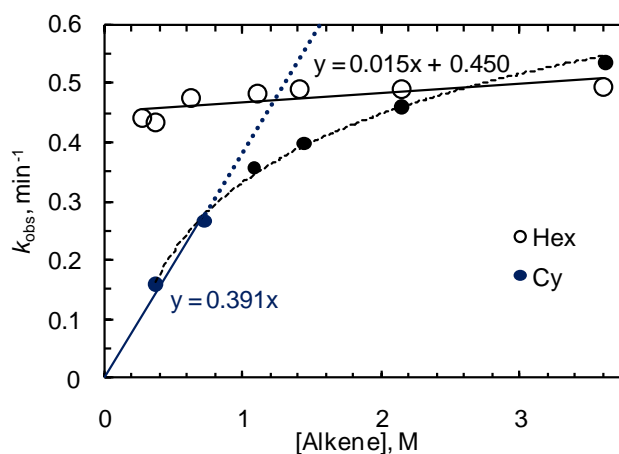


Figure VI-5. Dependence of pseudo first-order rate constant on alkene concentration for the reaction of 1-octene (0.26–3.75 M) (○) and vinylcyclohexane (0.29–3.75 M) (●) with PMPNHMe (**128d**) (0.29 M) in the presence of (*R*)-**127j-Nb** (0.017 M) in C₆D₆ at 150 °C. The solid lines represent the least-square fit to the data points, dotted lines are drawn as a guide for the eye.

Essentially no rate dependence on the concentration of 1-octene was observed, which indicates that alkene insertion (Scheme VI-9, step 2) is not rate-determining and is proceeding relatively fast within a large concentration interval of the alkene. Saturation behavior was observed in case of the sterically more demanding vinylcyclohexane with the rate being close to zero-order in alkene at high alkene concentrations, while first-order dependence was apparent at low alkene concentrations. Thus, insertion step 2 can serve as a rate-determining step as well. Based on these results an empirical rate law can be proposed (Eq. VI-2):

$$\text{rate} = k [\mathbf{127j-Nb}][\mathbf{128}][\text{alkene}]^{\alpha} \quad (\text{VI-2})$$

where $0 \leq \alpha \leq 1$

The insertion step (Scheme VI-9, step 2) is sensitive to the steric features of the alkene, however, compounds **128a–d** react with vinylcyclohexane and 1-octene with comparable rates in the saturation regime. The first-order rate dependence on the concentration of *N*-methyl-anilines **128a–d** (Figure VI-6, see also section VI.5 for more examples) is indicative of amide exchange (Scheme VI-9, step 4) becoming rate-determining at high alkene concentrations.

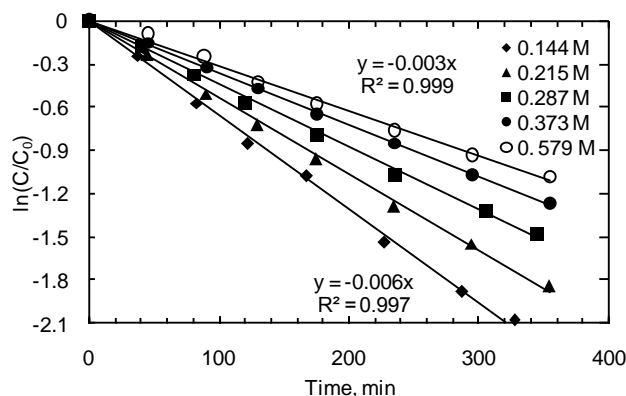
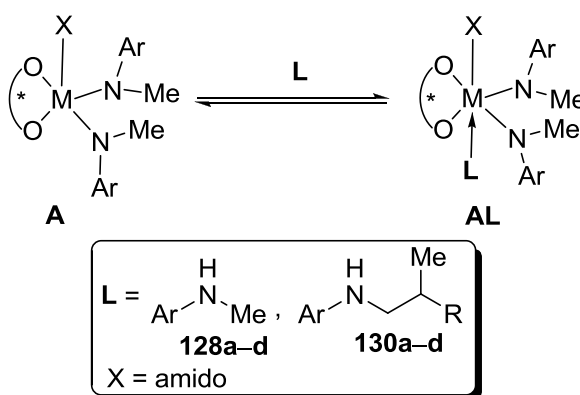


Figure VI-6. First-order kinetic plots for the reaction of 1-octene (0.613 M) with 4-FC₆H₄NHMe (**128b**) (0.144–0.579 M) in the presence of (*R*)-**127j-Nb** (0.017 M) in C₆D₆ at 150 °C. The solid lines represent the least-square fit to the data points.

In the presence of an excess of 1-octene (zero-order in alkene) the reaction can be adequately described as being first-order in amine **128** at all alkene concentrations. However, reactions at higher amine concentrations are significantly slower, which indicates a pronounced amine inhibition. This inhibition may originate from reversible metallaaziridine formation (step 1) or from other non-productive events which may involve catalytically relevant form of **127j-Nb** and free **128**. As clearly demonstrated above, although step 1 is reversible, the non-dissociative character of this transformation implies that neither the amine “elimination” step (Scheme VI-9, step 1) nor its reversal should depend on the concentration of free **128** and, therefore, this inhibition scenario can be ruled out. Instead, it seems more likely that the inhibition pathway involves reversible non-productive binding of the free amine (either **128** or **130**) to the catalytically active five-coordinate bis(anilide) **A** to form a “dormant” six-coordinate species **AL** (Scheme VI-15).

Scheme VI-15. Equilibrium between catalytic active five-coordinate species **A** and its “dormant” amine adduct **AL**.



The ability of the niobium center to adopt a six-coordinate environment is justified by the formation of the amine-coordinated aziridine (**A*PhNHMe**) elucidated by isotopic labeling. Furthermore, many of the precatalysts **127-M** include an additional coordinated amine molecule.^{23,24} The inhibition operating via non-productive binding of an additional substrate equivalent is also rather common in early transition metal-catalyzed hydroamination.^{30,33,34,51,52}

VI.2.5 Kinetic Isotope Effects

The determination of the kinetic isotope effect (KIE) has proven to be a very useful mechanistic tool, which has been applied in many studies of C–H activation by organometallic systems.^{53,54} We performed the reaction of **128a**, **128a-ND** and **128a-CD₃** with 1-octene in the presence of **127j-Nb**; however, in the absence of a complete mechanistic and kinetic model the observed “net” kinetic isotope effects for non-elementary transformations should be interpreted very carefully.

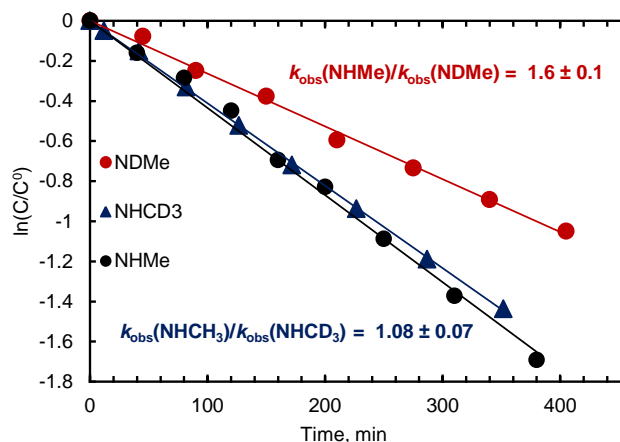


Figure VI-7. First-order kinetic plots for the reaction of 1-octene (1.89 M) with PhNHMe (**128a**) and its deuterated analogues (0.311 M) in the presence of (*R*)-**127j-Nb** (0.019 M) in C₆D₆ at 150 °C. The solid lines represent the least-square fit to the data points.

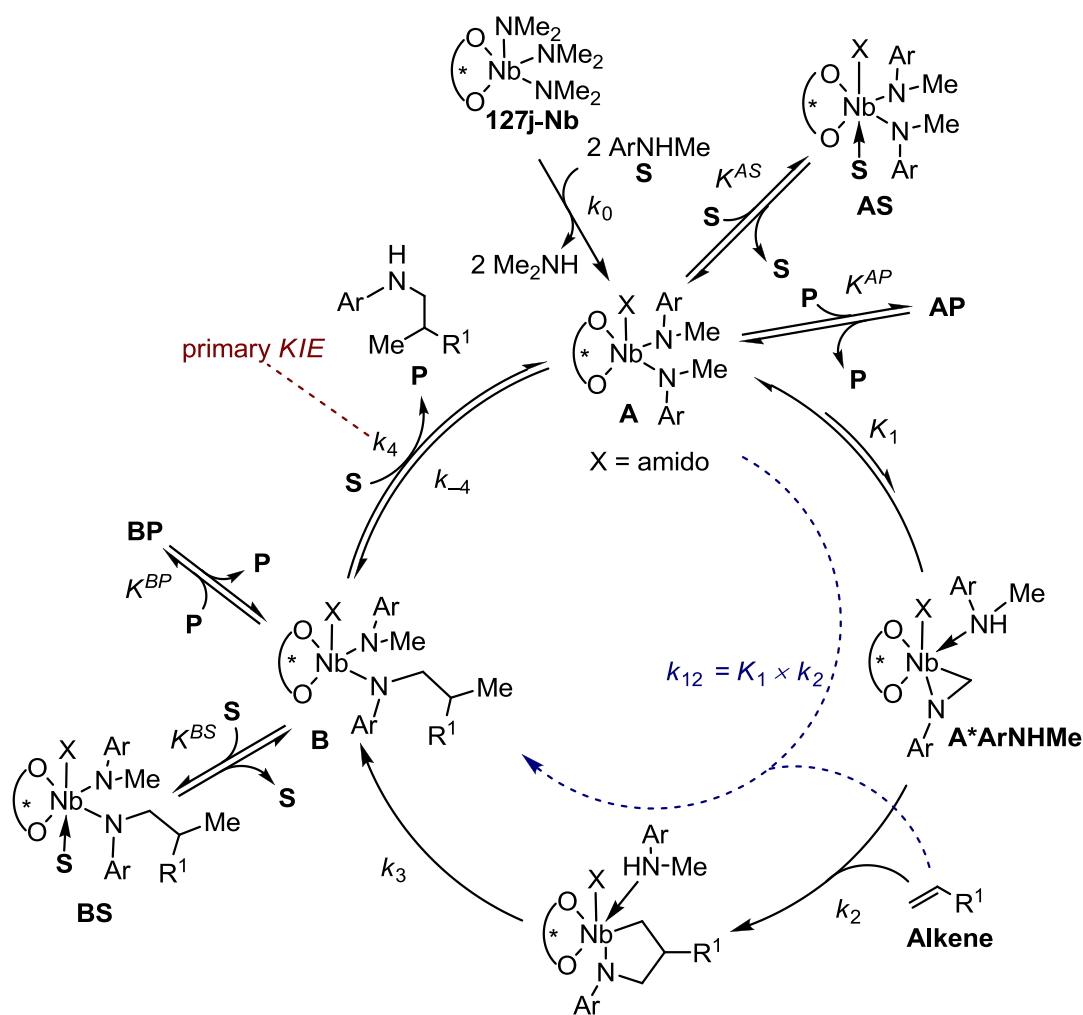
As shown in Figure VI-7, *N*-deuteration of **128a** resulted in a primary KIE of 1.6 ± 0.1 whereas deuteration of the methyl group in **128a-CD₃** did not significantly diminish the rate of the reaction. This result suggests that the C–H activation (step 1) is unlikely to be rate-determining under these conditions, whereas the rate-determining amide exchange (step 4) can account for the primary KIE as the N–H bond is being formed and broken during this step. These findings are in remarkable contrast to the strong primary isotope effect observed in intramolecular hydroaminoalkylation of a C–Deuterated aminoalkene by Doye.¹¹ More detailed and elaborate studies of the KIE's will be described below as we will proceed by introducing a plausible mechanistic model that will account for all mechanistic and kinetic observations.

VI.2.6 Mechanistic Model for Asymmetric Hydroaminoalkylation

The proposed mechanistic model is depicted in Scheme VI-16. Protonolysis of precatalyst **127j-Nb** with an excess of substrate **S** liberates two molecules of

dimethylamine and yields the bisamide **A**, which subsequently undergoes intramolecular rearrangement to the six-coordinate amine-bound metallaaziridine **A*ArNHMe**. The metallaaziridine undergoes intermolecular alkene insertion, followed by intramolecular protonolysis to yield the bisamide **B**, which may regenerate the bisamide **A** and release the product **P** via reversible amide exchange with an additional substrate molecule **S**. Reversible non-productive binding of **S** and **P** to bisamides **A** and **B** yields six-coordinate bisamides **AS**, **AP**, **BS** and **BP**.

Scheme VI-16. Proposed mechanism for the intermolecular hydroaminoalkylation.



It seems reasonable to make several justified assumptions in order to derive a relatively simple kinetic model. First, although a short induction period of 2–5 min was observed for most of the reactions with **128** at 150 °C, this value is negligible compared to the overall reaction time of 5–12 hrs. Therefore, it can be assumed that precatalyst activation is fast compared to catalytic turnover and that precatalyst **127j-Nb** is fully activated throughout the reaction. Thus, k_0 can be excluded from the kinetic model. Second, the quenching experiments along with the kinetic data and general considerations suggest that intramolecular protonolysis is fast compared to the intermolecular insertion ($k_3 \gg k_2[\text{alkene}]$), except for the reaction with norbornene or, alternatively, proceeds in a concerted fashion with this step, and, therefore, monomolecular protonolysis rate constant k_3 can be excluded as well. Third, based on our inability to detect **A*ArNHMe** under the reaction conditions, the equilibrium constant between the bisamide **A** and the metallaaziridine **A*ArNHMe** has to be small and can be estimated to $K_1 < 0.05$. The metallaaziridine **A*ArNHMe** does not contribute significantly to the material balance of all metal species and hence, the overall transformation from **A** to **B** via the sequence of C–H activation and insertion-protonolysis can be described with one bimolecular rate constant $k_{12} = K_1 \times k_2$

Thus, considering the following:

1. Catalyst activation is fast compared to catalytic turnover.
2. $K_1 < 0.05$ and the concentration of the metallaaziridine **A*ArNHMe** is small at all times.
3. The transformation from **A** to **B** can be described by a combined rate constant $k_{12} = K_1 \times k_2$.

We can write down an overall rate equation as:

$$Rate = \frac{d[P]}{dt} = k_4[B][S] - k_{-4}[A][P] \quad (VI-3)$$

Steady-state approximation for compound **A** (steady-state for **B** leads to a degenerate expression):

$$k_{12}[A][alkene] + k_{-4}[A][P] = k_4[B][S] \quad (VI-4)$$

Reversible amine binding is determined as follows:

$$K^{AS} = \frac{[AS]}{[A][S]}, \quad K^{AP} = \frac{[AP]}{[A][P]}, \quad K^{BS} = \frac{[BS]}{[B][S]}, \quad K^{BP} = \frac{[BP]}{[B][P]}$$

Material balance for the metal-containing species:

$$[cat]_0 = [A] + [B] + [AS] + [AP] + [BS] + [BP] \quad (VI-5)$$

Combining Eq. VI-5 with equilibrium constants:

$$\begin{aligned} [cat]_0 &= [A](1 + K^{AS}[S] + K^{AP}[P]) + [B](1 + K^{BS}[S] + K^{BP}[P]) = \\ &= [A]X + [B]Y \end{aligned} \quad (VI-6)$$

Where:

$$X = 1 + K^{AS}[S] + K^{AP}[P]$$

$$Y = 1 + K^{BS}[S] + K^{BP}[P]$$

Incorporation of Eq. VI-4 in Eq. VI-6:

$$\begin{aligned} [cat]_0 &= [A]X + \frac{k_{12}[A][alkene] + k_{-4}[A][P]}{k_4[S]} Y = \\ &= [A] \left\{ \frac{X k_4[S] + Y(k_{12}[alkene] + k_{-4}[P])}{k_4[S]} \right\} \end{aligned} \quad (VI-7)$$

Rewriting Eq. VI-7:

$$[A] = \frac{k_4[cat]_0[S]}{X k_4[S] + Y(k_{12}[alkene] + k_{-4}[P])} \quad (VI-8)$$

Modifying the general rate expression Eq. VI-3 considering Eq. VI-4:

$$\frac{d[P]}{dt} = k_{12}[A][alkene] \quad (VI-9)$$

Now we can incorporate Eq. VI-8 into Eq. VI-9:

$$\frac{d[P]}{dt} = \frac{k_{12}k_4[cat]_0[S][alkene]}{X k_4[S] + Y(k_{12}[alkene] + k_{-4}[P])} \quad (VI-10)$$

Finally, substituting X and Y :

$$\frac{d[P]}{dt} = \frac{k_{12}k_4[cat]_0[S][alkene]}{k_4[S](1 + K^{AS}[S] + K^{AP}[P]) + (k_{12}[alkene] + k_{-4}[P])(1 + K^{BS}[S] + K^{BP}[P])} \quad (VI-11)$$

Although Eq.VI-11 is derived from a steady-state assumption and additional considerations (1-3), it is still too complicated to be solved analytically.

We will make additional assumptions (4-6) which are in our view less justified than assumptions (1-3) however they are needed in order to make Eq.VI-11 more informative and applicable:

4. All inhibition equilibrium constants have similar values ($K^{AS} \approx K^{AP} \approx K^{BS} \approx K^{BP} \equiv K^{\text{dorm}}$), where K^{dorm} is a “general” equilibrium constant between 5- and 6- coordinate metal amido species.
5. The bimolecular amide exchange constants are very similar in value ($k_4 \approx k_{-4}$).
6. Catalyst loadings are low ($[cat]_0 \ll [S]_0$);

$$rate = \frac{k_{12}k_4[cat]_0[S][alkene]}{k_4[S]_0 + k_{12}[alkene]} \cdot \frac{1}{1 + K^{dorm}[S]_0} \quad (VI-12)$$

Eq VI-12 can be simplified for two limiting cases:

Alkene insertion is faster than amide exchange ($k_{12}[alkene] \gg k_4[S]_0$)

$$rate = k_{obs}[cat]_0[S] \quad (VI-13)$$

Where

$$k_{obs} = \frac{k_4}{1 + K^{dorm}[S]_0}$$

In this case the reaction will be limited by amide exchange and will display zero-order rate dependence on alkene concentration as it was experimentally observed for the fast insertion in the case of 1-octene and at high concentrations of vinylcyclohexane.

If alkene insertion is rate-limiting ($k_{12}[alkene] \ll k_4[S]_0$) one should observe an overall third order reaction (Eq VI-14):

$$rate = k_{obs}[cat]_0[S][alkene] \quad (VI-14)$$

$$\text{with } k_{obs} = \frac{k_{12}}{[S]_0(1 + K^{dorm}[S]_0)}$$

Although Eq VI-12 provides a formal description of all distinct kinetic patterns observed experimentally it should be remembered that it was derived using certain assumptions. While deriving a parent Eq VI-11, we proposed a steady-state in catalytic species and, and then the low catalyst loadings to obtain Eq VI-12, which were not always the case in a real experiment.* Furthermore, generally speaking, the assumptions

* In a typical experiment with 5% catalyst loading, up to 15% of substrate and product might be bound to the catalyst, therefore $[S] + [P] \neq [S]_0$

4, 5 are not justified by default, as individual amine exchange rates and reversible binding equilibrium constants should be different for various combinations of **A**, **B**, **S** and **P**.

A numerical nonlinear regression approach allows handling of complicated kinetic models without the aforementioned restrictions. Thus, analysis of kinetic data for the reaction of **128b** with 1-octene employing models of different complexity using the program DynaFit⁵⁵ allows evaluation of our assumptions on the relative turnover and equilibrium constant values.

Results for the data fit employing the models of different complexity using DynaFit⁵⁵ are shown in Table VI-5. Note, that none of these models include observed insertion constant k_{12} as the reactions are performed for the fast-inserting alkene. The most primitive model (assumption: $k_4 = k_{-4}$ and $K^{AS} = K^{AP} = K^{BS} = K^{BP} = K^{\text{dorm}}$) showed a good fit to the experimental data (Figure VI-8). Adding additional parameters to describe amide exchange (No 2) or catalyst inhibition (No 3) did not result in any substantial improvements (Table VI-5). In fact, additional kinetic parameters were fitted to the values which are very close to the original ones. Thus, we may conclude that model No 1 is accurate enough for the zero-order in alkene hydroaminoalkylation kinetics and our previous assumptions on the relative values of equilibrium and turnover constants are justified.

Table VI-5. Nonlinear fit to the models of various detalization levels.

No	Parameters	Results ^a	Weight, % ^b
1	$k_4 = k_{-4}$ $K^{AS} = K^{AP} = K^{BS} = K^{BP} = K^{\text{dorm}}$	$k_4 = (0.58 \pm 0.09) \text{ M}^{-1} \text{ min}^{-1}$ $K^{\text{dorm}} = (2.8 \pm 0.7) \text{ M}^{-1}$	61
2	$k_4 \neq k_{-4}$ $K^{AS} = K^{AP} = K^{BS} = K^{BP} = K^{\text{dorm}}$	$k_4 = (0.59 \pm 0.09) \text{ M}^{-1} \text{ min}^{-1}$ $k_{-4} = (0.5 \pm 0.2) \text{ M}^{-1} \text{ min}^{-1} \text{ }^c$ $K^{\text{dorm}} = (3.0 \pm 0.9) \text{ M}^{-1}$	21
3	$k_4 = k_{-4}$ $K^{AS} = K^{BS} = K^S$ $K^{AP} = K^{BP} = K^P$	$k_4 = (0.59 \pm 0.09) \text{ M}^{-1} \text{ min}^{-1}$ $K^S = (2.8 \pm 0.8) \text{ M}^{-1}$ $K^P = (2.7 \pm 1.3) \text{ M}^{-1}$	18

^a Nonlinear fit to the given model, confidence intervals for 95% probability. ^b Akaike statistical weight of the model. ^c Standard error.

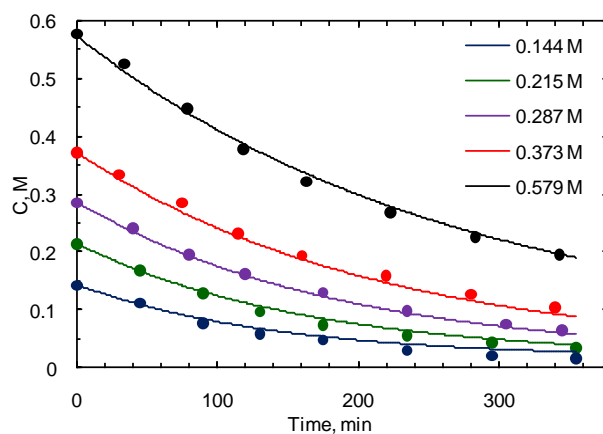
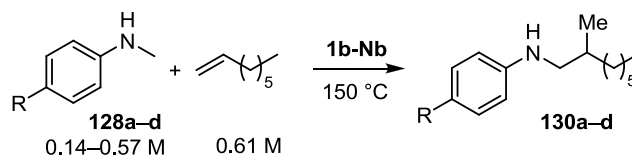


Figure VI-8. Experimental reaction progress data (dots) for the reaction of 1-octene (0.613 M) with **128b** (0.144–0.579 M) in the presence of (*R*)-**127j-Nb** (0.017 M) in C₆D₆ at 150 °C vs. the simulated reaction curves (lines) for $k_4 = 0.58 \pm 0.09 \text{ M}^{-1} \text{ min}^{-1}$, $K^{\text{dorm}} = 2.8 \pm 0.7 \text{ M}^{-1}$.

This kinetic model was also applied to the nonlinear regression analysis of the kinetic data of the reactions of 1-octene with other *N*-methyl-aniline derivatives (Table VI-6).

Table VI-6. Kinetic parameters for the reaction of **128a-d** with 1-octene.^a



Entry	R	k_4 , $\text{M}^{-1}\text{min}^{-1}$	K^{dorm} , M^{-1}
1	H (128a)	0.33 ± 0.02	1.6 ± 0.3
2	H (128a-CD₃)	0.38 ± 0.05	1.9 ± 0.5
3	H (128a-ND)	0.18 ± 0.03	1.1 ± 0.6
4	F (128b)	0.58 ± 0.09	2.8 ± 0.7
5	Cl (128c)	0.58 ± 0.15	7.8 ± 2.4
6	MeO (128d)	3.1 ± 1.2	14.4 ± 5.0

^a Nonlinear fit to a fast insertion model ($k_{12} \gg k_4 = k_{-4}$ and $K^{\text{AS}} = K^{\text{AP}} = K^{\text{BS}} = K^{\text{BP}} = K^{\text{dorm}}$), confidence intervals for 95% probability.

Deuteration of the *N*-methyl group in **128a-CD₃** did not result in a measurable KIE for k_4 or an equilibrium isotope effect (EIE) for K^{dorm} . Because k_4 describes the amide exchange reaction in which no C–H bond is formed or broken, the absence of a KIE matches the mechanistic expectations. In contrast, the *N*-deutero substrate **128a-ND** displayed a primary KIE of 1.8 ± 0.3 , which is in agreement with the value obtained from observed constants (Figure VI-7). The accuracy of the measurements is insufficient to decide whether an EIE for the reversible non-productive amine binding is present or not.

The dependence of kinetic parameters on the electronic properties of the para-substituent is nonlinear for both k_4 and K^{dorm} . *N*-methyl-aniline (**128a**) is less prone to

inhibition and is reacting slower than the more electron-accepting halide-substituted **128b** and **128c**, whereas the electron-donating methoxy-substituted **128d** is most reactive (Figure VI-9).

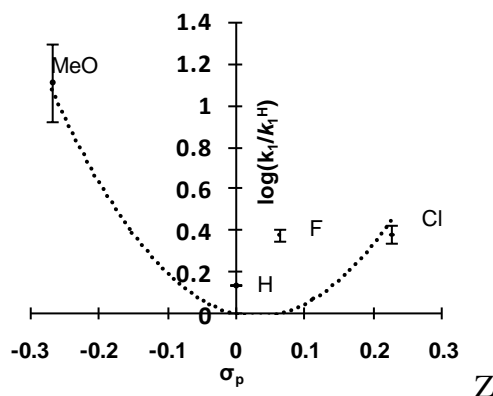


Figure VI-9. Hammett plot for turnover constant k_4 for the reaction of **128a–d** with 1-octene. Error bars indicate the error of the measurement. The dotted line is drawn as a guide for the eye.

It can be speculated that the observed nonlinearity may in part originate from the complex character of the interaction of **128** with **A** or **B** (Scheme VI-16), whether as an amide or amine. Indeed, the more nucleophilic and more Lewis-basic substrate **128d** should form stronger covalent and dative bonds to the metal than **128a**. While **128c** itself is more electron-deficient and should be less reactive, the corresponding species **A** contains two electron-deficient anilide ligands and is, therefore, more electrophilic and prone to amine inhibition. The overall reactivity is controlled by the interplay of the electronic features of ligand and starting material. Thus, we can expect that catalysts with a more electron-deficient ligand backbone should possess enhanced reactivity in amide exchange.

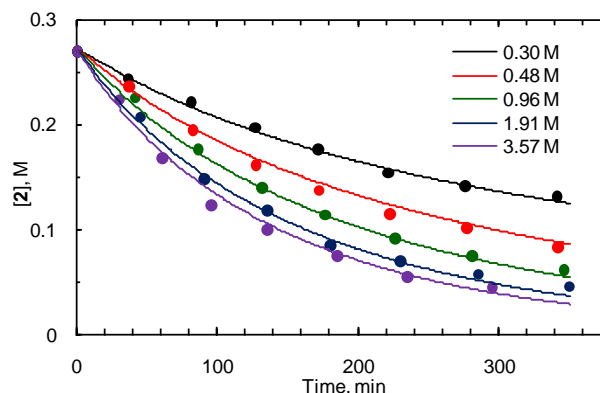


Figure VI-10. Experimental reaction progress data (dots) for the reaction of vinylcyclohexane (0.30–3.57 M) with PMPNHCH₃ (**128d**) (0.270 M) in the presence of (*R*)-**127j-Nb** (0.017 M) in C₆D₆ at 150 °C versus the simulated reaction curves (lines) for $k_4 = (3.7 \pm 0.2) \text{ M}^{-1} \text{ min}^{-1}$, $k_{12} = (0.81 \pm 0.05) \text{ M}^{-1} \text{ min}^{-1}$, $K^{\text{dorm}} = 14.4 \text{ M}^{-1}$. The value of K^{dorm} was obtained from the reaction with 1-octene.

An important observation is the negligible KIE for **128d**: $k_{12}(\text{CH}_3)/k_{12}(\text{CD}_3) = 1.19 \pm 0.14$. This suggests that no strong primary KIE or EIE is associated with the aziridine formation, as olefin insertion should not display any primary KIE. Alternatively, if the insertion proceeds in a concerted fashion with intramolecular protonolysis, this reaction can exhibit a primary KIE, because the hydrogen (respectively deuterium) in the N–H bond (respectively N–D bond) that is being broken originates from the methyl group of the *N*-methylaniline. The negligible net KIE can originate from the superposition of the primary KIE for insertion-protonolysis and the inverse EIE for the aziridine formation. At this point none of these scenarios can be ruled out with certainty. It should be noted that the absence of isotopic perturbation of enantioselectivity for the reaction involving 1-octene and vinylcyclohexane is a strong argument against a

concerted insertion-protonolysis mechanism. The stereodetermining step would involve cleavage of the N–H bond and one would expect some variation of stereoselectivity, which has been frequently observed in hydroamination reactions.^{30,33,37}

Although norbornene displayed a remarkable isotopic perturbation of enantioselectivity, it is prone to polymerization under the standard reaction conditions and reliable kinetic data could not be obtained. Overall, the absence of a primary KIE in the isolated reaction step directly involving the formation of the metallaaziridine is in remarkable contrast to literature precedence of metallaaziridine formation in titanium-catalyzed hydroaminoalkylations,¹¹ as well as in stoichiometric metallaaziridine formation via elimination of an alkane.^{56,57}

VI.3 Group 5 Metal Binaphtholates in Catalytic Asymmetric

Hydroamination

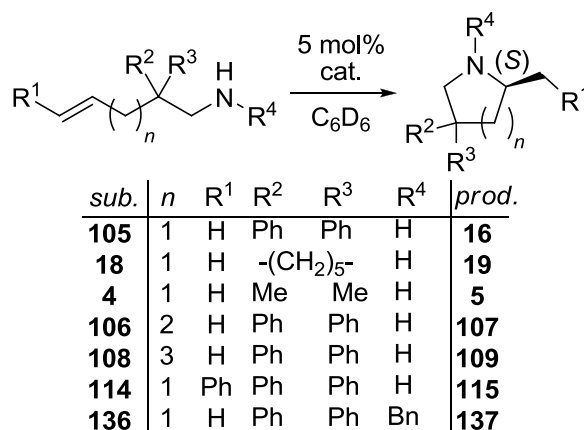
In the plethora of early transition metal-catalyzed hydroamination reaction studies the group 5 metal-based hydroamination catalysts have been relatively scarce⁵⁸⁻⁶³ and only the hydroamination of alkynes,⁵⁸ allenes^{58,62,63} and activated alkenes^{58,61} has been studied. The group 5 metal-catalyzed hydroamination of aminoalkenes has not been reported prior to our work and no niobium-based hydroamination catalysts were known.

A chiral tantalum catalyst system for the asymmetric hydroamination of aminoallenes in up to 74% ee was introduced only very recently.^{62,63}

Recent studies on titanium- and zirconium-catalyzed transformations of primary aminoalkenes have shown that the hydroaminoalkylation and hydroamination may occur concurrently, favoring one or the other process depending on the chain length of the aminoalkene.^{6,8,9,64} The reactivity of group 5 metal complexes in these reactions had not

been reported prior to our study. However, simultaneously to our original report,⁸⁴ Zi recently reported the application of tantalum bis(amidate) **126** and its analogues in asymmetric hydroamination of aminoalkenes with up to 80% ee.¹⁶ To our surprise we discovered that the binaphtholate tantalum complexes **127-Ta** readily catalyze the hydroamination/cyclization of various primary aminopentenes and aminohexenes (Table VI-8), but no hydroaminoalkylation products were detected.

Table VI-8. Catalytic asymmetric hydroamination/cyclization of aminoalkenes using binaphtholate tantalum and niobium complexes.



entry	subst.	cat.	<i>T</i> , °C; <i>t</i> , h ^b	% ee (config)
1	105	127a-Ta	100; 16	64 (<i>S</i>) ^c
2	105	127a-Nb	140; 18	50 (<i>S</i>)
3	105	127e-Ta	110; 14	<5 (<i>S</i>)
4	105	127k-Ta	100; 12	10 (<i>S</i>)
5	105	127j-Ta	100; 12	<5 (<i>S</i>)
6	105	127l-Ta	100; 11	21 (<i>S</i>)
7	18	127a-Ta	120; 30	81(<i>S</i>)
8	4	127a-Ta	140; 34	41 (<i>S</i>)
9	106	127a-Ta	120; 36	17
10	108	127a-M^d	170; 36	-- ^e

11	114	127a-Ta	170; 36	-- ^e
12	140	127a-Ta	170; 36	-- ^e

^a Reaction conditions: 5 mol% cat., C₆D₆, Ar atm. ^b >95% conv. based on ¹H NMR spectroscopy using ferrocene as internal standard. ^c 80% isolated yield. ^d M = Ta, Nb. ^e No reaction.

The cyclization of the *gem*-diphenyl activated aminopentene **105** proceeded with the tantalum catalysts at 100–110 °C with 5 mol% catalyst loading. The highest enantioselectivity for this substrate was 64% ee using the sterically most hindered catalyst **127a-Ta**. Less encumbered complexes showed higher activity but lower selectivity, and the niobium analogue was significantly less reactive (Table VI-8, entry 2). Other *gem*-dialkyl activated substrates were cyclized with selectivities of up to 81% ee (Table VI-8, entry 7). Similar to many previously known catalyst systems,^{17,20,51,65,66} the cyclization of aminohexene derivatives, such as **106**, proceeded with significantly diminished selectivity, due to the higher flexibility of the cyclization transition state relative to that of the cyclization of aminopentenes. While the catalytic activity of complexes **127-M** in the hydroamination/cyclization of aminoalkenes is significantly lower than that of rare-earth,^{51,67,68} alkaline,^{69,70} and alkaline earth^{32,38,71-73} metal-based hydroamination catalysts, the reactivity is quite comparable to many group 4 metal-based catalyst systems with an exception of few very reactive^{19,74} (See also Chapter 4) zirconium-based systems. However, there are only a limited number of catalyst systems that provide enantioselectivities exceeding 80% ee in these types of cyclization.^{17,33,51,65}

Attempts to cyclize aminoheptene **108e**, 1,2-disubstituted alkenylamine **114**, or the secondary aminoalkene **136** were unsuccessful. With only few exceptions⁷⁵⁻⁷⁷ most neutral group 4 metal-based catalysts are unable to cyclize secondary aminoalkenes,

which has been interpreted as evidence for a [2+2]-cycloaddition mechanism analogous to group 4 metal-catalyzed alkyne and allene hydroaminations,⁷⁸⁻⁸² as the secondary amine does not allow formation of a metal imido species required in this mechanism. However, previous mechanistic studies were unable to confirm an analogous [2+2]-cycloaddition mechanism in case of the amine addition to alkynes catalyzed by cationic tantalum imido complexes.^{58,59,83}

Examples of selective azepane ring formation through hydroamination are also rare^{19,77} and it is noteworthy that no hydroaminoalkylation was observed for **108** and **136** using either **127a-Ta** or **127a-Nb** in contrast to group 4 metal-based systems^{6,8,9,64} that often produce mixtures of hydroamination and hydroaminoalkylation products when applied to aminohexenes or aminoheptenes.

Overall, herein we have presented one of the the first examples of asymmetric aminoalkene hydroamination catalyzed by group 5 metal complexes. Although the reactivity was found to be low compared to the best catalysts in the field, the absence of competing hydroaminoalkylation was notable.

VI.4 Conclusions

Group 5 metal binaphtholate complexes are highly active catalysts in the intermolecular hydroaminoalkylation of unactivated alkenes with secondary amines. The reaction proceeds with high enantio- and regioselectivity (up to 98% ee, branched products formed exclusively). The strong preference to activate primary amine α -C-H bonds originate from steric constraints hampering alkene insertion, as demonstrated by isotopic labeling experiments. Mechanistic studies suggest that the reaction proceeds via a reversible, non-dissociative formation of a six-coordinate metallaaziridine species,

which undergoes facile alkene insertion and subsequent intramolecular protonolysis. Kinetic studies are supportive of a monometallic catalytic pathway with either alkene insertion or amide exchange serving as a rate-determining step. The amide exchange step is marked by a primary KIE whereas essentially no KIE was observed for the aziridine formation/olefin insertion/protonolysis sequence. The latter result is in remarkable contrast to previous findings in metallaaziridine chemistry and should originate from stereoelectronic effects of the binaphtholate ligand. Simulation experiments show a good fit of the proposed kinetic model to the original kinetic data. Reversible non-productive events include amine coordination to the catalytically active species and C–H activation of the aromatic ring by the tantalum catalysts. All turnover and equilibrium constants displayed nonlinear dependence on the electronic properties of the amine substrate. Evidence of an electron-acceptor ligand favoring the amide exchange process was obtained, which can be used as a guideline for future catalyst developments.

In addition, we have demonstrated a first example of an enantioselective (up to 81% ee) cyclohydroamination of aminoalkenes catalyzed by group 5 metal binaphtholates.

VI.5 Experimental

General considerations. All reactions with air- or moisture sensitive materials were performed in oven (120 °C) and flame-dried glassware under an inert atmosphere of argon, employing standard Schlenk and glovebox techniques. Hexanes, pentane and THF were sparged with argon for 1 h and then passed through a column with activated alumina prior to use. Alkenes, benzene and C₆D₆ were vacuum transferred from sodium/benzophenone ketyl. Amines were distilled twice from finely powdered CaH₂. The metal amides M(NMe₂)₅ (M = Nb, Ta) [Strem] and all other commercially available starting materials were used as received unless stated otherwise.

¹H, ²H{¹H}, ¹³C{¹H} and ¹⁹F NMR spectra were recorded on Varian (300, 400, 500 MHz) spectrometers at 25 °C unless stated otherwise. Chemical shifts are reported in ppm downfield from tetramethylsilane with the signal of the deuterated (¹³C, ²H) or undeuterated (¹H) portion of the solvent as internal standard. Mass spectra were recorded on a Finnigan LCQ-DUO mass spectrometer. HPLC analysis was carried out on an Agilent 1200 series instrument with multiple wavelength detector using Chiralcel OD-H, OJ-H, and Chiralpak AS-H columns (25 × 4.6 mm). Silica gel (230–400 mesh, Sorbent Technologies) and alumina (80–200 mesh, EMD) were used for column chromatography. Elemental analyses were performed by Robertson Microlit Laboratories, Inc., Ledgewood, NJ.

(*S*)-Mosher acid was transformed into the corresponding (*R*)-Mosher acid chloride according to a literature protocol.⁸⁵

The aminoalkene substrates 2,2-diphenylpent-4-enyl amine (**105**),⁸⁶ 2,2-dimethylpent-4-enyl amine (**4**),⁸⁷ (1-allylcyclohexyl)methylamine (**18**),⁸⁸ 2,2-diphenylhex-5-enyl

amine (**106**),⁸⁹ 2,2-diphenylhept-6-enyl amine (**108**),⁹⁰ 2,2,5-triphenylpent-4-enyl amine (**114**)⁹¹ and *N*-benzyl-2,2-diphenylpent-4-enyl amine (**140**)⁸⁸ were synthesized according to literature protocols. The hydroamination products 2,4,4-trimethylpyrrolidine (**5**),³⁰ 3-methyl-2-azaspiro[4,5]decane (**19**),⁹² 2-methyl-4,4-diphenylpyrrolidine (**16**),⁸⁶ and 2-methyl-5,5-diphenylpiperidine (**107**)⁸⁶ are known compounds and were identified by comparison to the literature NMR spectroscopic data. The absolute configuration of the hydroamination products were determined by comparison of the ¹⁹F NMR spectroscopic data with the assignments reported previously.⁵¹

Ligand Synthesis

Methyldiisopropylchlorosilane,⁹³ (*R*)-2,2'-bis(methoxymethoxy)-1,1'-binaphthyl,⁹⁴ (*R*)-3,3'-dibromo-2,2'-dihydroxy-1,1'-binaphthyl, (*R*)-3,3'-bis(triphenylsilyl)-2,2'-dihydroxy-1,1'-binaphthyl (**78a**), (*R*)-3,3'-bis[*tert*-butyl(dimethyl)silyl]-2,2'-dihydroxy-1,1'-binaphthyl (**78l**), and (*R*)-3,3'-bis(trimethylsilyl)-2,2'-dihydroxy-1,1'-binaphthyl (**78m**) were prepared according to literature protocols.⁹⁵ Proligand **78j** was prepared as described in Chapter 3.

Benzyldiphenylchlorosilane.⁹⁶ A solution of benzyl magnesium chloride (49 mmol), prepared from magnesium turnings (1.46 g, 60 mmol) and benzyl chloride (5.6 mL, 49 mmol) in Et₂O (50 mL), was added dropwise at 0°C to a solution of dichlorodiphenylsilane (9.9 mL, 50 mmol) in Et₂O (50 mL) over 30 min. The resulting suspension was heated to a reflux, and stirred at reflux for 2 h, cooled to room temperature and concentrated. The residue was dissolved in CH₂Cl₂ (100 mL) and

filtered through a short pad of celite. The filtrate was concentrated *in vacuo* and crystallized from pentane to yield 10.29 g (69%) of product in form of large off-white crystals. ^1H NMR (400 MHz, CDCl_3): δ = 7.59–7.51 (m, 4H), 7.49–7.32 (m, 6H), 7.19–7.05 (m, 3H), 7.00–6.93 (m, 2H, aryl-H), 2.89 (s, 2H, CH_2); $^{13}\text{C}\{^1\text{H}\}$ NMR (CDCl_3 , 100 MHz): δ = 135.8, 134.6, 132.7, 130.6, 129.2, 128.1, 128.0, 125.1 (aryl), 26.5 (CH_2).

General procedure for the preparation of ligands 78e and 78k. To a solution of (*R*)-3,3'-dibromo-2,2'-dihydroxy-1,1'-binaphthyl (400 mg, 0.90 mmol) in THF (20 mL) was added KH (80 mg, 2.0 mmol) under stirring. The mixture was stirred at room temperature for 30 minutes and then the trialkylchlorosilane (1.85 mmol) was added. The mixture was stirred overnight at room temperature, cooled down to $-78\text{ }^\circ\text{C}$ and a *t*-butyl lithium solution (2.5 mL, 3.7 mmol, 1.5 M in pentane) was added dropwise. The yellow solution was stirred for 5 min at $-78\text{ }^\circ\text{C}$ and was then allowed to reach room temperature slowly, after which it was stirred for an additional hour. The reaction was quenched with saturated aqueous NH_4Cl (50 mL) and the product was extracted with Et_2O ($3 \times 20\text{ mL}$). The combined organic layers were dried (Na_2SO_4) and concentrated. The product was purified using column chromatography on silica (hexanes/ CH_2Cl_2 70:30), to afford the pure diol proligand.

(*R*)-3,3'-Bis[benzyl(diphenyl)silyl]-2,2'-dihydroxy-1,1'-binaphthyl ((*R*)-**H₂BINOL-SiPh₂Bn, 78e**). White powder (350 mg, 47% overall yield); mp $129\text{--}132\text{ }^\circ\text{C}$. ^1H NMR (C_6D_6 , 400 MHz): δ = 8.11 (s, 2H), 7.7–7.59 (m, 8H), 7.38–7.32 (d, $^3J(\text{H,H}) = 7.9\text{ Hz}$, 2H), 7.31–6.90 (m, 28H), 4.83 (s, 2H, OH), 3.22 (d, $^2J(\text{H,H}) = 13.8\text{ Hz}$, 2H,

CH₂), 3.16 (d, $^2J(\text{H,H}) = 13.8$ Hz, 2H, CH₂); $^{13}\text{C}\{^1\text{H}\}$ NMR (C₆D₆, 125 MHz): $\delta = 157.2$ (CO), 142.0, 139.3, 136.4, 136.35, 135.3, 135.06, 135.01, 129.82, 129.78, 129.6, 129.4, 128.5, 128.43, 128.38, 128.29, 128.14, 128.08, 124.9, 124.18, 124.14, 110.6, 23.9 (CH₂).
 Anal. Calcd for C₅₈H₄₆O₂Si₂: C, 83.81; H, 5.58; Found: C, 83.71; H, 5.33.

((R)-3,3'-Bis[diisopropyl(methyl)silyl]-2,2'-dihydroxy-1,1'-binaphthyl ((R)-H₂BINOL-Si(*i*-Pr)₂Me, 78k). Viscous, colorless oil (417 mg, 65% yield), does not solidify after prolonged storage at -30 °C. ^1H NMR (CDCl₃, 500 MHz): $\delta = 8.06$ (s, 2H), 7.89 (d, $^3J(\text{H,H}) = 7.8$ Hz, 2H), 7.37–7.34 (m, 2H), 7.30–7.26 (m, 2H), 7.09 (d, $^3J(\text{H,H}) = 8.3$ Hz, 2H, aryl-H), 5.20 (s, 2H, OH), 1.44–1.36 (m, 4H, 4 CH(CH₃)₂), 1.06 (d, $^2J(\text{H,H}) = 2.6$ Hz, 6H, 2 CH₃CH), 1.05 (d, $^2J(\text{H,H}) = 2.6$ Hz, 6H, 2 CH₃CH), 0.98 (d, $^2J(\text{H,H}) = 4.4$ Hz, 6H, 2 CH₃CH), 0.97 (d, $^2J(\text{H,H}) = 4.4$ Hz, 6H, 2 CH₃CH), 0.37 (s, 6H, 2 SiCH₃); $^{13}\text{C}\{^1\text{H}\}$ NMR (CDCl₃, 125 MHz): $\delta = 157.0$ (CO), 139.4, 134.2, 129.2, 128.5, 127.6, 126.0, 123.8, 123.6, 109.4 (aryl), 18.53 (CH(CH₃)₂), 18.51 (CH(CH₃)₂), 18.23 (CH(CH₃)₂), 18.17 (CH(CH₃)₂), 12.0 (CH(CH₃)₂), 11.9 (CH(CH₃)₂), -9.8 (2 SiCH₃).

Complex Synthesis

Complex Syntheses – General Procedure for the NMR-Scale Preparation. To a mixture of diol proligand **78** (0.05 mmol) and M(NMe₂)₅ (M = Ta, Nb; 0.05 mmol) was added C₆D₆ (490 mg, 500 μL). The mixture was shaken vigorously and then left for 5 minutes at room temperature. Clean quantitative conversion to the diolate complex was confirmed by NMR spectroscopy. Aliquots of the resulting complex solution were used directly for the catalytic experiments.

[Ta{(R)-BINOL-SiPh₃}(NMe₂)₃(HNMe₂)] (127a-Ta). This known compound²³ was prepared in situ only. ¹H NMR (400 MHz, C₆D₆): δ = 8.09 (s, 2H), 7.85–7.80 (m, 12H), 7.40 (d, ³J(H,H) = 7.8 Hz, 2H), 7.28 (d, ³J(H,H) = 8.3 Hz, 2H), 7.15–7.09 (m, 18H), 6.93–6.85 (m, 4H, aryl-H), 2.79 (s, 18H, 3 NMe₂), 1.78 (s, 12H, 2 HNMe₂); ¹³C{¹H} NMR (100 MHz, C₆D₆): δ = 165.9 (CO), 141.5, 138.5, 137.1, 136.9, 129.3, 128.5, 128.4, 127.0, 126.3, 125.4, 122.5, 119.8 (aryl), 46.8 (3 NMe₂), 39.7 (2 HNMe₂).

[Nb{(R)-BINOL-SiPh₃}(NMe₂)₃(HNMe₂)] (127a-Nb). The proligand **78a** (49.0 mg, 0.061 mmol) and Nb(NMe₂)₅ (19.1 mg, 0.061 mmol) were dissolved in warm benzene (350 μL). The mixture was shaken vigorously and layered with pentane (400 μL). The vial was sealed and kept at room temperature overnight. The precipitate was filtered off and dried to yield 37.1 mg (56%) of **127a-Nb** in the form of dark-red crystals. ¹H NMR (500 MHz, C₆D₆): δ = 8.05 (s, 2H), 7.85–7.80 (m, 12H), 7.41 (d, ³J(H,H) = 7.8 Hz, 2H), 7.29 (d, ³J(H,H) = 8.6 Hz, 2H), 7.15–7.08 (m, 18H), 6.94–6.86 (m, 4H, aryl-H), 2.43 (s, 18H, 3 NMe₂), 2.01 (s, 6H, HNMe₂); ¹³C{¹H} NMR (125 MHz, C₆D₆): δ = 167.1 (CO), 141.0, 138.0, 137.2, 137.0, 129.3, 128.6, 128.3, 127.9, 126.5, 126.0, 122.5, 119.8 (aryl), 47.0 (3 NMe₂), 39.3 (HNMe₂). Anal. Calcd for C₆₄H₆₅N₄O₂Si₂Nb: C, 71.75; H, 6.12; N, 5.23. Found: C, 72.28; H, 6.51; N, 4.64.

[Ta{(R)-BINOL-SiPh₂Bn}(NMe₂)₃(HNMe₂)] (127e-Ta). The proligand **78e** (33.0 mg, 0.039 mmol) and Ta(NMe₂)₅ (13.9 mg, 0.039 mmol) were dissolved in warm benzene (250 μL). The mixture was shaken vigorously and layered with hexanes (200

μL). The vial was sealed and kept at room temperature overnight. The precipitate was filtered off and dried to yield 40.0 mg (86%) of **127e-Ta** in the form of yellow crystals. ^1H NMR (500 MHz, C_6D_6): δ = 8.03 (s, 2H), 7.75–7.70 (m, 4H), 7.38 (d, $^3J(\text{H,H})$ = 7.6 Hz, 2H), 7.35 (d, $^3J(\text{H,H})$ = 6.4 Hz, 4H), 7.29 (d, $^3J(\text{H,H})$ = 7.8 Hz, 4H), 7.23–7.18 (m, 10H), 7.14–7.11 (m, 4H), 7.06 (t, $^3J(\text{H,H})$ = 7.6 Hz, 4H), 7.01 (t, $^3J(\text{H,H})$ = 6.9 Hz, 4H), 6.97–6.91 (m, 6H, aryl-H), 3.69 (d, $^2J(\text{H,H})$ = 13.2 Hz, 2H, SiCH_2Ph), 2.84 (s, 18H, 3NMe₂), 2.83 (d, $^2J(\text{H,H})$ = 13.2 Hz, 2H, SiCH_2Ph), 2.06 (s, 6H, HNMe₂); $^{13}\text{C}\{^1\text{H}\}$ NMR (125 MHz, C_6D_6): δ = 165.4 (CO), 140.7, 139.7, 137.1, 136.7, 136.4, 135.9, 129.8, 129.6, 129.5, 129.4, 128.6, 128.5, 128.3, 128.2, 127.6, 127.0, 126.7, 126.4, 124.7, 123.1, 119.8 (aryl), 45.5 (3 NMe₂), 39.3 (HNMe₂), 23.8 (CH₂). Anal. Calcd for C₆₆H₆₉N₄O₂Si₂Ta: C, 66.76; H, 5.86; N, 4.72 Found: C, 66.95; H, 5.61; N, 4.18.

[Nb{(R)-BINOL-SiPh₂Bn}(NMe₂)₃(HNMe₂)] (**127e-Nb**). The proligand **78e** (60.0 mg, 0.072 mmol) and Nb(NMe₂)₅ (22.6 mg, 0.072 mmol) were dissolved in warm benzene (450 μL). The mixture was shaken vigorously and layered with pentane (300 μL). The vial was sealed and kept at room temperature overnight. The precipitate was filtered off and dried to yield 58.3 mg (74%) of **127e-Nb** in the form of orange crystals. ^1H NMR (500 MHz, C_6D_6): δ = 8.00 (s, 2H), 7.74–7.72 (m, 4H), 7.41–7.39 (m, 2H), 7.36–7.33 (m, 4H), 7.23–7.19 (m, 8H), 7.18–7.14 (m, 4H), 7.11–7.07 (m, 4H), 7.03 (t, $^3J(\text{H,H})$ = 7.6 Hz, 4H), 7.00–6.94 (m, 6H, aryl-H), 3.67 (d, $^2J(\text{H,H})$ = 13.2 Hz, 2H, SiCH_2Ph), 2.79 (d, $^2J(\text{H,H})$ = 13.2 Hz, 2H, SiCH_2Ph), 2.69 (s, 18H, 3 NMe₂), 2.15 (s, 6H, HNMe₂); $^{13}\text{C}\{^1\text{H}\}$ NMR (125 MHz, C_6D_6): δ = 166.9 (CO), 140.4, 139.6, 137.3, 137.1, 137.0, 136.3, 136.0, 129.7, 129.50, 129.45, 129.4, 128.6, 128.4, 128.3, 127.6, 126.9,

126.7, 126.1, 124.6, 122.9, 119.9 (aryl), 46.6 (3 NMe₂), 39.0 (HNMe₂), 24.0 (CH₂). Anal. Calcd for C₆₆H₆₉N₄O₂Si₂Nb: C, 72.11; H, 6.33; N, 5.10. Found: C, 72.24; H, 6.49; N, 4.72.

[Ta{(R)-BINOL-SiPh₂Me}(NMe₂)₃(HNMe₂)] (127j-Ta).²³ The proligrand (R)-H₂BINOL-SiPh₂Me **78j** (41.6 mg, 0.061 mmol) and Ta(NMe₂)₅ (24.6 mg, 0.061 mmol) were dissolved in warm benzene (350 μ L). The mixture was shaken vigorously and layered with hexanes (300 μ L). The vial was sealed and kept at room temperature overnight. The precipitate was filtered off and dried to yield 48.0 mg (76%) of **127j-Ta** in the form of yellow crystals. ¹H NMR (400 MHz, C₆D₆): δ = 7.93 (s, 2H), 7.71–7.65 (m, 8H), 7.38 (d, ³J(H,H) = 8.2 Hz, 2H), 7.26–7.22 (m, 8H), 7.09–7.06 (m, 6H), 6.94–6.85 (m, 4H, aryl-H), 2.94 (s, 18H, 3NMe₂), 1.96 (s, 6H, HNMe₂), 0.97 (s, 6H, 2 SiCH₃); ¹³C{¹H} NMR (100 MHz, C₆D₆): δ = 165.2 (CO), 139.9, 138.6, 138.0, 137.5, 136.1, 135.8, 129.4, 129.24, 129.16, 128.5, 128.2, 127.87, 127.85, 126.8, 126.6, 122.7, 119.5 (aryl), 46.3 (NMe₂), 39.9 (HNMe₂), –3.0 (Me).

[Nb{(R)-BINOL-SiPh₂Me}(NMe₂)₃(HNMe₂)] (127j-Nb). The proligrand (R)-H₂BINOL-SiPh₂Me **78j** (553.4 mg, 0.815 mmol) and Nb(NMe₂)₅ (255.0 mg, 0.815 mmol) were dissolved in warm benzene (2.0 mL). The mixture was stirred at 90 °C until complete dissolution. The mixture was cooled to room temperature, hexanes (1.0 mL) was layered on top of the solution and the vial was sealed and kept at room temperature overnight. The precipitate was filtered off and dried to yield 595 mg (77%) of **127j-Nb** as dark-red crystals. ¹H NMR (400 MHz, C₆D₆): δ = 7.91 (s, 2H), 7.69–7.62 (m, 8H), 7.40

(d, $^3J(\text{H,H}) = 7.8$ Hz, 2H), 7.31 (d, $^3J(\text{H,H}) = 8.2$ Hz, 2H), 7.22–7.19 (m, 6H), 6.96–6.88 (m, 6H), 6.94–6.85 (m, 4H, aryl-H), 2.70 (s, 18H, 3 NMe₂), 2.12 (s, 6H, HNMe₂), 0.95 (s, 6H, 2 SiCH₃); $^{13}\text{C}\{^1\text{H}\}$ NMR (100 MHz, C₆D₆): $\delta = 166.9$ (CO), 139.7, 138.5, 138.4, 137.3, 136.0, 135.7, 129.3, 129.2, 128.5, 128.1, 127.9, 127.6, 126.79, 126.76, 122.6, 119.6 (aryl), 47.1 (3 NMe₂) 39.1 (HNMe₂), –2.4 (SiMe). Anal. Calcd for C₅₄H₆₁N₄O₂Si₂Nb: C, 68.48; H, 6.49; N, 5.92. Found: C, 68.53; H, 6.71; N, 5.82.

[Ta{(R)-BINOL-Si*i*-Pr₂Me}(NMe₂)₃(HNMe₂)] (127k-Ta). To the solution of the proligand (R)-H₂BINOL-Si(*i*-Pr)₂Me **78k** (71.9 mg, 0.13 mmol) in pentane (200 μ L) was added a solution of Ta(NMe₂)₅ (53.1 mg, 0.13 mmol) in pentane (200 μ L). The vial was sealed and kept at –30°C overnight. The precipitate was collected and dried in vacuo to yield 50 mg (49%) of **127k-Ta** in the form of small yellow crystals. ^1H NMR (500 MHz, C₆D₆): $\delta = 8.09$ (s, 2H), 7.78 (d, $^3J(\text{H,H}) = 8.1$ Hz, 2H), 7.18–7.16 (m, 2H), 7.07 (t, $^3J(\text{H,H}) = 7.3$ Hz, 2H), 6.88 (t, $^3J(\text{H,H}) = 7.6$ Hz, 2H, aryl-H), 3.12 (s, 18H, 3 NMe₂), 2.13 (s, 6H, HNMe₂), 1.65 (sept, 2H, CH(CH₃)₂), 1.35 (sept, 2H, CH(CH₃)₂), 1.23 (d, $^2J(\text{H,H}) = 7.6$ Hz, 6H, 2 CH₃CH), 1.21–1.17 (m, 12H, 4 CH₃CH), 1.05 (d, $^2J(\text{H,H}) = 7.3$ Hz, 6H, 2 CH₃CH), 0.39 (s, 6H, 2 SiCH₃); $^{13}\text{C}\{^1\text{H}\}$ NMR (125 MHz, C₆D₆): $\delta = 165.0$ (CO), 136.8, 136.5, 129.4, 129.1, 128.1, 126.8, 126.4, 122.9, 119.4 (aryl), 45.7 (3 NMe₂), 39.1 (HNMe₂), 19.4, 19.2, 19.1, 18.6, 12.9, –9.8 (2 Si(CH₃)). Anal. Calcd for C₄₀H₆₂N₃O₂Si₂Ta (loss of HNMe₂): C, 56.25; H, 7.32; N, 4.92. Found: C, 54.78; H, 7.30; N, 4.68.

[Nb{(R)-BINOL-SiPr₂Me}(NMe₂)₃]□ (**127k-Nb**). To the solution of the proligand (R)-H₂BINOL-Si(*i*-Pr)₂Me **78k** (32.6 mg, 0.060 mmol) in pentane (200 μL) was added a solution of Nb(NMe₂)₅ (18.8 mg, 0.060 mmol) in pentane (200 μL). The vial was sealed and kept at -30°C overnight. The precipitate was collected and dried in vacuo to yield 17.0 mg (39%) of **127k-Nb** in the form of small orange crystals. ¹H NMR (500 MHz, C₆D₆): δ = 8.06 (s, 2H), 7.79 (d, ³J(H,H) = 8.1 Hz, 2H), 7.21 (d, ³J(H,H) = 8.6 Hz, 2H), 7.08 (t, ³J(H,H) = 7.4 Hz, 2H), 6.92–6.88 (m, 2H, aryl-H), 2.97 (s, 18H, 3 NMe₂), 1.60 (sept, 2H, CH(CH₃)₂), 1.31 (sept, 2H, CH(CH₃)₂), 1.22 (d, ²J(H,H) = 7.6 Hz, 6H, 2 CH₃CH), 1.21 (d, ²J(H,H) = 7.6 Hz, 6H, 2 CH₃CH), 1.21–1.17 (m, 9H, 3 CH₃CH), 1.05 (d, ²J(H,H) = 7.3 Hz, 6H, 2 CH₃CH), 0.35 (s, 6H, 2 SiCH₃); ¹³C{¹H} NMR (125 MHz, C₆D₆): δ = 166.7 (CO), 136.7, 136.6, 129.4, 128.8, 128.3, 126.8, 126.4, 122.7, 119.6 (aryl), 46.9 (3 NMe₂), 19.5, 19.2, 19.0, 18.6, 12.9, 11.8, -9.6 (2 SiCH₃). Anal. Calcd for C₄₀H₆₂N₃O₂Si₂Nb: C, 62.72; H, 8.16; N, 5.49. Found: C, 61.17; H, 7.93; N, 4.94.

[Ta{(R)-BINOL-SiMe₂*t*Bu}(NMe₂)₃] (**127l-Ta**). The proligand (R)-H₂BINOL-SiMe₂*t*Bu **78l** (42.7 mg, 0.082 mmol) and Ta(NMe₂)₅ (32.9 mg, 0.082 mmol) were dissolved in pentane (450 μL). The mixture was heated to 50 °C and slowly cooled to room temperature. The precipitate was filtered off and dried to yield 44.0 mg (64%) of **127l-Ta** as a yellow microcrystalline solid. ¹H NMR (400 MHz, C₆D₆): δ = 8.12 (s, 2H), 7.69 (d, ³J(H,H) = 7.8 Hz, 2H), 7.12 (d, ³J(H,H) = 8.6 Hz, 2H), 7.01 (vt, ³J(H,H) = 7.8, 7.0 Hz, 2H), 6.82 (t, ³J(H,H) = 7.8 Hz, 2H, aryl-H), 3.02 (s, 18H, 3 NMe₂), 1.06 (s, 18 H, 2 C(CH₃)₃), 0.49 (s, 6H, 2 SiCH₃), 0.43 (s, 6H, 2 SiCH₃); ¹³C{¹H} NMR (100 MHz, C₆D₆): δ = 165.1 (CO), 137.1, 136.5, 129.8, 129.3, 128.2, 126.9, 126.5, 123.0, 119.8

(aryl), 45.7 (3 NMe₂), 27.6 (2 C(CH₃)₃), 18.1 (2 C(CH₃)₃), -3.7 (SiCH₃), -4.0 (SiCH₃).
 Anal. Calcd for C₃₈H₅₈N₃O₂Si₂Ta: C, 55.25; H, 7.08; N, 5.09. Found: C, 54.68; H, 6.97; N, 4.96.

[Nb{(R)-BINOL-SiMe₂tBu}(NMe₂)₃] (127l-Nb). The proligand (R)-H₂BINOL-SiMe₂tBu **78l** (36.5 mg, 0.070 mmol) and Nb(NMe₂)₅ (22.2 mg, 0.070 mmol) were dissolved in hexanes (200 μL) and pentane (250 μL), respectively. After mixing, the solution was heated to 50 °C and slowly cooled to room temperature. The precipitate was filtered off and dried to yield 39.0 mg (75%) of **127l-Nb** as a yellow microcrystalline solid. ¹H NMR (400 MHz, C₆D₆): δ = 8.11 (s, 2H), 7.72 (d, ³J(H,H) = 8.2 Hz, 2H), 7.18 (d, ³J(H,H) = 8.6 Hz, 2H), 7.04 (vt, ³J(H,H) = 7.8 Hz, 7.0 Hz, 2H), 6.85 (t, ³J(H,H) = 7.8 Hz, 2H, aryl-H), 2.90 (s, 18H, 3 NMe₂), 1.08 (s, 18 H, 2 C(CH₃)₃), 0.49 (s, 6H, 2 SiCH₃), 0.40 (s, 6H, 2 SiCH₃); ¹³C{¹H} NMR (100 MHz, C₆D₆): δ = 166.8 (CO), 136.9, 136.7, 129.5, 129.2, 128.2, 127.6, 126.58, 126.5, 122.7, 120.0 (aryl), 47.1 (3 NMe₂), 27.6 (2 C(CH₃)₃), 18.1 (2 C(CH₃)₃), -3.6 (SiCH₃), -4.0 (SiCH₃). Anal. Calcd for C₃₈H₅₈N₃O₂Si₂Nb: C, 61.85; H, 7.92; N, 5.69. Found: C, 61.73; H, 8.13; N, 5.42.

[Ta{(R)-BINOL-SiMe₃}(NMe₂)₃(HNMe₂)] (127m-Ta).²³ To the solution of the proligand (R)-H₂BINOL-SiMe₃ **78m** (526 mg, 1.22 mmol) in hexanes (2 mL) was added a solution of Ta(NMe₂)₅ (488 mg, 1.22 mmol) in pentane (1 mL). The vial was sealed and heated to 80°C and then allowed to cool to room temperature. It was kept at this temperature overnight. The precipitate was collected and dried to yield 870 mg (89%) of **127m-Ta** in the form of large yellow crystals. ¹H NMR (500 MHz, C₆D₆): δ = 8.14 (s,

2H), 7.79 (d, $^3J(\text{H,H}) = 8.1$ Hz, 2H), 7.21 (d, $^3J(\text{H,H}) = 8.6$ Hz, 2H), 7.07 (vt, $^3J(\text{H,H}) = 7.8$, 6.9 Hz, 2H), 6.87 (vt, $^3J(\text{H,H}) = 8.6$, 6.9 Hz, 2H, aryl-H), 3.20 (s, 18H, 3 NMe₂), 2.00 (s, 3H, HNMe₂), 1.99 (s, 3H, HNMe₂), 1.04 (s, 1H, NH), 0.49 (s, 18H, 2 Si(CH₃)₃); ¹³C{¹H} NMR (125 MHz, C₆D₆): $\delta = 164.9$ (CO), 137.0, 136.1, 132.0, 129.2, 128.0, 127.0, 126.4, 122.7, 119.3 (aryl), 46.5 (3NMe₂), 40.0 (HNMe₂), -0.1 (Si(CH₃)₃).

[Nb{(R)-BINOL-SiMe₃}(NMe₂)₃(HNMe₂)] (127m-Nb). To the solution of the proligand (R)-H₂BINOL-SiMe₃ (431 mg, 1.10 mmol) in hexanes (2 mL) was added a solution of Nb(NMe₂)₅ (344 mg, 1.10 mmol) in pentane (2 mL). The vial was sealed and heated to 70°C and then allowed to cool to room temperature. It was kept at -30 °C overnight. The precipitate was collected and dried to yield 510 mg (66%) of **127m-Nb** in the form of dark-red crystals. ¹H NMR (500 MHz, C₆D₆): $\delta = 8.11$ (s, 2H), 7.79 (d, $^3J(\text{H,H}) = 7.8$ Hz, 2H), 7.28 (d, $^3J(\text{H,H}) = 8.6$ Hz, 2H), 7.09 (vt, $^3J(\text{H,H}) = 7.8$, 6.9 Hz, 2H), 6.89 (vt, $^3J(\text{H,H}) = 8.6$, 6.9 Hz, 2H, aryl-H), 2.97 (s, 18H, 3 NMe₂), 2.14 (s, 6H, HNMe₂), 0.46 (s, 18H, 2 Si(CH₃)₃); ¹³C{¹H} NMR (100 MHz, C₆D₆): $\delta = 166.6$ (CO), 136.8, 135.8, 132.1, 129.4, 127.6, 127.1, 126.3, 122.7, 119.4 (aryl), 47.3 (3 NMe₂), 39.2 (HNMe₂), 0.0 (Si(CH₃)₃). Anal.Calcd for C₃₂H₄₆N₃O₂Si₂Nb (loss of HNMe₂): C, 58.79; H, 7.09; N, 6.43. Found: C, 57.30; H, 7.17; N, 6.69.

General procedure for intermolecular hydroaminoalkylation. In a glovebox, a screw cap NMR tube was charged with amine (0.20 mmol), alkene (0.40 mmol, 2 equiv), and catalyst (0.01 mmol, 5 mol%) or an equivalent amount of 10 w% solution of the catalyst in C₆D₆. Additional C₆D₆ (0.3 mL) was added; the NMR tube was sealed,

removed from the glovebox and placed in the thermostated oil bath. The conversion was periodically monitored via ^1H NMR spectroscopy. After completion of the reaction, the crude reaction mixture was either concentrated or subjected to a column chromatography on silica or alumina or was subjected to *N*-benzoylation directly.

Derivatization of crude hydroaminoalkylation product (*Method A*). To a NMR tube containing the reaction mixture of a complete reaction was added CH_2Cl_2 (0.6 mL), followed by addition of DIPEA (77 mg, 0.6 mmol) and benzoyl chloride (56 mg, 0.4 mmol). The mixture was shaken and left at room temperature for 3 h. Volatiles were removed in vacuo and the residue was partitioned between Et_2O (2 mL) and 2M NaOH (2 mL). The resulting emulsion was stirred for 2 h, then the organic layer was separated, washed with brine (1 mL), dried (Na_2SO_4), and concentrated. Column chromatography on silica was performed to afford the target benzamide which was then used for HPLC analysis.

Derivatization of isolated hydroaminoalkylation product (*Method B*). The hydroaminoalkylation product (0.1 mmol) was dissolved in CH_2Cl_2 (1 mL) and then DIPEA (26 mg, 0.2 mmol) and benzoyl chloride (21 mg, 0.15 mmol) were added. The mixture was stirred at room temperature for 3 h. Volatiles were removed in vacuo and the residue was partitioned between Et_2O (2 mL) and 2M NaOH (2 mL). The resulting emulsion was stirred for 2 h and then the organic layer was separated, washed with brine (1 mL), dried (Na_2SO_4), and concentrated. The residue was purified by flash

chromatography on silica (CH_2Cl_2), if necessary, or was directly subjected to chiral HPLC analysis.

Determination of enantiomeric excess via Mosher amide formation. The isolated hydroaminoalkylation product (0.05 mmol) was dissolved in CHCl_3 (0.5 mL) and then DIPEA (52 mg, 0.4 mmol) and (*R*)-Mosher acid chloride (5 mg, 0.2 mmol) were added. The mixture was kept at 40 °C for 4 hours, after which the volatiles were removed. The residue was dissolved in Et_2O (2 mL) and passed through a short (0.5 cm) silica plug followed by eluting with additional 10 mL of Et_2O . The eluate was concentrated, dissolved in CDCl_3 or CD_3CN and the ^1H NMR spectrum was recorded to obtain the enantiomeric excess.

Determination of enantiomeric excess via debenzylation/Mosher amide formation sequence.²² The isolated hydroaminoalkylation product (0.03 mmol) was dissolved in absolute ethanol (2 mL). Ammonium formate (32 mg, 0.5 mmol) and 10% palladium on charcoal (11 mg, 0.01 mmol) were added, and the mixture was stirred at reflux for 40 min. The precipitate was filtered off, and the filtrate was treated with 1M HCl (2 mL). The volatiles were removed *in vacuo*, the residue was dissolved in water (10 mL) and then water was removed under reduced pressure. The residue was then dissolved in C_6D_6 (0.6 mL) and filtered through a short pad of celite into the NMR tube containing (*R*)-Mosher acid chloride (10 mg, 0.04 mmol) and DIPEA (26 mg, 0.2 mmol). A ^{19}F NMR spectrum was then taken to determine the enantiomeric excess.

***N*-(2-methyl-4-phenylbutyl)aniline (129).** Prepared from *N*-methylaniline and 4-phenyl-1-butene according to Table VI-4, entry 2. Purified by column chromatography on silica (hexanes/Et₂O 100:1). Yield 71%, colorless oil. ¹H NMR (500 MHz, CDCl₃): δ = 7.31–7.27 (m, 2H), 7.20–7.15 (m, 5H), 6.68 (t, ³*J*(H,H) = 7.3 Hz, 2H), 6.59 (d, ³*J*(H,H) = 8.6 Hz, aryl-H), 3.65 (br s, 1H, NH), 3.09 (dd, ²*J*(H,H) = 12.2 Hz, ³*J*(H,H) = 5.9 Hz, 1H, NCH₂), 2.95 (dd, ²*J*(H,H) = 12.2 Hz, ³*J*(H,H) = 6.9 Hz, 1H, NCH₂), 2.77–2.71 (m, 1H), 2.65–2.59 (m, 1H), 1.84–1.77 (m, 2H), 1.57–1.49 (m, 1H), 1.05 (d, ³*J*(H,H) = 6.6 Hz, 3H, CH₃); ¹³C{¹H} NMR (125 MHz, CDCl₃): δ = 148.5, 142.5 (*C*_{ipso}), 129.2, 128.34, 128.31, 125.8, 117.0, 112.6 (aryl-CH), 50.2 (CH₂N), 36.6 (CH), 33.3, 32.6, (CH₂), 18.0 (CH₃). MS (ESI): *m/z* 240.2 [M+ H]⁺.

***N*-(2-methyl-4-phenylbutyl)-*N*-phenylbenzamide.** Derivatization by method **B**. Purified by flash chromatography on silica (Hexanes/EtOAc 20:1) to give a colorless oil in 91% yield. HPLC (AS-H, hexane/2-propanol 98:2, 1.0 mL/min): *t*_R 39.0 min (major), 43.6 (minor); indicating 70% ee. ¹H NMR (500 MHz, CDCl₃): δ = 7.26–7.19 (m, 4H), 7.17–7.07 (m, 9H), 6.93 (d, ³*J*(H,H) = 7.8 Hz, 2H, aryl-H), 3.99 (dd, ²*J*(H,H) = 13.5 Hz, ³*J*(H,H) = 6.9 Hz, 1H, NCH₂), 3.85 (dd, ²*J*(H,H) = 13.5 Hz, ³*J*(H,H) = 7.7 Hz, 1H, NCH₂), 2.72–2.66 (m, 1H), 2.54–2.68 (m, 1H), 1.84–1.72 (m, 2H), 1.56–1.48 (m, 1H), 1.01 (d, ³*J*(H,H) = 6.1 Hz, 3H, CH₃); ¹³C{¹H} NMR (125 MHz, CDCl₃): δ = 170.7 (CO), 143.4, 142.5, 136.6 (*C*_{ipso}), 129.2, 129.0, 128.5, 128.4, 128.3, 127.7, 127.6, 126.5, 125.6 (aryl-CH), 55.2 (CH₂N), 36.2 (CH), 33.1, 31.3 (CH₂), 17.5 (CH₃). MS (ESI): *m/z* 240.2 [M-PhCO+ H]⁺.

***N*-(2-methyloctyl)-*N*-phenylbenzamide.**¹⁴ Prepared from *N*-methylaniline and 1-octene according to Table VI-3, entry 7. Derivatization by method **A**, gave a colorless oil in 92% yield. HPLC (AS-H, hexane/2-propanol 98.5:1.5, 0.5 mL/min): t_R 51.5 min (minor), 60.0 min (major); indicating 81% ee. ^1H NMR (400 MHz, CDCl_3): δ = 7.25–7.22 (m, 2H), 7.20–7.15 (m, 3H), 7.00 (d, $^3J(\text{H,H})$ = 7.1 Hz, 2H, aryl-H), 3.87–3.76 (m, 2H, CH_2N), 1.77–1.69 (m, 1H CHCH_3), 1.41–1.11 (m, 10H, 5 CH_2), 0.92 (d, $^3J(\text{H,H})$ = 6.7 Hz, 3H, CH_3CH), 0.84 (t, $^3J(\text{H,H})$ = 6.7 Hz, 3H, CH_3CH_2); $^{13}\text{C}\{^1\text{H}\}$ NMR (100 MHz, CDCl_3): δ = 170.7 (CO), 136.7, 129.2, 129.0, 128.5, 127.7, 127.6, 126.4 (aryl), 55.7 (CH_2N), 34.3, 31.8, 31.7, 29.5, 26.7, 22.6, 17.5 (CH_3CH), 14.1 (CH_3CH_2).

***N*-(4-fluorophenyl)-*N*-(2-methyloctyl)benzamide.** Prepared from 4-fluoro-*N*-methylaniline and 1-octene according to Table VI-4, entry 6. Derivatization by method **A**, gave a colorless oil in 89% yield. HPLC (AS-H, hexane/2-propanol 98.5:1.5, 1 mL/min): t_R 25.2 min (minor), 30.6 min (major); indicating 82% ee. ^1H NMR (500 MHz, CDCl_3 , 65 °C): δ = 7.26–7.15 (m, 5H), 7.02–6.98 (m, 2H), 6.80 (t, $^3J(\text{H,H})$ = 8.3 Hz, 2H, aryl-H), 3.81 (dd, $^2J(\text{H,H})$ = 13.5 Hz, $^3J(\text{H,H})$ = 8.5 Hz, 1H, NCH_2), 3.78 (dd, $^2J(\text{H,H})$ = 13.5 Hz, $^3J(\text{H,H})$ = 6.3 Hz, 1H, NCH_2), 1.82–1.76 (m, 1H CHCH_3), 1.45–1.19 (m, 10H, 5 CH_2), 0.96 (d, $^3J(\text{H,H})$ = 6.8 Hz, 3H, CH_3CH), 0.89 (t, $^3J(\text{H,H})$ = 6.7 Hz, 3H, CH_3CH_2); $^{13}\text{C}\{^1\text{H}\}$ NMR (125 MHz, CDCl_3 , 65 °C): δ = 170.8 (CO), 160.9 (d, $^1J(\text{C,F})$ = 247 Hz, CF), 140.0, 136.9, 129.4 (br), 128.5, 127.8, 115.9 (d, $^2J(\text{C,F})$ = 22 Hz, aryl), 56.1 (CH_2N), 34.6, 31.9, 31.8, 29.5, 26.8, 22.6, 17.6 (CH_3CH), 13.9 (CH_3CH_2). MS (ESI): m/z 342.2 $[\text{M} + \text{H}]^+$.

***N*-(4-chlorophenyl)-*N*-(2-methyloctyl)benzamide.** Prepared from 4-chloro-*N*-methylaniline and 1-octene according to Table VI-4, entry 7. Derivatization by method A, gave a colorless oil in 90% yield. HPLC (AS-H, hexane/2-propanol 98.5:1.5, 1 mL/min): t_R 21.1 min (minor), 25.7 min (major); indicating 67% ee. 1H NMR (500 MHz, $CDCl_3$): δ = 7.24–7.21 (m, 3H), 7.18–7.14 (m, 4H), 6.95 (d, $^3J(H,H)$ = 8.6 Hz, 2H, aryl-H), 3.81 (dd, $^2J(H,H)$ = 13.5 Hz, $^3J(H,H)$ = 8.5 Hz, 1H, NCH_2), 3.76 (dd, $^2J(H,H)$ = 13.5 Hz, $^3J(H,H)$ = 6.9 Hz, 1H, NCH_2), 1.75–1.67 (m, 1H $CHCH_3$), 1.41–1.12 (m, 10H, 5 CH_2), 0.92 (d, $^3J(H,H)$ = 6.6 Hz, 3H, CH_3CH), 0.86 (t, $^3J(H,H)$ = 6.6 Hz, 3H, CH_3CH_2); $^{13}C\{^1H\}$ NMR (125 MHz, $CDCl_3$, 65 °C): δ = 170.7 (CO), 142.7, 136.7, 132.2, 129.5, 129.2, 129.0, 128.5, 127.9 (aryl), 56.0 (CH_2N), 34.6, 32.0, 31.8, 29.5, 26.8, 22.6, 17.6 (CH_3CH), 13.9 (CH_3CH_2). MS (ESI): m/z 358.2 [$M+H$] $^+$.

***N*-(4-methoxyphenyl)-*N*-(2-methyloctyl)benzamide.** Prepared from 4-methoxy-*N*-methylaniline and 1-octene according to Table VI-4, entry 8. Derivatization by method A, gave a colorless oil in 89% yield. HPLC (OJ-H, hexane/2-propanol 99:1, 0.25 mL/min): t_R 46.0 min (minor), 52.1 min (major); indicating 74% ee. 1H NMR (400 MHz, $CDCl_3$, 65 °C): δ = 7.30–7.23 (m, 5H), 6.93 (d, $^3J(H,H)$ = 9.0 Hz, 2H), 6.73–6.70 (m, 2H, aryl-H), 3.85–3.75 (m, 2H, NCH_2), 3.73 (s, 3H, CH_3O), 1.84–1.75 (m, 1H, $CHCH_3$), 1.46–1.20 (m, 10H, 5 CH_2), 0.95 (d, $^3J(H,H)$ = 6.7 Hz, 3H, CH_3CH), 0.88 (t, $^3J(H,H)$ = 6.7 Hz, 3H, CH_3CH_2); $^{13}C\{^1H\}$ NMR (100 MHz, $CDCl_3$, 65 °C): δ = 170.8 (CO), 158.1, 137.3, 129.0, 128.9, 128.4, 127.6, 114.4, 114.2 (aryl), 56.1 (CH_3O), 55.4 (CH_2N), 34.6, 31.83, 31.77, 29.5, 26.8, 22.6, 17.6 (CH_3CH), 13.9 (CH_3CH_2). MS (ESI): m/z 354.2 [$M+H$] $^+$.

***N*-(3-cyclopentyl-2-methylpropyl)-4-methoxyaniline (131).** Prepared from *N*-methylaniline and allylcyclopentane according to Table VI-4, entry 10. Purified by column chromatography on alumina (hexanes/EtOAc 100:0.5) to give a yellow oil, which readily turns dark-brown in air, in 89% yield. ^1H NMR (400 MHz, CDCl_3): δ = 6.78 (d, $^3J(\text{H,H})$ = 9.0 Hz, 2H), 6.57 (d, $^3J(\text{H,H})$ = 9.0 Hz, 2H, aryl-H), 3.75 (s, 3H, CH_3O), 3.02 (dd, $^2J(\text{H,H})$ = 11.7 Hz, $^3J(\text{H,H})$ = 5.5 Hz, 1H, NCH_2), 2.83 (dd, $^2J(\text{H,H})$ = 11.7 Hz, $^3J(\text{H,H})$ = 7.4 Hz, 1H, NCH_2), 1.93–1.83 (m, 1H, CH), 1.80–1.71 (m, 3H), 1.64–1.49 (m, 4H), 1.41–1.35 (m, 1H), 1.26–1.19 (m, 2H), 1.13–1.00 (m, 3H), 0.97 (d, $^3J(\text{H,H})$ = 6.7 Hz, 3H, CH_3); $^{13}\text{C}\{^1\text{H}\}$ NMR (100 MHz, CDCl_3): δ = 151.8 (CO), 143.0 (C_{ipso}), 114.9, 113.9 (aryl-CH), 55.9 (CH_3O), 51.7 (CH_2N), 41.5, 37.6, 33.4, 32.6, 32.1, 25.13, 25.11, 18.3 (CH_3CH). MS (ESI): m/z 248.1 $[\text{M} + \text{H}]^+$.

***N*-(3-cyclopentyl-2-methylpropyl)-*N*-(4-methoxyphenyl)benzamide.**

Derivatization by method **B**. Purified by flash chromatography on silica (CH_2Cl_2) to give a colorless oil in 91% yield. HPLC (AS-H, hexane/2-propanol 90:10, 1 mL/min): t_R 20.7 min (major), 35.0 min (minor); indicating 81% ee. ^1H NMR (500 MHz, C_6D_6): δ = 7.47–7.44 (m, 2H), 6.93–6.88 m, 3H), 6.78 (d, $^3J(\text{H,H})$ = 9.0 Hz, 2H), 6.46 (d, $^3J(\text{H,H})$ = 9.0 Hz, 2H, aryl-H), 3.94 (dd, $^2J(\text{H,H})$ = 13.0 Hz, $^3J(\text{H,H})$ = 8.7 Hz, 1H, NCH_2), 3.87 (dd, $^2J(\text{H,H})$ = 13.0 Hz, $^3J(\text{H,H})$ = 6.4 Hz, 1H, NCH_2), 3.09 (s, 3H, CH_3O), 1.98–1.92 (m, 1H, CH), 1.83–1.77 (m, 1H), 1.74–1.69 (m, 1H), 1.66–1.60 (m, 1H), 1.58–1.51 (m, 2H), 1.49–1.39 (m, 3H), 1.07–0.93 (m, 2H), 1.04 (d, $^3J(\text{H,H})$ = 6.6 Hz, 3H, CH_3); $^{13}\text{C}\{^1\text{H}\}$ NMR (125 MHz, C_6D_6): δ = 170.1 (C=O), 158.0 (CO), 137.9, 137.3, 129.2, 129.1, 129.0,

114.4 (aryl), 56.2 (CH₃O), 54.7 (CH₂N), 41.5, 37.9, 33.7, 32.8, 31.3, 25.42, 25.39, 18.2 (CH₃CH). MS (ESI): m/z 352.3 [M+ H]⁺.

***N*-(2-cyclohexylpropyl)aniline (132a).** Prepared from *N*-methylaniline and vinylcyclohexane according to Table VI-4, entry 12. Purified by column chromatography on alumina (pentane). Yield 92%, colorless oil. ¹H NMR (400 MHz, CDCl₃): δ = 7.17 (vt, ³*J*(H,H) = 8.4, 7.4 Hz, 2H), 6.67 (vt, ³*J*(H,H) = 8.4, 7.4 Hz, 1H), 6.60 (d, ³*J*(H,H) = 8.4 Hz, 2H, aryl-H), 3.63 (br s, 1H, NH), 3.15 (dd, ²*J*(H,H) = 11.7 Hz, ³*J*(H,H) = 5.5 Hz, 1H, NCH₂), 2.88 (dd, ²*J*(H,H) = 11.7 Hz, ³*J*(H,H) = 7.5 Hz, 1H, NCH₂), 1.79–1.61 (m, 6H), 1.39–0.99 (m, 6H), 0.93 (d, ³*J*(H,H) = 7.0 Hz, 3H, CH₃); ¹³C{¹H} NMR (100 MHz, CDCl₃): δ = 148.7 (C_{ipso}), 129.2, 116.9, 112.6 (aryl-CH), 47.9 (CH₂N), 40.8 (CH), 38.0 (CH), 30.9, 28.6, 26.8, 26.71, 26.66 (CH₂, Cy), 14.8 (CH₃). MS (ESI): m/z 218.2 [M+ H]⁺.

***N*-(2-cyclohexylpropyl)-*N*-phenylbenzamide.¹⁴** Derivatization by method **B**. Purified by flash chromatography on silica (CH₂Cl₂) to give a colorless oil in 82% yield. HPLC (OD-H, hexane/2-propanol 99:1, 0.5 mL/min): t_R 24.8 min (minor), 26.2 (major); indicating 91% ee. ¹H NMR (400 MHz, CDCl₃): δ = 7.27–7.10 (m, 8H), 7.03 (d, ³*J*(H,H) = 7.4 Hz, 2H, aryl-H), 3.99 (dd, ²*J*(H,H) = 13.3 Hz, ³*J*(H,H) = 8.9 Hz, 1H, NCH₂), 3.85 (dd, ²*J*(H,H) = 13.3 Hz, ³*J*(H,H) = 5.9 Hz, 1H, NCH₂), 1.74–1.51 (m, 6H), 1.34–0.95 (m, 6H), 0.91 (d, ³*J*(H,H) = 7.1 Hz, 3H, CH₃); ¹³C{¹H} NMR (100 MHz, CDCl₃): δ = 170.7 (CO), 143.5 (C_{ipso}), 136.7 (C_{ipso}), 129.2, 128.9, 128.5, 127.7, 127.6, 126.4 (aryl-CH), 53.5 (CH₂N), 40.6 (CH), 36.6 (CH), 30.9, 28.2, 26.9, 26.7, 26.6 (CH₂, Cy), 13.9 (CH₃).

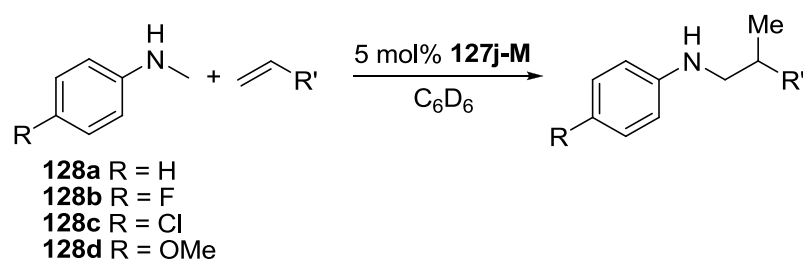
***N*-(2-cyclohexylpropyl)-4-fluoroaniline (132b).** Prepared from 4-fluoro-*N*-methylaniline and vinylcyclohexane according to Table VI-4, entry 13. Purified by column chromatography on alumina (hexanes) to give a colorless oil in 93% yield and 73% ee. ^1H NMR (400 MHz, CDCl_3): δ = 6.89–6.84 (m, 2H), 6.54–6.53 (m, 2H, aryl-H), 3.49 (br s, 1H, NH), 3.09 (dd, $^2J(\text{H,H}) = 12.1$ Hz, $^3J(\text{H,H}) = 5.5$ Hz, 1H, NCH_2), 2.84 (dd, $^2J(\text{H,H}) = 12.1$ Hz, $^3J(\text{H,H}) = 7.8$ Hz, 1H, NCH_2), 1.80–1.74 (m, 2H), 1.70–1.57 (m, 4H), 1.64–1.49 (m, 4H), 1.37–1.01 (m, 7H), 0.93 (d, $^3J(\text{H,H}) = 7.0$ Hz, 3H, CH_3); $^{13}\text{C}\{^1\text{H}\}$ NMR (100 MHz, CDCl_3): δ = 155.5 (d, $^1J(\text{C,F}) = 234.1$ Hz, CF), 145.0 (d, $^4J(\text{C,F}) = 2.0$ Hz, CN), 115.6 (d, $^2J(\text{C,F}) = 22.4$ Hz), 113.3 (d, $^3J(\text{C,F}) = 7.5$ Hz, aryl-CH), 48.6 (CH_2N), 40.8, 38.0, 30.9, 28.7, 26.8, 26.69, 26.65, 14.8 (CH_3CH). MS (ESI): m/z 236.3 $[\text{M} + \text{H}]^+$.

***N*-(2-cyclohexylpropyl)-4-chloroaniline (132c).** Prepared from 4-chloro-*N*-methylaniline and vinylcyclohexane according to Table VI-4, entry 14. Purified by column chromatography on alumina (hexanes:EtOAc 100:0.3) to give a colorless oil in 82% yield. HPLC (OJ-H, hexane/2-propanol 99.8:0.2, 1.5 mL/min): t_R 21 min (major), 24 min (minor); indicating 71% ee. ^1H NMR (500 MHz, CDCl_3): δ = 7.10 (d, $^3J(\text{H,H}) = 8.8$ Hz, 2H), 6.50 (d, $^3J(\text{H,H}) = 8.8$ Hz, 2H, aryl-H), 3.63 (br s, 1H, NH), 3.11 (dd, $^2J(\text{H,H}) = 12.1$ Hz, $^3J(\text{H,H}) = 5.5$ Hz, 1H, NCH_2), 2.85 (dd, $^2J(\text{H,H}) = 12.1$ Hz, $^3J(\text{H,H}) = 7.8$ Hz, 1H, NCH_2), 1.80–1.73 (m, 2H), 1.70–1.56 (m, 4H), 1.36–0.99 (m, 6H), 0.92 (d, $^3J(\text{H,H}) = 7.1$ Hz, 3H, CH_3); $^{13}\text{C}\{^1\text{H}\}$ NMR (125 MHz, CDCl_3): δ = 147.2 (CCl), 129.0

(CH), 121.3 (C_{ipso}), 113.6 (aryl), 48.0 (CH_2N), 40.7 (CH), 37.9 (CH), 30.8, 28.6, 26.8, 26.7, 26.6 (CH_2), 14.7 (CH_3). MS (ESI): m/z 252.1 $[M+H]^+$.

***N*-(2-cyclohexylpropyl)-4-methoxyaniline (132d).** Prepared from 4-methoxy-*N*-methylaniline and vinylcyclohexane according to Table VI-4

Table VI-4. Substrate scope in the intermolecular asymmetric hydroaminoalkylation catalyzed by **127j-M** (M = Ta, Nb).^a



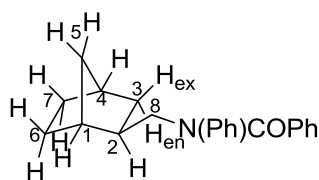
, entry 15. Purified by column chromatography on silica (hexanes/EtOAc 100:1.5) to give a yellow oil in 87% yield. HPLC (AS-H, hexane/2-propanol 95:5, 0.2 mL/min): t_R 36.4 min (minor), 39.8 min (major); indicating 75% ee. ^1H NMR (500 MHz, CDCl_3): δ = 6.78 (d, $^3J(\text{H,H})$ = 9.0 Hz, 2H), 6.57 (d, $^3J(\text{H,H})$ = 9.0 Hz, 2H, aryl-H), 3.74 (s, 3H, CH_3O), 3.37 (br s, 1H, NH), 3.10 (dd, $^2J(\text{H,H})$ = 11.7 Hz, $^3J(\text{H,H})$ = 5.4 Hz, 1H, NCH_2), 2.84 (dd, $^2J(\text{H,H})$ = 11.7 Hz, $^3J(\text{H,H})$ = 7.6 Hz, 1H, NCH_2), 1.79–1.72 (m, 2H), 1.70–1.58 (m, 4H), 1.64–1.49 (m, 4H), 1.36–1.00 (m, 7H), 0.93 (d, $^3J(\text{H,H})$ = 6.9 Hz, 3H, CH_3); $^{13}\text{C}\{^1\text{H}\}$ NMR (125 MHz, CDCl_3): δ = 151.8 (CO), 143.0 (C_{ipso}), 114.9, 113.9 (aryl-CH), 55.9 (CH_3O), 48.9 (CH_2N), 40.8, 38.0, 30.9, 28.7, 26.8, 26.71, 26.66, 14.8 (CH_3CH). MS (ESI): m/z 248.2 $[M+H]^+$.

***N*-(2-trimethylsilylpropyl)aniline (133).**¹² Prepared from *N*-methylaniline and vinyltrimethylsilane according to Table VI-4, entry 17. Purified by column chromatography on alumina (hexanes:EtOAc 100:0.5). Yield 82%, colorless oil. ¹H NMR (500 MHz, CDCl₃): δ = 7.18 (vt, ³*J*(H,H) = 8.2, 7.5 Hz, 2H), 6.69 (vt, ³*J*(H,H) = 8.2, 7.5 Hz, 1H), 6.60 (d, ³*J*(H,H) = 8.4 Hz, 2H, aryl-H), 3.64 (br s, 1H, NH), 3.31–3.27 (m, 1H, NCH₂), 2.95–2.89 (m, 1H, NCH₂), 1.06–1.01 (m, 4H), 0.05 (s, 9H, Si(CH₃)₃); ¹³C{¹H} NMR (125 MHz, CDCl₃): δ = 148.6 (*C*_{ipso}), 129.2, 117.0, 112.7 (aryl-CH), 46.6 (CH₂N), 20.5 (CH), 12.8 (CH₃CH), –3.1 (Si(CH₃)₃).

***N*-(2-trimethylsilylpropyl)-*N*-phenylbenzamide.** Derivatization by method **B**. Purified by column chromatography on silica (hexanes:EtOAc 100:3). Yield 90%, colorless oil. HPLC (AS-H, hexane/2-propanol 98.5:1.5, 1 mL/min): *t*_R 11.1 min (minor), 18.5 min (major); indicating 98% ee. ¹H NMR (300 MHz, CDCl₃): δ = 7.28–7.10 (m, 7H), 7.02 (d, ³*J*(H,H) = 7.3 Hz, 2H, aryl-H), 4.33–4.24 (m, 1H, NCH₂), 3.75 (dd, ²*J*(H,H) = 12.9 Hz, ³*J*(H,H) = 2.9 Hz, 1H, NCH₂), 1.05 (m, 1H, CH), 1.03 (d, ³*J*(H,H) = 2.6 Hz, 3H, CH₃), 0.01 (s, 9H, Si(CH₃)₃); ¹³C{¹H} NMR (75 MHz, CDCl₃): δ = 170.8 (CO), 143.2, 136.8, 129.2, 129.0, 128.5, 127.7, 127.6, 126.3 (aryl), 51.8 (CH₂N), 19.1 (CH), 12.3 (CH₃), –3.3 (Si(CH₃)₃).

***N*-phenyl-*N*-(2,3,3-trimethylbutyl)-*N*-benzamide.** Prepared from *N*-methylaniline and *tert*-butylethylene according to Table VI-4, entry 18. Derivatization by method **A**. Purified by column chromatography on silica (hexanes:EtOAc 100:2). Yield 70%, colorless oil. HPLC (AS-H, hexane/2-propanol 98:2, 1 mL/min): *t*_R 19.2 min

(minor), 25.0 min (major); indicating 81% ee. ^1H NMR (400 MHz, CDCl_3): δ = 7.26–7.00 (m, 8H), 7.02 (d, $^3J(\text{H,H})$ = 7.0 Hz, 2H, aryl-H), 4.23–4.16 (m, 1H, NCH_2), 3.75 (dd, $^2J(\text{H,H})$ = 13.3 Hz, $^3J(\text{H,H})$ = 3.5 Hz, 1H, NCH_2), 1.55–1.46 (m, 1H, CH), 0.96 (d, $^3J(\text{H,H})$ = 7.3 Hz, 3H, CH_3), 0.89 (s, 9H, $\text{C}(\text{CH}_3)_3$); $^{13}\text{C}\{^1\text{H}\}$ NMR (125 MHz, CDCl_3): δ = 170.8 (CO), 143.8, 137.2, 129.1, 128.9, 128.6, 127.8, 127.6, 126.3 (aryl), 52.0 (CH_2N), 41.1 (CHCH_3), 32.5 ($\text{C}(\text{CH}_3)_3$), 27.4 ($\text{C}(\text{CH}_3)_3$), 12.9 (CHCH_3) MS (ESI): m/z 296.2 [$\text{M} + \text{H}$] $^+$.



***N*-(bicyclo[2.2.1]hept-2-ylmethyl)-*N*-phenylbenzamide**

(139).¹⁴ Prepared from norbornene and *N*-methylaniline according to Table VI-4, entry 19, derivatization by method A.

Purified by flash chromatography on silica (hexanes/EtOAc 100:2) to give a colorless oil in 55% yield. HPLC (AS-H, hexane/2-propanol 98:2, 1 mL/min): t_R 29 min (minor), 39 min (major); indicating 61% ee. ^1H NMR (500 MHz, C_6D_6): δ = 7.27–7.11 (m, 8H), 7.03 (d, $^3J(\text{H,H})$ = 7.3 Hz, 2H, aryl-H), 3.93 (dd, $^2J(\text{H,H})$ = 13.5 Hz, $^3J(\text{H,H})$ = 9.0 Hz, 1H, $\text{NCH}_2\{\underline{8}\}$), 3.67 (dd, $^2J(\text{H,H})$ = 13.5 Hz, $^3J(\text{H,H})$ = 7.2 Hz, 1H, $\text{NCH}_2\{\underline{8}\}$), 2.23 (s, 1H, $\{\underline{4}\}$), 2.11 (s, 1H, $\{\underline{1}\}$), 1.71–1.66 (m, 1H, $\{\underline{2}\}$), 1.54–1.42 (m, 3H, $\{\text{exo-}\underline{6}, \text{exo-}\underline{7}, \underline{5}\}$), 1.31–1.24 (m, 1H, $\{\text{endo-}\underline{3}\}$), 1.19–1.12 (m, 2H, $\{\underline{5}, \text{exo-}\underline{3}\}$), 1.09–1.03 (m, 2H, $\{\text{endo-}\underline{6}, \text{endo-}\underline{7}\}$); $^{13}\text{C}\{^1\text{H}\}$ NMR (125 MHz, C_6D_6): δ = 170.7 (C=O), 143.4, 136.6, 129.2, 129.0, 128.5, 128.0, 127.6, 126.5 (aryl), 53.9 ($\text{CH}_2\text{N}\{\underline{8}\}$), 40.5 ($\text{CH}\{\underline{2}\}$), 39.0 ($\text{CH}\{\underline{1}\}$), 36.5 ($\text{CH}\{\underline{4}\}$), 35.5 ($\text{CH}_2\{\underline{3}\}$), 35.2 ($\text{CH}_2\{\underline{5}\}$), 29.6 ($\text{CH}_2\{\underline{6}, \underline{8}\}$), 28.9 ($\text{CH}_2\{\underline{6}, \underline{8}\}$).

***N*-((1-Methylcyclohexyl)methyl)aniline (136).**¹³ Prepared from *N*-methylaniline and methylenecyclohexane according to Table VI-4, entry 21. Purified by column chromatography on alumina (hexanes:EtOAc 100:0.4) to give a colorless oil in 72% yield. ¹H NMR (400 MHz, CDCl₃): δ = 7.15 (dd, ³*J*(H,H) = 8.6, 7.4 Hz, 2H), 7.65 (t, ³*J*(H,H) = 7.4 Hz, 1H), 6.62 (d, ³*J*(H,H) = 8.6 Hz, 2H, aryl-H), 3.57 (br s, 1H, NH), 2.93 (s, 2H, NCH₂), 1.54–1.25 (m, 10H, 5 CH₂), 0.97 (s, 3H, CH₃); ¹³C{¹H} NMR (100 MHz, CDCl₃): δ = 149.2 (C_{ipso}), 129.2 (CH), 116.8 (CH), 112.6 (CH, aryl), 54.7 (NCH₂), 35.8, 34.2, 26.4, 23.4, 21.9.

***N*-(4-Methoxyphenyl)-*N*-((2*S*)-2-phenylpropyl)amine (137).**⁹⁷ Prepared from 4-methoxy-*N*-methylaniline and styrene according to Table VI-4, entry 22. Isomer ratio >30:1. Purified by column chromatography on alumina (hexanes:EtOAc 100:2) to give a yellow oil in 73% yield. HPLC (OJ-H, hexane/2-propanol 90:10, 0.5 mL/min): *t*_R 42 min (*S*, major), 49 min (*R*, minor); indicating 71% ee. ¹H NMR (400 MHz, CDCl₃): δ = 7.25 (vt, ³*J*(H,H) = 8.1 Hz, 7.2 Hz, 2H), 7.17 (d, ³*J*(H,H) = 7.3 Hz, 1H), 7.14 (d, ³*J*(H,H) = 8.1 Hz, 2H), 6.69 (d, ³*J*(H,H) = 9.0 Hz, 2H), 6.46 (d, ³*J*(H,H) = 9.0 Hz, 2H, aryl-H), 3.66 (s, 3H, CH₃O), 3.22 (dd, ²*J*(H,H) = 12.1 Hz, ³*J*(H,H) = 6.2 Hz, 1H, NCH₂), 3.2 (br s, 1H, NH), 3.12 (dd, ²*J*(H,H) = 12.1 Hz, ³*J*(H,H) = 8.2 Hz, 1H, NCH₂), 2.96 (sext, ³*J*(H,H) = 7.1 Hz, 1H, CH), 1.25 (d, ³*J*(H,H) = 7.2 Hz, 3H, CH₃); ¹³C{¹H} NMR (100 MHz, CDCl₃): δ = 152.1 (CO), 144.6 (C_{ipso}), 142.3 (C_{ipso}), 128.6 (CH), 127.2 (CH), 126.6 (CH), 114.9 (CH), 114.3 (aryl), 55.8 (CH₃O), 52.0 (CH₂), 39.2 (CHCH₃), 19.8 (CH₃CH).

***N*-Benzyl-*N*-(2-cyclohexylpropyl)amine (138a).** Prepared from *N*-methylbenzylamine and vinylcyclohexane according to Scheme VI-5. The crude 8:1 mixture of regioisomers was purified by column chromatography on silica gel ($\text{CH}_2\text{Cl}_2/7\text{M NH}_3$ in MeOH 100:1) to give the pure major regioisomer **138a** as a colorless oil in 59% yield and 35% ee. ^1H NMR (500 MHz, CDCl_3): δ = 7.36–7.29 (m, 4H), 7.26–7.21 (m, 1H aryl-H), 3.79 (d, $^2J(\text{H,H})$ = 13.3 Hz, 1H, PhCH_2N), 3.75 (d, $^2J(\text{H,H})$ = 13.3 Hz, 1H, PhCH_2N), 2.62 (dd, $^2J(\text{H,H})$ = 11.5 Hz, $^3J(\text{H,H})$ = 5.6 Hz, 1H, NCH_2CH), 2.41 (dd, $^2J(\text{H,H})$ = 11.5 Hz, $^3J(\text{H,H})$ = 7.8 Hz, 1H, NCH_2CH), 1.74–1.70 (m, 2H), 1.65–1.61 (m, 1H), 1.59–1.48 (m, 4H), 1.30–0.91 (m, 7H), 0.86 (d, $^3J(\text{H,H})$ = 6.9 Hz, 3H, CH_3); $^{13}\text{C}\{^1\text{H}\}$ NMR (125 MHz, CDCl_3): δ = 140.7 (C_{ipso}), 128.3, 128.0, 126.8 (aryl-CH), 54.2 (PhCH_2N), 53.4 (NCH_2CH), 40.8 (CH), 38.4 (CH), 31.0, 28.5, 26.9, 26.8, 26.7 (CH_2 , Cy), 14.8 (CH_3). ^{19}F NMR of Mosher amide of 2-cyclohexylpropan-1-amine (470 MHz, C_6D_6 , 60 °C): δ = –69.45 (major), –69.48 (minor).

Characteristic signals of the minor regioisomer 2-cyclohexyl-*N*-methyl-1-phenylpropan-1-amine (**138b**) were obtained from ^1H NMR spectroscopic analysis of the crude reaction mixture which was concentrated *in vacuo* and dissolved in CDCl_3 . ^1H NMR (400 MHz, CDCl_3): δ = 3.50 (d, $^3J(\text{H,H})$ = 6.8 Hz, 1H, PhCHN), 2.23 (s, 3H, CH_3NH), other signals overlap with the signals of the major regioisomer.

General procedure for NMR-scale catalytic hydroamination/cyclization reactions. In the glovebox, a screw cap NMR tube was charged with ferrocene (6.0 mg, 32.3 μmol), C_6D_6 (0.4 mL), and the substrate (0.30 mmol). Then a solution of the catalyst, either prepared *in situ* or isolated, in C_6D_6 (10 w%) was added. The NMR tube

was sealed, removed from the glovebox and placed in the thermostated oil bath and the conversion was monitored by NMR spectroscopy by following the disappearance of the olefinic signals of the substrate relative to the internal standard ferrocene. The reaction time was recorded when a conversion of at least 95% was achieved.

General procedure for the determination of enantiomeric excess via Mosher amides. The amine (0.08–0.1 mmol) or the equivalent volume of the crude reaction mixture (approx 0.15 mL) was dissolved in CDCl₃ or toluene-*d*₈ (0.5 mL) in a NMR tube. DIPEA (2.5 equiv with respect to the amine) and (*R*)-Mosher acid chloride (1.5 equiv with respect to the amine) were added. Enantiomeric excess was then determined by ¹⁹F NMR spectroscopy at 60–100 °C.

Preparative-scale procedure for 2-methyl-4,4-diphenylpyrrolidine (16).⁸⁶ In the glovebox, a screw cap NMR tube was charged with aminoalkene (94 mg, 0.40 mmol), C₆D₆ (0.4 mL) and a solution of **127a-Ta** (223 mg, 10 w% in C₆D₆, 20 μmol, 5 mol%). The solution was then kept 100 °C overnight. The solution was diluted with CH₂Cl₂ (2 mL), and loaded onto a short silica pad. Dichloromethane was used to elute the proligand, and then CH₂Cl₂/7M NH₃ in MeOH (100:1) was used to elute the reaction product. Concentration *in vacuo* gave 75 mg of the target compound (80%) as a colorless oil in 61% ee according to ¹⁹F NMR spectroscopy of the Mosher amide. ¹H NMR (400 MHz, C₆D₆): δ = 7.22–7.20 (m, 2H), 7.14–7.08 (m, 6H), 7.04–7.00 (m, 2H, aryl-H), 3.51 (d, ²*J*(H,H) = 10.9 Hz, 1H, CH₂N), 3.34 (d, ²*J*(H,H) = 10.9 Hz, 1H, CH₂N), 3.16–3.11 (m, 1H, CHN), 2.39 (dd, ²*J*(H,H) = 12.4 Hz, ³*J*(H,H) = 6.3 Hz, 1H, CHCH₂), 1.80 (dd,

$^2J(\text{H,H}) = 12.3 \text{ Hz}$, $^3J(\text{H,H}) = 9.2 \text{ Hz}$, 1H, CHCH₂), 1.27 (br s, 1H, NH), 1.01 (d, $^3J(\text{H,H}) = 6.2 \text{ Hz}$, 3H, CH₃); $^{13}\text{C}\{^1\text{H}\}$ NMR (75.5 MHz, C₆D₆): $\delta = 148.8, 148.2, 128.4, 127.58, 127.51, 126.04, 126.00$ (aryl), 58.7 (CH₂NH), 57.3 (CPh₂), 53.1 (CH(CH₃)NH), 47.6 (CH₂), 22.5 (CH₃).

Isotopic labeling studies

Isotope exchange in the absence of alkene (typical procedure). In a glovebox, a screw cap NMR tube was charged with (*R*)-**127j-Ta** (3.9 mg, 5 μmol), *N*-(ethyl-*d*₅)-aniline (31.5 mg, 0.25 mmol), and C₆D₆ (500 μL). Ferrocene (5 mg) was added and the NMR tube was sealed and removed from the glovebox. The mixture was then placed into a thermostated oil bath and was monitored periodically by observing the aromatic signals in the ^1H NMR spectra compared to the signal of ferrocene as an internal standard. After 50 hours at 150 °C, the reaction mixture was cooled down, loaded on silica and concentrated. Flash column chromatography on a short silica pad (hexanes:EtOAc 100:1.5) gave 19 mg (60%) of the starting material as a colorless liquid. $^2\text{H}\{^1\text{H}\}$ NMR (CHCl₃ + 25 μL of CDCl₃, 46 MHz): $\delta = 6.67$ (s, 0.38 D, *o*-CD, aryl), 3.14 (s, 1.57D, CD₂), 1.22 (s, 3D, CD₃).

Isotope exchange in the catalytic process (example 1). In a glovebox, a screw cap NMR tube was charged with (*R*)-**127j-Nb** (0.10 M in C₆D₆, 20 μL , 2 μmol), *N*-(methyl-*d*₃)-aniline (22.0 mg, 0.20 mmol), 1-octene (44.8 mg, 0.40 mmol) and C₆D₆ (400

μL). Ferrocene (5 mg) was added and the NMR tube was sealed and removed from the glovebox. The mixture was then placed into a thermostated (150 °C) oil bath and was monitored periodically by observing the aromatic signals in the ^1H NMR spectra compared to the signal of ferrocene as an internal standard. After 30 hours at 150 °C, the reaction mixture was cooled down, loaded on alumina and concentrated. Column chromatography on alumina (hexanes) yielded the hydroaminoalkylation product **6a** (35.0 mg, 79%) as a colorless liquid. ^1H NMR (500 MHz, CDCl_3): δ = 7.16 (vt, $^3J(\text{H,H})$ = 8.4, 7.4 Hz, 2H), 6.67 (vt, $^3J(\text{H,H})$ = 8.4, 7.4 Hz, 1H), 6.59 (d, $^3J(\text{H,H})$ = 8.4 Hz, 2H, aryl-H), 3.61 (br s, 1H, NH), 3.16–3.12 (m, 0.05H, NCH_2), 2.90–2.85 (m, 0.05H, NCH_2), 1.79–1.61 (m, 6H), 1.39–0.99 (m, 6H), 0.93 (d, $^3J(\text{H,H})$ = 7.0 Hz, 0.12H, CH_3), 0.91 (dm, $^3J(\text{H,H})$ = 6.8 Hz, 1.92H, CH_2D); $^2\text{H}\{^1\text{H}\}$ NMR (46 MHz, CHCl_3 + 25 μL of CDCl_3): δ = 3.16 (s, 0.95D, N CD_2), 2.89 (s, 0.95D, N CD_2), 0.96 (s, 0.96D, CH_2D). After derivatization by method **B**: HPLC (OD-H, hexane/2-propanol 99:1, 0.5 mL/min): t_R 24.8 min (minor), 26.2 (major); indicating 79.5% ee.

Isotope exchange in the catalytic process (example 2). In a glovebox, a screw cap NMR tube was charged with (*R*)-**127j-Nb** (0.10 M in C_6D_6 , 20 μL , 2 μmol), *N*-(methyl- d_3)-aniline (22.0 mg, 0.20 mmol), norbornene (44.8 mg, 0.40 mmol) and C_6D_6 (400 μL). The mixture was then placed into a thermostated (140 °C) oil bath and was monitored periodically by observing the aromatic signals in ^1H NMR spectra compared to the signal of ferrocene as an internal standard. After 15 hours at 140 °C, the reaction mixture was cooled down, derivatized by method **A**, loaded on silica and concentrated. Column chromatography on silica (hexanes:EtOAc 100:2) yielded the

hydroaminoalkylation product **139-D** (33.6 mg, 55%) as a white solid. HPLC (AS-H, hexane/2-propanol 98:2, 1 mL/min): t_R 29 min (minor), 39 min (major); indicating 30% ee. ^1H NMR (500 MHz, C_6D_6): δ = 7.27–7.11 (m, 8H), 7.03 (d, $^3J(\text{H,H})$ = 7.3 Hz, 2H, aryl-H), 3.89 (m, 0.04H, NCH_2), 3.64 (m, 0.04H, NCH_2), 2.21 (s, 1H), 2.09 (s, 1H), 1.69–1.65 (m, 1H), 1.54–1.42 (m, 3H), 1.31–1.24 (m, 1H), 1.17–1.11 (m, 1H), 1.08–1.04 (m, 2H); $^2\text{H}\{^1\text{H}\}$ NMR (46 MHz, CHCl_3 + 25 μL of CDCl_3): δ = 3.89 (s, 0.96D, NCD_2), 3.68 (s, 0.96D, NCD_2), 1.17 (s, 0.9D, 3-*exo*-CHD).

Typical Kinetic procedure

In a glovebox, a screw cap NMR tube was charged with aliquots of standard solutions of **127j-Nb** (100 μL , 0.105M in C_6D_6) and *N*-methylaniline (100 μL , 1.62 M in C_6D_6), and then 1-octene (60 μL , 0.368 mmol) and C_6D_6 (340 μL) were added for a total volume of 600 μL . Ferrocene (5–8 mg) was added and the NMR tube was sealed and removed from the glovebox. The mixture was then placed into a thermostated oil bath and the disappearance of *N*-methylaniline was monitored periodically by observing the aromatic signals in ^1H NMR spectra compared to the signal of ferrocene as an internal standard.

Since the reactions were interrupted multiple times for taking the NMR spectra at room temperature a control experiment was performed with 3 identical reaction mixtures to confirm that interrupted reaction is representative to a “continuous” mode. Mixtures **I–III** were prepared as stated in the typical procedure (Table VI-9).

Table VI-9. Comparison of the “interrupted” and “continuous” reaction modes.

Sample	Kept @ 150 °C (single interval), min	Number of intervals	Kept @ rt between two runs, min	Total time @ 150 °C, min	Convers ion, %
I	300	1	-	300	62
II	150	2	30	300	63
III	50	6	14	300	60

As shown in Table VI-9, the conversion for mixtures I–III was nearly identical proving that the reaction can be interrupted and re-initiated multiple times without introducing significant error.

The reaction progress data was either directly transformed into conventional kinetic curves in appropriate coordinates or was subjected to nonlinear regression analysis using the Dynafit TM (version 3.28.070) package.⁵⁵ The fitting routine was supplied with the proposed mechanistic schemes, initial concentration data for alkene, amine and catalyst, data on the reaction progress and initial estimates for the rate constants.

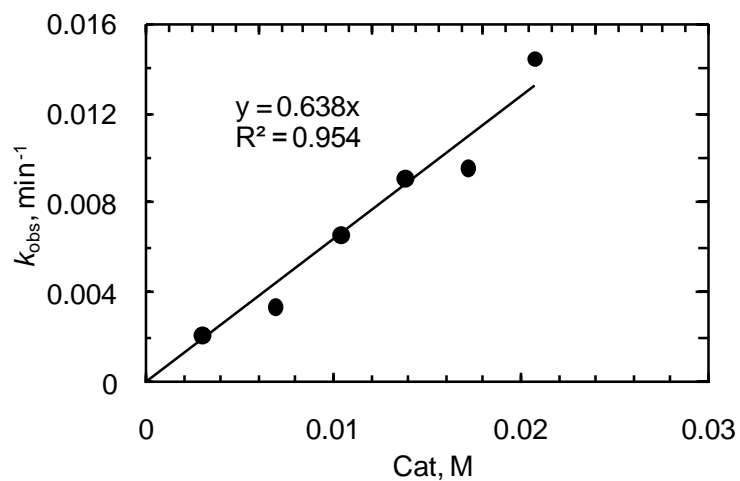


Figure VI-11. First order dependence of observed first-order reaction constant on catalyst concentration for the reaction of 1-octene (0.613 M) with PMPNHMe (**128d**) (0.20 M) in the presence of (*R*)-**127j-Nb** (0.003–0.022 M) in C₆D₆ at 150 °C.

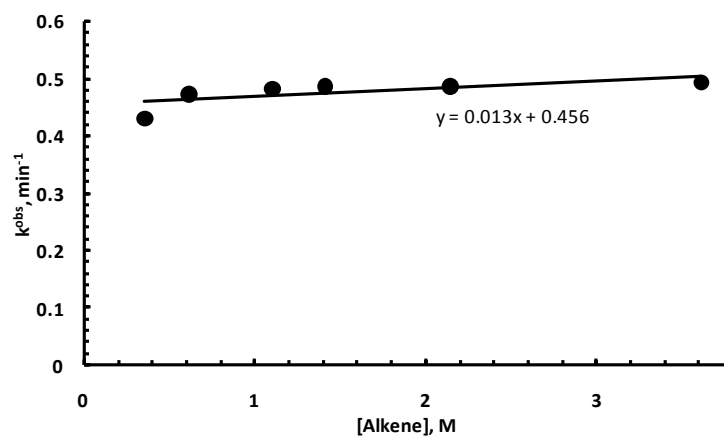


Figure VI-12. Zero order dependence of the first-order rate constant on the alkene concentration for the reaction of 1-octene (0.35–3.73 M) with PMPNHMe (**128d**) (0.290 M) in the presence of (*R*)-**127j-Nb** (0.017 M) in C₆D₆ at 150 °C.

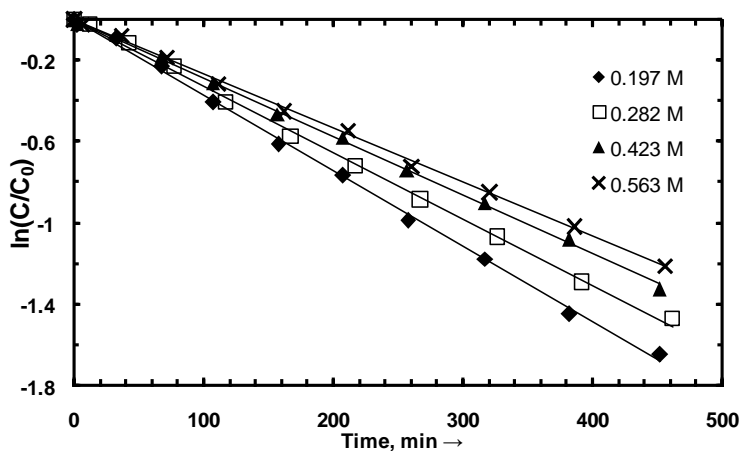


Figure VI-13. First order logarithmic plots for the reaction of 1-octene (0.613 M) with PhNHMe (**128a**) (0.197–0.563 M) in the presence of (*R*)-**127j-Nb** (0.017 M) in C₆D₆ at 150 °C.

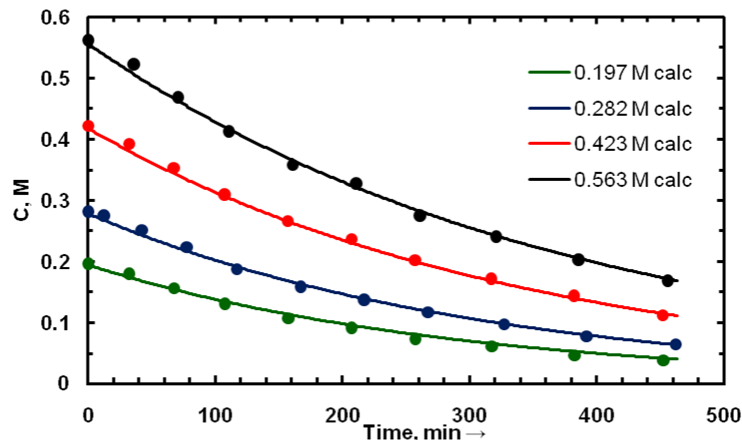


Figure VI-14. Experimental reaction progress data (dots) for the reaction of 1-octene (0.613 M) with PhNHMe (**128a**) (0.197–0.563 M) in the presence of (*R*)-**127j-Nb** (0.017 M) in C₆D₆ at 150 °C vs. the simulated reaction curves (lines) for $k_4 = (0.33 \pm 0.02) \text{ M}^{-1} \text{ min}^{-1}$, $K^{\text{dorm}} = (1.6 \pm 0.3) \text{ M}^{-1}$.

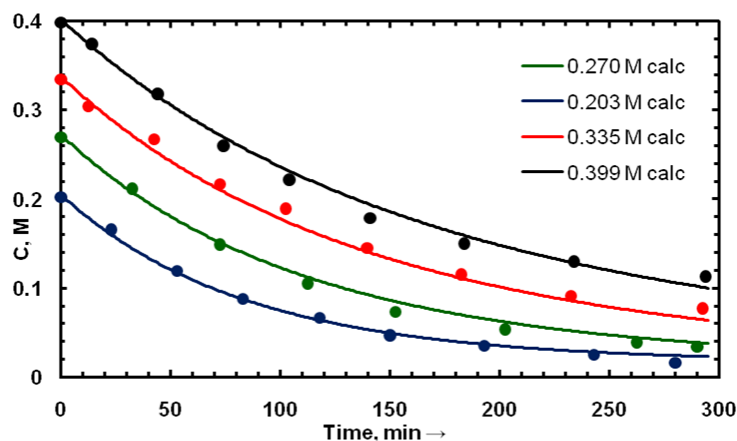


Figure VI-15. Experimental reaction progress data (dots) for the reaction of 1-octene (0.613 M) with PMPNHMe (**128d**) (0.203–0.399 M) in the presence of (*R*)-**127j-Nb** (0.017 M) in C₆D₆ at 150 °C vs. the simulated reaction curves (lines) for $k_4 = (3.1 \pm 1.2) \text{ M}^{-1} \text{ min}^{-1}$, $K^{\text{dorm}} = (14.5 \pm 5.0) \text{ M}^{-1}$.

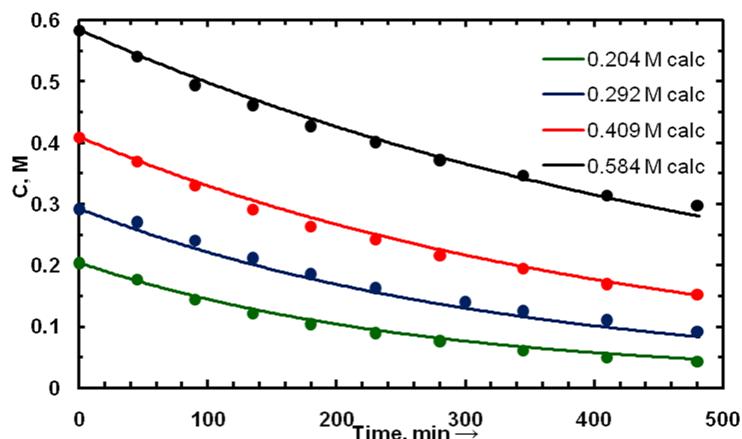


Figure VI-16. Experimental reaction progress data (dots) for the reaction of 1-octene (0.613 M) with *p*-ClC₆H₄NHMe (**128c**) (0.204–0.584 M) in the presence of (*R*)-**127j-Nb** (0.017 M) in C₆D₆ at 150 °C vs. the simulated reaction curves (lines) for $k_4 = (0.58 \pm 0.15) \text{ M}^{-1} \text{ min}^{-1}$, $K^{\text{dorm}} = (7.8 \pm 2.4) \text{ M}^{-1}$.

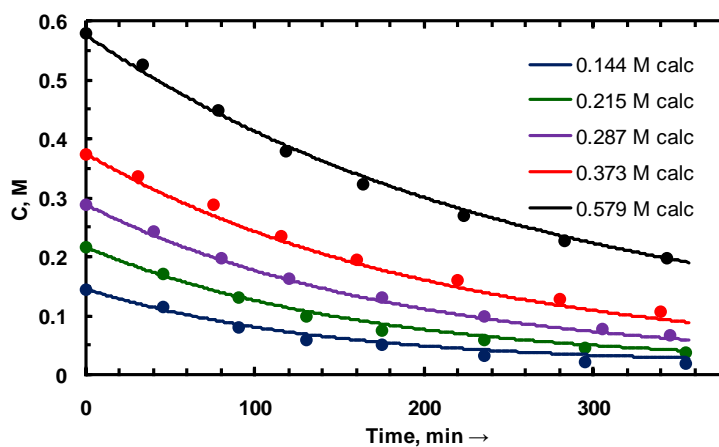


Figure VI-17. Experimental reaction progress data (dots) for the reaction of 1-octene (0.613 M) with *p*-FC₆H₄NHMe (**128b**) (0.144–0.579 M) in the presence of (*R*)-**127j-Nb** (0.017 M) in C₆D₆ at 150 °C vs. the simulated reaction curves (lines) for $k_4 = (0.58 \pm 0.09) \text{ M}^{-1} \text{ min}^{-1}$, $K^{\text{dorm}} = (2.8 \pm 0.7) \text{ M}^{-1}$.

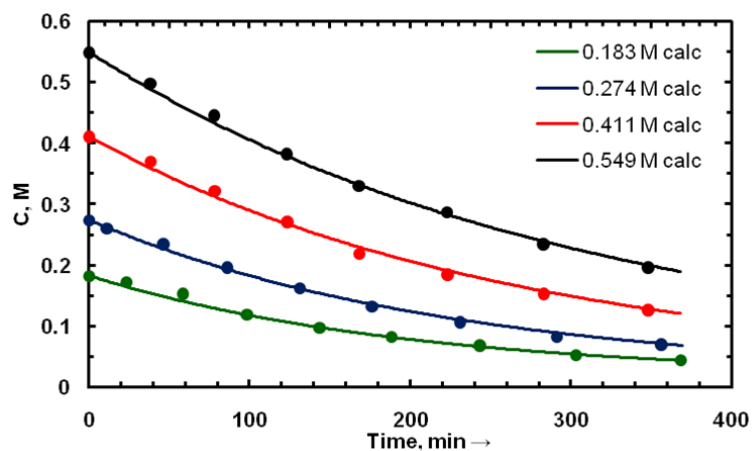


Figure VI-18. Experimental reaction progress data (dots) for the reaction of 1-octene (0.613 M) with PhNHCD₃ (**128a-CD₃**) (0.183–0.549 M) in the presence of (*R*)-**127j-Nb** (0.017 M) in C₆D₆ at 150 °C vs. the simulated reaction curves (lines) for $k_4 = (0.38 \pm 0.05) \text{ M}^{-1}\text{min}^{-1}$, $K^{\text{dorm}} = (1.9 \pm 0.5) \text{ M}^{-1}$.

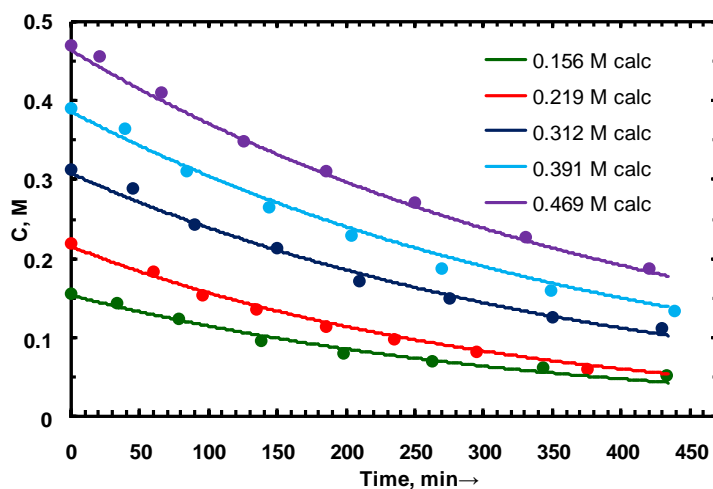


Figure VI-19. Experimental reaction progress data (dots) for the reaction of 1-octene (0.613 M) with PhNDMe (**128a-ND**) (0.156–0.469 M) in the presence of (*R*)-**127j-Nb** (0.020 M) in C₆D₆ at 150 °C vs. the simulated reaction curves (lines) for $k_4 = (0.33 \pm 0.02) \text{ M}^{-1}\text{min}^{-1}$, $K^{\text{dorm}} = (1.1 \pm 0.6) \text{ M}^{-1}$.

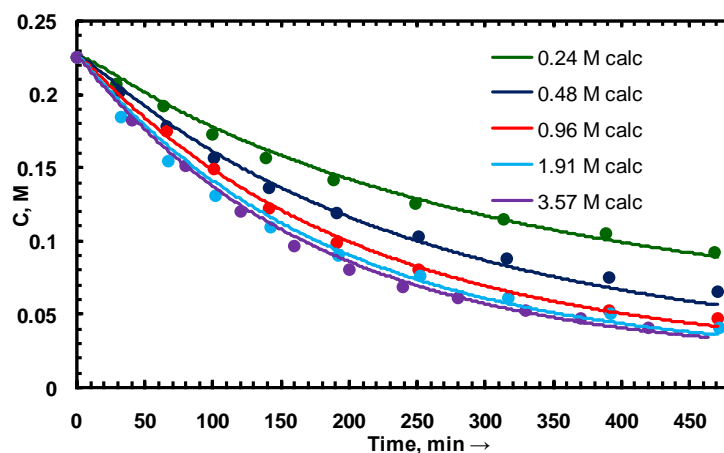


Figure VI-20. Experimental reaction progress data (dots) for the reaction of vinylcyclohexane (0.24–3.57 M) with PhNHMe (**128a**) (0.225 M) in the presence of (*R*)-**127j-Nb** (0.019 M) in C₆D₆ at 150 °C vs. the simulated reaction curves (lines) for $k_4 = (0.39 \pm 0.03) \text{ M}^{-1} \text{ min}^{-1}$, $k_{12} = (0.39 \pm 0.06) \text{ M}^{-1} \text{ min}^{-1}$, $K^{\text{dorm}} = 1.6 \text{ M}^{-1}$. The value of K^{dorm} was determined for 1-octene (see Figure VI-14).

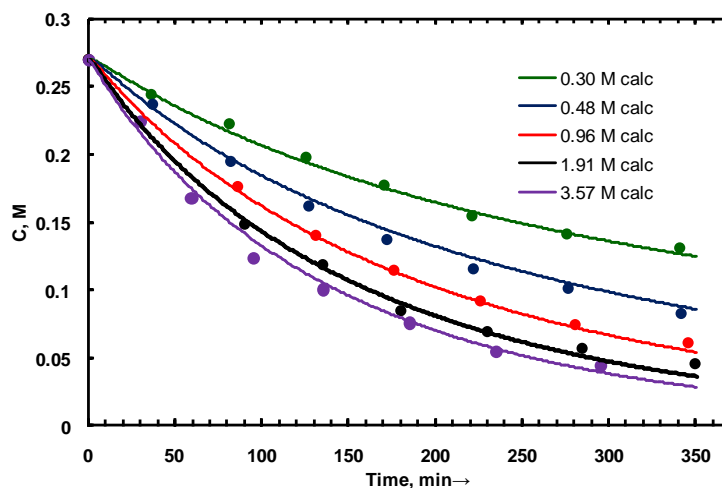


Figure VI-21. Experimental reaction progress data (dots) for the reaction of vinylcyclohexane (0.30–3.57 M) with *p*-FC₆H₄NHCH₃ (**128b**) (0.270 M) in the presence of (*R*)-**127j-Nb** (0.018 M) in C₆D₆ at 150 °C vs. the simulated reaction curves (lines) for

$k_4 = (0.89 \pm 0.05) \text{ M}^{-1}\text{min}^{-1}$, $k_{12} = (0.41 \pm 0.03) \text{ M}^{-1}\text{min}^{-1}$, $K^{\text{dorm}} = 2.8 \text{ M}^{-1}$. The value of K^{dorm} was determined for 1-octene (see Figure VI-17).

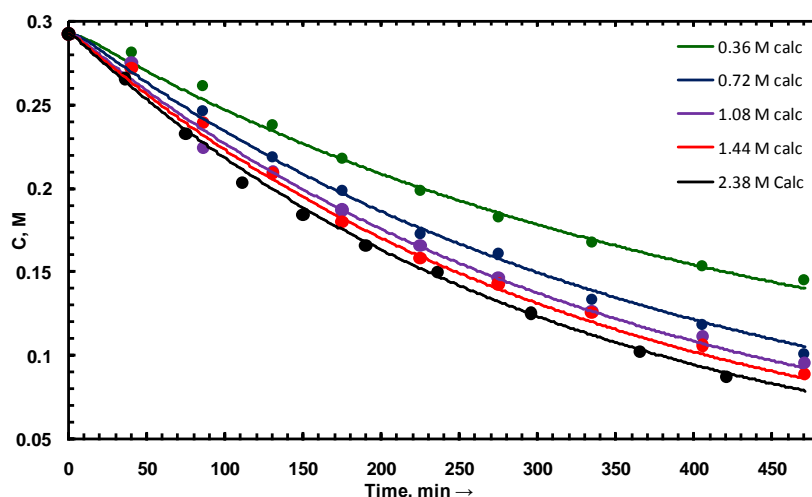


Figure VI-22. Experimental reaction progress data (dots) for the reaction of vinylcyclohexane (0.36–2.38 M) with $p\text{-ClC}_6\text{H}_4\text{NHCH}_3$ (**128c**) (0.292 M) in the presence of (*R*)-**127j-Nb** (0.017 M) in C_6D_6 at 150 °C vs. the simulated reaction curves (lines) for $k_4 = (0.67 \pm 0.03) \text{ M}^{-1}\text{min}^{-1}$, $k_{12} = (0.65 \pm 0.09) \text{ M}^{-1}\text{min}^{-1}$, $K^{\text{dorm}} = 7.8 \text{ M}^{-1}$. The value of K^{dorm} was determined for 1-octene (see Figure VI-16).

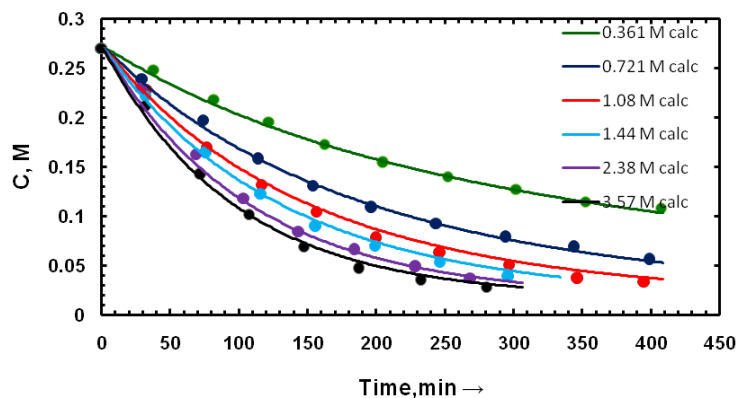


Figure VI-23. Experimental reaction progress data (dots) for the reaction of vinylcyclohexane (0.361–3.57 M) with PMPNHCH_3 (**128d**) (0.270 M) in the presence of (*R*)-**127j-Nb** (0.017 M) in C_6D_6 at 150 °C vs. the simulated reaction curves (lines) for k_4

$= (3.7 \pm 0.2) \text{ M}^{-1}\text{min}^{-1}$, $k_{12} = (0.92 \pm 0.05) \text{ M}^{-1}\text{min}^{-1}$, $K^{\text{dorm}} = 14.4 \text{ M}^{-1}$. The value of K^{dorm} was determined for 1-octene (see Figure VI-15).

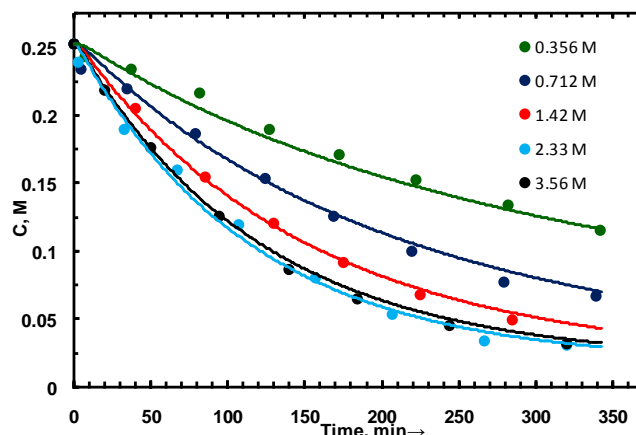


Figure VI-24. Experimental reaction progress data (dots) for the reaction of vinylcyclohexane (0.30–3.57 M) with PMPNHCD₃ (**128d-CD₃**) (0.253 M) in the presence of (*R*)-**127j-Nb** (0.017 M) in C₆D₆ at 150 °C vs. the simulated reaction curves (lines) for $k_4 = (3.0 \pm 0.3) \text{ M}^{-1}\text{min}^{-1}$, $k_{12} = (0.78 \pm 0.09) \text{ M}^{-1}\text{min}^{-1}$, $K^{\text{dorm}} = 14.5 \text{ M}^{-1}$. The value of K^{dorm} was determined for 1-octene/PMPNHCH₃ (Figure VI-15).

Crystallography. X-ray quality crystals of **127l-Ta** and **127l-Nb** were obtained by recrystallization from pentane solution at room temperature. Data were collected on a Bruker APEX-II CCD Diffractometer at 100(2) K, wavelength 0.71073 Å and are summarized in Table VI-10. Cell parameters were obtained from 7638 (**127l-Ta**), respectively 9870 (**127l-Nb**) reflections within the range $1.7 < \theta < 31.5^\circ$. Lorentz, polarization, and empirical absorption corrections were applied. The space group was determined from systematic absences. The structure was solved by direct methods (SHELXS program).⁹⁸ All positional and atomic displacement parameters (ADP) were

refined with all reflections data by full-matrix least squares on F^2 using SHELXL.⁹⁸ Non-hydrogen atoms were refined anisotropically. One of the silane groups and one the naphthyl rings are disordered occupationally (occupancy ratios 85:15 for **127I-Ta** and 91:9 for **127I-Nb**) and were refined as independent parts in SHELXL. Hydrogen atoms were constrained to idealized positions using a riding model. The absolute structure was refined using the Flack parameter.⁹⁹ The drawing of the molecule (Figure VI-25) was realized with the help of WinOrtep-3.¹⁰⁰

Table VI-10. Crystal structure and refinement data for **127I-Nb** and **127I-Ta**.

Compound	127I-Nb	127I-Ta
Empirical formula	$C_{38}H_{58}N_3O_2Si_2Nb$	$C_{38}H_{58}N_3O_2Si_2Ta$
Formula weight	737.96	826.00
Crystal system	Monoclinic	Monoclinic
Space group	$P2_1$	$P2_1$
Unit cell dimensions	$a = 10.7656(7) \text{ \AA}$, $\alpha = 90^\circ$ $b = 15.5456(10) \text{ \AA}$, $\beta = 95.076(1)^\circ$ $c = 11.9463(8) \text{ \AA}$, $\gamma = 90^\circ$	$a = 10.7857(5) \text{ \AA}$, $\alpha = 90^\circ$ $b = 15.5435(7) \text{ \AA}$, $\beta = 95.170(1)^\circ$ $c = 11.9546(6) \text{ \AA}$, $\gamma = 90^\circ$
Volume	$1991.5(2) \text{ \AA}^3$	$1996.01(16) \text{ \AA}^3$
Z	2	2
Density (calculated)	1.231 Mg/m^3	1.374 Mg/m^3
Absorption coefficient	0.396 mm^{-1}	2.847 mm^{-1}
F(000)	784	848
Crystal size	$0.18 \times 0.16 \times 0.12 \text{ mm}^3$	$0.23 \times 0.21 \times 0.14 \text{ mm}^3$
Θ range for data collection	1.90 to 31.50°	1.71 to 31.53°
Index ranges	$-15 \leq h \leq 15$, $-22 \leq k \leq 22$, $-17 \leq l \leq 17$	$-15 \leq h \leq 15$, $-22 \leq k \leq 22$, $-7 \leq l \leq 17$
Reflections collected	25295	25245

Independent reflections	12954 [R(int) = 0.0173]	12885 [R(int) = 0.0129]
Completeness to θ	99.9%	99.5 %
Absorption correction	Semi-empirical from equivalents	Semi-empirical from equivalents
Max. and min. transmission	0.4353 and 0.3950	0.730 and 0.574
Data / restraints / parameters	12954 / 11 / 490	12885 / 287 / 496
Goodness-of-fit on F^2	1.006	1.017
Final R indices [$I > 2\sigma(I)$]	R1 = 0.0245, wR2 = 0.0599	R1 = 0.0161, wR2 = 0.0386
R indices (all data)	R1 = 0.0254, wR2 = 0.0605	R1 = 0.0165, wR2 = 0.0388
Absolute structure parameter	−0.040(13)	−0.011(3)
Largest diff. peak and hole	0.566 and −0.210 e.Å ^{−3}	0.749 and −0.343 e.Å ^{−3}

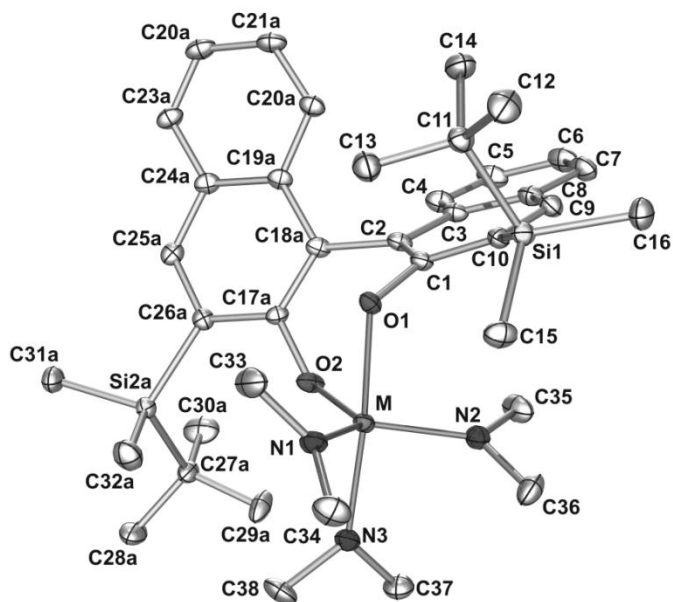


Figure VI-25. ORTEP diagram of the molecular structure of the isostructural complexes **127I-M** (M = Nb, Ta). Thermal ellipsoids are shown with a 50% probability level. Hydrogen atoms as well as one position of the disordered naphthyl ring and the silane group are omitted for clarity.

VI.6 References

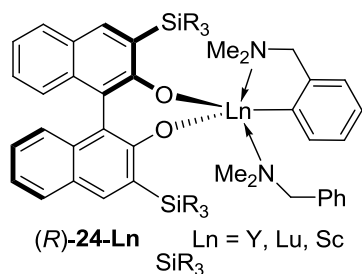
- (1) Roesky, P. W. *Angew. Chem., Int. Ed.* **2009**, *48*, 4892-4894.
- (2) Eisenberger, P.; Schafer, L. L. *Pure Appl. Chem.* **2010**, *82*, 1503-1515.
- (3) Clerici, M. G.; Maspero, F. *Synthesis* **1980**, 305-306.
- (4) Nugent, W. A.; Ovenall, D. W.; Holmes, S. J. *Organometallics* **1983**, *2*, 161-162.
- (5) Horrillo-Martínez, P.; Hultsch, K. C.; Gil, A.; Branchadell, V. *Eur. J. Org. Chem.* **2007**, 3311-3325.
- (6) Müller, C.; Saak, W.; Doye, S. *Eur. J. Org. Chem.* **2008**, 2731-2739.
- (7) Kubiak, R.; Prochnow, I.; Doye, S. *Angew. Chem. Int. Ed.* **2009**, *48*, 1153-1156.
- (8) Prochnow, I.; Kubiak, R.; Frey, O. N.; Beckhaus, R.; Doye, S. *ChemCatChem* **2009**, *1*, 162-172.
- (9) Bexrud, J. A.; Eisenberger, P.; Leitch, D. C.; Payne, P. R.; Schafer, L. L. *J. Am. Chem. Soc.* **2009**, *131*, 2116-2118.
- (10) Kubiak, R.; Prochnow, I.; Doye, S. *Angew. Chem. Int. Ed.* **2010**, *49*, 2626-2629.
- (11) Prochnow, I.; Zark, P.; Müller, T.; Doye, S. *Angew. Chem. Int. Ed.* **2011**, *50*, 6401-6405.
- (12) Herzon, S. B.; Hartwig, J. F. *J. Am. Chem. Soc.* **2007**, *129*, 6690-6691.
- (13) Herzon, S. B.; Hartwig, J. F. *J. Am. Chem. Soc.* **2008**, *130*, 14940-14941.
- (14) Eisenberger, P.; Ayinla, R. O.; Lauzon, J. M. P.; Schafer, L. L. *Angew. Chem. Int. Ed.* **2009**, *48*, 8361-8365.
- (15) Zi, G.; Zhang, F.; Song, H. *Chem. Commun.* **2010**, *46*, 6296-6298.
- (16) Zhang, F.; Song, H.; Zi, G. *Dalton Trans.* **2011**, *40*, 1547-1566.
- (17) Wood, M. C.; Leitch, D. C.; Yeung, C. S.; Kozak, J. A.; Schafer, L. L. *Angew. Chem. Int. Ed.* **2007**, *46*, 354-358.
- (18) Gott, A. L.; Clarke, A. J.; Clarkson, G. J.; Scott, P. *Organometallics* **2007**, *26*, 1729-1737.
- (19) Reznichenko, A. L.; Hultsch, K. C. *Organometallics* **2010**, *29*, 24-27.
- (20) Ayinla, R. O.; Gibson, T.; Schafer, L. L. *J. Organomet. Chem.* **2011**, *696*, 50-60.
- (21) Cummings, S.; Tunge, J. A.; Norton, J. R. *Top. Organomet. Chem.* **2005**, *10*, 1-41.
- (22) Reznichenko, A. L.; Nguyen, H. N.; Hultsch, K. C. *Angew. Chem., Int. Ed.* **2010**, *49*, 8984-8987.
- (23) Thorn, M. G.; Moses, J. E.; Fanwick, P. E.; Rothwell, I. P. *J. Chem. Soc., Dalton Trans.* **2000**, 2659-2660.
- (24) Ru Son, A. J.; Schweiger, S. W.; Thorn, M. G.; Moses, J. E.; Fanwick, P. E.; Rothwell, I. P. *Dalton Trans.* **2003**, 1620-1627.
- (25) Watson, P. L.; Parshall, G. W. *Acc. Chem. Res.* **1985**, *18*, 51-56.
- (26) Thompson, M. E.; Baxter, S. M.; Bulls, A. R.; Burger, B. J.; Nolan, M. C.; Santarsiero, B. D.; Schaefer, W. P.; Bercaw, J. E. *J. Am. Chem. Soc.* **1987**, *109*, 203-219.
- (27) Fendrick, C. M.; Marks, T. J. *J. Am. Chem. Soc.* **1986**, *108*, 425-437.

- (28) Sadow, A. D.; Tilley, T. D. *J. Am. Chem. Soc.* **2003**, *125*, 7971-7977.
- (29) Sadow, A. D.; Tilley, T. D. *Angew. Chem., Int. Ed.* **2003**, *42*, 803-805.
- (30) Gagné, M. R.; Stern, C. L.; Marks, T. J. *J. Am. Chem. Soc.* **1992**, *114*, 275-294.
- (31) Allan, L. E. N.; Clarkson, G. J.; Fox, D. J.; Gott, A. L.; Scott, P. *J. Am. Chem. Soc.* **2010**, *132*, 15308-15320.
- (32) Dunne, J. F.; Fulton, D. B.; Ellern, A.; Sadow, A. D. *J. Am. Chem. Soc.* **2010**, *132*, 17680-17683.
- (33) Manna, K.; Xu, S.; Sadow, A. D. *Angew. Chem. Int. Ed.* **2011**, *50*, 1865-1868.
- (34) Arrowsmith, M.; Crimmin, M. R.; Barrett, A. G. M.; Hill, M. S.; Kociok-Köhn, G.; Procopiou, P. A. *Organometallics* **2011**, *30*, 1493-1506.
- (35) Leitch, D. C.; Platel, R. H.; Schafer, L. L. *J. Am. Chem. Soc.* **2011**, *133*, 15453-15463.
- (36) Hangaly, N. K.; Petrov, A. R.; Rufanov, K. A.; Harms, K.; Elffferding, M.; Sundermeyer, J. *Organometallics* **2011**, *30*, 4544-4554.
- (37) Manna, K.; Kruse, M. L.; Sadow, A. D. *ACS Catal.* **2011**, *1*, 1637-1642.
- (38) Zhang, X.; Emge, T. J.; Hultzs, K. C. *Angew. Chem. Int. Ed.* **2012**, *51*, 394-398.
- (39) Hanley, P. S.; Markovic, D.; Hartwig, J. F. *J. Am. Chem. Soc.* **2010**, *132*, 6302-6303.
- (40) Hanley, P. S.; Hartwig, J. F. *J. Am. Chem. Soc.* **2011**, *133*, 15661-15673.
- (41) Neukom, J. D.; Perch, N. S.; Wolfe, J. P. *J. Am. Chem. Soc.* **2010**, *132*, 6276-6277.
- (42) Neukom, J. D.; Perch, N. S.; Wolfe, J. P. *Organometallics* **2011**, *30*, 1269-1277.
- (43) White, P. B.; Stahl, S. S. *J. Am. Chem. Soc.* **2011**, *133*, 18594-18597.
- (44) Zhang, J.; Yang, C.-G.; He, C. *J. Am. Chem. Soc.* **2006**, *128*, 1798-1799.
- (45) McKinney Brooner, R. E.; Widenhoefer, R. A. *Chem. Eur J.* **2011**, *17*, 6170-6178.
- (46) Casalnuovo, A. L.; Calabrese, J. C.; Milstein, D. *J. Am. Chem. Soc.* **1988**, *110*, 6738-6744.
- (47) Gallazzi, M. C.; Porri, L.; Vitulli, G. *J. Organomet. Chem.* **1975**, *97*, 131-138.
- (48) Catellani, M.; Motti, E.; Della Ca, N. *Acc. Chem. Res.* **2008**, *41*, 1512-1522.
- (49) Martins, A.; Mariampillai, B.; Lautens, M.; Yu, J.-Q.; Shi, Z. *Top. Curr. Chem.* **2010**, *292*, 1-33.
- (50) Tobisch, S. *Chem. Eur J.* **2011**, *17*, 14974-14986.
- (51) Gribkov, D. V.; Hultzs, K. C.; Hampel, F. *J. Am. Chem. Soc.* **2006**, *128*, 3748-3759.
- (52) Hong, S.; Kawaoka, A. M.; Marks, T. J. *J. Am. Chem. Soc.* **2003**, *125*, 15878-15892.
- (53) Parkin, G. *Acc. Chem. Res.* **2009**, *42*, 315-325.
- (54) Gómez-Gallego, M.; Sierra, M. A. *Chem. Rev.* **2011**, *111*, 4857-4963.
- (55) Kuzmič, P. *Anal. Biochem.* **1996**, *237*, 260-273.

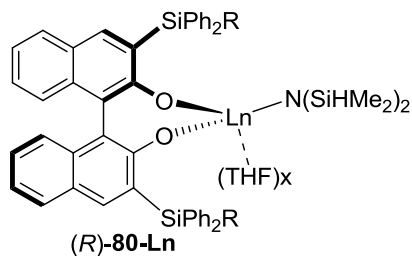
- (56) Coles, N.; Harris, M. C. J.; Whitby, R. J.; Blagg, J. *Organometallics* **1994**, *13*, 190-199.
- (57) Mayer, J. M.; Curtis, C. J.; Bercaw, J. E. *J. Am. Chem. Soc.* **1983**, *105*, 2651-2660.
- (58) Anderson, L. L.; Arnold, J.; Bergman, R. G. *Org. Lett.* **2004**, *6*, 2519-2522.
- (59) Anderson, L. L.; Arnold, J.; Bergman, R. G. *Org. Lett.* **2006**, *8*, 2445.
- (60) Lorber, C.; Choukroun, R.; Vendier, L. *Organometallics* **2004**, *23*, 1845-1850.
- (61) Maurya, M. R.; Arya, A.; Kumar, U.; Kumar, A.; Avecilla, F.; Pessoa, J. C. *Dalton Trans.* **2009**, 9555-9566.
- (62) Near, K. E.; Chapin, B. M.; McAnnally-Linz, D. C.; Johnson, A. R. *J. Organomet. Chem.* **2011**, *696*, 81-86.
- (63) Hansen, M. C.; Heusser, C. A.; Narayan, T. C.; Fong, K. E.; Hara, N.; Kohn, A. W.; Venning, A. R.; Rheingold, A. L.; Johnson, A. R. *Organometallics* **2011**, *30*, 4616-4623.
- (64) Bexrud, J. A.; Schafer, L. L. *Dalton Trans.* **2010**, *39*, 361-363.
- (65) Shen, X.; Buchwald, S. L. *Angew. Chem. Int. Ed.* **2010**, *49*, 564-567.
- (66) Giardello, M. A.; Conticello, V. P.; Brard, L.; Gagné, M. R.; Marks, T. J. *J. Am. Chem. Soc.* **1994**, *116*, 10241-10254.
- (67) Müller, T. E.; Hultsch, K. C.; Yus, M.; Foubelo, F.; Tada, M. *Chem. Rev.* **2008**, *108*, 3795-3892.
- (68) Hong, S.; Marks, T. J. *Acc. Chem. Res.* **2004**, *37*, 673-686.
- (69) Quinet, C.; Jourdain, P.; Hermans, C.; Ates, A.; Lucas, I.; Markó, I. E. *Tetrahedron* **2008**, *64*, 1077-1087.
- (70) Horrillo Martínez, P.; Hultsch, K. C.; Hampel, F. *Chem. Commun.* **2006**, 2221-2223.
- (71) Datta, S.; Gamer, M. T.; Roesky, P. W. *Organometallics* **2008**, *27*, 1207-1213.
- (72) Crimmin, M. R.; Arrowsmith, M.; Barrett, A. G. M.; Casely, I. J.; Hill, M. S.; Procopiou, P. A. *J. Am. Chem. Soc.* **2009**, *131*, 9670-9685.
- (73) Zhang, X.; Emge, T. J.; Hultsch, K. C. *Organometallics* **2010**, *29*, 5871-5877.
- (74) Manna, K.; Ellern, A.; Sadow, A. D. *Chem. Commun.* **2010**, *46*, 339-341.
- (75) Stubbert, B. D.; Marks, T. J. *J. Am. Chem. Soc.* **2007**, *129*, 6149-6167.
- (76) Majumder, S.; Odom, A. L. *Organometallics* **2008**, *27*, 1174-1177.
- (77) Leitch, D. C.; Payne, P. R.; Dunbar, C. R.; Schafer, L. L. *J. Am. Chem. Soc.* **2009**, *131*, 18246-18247.
- (78) Walsh, P. J.; Baranger, A. M.; Bergman, R. G. *J. Am. Chem. Soc.* **1992**, *114*, 1708-1719.
- (79) Baranger, A. M.; Walsh, P. J.; Bergman, R. G. *J. Am. Chem. Soc.* **1993**, *115*, 2753-2763.
- (80) Johnson, J. S.; Bergman, R. G. *J. Am. Chem. Soc.* **2001**, *123*, 2923-2924.
- (81) Pohlki, F.; Doye, S. *Angew. Chem. Int. Ed.* **2001**, *40*, 2305-2308.
- (82) Straub, B. F.; Bergman, R. G. *Angew. Chem. Int. Ed.* **2001**, *40*, 4632-4635.

- (83) Anderson, L. L.; Schmidt, J. A. R.; Arnold, J.; Bergman, R. G. *Organometallics* **2006**, *25*, 3394-3406.
- (84) Reznichenko, A. L.; Emge, T. J.; Audörsch, S.; Klauber, E. G.; Hultsch, K. C.; Schmidt, B. *Organometallics* **2011**, *30*, 921-924.
- (85) Smith, P. M.; Thomas, E. J. *J. Chem. Soc., Perkin Trans. 1* **1998**, 3541-3556.
- (86) Hong, S.; Tian, S.; Metz, M. V.; Marks, T. J. *J. Am. Chem. Soc.* **2003**, *125*, 14768-14783.
- (87) Tamaru, Y.; Hojo, M.; Higashimura, H.; Yoshida, Z. *J. Am. Chem. Soc.* **1998**, *110*, 3994-4002.
- (88) Bender, C. F.; Widenhoefer, R. A. *J. Am. Chem. Soc.* **2005**, *127*, 1070-1071.
- (89) Kondo, T.; Okada, T.; Mitsudo, T.-a. *J. Am. Chem. Soc.* **2002**, *124*, 186-187.
- (90) Bexrud, J. A.; Beard, J. D.; Leitch, D. C.; Schafer, L. L. *Org. Lett.* **2005**, *7*, 1959-1962.
- (91) Black, D. S. C.; Doyle, J. E. *Austr. J. Chem.* **1978**, *31*, 2247-2257.
- (92) Collin, J.; Daran, J.-D.; Jacquet, O.; Schulz, E.; Trifonov, A. *Chem. Eur. J.* **2005**, *11*, 3455-3462.
- (93) Masaoka, S.; Banno, T.; Ishikawa, M. *J. Organomet. Chem.* **2006**, *691*, 174-181.
- (94) Totland, K. M.; Boyd, T. J.; Lavoie, G. G.; Davis, W. M.; Schrock, R. R. *Macromolecules* **1996**, *29*, 6114-6125.
- (95) Maruoka, K.; Ito, T.; Araki, Y.; Shirasaka, T.; Yamamoto, H. *Bull. Chem. Soc. Jpn.* **1988**, *61*, 2975-2976.
- (96) Lyčka, A.; Šnobl, D.; Handlír, K.; Holeček, J.; Nádvorník, M. *Collect. Czech. Chem. Commun.* **1982**, *47*, 603-612.
- (97) Hoffmann, S.; Nicoletti, M.; List, B. *J. Am. Chem. Soc.* **2006**, *128*, 13074-13075.
- (98) Sheldrick, G. *Acta Crystallogr.* **2008**, *A64*, 112-122.
- (99) Flack, H. *Acta Cryst.* **1983**, *A39*, 876-881.
- (100) Farrugia, L. J. *J. Appl. Cryst.* **1997**, *30*, 565.

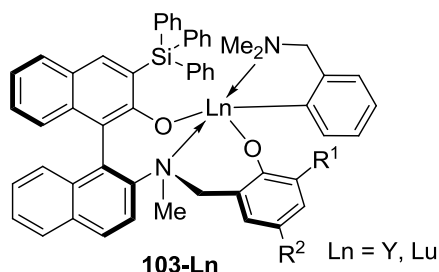
Appendix A. Structures of complexes.



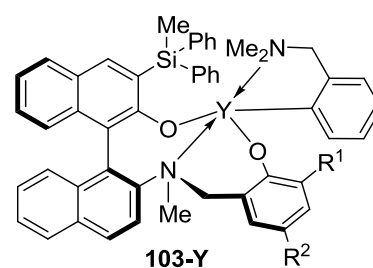
	SiR ₃
(<i>R</i>)- 24a-Ln	SiPh ₃
(<i>R</i>)- 24b-Y	Si(3,5-Me ₂ C ₆ H ₃) ₃
(<i>R</i>)- 24c-Y	SiPh ₂ tBu
(<i>R</i>)- 24d-Y	SiPh ₂ Cy
(<i>R</i>)- 24e-Y	SiPh ₂ Bn
(<i>R</i>)- 24f-Y	SiPh ₂ (2-PhC ₆ H ₄)
(<i>R</i>)- 24g-Y	SiPh ₂ (4-MeOC ₆ H ₄)
(<i>R</i>)- 24h-Y	Si(4- <i>t</i> -BuC ₆ H ₄) ₄
(<i>R</i>)- 24i-Y	Si(<i>i</i> -Pr) ₃



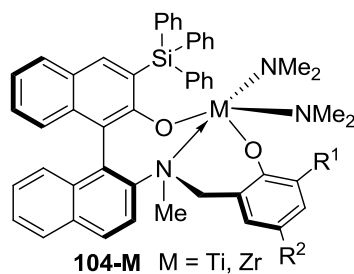
(<i>R</i>)- 80a-Y	R = Ph, x = 2
(<i>R</i>)- 80a-La	R = Ph, x = 0
(<i>R</i>)- 80j-Y	R = Me, x = 2



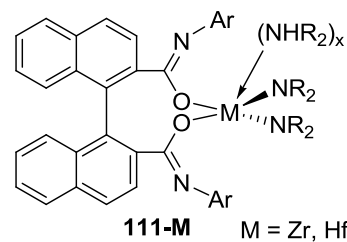
	R ¹	R ²
(<i>S</i>)- 103a-Ln	<i>t</i> -Bu	<i>t</i> -Bu
(<i>S</i>)- 103b-Ln	SiPh ₂ Me	Me
(<i>S</i>)- 103c-Ln	SiPh ₃	Me
(<i>R</i>)- 103d-Ln	Si(3,5-Me ₂ C ₆ H ₃) ₃	Me
(<i>S</i>)- 103e-Ln	Si(<i>t</i> -BuPh ₂)	Me



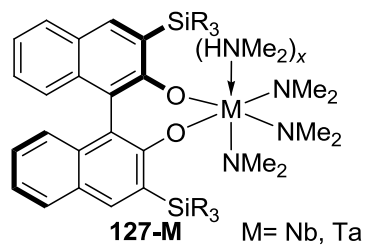
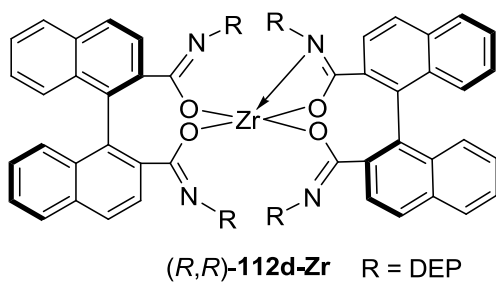
	R ¹	R ²
(<i>S</i>)- 103f-Y	<i>t</i> -Bu	<i>t</i> -Bu
(<i>S</i>)- 103g-Y	SiPh ₂ Me	Me



	R ¹	R ²
(<i>S</i>)- 104a-Zr	<i>t</i> -Bu	<i>t</i> -Bu
(<i>S</i>)- 104b-M	SiPh ₂ Me	Me
(<i>S</i>)- 104c-Zr	SiPh ₃	Me
(<i>R</i>)- 104d-Zr	Si(3,5-Me ₂ C ₆ H ₃) ₃	Me
(<i>S</i>)- 104e-Zr	Si(<i>t</i> -BuPh ₂)	Me

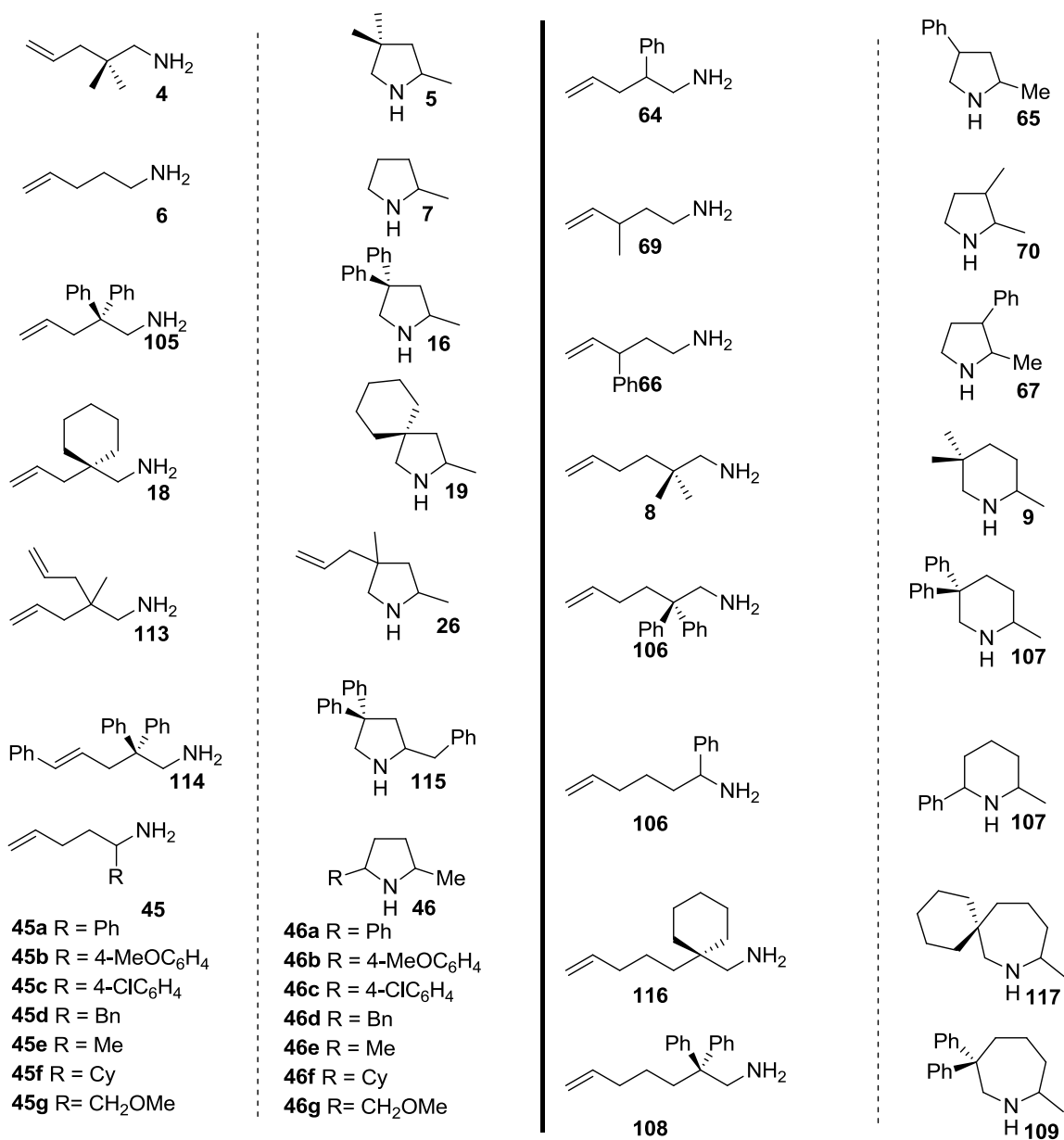


	Ar	R	x
(<i>S</i>)- 111c-Zr	Mes	Me	2
(<i>R</i>)- 111ca-Zr	Mes	Et	1
(<i>R</i>)- 111d-M	DEP	Me	2
(<i>S</i>)- 111e-Zr	DiPP	Me	1
(<i>S</i>)- 111g-Zr	2,4,6-MeO ₃ C ₆ H ₂	Me	2
(<i>R</i>)- 111h-Zr	2-Me-1-Naphthyl	Me	2



	SiR ₃	x, M = Ta	x, M = Nb
(<i>S</i>)- 127a-M	SiPh ₃	1	1
(<i>R</i>)- 127e-M	SiPh ₂ Bn	1	1
(<i>R</i>)- 127j-M	SiPh ₂ Me	1	1
(<i>S</i>)- 127k-M	Si(<i>i</i> -Pr) ₂ Me	1	0
(<i>S</i>)- 127l-M	SiMe ₂ <i>t</i> -Bu	0	0
(<i>R</i>)- 127m-M	SiMe ₃	1	1

Appendix B. Structures of aminoalkenes and the corresponding hydroamination/cyclization products.



Curriculum Vitae

Alexander Reznichenko

Education

10/2012	Ph.D. in Chemistry, Department of Chemistry & Chemical Biology, Rutgers University, Piscataway, NJ
09/2007-06/2012	Doctoral Candidate, Rutgers University
11/2006-06/2007	Graduate research assistant at the Institute of Organic Chemistry, Friedrich-Alexander University of Erlangen-Nuremberg, Germany.
2006	Diploma in Chemistry, Moscow State University, Russia
2001-2006	Moscow State University, Department of Chemistry, Organic Chemistry major

Doctoral Publications

1. Reznichenko, A. L.; Hultzs, K. C. "Group 5 Metal Binaphtholate Complexes as Highly Enantioselective Catalysts for Asymmetric Hydroaminoalkylation: A Mechanistic Study" *J. Am. Chem. Soc.* **2012**, *134*, 3300-3311.
2. Reznichenko, A. L.; Hultzs, K. C. "Hydroamination of Alkenes" *Organic Reactions* [submitted for publication].
3. Reznichenko, A. L.; Hultzs, K. C. Early Transition Metal and Main Group Metal Catalyzed Hydroamination" *Top. Organomet. Chem.* **2012** [in press].
4. Reznichenko, A. L.; Emge, T. J., Audörsch, S.; Klauber, E. G.; Hultzs, K. C.; Schmidt, B. "Group 5 Metal Binaphtholate Complexes for the Catalytic Asymmetric Hydroaminoalkylation and Hydroamination/Cyclization" *Organometallics* **2011**, *30*, 921-924.
5. Reznichenko, A. L.; Nguyen, H. N.; Hultzs, K. C. "Asymmetric Intermolecular Hydroamination of Unactivated Alkenes with Simple Amines" *Angew. Chem. Int. Ed.* **2010**, *49*, 8984-8987; *Angew. Chem.* **2010**, *122*, 9168-9171.
6. Reznichenko, A. L.; Hultzs, K. C. "Hydroamination, Hydrophosphination, Hydrophosphinylation, and Hydrophosphonylation of Carbon-Carbon Double Bonds" in *Science of Synthesis, Vol. 1*. Ed. de Vries, J. G. Thieme, **2010**, 689-729.
7. Reznichenko, A. L.; Hultzs, K. C. "Catalytic σ -Bond Metathesis" *Struct. Bond.* **2010**, *137*, 1-48.
8. Reznichenko, A. L.; Hultzs, K. C. " C_2 -Symmetric Zirconium Bis(Amidate) Complexes with Enhanced Reactivity in Aminoalkene Hydroamination" *Organometallics* **2010**, *29*, 24-27.
9. Reznichenko, A. L.; Hultzs, K. C. "Asymmetric Hydroamination" in *Chiral Amine Synthesis: Methods, Developments and Applications*. Ed. Nugent, T. Wiley, **2010**, 341-376.
10. Reznichenko, A. L.; Hampel, F.; Hultzs, K. C. "Kinetic Resolution of Aminoalkenes by Asymmetric Hydroamination: A Mechanistic Study" *Chem. Eur. J.*, **2009**, *15*, 12819-12827.